DOT/FAA/TC-17/7

Federal Aviation Administration
William J. Hughes Technical Center
Aviation Research Division
Atlantic City International Airport
New Jersey 08405

Mode I (G1c) Fracture Toughness of Composite Sandwich Structures for Use in Damage Tolerance Design and Analysis: Vol. III Supplemental Static Testing

March 2018

Final Report

This document is available to the U.S. public through the National Technical Information Services (NTIS), Springfield, Virginia 22161.

This document is also available from the Federal Aviation Administration William J. Hughes Technical Center at actlibrary.tc.faa.gov.

U.S. Department of Transportation
Federal Aviation Administration

NOTICE

Technical Report Documentation Page

1. Report No.	2. Government Accession No.	3. Recipient's Catalog No.
DOT/FAA/TC-17/7		

4. Title and Subtitle	5. Report Date
MODE I (G1C) FRACTURE TOUGHNESS OF COMPOSITE SANDWICH STRUCTURES FOR USE IN DAMAGE TOLERANCE DESIGN AND ANALYSIS: VOL. III SUPPLEMENTAL STATIC TESTING	March 2018
	6. Performing Organization Code

7. Author(s)	8. Performing Organization Report No.
John S. Tomblin, Waruna Seneviratne, and Shawn Denning	

9. Performing Organization Name and Address	10. Work Unit No. (TRAIS)
	11. Contract or Grant No.

12. Sponsoring Agency Name and Address	13. Type of Report and Period Covered
FAA Northwest Mountain Regional Office 1601 Lind Ave SW Renton, WA 98057	14. Sponsoring Agency Code AIR-100

15. Supplementary Notes

The FAA William J. Hughes Technical Center Aviation Research Division CORs were Lynn Pham and Curtis Davies.

16. Abstract

This report, Volume III in a set of three volumes, contains results of Mode I static testing of composite sandwich structures for sandwich variables not tested in Volume I. The first volume contains results of Mode I static testing, and the second volume contains results of Mode I fatigue testing. This report contains the supplemental static test results of an investigation carried out to further understand the influence of sandwich parameters–such as core type, cell size, core density, disbond location, fabrication process, ribbon direction, and crack-tip location–on the onset and growth of damage in sandwich composites. Core properties such as core density, cell size, and core type influenced fracture toughness. Fabrication processes had no effect on fracture toughness. The information gathered throughout this research will be instrumental in developing analytical methods and validating finite element analysis procedures to further investigate the damage growth mechanics of sandwich composite structures. The data can also be used in the design of sandwich structures constructed from similar materials and geometries tested here.

17. Key Words	18. Distribution Statement
Progressive damage growth, Composite sandwich, Fracture mechanics, Mode I, Core properties	This document is available to the U.S. public through the National Technical Information Service (NTIS), Springfield, Virginia 22161. This document is also available from the Federal Aviation Administration William J. Hughes Technical Center at actlibrary.tc.faa.gov.

19. Security Classif. (of this report)	20. Security Classif. (of this page)	21. No. of Pages	22. Price
Unclassified	Unclassified	345	

ACKNOWLEDGEMENTS

This research program was funded by FAA William J. Hughes Technical Center, Atlantic City, NJ. The authors would like to thank Curtis Davies, FAA William J. Hughes Technical Center, and Dr. Larry Ilcewicz, FAA Seattle Aircraft Certification Office, for technical guidance. In addition, the support from Cessna Aircraft, Bombardier Aerospace, Hawker Beechcraft, and Spirit Aerosystems is appreciated.

The authors also would like to thank the National Institute for Aviation Research Composites and Structures Laboratory staff, namely Janith Senaratne, Chee-Kuen Chan, Jason Koehn, Sheun-Wuay Cheng, Kenny Yee, and Chandi Dahal for their commitment, hard work, and support during test specimen fabrication, testing, and data reduction.

TABLE OF CONTENTS

LIST OF FIGURES

LIST OF TABLES

LIST OF SYMBOLS AND ACRONYMS

5%/max	5% radial offset or max load onset of crack growth
β	Geometric Correction Parameter
δ	End displacement of cantilever beam
Δa	Additional crack length required to correct for cantilever beam not being perfectly built in
ΔA	Overall change in crack length
σ	Stress
ε	Strain
a	Crack length
a_o	Prescribed crack length
b	Specimen width
B	*y*-Intercept
E	Stiffness
F	Large displacement correction factor
G	Strain energy release rate
Gc	Fracture toughness or critical strain energy release rate
GIC	Mode I fracture toughness
GIC (NL)	Mode I fracture toughness measured at non-linear onset of crack growth
GIC (VIS)	Mode I fracture toughness measured at visual onset of crack growth
GIC (5%/max)	Mode I fracture toughness measured at 5% radial offset or max load onset of crack growth
I	Second moment of inertia of cantilever beam
L	Length of specimen
M	Moment applied to cantilever beam
P	Load applied to cantilever beam
t	Distance from bottom surface of cantilever beam to load line in piano hinge
V	Volume
x	Axial direction of cantilever beam
y	Normal-to-axial direction of cantilever beam
AM	Area method
APO	Adhesive pullout failure
C	Tensile core failure
CCFS	Co-cured facesheet(s)
CDT	Critical damage threshold
CPO	Core pullout failure
DCB	Double-cantilever beam
FPD	First-ply delamination
FSF	Facesheet shear failure
HX	Hexagonal core
IFD	Interlaminar facesheet delamination
MBT	Modified beam theory
NL	Non-linear
OX	Over-expanded core
PCFS	Pre-cured facesheet(s)

SCB	Single-cantilever beam
SERR	Strain energy release rate
VIS	Visual

EXECUTIVE SUMMARY

This report contains the supplemental static test results of an investigation carried out to further understand the influence of sandwich parameters—such as core type, cell size, core density, disbond location, fabrication process, ribbon direction, and crack tip location—on the onset damage in sandwich composites. This investigation was conducted using single-cantilever beam static and fatigue testing for Mode I fracture toughness of a core-facesheet disbond. The initial static test data, including fluid-ingression data and fatigue test data, were published as Volumes I and II. Core properties, such as core density, cell size, and core type, influenced fracture toughness, whereas fabrication processes had no effect. The information gathered through this research will be instrumental in developing analytical methods and validating finite element analysis procedures to further investigate the damage growth mechanics of sandwich composite structures. The data can also be used in the design of composite sandwich structures constructed with materials and geometries similar to those tested here.

1. INTRODUCTION

Over the past 25 years, the use of advanced composite materials in aircraft primary structures has increased significantly. In 1994, with the Advanced General Aviation Transport Experiments program, NASA and the FAA revitalized the use of composites in general and commercial aviation. Driven by the demand for fuel-efficient, lightweight, and high-stiffness structures that have fatigue durability and corrosion resistance, large modern commercial aircraft are designed with more than 50% composite materials. The certification for composites must meet rigorous structural integrity, safety, and durability requirements. Despite the many advantages of composite structures, composite structural certification becomes challenging because of the lack of experience involving large-scale structures, complex interactive failure mechanisms, sensitivity to temperature and moisture, and scatter in the data, especially fatigue data.

The onset of damage propagation and the critical damage threshold (CDT) is a function of the stress level for a particular damage configuration. Typically, certification programs adopt the "no-growth" damage-tolerant design concept, whereby a composite structure is required to demonstrate the ability to contain intrinsic manufacturing defects and the maximum allowable service damage(s) in adverse operational conditions and throughout the design life of the structure (i.e., the allowable damage limit is selected so that the fatigue stress level corresponding to the limit load of the structure will not cause the onset of damage propagation prior to a life corresponding to the design service goal). In contrast, a "stable-growth" damage-tolerance design concept must consider the damage growth only if all of the following apply:

1. Damage growth is stable or an arrest mechanism is in place prior to the damage reaching CDT.
2. Damage growth can be predicted through analysis and can be verified by testing.
3. At least two inspection intervals occur prior to the damage reaching the CDT, if applicable.

Because the onset of damage propagation depends on several design parameters, such as load spectrum/severity, damage configuration, environmental exposure, facesheet parameters, and sandwich core parameters, the application of load-enhancement factors to a structure that exhibits stable damage growth during test substantiation may significantly alter the fatigue life. Damage-tolerance substantiation through the stable-growth approach for a specific structure requires knowledge of the onset (initiation) and growth rate (propagation) of damage as well as factors that influence both of them. Based on experimental validation, fracture toughness of the adhesive or core can be used to predict the damage initiation [1]. The influence of key parameters, such as initial damage configuration, environmental exposure, facesheet parameters, and sandwich core parameters on both initiation and propagation must be studied in detail and incorporated into the certification process to mitigate risks associated with the stable-growth approach. The data contained in this report and the preceding volumes (I and II) encompass information regarding the fracture toughness of sandwich structures; the influence of facesheet and core parameters provide an understanding of sandwich structure design space and failure mechanism. The influence of sandwich parameters, such as core type, cell size, core density, disbond location, fabrication process, ribbon direction, and crack tip location on the onset and damage growth of sandwich composites was investigated. These sandwich variables were not investigated in tests reported in Volume I. This investigation used single-cantilever beam (SCB) static testing for Mode I fracture

toughness (GIC) of a core-facesheet construction, because the failures occurred in core, core adhesive interface, and adhesive. The effects of fluid ingression will not be evaluated in this report; those results are found in Volume I. The flow chart (see figure 1) demonstrates how the data generated in this program will result in guidance for durability and damage tolerance of sandwich composite structures.

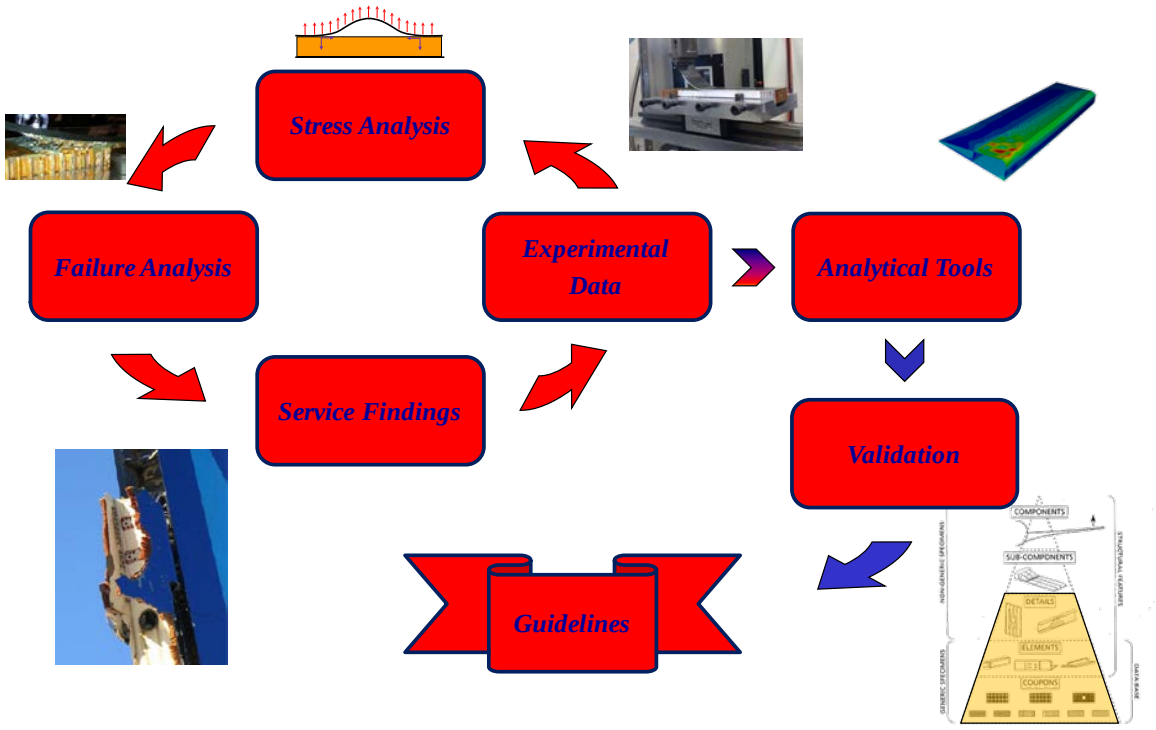

Figure 1. Objective of current research program

Crack growth can be characterized by three modes [2, 3]: Mode I (opening mode), Mode II (sliding or in-plane shear mode), and Mode III (tearing or out-of-plane shear mode), as shown in figure 2. It is common for combinations of these three modes to be present at a crack tip unless care is taken to isolate them, especially in coupon-level testing. All three volumes of these test reports address the Mode I (opening mode) fracture toughness of sandwich structures.

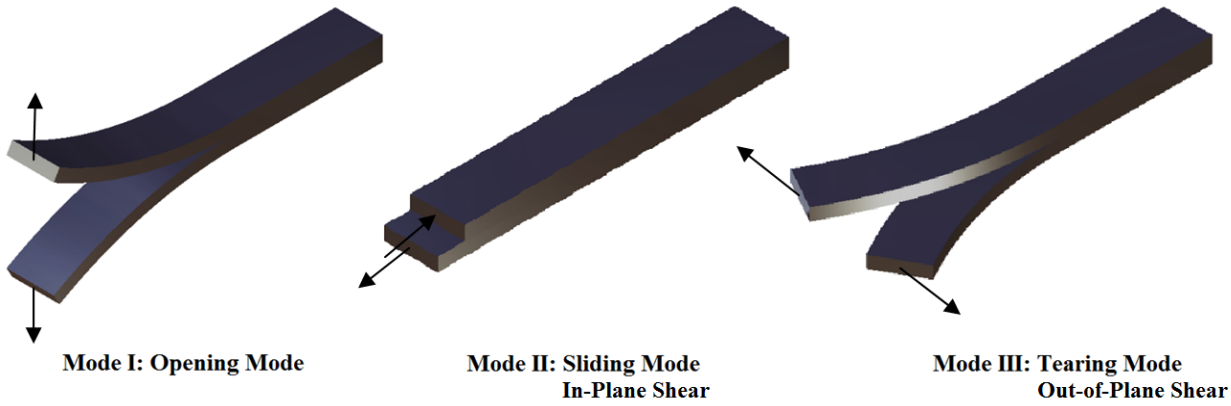

Figure 2. Fracture modes

GIC opening mode is considered a material property. For the tests performed here, GIC has a broader meaning. It should be best understood as a structural property of a given sandwich construction. Different failure modes are encountered and, therefore, a strict definition of a material property does not apply.

2. EXPERIMENTAL PROCEDURE

It is important to note that the procedures involved in testing sandwich composite specimens for strain energy release rate (SERR or G) has no engineering standard dictating proper methods. Similar test procedures and data reduction themes were investigated [4–8], and a new procedure was developed modifying the existing procedure for testing laminate double-cantilever beam (DCB) specimens in combination with work done by Cantwell and Davies on SCB specimens [7, 8].

2.1 SANDWICH SCB TEST

The primary objective of this report was to determine the GIC of several sandwich composite material systems. Therefore, it was imperative to develop and use a test configuration that isolated Mode I crack propagation and mitigated Mode II-/Mode III-induced crack growth. Volume I presented an in-depth analysis of how the test procedure was selected, so only a brief synopsis is contained herein. The DCB test method was compared with the SCB test, as shown in figure 3. It was determined that the DCB test was unsuitable for sandwich testing because of unsymmetric loading and a stiffness mismatch. The SCB test proved to mitigate the unfavorable conditions found in DCB testing. Furthermore, once the SCB test was placed on a sliding foundation, as shown in figure 4, mode mixity was mitigated, and Mode I loading was obtained.

(a) (b)

Figure 3. The (a) DCB and (b) SCB test configurations [9]

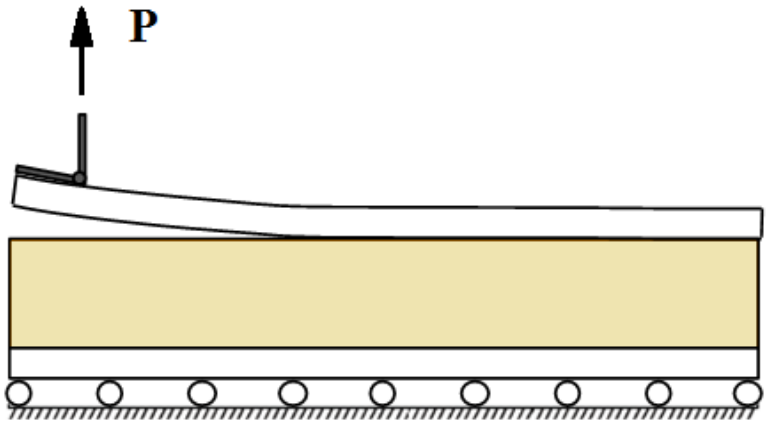

Figure 4. Sandwich SCB test

2.1.1 Test Fixture

As determined in Volume I, the SCB test method provides a reliable means of determining GIC. Furthermore, the SCB test diminishes the effects of the unsymmetric loading of sandwich specimens and the effects of a stiffness mismatch. In addition, it reduces the effects of mode mixity. This mode mixity can be further mitigated by creating a very long loading arm, thereby reducing the component of force in the shear direction, or by placing the specimen on a sliding foundation, which releases the force in the shear direction every time it overcomes static friction. The latter was used in the design of this test configuration. Also, the clamping method could be carried out in many ways. For example, each specimen could be perfectly bonded to the sliding foundation; however, this is illogical and time and cost intensive. Instead an adjustable clamping system was used, as shown in figure 5.

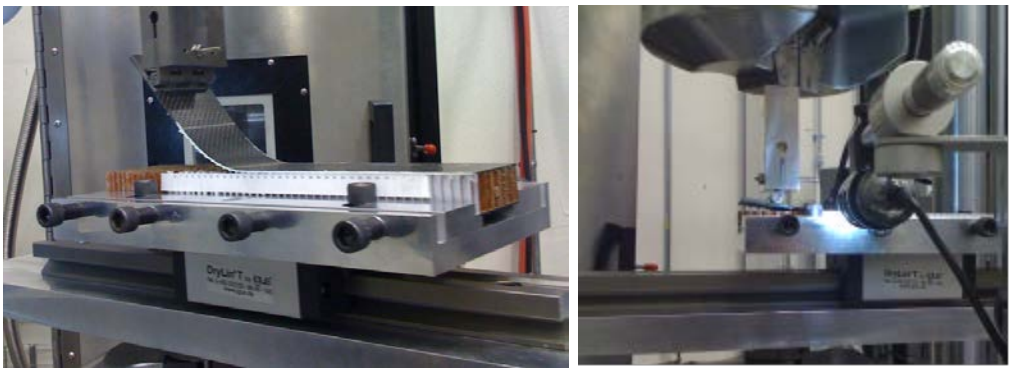

Figure 5. Sliding SCB test fixture design

The SCB test fixture shown in figure 5 holds the bottom facesheet while loading the hinge bonded to the facesheet closest to the prescribed crack. The assembly is mounted onto a traveling stage so that Mode II loading, which develops during crack-opening displacement, is relieved. This test setup prevents mixed-mode mechanics.

2.1.2 Test Specimen

Test specimens consisted of a sandwich core bonded between two composite facesheets. Specimen sizing was based on the sizing results and conclusions determined both empirically (large deflections during testing) and theoretically (based on methods presented by Ratcliffe [10]) during the first round of testing (i.e., Volume I). It was determined that the specimens would have a 1.0″ prescribed crack length (a_o), identical to the shortened specimens from Volume I; furthermore, the overall dimensions were reduced from 2″ in width (b) by 10″ in length (L), as those tested in Volume I, to 8″ in L. Specimen geometry is seen in figure 6.

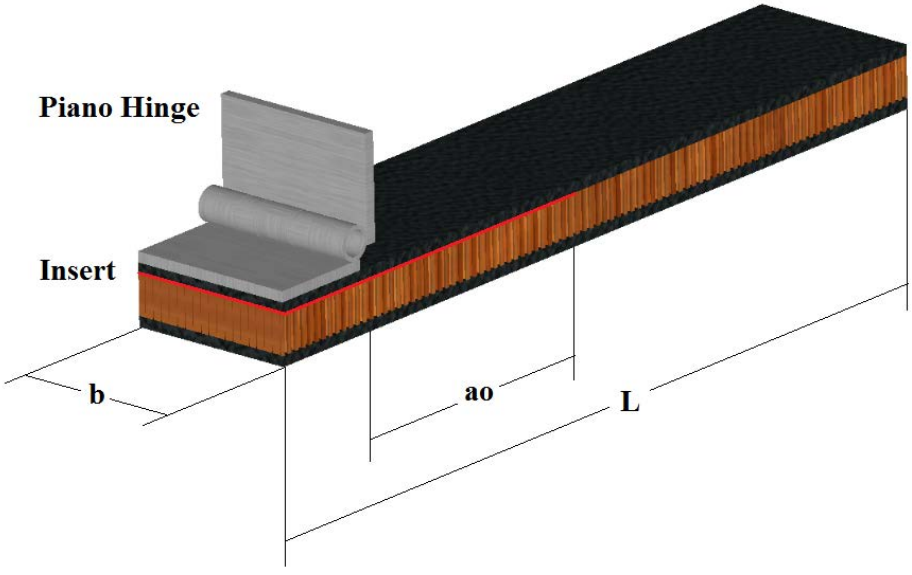

Figure 6. Sandwich SCB specimen geometry

2.2 TEST MATRIX

Experiments proposed in the current task were carried out using four-ply Cytec 5320-T650-3K plain-weave facesheets bonded to Hexcel HexWeb HRH-10 aramid fiber/phenolic honeycomb core using Cytec FM300-2 film adhesive. Sandwich SCB specimens were 2″ x 8″ with an a_o of 1.0″. Table 1 shows the test matrix for determining the GIC of sandwich specimens using the SCB test configuration. As shown, two different core types (hexagonal and over-expanded), three different cell sizes (1/8″, 3/16″, and 3/8″), and three different core densities (2.0, 3.0, and 6.0 pcf) were selected. The 1/8″ 2.0 pcf core was actually 1.8 pcf, but was assumed to be 2.0 for comparisons. Typical nomenclature for the core designation is material-cell size-density (i.e., HRH-10–1/8–3.0) indicating HRH-10 hexagonal honeycomb material with 1/8″ cell size, and 3.0 lb/ft^3 (pcf) density. In addition, two different disbond locations (top and bottom), two different fabrication processes (pre-cured facesheets [PCFS] and co-cured facesheets [CCFS]), two ribbon directions (longitudinal and lateral), and two different crack tip locations (center and edge of the core) were selected. The test matrix was reduced so that a design of experiments model could be used for evaluating other (untested) combinations within the design space considered in table 1. To uniquely identify different specimen configurations, the nomenclature shown in figure 7 was used.

Table 1. SCB sandwich specimen test matrix

Core Type	Cell Size (in)	Core Density (pcf)	Disbond Location	Fabrication Process	Ribbon Direction	Crack Tip Location	Number of Specimens
HX	1/8	1.8 ≈ 2.0	T	PCFS	LONG	C	6
			B				6
		3.0	T	PCFS	LONG	C	6
			B				6
						E	6
			T		LAT	C	6
			B				6
						E	6
			T	CCFS	LONG	C	6
			B				6
		6.0	T	PCFS	LONG	C	6
			B				6
	3/16	2.0	T	PCFS	LONG	C	6
			B				6
		3.0	T	PCFS	LONG	C	6
			B				6
			T		LAT	C	6
			B				6
		6.0	T	PCFS	LONG	C	6
			B				6
	3/8	2.0	T	PCFS	LONG	C	6
			B				6
		3.0	T	PCFS	LONG	C	6
			B				6
						E	6
			T		LAT	C	6
			B				6
						E	6
			T	CCFS	LONG	C	6
			B				6
OX	3/16	3.0	T	PCFS	LONG	C	6
			B				6
			T		LAT	C	6
			B				6

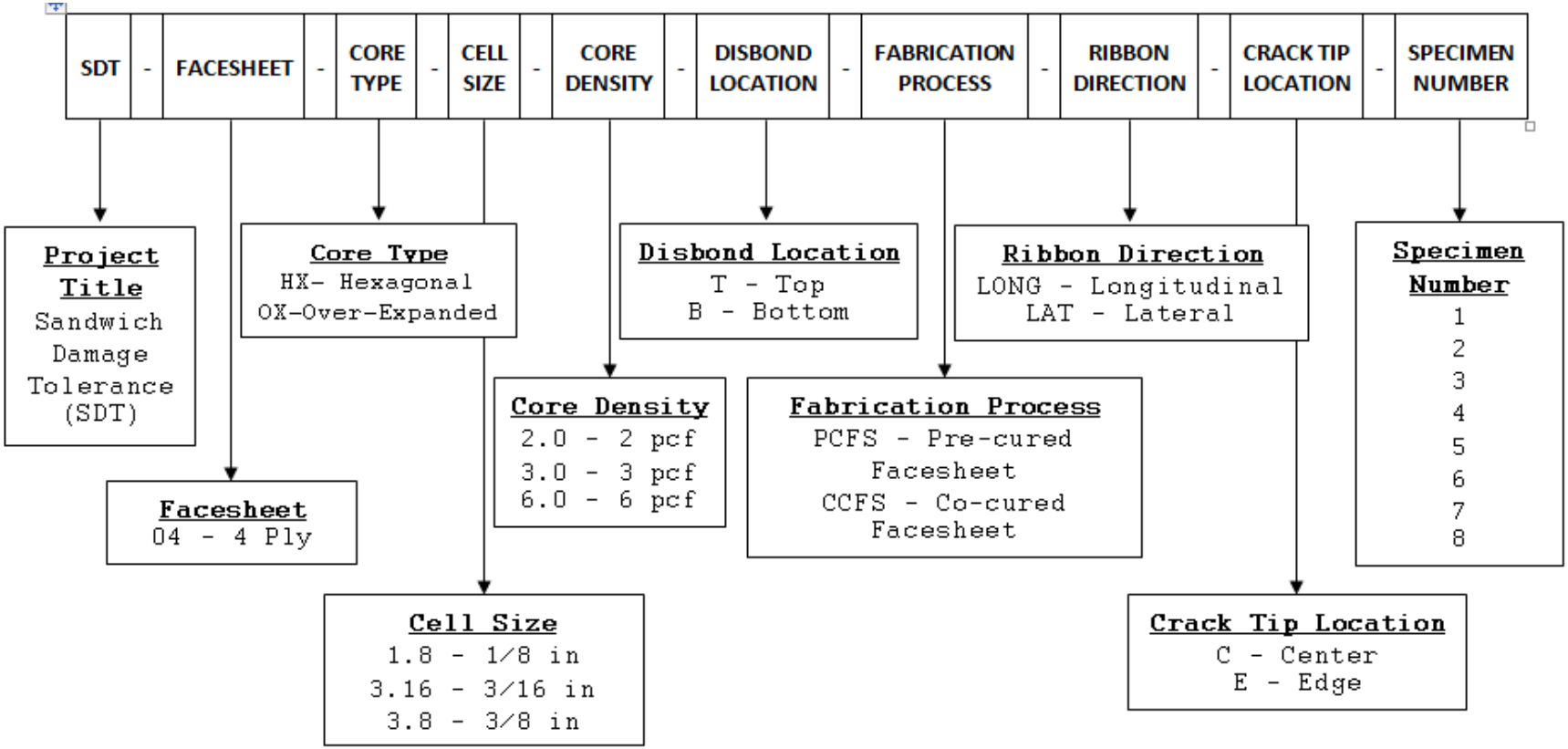

Figure 7. Specimen nomenclature

Figure 8 shows the basic core geometry for both the hexagonal (HX) core and over-expanded (OX) core. Note that the OX cell size is the normal HX cell size before expansion/compression to the rectangular shape. Figure 9 illustrates how both cell size and core density are determined. Figure 10 illustrates the disbond (Teflon™ insert) location during the final layup and curing process. It is important to note that both disbond locations were tested with the piano hinge being bonded to the facesheet closest to the disbond (i.e., so that the facesheet would act as the cantilevered beam and the facesheet/core would be clamped onto the fixture). The purpose of the different Teflon locations was to interrogate cure processes on the disbond. Figure 11 shows the two fabrication processes: PCFS are first laid up and cured in a preliminary cure process and then secondarily bonded to the core, whereas CCFS are laid up in conjunction with the core and cured in a single process. Figure 12 shows the ribbon direction with respect to crack growth direction for both hexagonal and over-expanded cores, with longitudinal defined as when the ribbon direction is aligned with the crack growth direction, and lateral defined as when the ribbon direction is normal to the crack growth direction. Finally, figure 13 shows the crack tip location (i.e., where the front edge of the Teflon insert is located with respect to cell geometry) for both ribbon directions.

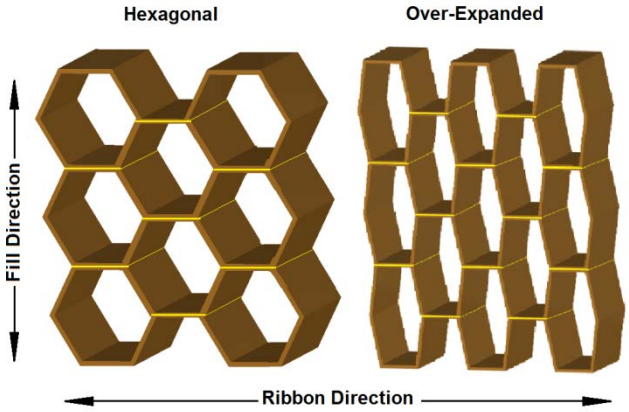

Figure 8. Core types: hexagonal vs. over-expanded core

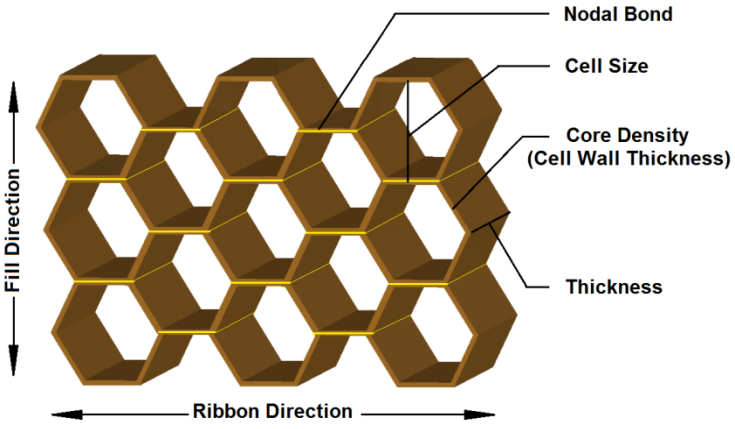

Figure 9. Cell size and core density

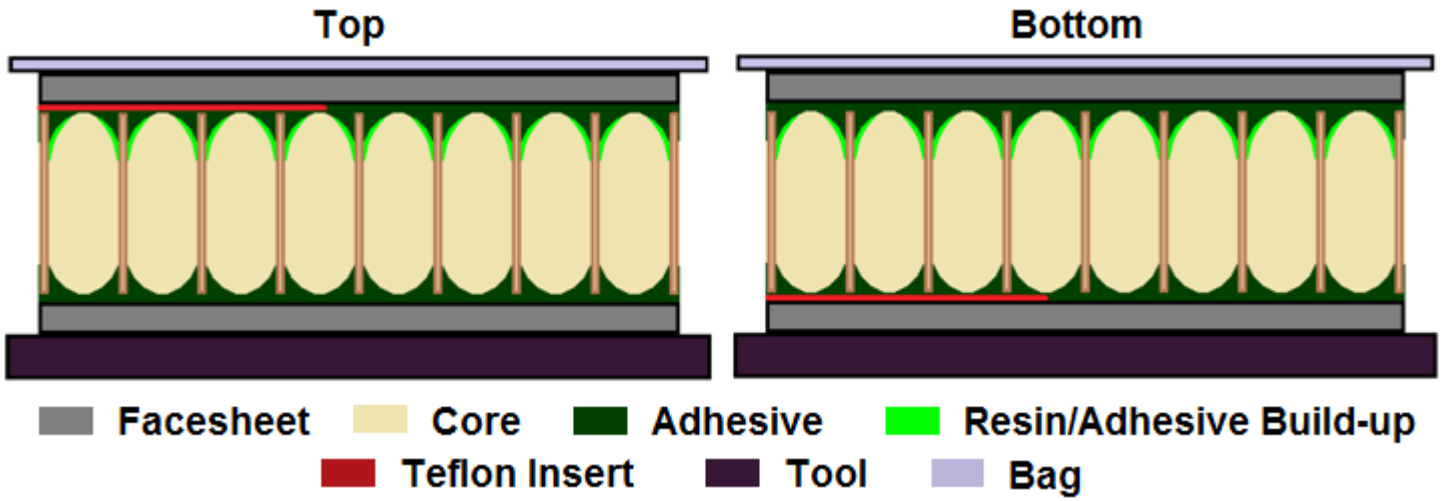

Figure 10. Disbond location, determined with respect to final layup and cure

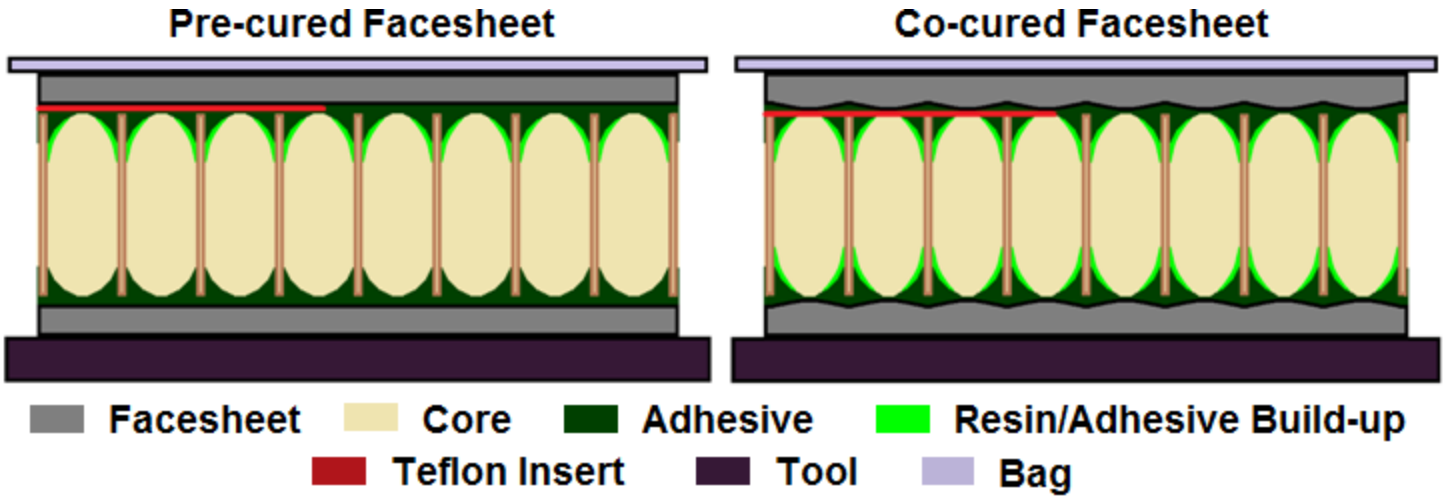

Figure 11. Fabrication process

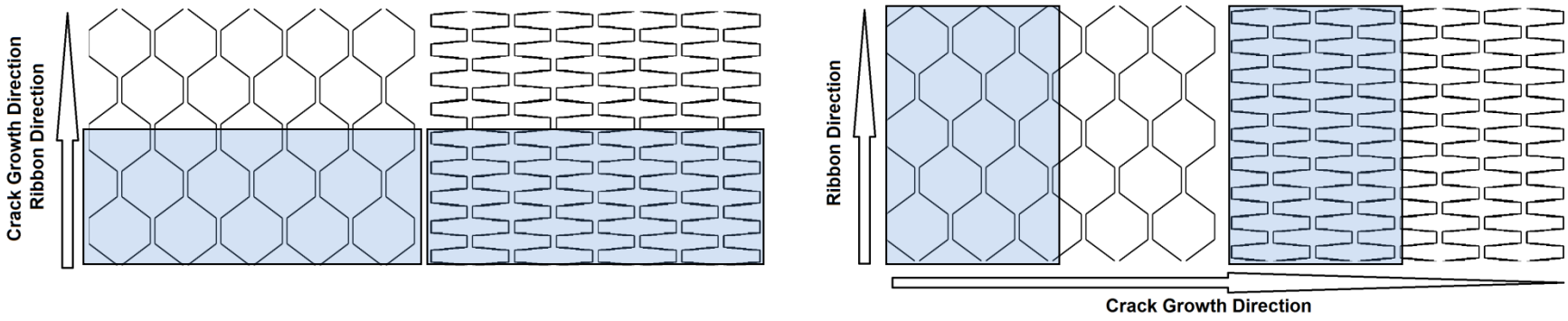

(a) (b)

Figure 12. Ribbon direction: (a) longitudinal vs. (b) lateral

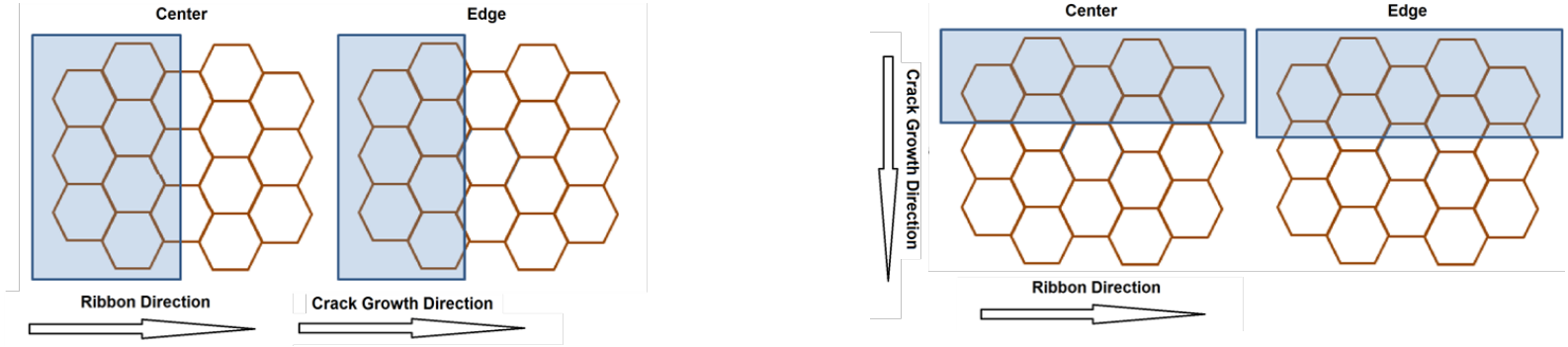

(a) (b)

Figure 13. Crack tip location for ribbon direction, center vs. edge: (a) longitudinal vs. (b) lateral

2.3 SPECIMEN FABRICATION

Specimens were fabricated in 13 panels. The Cytec 5320-T650-3K plain weave facesheet material was cut and kitted, and the Hexcel HexWeb HRH-10 aramid fiber/phenolic honeycomb core was cut, cleaned with compressed air, dried, and kitted separately from the facesheet material.

For the PCFS, the facesheet material was laid up with a $[0/45]_s$ ply sequence, then cured. Once cured, the facesheet was laid up with film adhesive. The core then had Teflon inserts attached (using tape placed in the trim area) at the predefined locations (top/bottom, longitudinal/lateral and center/edge). The core was then added to the layup, film adhesive and the other facesheet were added, and the final layup was cured, as shown in table 2.

Table 2. Panel layups

Preliminary-Cure Cycle			
	Top Facesheet		Bottom Facesheet
Stacking Sequence	0°		0°
	45°		45°
	45°		45°
	0°		0°
Secondary-Cure Cycle			
Stacking Sequence	Top facesheet		
	Film adhesive		
	Teflon insert		
	Core		
	Teflon insert		
	Film adhesive		
	Bottom facesheet		

Single-Cure Cycle	
Stacking Sequence	0°
	45°
	45°
	0°
	Film adhesive
	Teflon insert
	Core
	Teflon insert
	Film adhesive
	0°
	45°
	45°
	0°

For the CCFS, the facesheet material was laid up with a $[0/45]_s$ ply sequence, and film adhesive was added. Teflon inserts were then attached to the core (using tape placed in the trim area) at the predefined locations (top/bottom, longitudinal/lateral, and center/edge). The core was added to the layup, film adhesive was added, and the other facesheet was laid up with the same ply sequence as previously. The layup was then cured, as shown in table 2.

Both cure cycles for PCFS and the single-cure cycle for CCFS all followed the same procedure. The layup was vacuum bagged and cured at 250°F for 75 minutes, then 300°F for 120 minutes, with ramp rates of 5°F per minute. The cure cycle is shown in figure 14. Once the panels underwent the final cure cycle, they were c-scanned, and no issues were observed.

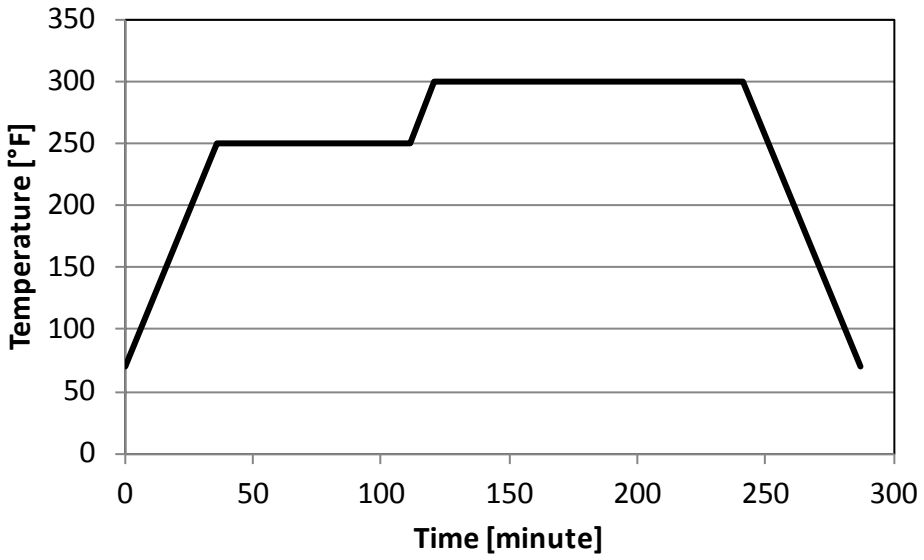

Figure 14. Cure cycle

The prescribed crack locations were then identified and confirmed by removing just the facesheet from the trim areas (leaving the core and Teflon insert). The crack tip location was indicated by drawing a line across the panel, which was used as the reference datum during machining. The panels were then machined into individual test specimens. Following this, the specimens underwent a quality control inspection to ensure crack tip location and overall dimensions. Lastly, the specimens had the piano hinges bonded to the facesheet closest to the insert. EA 9394 paste adhesive was used, and the specimens underwent an accelerated cure.

2.4 TEST PROCEDURE

The fracture toughness was measured using the SERR, because this is the most applicable with the specimen test configuration and geometry. Furthermore, the fracture toughness is often represented graphically by a resistance curve (R-curve). The fracture behavior of a material for a given mode was studied by developing an R-curve that could be used to predict the load required for propagation. The R-curve is traditionally the SERR plotted against the crack extension for a given material. It provides a basic description of how a fracture behaves in a particular material because it depicts the energy required for a crack to propagate. Furthermore, an R-curve can predict the stable/unstable regions of the propagation by plotting the driving force against crack length over the R-curve, as shown in figure 15 [2].

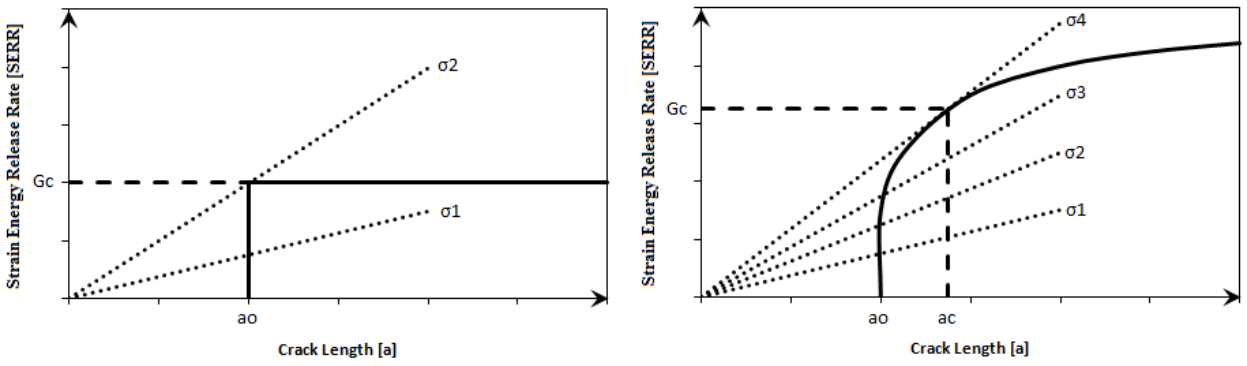

Figure 15. Driving force/R-curve: (a) flat R-curve and (b) rising R-curve [2]

R-curves for two types of materials are shown. The first case, as shown in figure 15(a), is a material with a flat curve, indicating brittle behavior. The crack does not extend for the first stress level and becomes unstable once the driving force increases beyond the second stress level, but the resistance remains constant. The second case, as shown in figure 15(b), is a material with a rising curve, indicating ductile behavior. The crack propagates slowly with increasing stress levels (1st through 4th) until it reaches a critical point (4th stress level) and becomes unstable as the rate of change in the driving force exceeds the slope of the R-curve. In both cases, the fracture toughness is represented by Gc (critical SERR).

2.4.1 Static Test Procedure

The static test procedure for determining GIC was based very closely on the ASTM standard for Mode I Interlaminar Fracture Toughness of Unidirectional Fiber-Reinforced Polymer Matrix Composites (D5528). Excluding the test specimen configuration (SCB vs. DCB) and data-reduction method, the test procedures are nearly identical.

Similarly to the practices outlined in the D5528 standard, the side of each specimen was painted white so that the crack propagation would be clearly visible. Because the edge was not planar but rather contoured with the honeycomb core, shadowing and depth played a part in visually determining the crack tip location and crack propagation; therefore, crack length was a subjective measurement. Crack tip location was monitored using a traveling digital microscope, setting the magnification to 20x, as shown in figure 5.

One key difference in the test setup was the SCB test fixture. Specimens were clamped in the widthwise direction into the test fixture, and the torque value was determined empirically so that the facesheets were not damaged. The clamping torque was 20–25 in.-lbs.

As recommended in the D5528 standard, the specimen was preloaded to produce a natural (sharp) crack tip. This test was conducted under a displacement control mode with a crosshead speed of 2 mm/min, while continuously recording the load and actuator displacement. Actuator displacement was assumed to be equal to the crack opening displacement (δ). The crack was then propagated for approximately 5 mm, and the data collected during this phase were used for determining the

precrack fracture toughness. The specimen was then reloaded and the crack propagated for approximately 50 mm.

Three distinct values of GIC were determined from the sandwich SCB test. The first and most conservative value was the non-linear (NL) GIC, based on the load at onset of nonlinearity in the load versus displacement curve. The second and most subjective value was the visual (VIS) GIC, which corresponds to the load at which the crack initiates (visible crack). Lastly, the 5% offset or max load GIC (5%/max) was determined by plotting the intersection of the load versus displacement curve and a 5% radial offset curve or the maximum load, whichever occurs first. These three values as well as all propagation points were then plotted, producing an R-curve, as shown in figure 16. The D5528 standard procedure includes details for determining these three values of GICs.

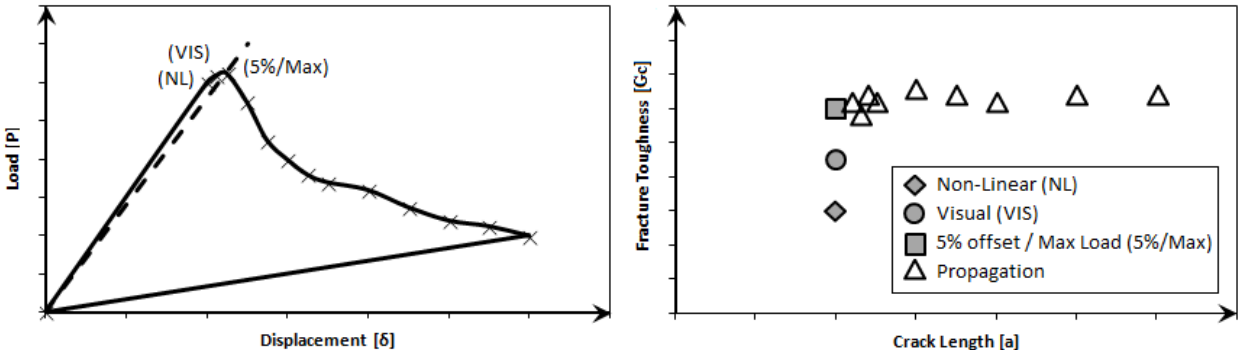

(a) (b)

Figure 16. Image of sample (a) load vs. displacement diagram and (b) resistance curve

2.5 DATA REDUCTION

2.5.1 Modified Beam Theory

The modified beam theory (MBT) data-reduction scheme is identical to that used in Volume I. It is repeated here for convenience.

2.5.1.1 GIC Derivation

The SERR is the energy dissipated during crack growth normalized by the newly created fracture surface. Several data-reduction methodologies can be used to determine the SERR, the most common of which is derived from beam theory [11, 12].

The SERR or G is a material (and geometric) constant that characterizes the amount of energy required to open the crack. It is best to start the derivation process in its simplest form [2] as:

$$G = \beta \frac{\partial U}{\partial a} \tag{1}$$

First, the strain energy (U) is reviewed, which is defined as the volume integral [11, 12]:

$$U = \frac{1}{2}\int_V \sigma\varepsilon \, dV \tag{2}$$

Consider these relationships and assume that the stiffness and cross-sectional area remain constant [11, 12] as:

$$\varepsilon = \frac{\sigma}{E} \tag{3}$$

then,

$$U = \frac{1}{2E}\int_V \sigma^2 \, dV \tag{4}$$

$$\sigma = \frac{My}{I} \tag{5}$$

$$U = \frac{1}{2E}\int_V \frac{M^2y^2}{I^2} \, dV \tag{6}$$

$$I = \int_A y^2 \, dA \tag{7}$$

$$U = \frac{1}{2EI}\int_x M^2 \, dx \tag{8}$$

Consider only the beam from the crack tip to the end load and the following relationships:

$$M = P\,(a - x) \tag{9}$$

$$U = \frac{1}{2EI}\int_0^a [P(a - x)]^2 \, dx \tag{10}$$

Solve for strain energy:

$$U = \frac{P^2a^3}{6EI} \tag{11}$$

Normalize by the crack front width:

$$\beta = \frac{1}{b} \tag{12}$$

Solve for SERR:

$$GIC = \beta\frac{\partial U}{\partial a} = \frac{P^2a^2}{2EIb} \tag{13}$$

Consider crack-opening displacement, derived from the Euler-Bernoulli beam theory [11, 12], as:

$$\delta = \frac{Pa^3}{3EI} \tag{14}$$

Substituting, the SERR's final form is obtained as:

$$GIC = \frac{3P\delta}{2ba} \tag{15}$$

2.5.1.2 "Δa" Crack Tip Rotation Correction

Beam theory has many assumptions, one of which is being perfectly built in or clamped. This implies that the crack front is perfectly normal to the loading direction and that there is no rotation or displacement. In reality, however, the crack front does rotate and may be displaced vertically. To remedy this issue, the crack is theoretically lengthened, Δa, to the point at which the crack front would be normal to the loading direction. When this adjustment is applied to beam theory, it is called the MBT.

Start by considering the displacement derived by Euler-Bernoulli beam theory [11, 12]:

$$\delta = \frac{Pa^3}{3EI} \tag{16}$$

Consider compliance:

$$C = \frac{\delta}{P} \tag{17}$$

$$C = \frac{a^3}{3EI} \tag{18}$$

Rewrite:

$$C^{1/3} = \left(\frac{1}{3EI}\right)^{1/3} a + 0 \tag{19}$$

Consider the function of a line:

$$y = mx + B \tag{20}$$

Ideally the *y*-intercept would be zero and the line would intersect the origin; however, because the Euler beam is not perfectly built in (displacement and rotation at the crack tip do not equal zero), the curve does not intersect the origin. Therefore, additional terms are added to the above equations to shift the experimental dataset and force the curve to intercept the origin.

Increase the crack length by Δa:

$$\delta = \frac{P(a+\Delta a)^3}{3EI} \tag{21}$$

Consider compliance and rewrite:

$$C^{1/3} = \left(\frac{1}{3EI}\right)^{1/3} (a + \Delta a) + B \tag{22}$$

Solve for Δa, where B is obtained empirically:

$$(3CEI)^{1/3} - B(3EI)^{1/3} - a = \Delta a \tag{23}$$

Set $C^{1/3}$ and a to zero (forcing the function to pass through the origin):

$$B(3EI)^{1/3} = \Delta a \tag{24}$$

Solve either analytically or graphically using a plot similar to the one in figure 17.

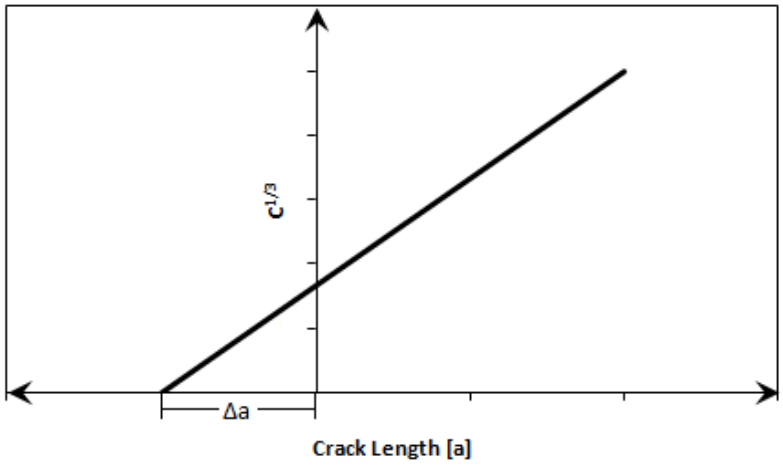

Figure 17. Graphical solution for Δ*a*

2.5.1.3 "*F*" Large Deflection Correction

Another assumption associated with beam theory entails small deflections. This implies that the tip deflection cannot be larger than one-tenth of the beam length. Large deflection causes two distinct issues. The first is the direction of the load application. Because load is applied through a piano hinge, the loading direction is always perfectly normal to the crack front. The second is an artificial shortening of the moment arm. To remedy this issue, a correction factor, *F*, is applied to reduce the moment arm or the force felt at the crack tip.

Start by considering the correction factor *F* presented by the ASTM standard. The first variable term refers to shortening caused by the beam in large deflection, and the second refers to shortening caused by the piano hinge in large deflection:

$$F = 1 - \frac{3}{10}\left(\frac{\delta}{a}\right)^2 - \frac{3}{2}\left(\frac{\delta t}{a^2}\right) \tag{25}$$

Now recall that the ASTM standard refers to DCBs, and δ refers to the total displacement, which is the displacement of both the top and bottom beams. Therefore, the δ in the above equation must be replaced with 2δ:

$$F = 1 - \frac{3}{10}\left(\frac{2\delta}{a}\right)^2 - \frac{3}{2}\left(\frac{2\delta t}{a^2}\right) \tag{26}$$

Reduce:

$$F = 1 - \frac{6}{5}\left(\frac{\delta}{a}\right)^2 - 3\left(\frac{\delta t}{a^2}\right) \tag{27}$$

To further validate the correction factor, it was compared to an analytical model developed by Williams [13]. The two solutions are shown in figure 18.

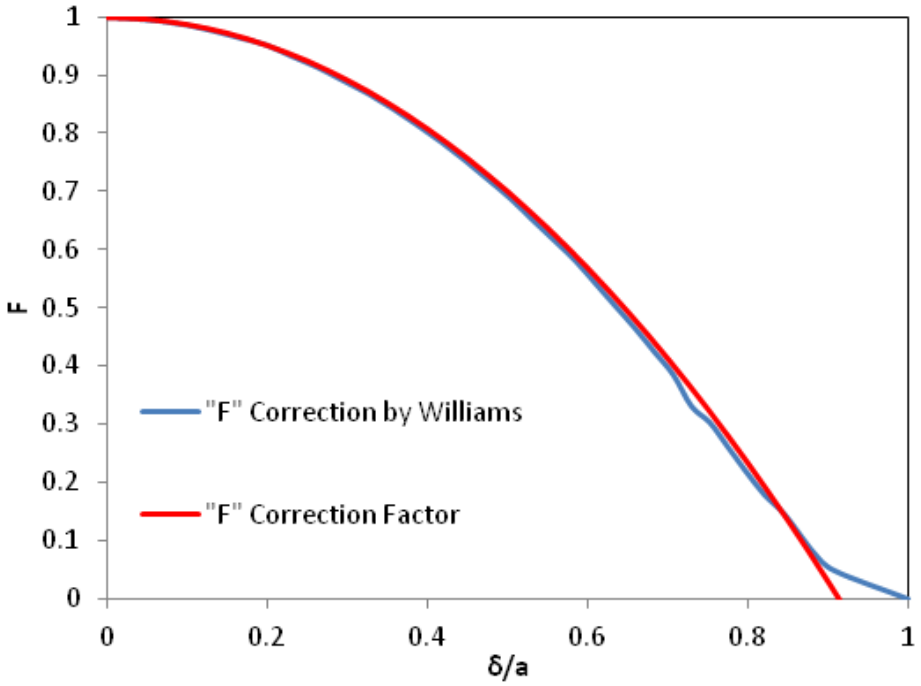

Figure 18. Comparison of correction factor (*F*) and analytical solution

2.5.2 Area Method

2.5.2.1 GIC Derivation

Once more, the derivation process is started in its simplest form:

$$G = \beta \frac{\partial U}{\partial a} \tag{28}$$

The differential change in strain energy with respect to the differential change in crack length will be approximated by considering the overall change in strain energy with respect to the overall change in crack length:

$$G = \beta \frac{\Delta U}{\Delta A} \tag{29}$$

The overall change in strain energy will be determined by finding the area under the load versus displacement curve, whereas the overall change in crack length will be taken from the test sheets [14], as shown in figure 19.

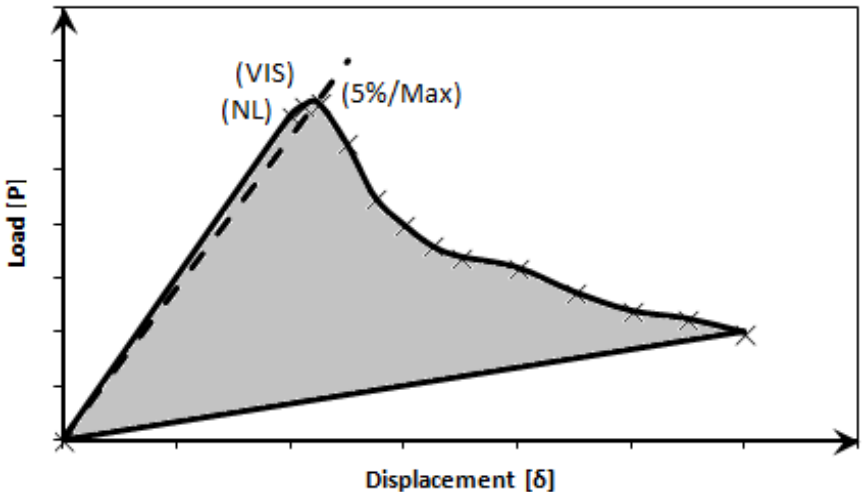

Figure 19. Change in strain energy; area under load vs. displacement curve

Normalize by twice the crack front width, and substitute to obtain the final form:

$$G = \frac{\text{Area}}{2\text{b}\Delta A} \tag{30}$$

This report determined only the AREA GIC for specimens with an overall change in crack length of approximately 2″, within a 10% tolerance.

2.6 FAILURE MODES

2.6.1 Adhesive Interface Disbond

Adhesive interface disbond or adhesion failure, occurs when a crack is formed between the adhesive and the facesheet (see figure 20). This failure, identified by the letter *A* in this report, is typically an indication of poor adhesion of film adhesive to the facesheet during the curing (bonding) process.

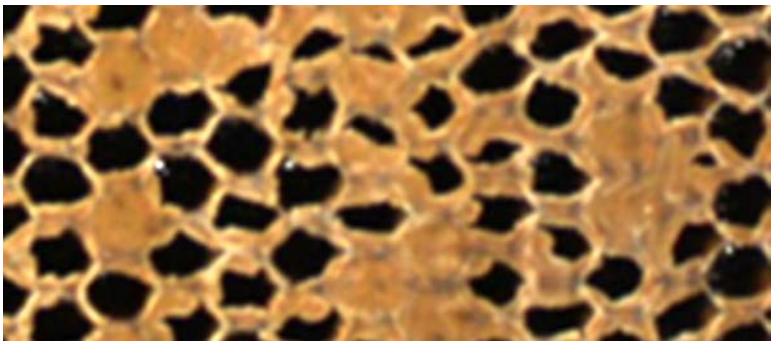

(a)

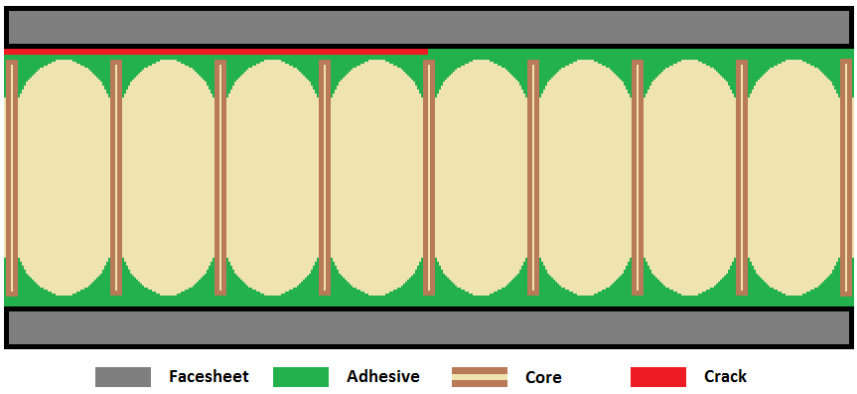

(b)

Figure 20. The (a) adhesive interface failure surface and (b) side view

2.6.2 Adhesive Pullout Failure

Adhesive pullout failure (APO) (or pullout failure) occurs when a crack is formed within the adhesive (see figure 21). This type of failure often takes place in combination with an adhesive interface disbond.

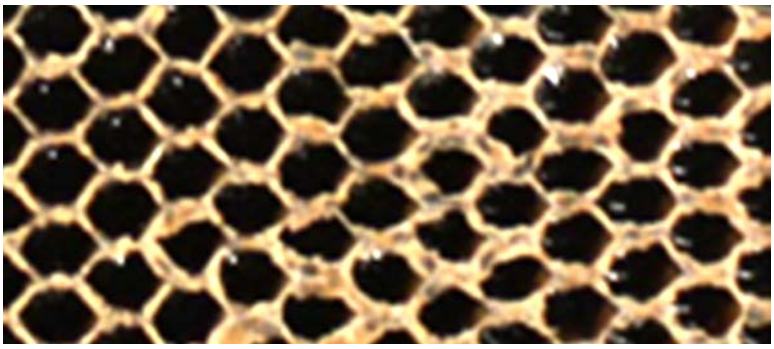

(a)

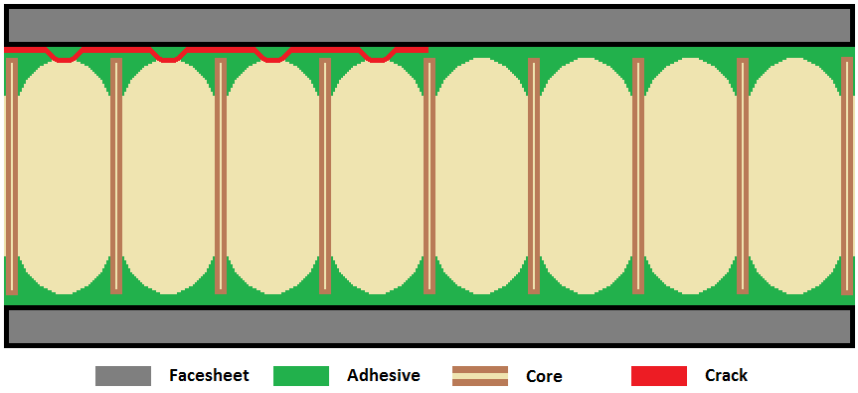

(b)

Figure 21. The (a) APO surface and (b) side view

2.6.3 Tensile Core Failure

Tensile core failure (or core failure) (C) occurs when a crack is formed within the core (see figure 22). Soon after initiation, the crack propagates into the core and often stays there.

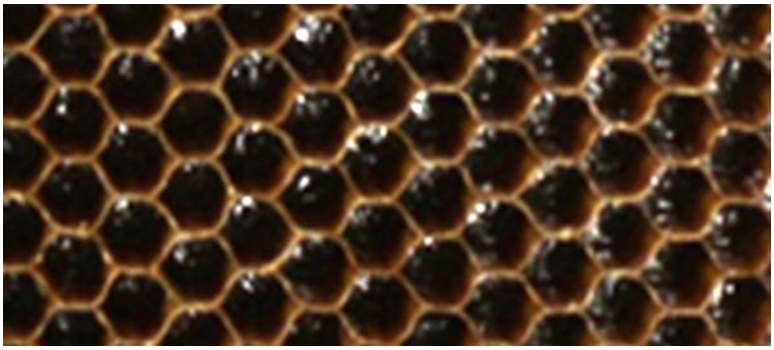

(a)

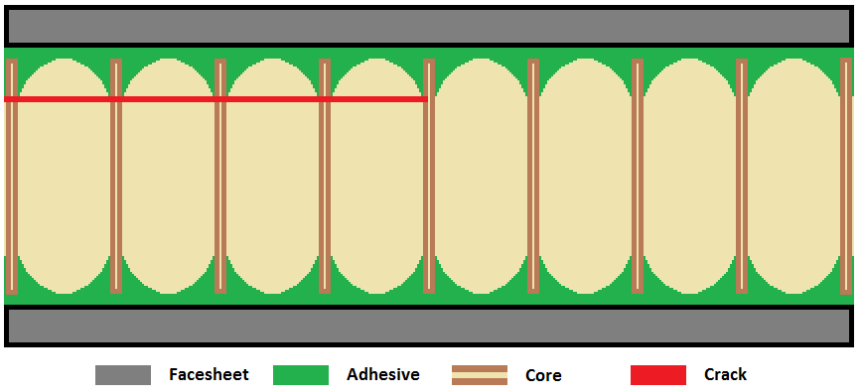

(b)

Figure 22. The (a) tensile core failure surface and (b) side view

2.6.4 Tensile Core Pullout Failure

Tensile core pullout failure (CPO) occurs when a crack is formed between the adhesive and the core (see figure 23). This failure mode was not seen during this program but can occur because of improper core preparation (i.e., a roughly cut/dry sanded core).

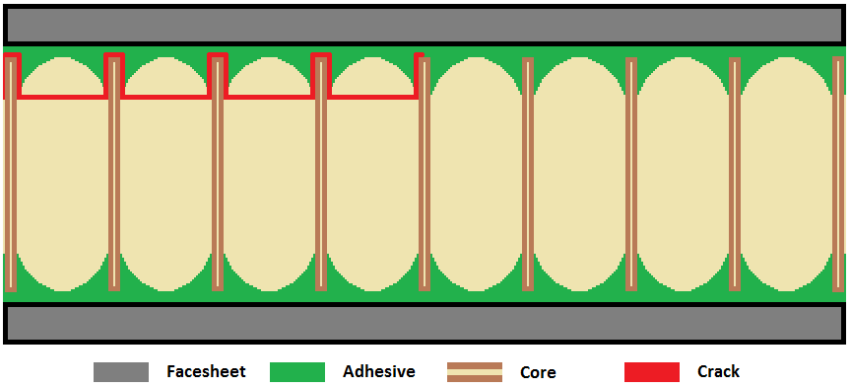

Figure 23. CPO

2.6.5 Adherend First-Ply Facesheet Delamination

An adherend first-ply facesheet delamination (FPD) (adherend failure) is very rare and occurs when a crack is formed between the first ply and the remaining plies of a composite facesheet and propagates through the laminate (see figure 24). This failure mode was not seen in this report.

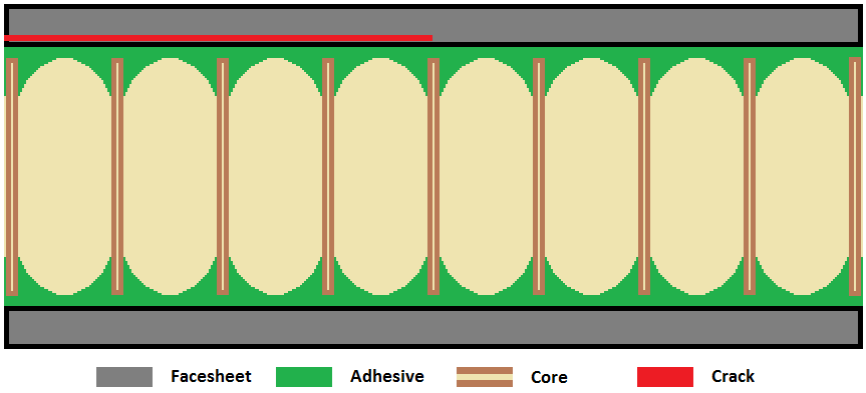

Figure 24. Adherend FPD and interlaminar facesheet delamination

2.6.6 Interlaminar Facesheet Delamination

Typically, interlaminar facesheet delamination (IFD) often forms on very thick facesheets (see figure 24) when a crack is formed within the laminate. This crack is predominantly caused by shear (Mode II) loads, whereas a facesheet is in the process of bending. This failure mode was not seen in this report.

2.6.7 Facesheet Shear Failure

Facesheet shear failure (FSF) occurs when the crack abruptly changes from one of the aforementioned failure modes and propagates through the thickness of the facesheet (see figure 25). This failure mode is a result of large displacements and shear loads within the facesheet.

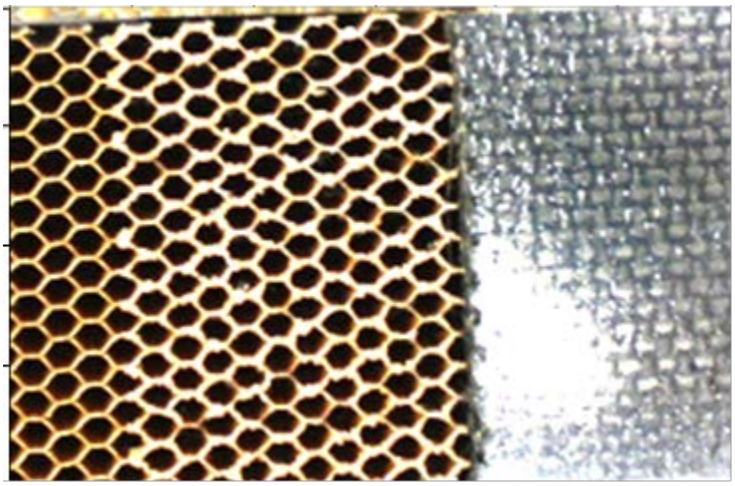

(a)

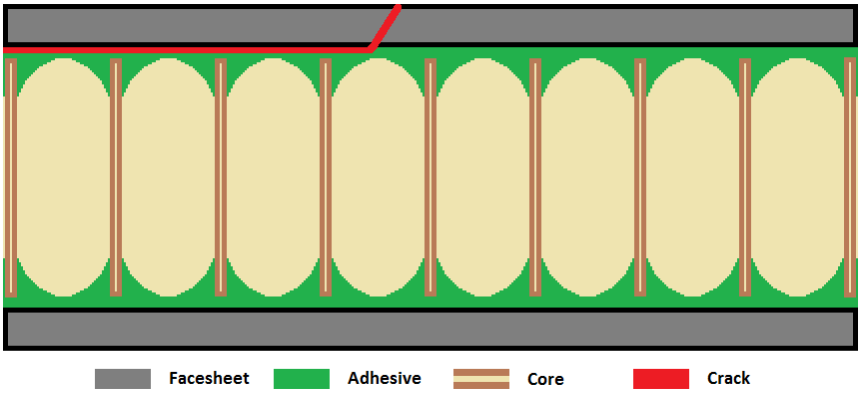

(b)

Figure 25. The (a) FSF and (b) side view

3. RESULTS AND DISCUSSION

Tables 3 and 4 represent the fracture toughness obtained for different sandwich parameters in terms of average values. Figures 26–30 show a graphical comparison of these results. Test data include the GIC values for different core types, cell sizes, and core densities. In addition, the test data include the GIC values for differing disbond locations, fabrication processes, ribbon directions, and crack tip locations at growth onset. It is important to note that other variables can contribute to GIC, such as paper thickness.[1] Therefore, the discussion and conclusions herein are solely based on the results included in this report. Individual test results, including failure modes, are found in appendices A–C.

Though the master summary tables and charts show a comparison of GICs, the effects of these variables on fracture toughness are coupled across different variables and require detailed data analysis for determining the impact of each variable. This section discusses the impact of the following sandwich parameters on GIC in detail:

a. Core type—HX versus OX
b. Cell size—1/8″ versus 3/16″ versus 3/8″
c. Core density—2.0 pcf versus 3.0 pcf versus 6.0 pcf
d. Disbond location—top (T) versus bottom (B)
e. Fabrication process—PCFS versus CCFS
f. Ribbon direction—longitudinal (LONG) versus lateral (LAT)
g. Crack tip location at onset—center (C) versus edge (E)

Furthermore, the failure modes for each specimen are included. In the appendices, the progressive failure modes are compared against the SERR as the crack propagates so that the change in SERR can be attributed to corresponding changes in failure mode(s).

Finally, a comparison between the two data-reduction methods is included.

[1] Hexweb® HRH-10 is manufactured from NOMEX® aramid fiber sheets, referred to as paper. A thermosetting adhesive is used to bond these sheets at the nodes and after expanding to the hexagonal or OX-Core® configuration, the block is dipped in phenolic resin to obtain targeted density.

Table 3. Master summary [English units]

Core Type	Cell Size (in)	Core Density (pcf)	Disbond Location	Fabrication Process	Ribbon Direction	Crack Tip Location	GIC (in-lb/in^2)						
							Pre-crack			Crack			AREA
							NL	VIS	5%/Max	NL	VIS	5%/Max	AVE
HX	1/8	2.0	T	PCFS	LONG	C	1.11	1.81	2.11	0.93	2.11	2.51	2.86
			B				1.43	1.88	2.06	0.85	2.21	2.90	2.79
		3.0	T		LONG	C	2.10	3.25	3.34	1.27	3.00	3.69	3.54
			B				1.86	N/A	2.89	0.93	3.19	3.27	3.63
						E	1.54	2.37	2.73	1.07	2.26	2.45	5.26
			T		LAT	C	1.70	N/A	2.56	0.66	2.68	2.78	4.03
			B				1.29	2.19	2.28	0.58	2.30	2.25	4.06
						E	1.22	3.15	2.58	0.80	2.55	2.38	4.23
			T	CCFS	LONG	C	1.42	3.34	2.66	0.71	2.89	2.96	3.54
			B				1.68	N/A	2.70	0.79	3.15	3.41	4.02
		6.0	T	PCFS	LONG	C	1.75	3.72	3.47	0.91	3.43	3.48	7.20
			B				1.77	3.75	3.65	0.61	3.01	3.16	7.65
	3/16	2.0	T	PCFS	LONG	C	1.03	1.67	1.62	0.68	1.92	2.22	2.53
			B				1.34	2.02	1.93	0.87	2.24	2.34	2.31
		3.0	T	PCFS	LONG	C	1.91	2.06	2.57	0.93	2.68	2.80	3.69
			B				1.49	2.32	2.41	1.28	2.36	2.67	3.20
			T		LAT	C	1.64	2.30	2.32	0.87	N/A	2.11	3.44
			B				1.64	2.70	2.53	0.89	2.17	2.38	3.65
		6.0	T	PCFS	LONG	C	1.26	2.27	2.28	0.63	2.17	2.05	4.71
			B				1.36	N/A	2.36	0.74	2.24	2.51	3.60
	3/8	2.0	T	PCFS	LONG	C	0.90	1.06	1.22	0.59	1.11	1.30	1.30
			B				0.87	2.22	2.22	0.44	1.43	1.57	1.40
		3.0	T	PCFS	LONG	C	0.56	N/A	0.86	0.55	2.34	2.43	2.29
			B				1.40	2.19	2.03	0.79	2.06	1.82	2.16
						E	1.16	1.78	1.59	0.68	1.77	1.91	2.13
			T		LAT	C	1.11	1.75	1.91	0.67	1.44	1.62	2.93
			B				1.32	2.41	1.89	0.86	1.65	1.82	2.48
						E	1.15	2.52	2.59	0.79	2.01	1.87	2.30
			T	CCFS	LONG	C	1.36	N/A	2.01	1.03	2.63	2.84	4.02
			B				0.84	1.96	1.40	0.41	2.14	2.36	3.97
OX	3/16	3.0	T	PCFS	LONG	C	1.67	N/A	2.31	0.87	2.41	2.51	2.86
			B				1.43	2.17	2.24	0.64	2.39	2.13	2.88
			T		LAT	C	1.76	N/A	2.55	0.84	3.02	2.89	3.46
			B				1.50	1.79	1.88	0.92	1.74	1.72	3.86

Table 4. Master summary [SI units]

Core Type	Cell Size (in)	Core Density (pcf)	Disbond Location	Fabrication Process	Ribbon Direction	Crack Tip Location	GIC (KJ/m^2)						
							Precrack			Crack			AREA
							NL	VIS	5%/Max	NL	VIS	5%/Max	AVE
HX	1/8	2.0	T	PCFS	LONG	C	0.20	0.32	0.37	0.16	0.37	0.44	0.50
			B				0.25	0.33	0.36	0.15	0.39	0.51	0.49
		3.0	T	PCFS	LONG	C	0.37	0.57	0.59	0.22	0.53	0.65	0.62
			B				0.33	N/A	0.51	0.16	0.56	0.57	0.64
						E	0.27	0.41	0.48	0.19	0.40	0.43	0.92
			T		LAT	C	0.30	N/A	0.45	0.11	0.47	0.49	0.71
			B				0.23	0.38	0.40	0.10	0.40	0.39	0.71
						E	0.21	0.55	0.45	0.14	0.45	0.42	0.74
			T	CCFS	LONG	C	0.25	0.59	0.47	0.12	0.51	0.52	0.62
			B				0.29	N/A	0.47	0.14	0.55	0.60	0.70
		6.0	T	PCFS	LONG	C	0.31	0.65	0.61	0.16	0.60	0.61	1.26
			B				0.31	0.66	0.64	0.11	0.53	0.55	1.34
	3/16	2.0	T	PCFS	LONG	C	0.18	0.29	0.28	0.12	0.34	0.39	0.44
			B				0.24	0.35	0.34	0.15	0.39	0.41	0.40
		3.0	T	PCFS	LONG	C	0.33	0.36	0.45	0.16	0.47	0.49	0.65
			B				0.26	0.41	0.42	0.22	0.41	0.47	0.56
			T		LAT	C	0.29	0.40	0.41	0.15	N/A	0.37	0.60
			B				0.29	0.47	0.44	0.16	0.38	0.42	0.64
		6.0	T	PCFS	LONG	C	0.22	0.40	0.40	0.11	0.38	0.36	0.82
			B				0.24	N/A	0.41	0.13	0.39	0.44	0.63
	3/8	2.0	T	PCFS	LONG	C	0.16	0.19	0.21	0.10	0.20	0.23	0.23
			B				0.15	0.39	0.39	0.08	0.25	0.28	0.24
		3.0	T	PCFS	LONG	C	0.10	N/A	0.15	0.10	0.41	0.43	0.40
			B				0.25	0.38	0.36	0.14	0.36	0.32	0.38
						E	0.20	0.31	0.28	0.12	0.31	0.33	0.37
			T		LAT	C	0.19	0.31	0.33	0.12	0.25	0.28	0.51
			B				0.23	0.42	0.33	0.15	0.29	0.32	0.43
						E	0.20	0.44	0.45	0.14	0.35	0.33	0.40
			T	CCFS	LONG	C	0.24	N/A	0.35	0.18	0.46	0.50	0.70
			B				0.15	0.34	0.25	0.07	0.37	0.41	0.70
OX	3/16	3.0	T	PCFS	LONG	C	0.29	N/A	0.40	0.15	0.42	0.44	0.50
			B				0.25	0.38	0.39	0.11	0.42	0.37	0.50
			T		LAT	C	0.31	N/A	0.45	0.15	0.53	0.51	0.61
			B				0.26	0.31	0.33	0.16	0.30	0.30	0.68

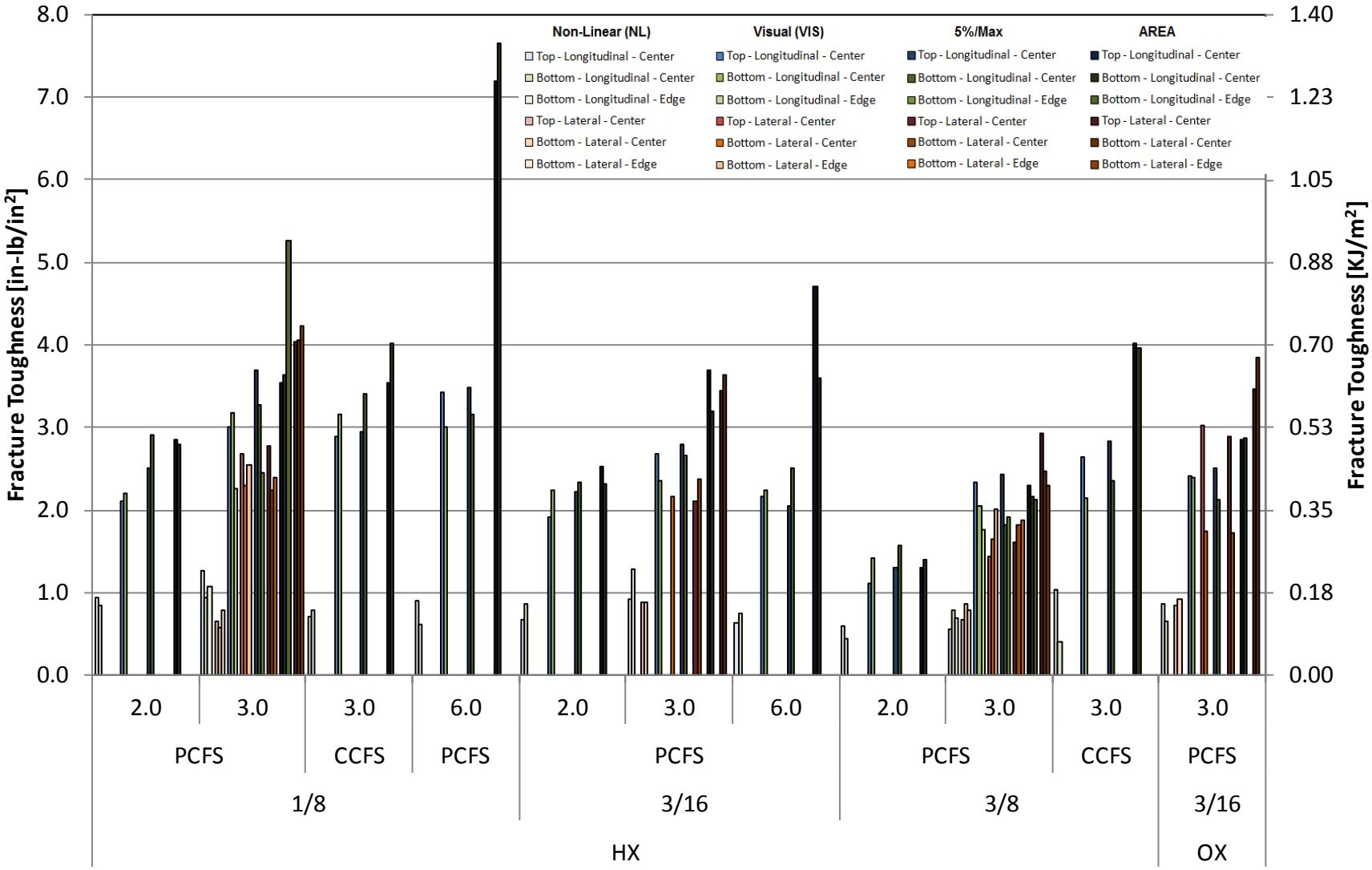

Figure 26. Fracture toughness master summary

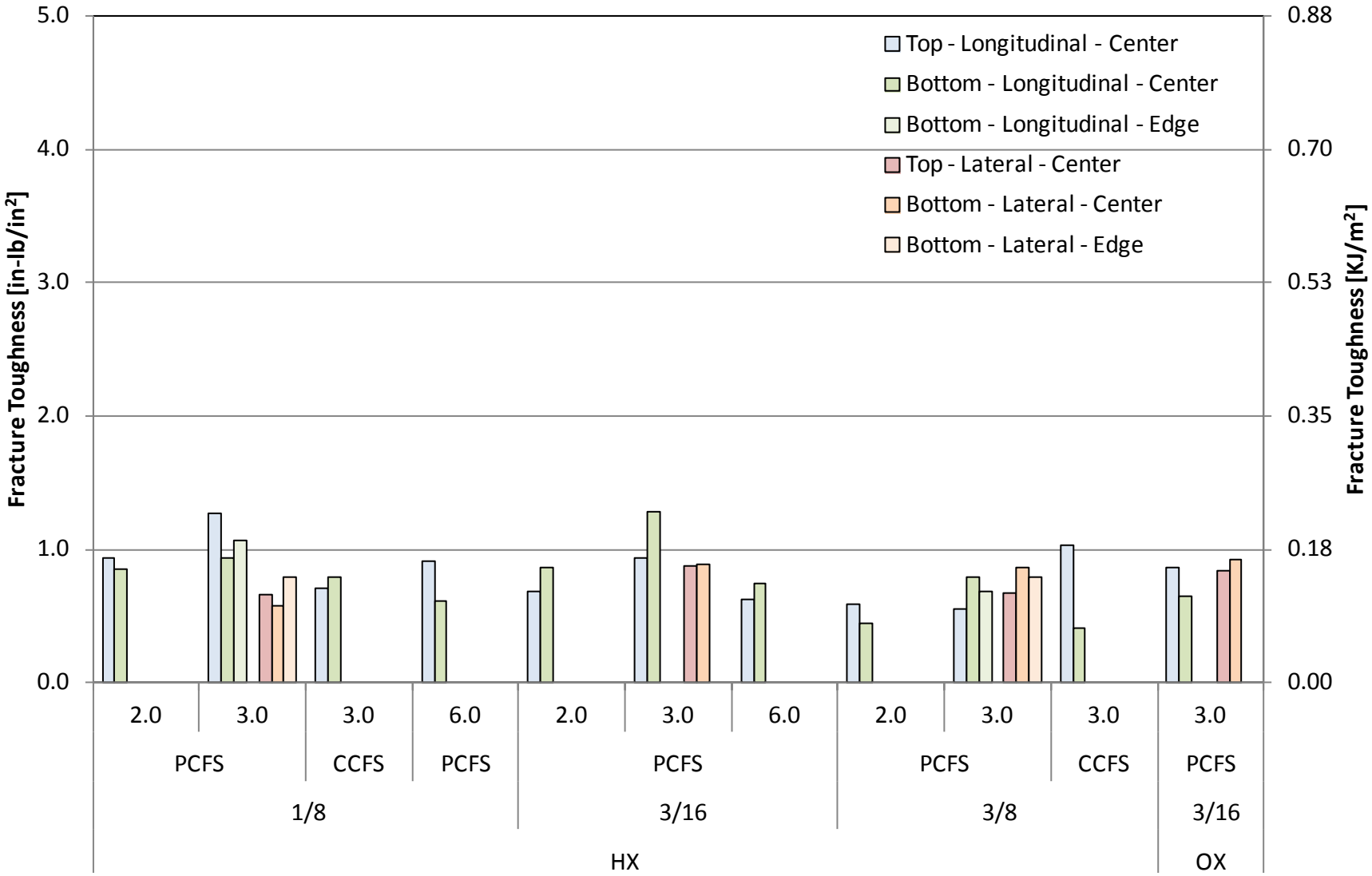

Figure 27. Fracture toughness (NL) master summary

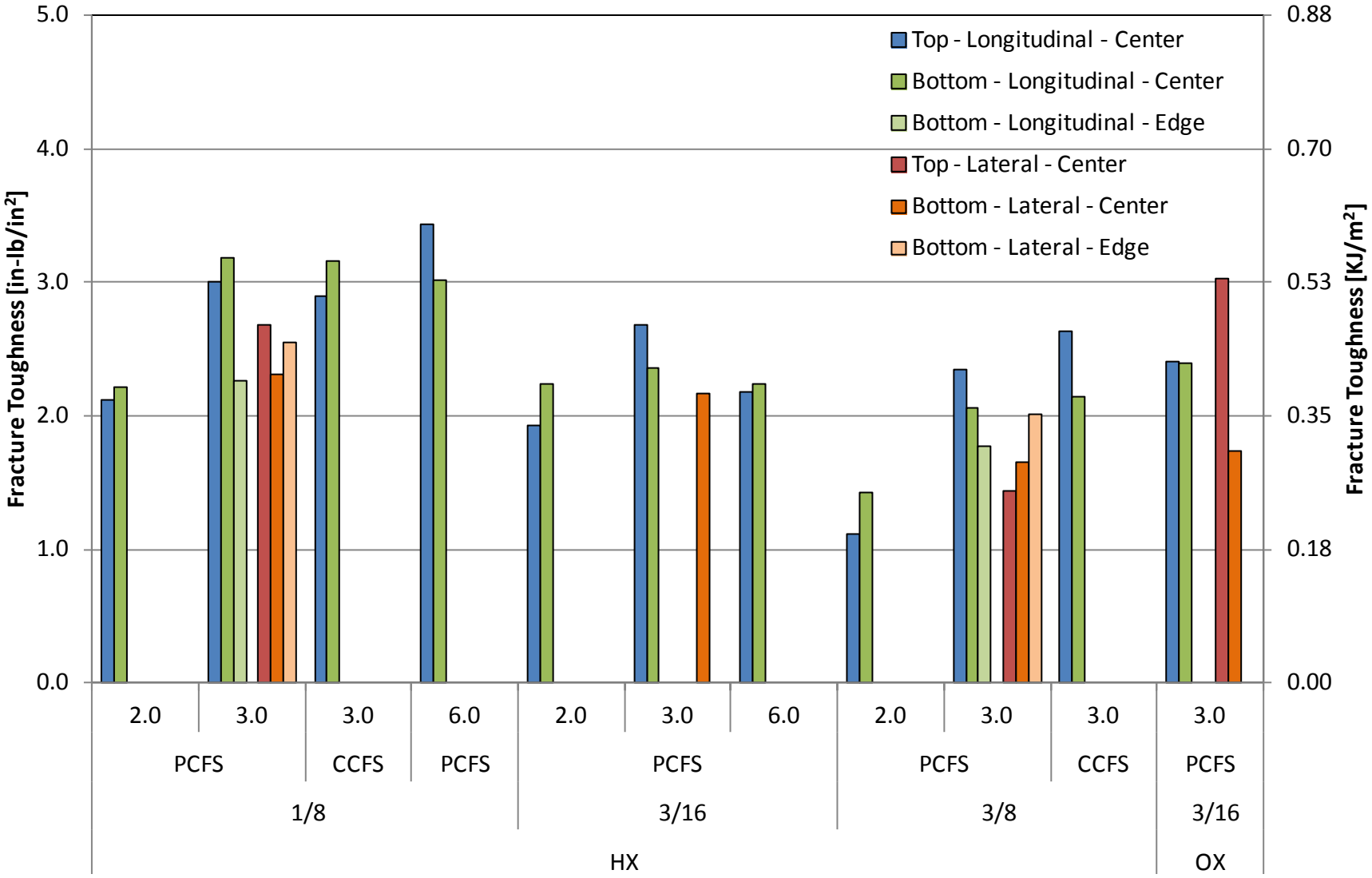

Figure 28. Fracture toughness (VIS) master summary

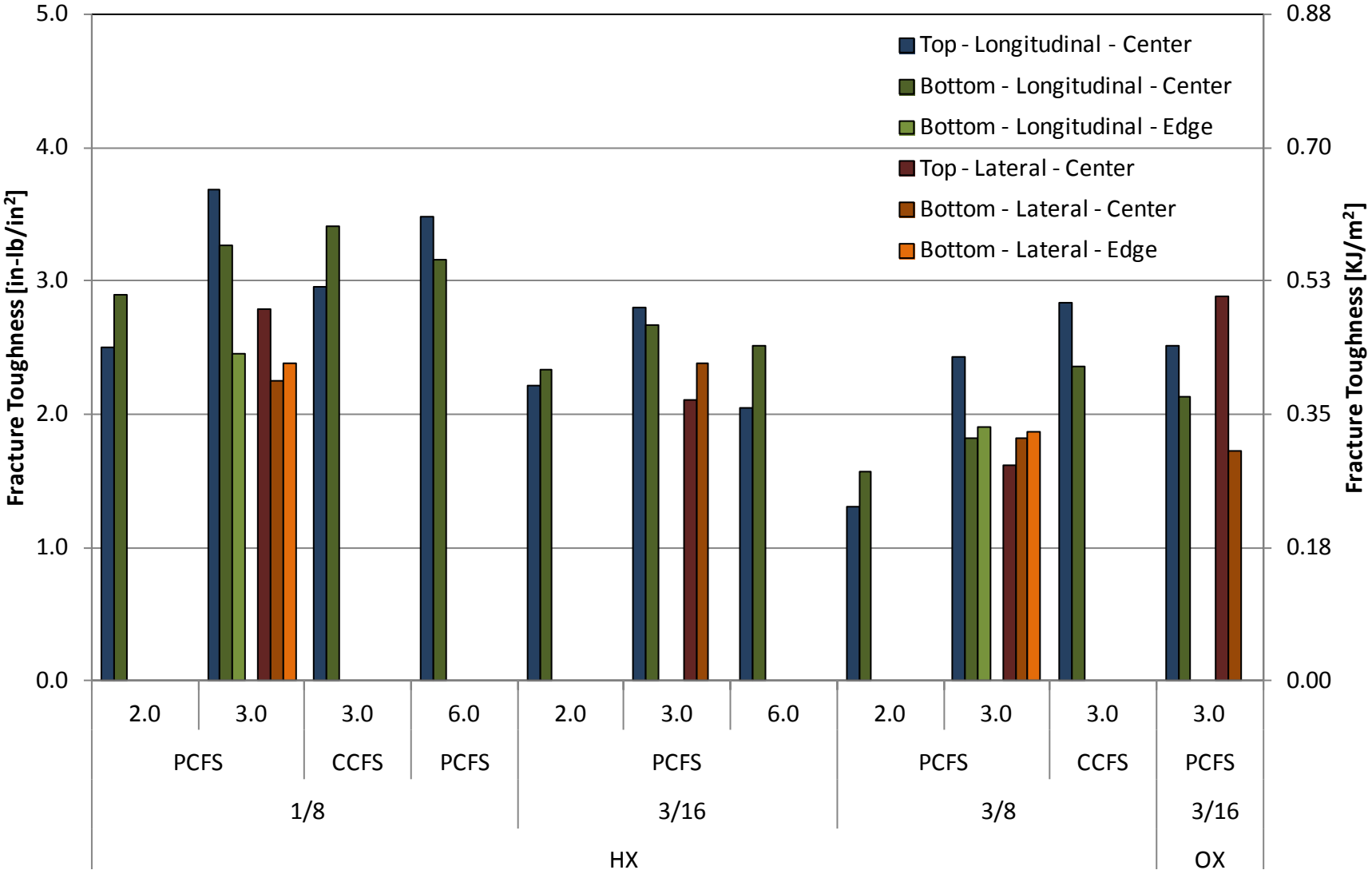

Figure 29. Fracture toughness (5%/max) master summary

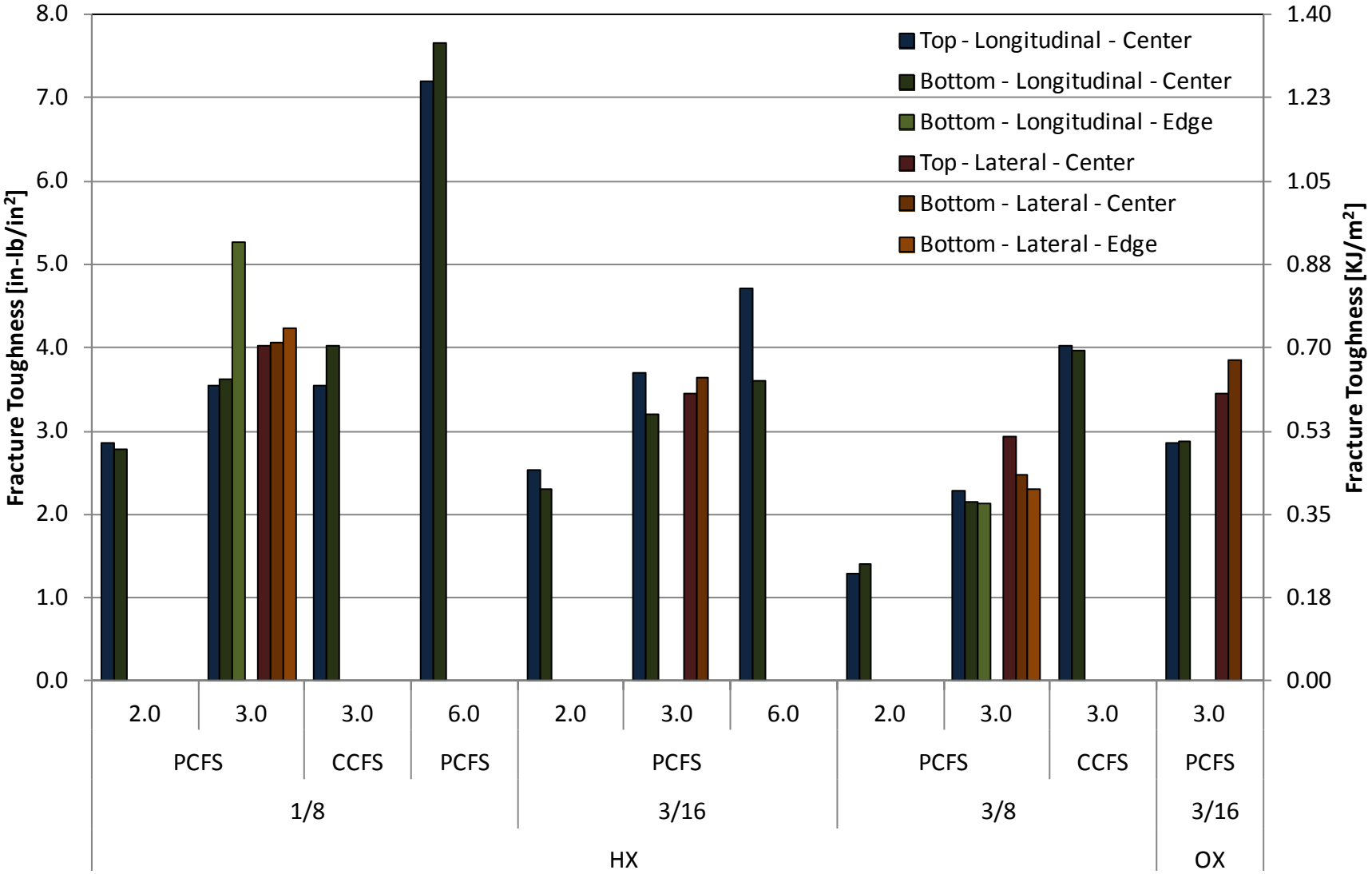

Figure 30. Fracture toughness (AREA) master summary

3.1 EFFECTS OF CORE TYPE

Two hexagonal and over-expanded core types were tested, both of which had the same cell size of 3/16″ and core density of 3.0 pcf. Each core was tested with two disbond locations, top and bottom, and two ribbon directions, longitudinal and lateral. In addition, both cores, with both disbond locations and both ribbon directions, had an initial crack tip location at the center of the cell. Furthermore, both cores, with both disbond locations and both ribbon directions, were fabricated with PCFS. The combination of the above parameters resulted in four distinct datasets, as presented in table 5.

Table 5. Core type test matrix

	Facesheet	Core Type	Cell Size (in)	Core Density (pcf)	Disbond Location	Fabrication Process	Ribbon Direction	Crack Tip Location	No. of Specimens
CORE TYPE	4	HX	3/16	3	TOP	PCFS	LONG	CENTER	6
	4	OX	3/16	3	TOP	PCFS	LONG	CENTER	6
	4	HX	3/16	3	BOTTOM	PCFS	LONG	CENTER	6
	4	OX	3/16	3	BOTTOM	PCFS	LONG	CENTER	6
	4	HX	3/16	3	TOP	PCFS	LAT	CENTER	6
	4	OX	3/16	3	TOP	PCFS	LAT	CENTER	6
	4	HX	3/16	3	BOTTOM	PCFS	LAT	CENTER	6
	4	OX	3/16	3	BOTTOM	PCFS	LAT	CENTER	6

First, when considering the NL data, no distinct pattern emerges. When examining the longitudinal data, it can be seen that the HX has greater fracture toughness than the over-expanded core; the opposite appears to be true for the lateral data (see figure 31).

Second, when investigating the VIS data, similar relationships may be ascertained, once more correlating to ribbon direction. When considering longitudinal data, the HX again has a greater fracture toughness than the over-expanded core. However, when looking at the lateral data, the disbond location has an additional effect. The top disbond data results in the HX having a greater fracture toughness than the over-expanded core, with the opposite true for the bottom disbond data (see figure 31).

Third, when examining the 5% offset/max load (5%/max) data, it can be seen that the same patterns occur as in the VIS data (see figure 31).

Fourth, when taking the AREA data into account a single distinct relationship was identified. The HX had a greater fracture toughness than the over-expanded core (see figure 31).

Fifth, when considering the behavior of the entire R-curve, two distinct patterns emerge, once again correlating to ribbon direction. When studying longitudinal data, the HX was identified as being slightly more fracture resistant than the over-expanded core, regardless of crack length, whereas the lateral data suggest that both the hexagonal and over-expanded cores have

approximately the same fracture toughness with respect to crack length. In addition, the core type seems to have little effect on the shape of the R-curve. Approximate R-curves representing this behavior are shown in figure 32.

Sixth, when considering load-versus-displacement plots, a similar relationship to the R-curves was identified. For longitudinal data, the HX appears to have slightly larger loads than the over-expanded core at corresponding displacements, whereas for lateral data, the hexagonal and over-expanded cores appear to have approximately the same loads at corresponding displacements. In addition, it should be noted that both hexagonal and over-expanded cores have stable load displacement curves, with very small or no load drops, representing slow crack growth. Approximate load-versus-displacement curves representing this behavior are shown in figure 33.

Lastly, when examining the failure modes, it can be seen that both hexagonal and over-expanded cores failed in a similar manner, primarily in the core, with some cells partially in adhesive pull out. An in-depth failure mode analysis is found in appendices A and C.

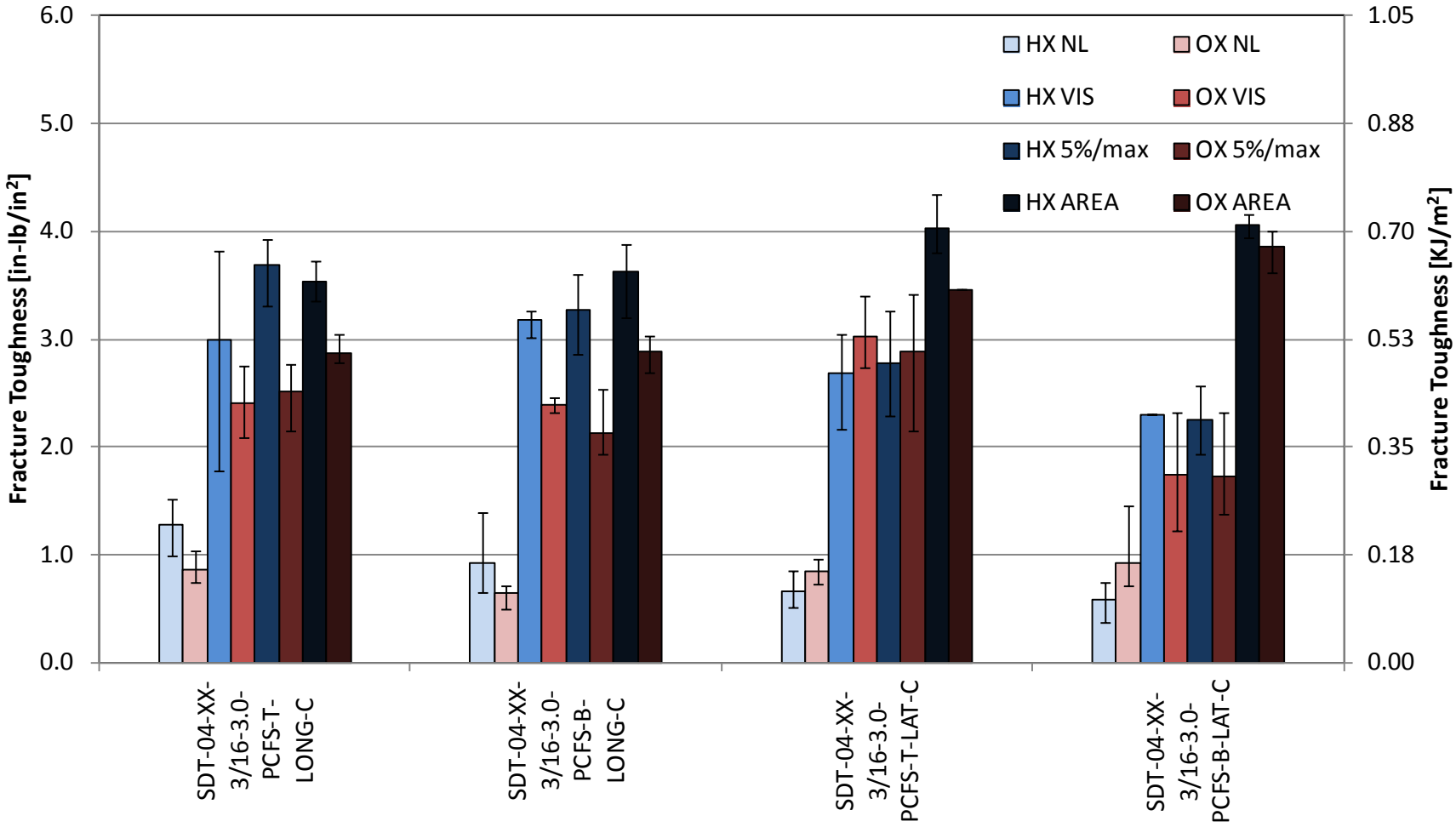

Figure 31. NL, VIS, and 5%/max fracture toughness between both core types

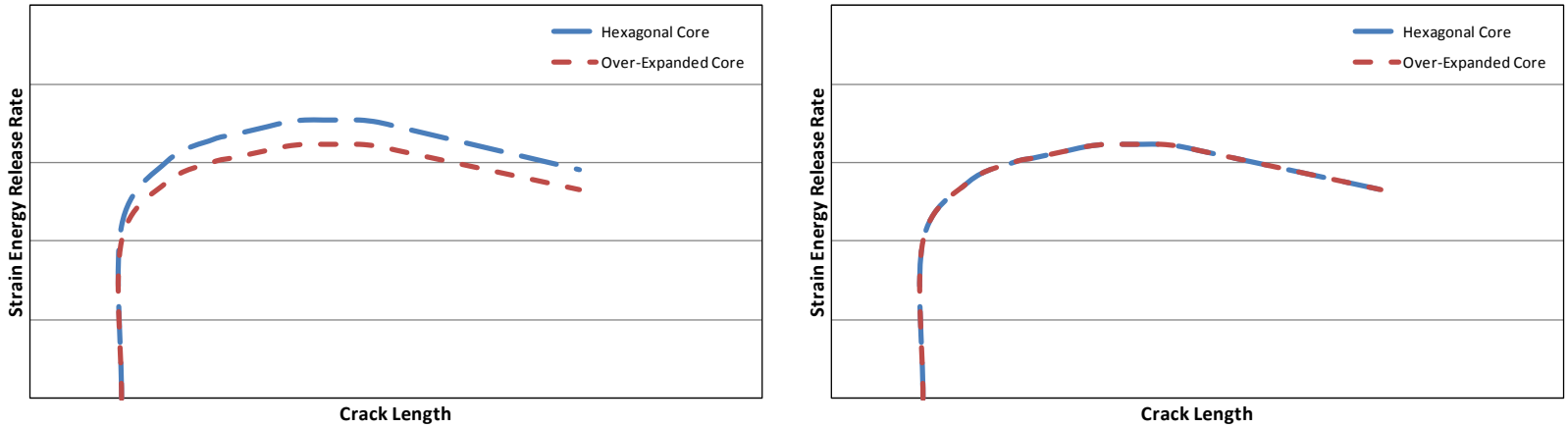

Figure 32. Typical R-curve pattern between both core types: (a) for longitudinal ribbon direction and (b) for lateral ribbon direction

\

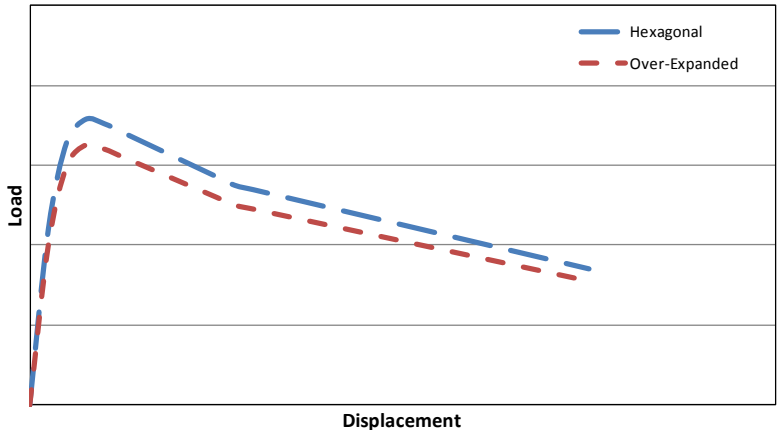

(a)

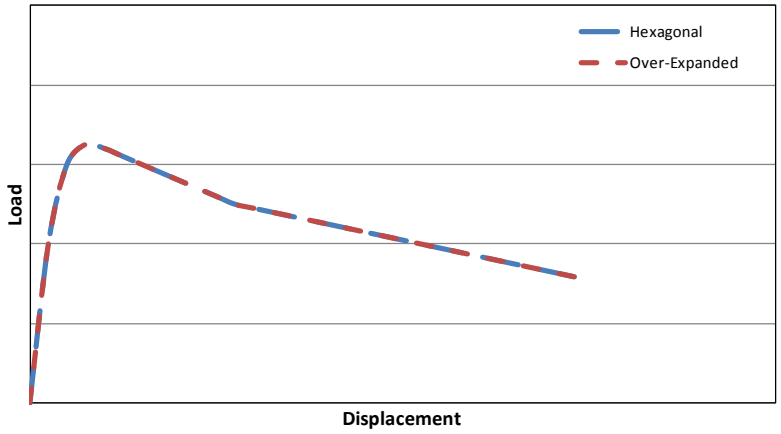

(b)

Figure 33. Typical load vs. displacements pattern between both core types: (a) longitudinal ribbon direction and (b) lateral ribbon direction

3.2 EFFECTS OF CELL SIZE

Three cell sizes of 1/8″, 3/16″, and 3/8″ were tested. All cell sizes had the same core type (HX), and were tested at three core densities of 2.0 pcf, 3.0 pcf, and 6.0 pcf (6.0 pcf was not tested for 3/8″). Each cell size was tested with two disbond locations, top and bottom. All three of the cell sizes at all three core densities and with both disbond locations were tested with the longitudinal ribbon direction. All three cell sizes (with a core density of 3.0 pcf) and both disbond locations were tested with the lateral ribbon direction. In addition, all three cell sizes at all three densities with both disbond locations and both ribbon directions had an initial crack tip location at the center of the cell. Two 1/8″ and 3/8″cell sizes with core densities of 3.0 pcf, bottom disbond locations, and both ribbon directions had initial crack tip locations at the edge of the cells. Furthermore, all three cell sizes at all three core densities with both disbond locations, both ribbon directions, and both crack tip locations were fabricated with PCFS. Two 1/8″ and 3/8″ cell sizes with core densities of 3.0 pcf, both disbond locations, longitudinal ribbon directions, and initial crack tip locations at the center of the cells were fabricated with CCFS. The combination of the above parameters resulted in 12 distinct datasets, as presented in table 6.

Table 6. Cell size test matrix

	Facesheet	Core Type	Cell Size (in)	Core Density (pcf)	Disbond Location	Fabrication Process	Ribbon Direction	Crack Tip Location	No. of Specimens
CELL SIZE	4	HX	1/8	1.8≈2	TOP	PCFS	LONG	CENTER	6
	4	HX	3/16	2	TOP	PCFS	LONG	CENTER	6
	4	HX	3/8	2	TOP	PCFS	LONG	CENTER	6
	4	HX	1/8	1.8≈2	BOTTOM	PCFS	LONG	CENTER	6
	4	HX	3/16	2	BOTTOM	PCFS	LONG	CENTER	6
	4	HX	3/8	2	BOTTOM	PCFS	LONG	CENTER	6
	4	HX	1/8	3	TOP	PCFS	LONG	CENTER	6
	4	HX	3/16	3	TOP	PCFS	LONG	CENTER	6
	4	HX	3/8	3	TOP	PCFS	LONG	CENTER	6
	4	HX	1/8	3	BOTTOM	PCFS	LONG	CENTER	6
	4	HX	3/16	3	BOTTOM	PCFS	LONG	CENTER	6
	4	HX	3/8	3	BOTTOM	PCFS	LONG	CENTER	6
	4	HX	1/8	3	BOTTOM	PCFS	LONG	EDGE	6
	4	HX	3/8	3	BOTTOM	PCFS	LONG	EDGE	6
	4	HX	1/8	3	TOP	PCFS	LAT	CENTER	6
	4	HX	3/16	3	TOP	PCFS	LAT	CENTER	6
	4	HX	3/8	3	TOP	PCFS	LAT	CENTER	6
	4	HX	1/8	3	BOTTOM	PCFS	LAT	CENTER	6
	4	HX	3/16	3	BOTTOM	PCFS	LAT	CENTER	6
	4	HX	3/8	3	BOTTOM	PCFS	LAT	CENTER	6
	4	HX	1/8	3	BOTTOM	PCFS	LAT	EDGE	6
	4	HX	3/8	3	BOTTOM	PCFS	LAT	EDGE	6
	4	HX	1/8	3	TOP	CCFS	LONG	CENTER	6
	4	HX	3/8	3	TOP	CCFS	LONG	CENTER	6
	4	HX	1/8	3	BOTTOM	CCFS	LONG	CENTER	6
	4	HX	3/8	3	BOTTOM	CCFS	LONG	CENTER	6
	4	HX	1/8	6	TOP	PCFS	LONG	CENTER	6
	4	HX	3/16	6	TOP	PCFS	LONG	CENTER	6
	4	HX	1/8	6	BOTTOM	PCFS	LONG	CENTER	6
	4	HX	3/16	6	BOTTOM	PCFS	LONG	CENTER	6

First, when considering the NL data, no clear pattern emerges, suggesting that cell size has little impact on non-linearity and that the other parameters play a much more significant role (see figure 34).

Second, when investigating the VIS data, a clear relationship materializes. The fracture toughness typically decreases with respect to cell size (i.e., 1/8″ is larger than 3/16″, which in turn is larger than 3/8″) (see figure 34).

Third, the 5% offset/max load (5%/max) data are shown to behave similarly to the VIS data (see figure 34).

Fourth, when taking the AREA data into account, the same relationship as the VIS and 5%/max data was identified (see figure 34).

Fifth, when considering the behavior of the entire R-curve, a distinct pattern similar to the VIS and 5%/max relationship was identified. The overall fracture resistance decreased with respect to cell size, 1/8″ is larger than 3/16″, which in turn is larger than 3/8″; however, the magnitude of difference between the cell sizes decreased with respect to crack length (i.e., the shorter the crack length, the more profound the impact of cell size). Furthermore, it should be noted that the overall shape of the resistance curve changed with cell size. The 1/8″ cell size had a sharp rising region (stable growth) followed by a sharp falling region (unstable growth). The 3/16″ cell size also had a modest rising region (stable growth) followed by a modest falling region (unstable growth). The 3/8″ cell size had a slightly rising region (stable growth) followed by a flat region (unstable growth) and slightly falling region (unstable growth). When considering all three cell sizes, it becomes apparent that as the cell size increases, the material system behaves in a more brittle manner, or as the cell size decreases, it behaves in a more ductile manner. The one exception to this behavior was found in the co-cured specimens where cell size seemed to be coupled and played a more complex role diminishing the effects; this coupling could explain the ambiguity found in the Volume I test results. Approximate R-curves representing this behavior are shown in figure 35.

Sixth, when considering load versus displacement plots, a similar relationship to the R-curves may be observed, the overall loads decreased with respect to cell size, 1/8″ is larger than 3/16″, which in turn is larger than 3/8″, at corresponding displacements. The one exception can once more be found among the co-cured specimens, which seemed to be coupled with the fabrication process and resulted in a much smaller difference in load between 1/8″ and 3/8″. In addition, it should be noted that 1/8″ and 3/16″ cores had stable load displacement curves, with very small or no-load drops, representing slow crack growth, except in the case of the 3/16″ core at 6.0 pcf, which had moderate load drops representing abrupt crack growth, whereas 3/8″ cores had small (for 2.0 pcf) and large (for 3.0 pcf) load drops representing abrupt crack growth. Approximate load versus displacement curves representing this behavior are shown in figure 36.

Lastly, when examining the failure modes, it can be observed that the failure mode varied among cell sizes and was coupled with core density. The 1/8″core with core densities of 2.0 pcf and 3.0 pcf typically failed in the core, and a core density of 6.0 pcf failed in adhesive pullout. The 3/16″ core with a core density of 2.0 pcf typically failed in the core, as did a core density of 3.0 pcf, with some cells partially in adhesive pullout; a core density of 6.0 pcf failed in adhesive pullout. The 3/8″ core with a core density of 2.0 pcf typically failed in adhesive pullout, with some core failure below the crack surface; a core density of 3.0 pcf typically failed in adhesive pullout. When considering all failure modes, an overall pattern does emerge—as the cell size increases the failure mode moves from the core to a mix of core and adhesive pullout to adhesive pullout, with the magnitude of change being dictated by core density. An in-depth failure mode analysis is in appendices A and B.

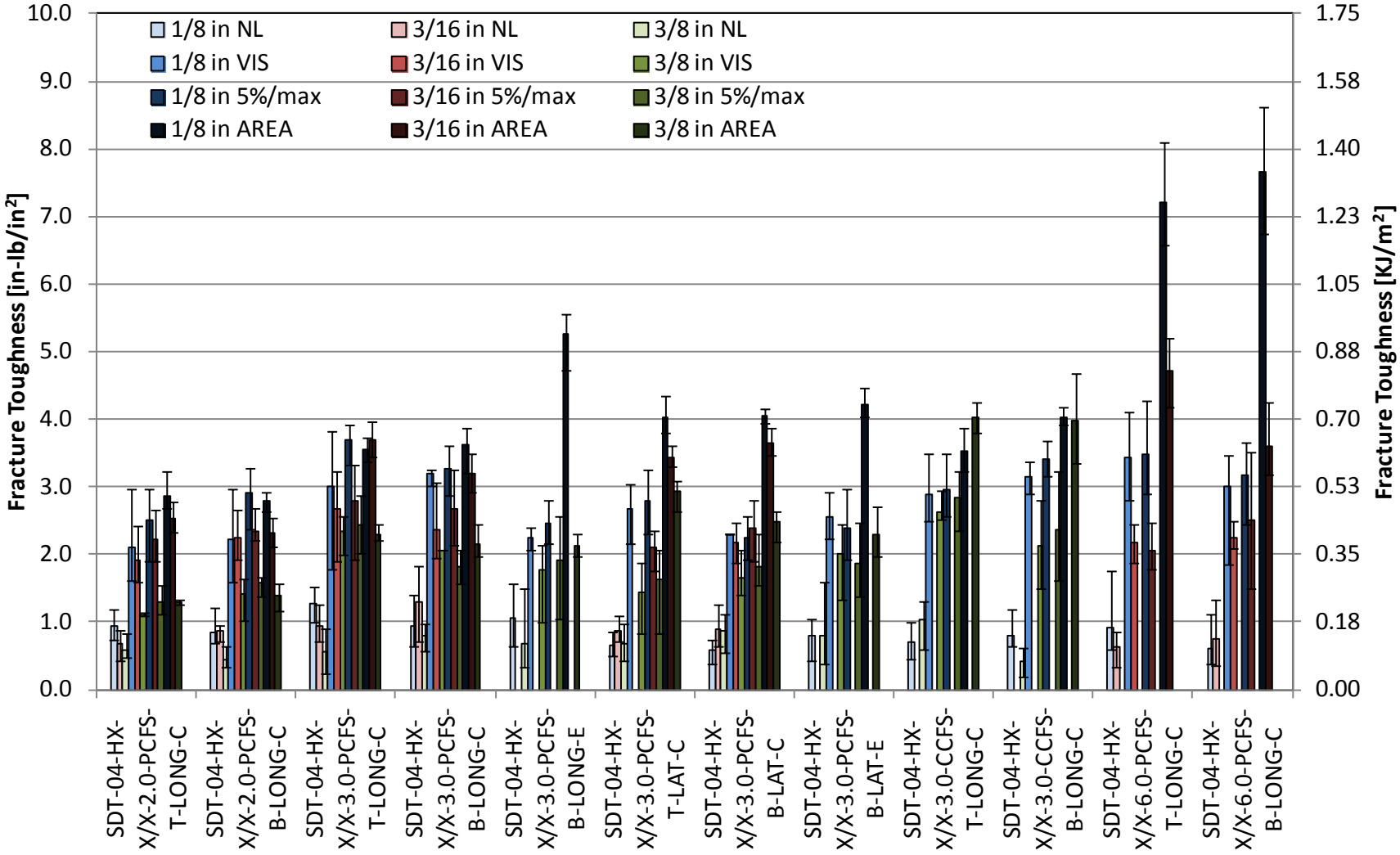

Figure 34. NL, VIS, and 5%/max fracture toughness among various cell sizes

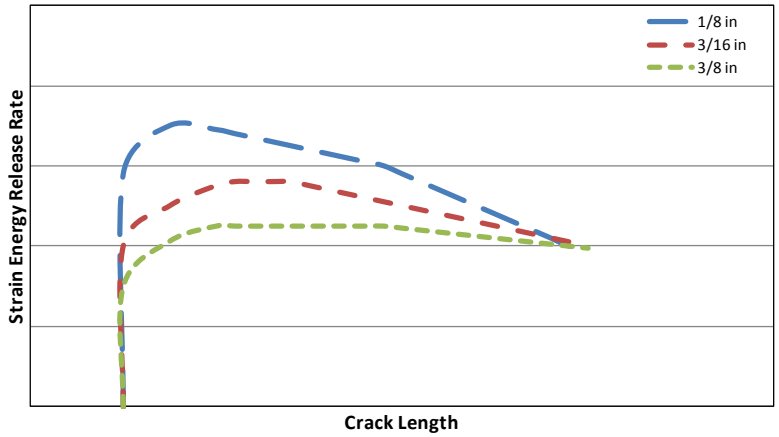

(a)

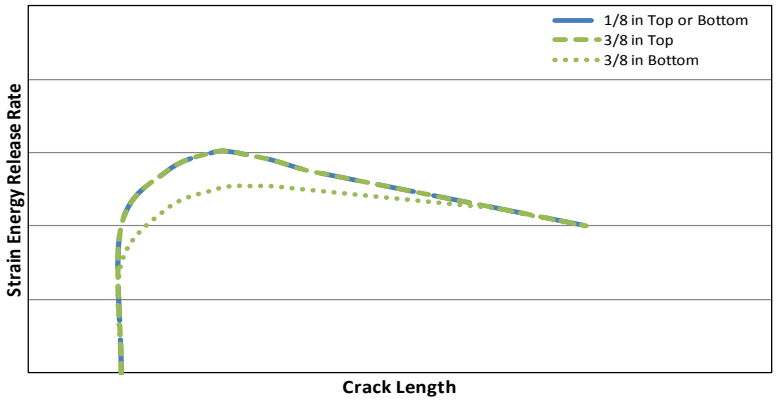

(b)

Figure 35. Typical R-curve pattern among various cell sizes

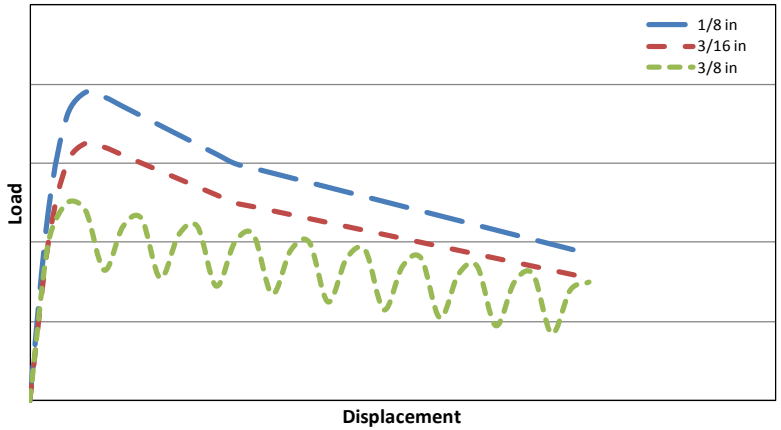

(a)

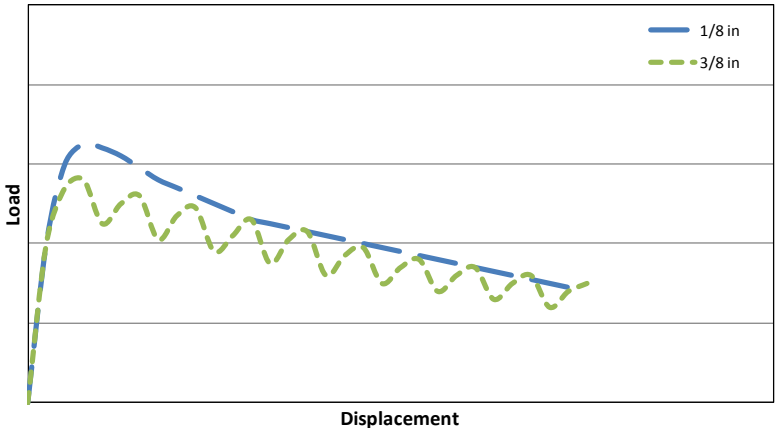

(b)

Figure 36. Typical load vs. displacement pattern among various cell sizes

3.3 EFFECTS OF CORE DENSITY

Three core densities of 2.0 pcf, 3.0 pcf, and 6.0 pcf were tested, all having the same core type, hexagonal, and all tested at three cell sizes of 1/8″, 3/16″, and 3/8″ (except 3/8″ cell size with core density of 6.0 pcf was not tested). All three core densities at all three cell sizes were tested with two disbond locations, top and bottom. All three core densities at all three cell sizes and at both disbond locations were tested with the longitudinal ribbon direction. In addition, all three core densities at all three cell sizes and with both disbond locations had an initial crack tip location at the center of the cell. Furthermore, all three core densities at all three cell sizes and with both disbond locations were fabricated with PCFS. The combination of the above parameters resulted in six distinct datasets as presented in table 7.

Table 7. Core density test matrix

	Facesheet	Core Type	Cell Size (in)	Core Density (pcf)	Disbond Location	Fabrication Process	Ribbon Direction	Crack Tip Location	No. of Specimens
CORE DENSITY	4	HX	1/8	1.8 ≈ 2	TOP	PCFS	LONG	CENTER	6
	4	HX	1/8	3	TOP	PCFS	LONG	CENTER	6
	4	HX	1/8	6	TOP	PCFS	LONG	CENTER	6
	4	HX	1/8	1.8 ≈ 2	BOTTOM	PCFS	LONG	CENTER	6
	4	HX	1/8	3	BOTTOM	PCFS	LONG	CENTER	6
	4	HX	1/8	6	BOTTOM	PCFS	LONG	CENTER	6
	4	HX	3/16	2	TOP	PCFS	LONG	CENTER	6
	4	HX	3/16	3	TOP	PCFS	LONG	CENTER	6
	4	HX	3/16	6	TOP	PCFS	LONG	CENTER	6
	4	HX	3/16	2	BOTTOM	PCFS	LONG	CENTER	6
	4	HX	3/16	3	BOTTOM	PCFS	LONG	CENTER	6
	4	HX	3/16	6	BOTTOM	PCFS	LONG	CENTER	6
	4	HX	3/8	2	TOP	PCFS	LONG	CENTER	6
	4	HX	3/8	3	TOP	PCFS	LONG	CENTER	6
	4	HX	3/8	2	BOTTOM	PCFS	LONG	CENTER	6
	4	HX	3/8	3	BOTTOM	PCFS	LONG	CENTER	6

It is important to note that core density is a function of both paper thickness and resin. The distinction of which element is impacting the data is beyond the scope of this program.

First, when considering the NL data, a distinct pattern emerges. The fracture toughness first increases between 2.0 pcf and 3.0 pcf cores and then decreases between 3.0 pcf and 6.0 pcf cores (see figure 37).

Second, when investigating the VIS data, a similar relationship to the NL data may be ascertained (see figure 37).

Third, when examining the 5% offset/max load (5%/max) data, similar behavior to both the NL and VIS data was identified (see figure 37).

Fourth, when taking the AREA data into account, a single distinct relationship was identified. The fracture toughness increased as core density increased. This was due to the large loads found at higher displacements in the 6.0 pcf cores (see figure 37).

Fifth, when considering the behavior of the entire R-curve, three patterns emerge, each coupled with cell size. In 1/8″ cores, the fracture toughness increased with cell density from 2.0 pcf to 3.0 pcf, then leveled off from 3.0 pcf to 6.0 pcf, with 3.0 pcf and 6.0 pcf being approximately the same. In 3/16″ cores, the fracture resistance behaved in a manner similar to NL, VIS, and 5%/max data, first increasing with density, from 2.0 pcf to 3.0 pcf, then decreasing with density, from 3.0 pcf to 6.0 pcf, where 2.0 pcf and 6.0 pcf were approximately the same. Furthermore, the magnitude of the difference decreased as the crack length increased. Lastly, in 3/8″ cores, the fracture toughness increased from 2.0 pcf to 3.0 pcf; however, no 6.0 pcf core was tested, so there is no way of determining how the fracture resistance responded between 3.0 pcf and 6.0 pcf. In addition, it should be noted that the shape of the resistance curves was unaffected by core density and only varied with cell size. Approximate R-curves representing this behavior are shown in figure 38.

Sixth, when considering load versus displacement plots, three distinct relationships emerge, differing from those identified in the NL, VIS, and 5%/max data as well as the R-curves. Once more, each relationship is coupled with cell size. The 1/8″ core produced load versus displacement curves that increased with core density, with stable load displacement curves having very small or no-load drops, representing slow crack growth. The 3/16″ cores resulted in load versus displacement curves that increased between 2.0 pcf and 3.0 pcf, where both 2.0 pcf and 3.0 pcf had stable load displacement curves, with very small or no-load drops, representing slow crack growth; however, the 6.0 pcf core initially was between 2.0 pcf and 3.0 pcf at small displacements, but as the displacements increased, the 6.0 pcf core loads were less affected than those of the 2.0 pcf and 3.0 pcf cores, resulting in higher corresponding loads. In addition, the 6.0 pcf core had moderate load drops representing abrupt crack growth. The 3/8″ cores had load displacement curves that increased between 2.0 pcf and 3.0 pcf, whereas the 2.0 pcf core had small load drops representing abrupt crack growth, and the 3.0 pcf core had large load drops, representing more severe abrupt crack growth. Approximate load versus displacement curves representing in this behavior are shown in figure 39.

Lastly, when examining the failure modes, it can be seen that the failure mode varied between core densities and was coupled with cell size. The 2.0 pcf with 1/8″ and 3/16″ cores failed in the core, and the 3/8″ core typically failed in adhesive pullout, with some core failure below the crack surface. The 3.0 pcf with 1/8″ core primarily failed in the core, and 3/16″ and 3/8″ cores typically failed in adhesive pullout. The 6.0 pcf with a 1/8″ and 3/16″ cores failed in adhesive pullout. When considering all failure modes, an overall pattern emerges—as the core density increases, the failure mode moves from the core to a mix of core and adhesive pullout, to adhesive pullout, with the magnitude of change being dictated by cell size. An in-depth failure mode analysis is found in appendix A.

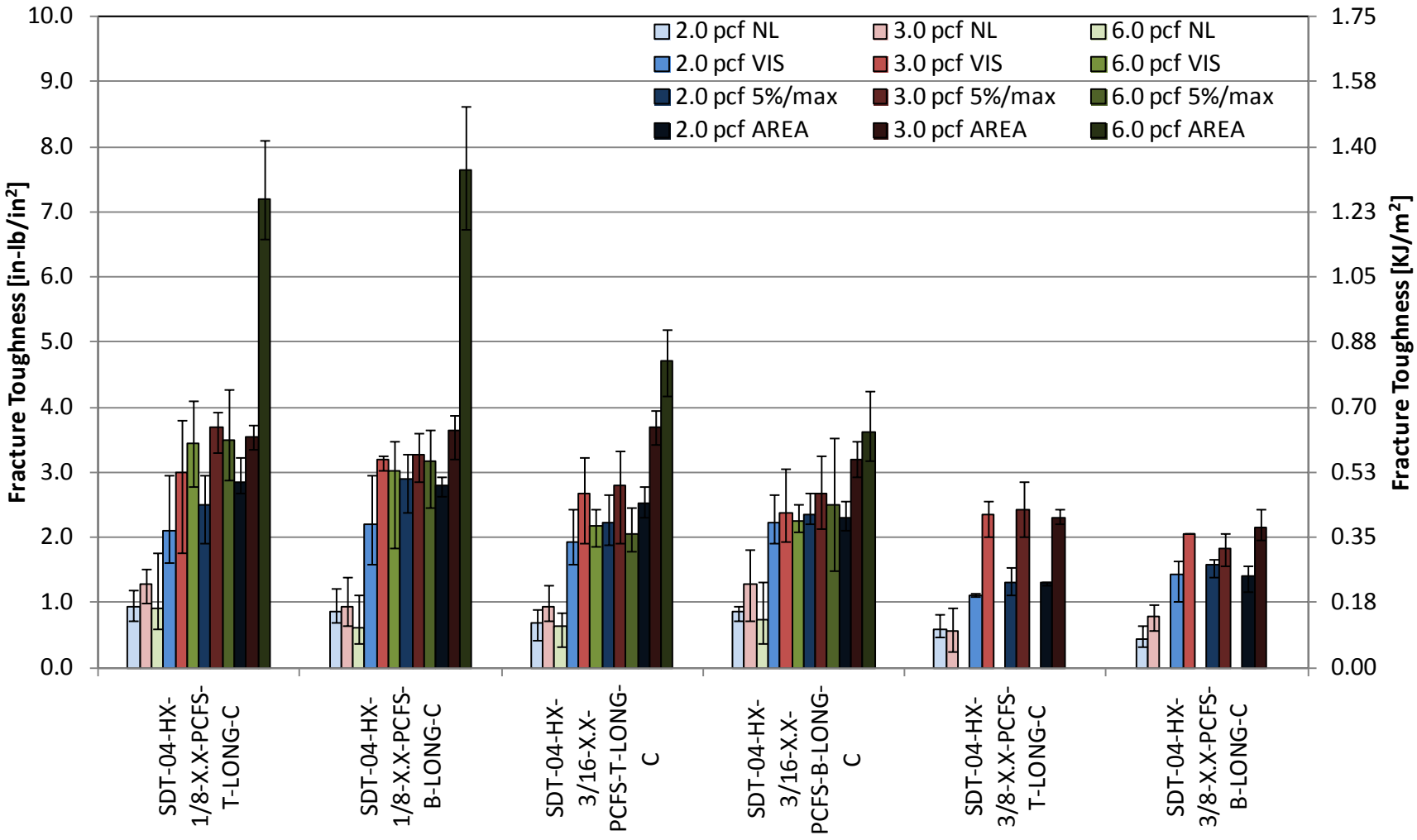

Figure 37. NL, VIS, and 5%/max fracture toughness among various core densities

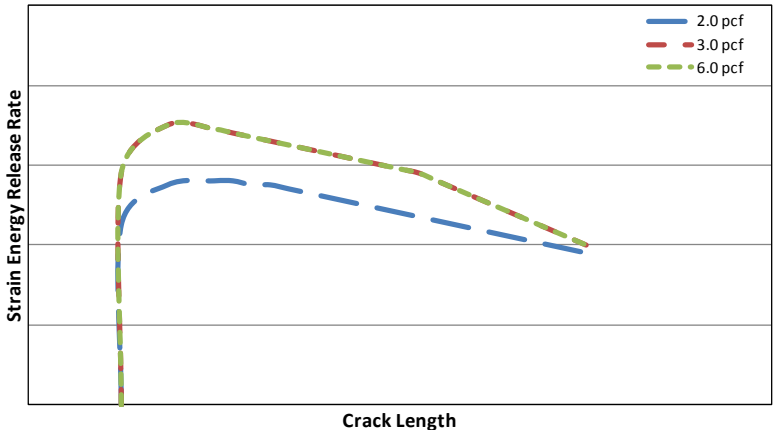

(a) R-curve for 1/8″ cores

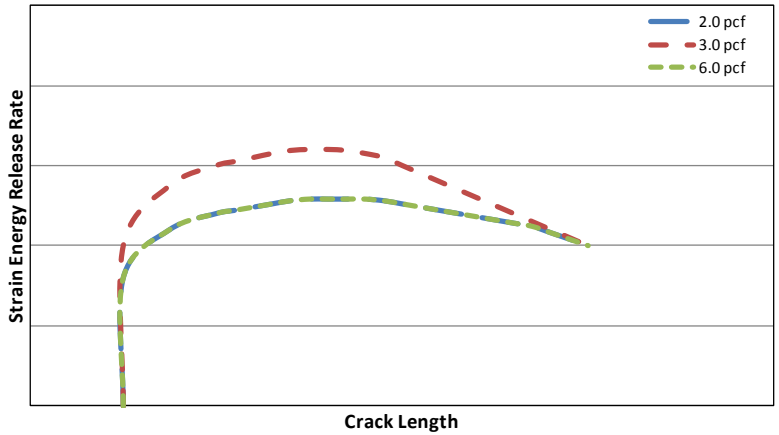

(b) R-curve for 3/16″ cores

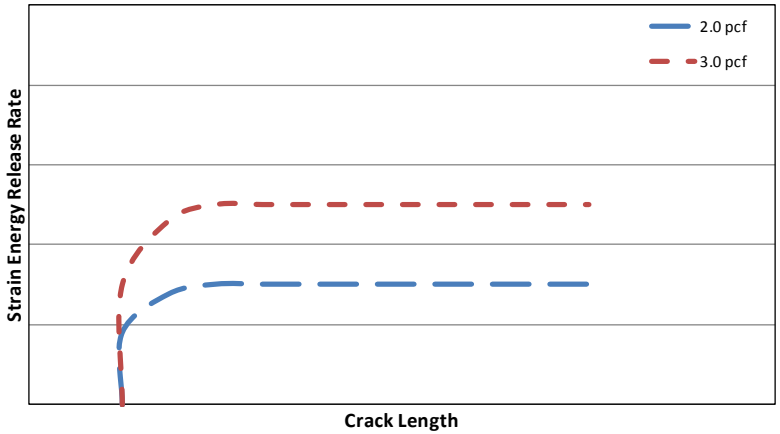

(c) R-curve for 3/8″ cores

Figure 38. Typical R-curve patterns among various core densities

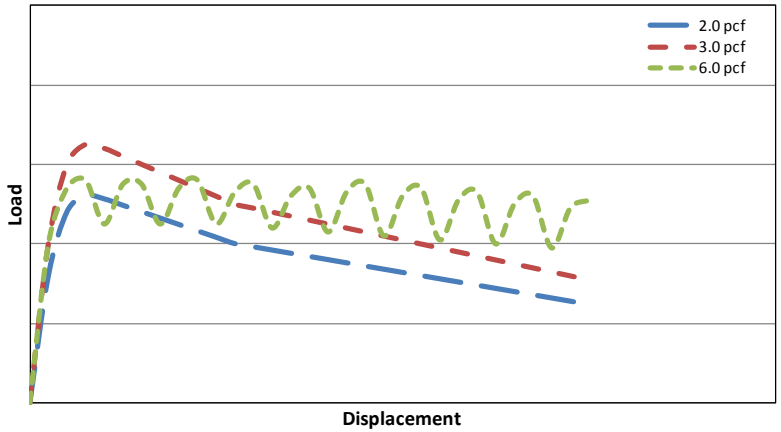

(a) Load vs. displacement 1/8″ cores

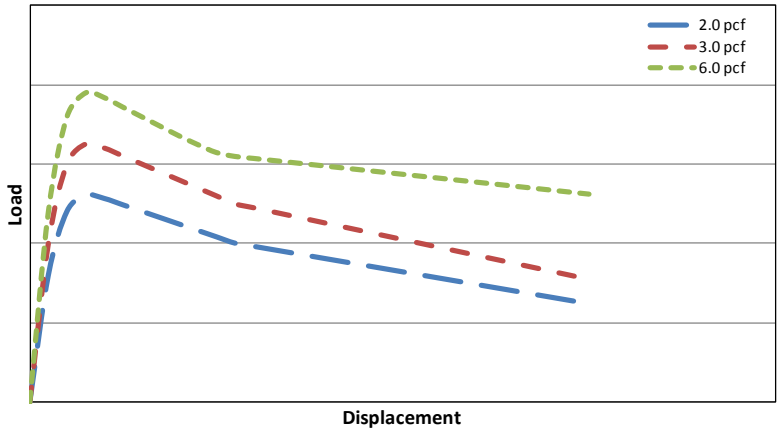

(b) Load vs. displacement 3/16″ cores

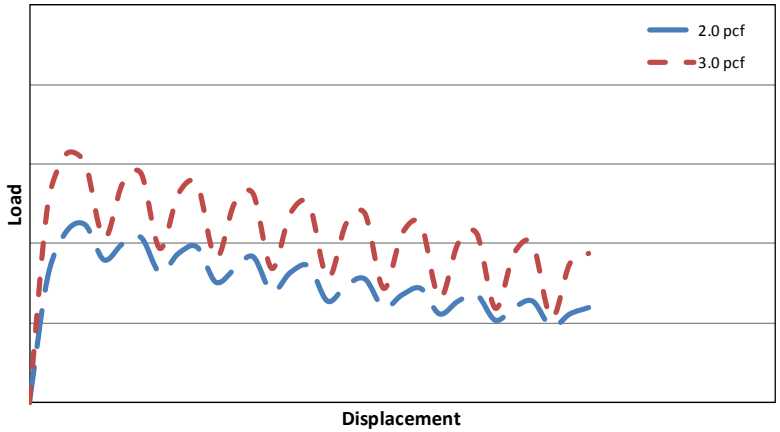

(c) Load vs. displacement 3/8″ cores

Figure 39. Typical load vs. displacement patterns among various core densities

3.4 EFFECTS OF DISBOND LOCATION

Two disbond locations, top and bottom, were tested. Both disbond locations were tested with a HX with all three cell sizes of 1/8″, 3/16″, and 3/8″, and three core densities of 2.0 pcf, 3.0 pcf, and 6.0 pcf (except 3/8″ cell size with core density of 6.0 pcf was not tested). Both disbond locations were tested with an over-expanded core, a cell size of 3/16″, and a core density of 3.0 pcf. Both disbond locations with both core types, all three cell sizes, and all three core densities were tested with the longitudinal ribbon direction. Both disbond locations with both core types, all three cell sizes, and 3.0 pcf were tested with the lateral ribbon direction. In addition, both disbond locations with both core types, all three cell sizes, all three core densities, and both ribbon directions had an initial crack tip location at the center of the cell. Furthermore, both disbond locations, with both core types, all three cell sizes, all three core densities, and both ribbon directions were fabricated with PCFS. Both disbond locations with an HX, two 1/8″ and 3/8″ cell sizes, a core density of 3.0 pcf, and a longitudinal ribbon were fabricated with CCFS. The combination of the above parameters resulted in 15 distinct datasets, as presented in table 8.

Table 8. Disbond location test matrix

	Facesheet	Core Type	Cell Size (in)	Core Density (pcf)	Disbond Location	Fabrication Process	Ribbon Direction	Crack Tip Location	No. of Specimens
DISBOND LOCATION	4	HX	1/8	1.8 ≈ 2	TOP	PCFS	LONG	CENTER	6
	4	HX	1/8	1.8 ≈ 2	BOTTOM	PCFS	LONG	CENTER	6
	4	HX	1/8	3	TOP	PCFS	LONG	CENTER	6
	4	HX	1/8	3	BOTTOM	PCFS	LONG	CENTER	6
	4	HX	1/8	3	TOP	PCFS	LAT	CENTER	6
	4	HX	1/8	3	BOTTOM	PCFS	LAT	CENTER	6
	4	HX	1/8	3	TOP	CCFS	LONG	CENTER	6
	4	HX	1/8	3	BOTTOM	CCFS	LONG	CENTER	6
	4	HX	1/8	6	TOP	PCFS	LONG	CENTER	6
	4	HX	1/8	6	BOTTOM	PCFS	LONG	CENTER	6
	4	HX	3/16	2	TOP	PCFS	LONG	CENTER	6
	4	HX	3/16	2	BOTTOM	PCFS	LONG	CENTER	6
	4	HX	3/16	3	TOP	PCFS	LONG	CENTER	6
	4	HX	3/16	3	BOTTOM	PCFS	LONG	CENTER	6
	4	HX	3/16	3	TOP	PCFS	LAT	CENTER	6
	4	HX	3/16	3	BOTTOM	PCFS	LAT	CENTER	6
	4	HX	3/16	6	TOP	PCFS	LONG	CENTER	6
	4	HX	3/16	6	BOTTOM	PCFS	LONG	CENTER	6
	4	HX	3/8	2	TOP	PCFS	LONG	CENTER	6
	4	HX	3/8	2	BOTTOM	PCFS	LONG	CENTER	6
	4	HX	3/8	3	TOP	PCFS	LONG	CENTER	6
	4	HX	3/8	3	BOTTOM	PCFS	LONG	CENTER	6
	4	HX	3/8	3	TOP	PCFS	LAT	CENTER	6
	4	HX	3/8	3	BOTTOM	PCFS	LAT	CENTER	6
	4	HX	3/8	3	TOP	CCFS	LONG	CENTER	6
	4	HX	3/8	3	BOTTOM	CCFS	LONG	CENTER	6
	4	OX	3/16	3	TOP	PCFS	LONG	CENTER	6
	4	OX	3/16	3	BOTTOM	PCFS	LONG	CENTER	6
	4	OX	3/16	3	TOP	PCFS	LAT	CENTER	6
	4	OX	3/16	3	BOTTOM	PCFS	LAT	CENTER	6

First, when considering NL data, no consistent patterns explaining the effects of the disbond location could be identified, because the effects of core type, cell size, core density, fabrication process, and ribbon direction became coupled and obscured any influence of the disbond location (see figure 40).

Second, when investigating the VIS data, once again no consistent relationships explaining the effects of the disbond location were observed, because the effects of core type, cell size, core density, fabrication process, and ribbon direction became coupled and clouded any influence of

the disbond location. It is important to note that the VIS relationships differ from those found in the NL data (see figure 40).

Third, when examining the 5% offset/max load (5%/max) data, once more, no consistent behavior explaining the effects of the disbond location was found, because the effects of core type, cell size, core density, fabrication process, and ribbon direction became coupled and masked any influence of the disbond location. However, it is worth noting that the patterns found in the 5%/max data are consistent with those found in the VIS data (see figure 40).

Fourth, when taking the AREA data into account, as before, no consistent behavior explaining the effects of the disbond location was found, because the effects of core type, cell size, core density, fabrication process, and ribbon direction became coupled and diluted any influence of the disbond location. It is important to note that the AREA relationships differ from those found in the NL, VIS and 5%/max data (see figure 40).

Fifth, when considering the behavior of the entire R-curve, two relationships correlating to core type were observed. The HX resulted in both the top disbond and bottom disbond locations, resulting in approximately the same fracture resistance. However, within the over-expanded core, the top disbond location specimens resulted in a greater fracture toughness for small crack lengths than the bottom disbond location specimens, and the R-curves quickly converged to larger crack lengths. The shape of the R-curves, however, was dictated by cell size. Approximate R-curves representing this behavior are shown in figure 41.

Sixth, when considering load versus displacement plots, it was observed that, for most cases, both the top and bottom disbond locations resulted in approximately the same load displacement plots, inferring that disbond location played little to no role in load versus displacement plots. The exception to this rule was found in the hexagonal, 3/16″, 6.0-pcf core, where the top disbond location data resulted in higher loads than the bottom disbond location specimens, regardless of corresponding displacements. Approximate load versus displacement curves representing this behavior are shown in figure 42.

Lastly, when examining the failure modes, it became apparent that disbond location played little to no role and the coupled effect of cell size and core density dictated the failure mode. An in-depth failure mode analysis is found in appendices – C.

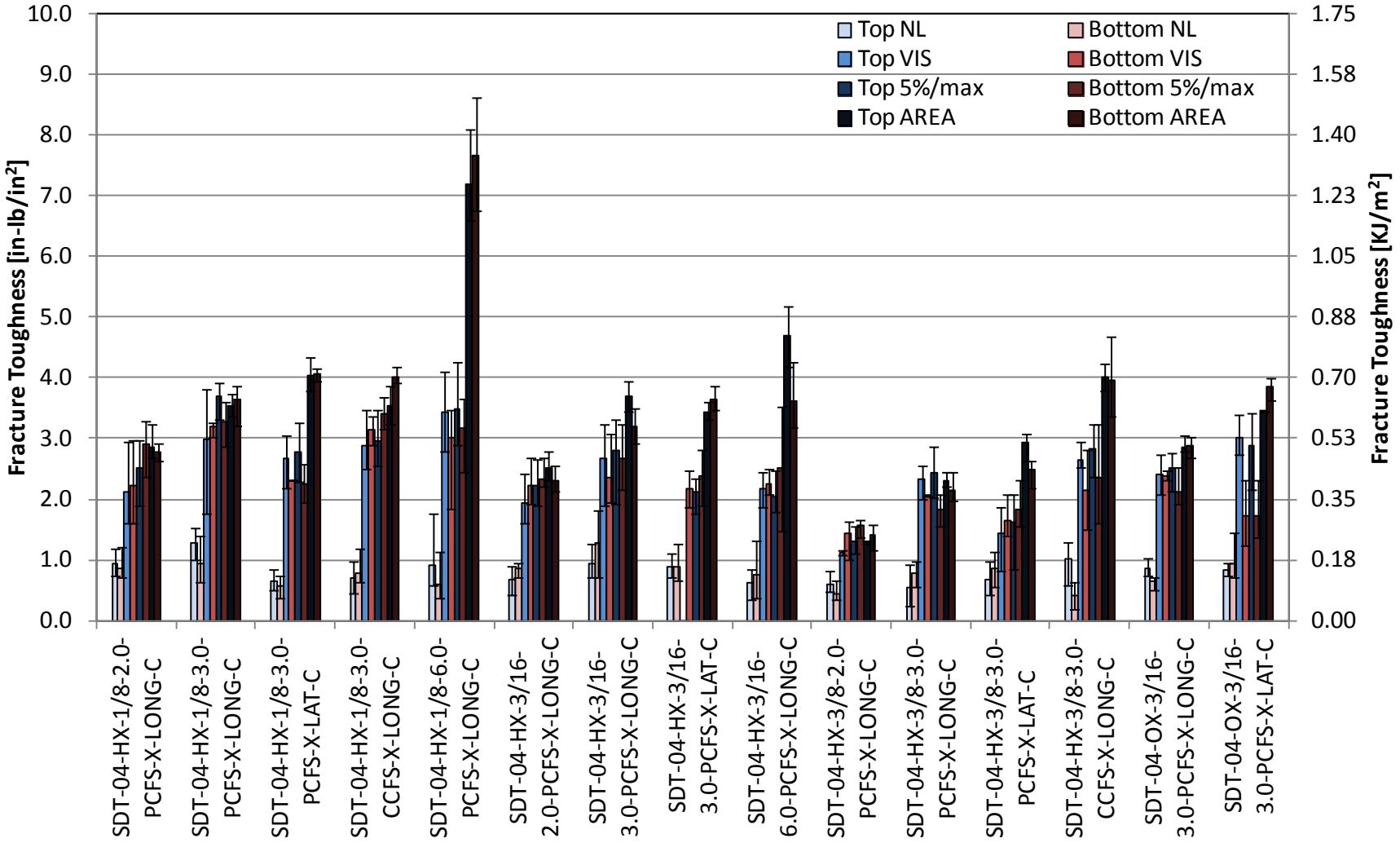

Figure 40. NL, VIS, and 5%/max fracture toughness between both disbond locations

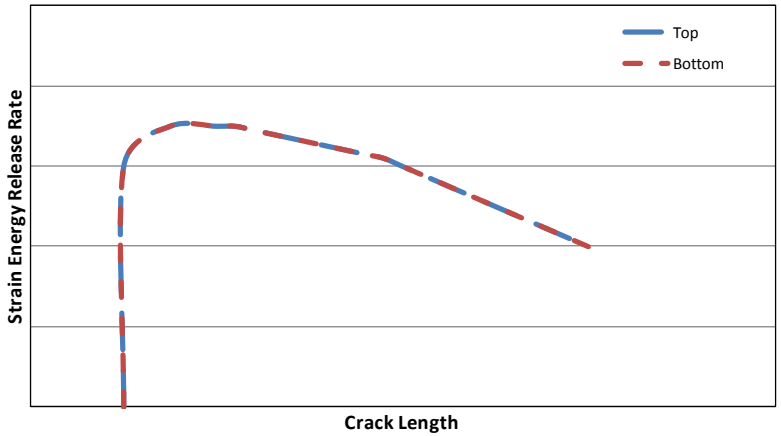

(a) R-curve for hexagonal 1/8″ cores

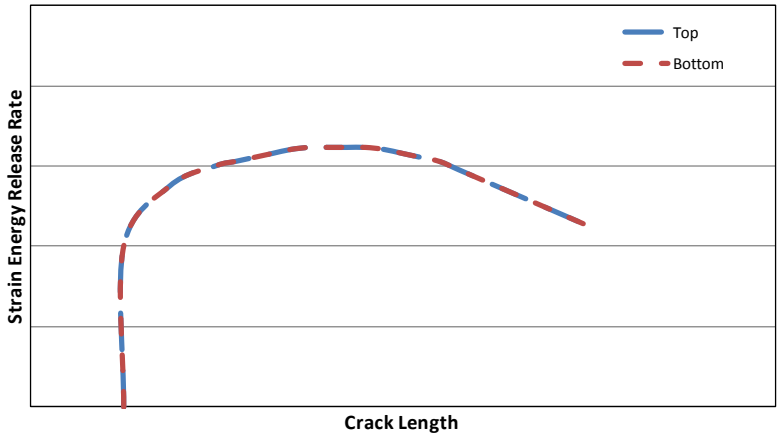

(b) R-curve for hexagonal 3/16″ cores

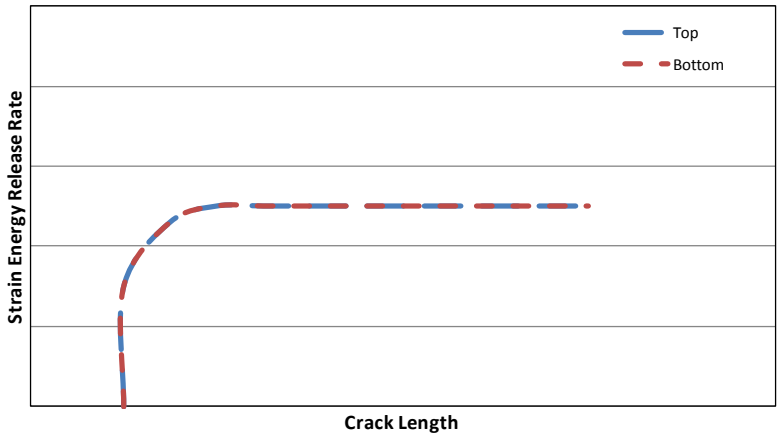

(c) R-curve for hexagonal 3/8″ cores

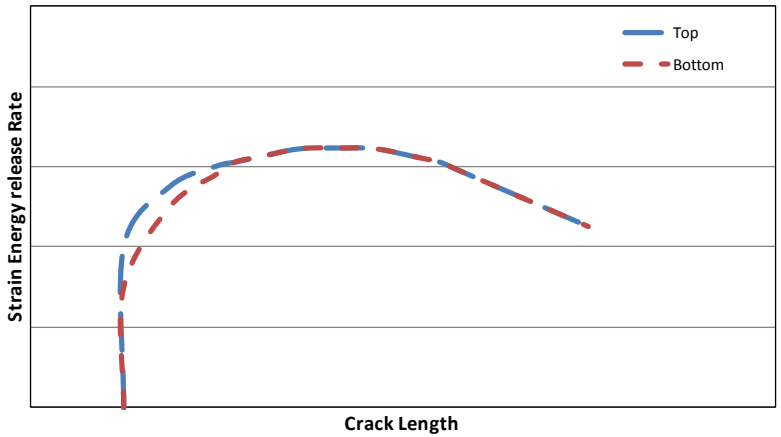

(d) R-curve for over-expanded 3/16″ cores

Figure 41. Typical R-curve pattern between both disbond locations

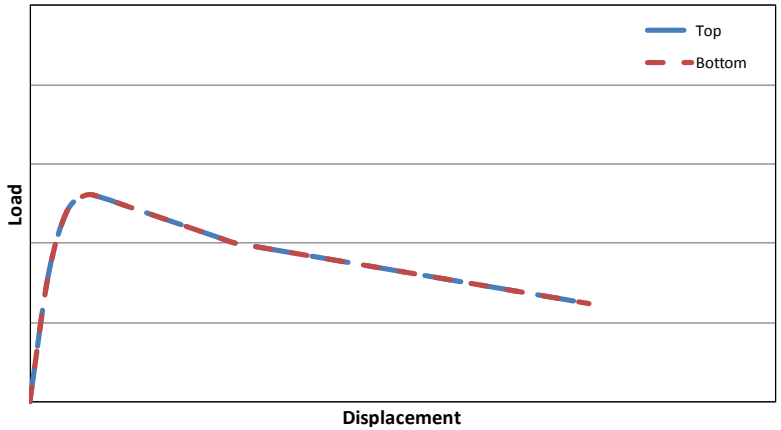

(a) Load vs. displacement for 2.0 pcf core
(3/8″ load drops not shown)

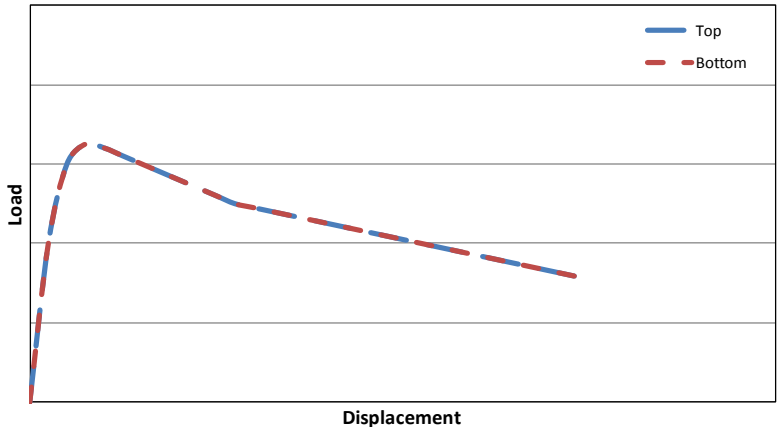

(b) Load vs. displacement for 3.0 pcf core
(3/8″ load drops not shown, similar to OX core)
(c)

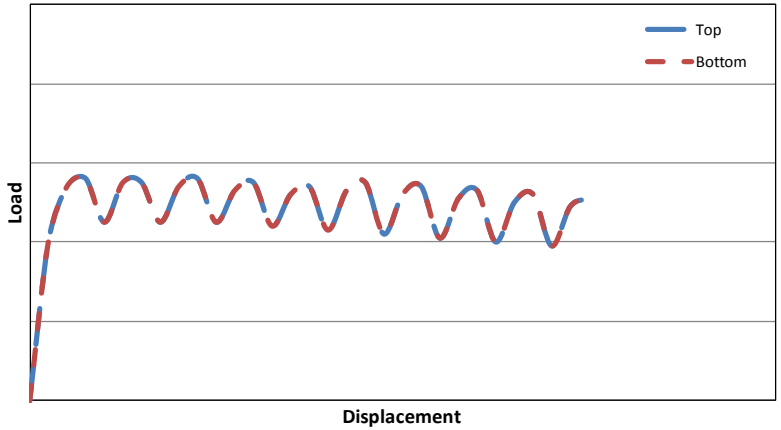

(d) Load vs. displacement for 6.0 pcf 1/8″ core

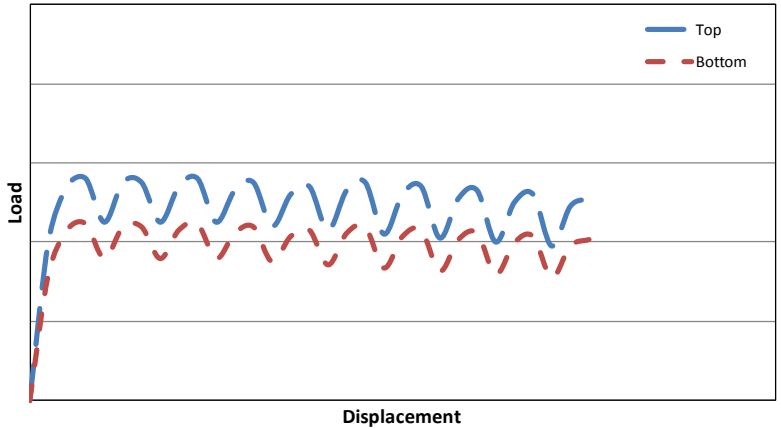

(e) Load vs. displacement for 6.0 pcf 3/16″ core

Figure 42. Typical load vs. displacement pattern between both disbond locations

3.5 EFFECTS OF FABRICATION PROCESS

Two fabrication processes, PCFS and CCFS, were tested, both with the same HX type, two cell sizes of 1/8″ and 3/8″, and same core density of 3.0 pcf. Both fabrication processes of both cell sizes were tested with two disbond locations, top and bottom, and the same longitudinal ribbon direction. In addition, both fabrication processes of both cell sizes at both disbond locations had an initial crack tip location, at the center of the cell. The combination of these parameters resulted in four distinct datasets, as presented in table 9.

Table 9. Fabrication process test matrix

	Facesheet	Core Type	Cell Size (in)	Core Density (pcf)	Disbond Location	Fabrication Process	Ribbon Direction	Crack Tip Location	No. of Specimens
FABRICATION PROCESS	4	HX	1/8	3	TOP	PCFS	LONG	CENTER	6
	4	HX	1/8	3	TOP	CCFS	LONG	CENTER	6
	4	HX	1/8	3	BOTTOM	PCFS	LONG	CENTER	6
	4	HX	1/8	3	BOTTOM	CCFS	LONG	CENTER	6
	4	HX	3/8	3	TOP	PCFS	LONG	CENTER	6
	4	HX	3/8	3	TOP	CCFS	LONG	CENTER	6
	4	HX	3/8	3	BOTTOM	PCFS	LONG	CENTER	6
	4	HX	3/8	3	BOTTOM	CCFS	LONG	CENTER	6

First, when considering the NL data, it was observed that the PCFS specimens typically had a greater fracture toughness than the CCFS specimens (in all but one case) (see figure 43).

Second, when investigating the VIS data, two distinct patterns emerged, each correlating to cell size. When examining the 1/8″ core, it became apparent that fracture toughness in the PCFS specimens was greater than in the CCFS specimens, whereas the opposite was true for specimens with a 3/8″ core (see figure 43).

Third, when examining the 5% offset/max load (5%/max) data, two similar relationships may be observed, once more correlating to cell size. However, when looking at the 1/8″ core, the disbond location appears to be having an additional effect. The PCFS specimens with a top disbond had a greater fracture toughness than the CCFS specimens, and the opposite appears to be true for bottom disbond data. When considering the 3/8″ core data, it appears that the CCFS specimens had a greater fracture toughness than the PCFS specimens (see figure 43).

Fourth, when taking the AREA data into account, two similar behaviors may be observed, once more correlating to cell size. When considering the 1/8″ core, the PCFS specimens had approximately the same or slightly less fracture toughness than the CCFS specimens. When considering 3/8″ core data, it appears that the CCFS specimens had greater fracture toughness than the PCFS specimens (see figure 43).

Fifth, when considering the behavior of the entire R-Curve, two patterns were observed, similar to those found in the 5%/max data, again correlating to cell size. When looking at the 1/8″ core, the

PCFS specimens had a larger fracture resistance than the CCFS specimens, regardless of crack length. However, within the 3/8″ core, it appears that the CCFS specimens had a larger fracture resistance than the PCFS specimens, regardless of crack length. In addition, the fabrication process seems to have little to no effect on the shape of the R-curve, with cell size seeming to play the dominate role. Approximate R-curves representing this behavior can be found in figure 44.

Sixth, when considering load versus displacement plots, similar behaviors were observed, once more correlating to cell size. The 1/8″ core initially had larger loads for the PCFS specimens than for the CCFS specimens at small displacements, but the curves quickly converged as the displacements increased. However, the 3/8″ core produced CCFS loads that were higher than PCFS loads at corresponding displacements. Furthermore, when considering the shape of the load versus displacement curves, it becomes apparent that the fabrication process coupled with cell size and the 1/8″ core had stable load displacement curves, with very small or no load drops, representing slow crack growth, whereas the 3/8″ core had small (PCFS) and large (CCFS) load drops, representing abrupt crack growth. The fabrication process clearly affected the magnitude of the load drops except of the greater AREA GIC for co-cured facesheet fabrication has no effect. Approximate load versus displacement curves representing this behavior can be found in figure 45.

Lastly, when examining the failure modes, it becomes apparent that the fabrication process plays no role, and that failure mode is primarily affected by cell size. An in-depth failure mode analysis is found in appendices A and C.

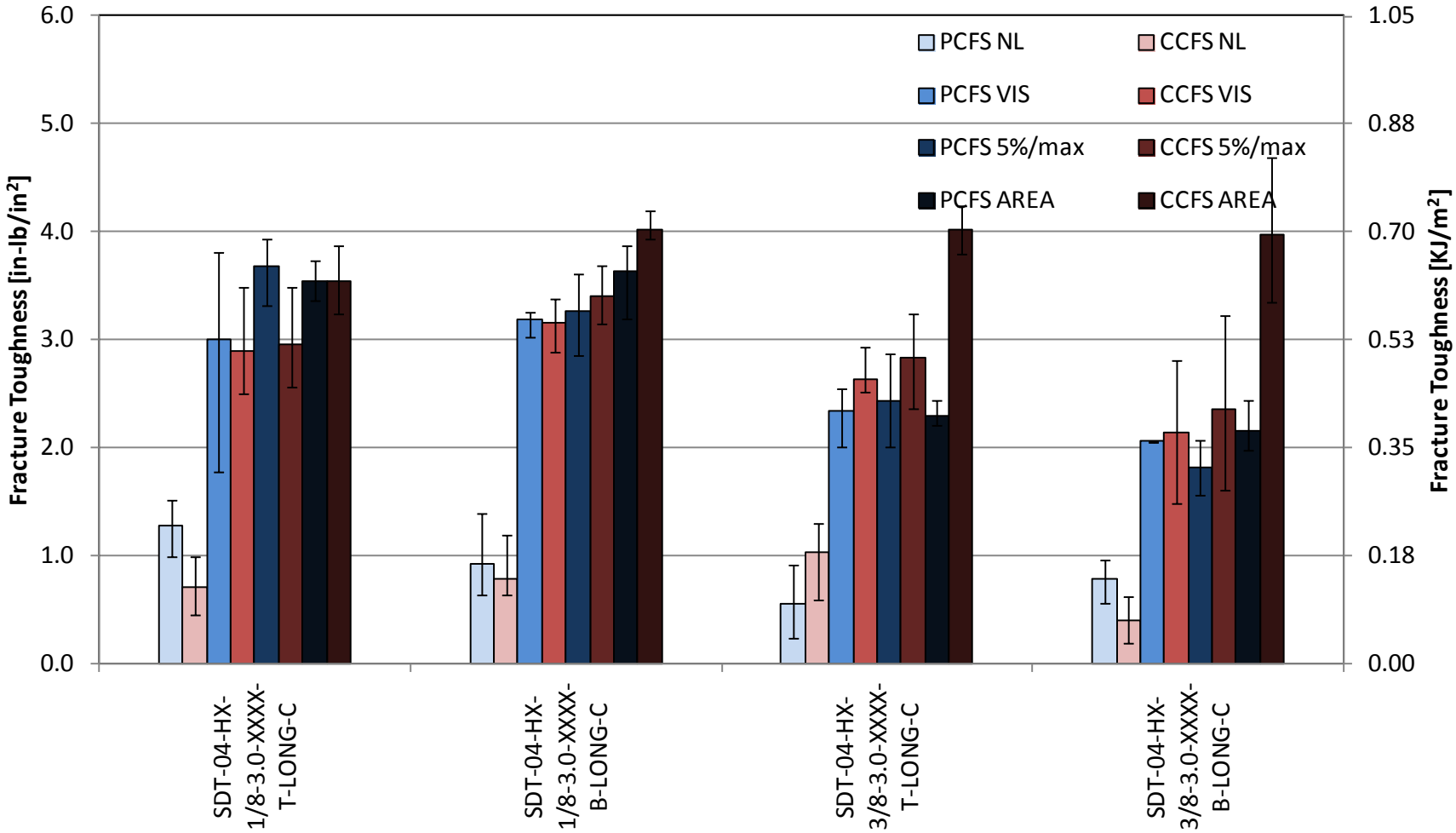

Figure 43. NL, VIS, and 5%/max fracture toughness and AREA between both fabrication processes

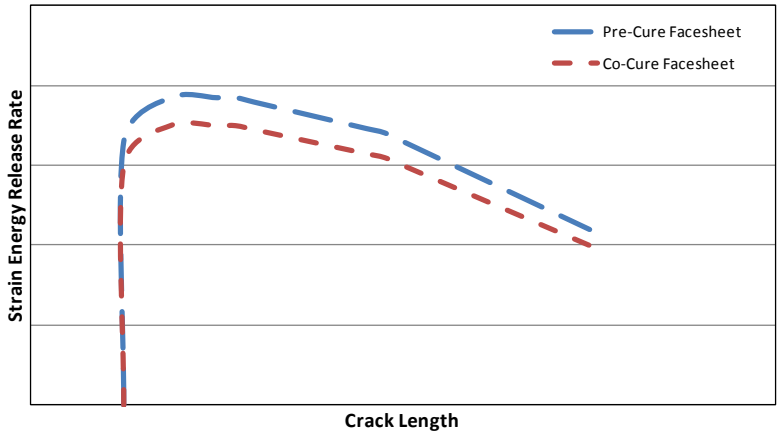

(a) R-curve for 1/8″ core

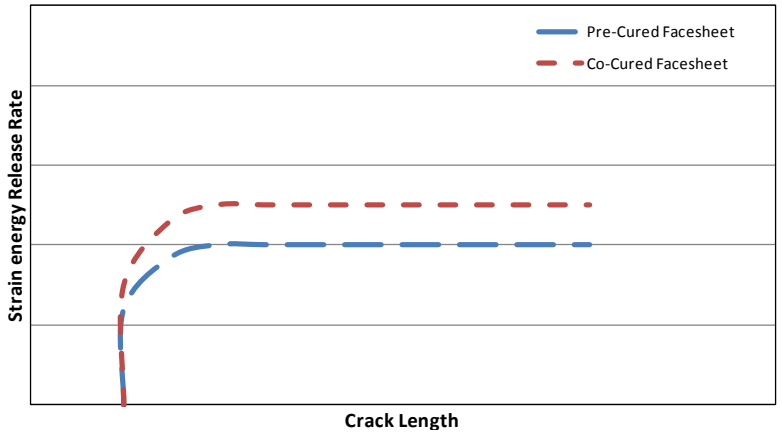

(b) R-curve for 3/8″ core

Figure 44. Typical R-curve pattern between both fabrication processes

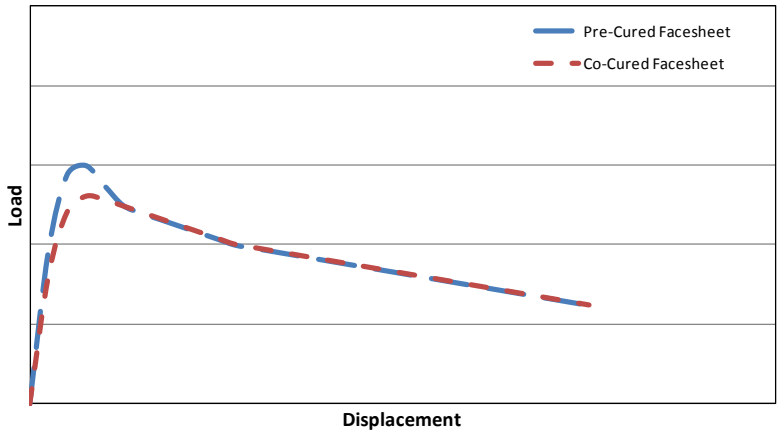

(a) Load vs. displacement for 1/8″ core

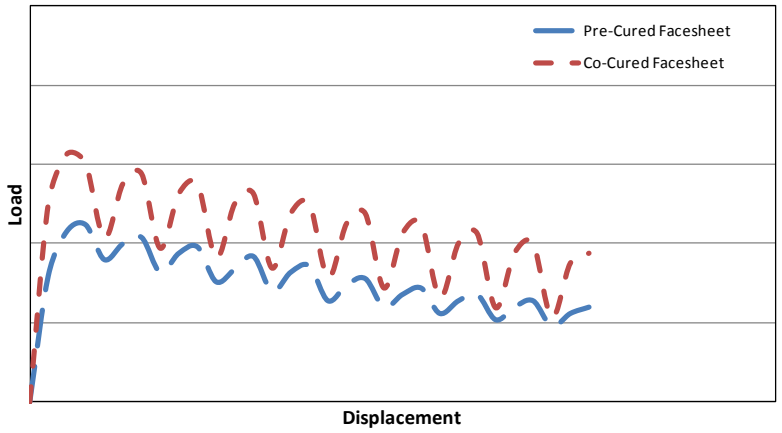

(b) Load vs. displacement for 3/8″ core

Figure 45. Typical load vs. displacement pattern between both fabrication processes

3.6 EFFECTS OF RIBBON DIRECTION

Two ribbon directions were tested (longitudinal and lateral). Both ribbon directions were tested with an HX at all three cell sizes, 1/8″, 3/16″ and 3/8″, and the same core density, 3.0 pcf. Both ribbon directions were tested with an over-expanded core, at the same cell size, 3/16″, and the same core density, 3.0 pcf. Both of the ribbon directions, with both core types and at all cell sizes, were tested with two disbond locations, top and bottom. In addition, both ribbon directions, with both core types at all three cell sizes and with both disbond locations, had an initial crack tip location at the center of the cell. Both ribbon directions (and with an HX) at two cell sizes, 1/8″ and 3/8″, the same core density, 3.0 pcf, and with a bottom disbond location, had an initial crack tip location at the edge of the cell. Furthermore, both ribbon directions, with both core types, at all three cell sizes, at all three densities, with both disbond locations, and with both crack tip locations, were fabricated with PCFS. The combination of the above parameters resulted in ten distinct datasets as presented in table 10.

Table 10. Ribbon direction test matrix

	Facesheet	Core Type	Cell Size (in)	Core Density (pcf)	Disbond Location	Fabrication Process	Ribbon Direction	Crack Tip Location	No. of Specimens
RIBBON DIRECTION	4	HX	1/8	3	TOP	PCFS	LONG	CENTER	6
	4	HX	1/8	3	TOP	PCFS	LAT	CENTER	6
	4	HX	1/8	3	BOTTOM	PCFS	LONG	CENTER	6
	4	HX	1/8	3	BOTTOM	PCFS	LAT	CENTER	6
	4	HX	1/8	3	BOTTOM	PCFS	LONG	EDGE	6
	4	HX	1/8	3	BOTTOM	PCFS	LAT	EDGE	6
	4	HX	3/16	3	TOP	PCFS	LONG	CENTER	6
	4	HX	3/16	3	TOP	PCFS	LAT	CENTER	6
	4	HX	3/16	3	BOTTOM	PCFS	LONG	CENTER	6
	4	HX	3/16	3	BOTTOM	PCFS	LAT	CENTER	6
	4	HX	3/8	3	TOP	PCFS	LONG	CENTER	6
	4	HX	3/8	3	TOP	PCFS	LAT	CENTER	6
	4	HX	3/8	3	BOTTOM	PCFS	LONG	CENTER	6
	4	HX	3/8	3	BOTTOM	PCFS	LAT	CENTER	6
	4	HX	3/8	3	BOTTOM	PCFS	LONG	EDGE	6
	4	HX	3/8	3	BOTTOM	PCFS	LAT	EDGE	6
	4	OX	3/16	3	TOP	PCFS	LONG	CENTER	6
	4	OX	3/16	3	TOP	PCFS	LAT	CENTER	6
	4	OX	3/16	3	BOTTOM	PCFS	LONG	CENTER	6
	4	OX	3/16	3	BOTTOM	PCFS	LAT	CENTER	6

First, when considering the NL data, four distinct patterns emerged based on core type, cell size, and disbond location. The HX exhibited two patterns: the longitudinal 1/8″ and 3/16″ core specimens typically had a larger fracture toughness than the lateral specimens, whereas the 3/8″ specimens demonstrated the opposite, with lateral specimens exhibiting a higher fracture

toughness than the longitudinal specimens. The over-expanded core exhibited two patterns. The top disbond had little or no effect on fracture toughness between longitudinal and lateral specimens. However, the bottom disbond resulted in the lateral specimens having a greater fracture toughness than the longitudinal specimens (see figure 46).

Second, when investigating the VIS data, four relationships were ascertained, based on core type, crack tip location, and disbond location. The HXs with a center disbond location (which should have played little to no role after the pre-crack) resulted in the longitudinal specimens having a greater fracture toughness than the lateral specimens; the opposite was true for specimens with an edge crack tip location. This could be due to the pre-crack being 1–5 mm, because the effect was not noticed in the entire R-curve. The over-expanded core with a top disbond location resulted in the lateral specimens having higher fracture toughness, with the opposite being true for the bottom disbond location (see figure 46).

Third, when examining the 5% offset/max load (5%/max) data, four patterns similar to those found in the VIS data were observed. The HX with a center disbond was the same as the VIS response. However, the edge crack location resulted in both longitudinal and lateral specimens having approximately the same fracture toughness. The over-expanded core had a similar response to the VIS data (see figure 46).

Fourth, when taking the AREA data into account, a general relationship was identified. The longitudinal specimens appeared to have a smaller fracture toughness than the lateral specimens. This was true in all but two cases: hexagonal 1/8″ core with a bottom disbond and edge crack tip location, and hexagonal 3/16″ core with a top disbond location (see figure 46).

Fifth, when considering the behavior of the entire R-curve, three relationships were identified, based on core type and cell size. The hexagonal 1/8″ and 3/16″ cores both resulted in the longitudinal core being more fracture resistant than the lateral core, regardless of crack length, and the hexagonal 3/8″ core resulted in both longitudinal and lateral fracture toughness being approximately the same, regardless of crack length. Within the over-expanded core, the lateral specimens were more fracture resistant than the longitudinal specimens, regardless of crack length. In addition, the shape of the resistance curves was dictated by the cell size, and ribbon direction had little to no impact. Approximate R-curves representing this behavior can be found in figure 47.

Sixth, when considering load versus displacement plots, six distinct patterns emerged, corresponding to core type, cell size, disbond location, and crack tip location. The hexagonal 1/8″core with a center disbond location had higher loads for longitudinal specimens than lateral specimens at small corresponding displacements, and then approximately the same loads between longitudinal and lateral specimens for larger corresponding displacements; furthermore, those cores with an edge disbond location had approximately the same loads between longitudinal and lateral specimens for small corresponding displacements, and the longitudinal specimens had higher loads than the lateral specimens for larger corresponding displacements. This behavior is peculiar because once past the pre-crack region, both datasets should be the same. The reason for this divergence is not yet understood and beyond the scope of this report. The hexagonal 3/16″ core with a top disbond had a response similar to the 1/8″ center crack tip location specimens, and

the bottom disbond specimens resulted in approximately the same loads between the longitudinal and lateral specimens for the same corresponding displacements. Between the 1/8″ and 3/16″ cores, ribbon direction seemed to play little or no role in the shape of the load displacement curve. The 3/8″ core resulted in the same average load between longitudinal and lateral specimens, with varying peak and valley loads, meaning ribbon direction influenced the shape of the load displacement curve with large (longitudinal) and small (lateral) load drops representing abrupt crack growth. The over-expanded core resulted in lateral specimens having larger loads than longitudinal specimens for all corresponding displacements. Within the over-expanded core, ribbon direction seemed to play little or no role in the shape of the load displacement curve. Approximate load versus displacement curves representing this behavior can be found in figures 48 and 49.

Lastly, when examining the failure modes, the ribbon direction had little to no effect; cell size dictated failure mode instead. An in-depth failure mode analysis is found in appendices A and B.

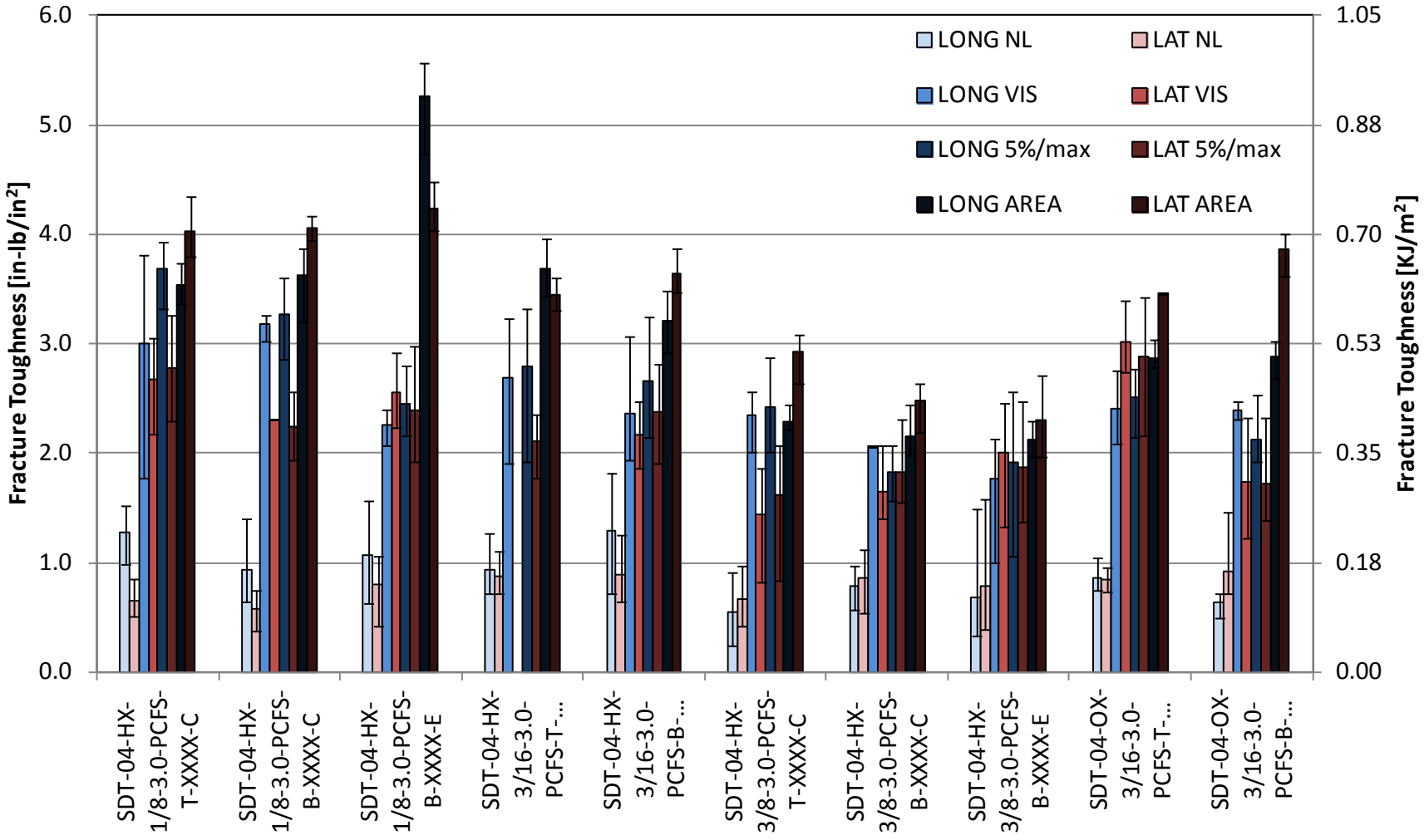

Figure 46. NL, VIS, and 5%/max fracture toughness between both ribbon directions

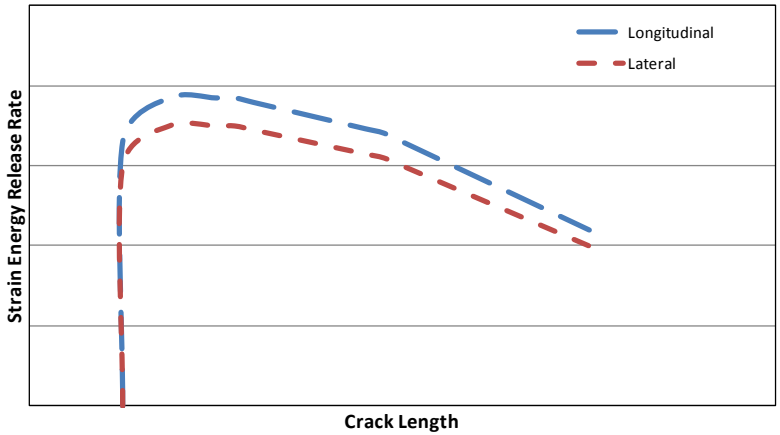

(a) R-curve for hexagonal 1/8″ core

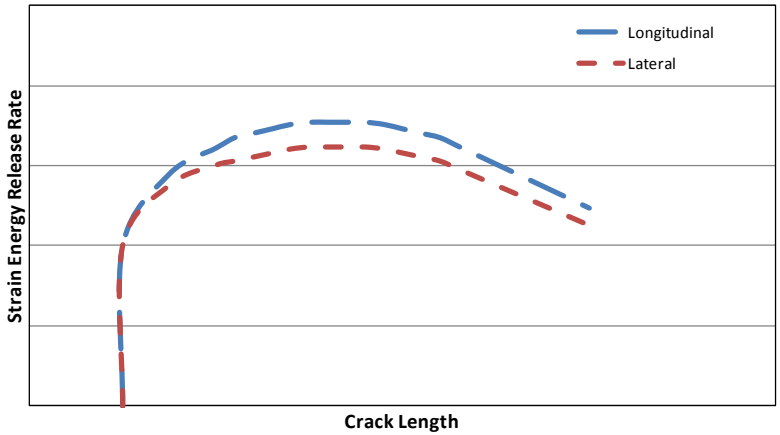

(b) R-curve for hexagonal 3/16″ core

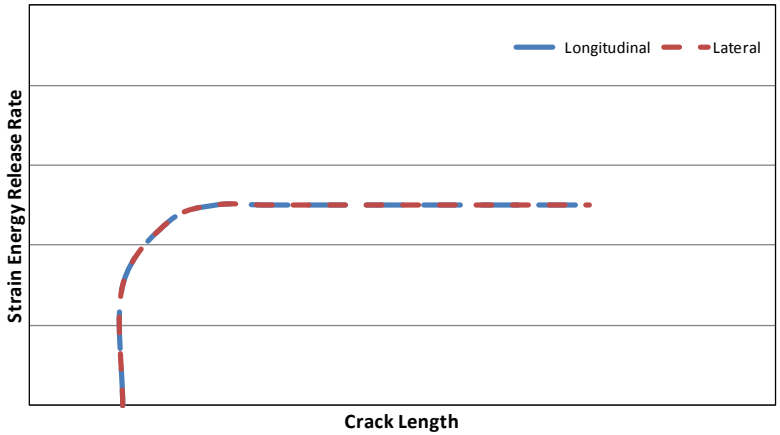

(c) R-curve for hexagonal 3/8″ core

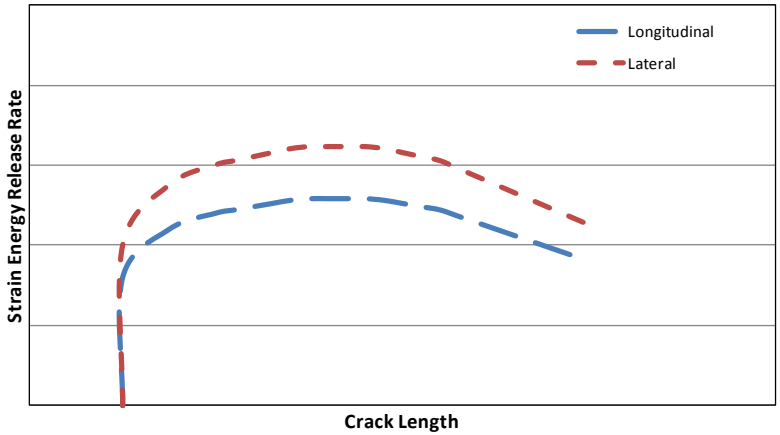

(d) R-curve for over-expanded 3/16″ core

Figure 47. Typical R-curve pattern between both ribbon directions

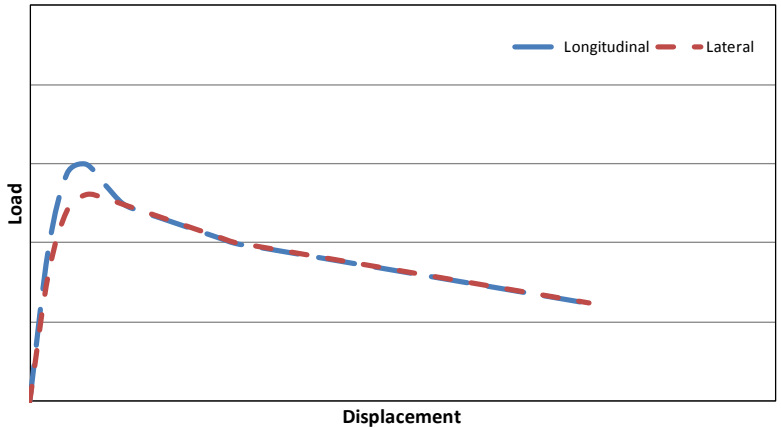

(a) Load vs. displacement for hexagonal 1/8″ core with center crack tip

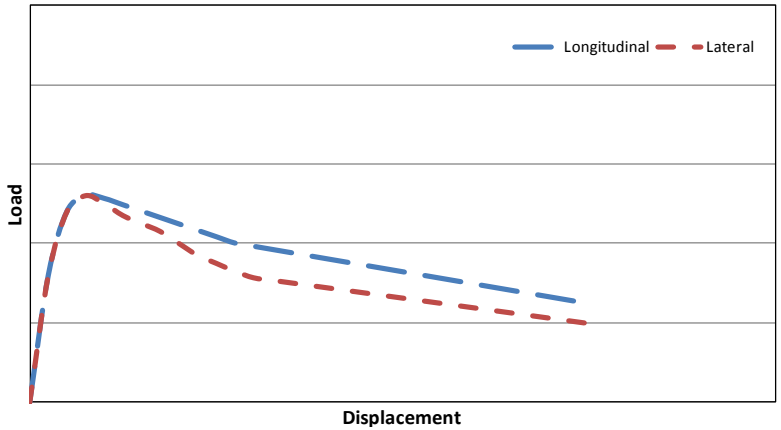

(b) Load vs. displacement for hexagonal 1/8″ core with edge crack tip

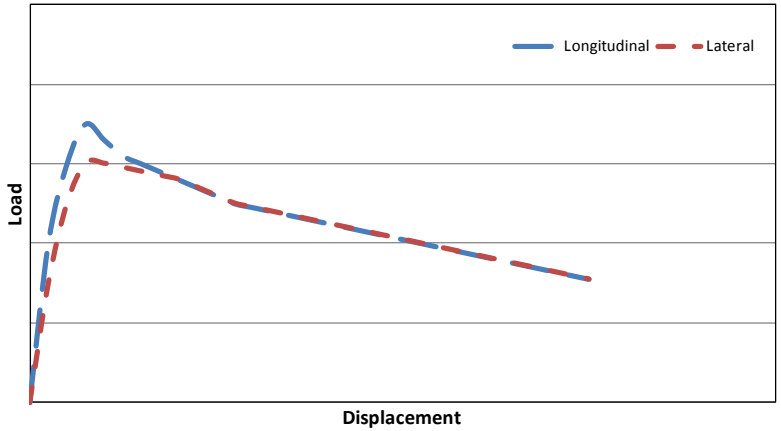

(c) Load vs. displacement for hexagonal 3/16″ core with top disbond

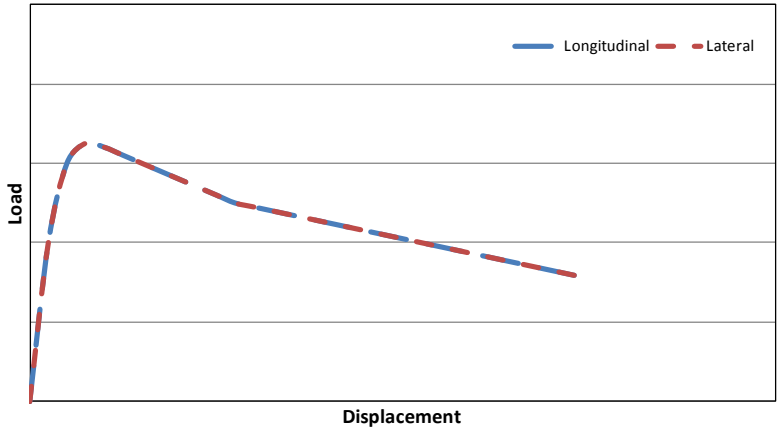

(d) Load vs. displacement for hexagonal 3/16″ core with bottom disbond

Figure 48. Typical load vs. displacement pattern between both ribbon directions

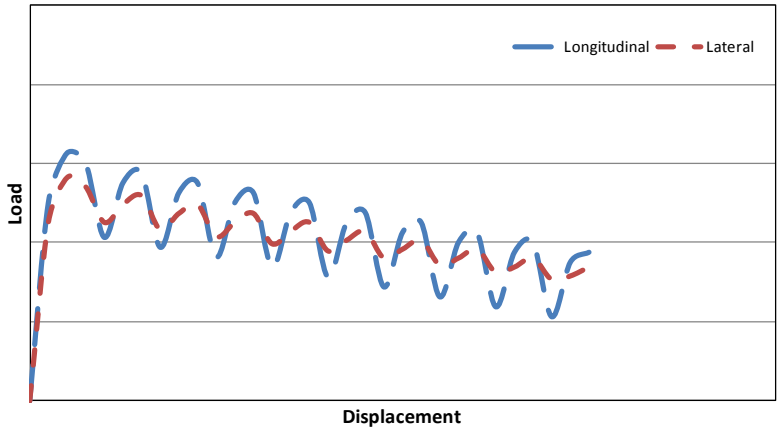

(e) Load vs. displacement for hexagonal 3/8″ core

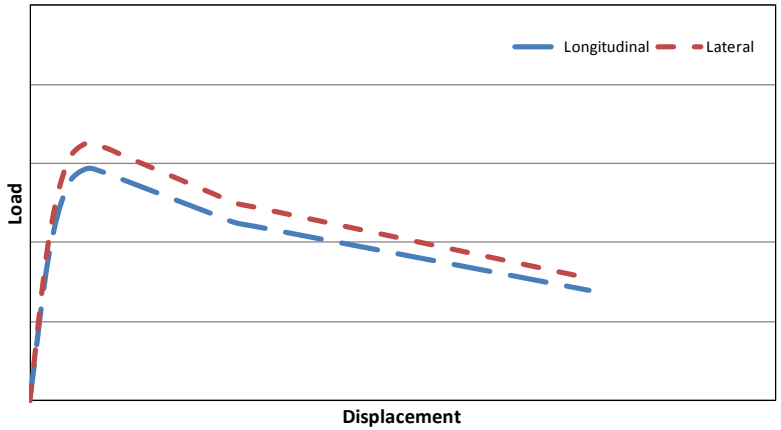

(f) Load vs. displacement for over-expanded 3/16″ core

Figure 49. Typical load vs. displacement pattern between both ribbon directions (continued)

3.7 EFFECTS OF CRACK TIP LOCATION

Two crack tip locations, center and edge, were tested with the same HX type, two cell sizes of 1/8″ and 3/8″, and the same core density of 3.0 pcf. Both crack tip locations of both cell sizes were tested with a bottom disbond location, and two ribbon directions, longitudinal and lateral. In addition, crack tip locations of both cell sizes in both ribbon directions were fabricated with PCFS. The combination of the above parameters resulted in four distinct datasets, as presented in table 11.

Table 11. Crack tip location test matrix

	Facesheet	Core Type	Cell Size (in)	Core Density (pcf)	Disbond Location	Fabrication Process	Ribbon Direction	Crack Tip Location	No. of Specimens
CRACK TIP LOCATION	4	HX	1/8	3	BOTTOM	PCFS	LONG	CENTER	6
	4	HX	1/8	3	BOTTOM	PCFS	LONG	EDGE	6
	4	HX	1/8	3	BOTTOM	PCFS	LAT	CENTER	6
	4	HX	1/8	3	BOTTOM	PCFS	LAT	EDGE	6
	4	HX	3/8	3	BOTTOM	PCFS	LONG	CENTER	6
	4	HX	3/8	3	BOTTOM	PCFS	LONG	EDGE	6
	4	HX	3/8	3	BOTTOM	PCFS	LAT	CENTER	6
	4	HX	3/8	3	BOTTOM	PCFS	LAT	EDGE	6

The effects of crack tip location were evaluated for both test runs, the most significant being the pre-crack test run, which grew the crack for 1–5 mm, thereby producing a sharp crack tip. The first evaluation determined if the crack tip location affected the amount of energy required to start the crack.

First, when considering the NL data, it was observed that the center crack tip location specimens resulted in greater fracture toughness than the edge crack tip location specimens (see figure 50).

Second, when investigating the VIS data, two distinct relationships emerge, both correlating to ribbon direction. Within longitudinal cores, the center crack tip location specimens resulted in a larger fracture toughness than the edge crack tip location specimens, whereas the opposite was observed in lateral cores (see figure 50).

Third, when examining the 5% offset/max load (5%/max) data, a similar behavior to the VIS data was identified (see figure 50).

Lastly, when examining the failure modes, it becomes apparent that the effects of crack tip location were coupled with cell size and ribbon direction. Within the 1/8″ cores with longitudinal ribbon direction, the center crack tip location specimens failed primarily in the core, whereas the edge crack tip specimens failed in a mix of adhesive and core. Within the 1/8″ core with lateral ribbon direction, crack tip location seemed to have little or no effect, because both failed in a mix of adhesive and core. Within the 3/8″ core, regardless of ribbon direction, crack tip location appeared

to have little to no effect, with both failing primarily in adhesive pullout. An in-depth failure mode analysis is found in appendix A.

The second evaluation was the crack propagation test run, which grew the crack to approximately 50 mm. Theoretically, the crack tip at this point should be random, and the data from both the center and edge crack tip locations should be identical. This analysis investigated the resultant behaviors.

First, when considering the NL data, two distinct patterns emerged, correlating to cell size. Within the 1/8″ core, it was observed that the center crack tip location specimens had a slightly higher fracture toughness than the edge crack tip location specimens, whereas the opposite was observed among 3/8″ cores. These differences could be attributed to the small pre-crack region (1–5 mm) and the crack tip location still influencing the fracture toughness (i.e., the crack front not yet being random) (see figure 51).

Second, when investigating the VIS data, two distinct relationships correlating to ribbon direction were ascertained. Within longitudinal cores, the center crack tip location specimens resulted in a greater fracture toughness than the edge crack tip location specimens, whereas the opposite was observed in the lateral cores. These differences could be attributed to the small pre-crack region (1–5 mm) and the crack tip location still influencing the fracture toughness (i.e., the crack front not yet being random) (see figure 51).

Third, when examining the 5% offset/max load (5%/max) data, it became apparent that the crack tip location played little or no effect on fracture toughness, because both the center crack tip location specimens and edge crack tip location specimens were approximately the same in all but one case—the 1/8″ longitudinal ribbon direction (see figure 51).

Fourth, when taking the AREA data into account, a general relationship similar to the 5%/max data was identified (see figure 51).

Fifth, when considering the behavior of the entire R-curve, it was observed that regardless of crack tip location, both center and edge crack tip location specimens produced identical R-curves, which was to be expected, especially once past the pre-crack region. However, one set of data did not follow this pattern. The 1/8″ core with lateral ribbon direction resulted in the fracture toughness being higher within the edge crack tip location specimens than the center crack tip location specimens, regardless of crack tip location. This behavior is unexplained and beyond the scope of this program. Approximate R-curves representing this behavior can be found in figure 52.

Sixth, when considering load versus displacement plots, it was observed that regardless of crack tip location, both center and edge crack tip location specimens produced similar load versus displacement curves, which was to be expected, especially once past the pre-crack region. However, one set of data did not follow this pattern. The 1/8″ core with longitudinal ribbon direction resulted in loads that were higher for the center crack tip location specimens than for the edge crack tip location specimens, regardless of corresponding displacements. This behavior is unexplained and beyond the scope of this program. In addition, it should be noted that crack tip

location seemed to play little to no role in the shape of the load versus displacement curves, with cell size and ribbon direction playing dominant roles. Approximate load-versus-displacement curves representing this behavior can be found in figure 53.

Lastly, when examining the failure modes, it becomes apparent that crack tip location plays no role and that failure mode is primarily affected by cell size. An in-depth failure mode analysis is found in appendix A.

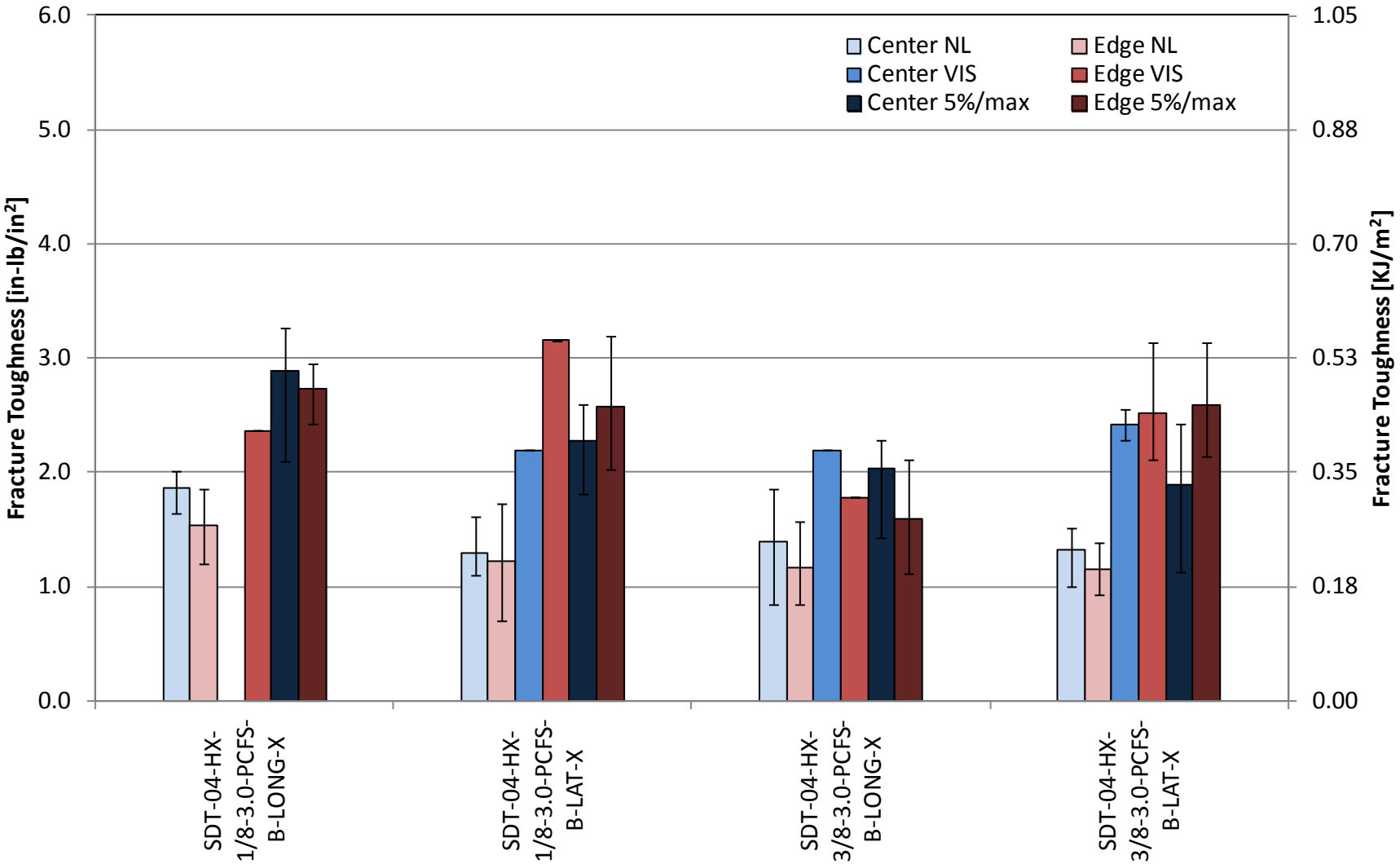

Figure 50. Pre-crack NL, VIS, and 5%/max fracture toughness between both crack tip locations

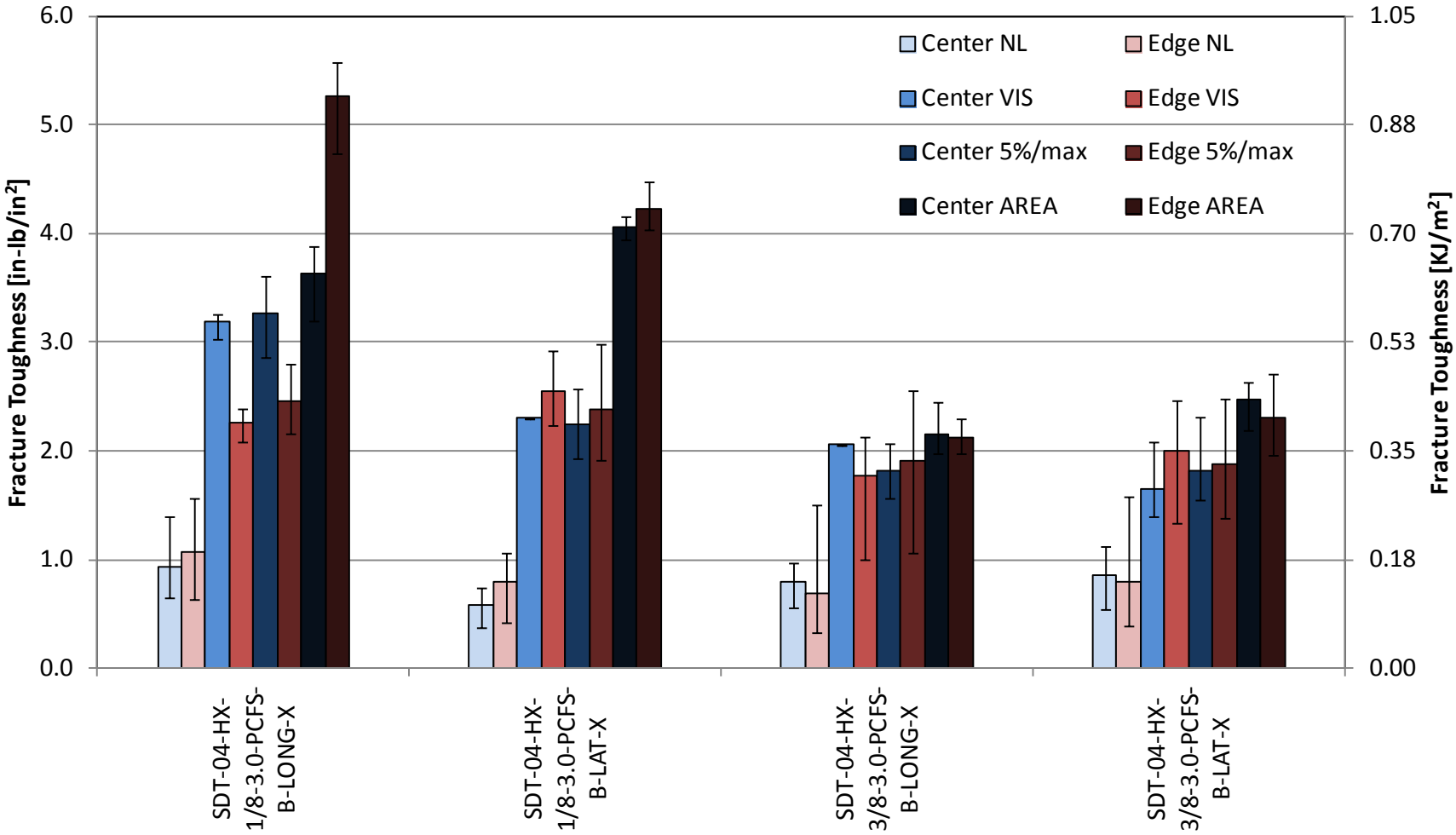

Figure 51. NL, VIS, and 5%/max fracture toughness between both crack tip locations

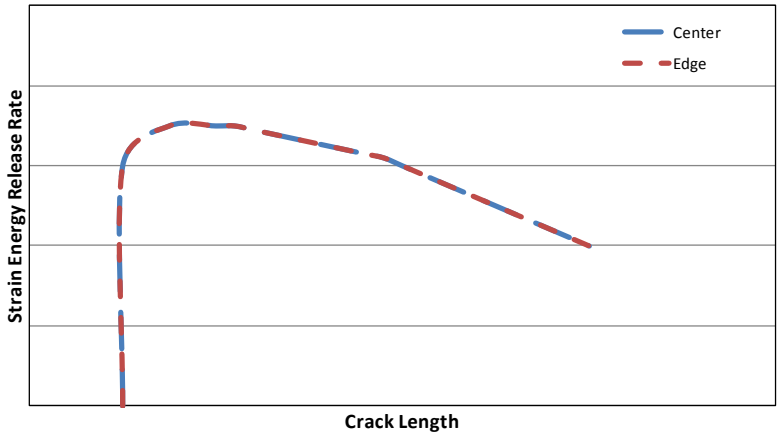

(a) R-curve for 1/8″ core with longitudinal ribbon

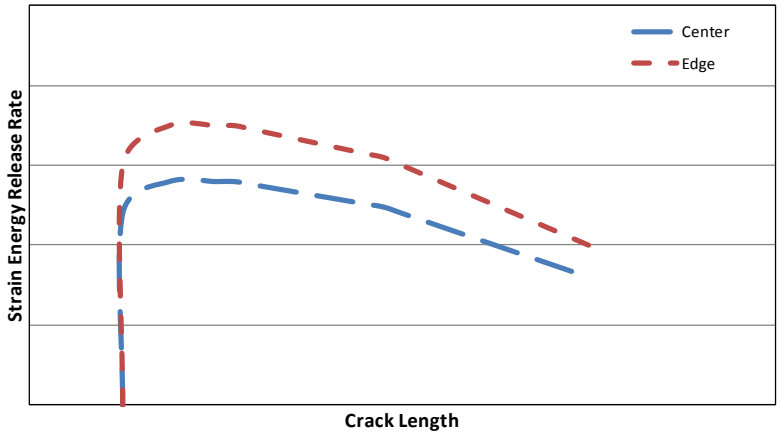

(b) R-curve for 1/8″ core with lateral ribbon

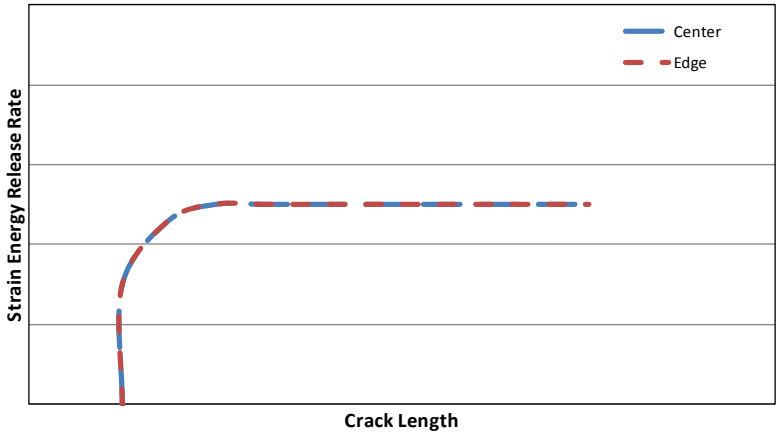

(c) R-curve for 3/8″ core

Figure 52. Typical R-curve pattern between both crack tip locations (a) with longitudinal ribbon, (b) with lateral ribbon, and (c) for 3/8″ core

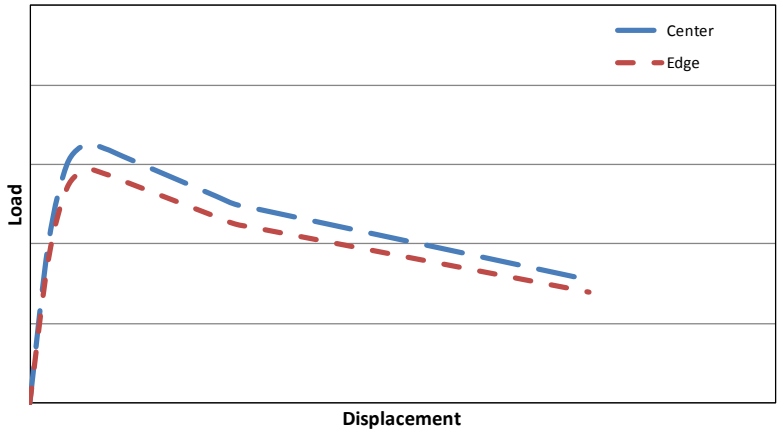

(a) Load vs. displacement for 1/8″ core with longitudinal ribbon

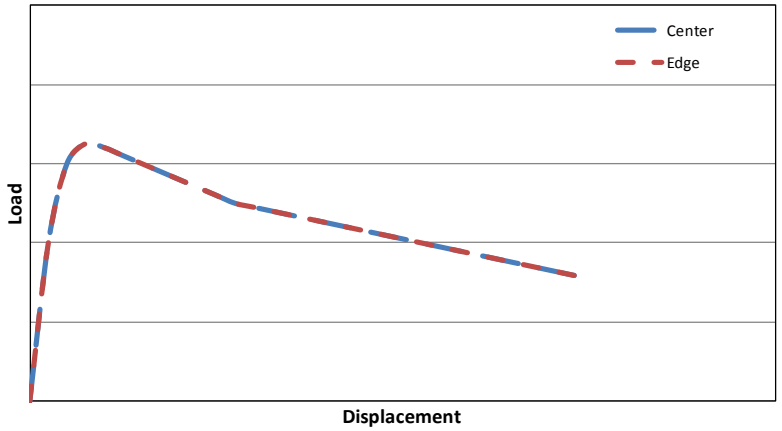

(b) Load vs. displacement for 1/8″ core with lateral ribbon

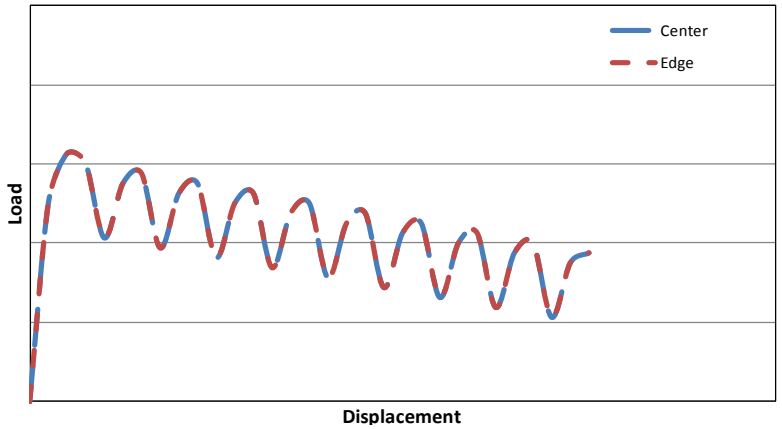

(c) Load vs. displacement for 3/8″ core with longitudinal ribbon

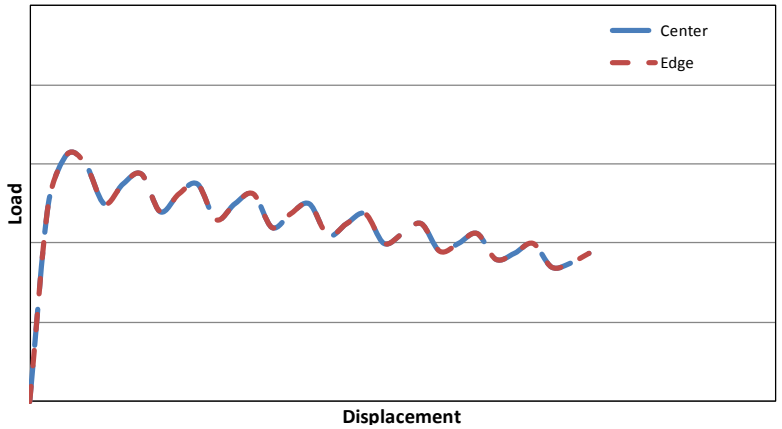

(d) Load vs. displacement for 3/8″ core with lateral ribbon

Figure 53. Typical load vs. displacement pattern: (a) for 1/8″ core with longitudinal ribbon, (b) for 1/8″ core with lateral ribbon, (c) between both crack tip locations, and (d) for 3/8″ core with lateral ribbon

3.8 EFFECT OF FAILURE MODES

The failure mode was dictated by both cell size and core density. When considering cell size with respect to core density, the failure modes were as follows: the 1/8″ core with densities of 2.0 pcf and 3.0 pcf typically failed in the core, whereas the 1/8″ core with a density of 6.0 pcf failed in adhesive pullout. The 3/16″ core with a density of 2.0 pcf typically failed in the core; the 3/16″ core with a core density of 3.0 pcf primarily failed in the core with some cells partially in adhesive pullout; and the 3/16″ core with a core density of 6.0 pcf failed in adhesive pullout. The 3/8″ core with a density of 2.0 pcf typically failed in adhesive pullout with some core failure below the crack surface, whereas the 3/8″ core with a density of 3.0 pcf typically failed in adhesive pullout. When considering all failure modes, an overall pattern emerged: as the cell size increases, the failure mode moves from the core to a mix of core and adhesive pullout, to adhesive pullout, with the magnitude of change being dictated by core density. When considering core density with respect to cell size, the failure modes were as follows: The 1/8″ and 3/16″ cores with a density of 2.0 pcf failed in the core, whereas the 3/8″ core with a density of 2.0 pcf typically failed in adhesive pullout with some core failure below the crack surface. The 1/8″ core with a density of 3.0 pcf primarily failed in the core, and the 3/16″ and 3/8″ cores with densities of 3.0 pcf typically failed in adhesive pullout. The 1/8″ and 3/16″ cores with densities of 6.0 pcf failed in adhesive pullout. When considering all failure modes, an overall pattern emerged: as the core density increased, the failure mode moved from the core to a mix of core and adhesive pullout, to adhesive pullout, with the magnitude of change being dictated by cell size. The interdependency of both cell size and core density can be found in table 12. Figures 54–68 show these failure modes. The (1) and (2) in the figure captions refer to longitudinal crack growth that aligns with ribbon direction and to lateral crack growth that aligns with fill direction, respectively. An in-depth failure mode analysis is found in appendices A and B.

Table 12. Failure mode

Failure Mode		Cell Size [in]		
		1/8	3/16	3/8
Core Density [pcf]	2.0	C	C	C and APO
	3.0	C	APO	APO
	6.0	APO	APO and A	

SDT-04-HX-1.8-2-T-PCFS-LONG-C-X

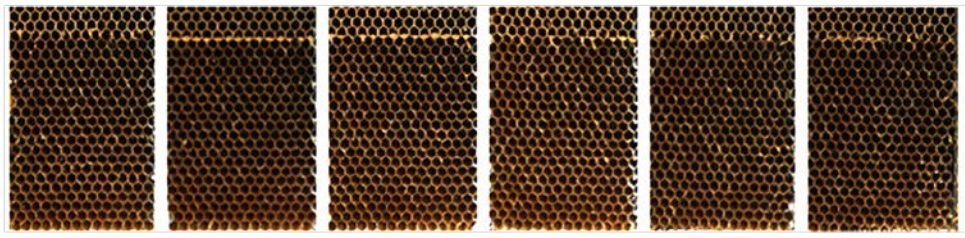

SDT-04-HX-1.8-2-B-PCFS-LONG-C-X

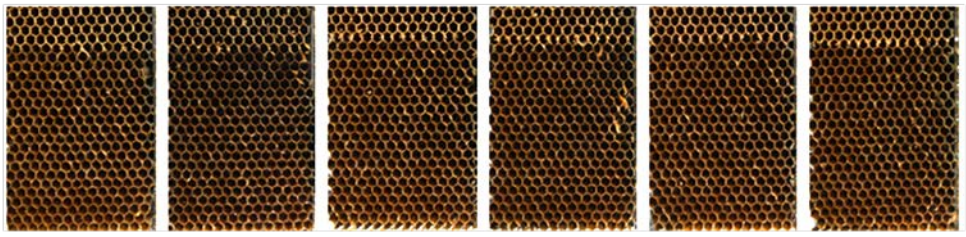

Figure 54. Core failure modes for specimens with PCFS and HRH-10–1/8–2.0 core

SDT-04-HX-1.8-3-T-PCFS-LONG-C-X

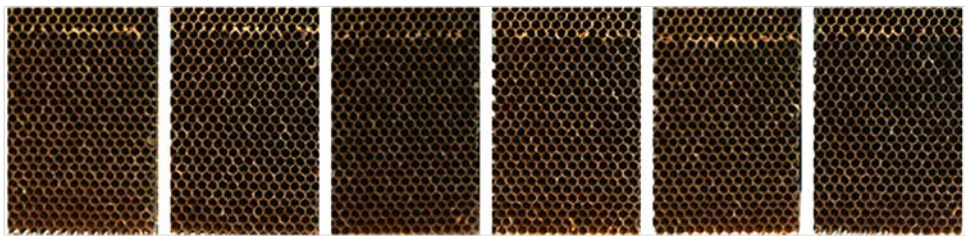

SDT-04-HX-1.8-3-B-PCFS-LONG-C-X

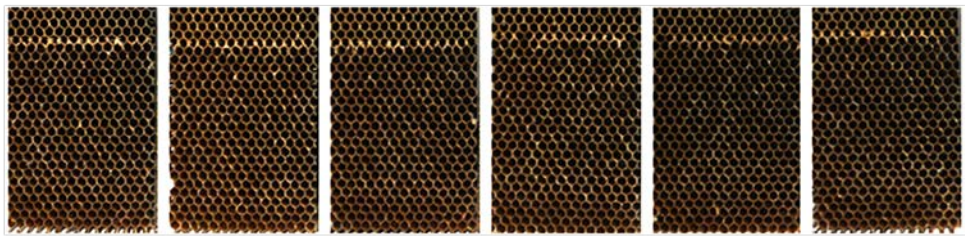

SDT-04-HX-1.8-3-T-PCFS-LONG-E-X

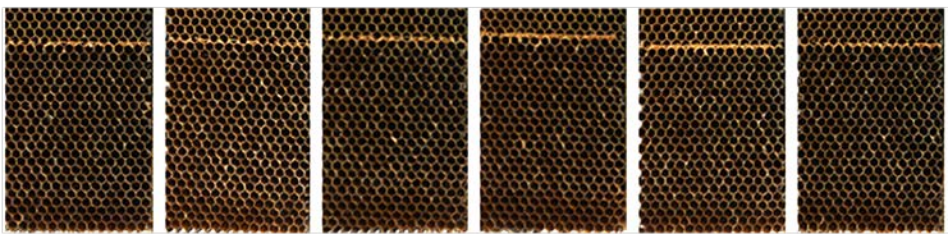

Figure 55. Core failure modes for specimens with PCFS and HRH-10–1/8–3.0 core (1)

SDT-04-HX-1.8-3-T-PCFS-LAT-C-X

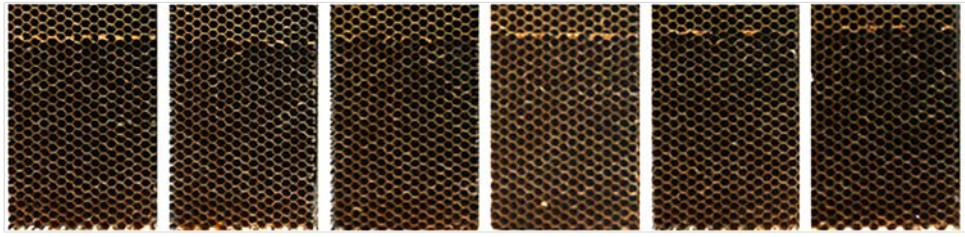

SDT-04-HX-1.8-3-B-PCFS-LAT-C-X

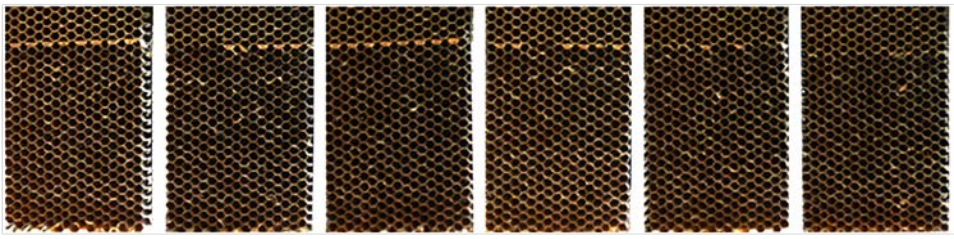

SDT-04-HX-1.8-3-B-PCFS-LAT-E-X

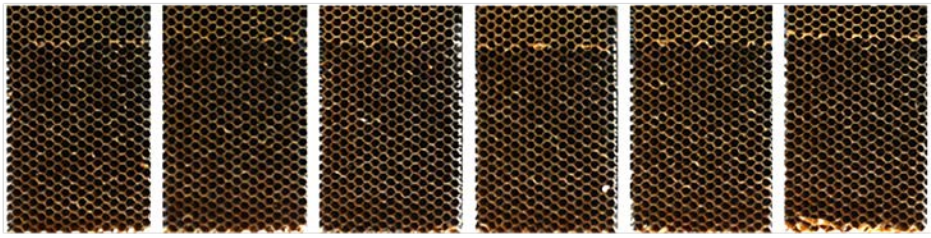

Figure 56. Core failure modes for specimens with PCFS and HRH-10–1/8–3.0 core (2)

SDT-04-HX-1.8-3-T-CCFS-LONG-C-X

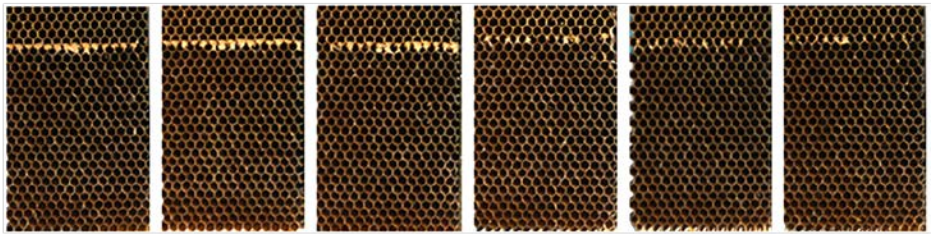

SDT-04-HX-1.8-3-B-CCFS-LONG-C-X

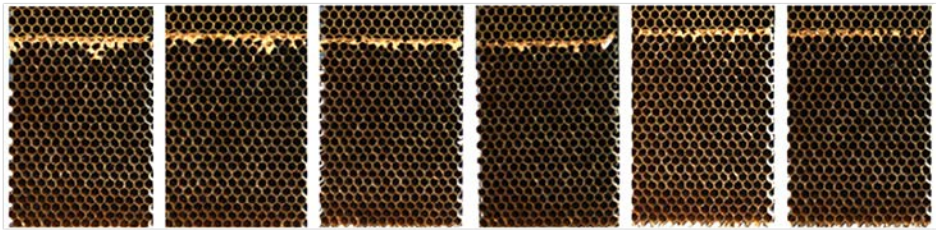

Figure 57. Core failure modes for specimens with CCFS and HRH-10–1/8–3.0 core

SDT-04-HX-1.8-6-T-PCFS-LONG-C-X

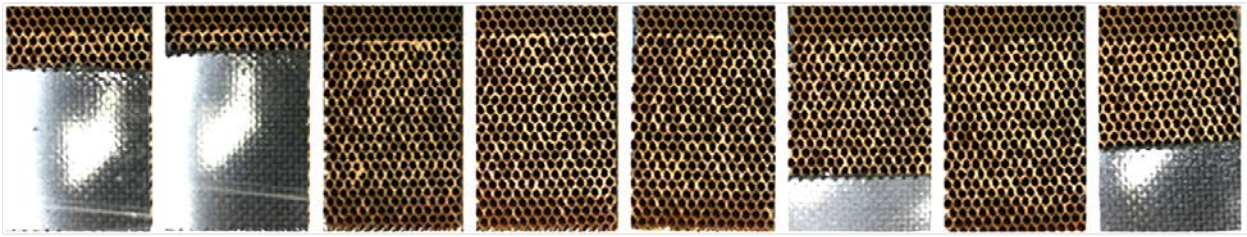

SDT-04-HX-1.8-6-B-PCFS-LONG-C-X

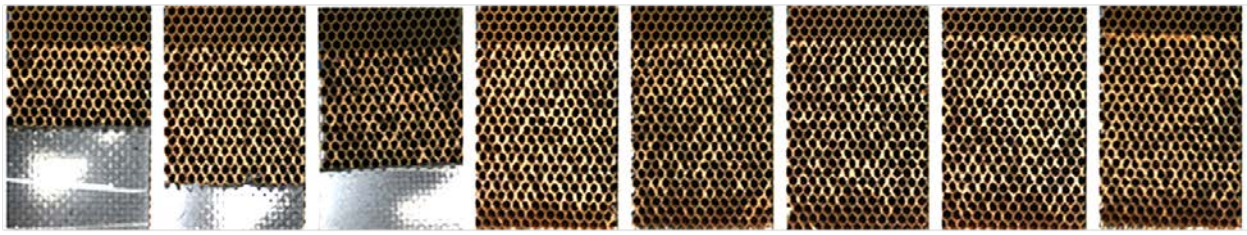

Figure 58. APO and core failure modes for specimens with PCFS and HRH-10–1/8–6.0 core

SDT-04-HX-3.16-2-T-PCFS-LONG-C-X

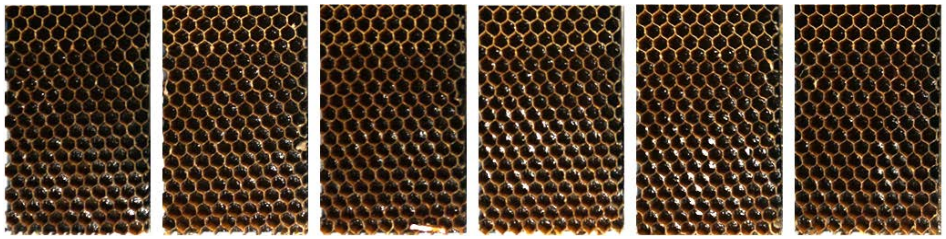

SDT-04-HX-3.16-2-B-PCFS-LONG-C-X

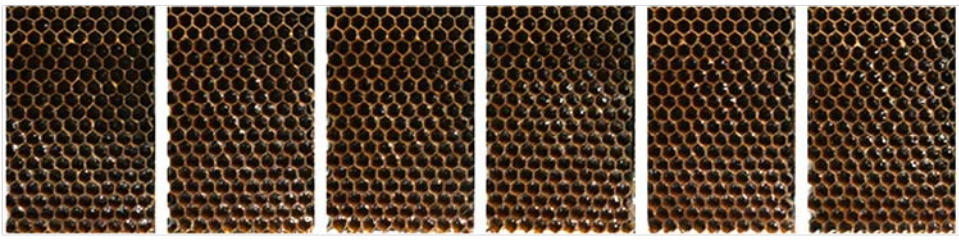

Figure 59. Core failure modes for specimens with PCFS and HRH-10–3/16–2.0 core

SDT-04-HX-3.16-3-T-PCFS-LONG-C-X

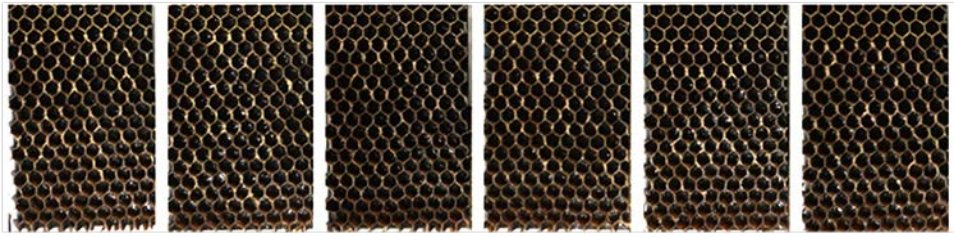

SDT-04-HX-3.16-3-B-PCFS-LONG-C-X

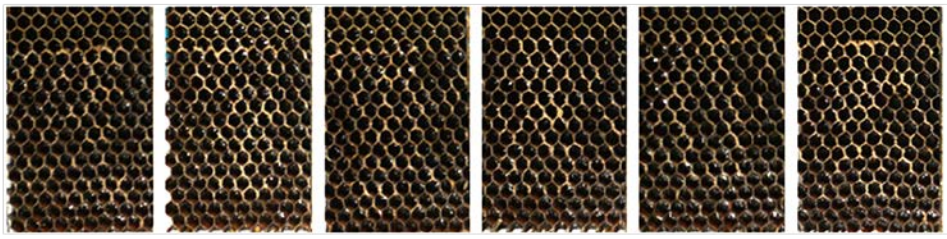

Figure 60. APO modes for specimens with PCFS and HRH-10–3/16–3.0 core (1)

SDT-04-HX-3.16-3-T-PCFS-LAT-C-X

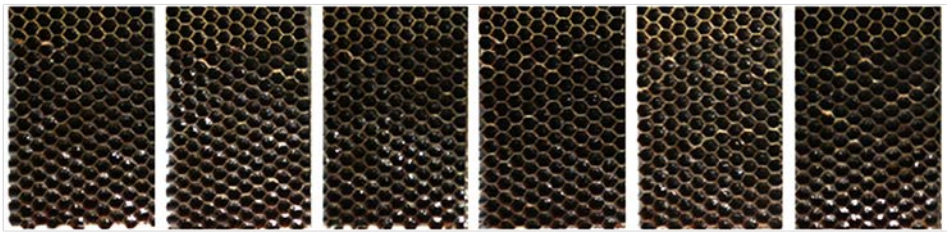

SDT-04-HX-3.16-3-B-PCFS-LAT-C-X

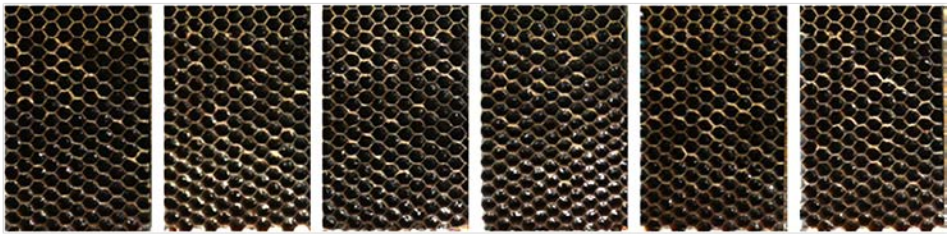

Figure 61. Failure modes for specimens with PCFS and HRH-10–3/16–3.0 core (2)

SDT-04-HX-3.16-6-T-PCFS-LONG-C-X

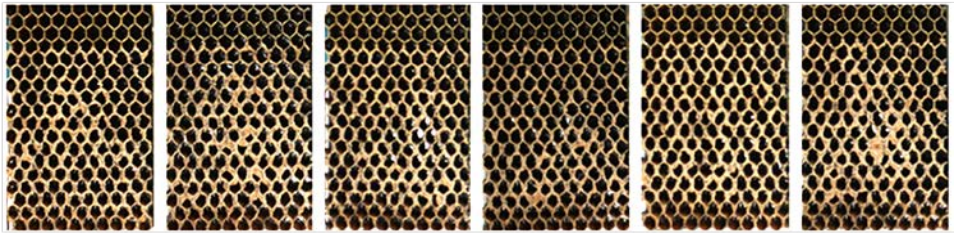

SDT-04-HX-3.16-6-B-PCFS-LONG-C-X

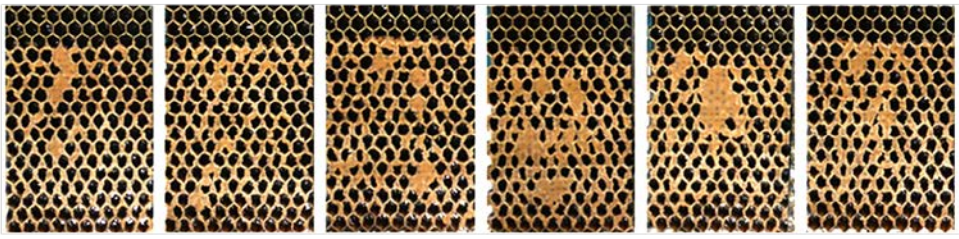

Figure 62. Adhesion failure modes for specimens with PCFS and HRH-10–3/16–6.0 core

SDT-04-HX-3.8-2-T-PCFS-LONG-C-X

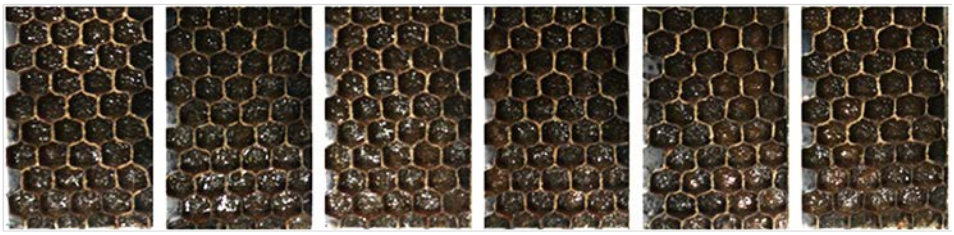

SDT-04-HX-3.8-2-B-PCFS-LONG-C-X

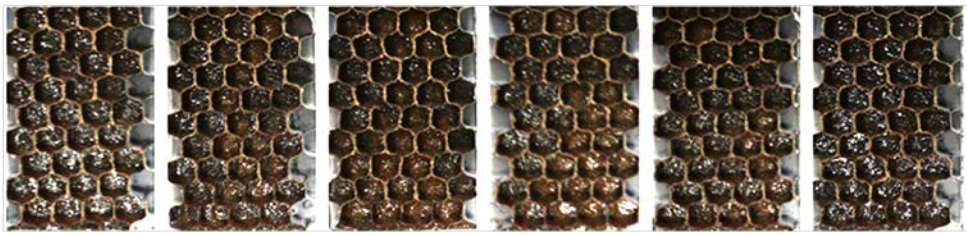

Figure 63. APO and core failure modes for specimens with PCFS and HRH-10–3/8–2.0 core

SDT-04-HX-3.8-3-T-PCFS-LONG-C-X

SDT-04-HX-3.8-3-B-PCFS-LONG-C-X

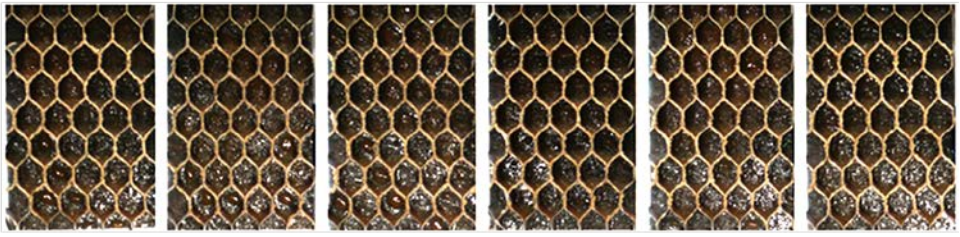

SDT-04-HX-3.8-3-B-PCFS-LONG-E-X

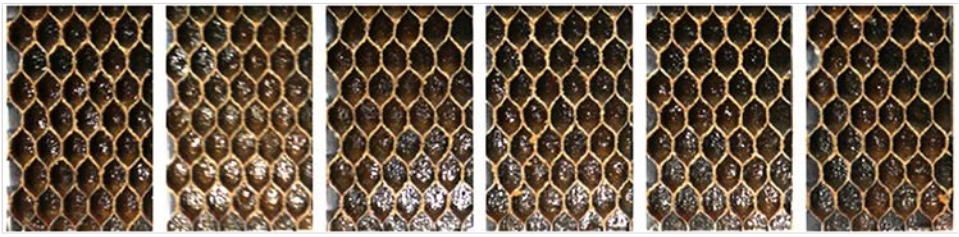

Figure 64. APO modes for specimens with PCFS and HRH-10–3/8–3.0 core (1)

SDT-04-HX-3.8-3-T-PCFS-LAT-C-X

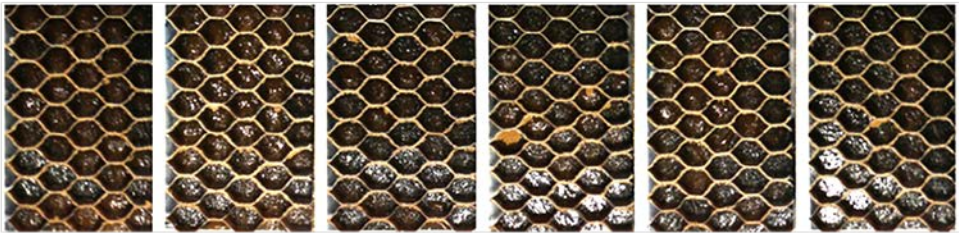

SDT-04-HX-3.8-3-B-PCFS-LAT-C-X

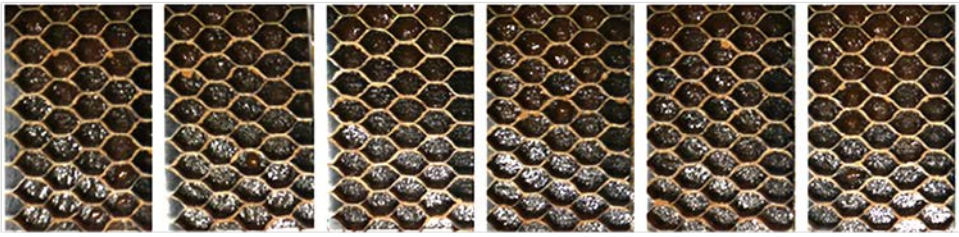

SDT-04-HX-3.8-3-B-PCFS-LAT-E-X

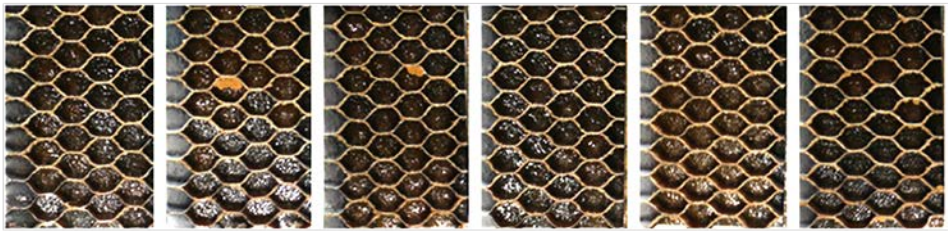

Figure 65. APO modes for specimens with PCFS and HRH-10–3/8–3.0 core (2)

SDT-04-HX-3.8-3-T-CCFS-LONG-C-X

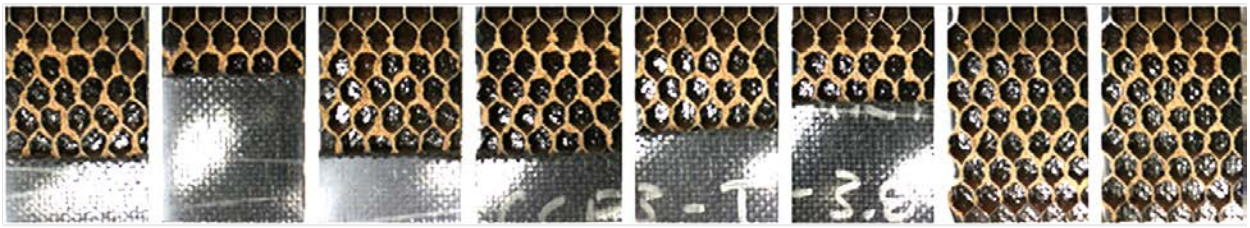

SDT-04-HX-3.8-3-B-CCFS-LONG-C-X

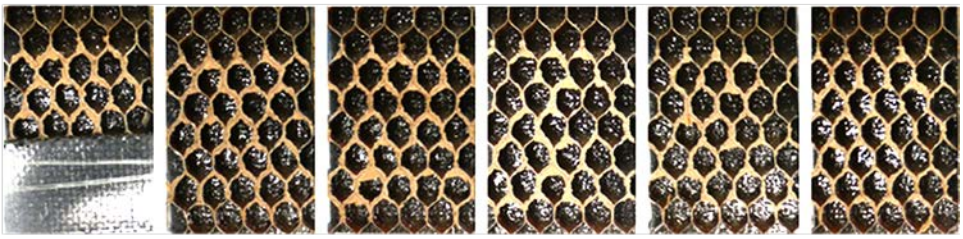

Figure 66. APO modes for specimens with CCFS and HRH-10–3/8–3.0 core

SDT-04-OX-3.16-3-T-PCFS-LONG-C-X

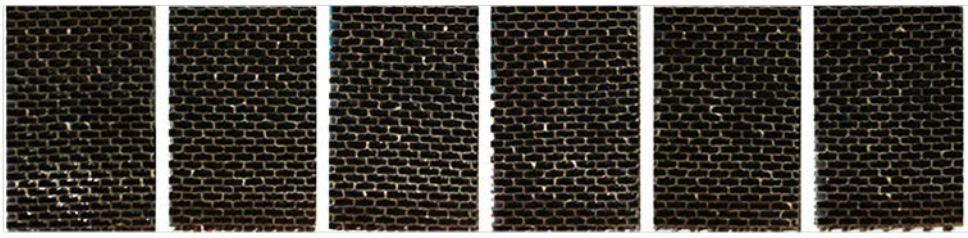

SDT-04-OX-3.16-3-B-PCFS-LONG-C-X

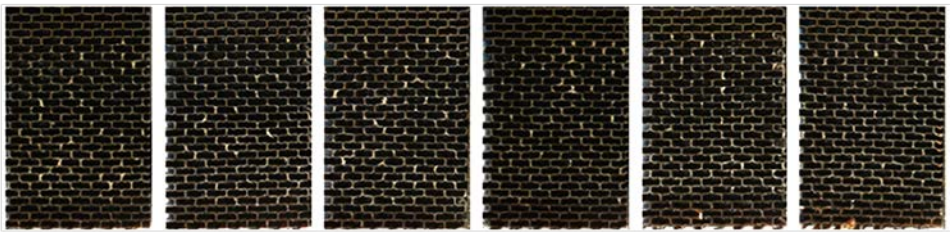

Figure 67. Core failure modes for specimens with PCFS and HRH-10/OX–3/16–3.0 core (1)

SDT-04-OX-3.16-3-T-PCFS-LAT-C-X

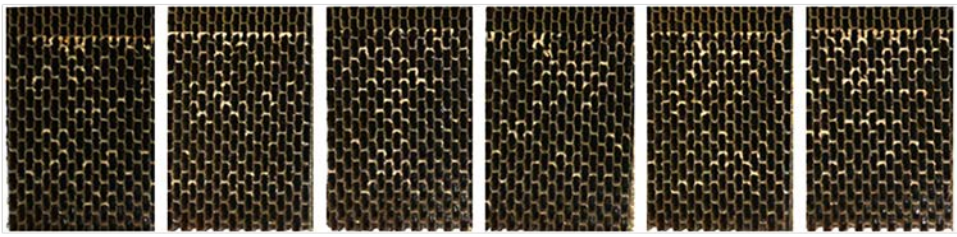

SDT-04-OX-3.16-3-B-PCFS-LAT-C-X

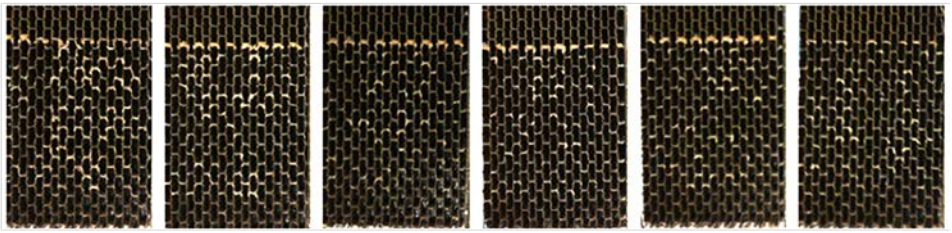

Figure 68. Core failure modes for specimens with PCFS and HRH-10/OX–3/16–3.0 core (2)

3.9 EFFECTS OF DATA REDUCTION METHOD

As presented in the data reduction section (2.5), two distinct reduction methods were used. MBT was used to find the instantaneous fracture toughness at each discrete crack propagation location. This method was applied in determining the recorded values (NL, VIS, and 5%/max). An area method (AM) was used to obtain the average fracture toughness across the entire crack area. The two methods were compared (5%/max and AREA).

When comparing the two data-reduction methods, it became apparent that they correlated primarily with core density and secondarily with ribbon direction and the fabrication process. When investigating the hexagonal 2.0 pcf core, it became apparent that both data-reduction methods yielded approximately the same fracture toughness (see figure 69). It is important to note that the 2.0 pcf core resulted in the most stable failure mode (core failure). When considering the hexagonal 3.0 pcf core with PCFS, the AM resulted in larger fracture toughness than MBT. The ribbon direction seemed to play a secondary role, with the longitudinal ribbon direction typically resulting in a small difference between the AM and MBT, whereas the lateral ribbon direction had a significant difference between AM and MBT (see figure 70). The hexagonal 3.0 pcf core with CCFS resulted in the AM being significantly larger than the MBT (see figure 71). When examining the hexagonal 6.0 pcf core, it was apparent that the AM resulted in significantly larger fracture toughness than the MBT (see figure 72). It is important to note that the 6.0 pcf cores resulted in the most unstable failure mode (APO). Lastly the over-expanded 3.0 pcf core resulted in the AM fracture toughness being larger than the MBT (see figure 73).

MBT method is more suitable to determine crack growth initiation, whereas the AM method provides a measure of ductility and stable growth potential.

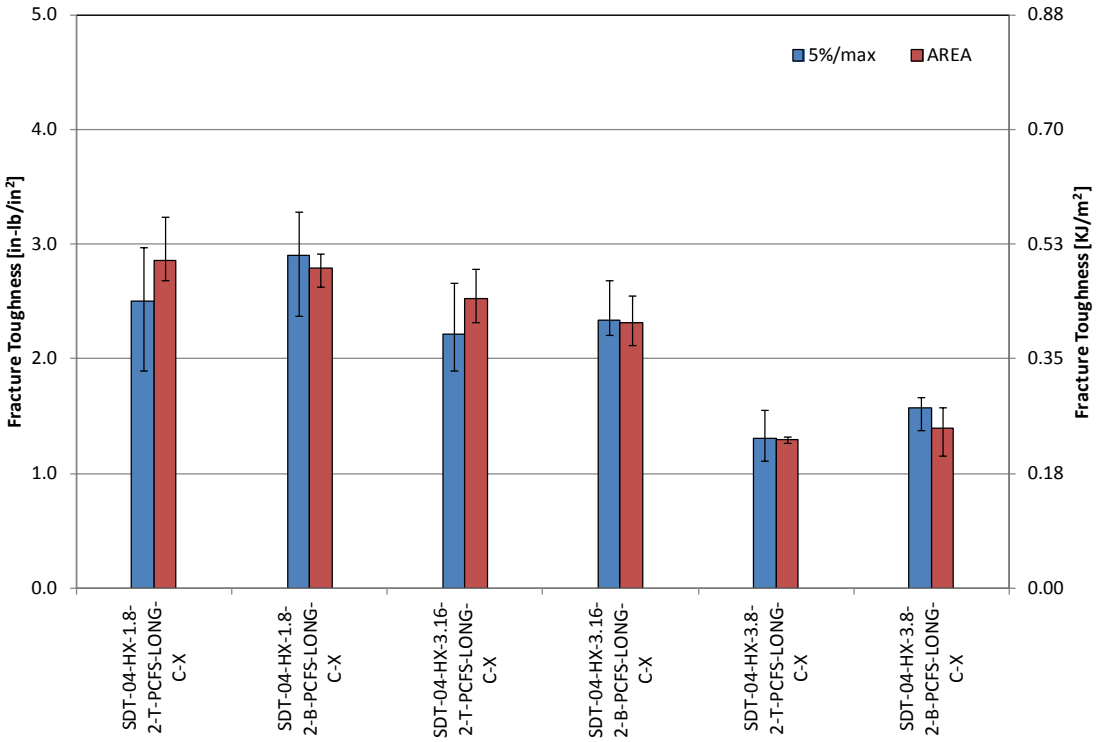

Figure 69. Fracture toughness of hexagonal 2.0 pcf PCFS cores

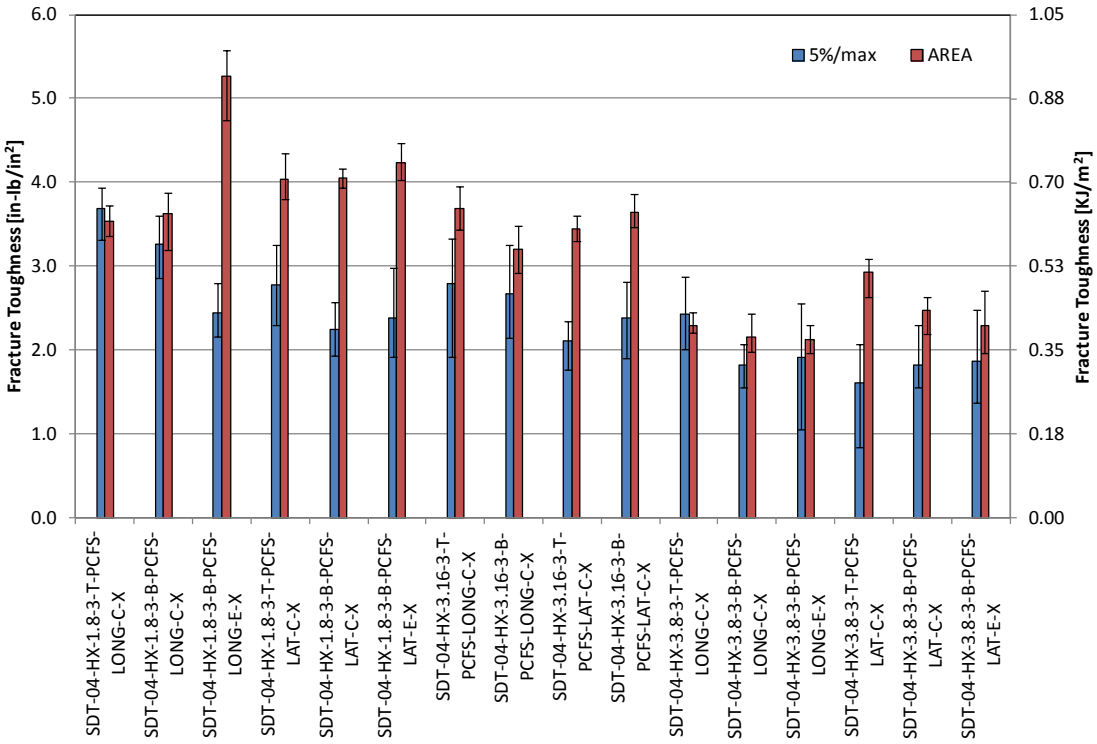

Figure 70. Fracture toughness of hexagonal 3.0 pcf PCFS cores

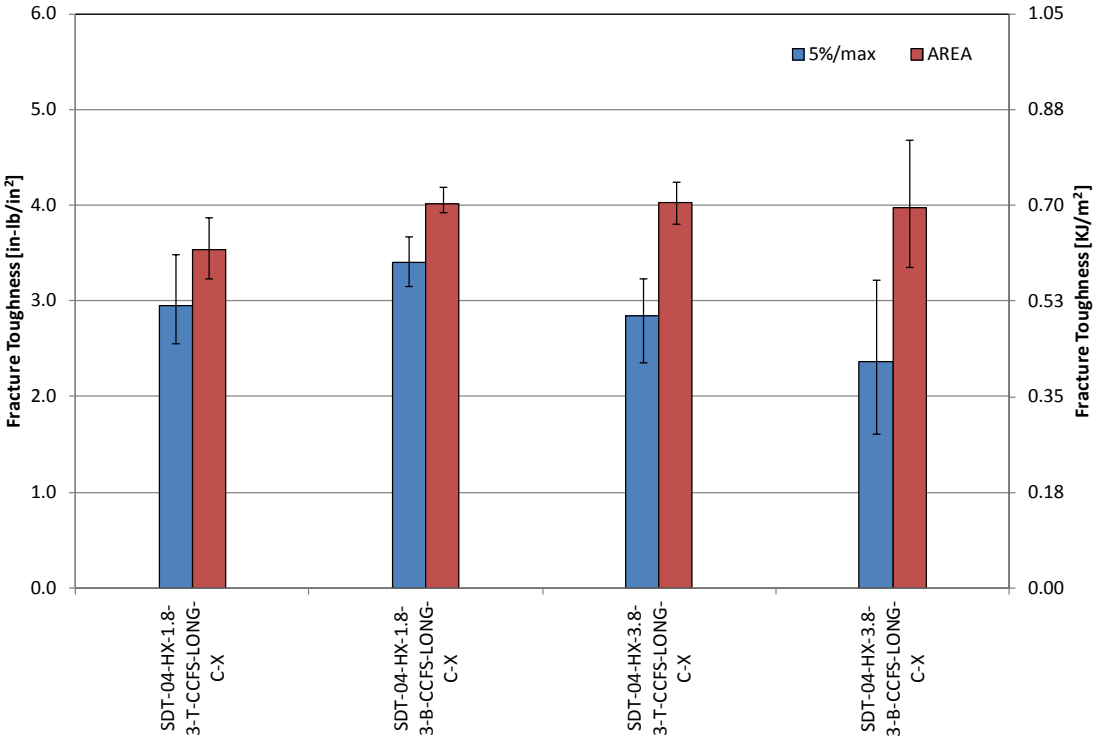

Figure 71. Fracture toughness of hexagonal 3.0 pcf CCFS cores

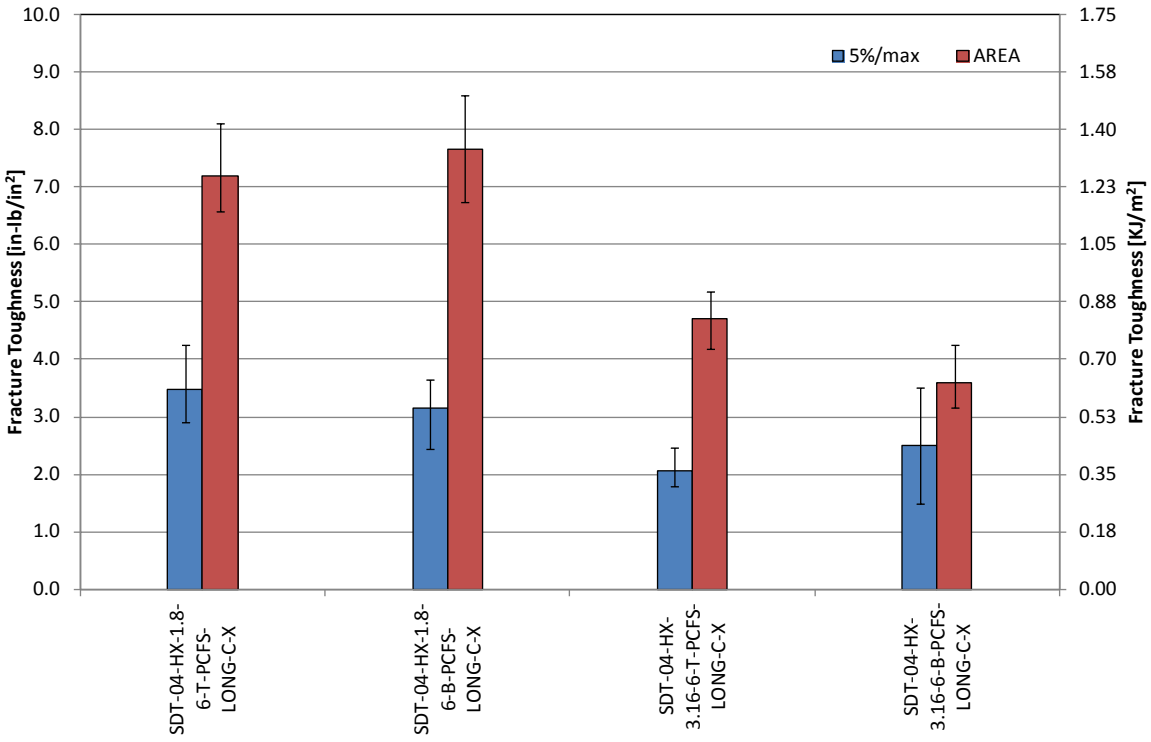

Figure 72. Fracture toughness of hexagonal 6.0 pcf PCFS cores

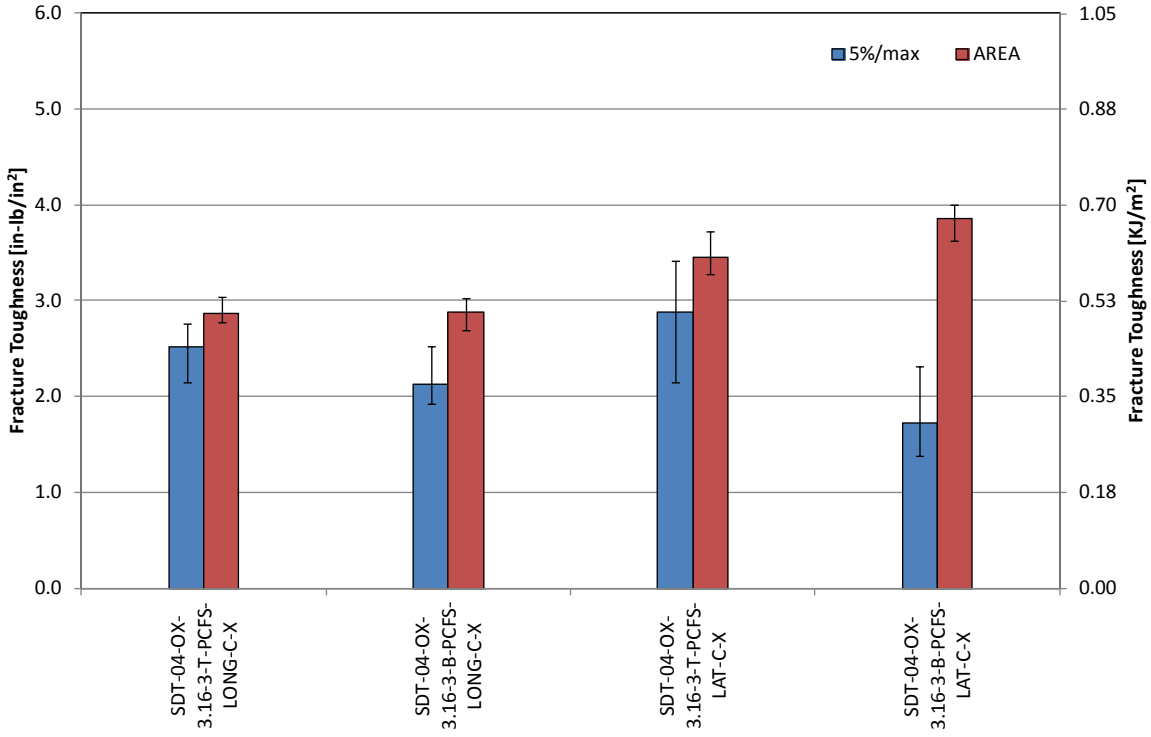

Figure 73. Fracture toughness of over-expanded 3.0 pcf PCFS cores

4. CONCLUSION AND RECOMMENDATIONS

A research program was conducted regarding the effects of configurations not tested in Volume I on fracture toughness of composite sandwich structures. The SCB specimens were found to be the most suitable for determining the Mode I fracture toughness (GIC) of composite sandwich specimens. The SCB test fixture with a traveling stage prevents mixed-mode mechanics. The immaturity of the test procedure and the variation in the initial flaw can also contribute to the data scatter. Note that the SCB test configuration does not directly relate to the sandwich damage growth phenomenon in a structure, because the realistic damage is often a mixed-mode fracture, but it provides a set of comparative data for identifying the effects of different core parameters on Mode I damage growth. In addition, the data will be used for analytical models that in turn will be used for predicting the growth phenomenon. This research will be expanded to larger and more realistic specimen configurations that are representative of aircraft structures under ground-air-ground cycles.

The impact of several key sandwich parameters on GIC and propagation values, which was not considered in Volume I, was studied. These included: (1) core type, (2) cell size, (3) core density, (4) disbond location, (5) fabrication process, (6) ribbon direction, and (7) crack tip location. It is important to note that several other variables can contribute to GIC; therefore, the conclusions are solely based on the results of this report. Though the master summary tables and charts show a comparison of GICs, the effects of these variables on GIC are coupled across different variables and required detailed data analysis for determining the impact of each variable. The results of these tests/analyses are summarized below:

- Core type in conjunction with ribbon direction played a key role in fracture toughness. When considering longitudinal ribbon direction, the HX was more fracture resistant than the over-expanded core; however, when considering lateral ribbon direction, the opposite was true. This relationship was prevalent in both the recorded values (NL, VIS, and 5%/max) and the R-curve.
- Cell size played a prominent role in fracture toughness. Fracture resistance decreased as cell size increased. This behavior manifested itself in both the recorded values and the R-curve. Furthermore, cell size dictated the shape of the R-curve and, in combination with core density, governed failure modes. In addition, cell size controlled the shape of the load displacement curves.
- Core density also played an important role in fracture toughness. Fracture toughness initially increased between low and moderate core densities, but then decreased between moderate and high core densities. This relationship may be observed in both the recorded values and the R-curve. Furthermore, in combination with cell size, core density governed failure modes. In addition, core density determined the magnitude of the load displacement curve.
- Disbond location edge or center of core cell played little to no role. This was ascertained by the lack of any clear and consistent pattern in the recorded values among R-curves and load displacement curves.
- In combination with cell size, the fabrication process did not play a large role in fracture toughness. When considering the 1/8″ cell size, the PCFS were approximately the same or slightly more fracture resistant than the CCFS. The 3/8″ cell size CCFS were significantly

more fracture resistant by AREA measurement than the PCFS. This behavior was identified in both the recorded values and the R-curve.

- Ribbon direction played a complex role in combination with core type on fracture toughness. When considering the HX, the longitudinal ribbon direction was more fracture resistant than the lateral ribbon direction; however, when considering the over-expanded core, the opposite was generally true. This relationship was observed in the recorded values and the R-curve.
- Crack tip location in conjunction with ribbon direction played no role in the pre-crack fracture toughness. When considering longitudinal ribbon direction, the center of the core cell crack tip location was more fracture resistant than the core cell edge crack tip location; however, the opposite was observed for the lateral ribbon direction. This behavior was identified in the pre-crack recorded values. However, because of scatter, this conclusion is speculative.

Failure mode and type in the core or adhesive was a function of the combined effects of cell size and core density. The smaller the core density and cell size, the greater the likelihood of core failure.

The MBT data-reduction method resulted in a more conservative fracture toughness than the AM. The differences between the two methods were correlated with core density; the AM resulted in significantly larger fracture toughness than the MBT as the core density increased.

5. REFERENCES

1. Seneviratne, W., Tomblin, J., and Gunawardana, S. (2007). Experimental fracture mechanics for adhesive joint design. *International Conference on Computational & Experimental Engineering and Sciences (ICCES)*, 4(2), pp. 81–86.

2. Anderson, T. L. (1995). *Fracture mechanics: fundamentals and applications*. (2nd ed.). CRC Press, pp. 12–15.

3. Smith, B. L. (2010). Mechanics of damage tolerance: Residual strength, fracture crack propagation and damage tolerance evaluation. Wichita State University, pp. 13–18.

4. Aviles, F. and Carlsson, L. A. (2008). Analysis of the sandwich DCB specimen for debond characterization. *Engineering Fracture Mechanics*, 75(2), pp. 153–168.

5. Li, X. and Carlsson, L. A. (2000). Elastic foundation analysis of tilted sandwich debond (TSD) specimen. *Journal of Sandwich Structures and Materials*, 2(1), pp. 3–32.

6. Shivakumar, K., Chen, H., and Smith, S. A. (2005). An evaluation of data reduction methods for opening mode fracture toughness of sandwich panels. *Journal of Sandwich Structures and Materials*, 7(1), pp. 77–90.

7. Cantwell, W. J. and Davies, P. (1994). A test technique for assessing core-skin adhesion in composite sandwich structures. *Journal of Material Science Letters,* 13(3), pp. 203–205.

8. Cantwell, W. J. and Davies, P. (1996). A study of skin-core adhesion in glass fiber reinforced sandwich materials. *Applied Composite Materials,* 3(6), pp. 407–420.

9. Seneviratne, W. and Tomblin, J. (2011). Damage growth in fluid-ingressed sandwich structures. *First Technical Workshop for Safety Management Initiative for Sandwich Disbond Growth*, Hampton, VA.

10. Ratcliffe, J. G. (2010). Sizing Single cantilever beam specimens for characterizing facesheet/core peel debonding in sandwich structure. NASA/TP-2010-216169, National Institute of Aerospace, Langley Research Center, Hampton, VA.

11. Boresi, A. P. and Schmidt, R. J. (2003). *Advanced mechanics of materials*. (6th ed.). John Wiley & Sons, Inc., pp. 3–4, 79–90, and 158–160).

12. Hibbler, R. C. (2005). *Mechanic of materials*. (6^{th} ed.). Pearson Prentice Hall, pp. 585–592 and 725–740.

13. Williams, J. G. (1987). Large displacement and end block effects in 'DCB' interlaminar test in modes I and II. *Journal of Composite Materials*, 21(4), pp. 330–347.

14. Southward, T. (2009). Buckling and growth of disbonds in honeycomb sandwich structure. VDM Verlag, Dr. Muller Aktiengesellschaft & Co., KG, pp. 1–9.

APPENDIX A—STATIC RESULTS FOR THIN PRE-CURED FACESHEET (4-PLY)
AND SECONDARILY BONDED HRH-10 HEXAGONAL CORES TESTED
AS SINGLE-CANTILEVER BEAMS

A.1 HRH-10–1/8–2.0 DATA

A.1.1 HRH-10–1/8–2.0 LONGITUDINAL RIBBON DIRECTION WITH TOP DISBOND (CENTER) DATA

Table A-1. Test summary for HRH-10–1/8–2.0 longitudinal ribbon direction with top disbond (center) pre-crack

Specimen	GIC (in-lb/in^2)			GIC (KJ/m^2)			Failure Mode
	NL	VIS	5%/max	NL	VIS	5%/max	
SDT-04-HX-1.8-2-T-PCFS-LONG-C-1							
SDT-04-HX-1.8-2-T-PCFS-LONG-C-2	1.321	N/A	2.078	0.231	N/A	0.364	Primarily C
SDT-04-HX-1.8-2-T-PCFS-LONG-C-3	0.832	1.691	1.691	0.146	0.296	0.296	Half a cell in A, then C
SDT-04-HX-1.8-2-T-PCFS-LONG-C-4	0.803	1.927	1.927	0.141	0.337	0.337	Half a cell in A, then C
SDT-04-HX-1.8-2-T-PCFS-LONG-C-5	1.184	N/A	2.105	0.207	N/A	0.369	Primarily C, with a couple of cells half A, then C
SDT-04-HX-1.8-2-T-PCFS-LONG-C-6	1.173	N/A	2.581	0.205	N/A	0.452	Primarily C
SDT-04-HX-1.8-2-T-PCFS-LONG-C-7	1.372	N/A	2.251	0.240	N/A	0.394	Primarily C
SDT-04-HX-1.8-2-T-PCFS-LONG-C-8							
AVERAGE GIC	1.114	1.809	2.105	0.195	0.317	0.369	
STANDARD DEVIATION	0.243	0.167	0.301	0.042	0.029	0.053	
COEFFICIENT OF VARIATION (%)	21.769	9.239	14.283	21.769	9.239	14.283	

Table A-2. Test summary for HRH-10–1/8–2.0 longitudinal ribbon direction with top disbond (center)

Specimen	GIC (in-lb/in^2)				GIC (KJ/m^2)				Failure Mode
	NL	VIS	5%/max	AREA	NL	VIS	5%/max	AREA	
SDT-04-HX-1.8-2-T-PCFS-LONG-C-1									
SDT-04-HX-1.8-2-T-PCFS-LONG-C-2	0.908	1.744	2.110	2.798	0.159	0.305	0.370	0.490	Primarily in C
SDT-04-HX-1.8-2-T-PCFS-LONG-C-3	1.188	1.615	2.848	2.689	0.208	0.283	0.499	0.471	Primarily in C
SDT-04-HX-1.8-2-T-PCFS-LONG-C-4	0.792	1.756	1.904	2.845	0.139	0.307	0.333	0.498	Primarily in C
SDT-04-HX-1.8-2-T-PCFS-LONG-C-5	0.883	2.036	2.442	2.847	0.155	0.357	0.428	0.499	Primarily in C
SDT-04-HX-1.8-2-T-PCFS-LONG-C-6	1.091	2.566	2.774	2.717	0.191	0.449	0.486	0.476	Primarily in C
SDT-04-HX-1.8-2-T-PCFS-LONG-C-7	0.730	2.959	2.969	3.239	0.128	0.518	0.520	0.567	Primarily in C
SDT-04-HX-1.8-2-T-PCFS-LONG-C-8									
AVERAGE GIC	0.932	2.113	2.508	2.856	0.163	0.370	0.439	0.500	
STANDARD DEVIATION	0.176	0.537	0.431	0.199	0.031	0.094	0.075	0.035	
COEFFICIENT OF VARIATION (%)	18.828	25.396	17.169	6.964	18.828	25.396	17.169	6.964	

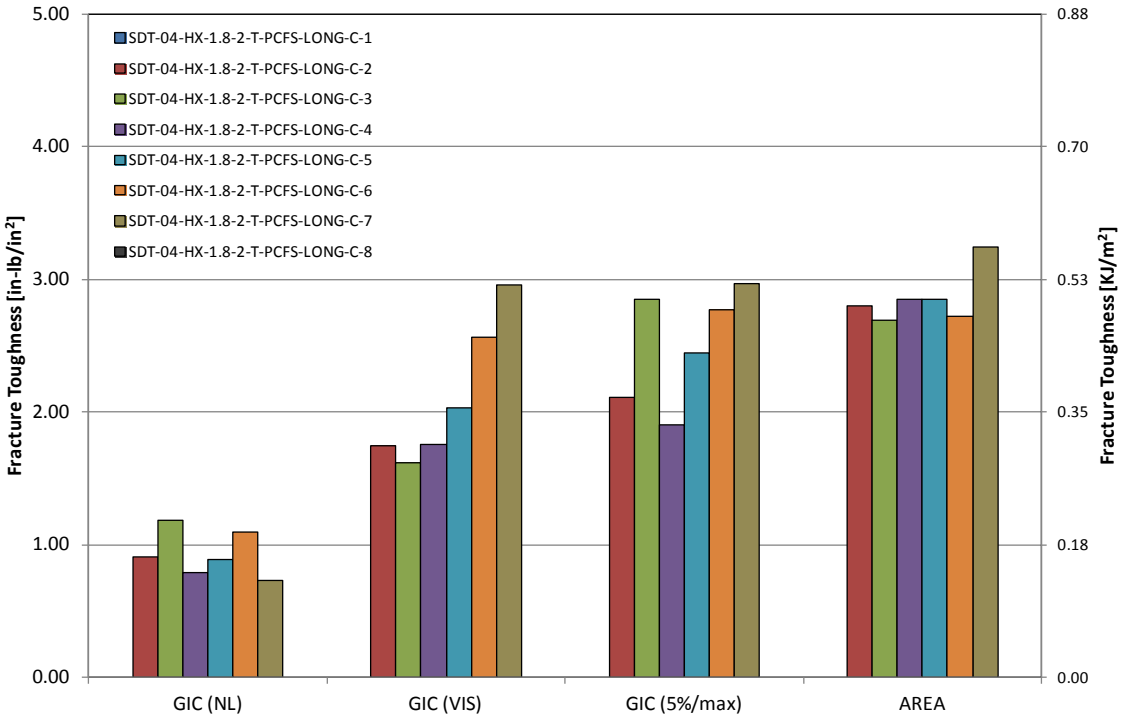

Figure A-1. GIC for HRH-10–1/8–2.0 longitudinal ribbon direction with top disbond (center)

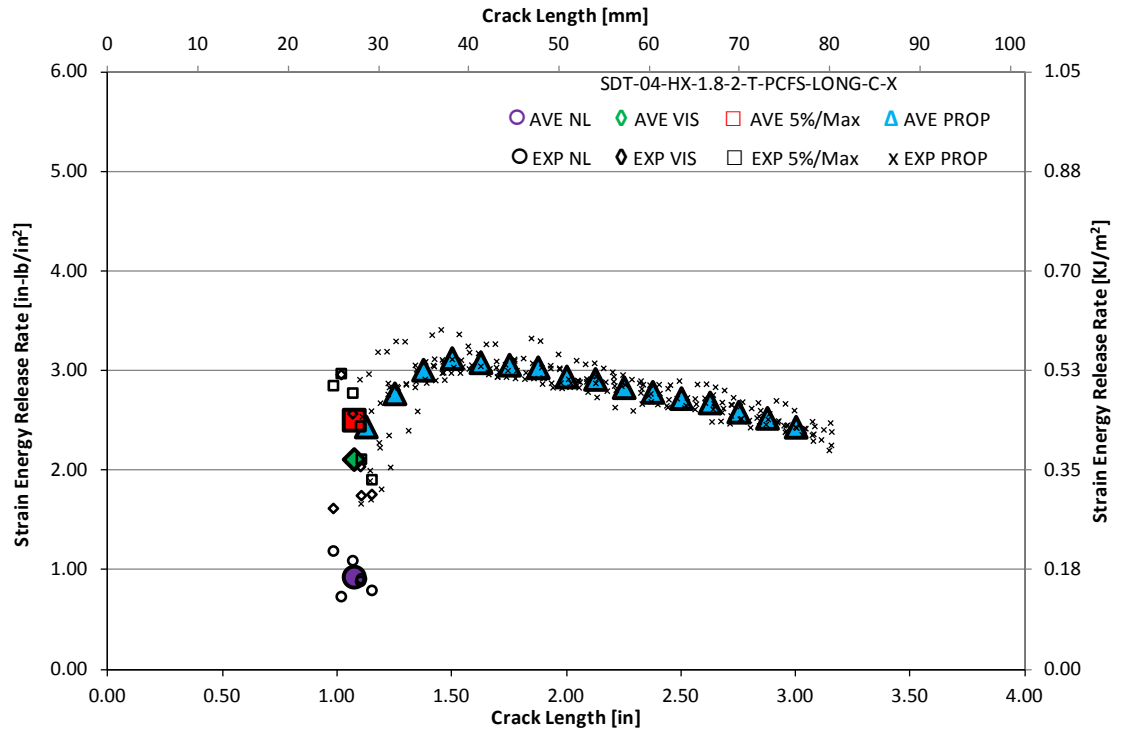

Figure A-2. Resistance curve for HRH-10–1/8–2.0 longitudinal ribbon direction with top disbond (center)

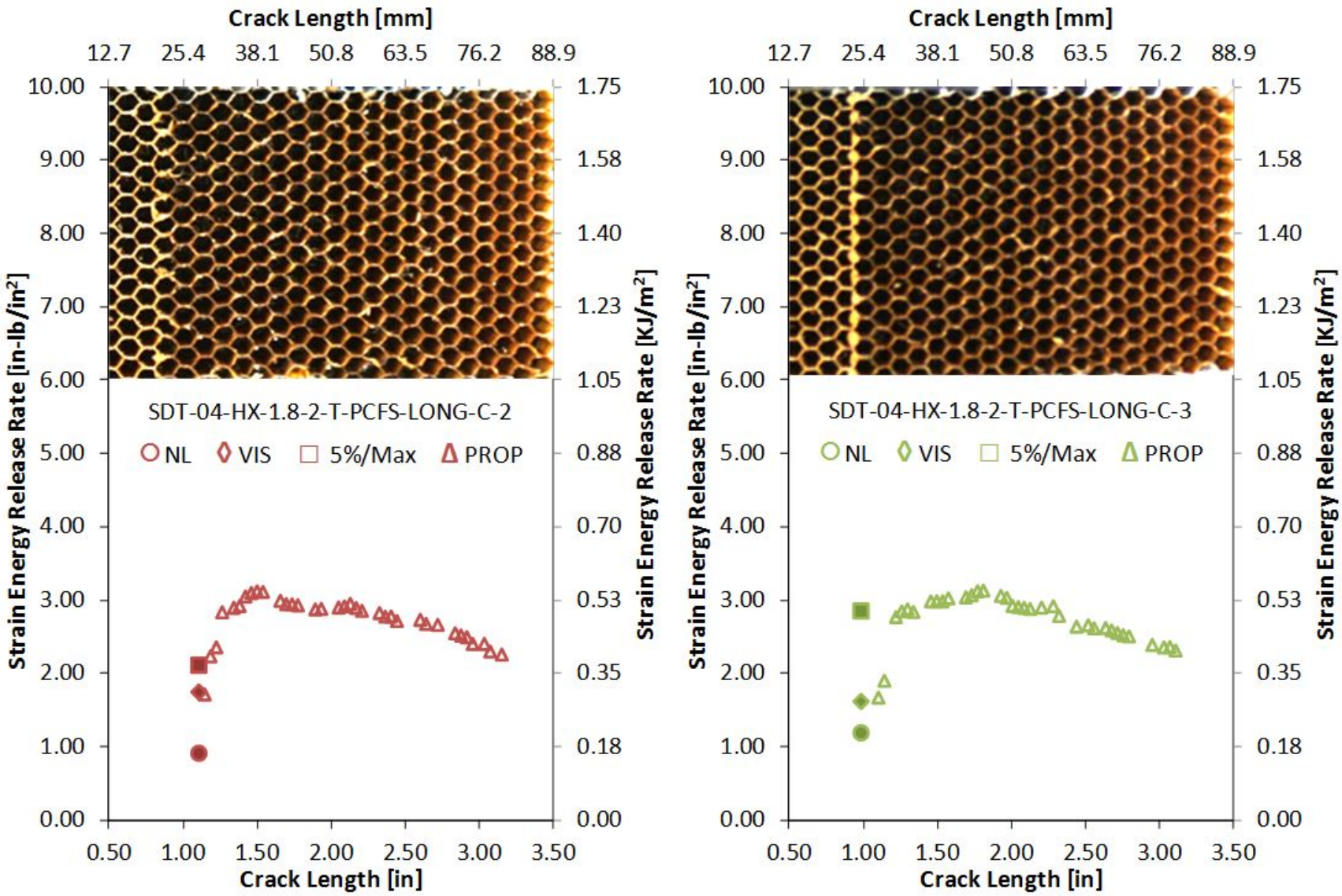

Figure A-3. Failure mode image and resistance curve of SDT-04-HX-1.8-2-T-PCFS-LONG-C-X #2 and #3

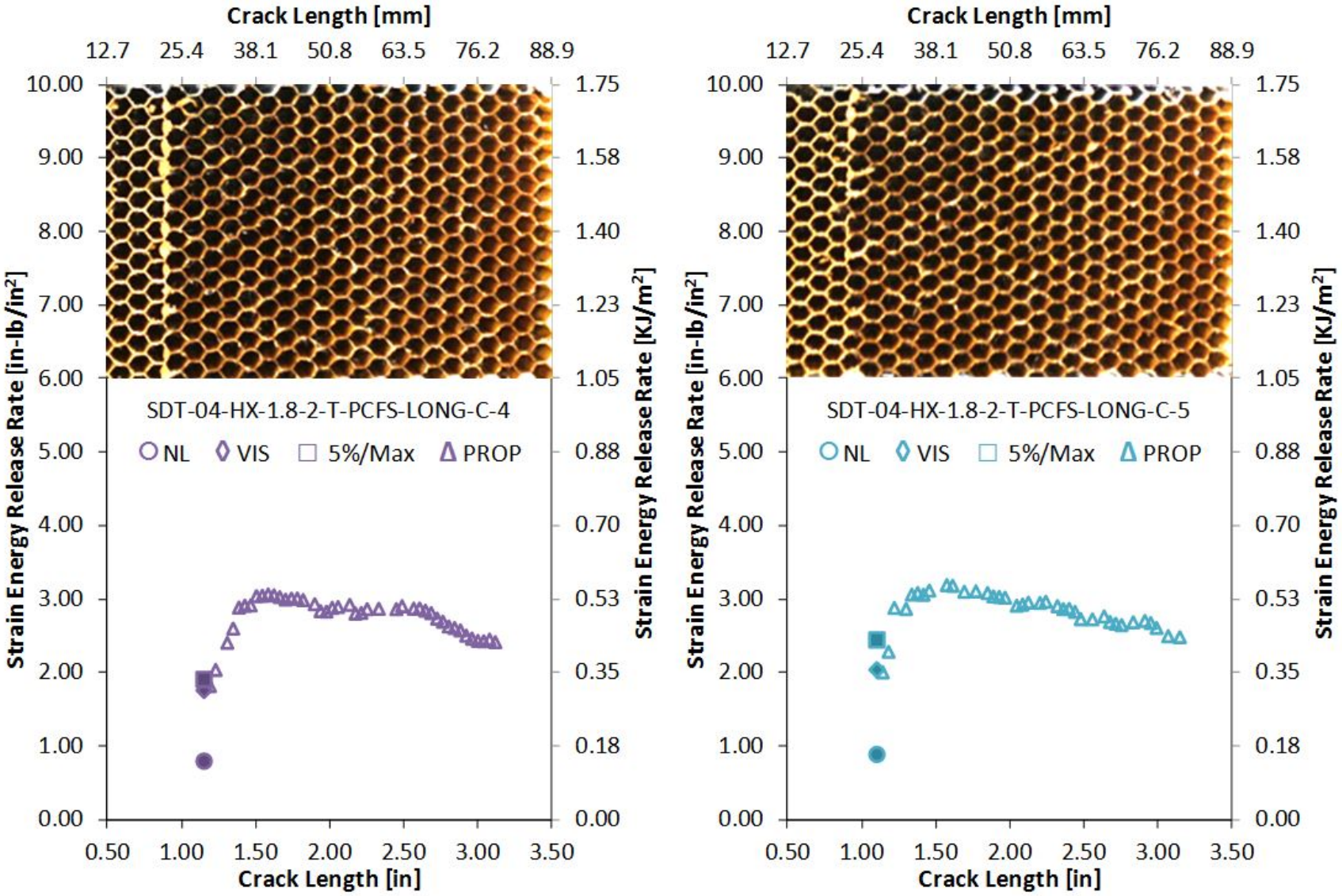

Figure A-4. Failure mode image and resistance curve of SDT-04-HX-1.8-2-T-PCFS-LONG-C-X #4 and #5

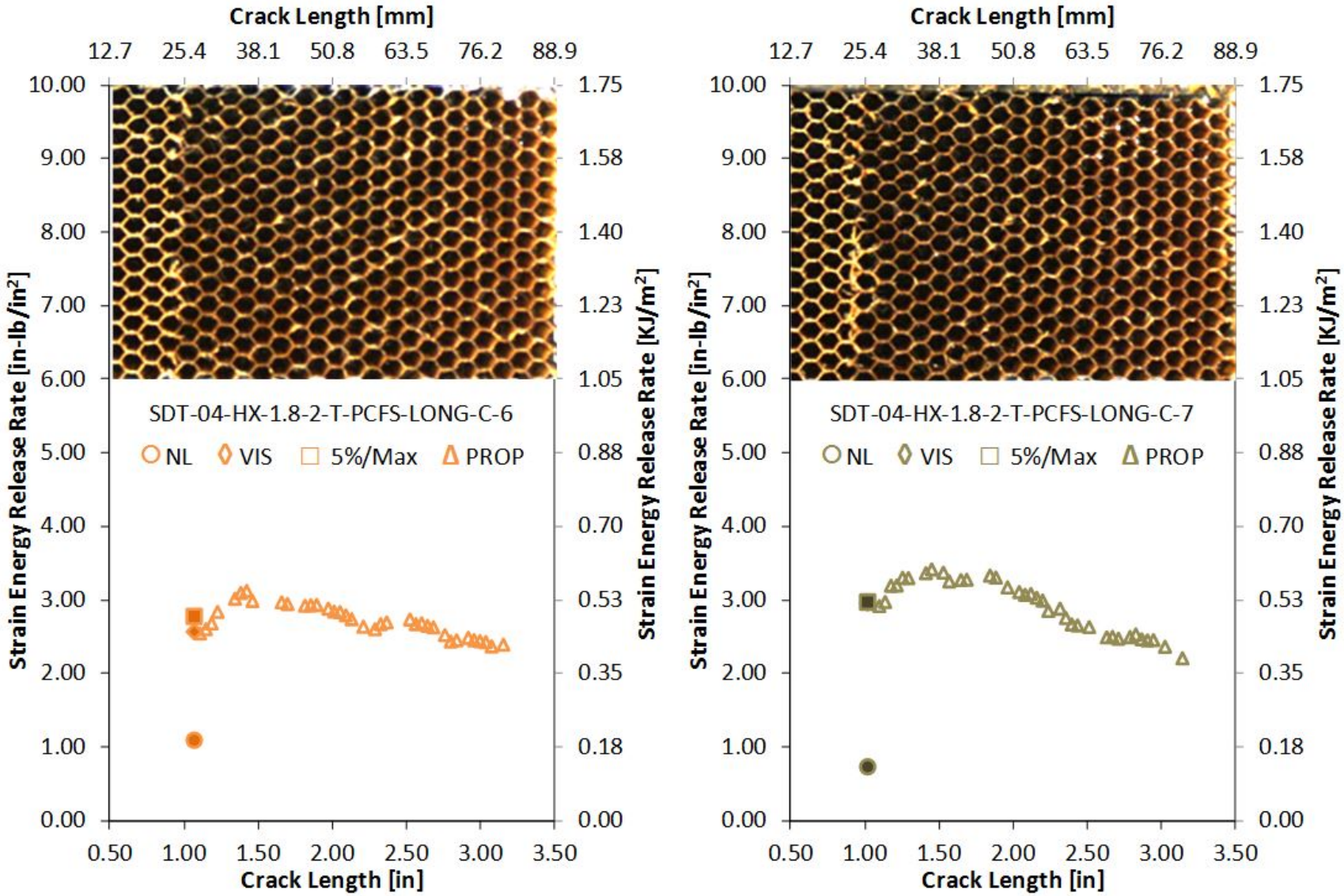

Figure A-5. Failure mode image and resistance curve of SDT-04-HX-1.8-2-T-PCFS-LONG-C-X #6 and #7

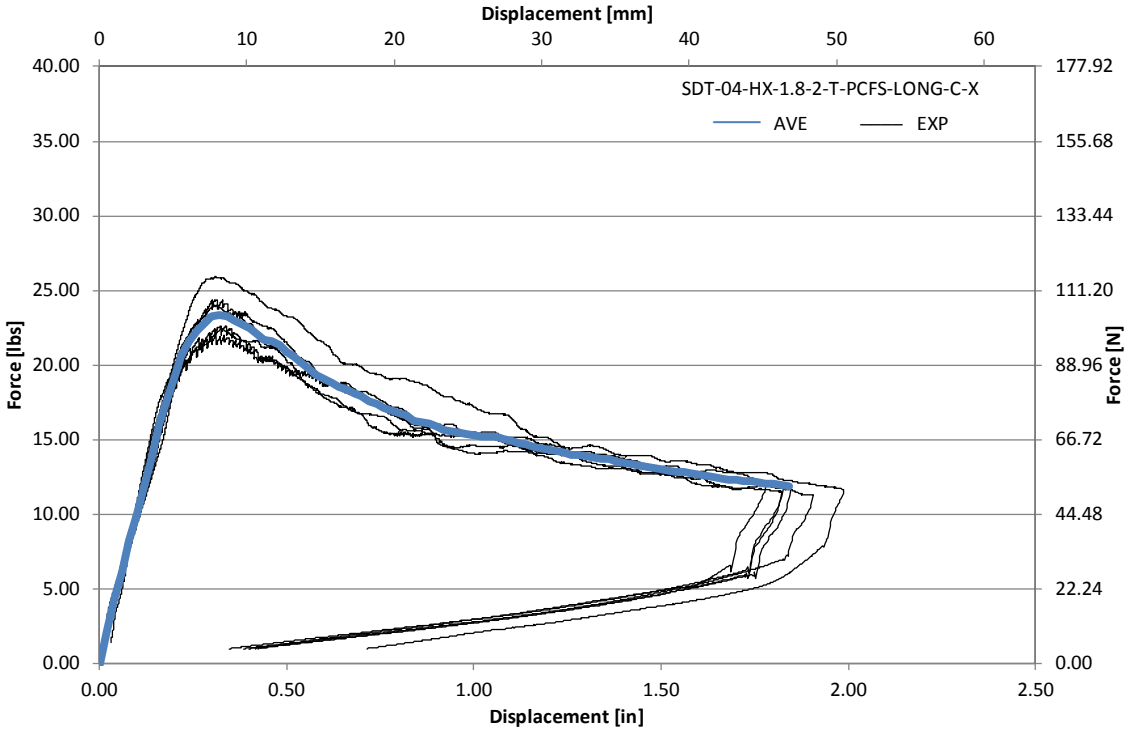

Figure A-6. Load vs. displacement curve for HRH-10–1/8–2.0 longitudinal ribbon direction with top disbond (center)

A.1.2 HRH-10–1/8–2.0 LONGITUDINAL RIBBON DIRECTION WITH BOTTOM DISBOND (CENTER) DATA

Table A-3. Test summary for HRH-10–1/8–2.0 longitudinal ribbon direction with bottom disbond (center) pre-crack

Specimen	GIC (in-lb/in^2)			GIC (KJ/m^2)			Failure Mode
	NL	VIS	5%/max	NL	VIS	5%/max	
SDT-04-HX-1.8-2-B-PCFS-LONG-C-1	1.409	N/A	2.021	0.247	N/A	0.354	Primarily C
SDT-04-HX-1.8-2-B-PCFS-LONG-C-2	1.226	N/A	1.921	0.215	N/A	0.336	Primarily C
SDT-04-HX-1.8-2-B-PCFS-LONG-C-3	1.707	N/A	2.377	0.299	N/A	0.416	Primarily C
SDT-04-HX-1.8-2-B-PCFS-LONG-C-4	1.498	N/A	1.995	0.262	N/A	0.349	Primarily C
SDT-04-HX-1.8-2-B-PCFS-LONG-C-5	1.581	N/A	2.142	0.277	N/A	0.375	Primarily C
SDT-04-HX-1.8-2-B-PCFS-LONG-C-6	1.151	1.877	1.877	0.202	0.329	0.329	Primarily C
SDT-04-HX-1.8-2-B-PCFS-LONG-C-7							
SDT-04-HX-1.8-2-B-PCFS-LONG-C-8							
AVERAGE GIC	1.429	1.877	2.056	0.250	0.329	0.360	
STANDARD DEVIATION	0.212	N/A	0.182	0.037	N/A	0.032	
COEFFICIENT OF VARIATION (%)	14.823	N/A	8.853	14.823	N/A	8.853	

Table A-4. Test Summary for HRH-10–1/8–2.0 longitudinal ribbon direction with bottom disbond (center)

Specimen	GIC (in-lb/in^2)				GIC (KJ/m^2)				Failure Mode
	NL	VIS	5%/max	AREA	NL	VIS	5%/max	AREA	
SDT-04-HX-1.8-2-B-PCFS-LONG-C-1	0.740	1.598	3.285	2.782	0.130	0.280	0.575	0.487	Primarily in C
SDT-04-HX-1.8-2-B-PCFS-LONG-C-2	0.777	2.222	2.378	2.845	0.136	0.389	0.417	0.498	Primarily in C
SDT-04-HX-1.8-2-B-PCFS-LONG-C-3	0.702	N/A	2.763	2.824	0.123	N/A	0.484	0.494	Primarily in C
SDT-04-HX-1.8-2-B-PCFS-LONG-C-4	0.906	2.966	2.966	2.719	0.159	0.519	0.519	0.476	Primarily in C
SDT-04-HX-1.8-2-B-PCFS-LONG-C-5	0.783	N/A	2.849	2.628	0.137	N/A	0.499	0.460	Primarily in C
SDT-04-HX-1.8-2-B-PCFS-LONG-C-6	1.209	2.061	3.173	2.923	0.212	0.361	0.556	0.512	Primarily in C
SDT-04-HX-1.8-2-B-PCFS-LONG-C-7									
SDT-04-HX-1.8-2-B-PCFS-LONG-C-8									
AVERAGE GIC	0.853	2.212	2.902	2.787	0.149	0.387	0.508	0.488	
STANDARD DEVIATION	0.188	0.568	0.323	0.103	0.033	0.099	0.057	0.018	
COEFFICIENT OF VARIATION (%)	22.014	25.682	11.120	3.689	22.014	25.682	11.120	3.689	

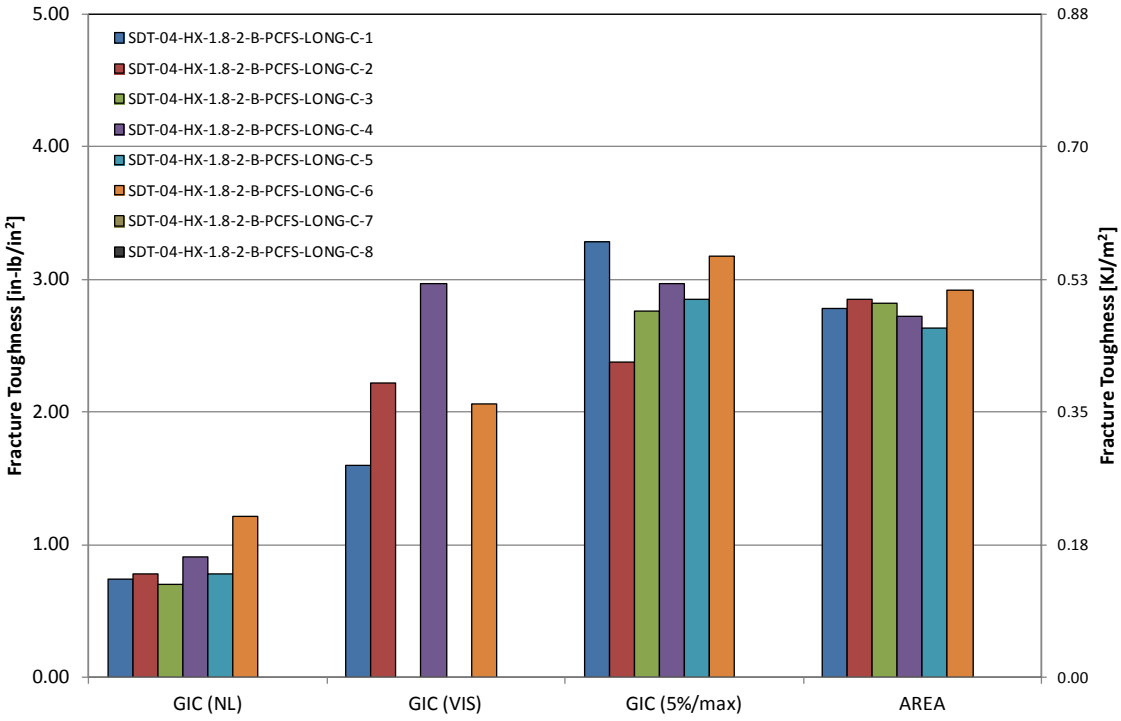

Figure A-7. GIC for HRH-10–1/8–2.0 longitudinal ribbon direction with bottom disbond (center)

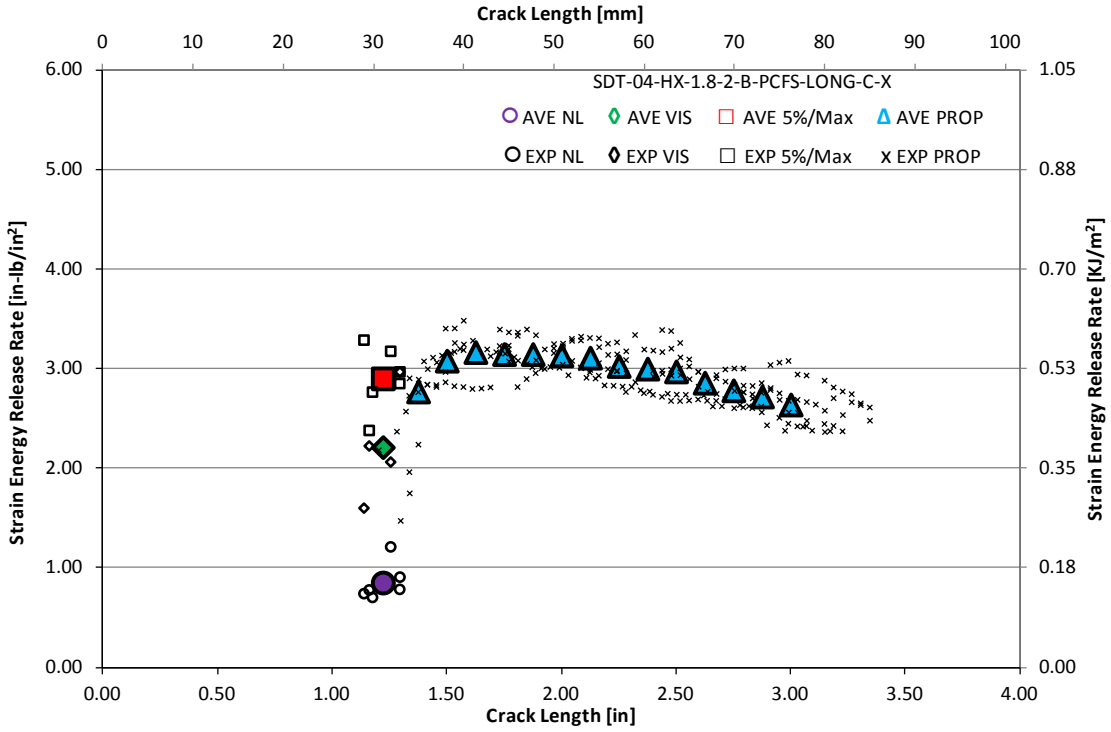

Figure A-8. Resistance curve for HRH-10–1/8–2.0 longitudinal ribbon direction with bottom disbond (center)

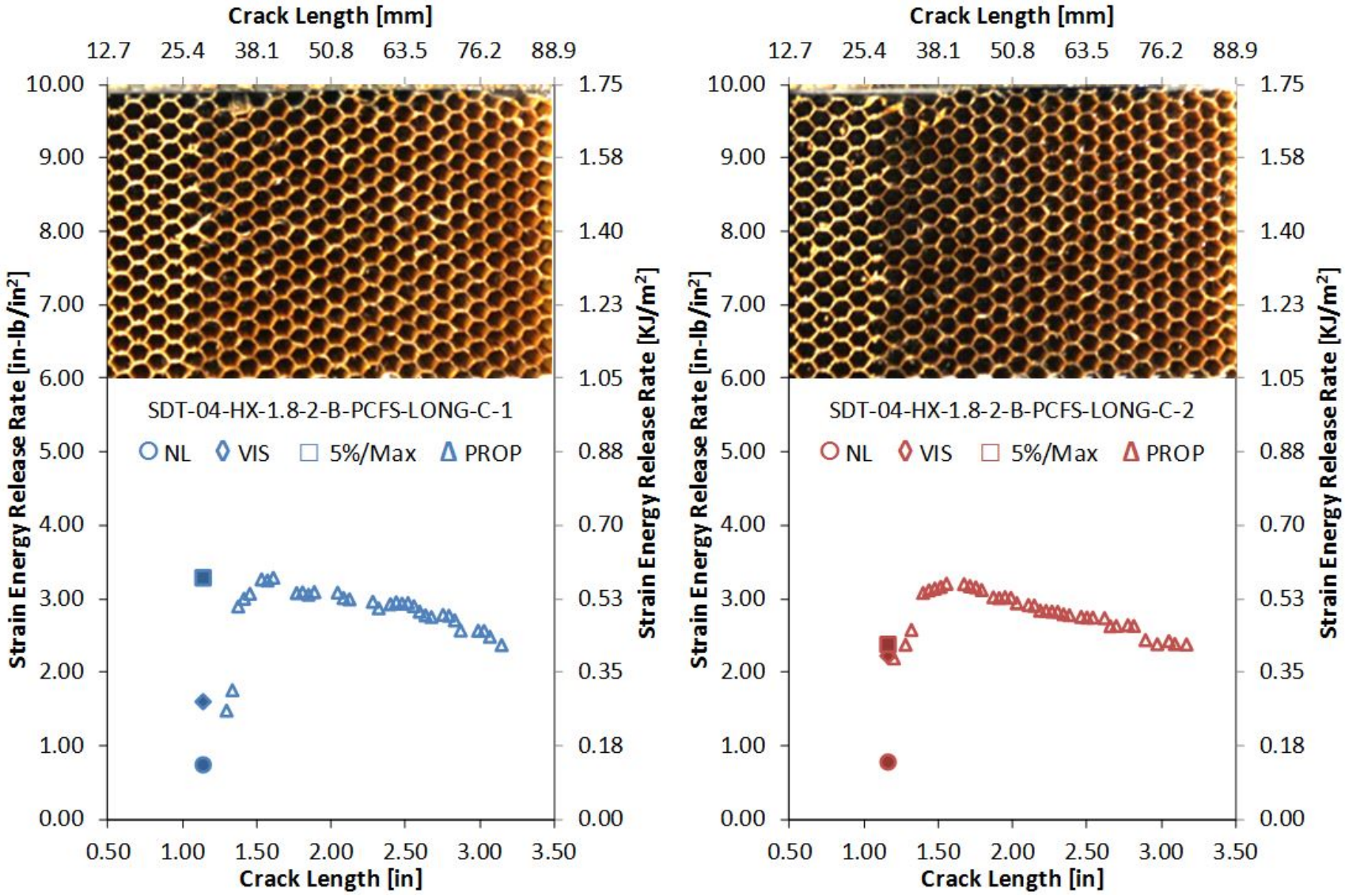

Figure A-9. Failure mode image and resistance curve of SDT-04-HX-1.8-2-B-PCFS-LONG-C-X #1 and #2

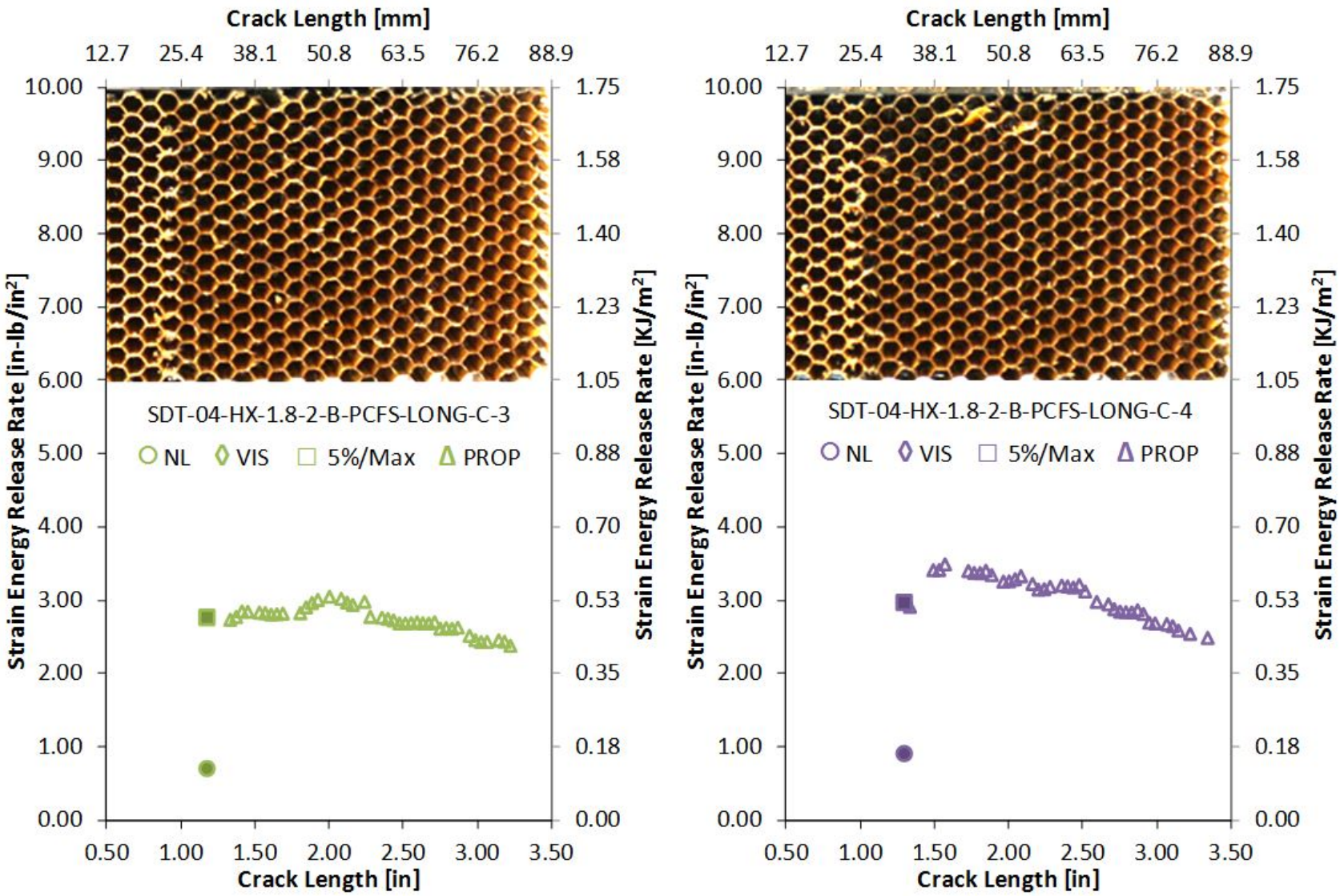

Figure A-10. Failure mode image and resistance curve of SDT-04-HX-1.8-2-B-PCFS-LONG-C-X #3 and #4

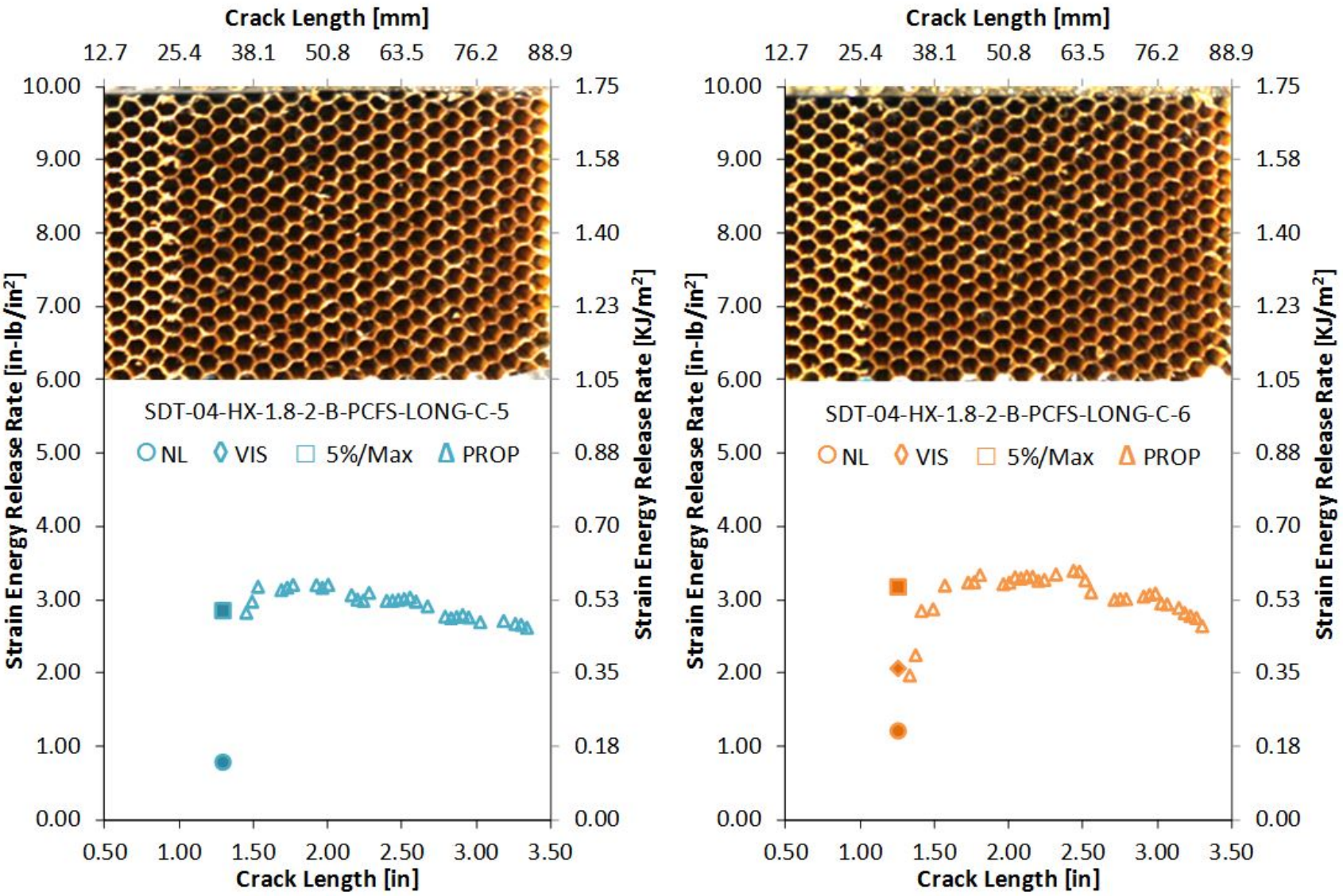

Figure A-11. Failure mode image and resistance curve of SDT-04-HX-1.8-2-B-PCFS-LONG-C-X #5 and #6

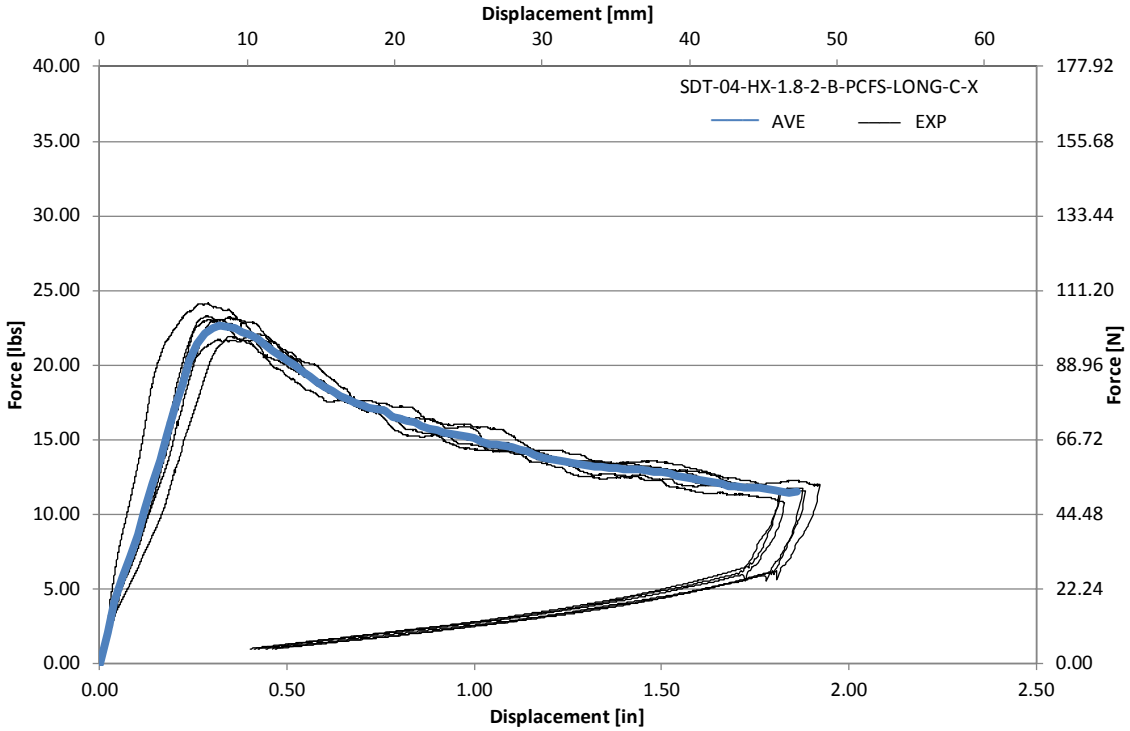

Figure A-12. Load vs. displacement curve for HRH-10–1/8–2.0 longitudinal ribbon direction with bottom disbond (center)

A.2 HRH-10–1/8–3.0 DATA

A.2.1 HRH-10–1/8–3.0 LONGITUDINAL RIBBON DIRECTION WITH TOP DISBOND (CENTER) DATA

Table A-5. Test summary for HRH-10–1/8–3.0 longitudinal ribbon direction with top disbond (center) pre-crack

Specimen	GIC (in-lb/in^2)			GIC (KJ/m^2)			Failure Mode
	NL	VIS	5%/max	NL	VIS	5%/max	
SDT-04-HX-1.8-3-T-PCFS-LONG-C-1	2.243	N/A	3.696	0.393	N/A	0.647	Primarily C
SDT-04-HX-1.8-3-T-PCFS-LONG-C-2	2.304	N/A	3.345	0.404	N/A	0.586	Primarily C
SDT-04-HX-1.8-3-T-PCFS-LONG-C-3	2.261	3.254	3.254	0.396	0.570	0.570	Primarily C
SDT-04-HX-1.8-3-T-PCFS-LONG-C-4	2.305	N/A	3.146	0.404	N/A	0.551	Primarily C
SDT-04-HX-1.8-3-T-PCFS-LONG-C-5	1.862	N/A	3.002	0.326	N/A	0.526	Primarily C
SDT-04-HX-1.8-3-T-PCFS-LONG-C-6	1.628	N/A	3.615	0.285	N/A	0.633	Primarily C
SDT-04-HX-1.8-3-T-PCFS-LONG-C-7							
SDT-04-HX-1.8-3-T-PCFS-LONG-C-8							
AVERAGE GIC	2.101	3.254	3.343	0.368	0.570	0.585	
STANDARD DEVIATION	0.286	N/A	0.269	0.050	N/A	0.047	
COEFFICIENT OF VARIATION (%)	13.625	N/A	8.045	13.625	N/A	8.045	

Table A-6. Test summary for HRH-10–1/8–3.0 longitudinal ribbon direction with top disbond (center)

Specimen	GIC (in-lb/in^2)				GIC (KJ/m^2)				Failure Mode
	NL	VIS	5%/max	AREA	NL	VIS	5%/max	AREA	
SDT-04-HX-1.8-3-T-PCFS-LONG-C-1	1.108	3.814	3.931	3.511	0.194	0.668	0.688	0.615	Primarily in C
SDT-04-HX-1.8-3-T-PCFS-LONG-C-2	1.484	N/A	3.922	3.547	0.260	N/A	0.687	0.621	Primarily in C
SDT-04-HX-1.8-3-T-PCFS-LONG-C-3	1.376	N/A	3.314	3.543	0.241	N/A	0.580	0.621	Primarily in C
SDT-04-HX-1.8-3-T-PCFS-LONG-C-4	1.167	3.405	3.423	3.363	0.204	0.596	0.600	0.589	Primarily in C
SDT-04-HX-1.8-3-T-PCFS-LONG-C-5	1.516	N/A	3.612	3.547	0.266	N/A	0.633	0.621	Primarily in C
SDT-04-HX-1.8-3-T-PCFS-LONG-C-6	0.991	1.777	3.919	3.732	0.174	0.311	0.686	0.654	Primarily in C
SDT-04-HX-1.8-3-T-PCFS-LONG-C-7									
SDT-04-HX-1.8-3-T-PCFS-LONG-C-8									
AVERAGE GIC	1.274	2.999	3.687	3.540	0.223	0.525	0.646	0.620	
STANDARD DEVIATION	0.216	1.077	0.277	0.118	0.038	0.189	0.048	0.021	
COEFFICIENT OF VARIATION (%)	16.920	35.930	7.506	3.321	16.920	35.930	7.506	3.321	

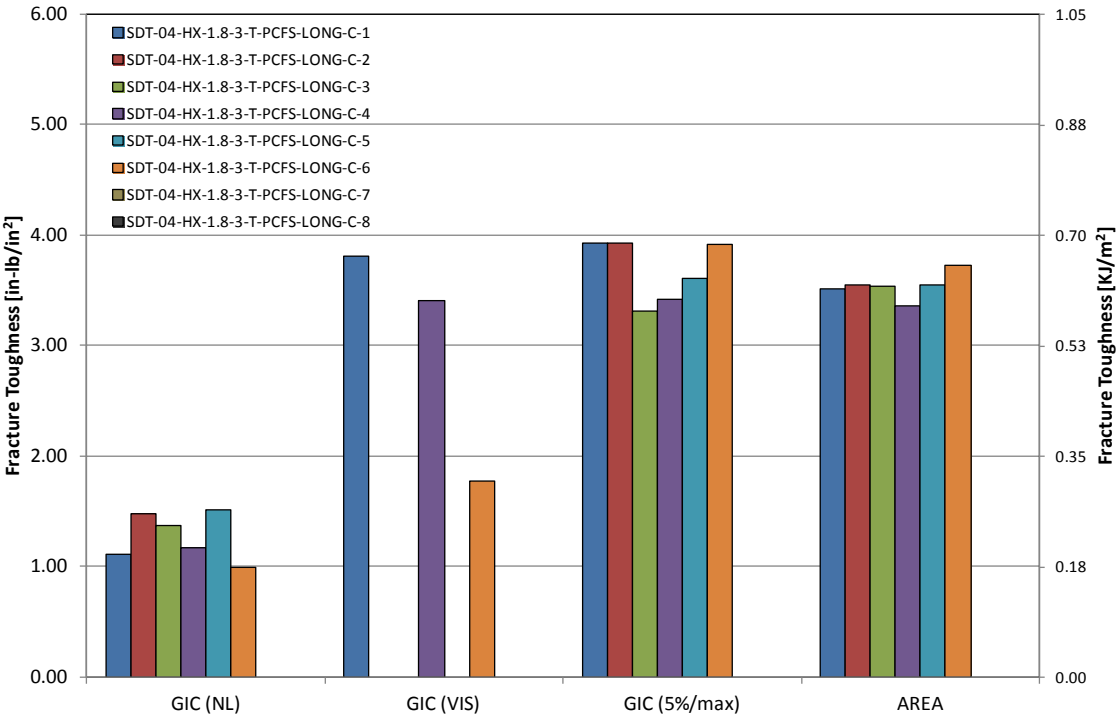

Figure A-13. GIC for HRH-10–1/8–3.0 longitudinal ribbon direction with top disbond (center)

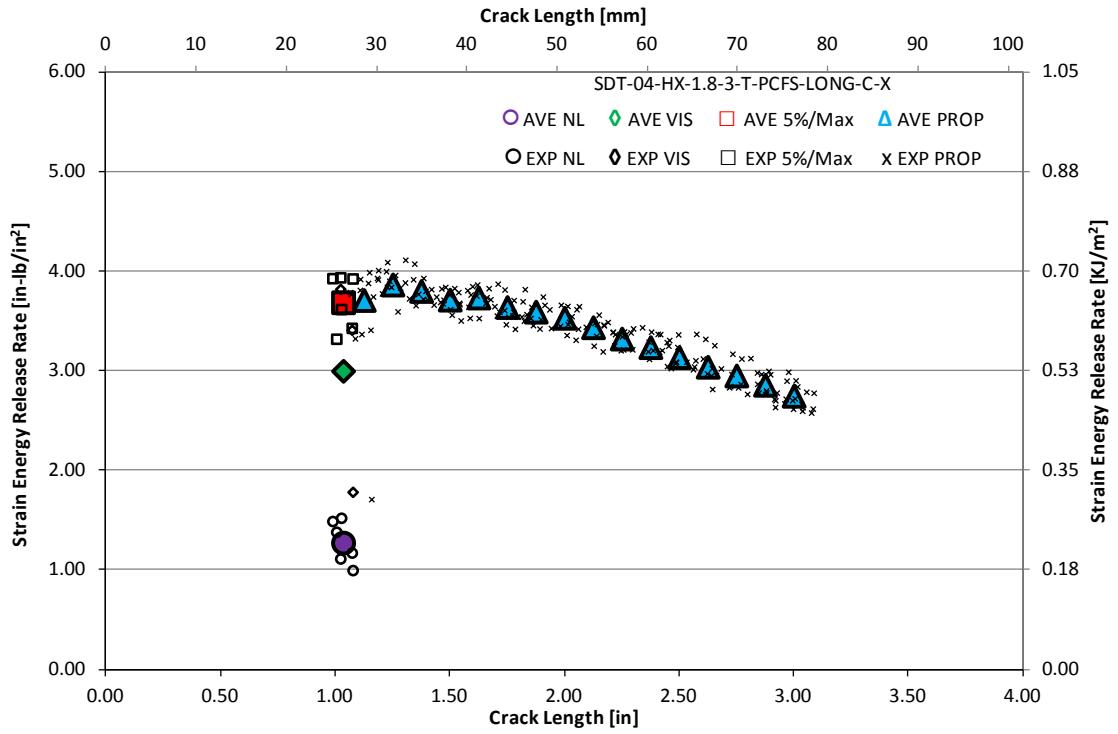

Figure A-14. Resistance curve for HRH-10–1/8–3.0 longitudinal ribbon direction with top disbond (center)

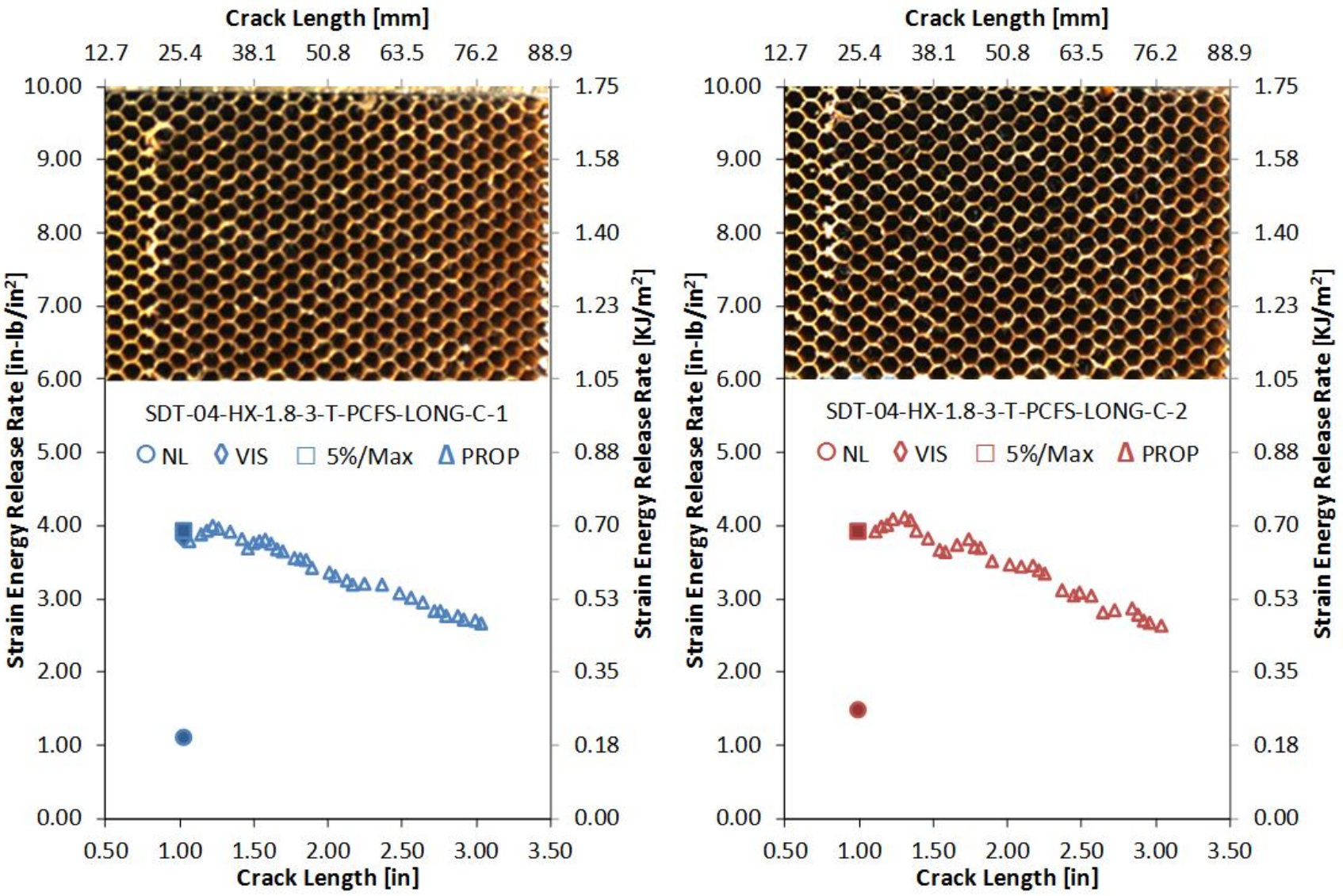

Figure A-15. Failure mode image and resistance curve of SDT-04-HX-1.8-3-T-PCFS-LONG-C-X #1 and #2

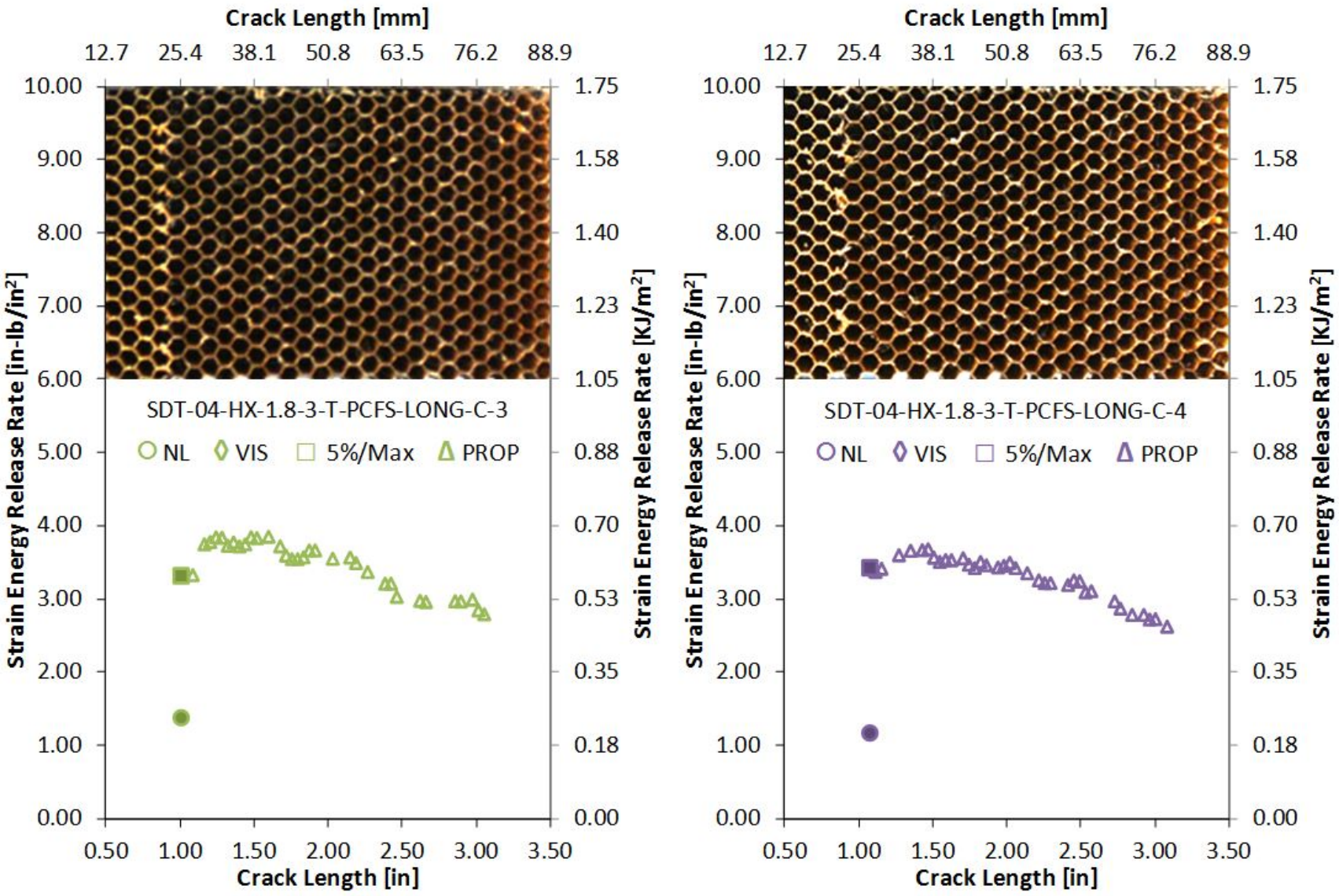

Figure A-16. Failure mode image and resistance curve of SDT-04-HX-1.8-3-T-PCFS-LONG-C-X #3 and #4

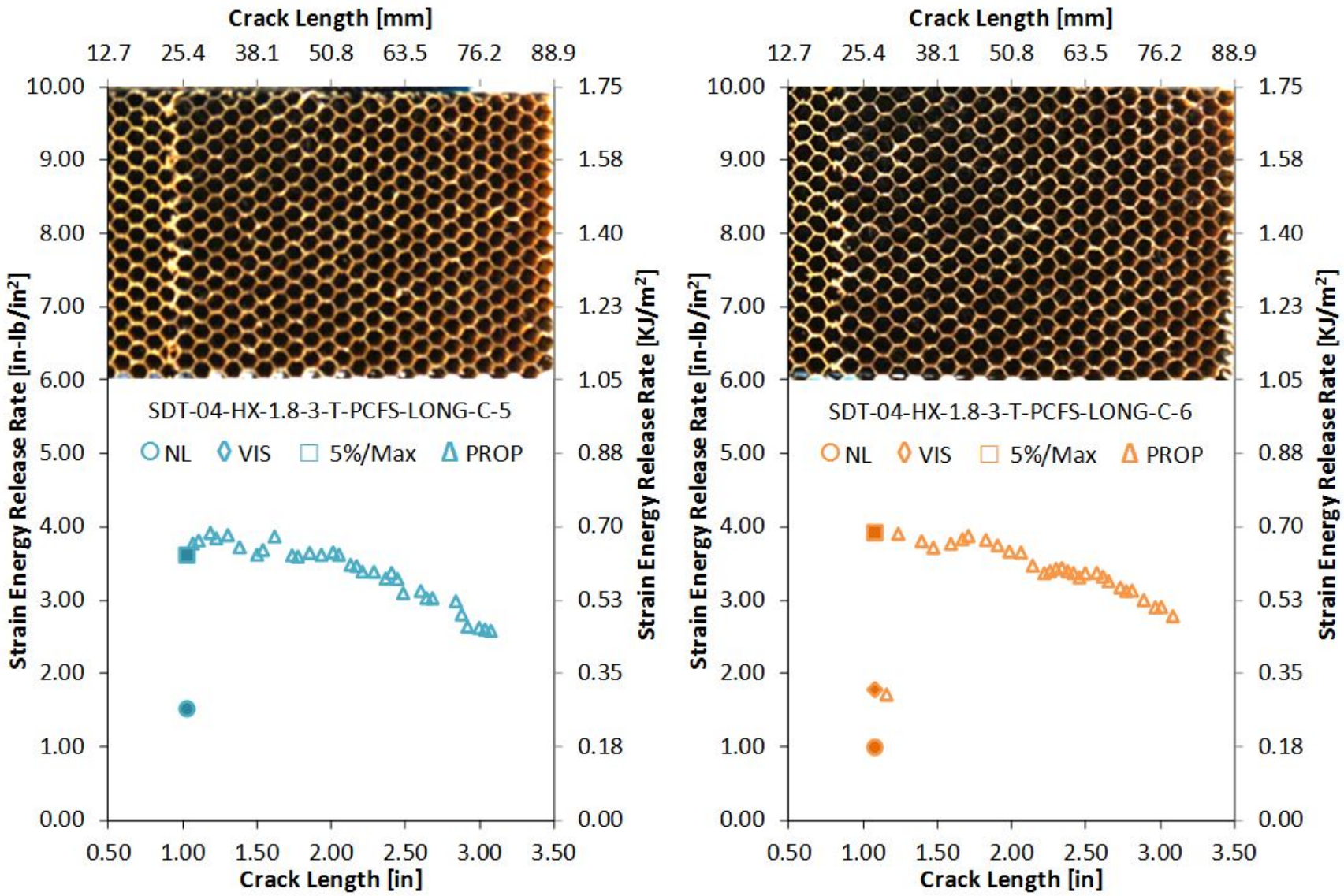

Figure A-17. Failure mode image and resistance curve of SDT-04-HX-1.8-3-T-PCFS-LONG-C-X #5 and #6

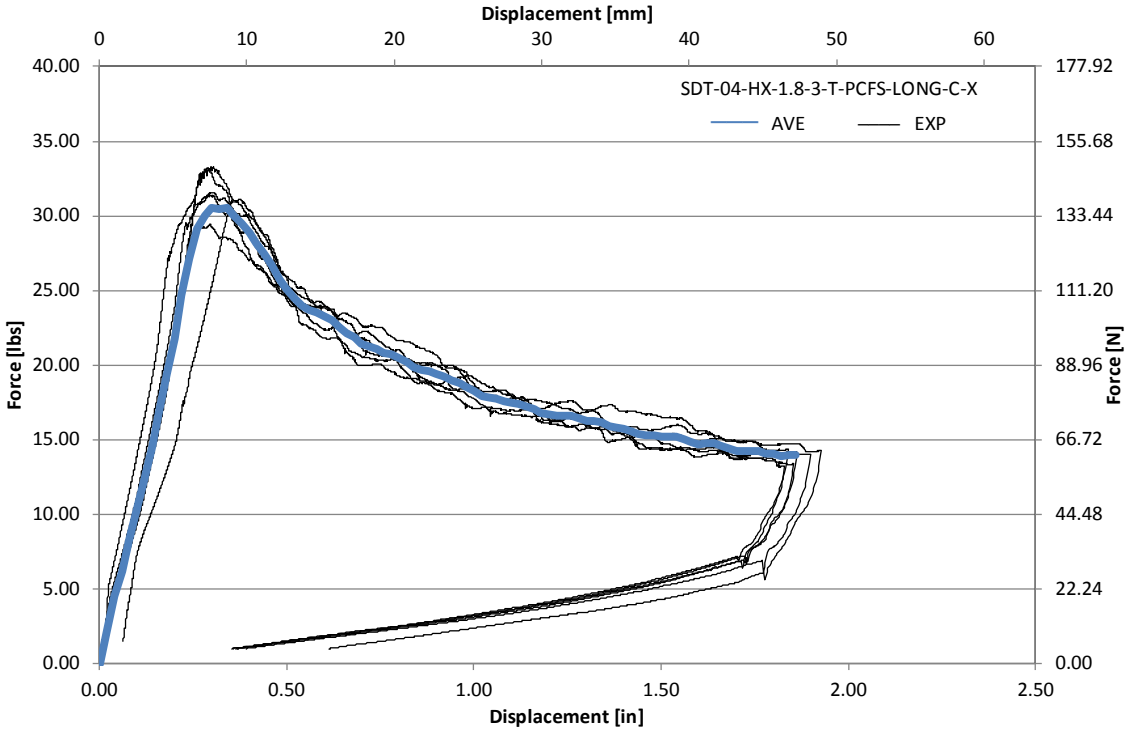

Figure A-18. Load vs. displacement curve for HRH-10–1/8–3.0 longitudinal ribbon direction with top disbond (center)

A.2.2 HRH-10–1/8–3.0 LONGITUDINAL RIBBON DIRECTION WITH A BOTTOM DISBOND (CENTER) DATA

Table A-7. Test summary for HRH-10–1/8–3.0 longitudinal ribbon direction with bottom disbond (center) pre-crack

Specimen	GIC (in-lb/in^2)			GIC (KJ/m^2)			Failure Mode
	NL	VIS	5%/max	NL	VIS	5%/max	
SDT-04-HX-1.8-3-B-PCFS-LONG-C-1							
SDT-04-HX-1.8-3-B-PCFS-LONG-C-2	1.639	N/A	2.096	0.287	N/A	0.367	Primarily C
SDT-04-HX-1.8-3-B-PCFS-LONG-C-3	1.737	N/A	2.700	0.304	N/A	0.473	Primarily C
SDT-04-HX-1.8-3-B-PCFS-LONG-C-4	1.925	N/A	3.088	0.337	N/A	0.541	Primarily C
SDT-04-HX-1.8-3-B-PCFS-LONG-C-5	1.952	N/A	3.146	0.342	N/A	0.551	Primarily C
SDT-04-HX-1.8-3-B-PCFS-LONG-C-6	1.898	N/A	3.033	0.332	N/A	0.531	Primarily C
SDT-04-HX-1.8-3-B-PCFS-LONG-C-7	2.010	N/A	3.263	0.352	N/A	0.571	Primarily C
SDT-04-HX-1.8-3-B-PCFS-LONG-C-8							
AVERAGE GIC	1.860	N/A	2.888	0.326	N/A	0.506	
STANDARD DEVIATION	0.142	N/A	0.431	0.025	N/A	0.076	
COEFFICIENT OF VARIATION (%)	7.620	N/A	14.941	7.620	N/A	14.941	

Table A-8. Test summary for HRH-10–1/8–3.0 longitudinal ribbon direction with bottom disbond (center)

Specimen	GIC (in-lb/in^2)				GIC (KJ/m^2)				Failure Mode
	NL	VIS	5%/max	AREA	NL	VIS	5%/max	AREA	
SDT-04-HX-1.8-3-B-PCFS-LONG-C-1									
SDT-04-HX-1.8-3-B-PCFS-LONG-C-2	1.399	3.227	3.604	3.770	0.245	0.565	0.631	0.660	Primarily in C
SDT-04-HX-1.8-3-B-PCFS-LONG-C-3	0.647	N/A	3.352	3.838	0.113	N/A	0.587	0.672	Primarily in C
SDT-04-HX-1.8-3-B-PCFS-LONG-C-4	0.921	3.021	3.059	3.316	0.161	0.529	0.536	0.581	Primarily in C
SDT-04-HX-1.8-3-B-PCFS-LONG-C-5	0.810	N/A	2.863	3.875	0.142	N/A	0.501	0.679	Primarily in C
SDT-04-HX-1.8-3-B-PCFS-LONG-C-6	0.906	3.257	3.288	3.782	0.159	0.570	0.576	0.662	Primarily in C
SDT-04-HX-1.8-3-B-PCFS-LONG-C-7	0.903	3.236	3.430	3.202	0.158	0.567	0.601	0.561	Primarily in C
SDT-04-HX-1.8-3-B-PCFS-LONG-C-8									
AVERAGE GIC	0.931	3.185	3.266	3.631	0.163	0.558	0.572	0.636	
STANDARD DEVIATION	0.251	0.110	0.266	0.292	0.044	0.019	0.047	0.051	
COEFFICIENT OF VARIATION (%)	27.004	3.456	8.151	8.049	27.004	3.456	8.151	8.049	

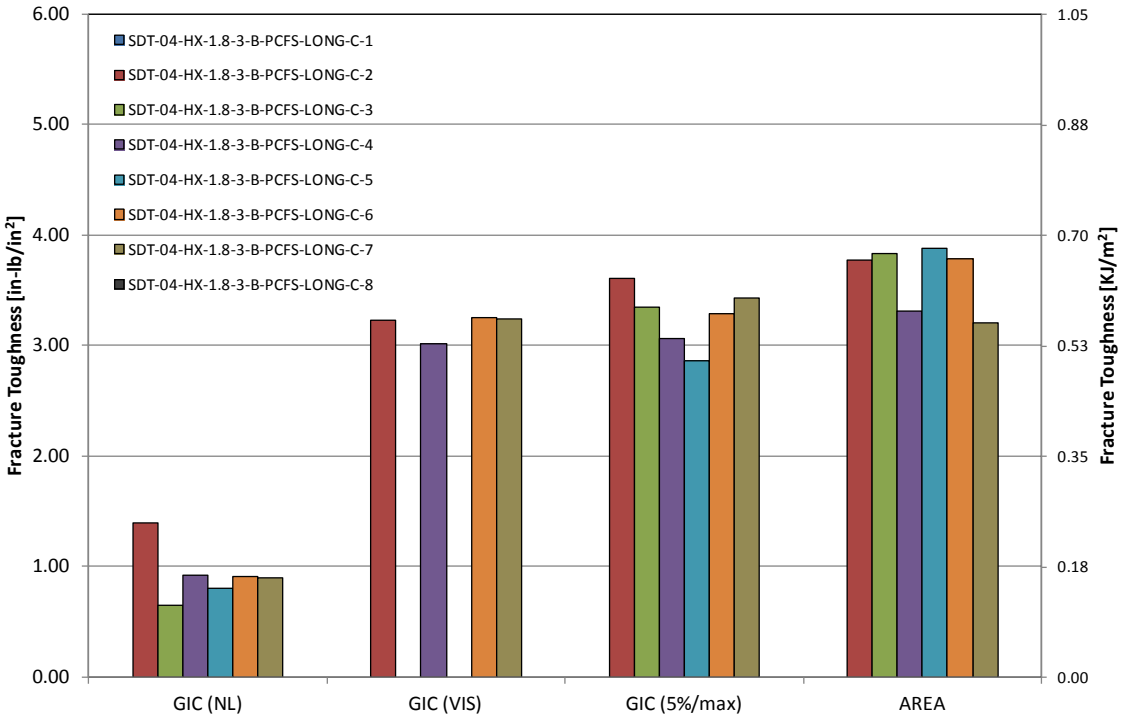

Figure A-19. GIC for HRH-10–1/8–3.0 longitudinal ribbon direction with bottom disbond (center)

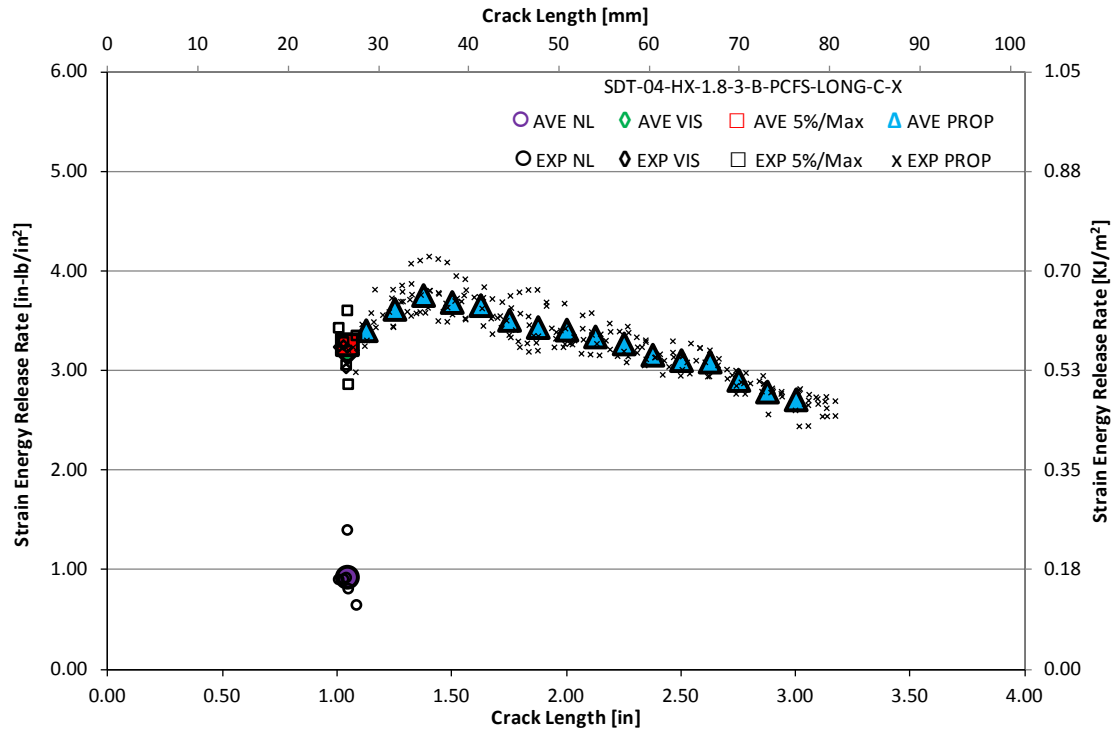

Figure A-20. Resistance curve for HRH-10–1/8–3.0 longitudinal ribbon direction with bottom disbond (center)

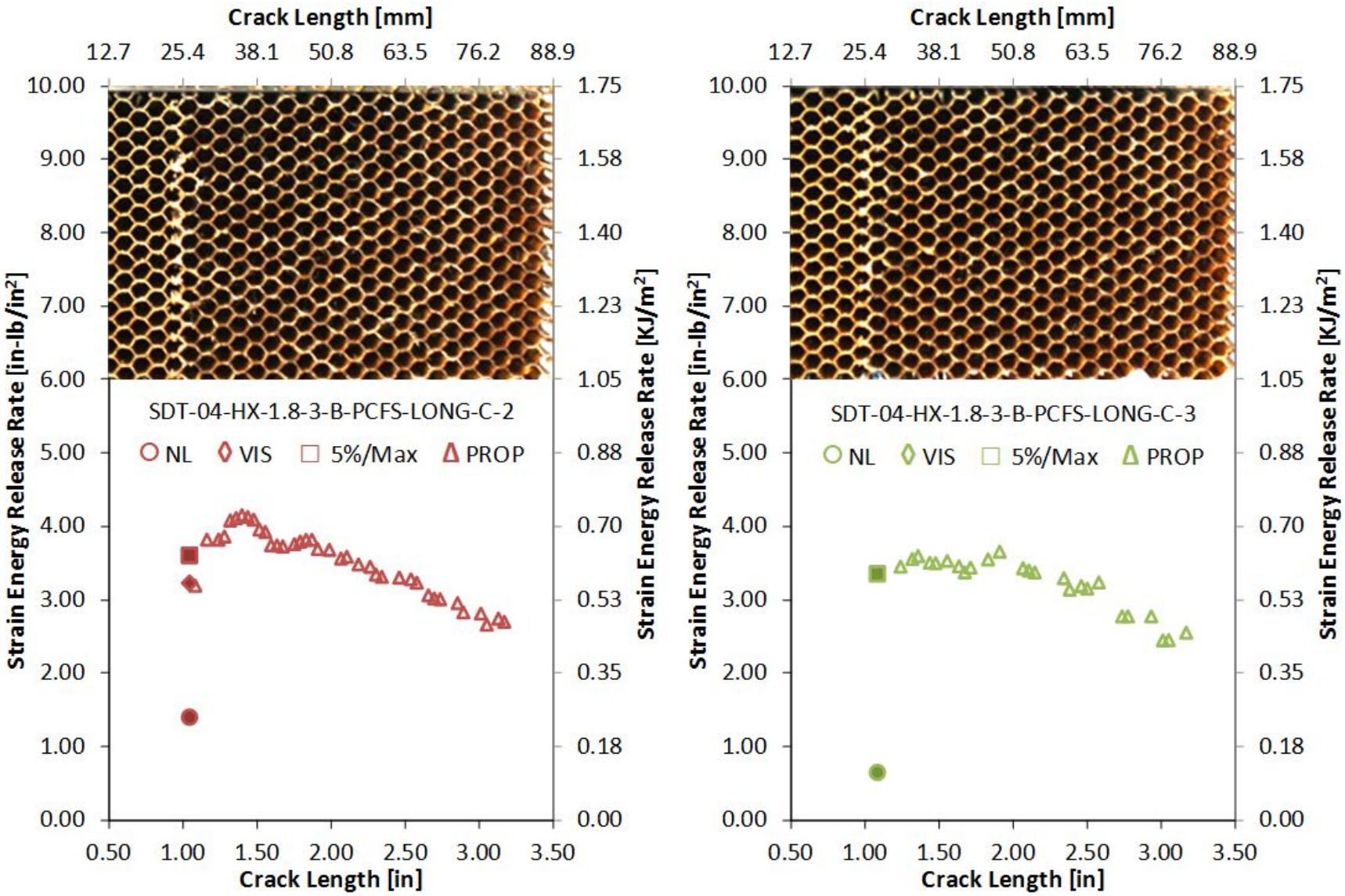

Figure A-21. Failure mode image and resistance curve of SDT-04-HX-1.8-3-B-PCFS-LONG-C-X #2 and #3

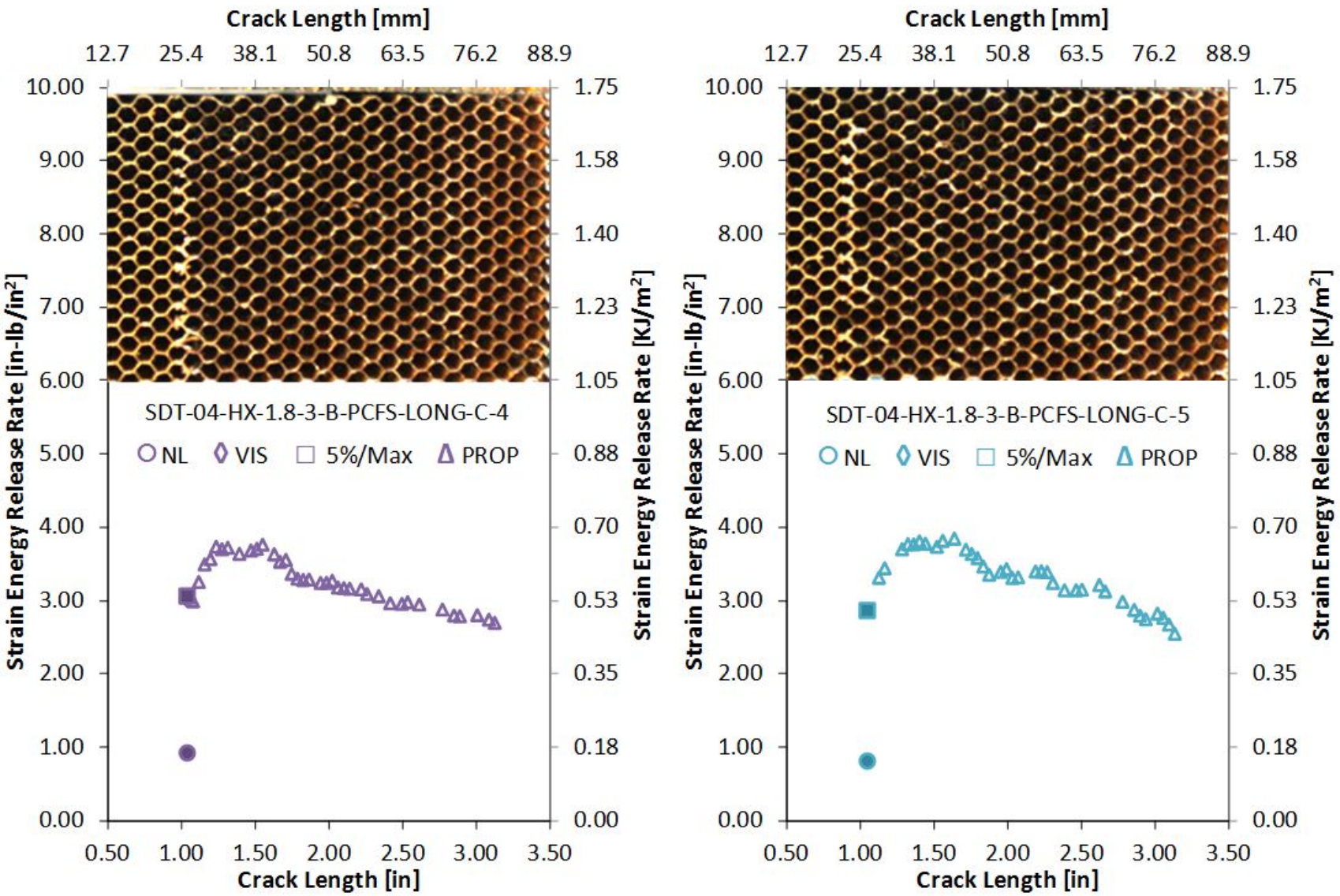

Figure A-22. Failure mode image and resistance curve of SDT-04-HX-1.8-3-B-PCFS-LONG-C-X #4 and #5

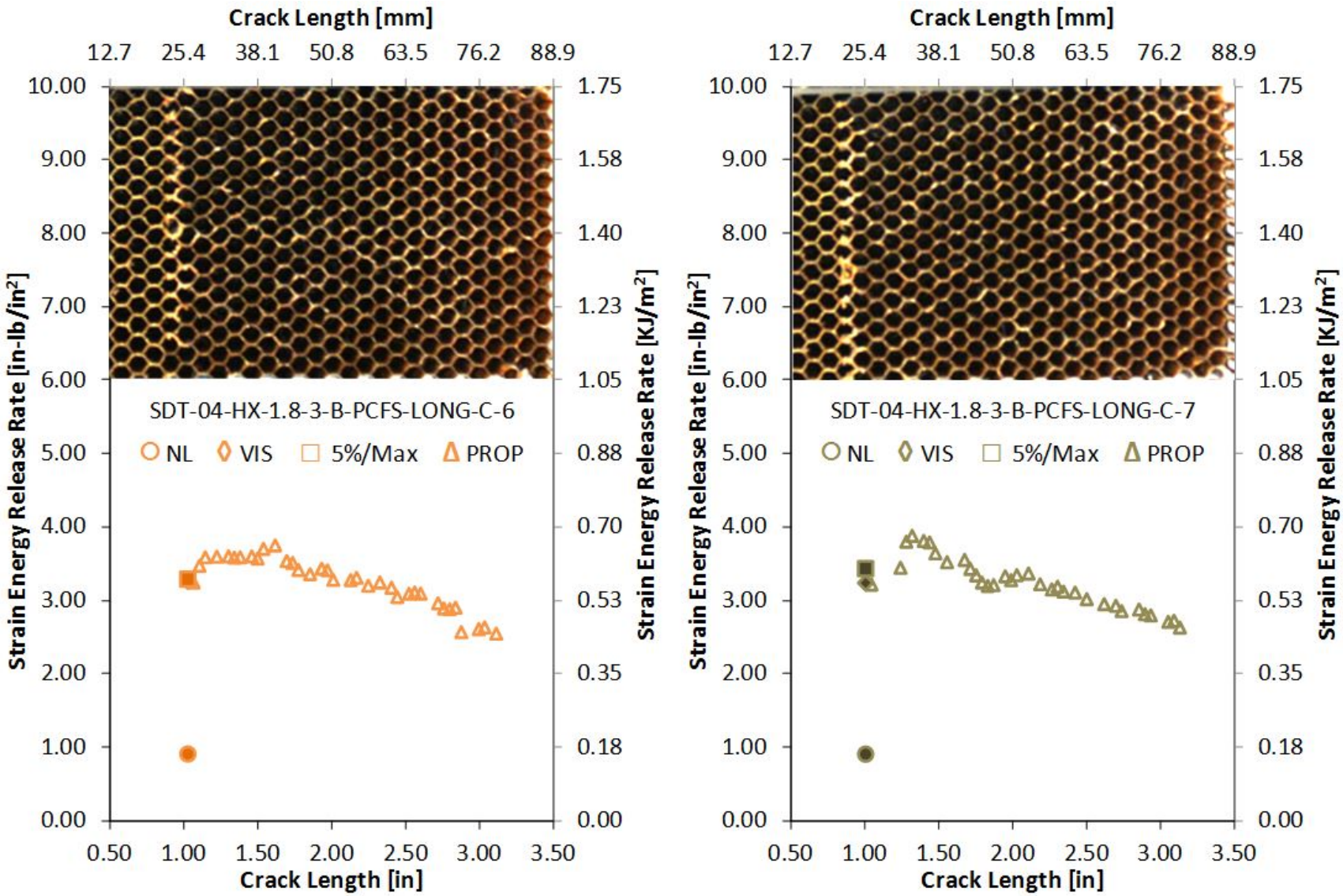

Figure A-23. Failure mode image and resistance curve of SDT-04-HX-1.8-3-B-PCFS-LONG-C-X #6 and #7

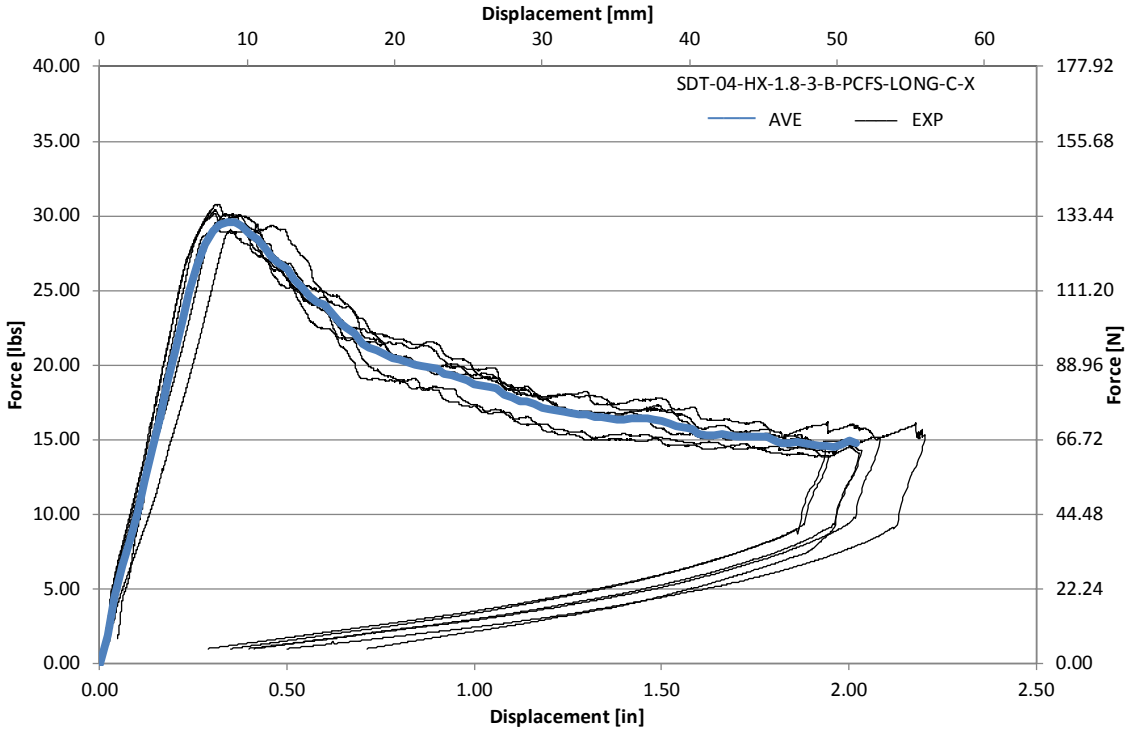

Figure A-24. Load vs. displacement curve for HRH-10–1/8–3.0 longitudinal ribbon direction with bottom disbond (center)

A.2.3 HRH-10–1/8–3.0 LONGITUDINAL RIBBON DIRECTION WITH BOTTOM DISBOND (EDGE) DATA

Table A-9. Test summary for HRH-10–1/8–3.0 longitudinal ribbon direction with bottom disbond (edge) pre-crack

Specimen	GIC (in-lb/in^2)			GIC (KJ/m^2)			Failure Mode
	NL	VIS	5%/max	NL	VIS	5%/max	
SDT-04-HX-1.8-3-B-PCFS-LONG-E-1	1.495	N/A	2.929	0.262	N/A	0.513	Half a cell in A, then C
SDT-04-HX-1.8-3-B-PCFS-LONG-E-2	1.827	N/A	2.956	0.320	N/A	0.518	Half a cell in A, then C
SDT-04-HX-1.8-3-B-PCFS-LONG-E-3	1.572	N/A	2.777	0.275	N/A	0.486	Half a cell in A, then C
SDT-04-HX-1.8-3-B-PCFS-LONG-E-4	1.859	N/A	2.760	0.326	N/A	0.483	Half a cell in A, then C
SDT-04-HX-1.8-3-B-PCFS-LONG-E-5	1.298	2.367	2.422	0.227	0.415	0.424	Half a cell in A, then C
SDT-04-HX-1.8-3-B-PCFS-LONG-E-6	1.201	N/A	2.541	0.210	N/A	0.445	Half a cell in A, then C
SDT-04-HX-1.8-3-B-PCFS-LONG-E-7							
SDT-04-HX-1.8-3-B-PCFS-LONG-E-8							
AVERAGE GIC	1.542	2.367	2.731	0.270	0.415	0.478	
STANDARD DEVIATION	0.269	N/A	0.212	0.047	N/A	0.037	
COEFFICIENT OF VARIATION (%)	17.411	N/A	7.757	17.411	N/A	7.757	

Table A-10. Test summary for HRH-10–1/8–3.0 longitudinal ribbon direction with bottom disbond (edge)

Specimen	GIC (in-lb/in^2)				GIC (KJ/m^2)				Failure Mode
	NL	VIS	5%/max	AREA	NL	VIS	5%/max	AREA	
SDT-04-HX-1.8-3-B-PCFS-LONG-E-1	0.755	2.392	2.516	5.131	0.132	0.419	0.441	0.899	Primarily in C
SDT-04-HX-1.8-3-B-PCFS-LONG-E-2	1.419	N/A	2.246	5.376	0.249	N/A	0.393	0.941	Primarily in C
SDT-04-HX-1.8-3-B-PCFS-LONG-E-3	1.564	2.076	2.164	5.226	0.274	0.364	0.379	0.915	Primarily in C
SDT-04-HX-1.8-3-B-PCFS-LONG-E-4	1.377	N/A	2.802	4.737	0.241	N/A	0.491	0.830	Primarily in C
SDT-04-HX-1.8-3-B-PCFS-LONG-E-5	0.660	2.298	2.316	5.569	0.116	0.402	0.406	0.975	Primarily in C
SDT-04-HX-1.8-3-B-PCFS-LONG-E-6	0.633	N/A	2.666	5.512	0.111	N/A	0.467	0.965	Primarily in C
SDT-04-HX-1.8-3-B-PCFS-LONG-E-7									
SDT-04-HX-1.8-3-B-PCFS-LONG-E-8									
AVERAGE GIC	1.068	2.256	2.452	5.258	0.187	0.395	0.429	0.921	
STANDARD DEVIATION	0.429	0.162	0.251	0.304	0.075	0.028	0.044	0.053	
COEFFICIENT OF VARIATION (%)	40.133	7.199	10.252	5.790	40.133	7.199	10.252	5.790	

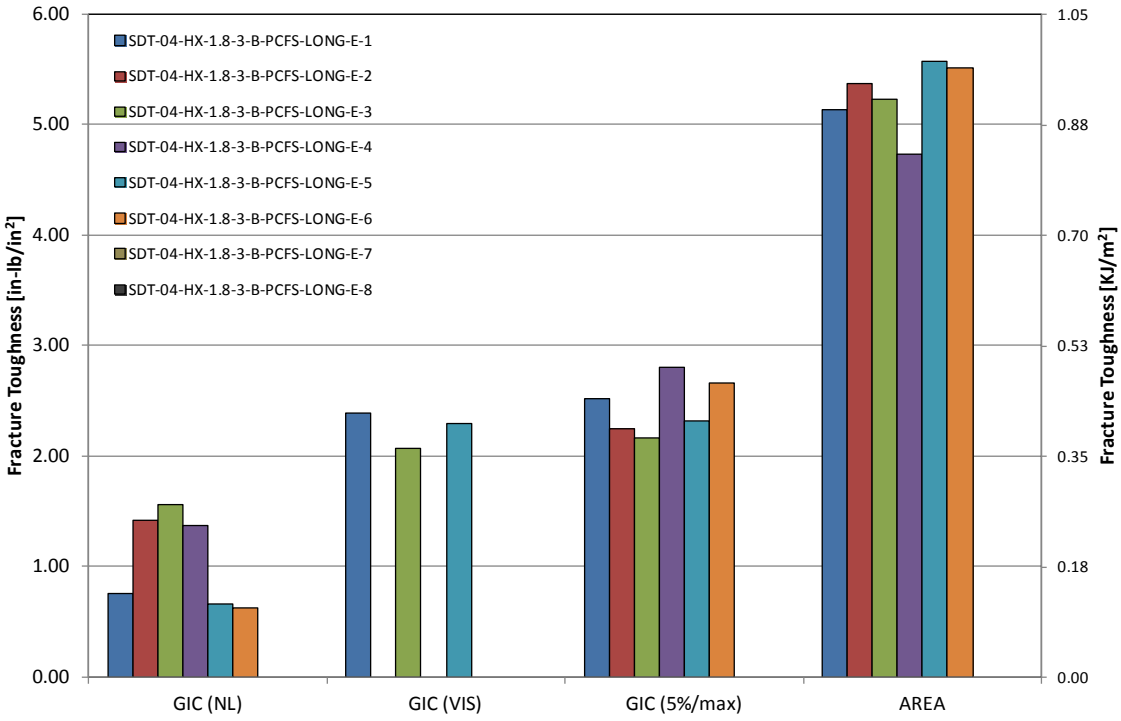

Figure A-25. GIC for HRH-10–1/8–3.0 longitudinal ribbon direction with bottom disbond (edge)

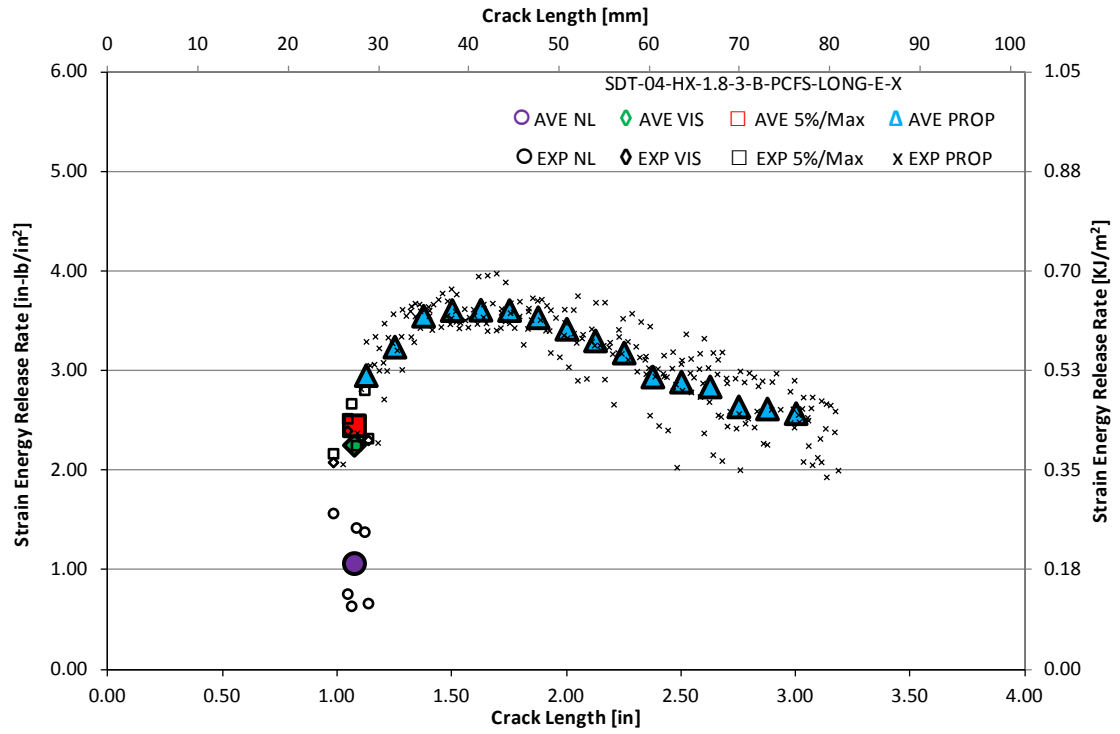

Figure A-26. Resistance curve for HRH-10–1/8–3.0 longitudinal ribbon direction with bottom disbond (edge)

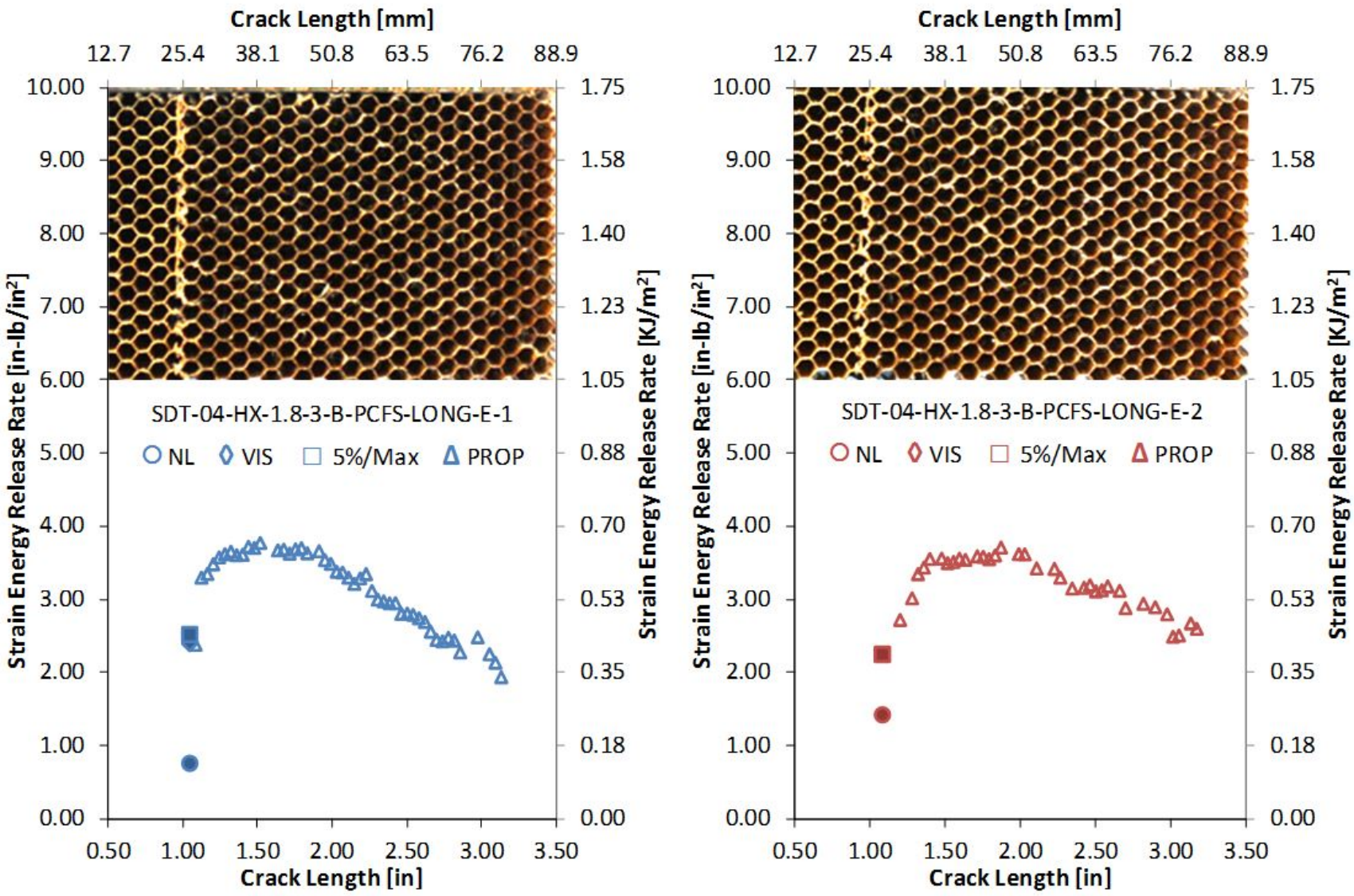

Figure A-27. Failure mode image and resistance curve of SDT-04-HX-1.8-3-B-PCFS-LONG-E-X #1 and #2

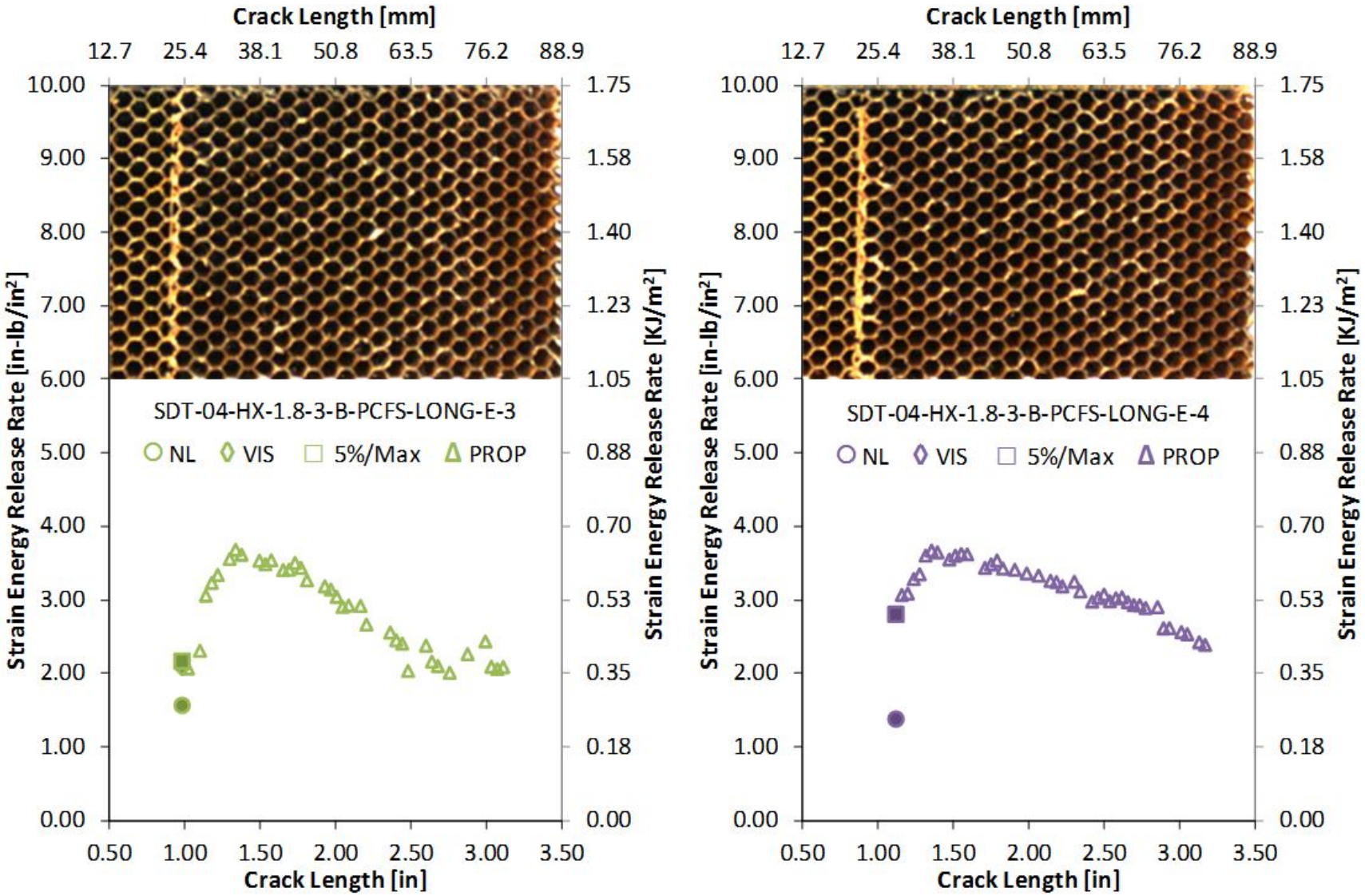

Figure A-28. Failure mode image and resistance curve of SDT-04-HX-1.8-3-B-PCFS-LONG-E-X #3 and #4

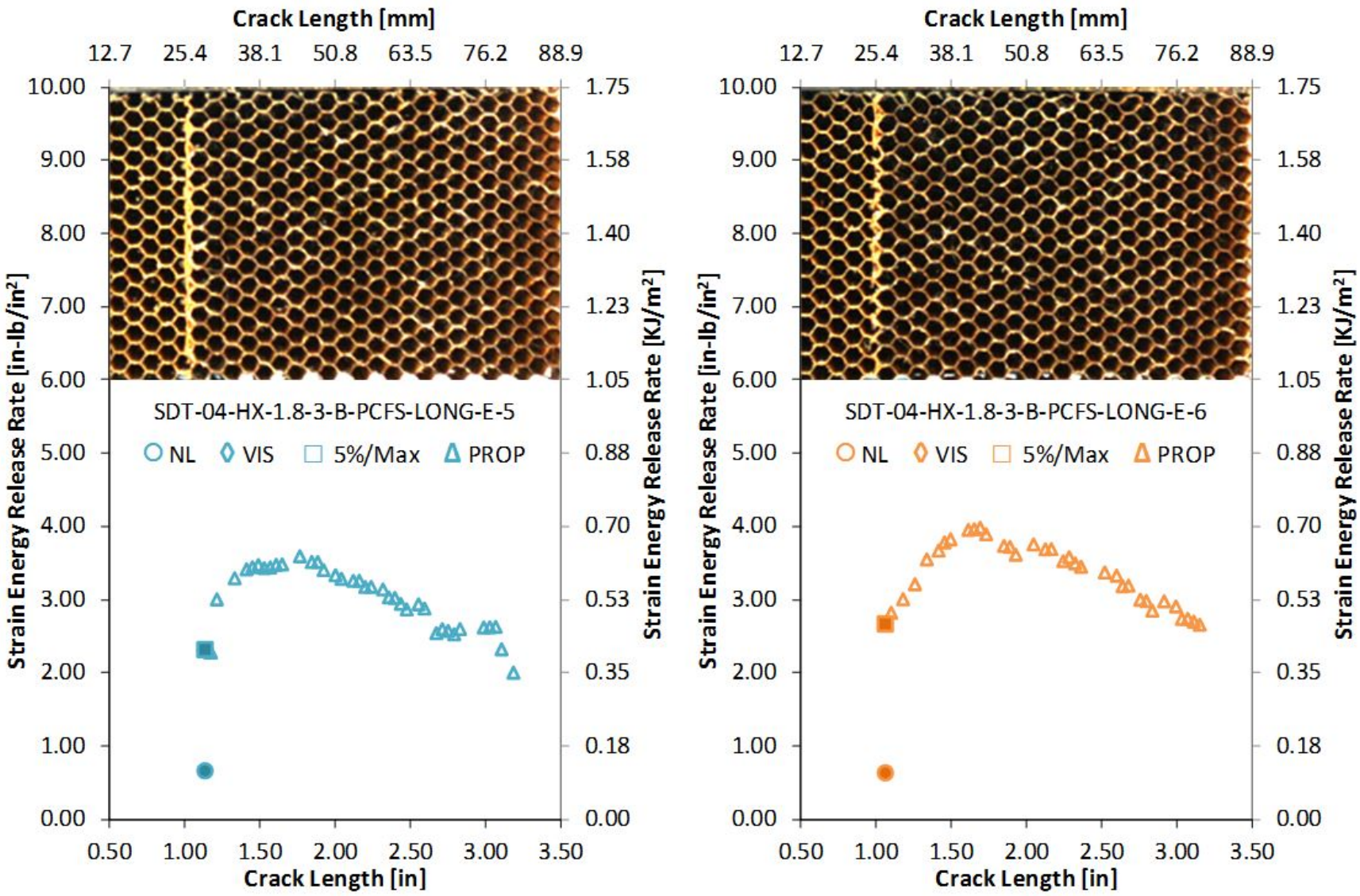

Figure A-29. Failure mode image and resistance curve of SDT-04-HX-1.8-3-B-PCFS-LONG-E-X #5 and #6

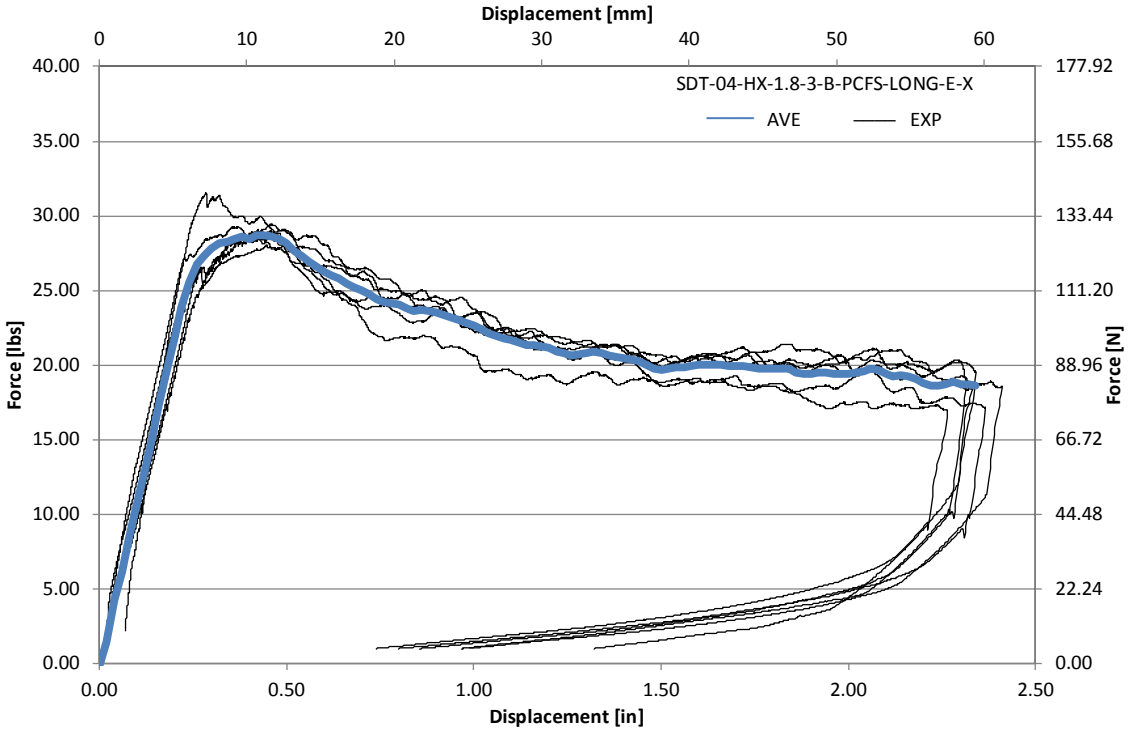

Figure A-30. Load vs. displacement curve for HRH-10–1/8–3.0 longitudinal ribbon direction with bottom disbond (edge)

A.2.4 HRH-10–1/8–3.0 LATERAL RIBBON DIRECTION WITH TOP DISBOND (CENTER) DATA

Table A-11. Test summary for HRH-10–1/8–3.0 lateral ribbon direction with top disbond (center) pre-crack

Specimen	GIC (in-lb/in^2)			GIC (KJ/m^2)			Failure Mode
	NL	VIS	5%/max	NL	VIS	5%/max	
SDT-04-HX-1.8-3-T-PCFS-LAT-C-1							
SDT-04-HX-1.8-3-T-PCFS-LAT-C-2	1.824	N/A	2.643	0.319	N/A	0.463	Primarily C
SDT-04-HX-1.8-3-T-PCFS-LAT-C-3	2.019	N/A	2.695	0.354	N/A	0.472	Primarily C
SDT-04-HX-1.8-3-T-PCFS-LAT-C-4	1.851	N/A	2.793	0.324	N/A	0.489	Primarily C
SDT-04-HX-1.8-3-T-PCFS-LAT-C-5	1.485	N/A	2.669	0.260	N/A	0.467	Primarily C, with a few cells half A
SDT-04-HX-1.8-3-T-PCFS-LAT-C-6	1.477	N/A	2.314	0.259	N/A	0.405	Primarily C, with a couple of cells half A
SDT-04-HX-1.8-3-T-PCFS-LAT-C-7							
SDT-04-HX-1.8-3-T-PCFS-LAT-C-8	1.531	N/A	2.241	0.268	N/A	0.392	Primarily C
AVERAGE GIC	1.698	N/A	2.559	0.297	N/A	0.448	
STANDARD DEVIATION	0.230	N/A	0.225	0.040	N/A	0.039	
COEFFICIENT OF VARIATION (%)	13.558	N/A	8.807	13.558	N/A	8.807	

Table A-12. Test summary for HRH-10–1/8–3.0 lateral ribbon direction with top disbond (center)

Specimen	GIC (in-lb/in^2)				GIC (KJ/m^2)				Failure Mode
	NL	VIS	5%/max	AREA	NL	VIS	5%/max	AREA	
SDT-04-HX-1.8-3-T-PCFS-LAT-C-1									
SDT-04-HX-1.8-3-T-PCFS-LAT-C-2	0.599	2.519	3.257	3.974	0.105	0.441	0.570	0.696	Primarily in C
SDT-04-HX-1.8-3-T-PCFS-LAT-C-3	0.529	2.173	2.332	3.800	0.093	0.381	0.408	0.665	Primarily in C
SDT-04-HX-1.8-3-T-PCFS-LAT-C-4	0.509	N/A	2.296	4.344	0.089	N/A	0.402	0.761	Primarily in C
SDT-04-HX-1.8-3-T-PCFS-LAT-C-5	0.744	2.918	2.937	4.070	0.130	0.511	0.514	0.713	Primarily in C
SDT-04-HX-1.8-3-T-PCFS-LAT-C-6	0.698	2.718	2.727	4.113	0.122	0.476	0.478	0.720	Primarily in C
SDT-04-HX-1.8-3-T-PCFS-LAT-C-7									
SDT-04-HX-1.8-3-T-PCFS-LAT-C-8	0.858	3.052	3.152	3.886	0.150	0.535	0.552	0.681	Primarily in C
AVERAGE GIC	0.656	2.676	2.783	4.031	0.115	0.469	0.487	0.706	
STANDARD DEVIATION	0.135	0.346	0.407	0.192	0.024	0.061	0.071	0.034	
COEFFICIENT OF VARIATION (%)	20.586	12.936	14.618	4.759	20.586	12.936	14.618	4.759	

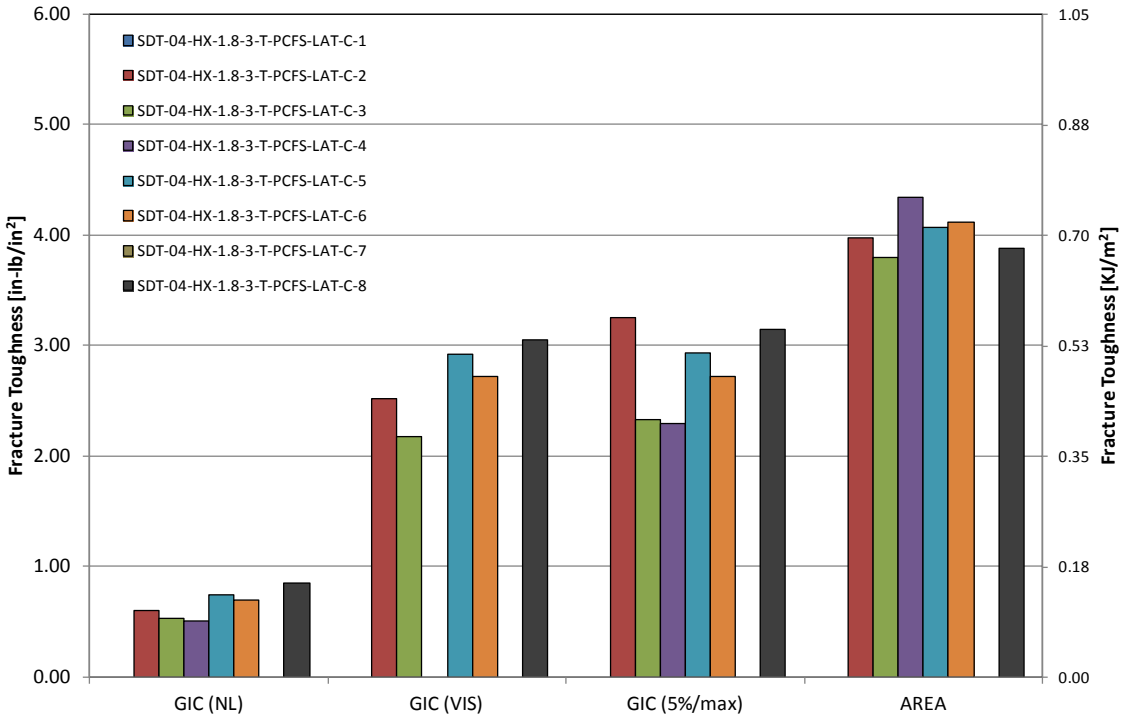

Figure A-31. GIC for HRH-10–1/8–3.0 lateral ribbon direction with top disbond (center)

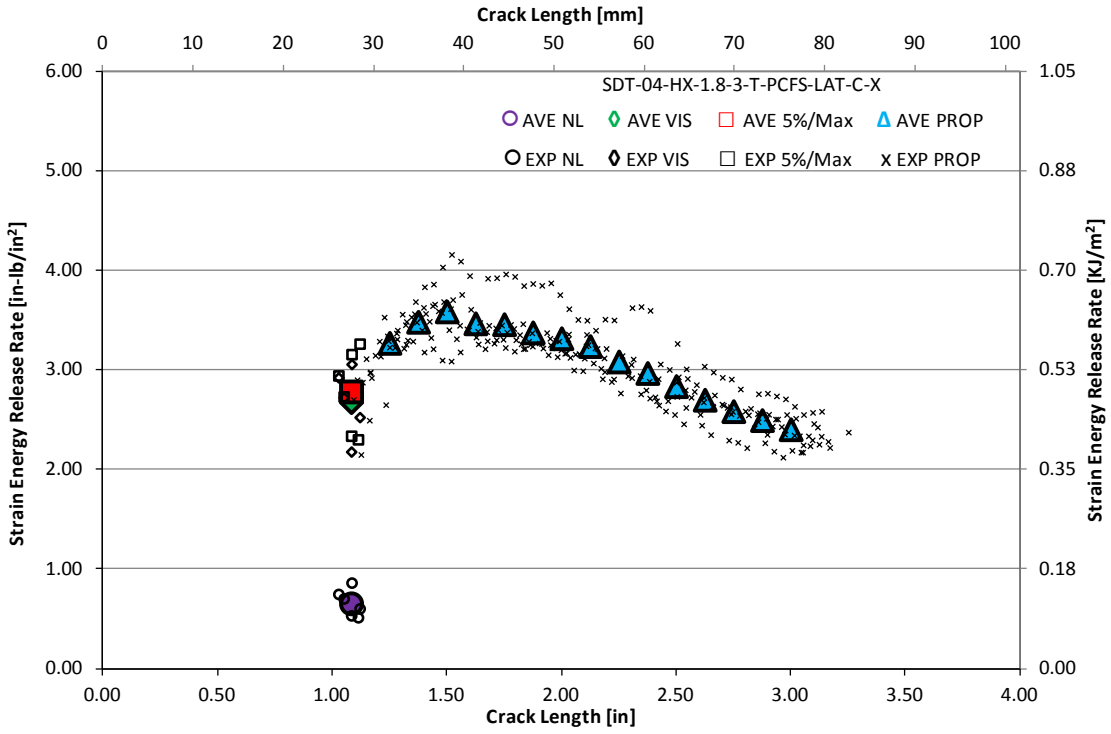

Figure A-32. Resistance curve for HRH-10–1/8–3.0 lateral ribbon direction with top disbond (center)

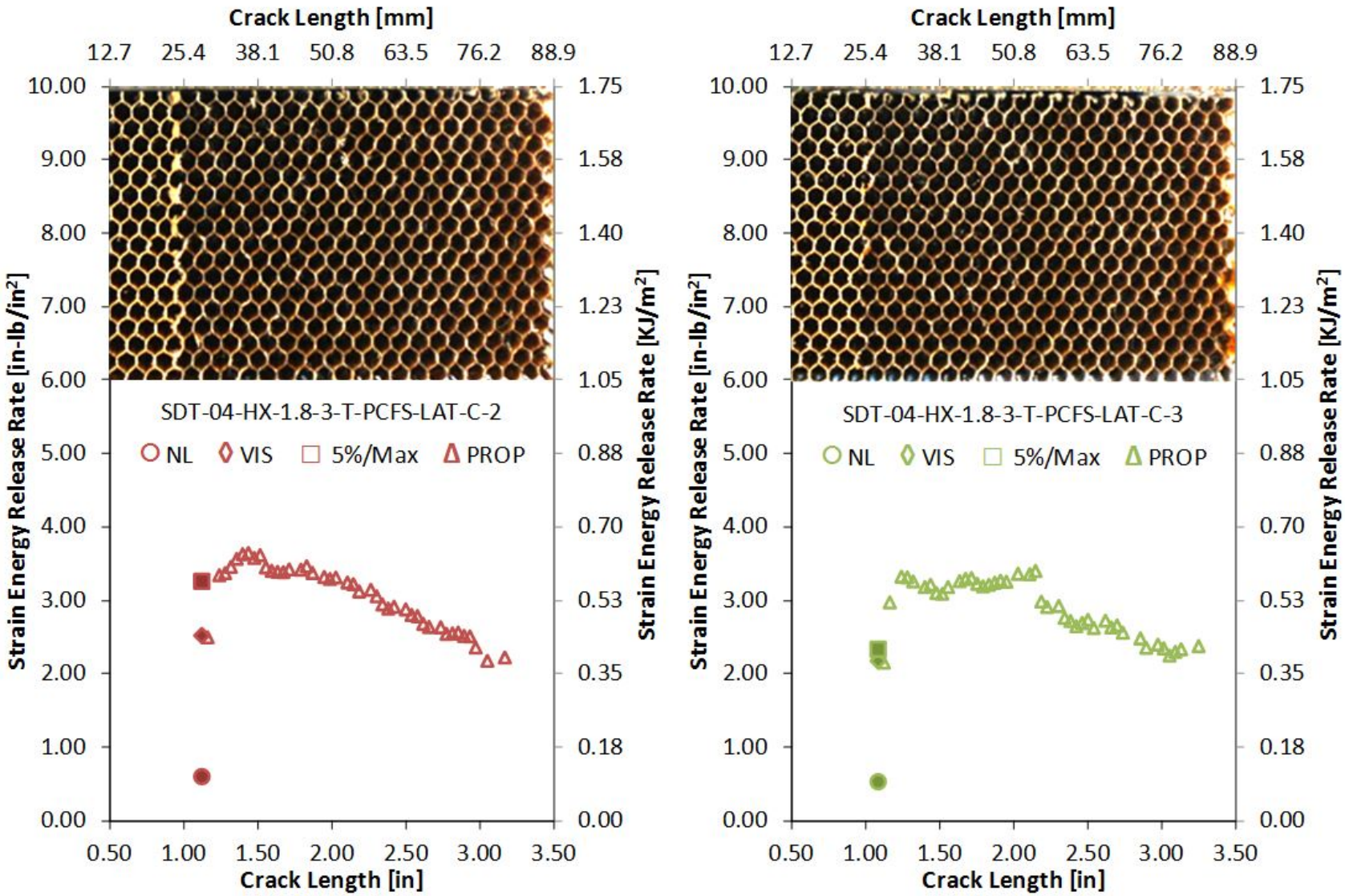

Figure A-33. Failure mode image and resistance curve of SDT-04-HX-1.8-3-T-PCFS-LAT-C-X #2 and #3

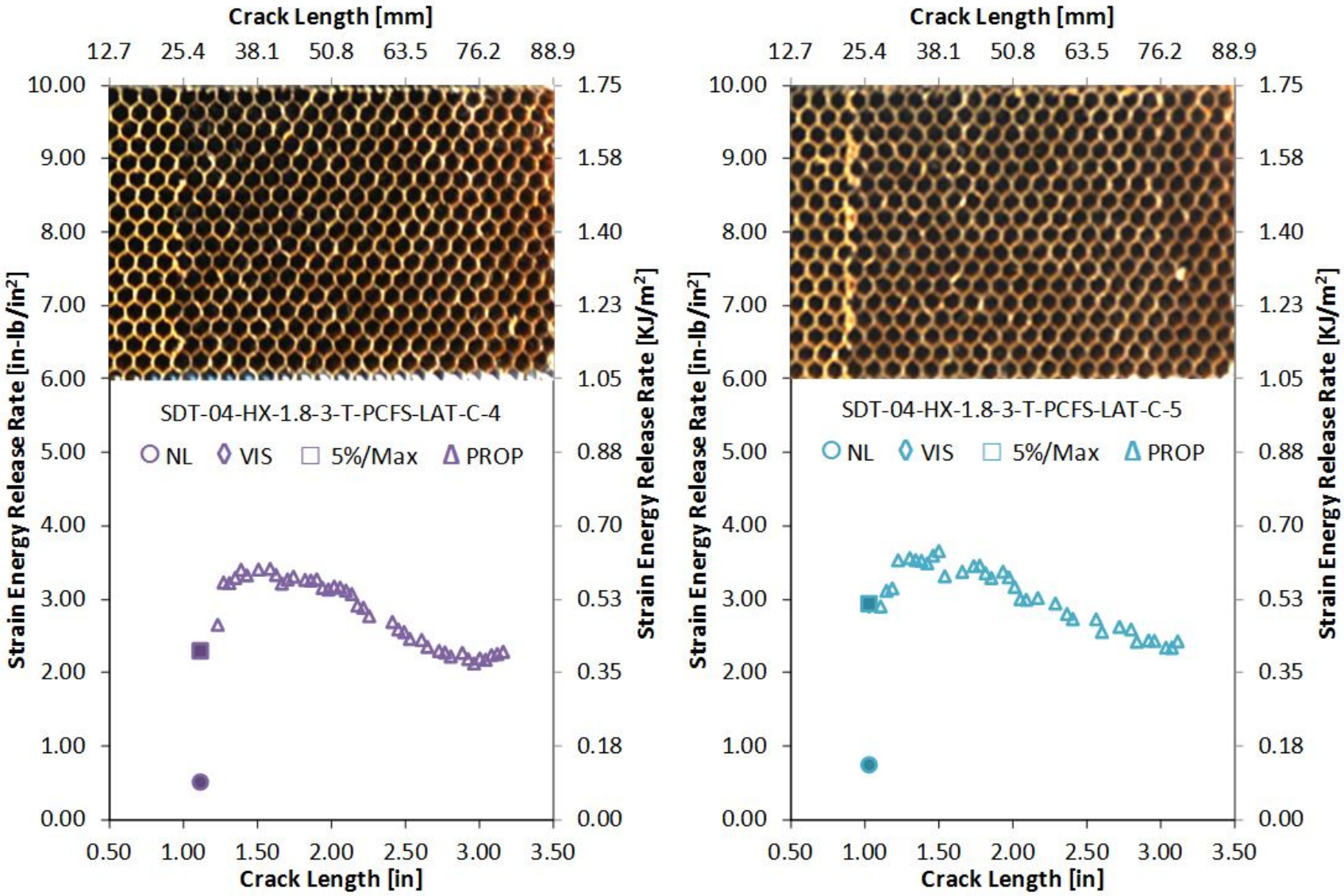

Figure A-34. Failure mode image and resistance curve of SDT-04-HX-1.8-3-T-PCFS-LAT-C-X #4 and #5

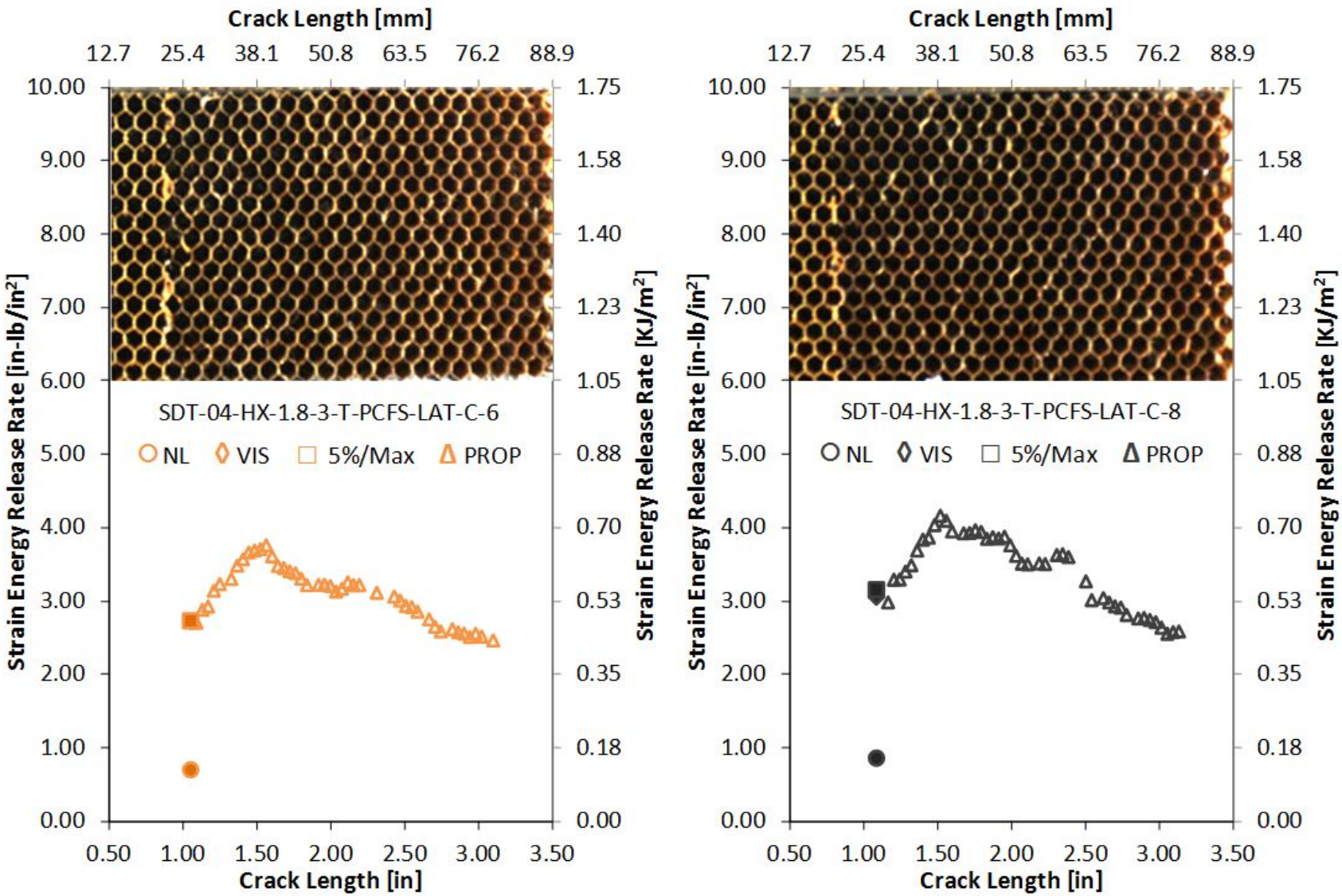

Figure A-35. Failure mode image and resistance curve of SDT-04-HX-1.8-3-T-PCFS-LAT-C-X #6 and #8

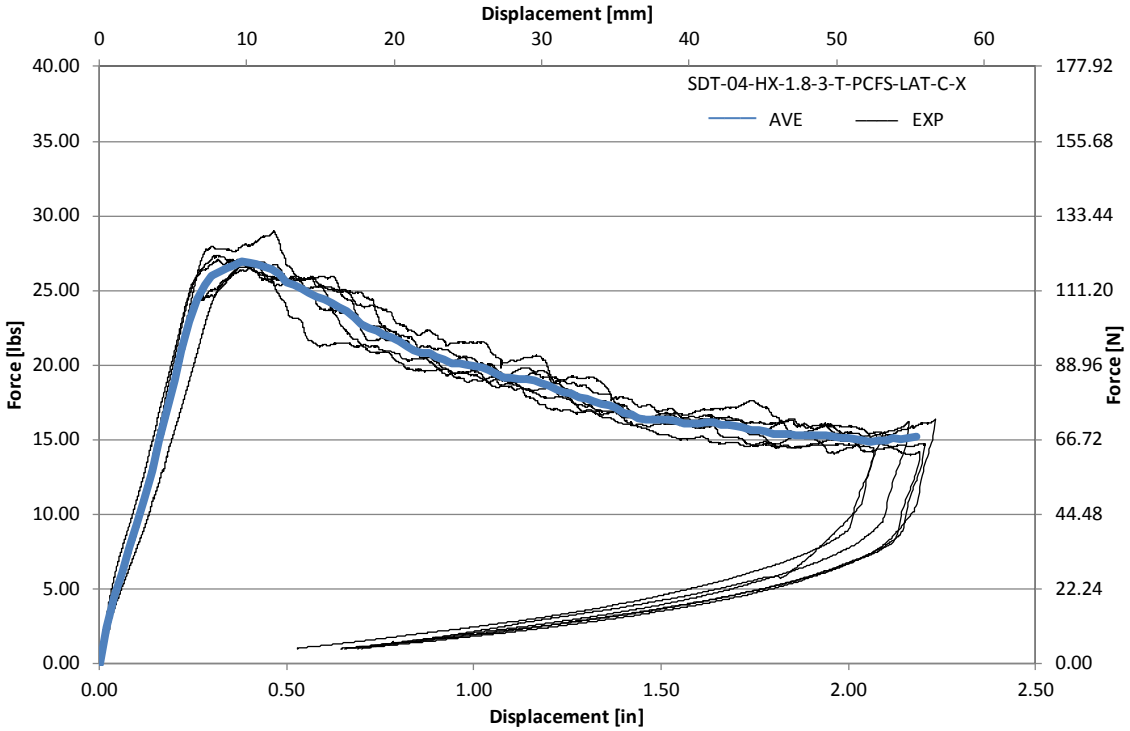

Figure A-36. Load vs. displacement curve for HRH-10–1/8–3.0 lateral ribbon direction with top disbond (center)

A.2.5 HRH-10–1/8–3.0 LATERAL RIBBON DIRECTION WITH A BOTTOM DISBOND (CENTER) DATA

Table A-13. Test summary for HRH-10–1/8–3.0 lateral ribbon direction with bottom disbond (center) pre-crack

Specimen	GIC (in-lb/in^2)			GIC (KJ/m^2)			Failure Mode
	NL	VIS	5%/max	NL	VIS	5%/max	
SDT-04-HX-1.8-3-B-PCFS-LAT-C-1							
SDT-04-HX-1.8-3-B-PCFS-LAT-C-2	1.613	N/A	2.595	0.283	N/A	0.454	Half a cell in A, then C
SDT-04-HX-1.8-3-B-PCFS-LAT-C-3	1.289	N/A	2.424	0.226	N/A	0.425	Primarily C, with several half A
SDT-04-HX-1.8-3-B-PCFS-LAT-C-4	1.250	2.195	2.195	0.219	0.384	0.384	Half a cell in A, then C
SDT-04-HX-1.8-3-B-PCFS-LAT-C-5	1.234	N/A	2.394	0.216	N/A	0.419	Primarily C, with several half A
SDT-04-HX-1.8-3-B-PCFS-LAT-C-6	1.262	N/A	2.265	0.221	N/A	0.397	Primarily C, with a couple of cells half A
SDT-04-HX-1.8-3-B-PCFS-LAT-C-7	1.095	N/A	1.813	0.192	N/A	0.317	Primarily C
SDT-04-HX-1.8-3-B-PCFS-LAT-C-8							
AVERAGE GIC	1.290	2.195	2.281	0.226	0.384	0.399	
STANDARD DEVIATION	0.172	N/A	0.268	0.030	N/A	0.047	
COEFFICIENT OF VARIATION (%)	13.336	N/A	11.743	13.336	N/A	11.743	

Table A-14. Test summary for HRH-10–1/8–3.0 lateral Ribbon direction with bottom disbond (center)

Specimen	GIC (in-lb/in^2)				GIC (KJ/m^2)				Failure Mode
	NL	VIS	5%/max	AREA	NL	VIS	5%/max	AREA	
SDT-04-HX-1.8-3-B-PCFS-LAT-C-1									
SDT-04-HX-1.8-3-B-PCFS-LAT-C-2	0.697	N/A	2.196	4.083	0.122	N/A	0.385	0.715	Primarily in C
SDT-04-HX-1.8-3-B-PCFS-LAT-C-3	0.746	N/A	2.441	4.073	0.131	N/A	0.428	0.713	Primarily in C
SDT-04-HX-1.8-3-B-PCFS-LAT-C-4	0.656	N/A	1.936	3.940	0.115	N/A	0.339	0.690	Primarily in C
SDT-04-HX-1.8-3-B-PCFS-LAT-C-5	0.476	2.304	2.568	4.008	0.083	0.403	0.450	0.702	Primarily in C
SDT-04-HX-1.8-3-B-PCFS-LAT-C-6	0.383	N/A	2.371	4.161	0.067	N/A	0.415	0.729	Primarily in C
SDT-04-HX-1.8-3-B-PCFS-LAT-C-7	0.529	N/A	1.986	4.073	0.093	N/A	0.348	0.713	Primarily in C
SDT-04-HX-1.8-3-B-PCFS-LAT-C-8									
AVERAGE GIC	0.581	2.304	2.250	4.056	0.102	0.403	0.394	0.710	
STANDARD DEVIATION	0.141	N/A	0.254	0.075	0.025	N/A	0.045	0.013	
COEFFICIENT OF VARIATION (%)	24.247	N/A	11.310	1.846	24.247	N/A	11.310	1.846	

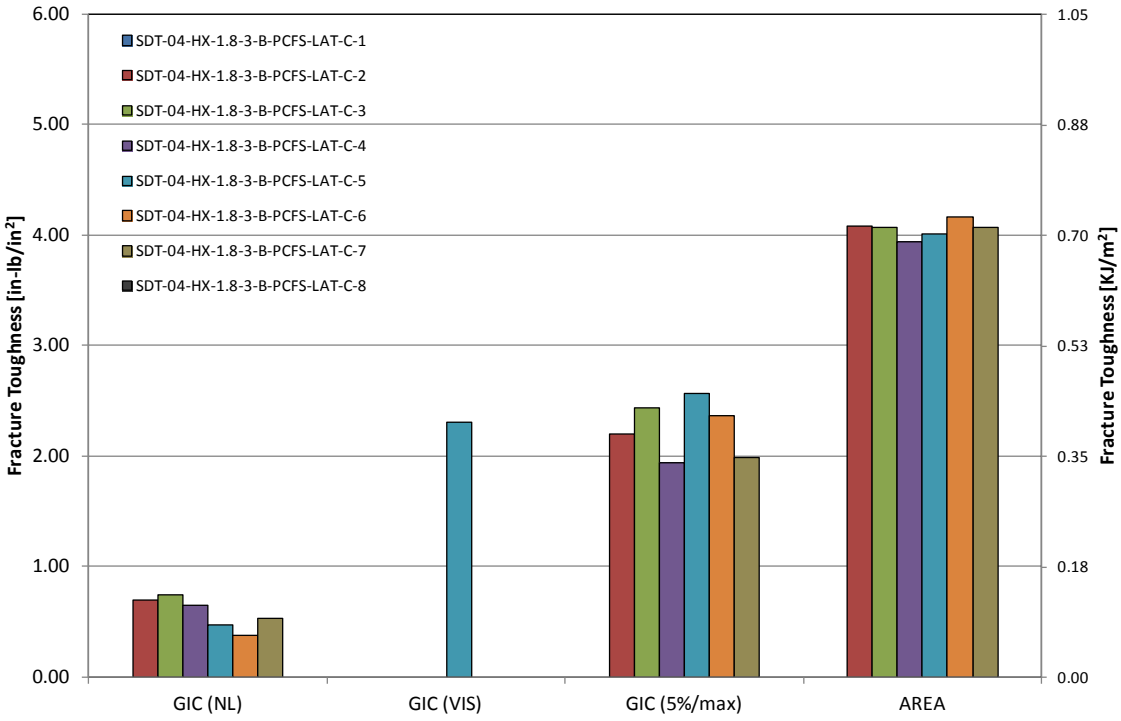

Figure A-37. GIC for HRH-10–1/8–3.0 lateral ribbon direction with bottom disbond (center)

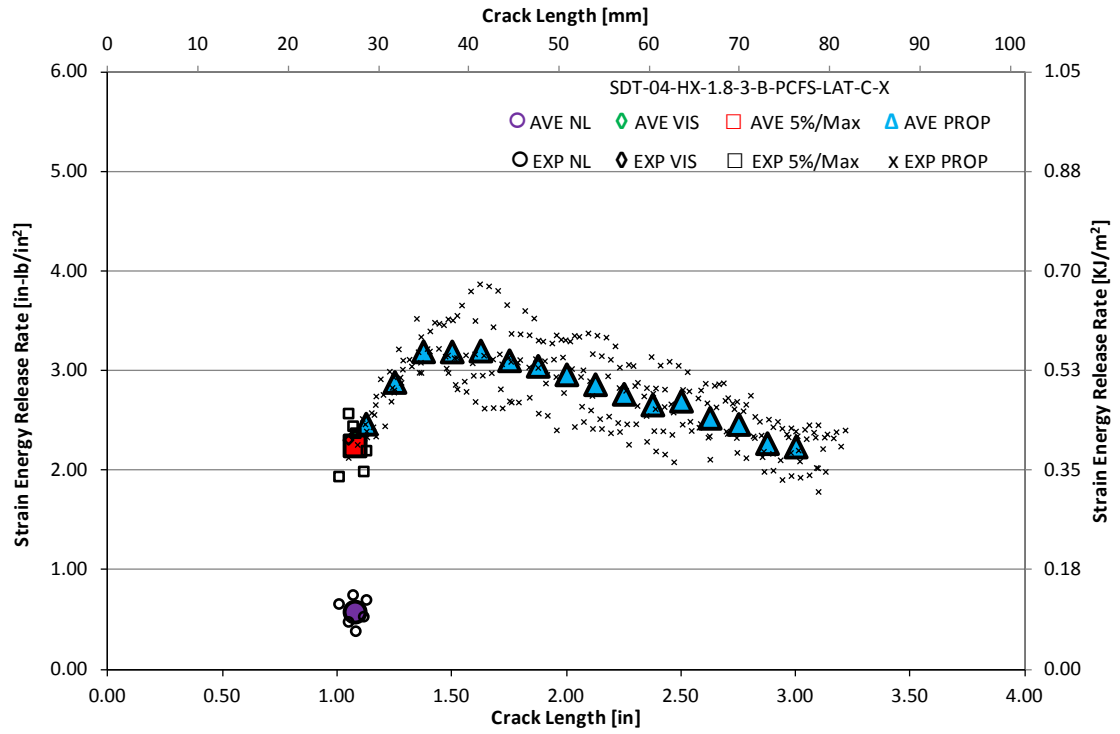

Figure A-38. Resistance curve for HRH-10–1/8–3.0 lateral ribbon direction with bottom disbond (center)

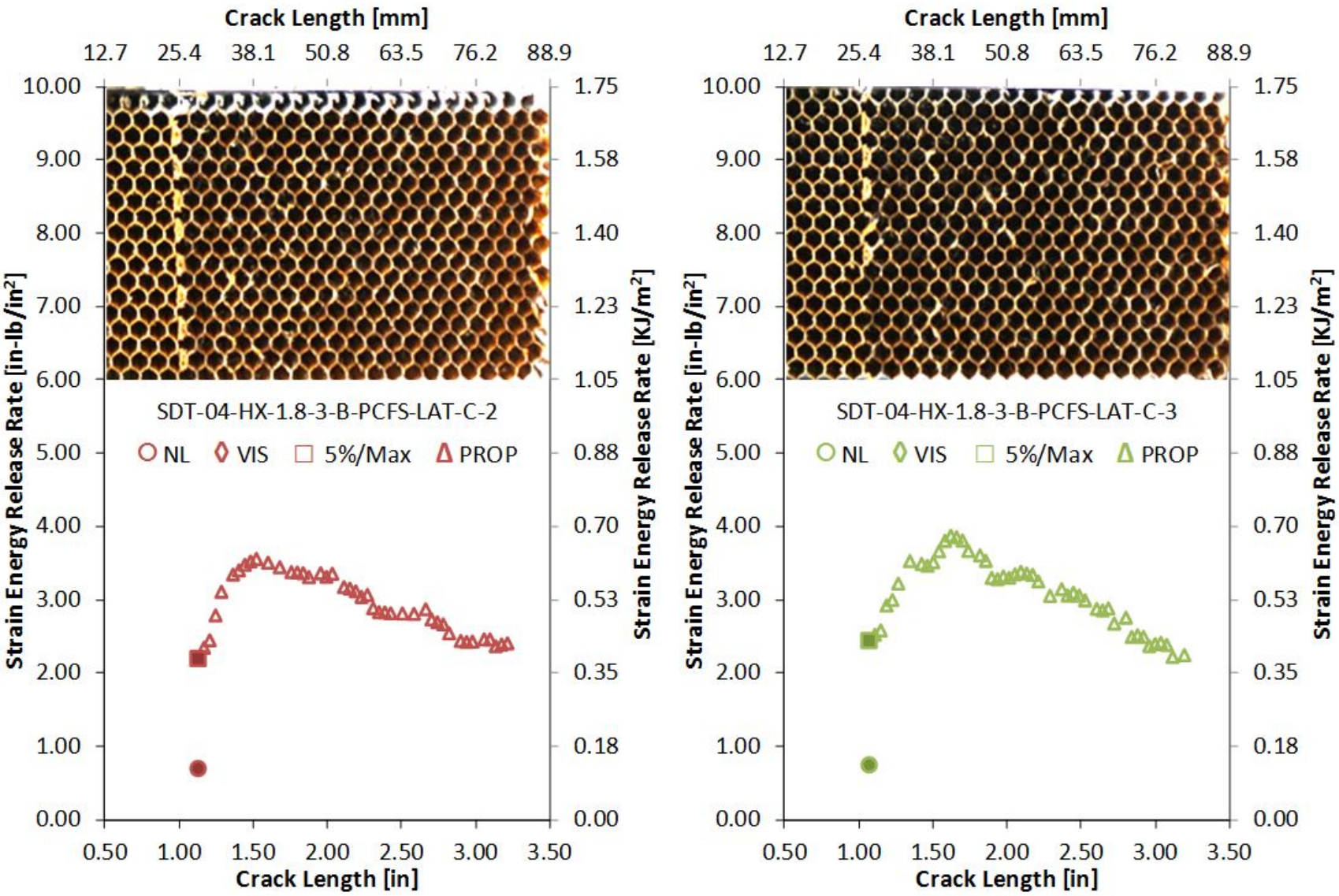

Figure A-39. Failure mode image and resistance curve of SDT-04-HX-1.8-3-B-PCFS-LAT-C-X #2 and #3

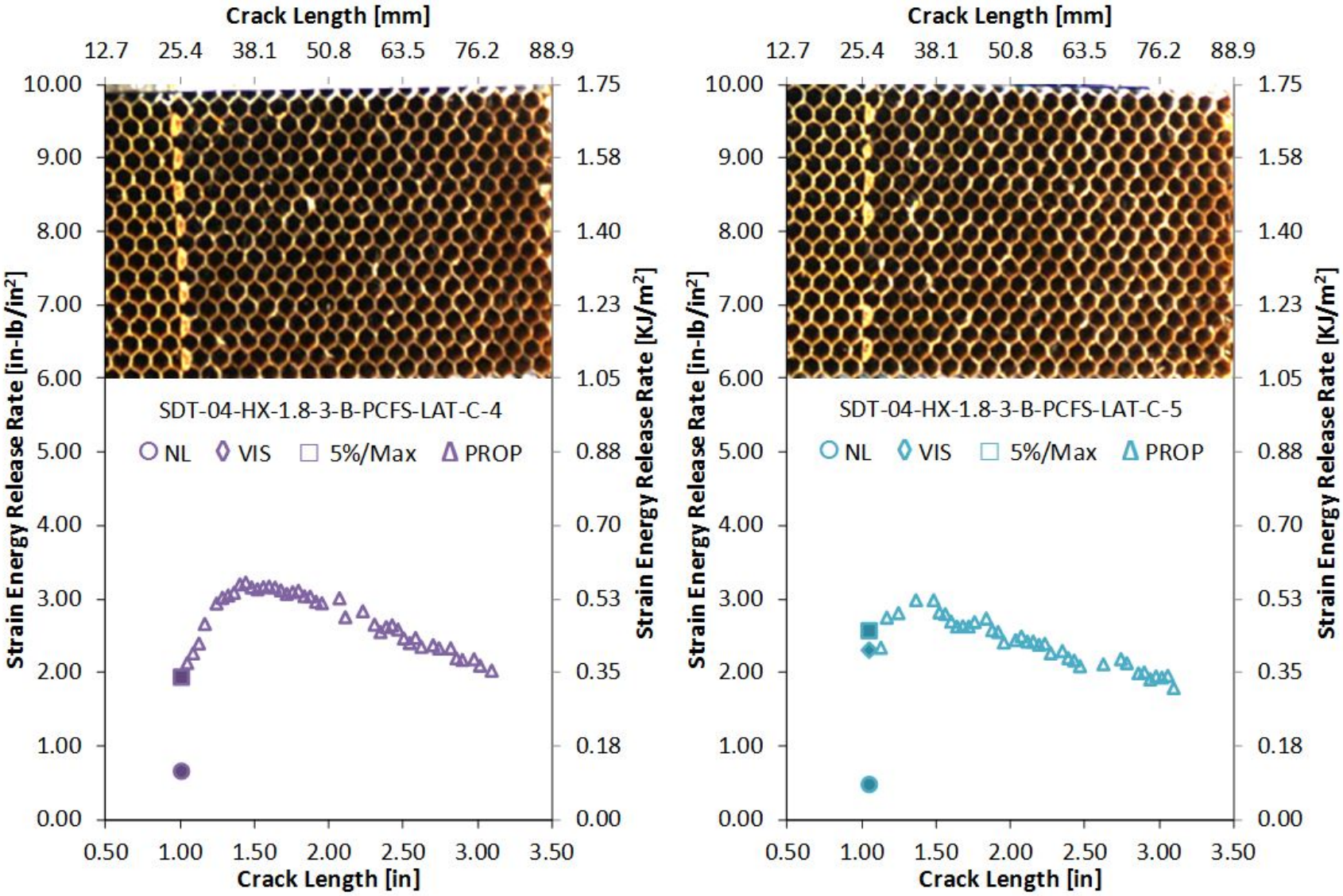

Figure A-40. Failure mode image and resistance curve of SDT-04-HX-1.8-3-B-PCFS-LAT-C-X #4 and #5

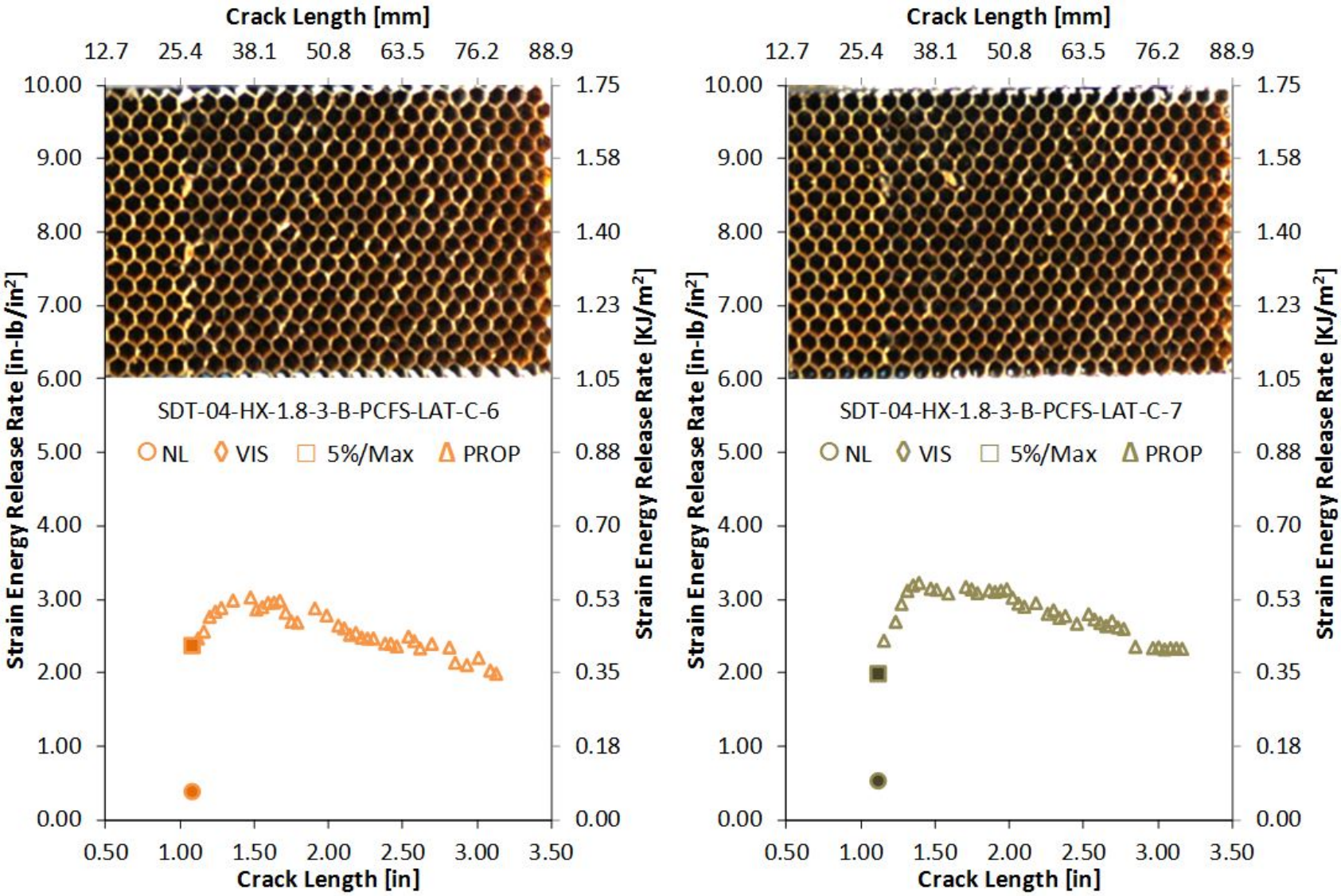

Figure A-41. Failure mode image and resistance curve of SDT-04-HX-1.8-3-B-PCFS-LAT-C-X #6 and #7

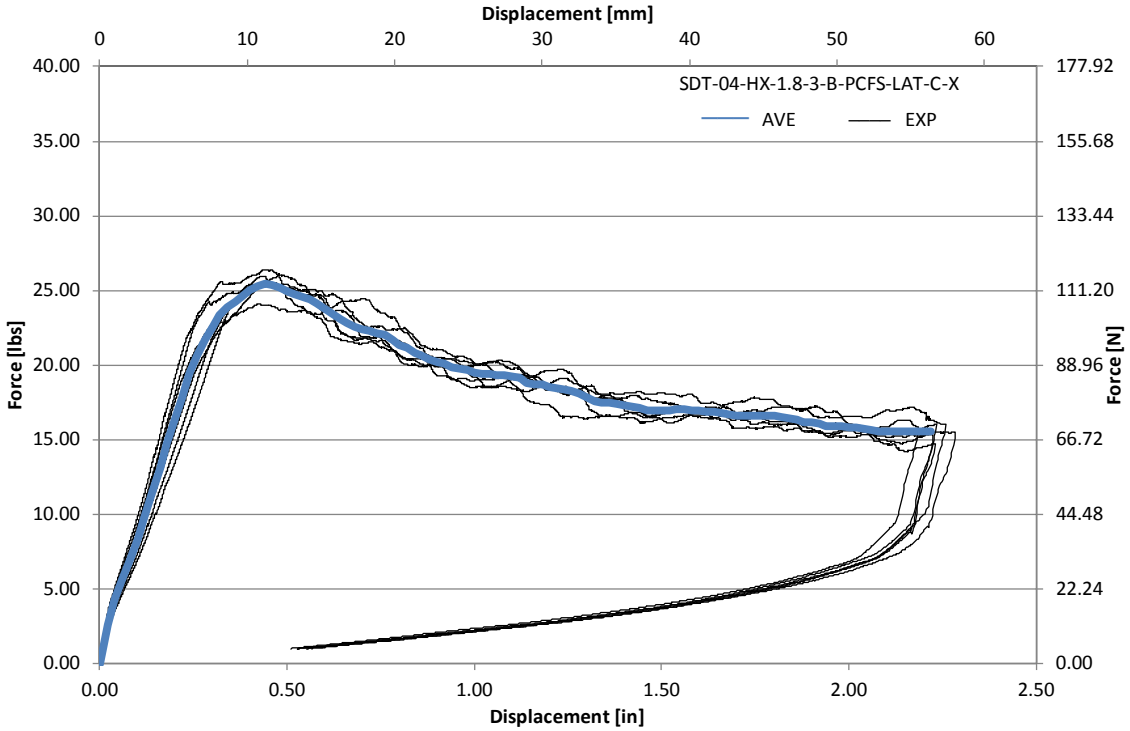

Figure A-42. Load vs. displacement curve for HRH-10–1/8–3.0 lateral ribbon direction with bottom disbond (center)

A.2.6 HRH-10–1/8–3.0 LATERAL RIBBON DIRECTION WITH BOTTOM DISBOND (EDGE) DATA

Table A-15. Test summary for HRH-10–1/8–3.0 lateral ribbon direction with bottom disbond (edge) pre-crack

Specimen	GIC (in-lb/in^2)			GIC (KJ/m^2)			Failure Mode
	NL	VIS	5%/max	NL	VIS	5%/max	
SDT-04-HX-1.8-3-B-PCFS-LAT-E-1	0.942	N/A	2.492	0.165	N/A	0.436	Primarily C
SDT-04-HX-1.8-3-B-PCFS-LAT-E-2	0.959	N/A	2.031	0.168	N/A	0.356	Primarily C
SDT-04-HX-1.8-3-B-PCFS-LAT-E-3	1.559	N/A	2.816	0.273	N/A	0.493	Primarily C
SDT-04-HX-1.8-3-B-PCFS-LAT-E-4							
SDT-04-HX-1.8-3-B-PCFS-LAT-E-5							
SDT-04-HX-1.8-3-B-PCFS-LAT-E-6	1.725	N/A	2.637	0.302	N/A	0.462	Primarily C, with a couple of cells half A
SDT-04-HX-1.8-3-B-PCFS-LAT-E-7	0.705	3.152	3.200	0.123	0.552	0.560	Primarily C, with a couple of cells half A
SDT-04-HX-1.8-3-B-PCFS-LAT-E-8	1.413	N/A	2.286	0.247	N/A	0.400	Primarily C, with a couple of cells half A
AVERAGE GIC	1.217	3.152	2.577	0.213	0.552	0.451	
STANDARD DEVIATION	0.405	N/A	0.410	0.071	N/A	0.072	
COEFFICIENT OF VARIATION (%)	33.242	N/A	15.892	33.242	N/A	15.892	

Table A-16. Test summary for HRH-10–1/8–3.0 lateral ribbon direction with bottom disbond (edge)

Specimen	GIC (in-lb/in^2)				GIC (KJ/m^2)				Failure Mode
	NL	VIS	5%/max	AREA	NL	VIS	5%/max	AREA	
SDT-04-HX-1.8-3-B-PCFS-LAT-E-1	0.778	2.923	2.978	4.029	0.136	0.512	0.522	0.706	Primarily in C
SDT-04-HX-1.8-3-B-PCFS-LAT-E-2	0.902	2.496	2.649	4.123	0.158	0.437	0.464	0.722	Primarily in C
SDT-04-HX-1.8-3-B-PCFS-LAT-E-3	1.055	2.236	2.340	4.284	0.185	0.392	0.410	0.750	Primarily in C
SDT-04-HX-1.8-3-B-PCFS-LAT-E-4									
SDT-04-HX-1.8-3-B-PCFS-LAT-E-5									
SDT-04-HX-1.8-3-B-PCFS-LAT-E-6	0.801	N/A	2.044	4.473	0.140	N/A	0.358	0.783	Primarily in C
SDT-04-HX-1.8-3-B-PCFS-LAT-E-7	0.427	N/A	1.919	4.322	0.075	N/A	0.336	0.757	Primarily in C
SDT-04-HX-1.8-3-B-PCFS-LAT-E-8	0.817	N/A	2.378	4.132	0.143	N/A	0.416	0.724	Primarily in C
AVERAGE GIC	0.797	2.552	2.385	4.227	0.140	0.447	0.418	0.740	
STANDARD DEVIATION	0.208	0.347	0.389	0.162	0.036	0.061	0.068	0.028	
COEFFICIENT OF VARIATION (%)	26.065	13.606	16.314	3.842	26.065	13.606	16.314	3.842	

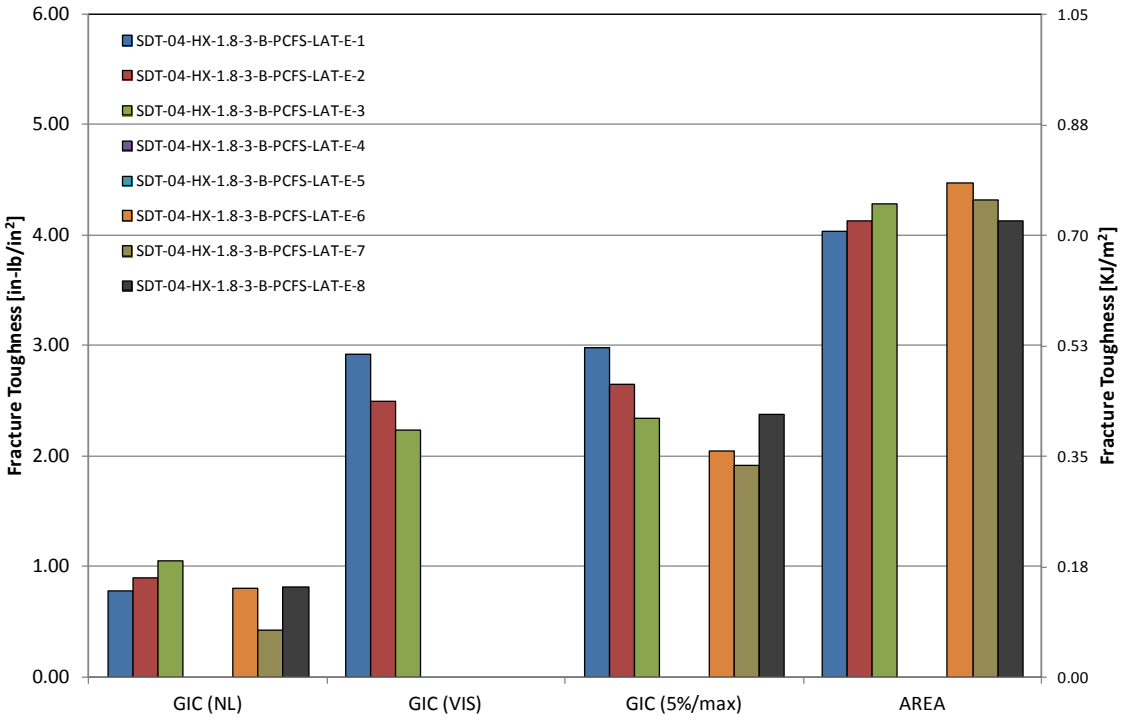

Figure A-43. GIC for HRH-10–1/8–3.0 lateral ribbon direction with bottom disbond (edge)

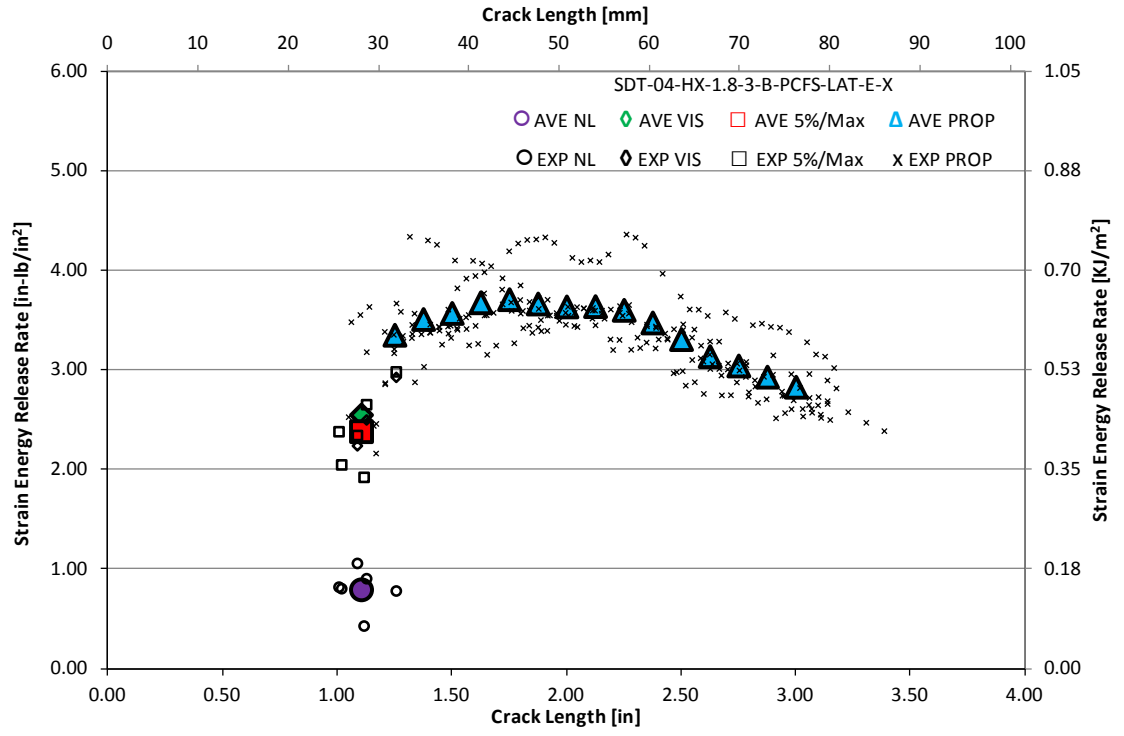

Figure A-44. Resistance curve for HRH-10–1/8–3.0 lateral ribbon direction with bottom disbond (edge)

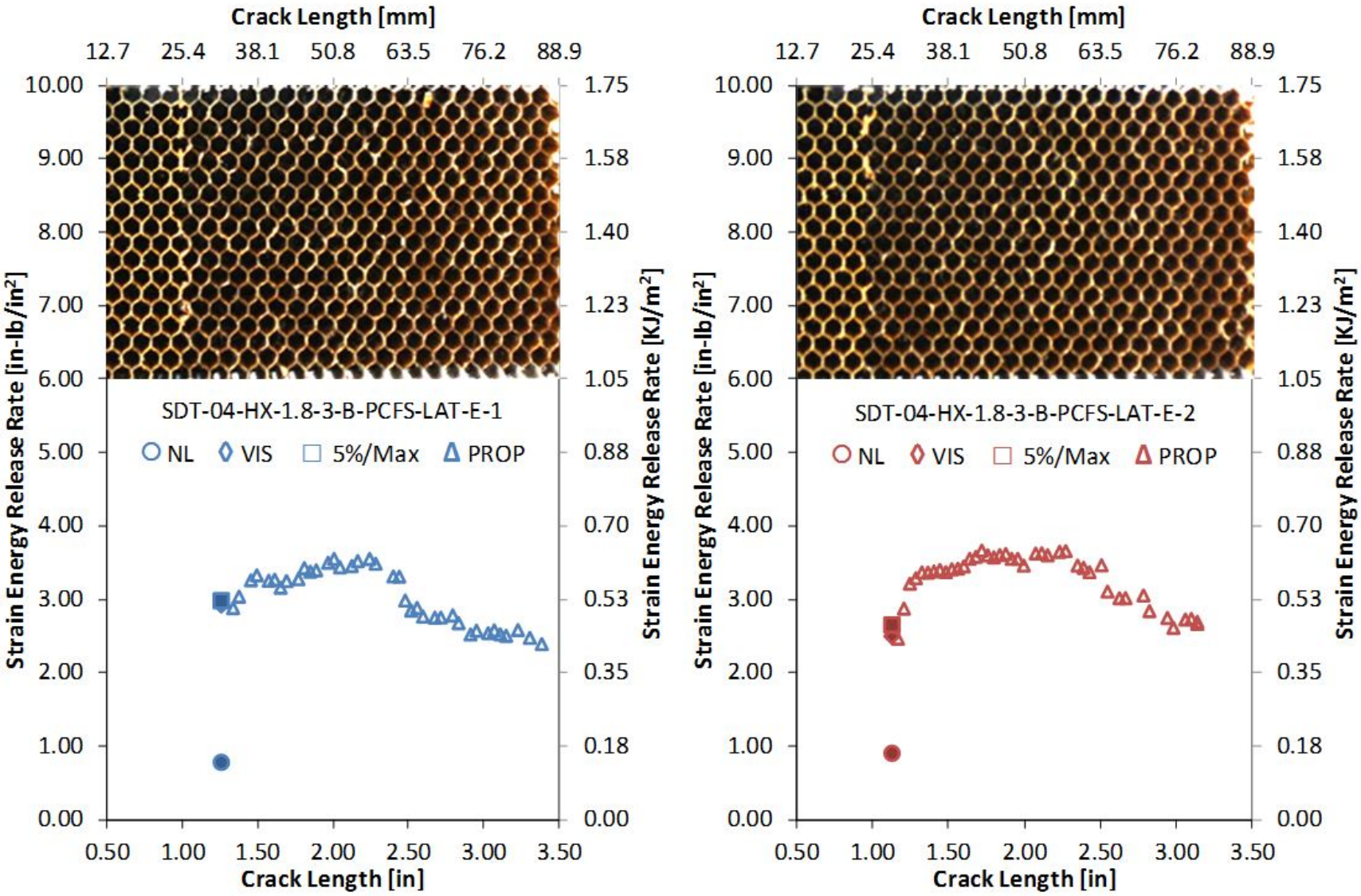

Figure A-45. Failure mode image and resistance curve of SDT-04-HX-1.8-3-B-PCFS-LAT-E-X #1 and #2

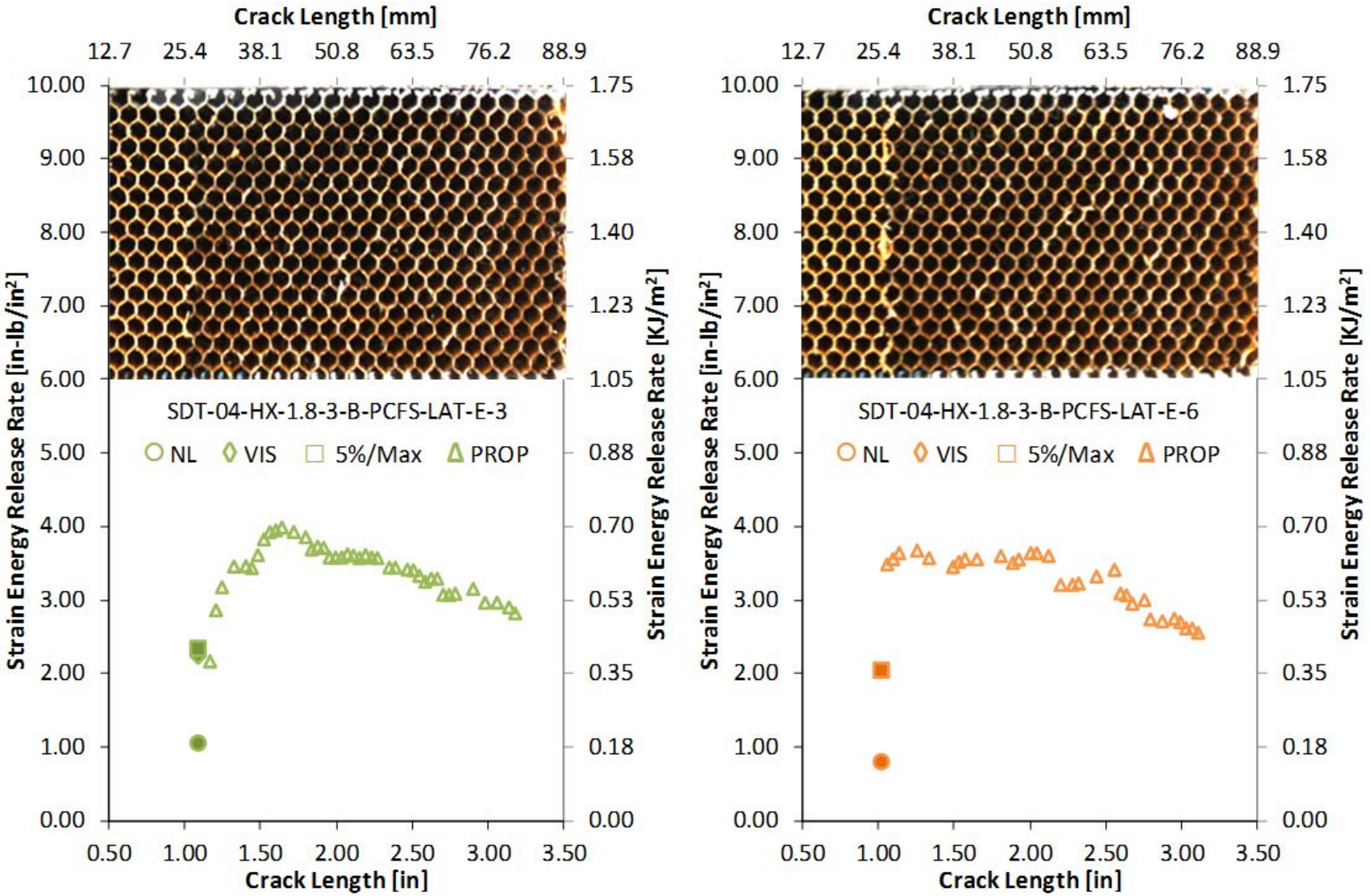

Figure A-46. Failure mode image and resistance curve of SDT-04-HX-1.8-3-B-PCFS-LAT-E-X #3 and #6

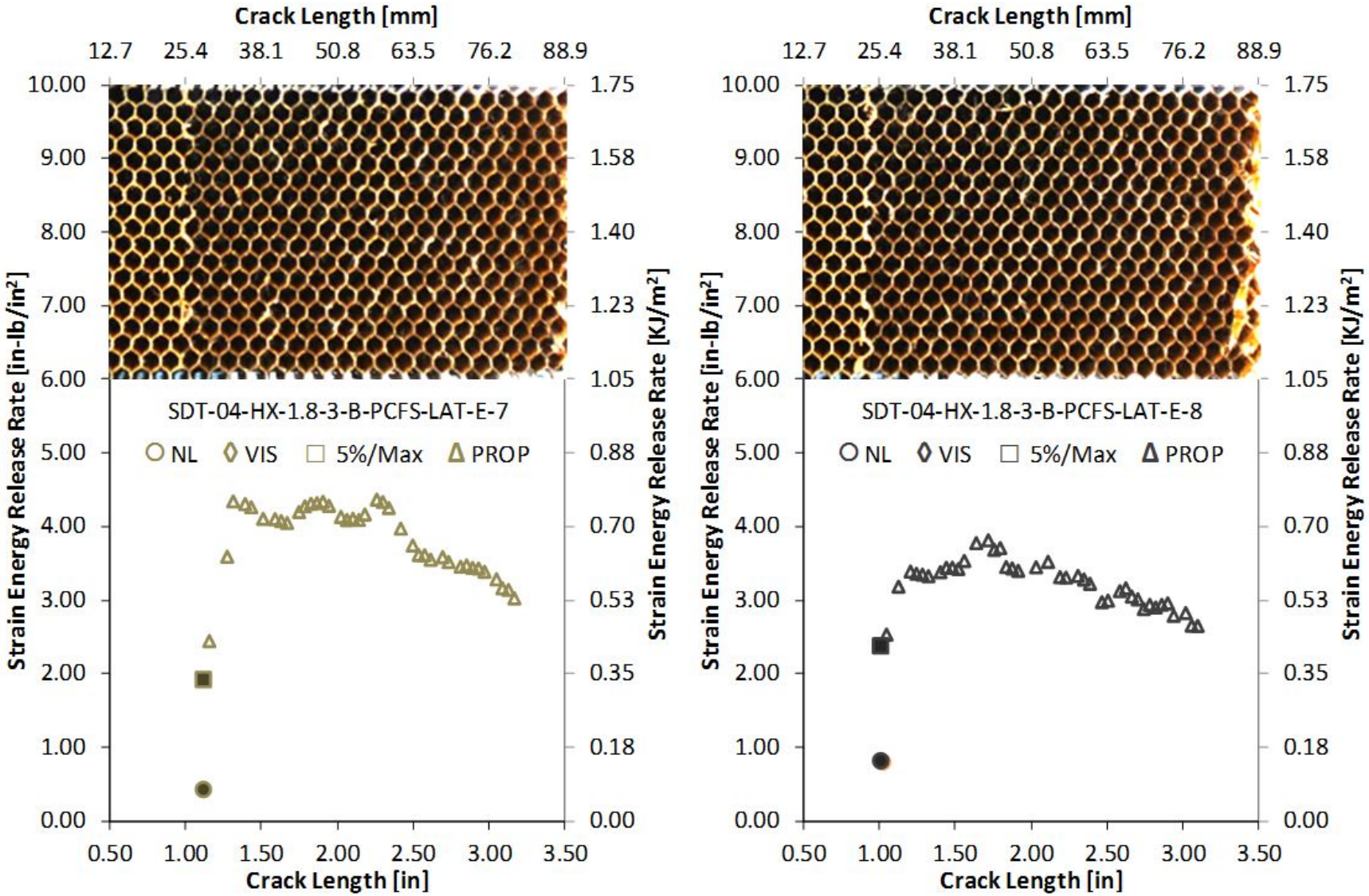

Figure A-47. Failure mode image and resistance curve of SDT-04-HX-1.8-3-B-PCFS-LAT-E-X #7 and #8

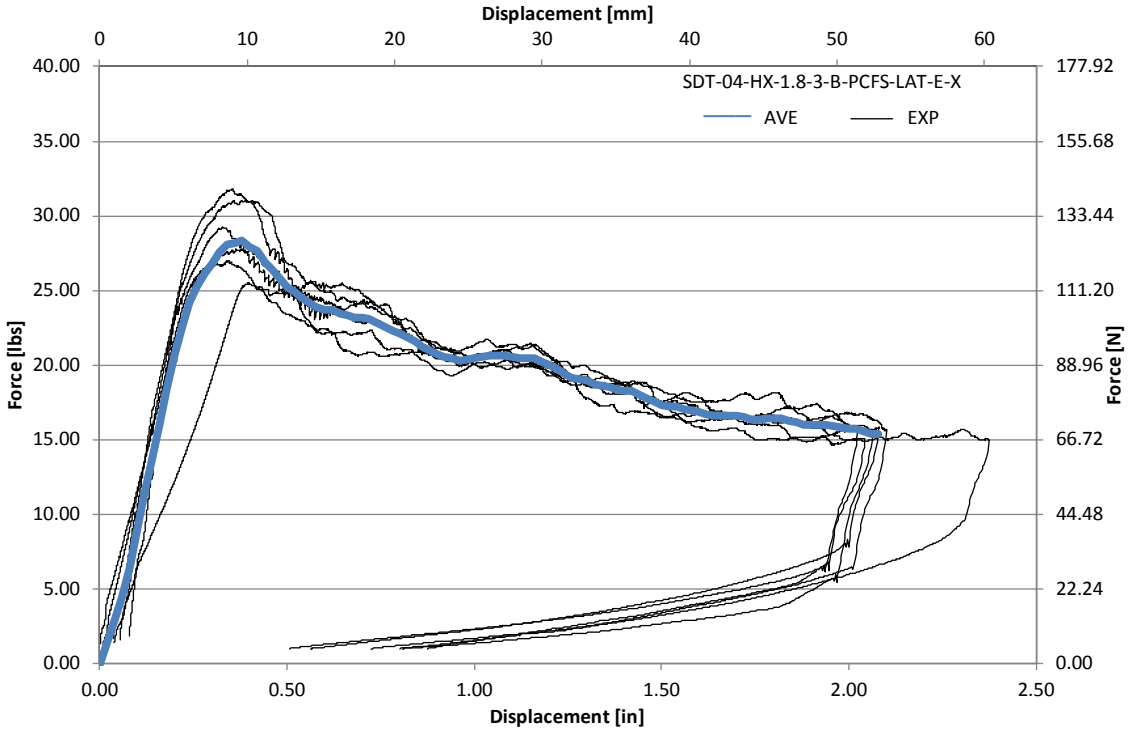

Figure A-48. Load vs. displacement curve for HRH-10–1/8–3.0 lateral ribbon direction with bottom disbond (edge)

A.3 HRH-10–1/8–6.0 DATA

A.3.1 HRH-10–1/8–6.0 LONGITUDINAL RIBBON DIRECTION WITH TOP DISBOND (CENTER) DATA

Table A-17. Test summary for HRH-10–1/8–6.0 longitudinal ribbon direction with top disbond (center) pre-crack

Specimen	GIC (in-lb/in^2)			GIC (KJ/m^2)			Failure Mode
	NL	VIS	5%/max	NL	VIS	5%/max	
SDT-04-HX-1.8-6-T-PCFS-LONG-C-1	1.891	N/A	3.933	0.331	N/A	0.689	Primarily APO
SDT-04-HX-1.8-6-T-PCFS-LONG-C-2	1.931	3.725	3.725	0.338	0.652	0.652	Primarily APO
SDT-04-HX-1.8-6-T-PCFS-LONG-C-3	2.085	N/A	3.358	0.365	N/A	0.588	Primarily APO
SDT-04-HX-1.8-6-T-PCFS-LONG-C-4	1.505	N/A	2.716	0.264	N/A	0.476	Primarily APO
SDT-04-HX-1.8-6-T-PCFS-LONG-C-5	2.387	N/A	3.631	0.418	N/A	0.636	Primarily APO
SDT-04-HX-1.8-6-T-PCFS-LONG-C-6	1.397	N/A	3.458	0.245	N/A	0.606	Primarily APO
SDT-04-HX-1.8-6-T-PCFS-LONG-C-7	1.799	N/A	3.295	0.315	N/A	0.577	Primarily APO
SDT-04-HX-1.8-6-T-PCFS-LONG-C-8	0.995	N/A	3.678	0.174	N/A	0.644	Primarily APO
AVERAGE GIC	1.749	3.725	3.474	0.306	0.652	0.608	
STANDARD DEVIATION	0.435	N/A	0.370	0.076	N/A	0.065	
COEFFICIENT OF VARIATION (%)	24.893	N/A	10.662	24.893	N/A	10.662	

Table A-18. Test summary for HRH-10–1/8–6.0 longitudinal ribbon direction with top disbond (center)

Specimen	GIC (in-lb/in^2)				GIC (KJ/m^2)				Failure Mode
	NL	VIS	5%/max	AREA	NL	VIS	5%/max	AREA	
SDT-04-HX-1.8-6-T-PCFS-LONG-C-1	1.763	4.101	4.266	N/A	0.309	0.718	0.747	N/A	Primarily APO, then FSF
SDT-04-HX-1.8-6-T-PCFS-LONG-C-2	1.054	N/A	2.975	N/A	0.185	N/A	0.521	N/A	Primarily APO, then FSF
SDT-04-HX-1.8-6-T-PCFS-LONG-C-3	0.674	2.795	2.896	7.100	0.118	0.490	0.507	1.243	Primarily APO
SDT-04-HX-1.8-6-T-PCFS-LONG-C-4	0.814	N/A	3.497	7.154	0.143	N/A	0.612	1.253	Primarily APO
SDT-04-HX-1.8-6-T-PCFS-LONG-C-5	0.916	N/A	3.580	6.591	0.160	N/A	0.627	1.154	Primarily APO
SDT-04-HX-1.8-6-T-PCFS-LONG-C-6	0.760	3.241	3.142	8.105	0.133	0.568	0.550	1.419	Primarily APO, then FSF
SDT-04-HX-1.8-6-T-PCFS-LONG-C-7	0.586	3.406	3.444	7.062	0.103	0.596	0.603	1.237	Primarily APO
SDT-04-HX-1.8-6-T-PCFS-LONG-C-8	0.713	3.629	4.075	N/A	0.125	0.636	0.714	N/A	Primarily APO, then FSF
AVERAGE GIC	0.910	3.434	3.484	7.202	0.159	0.601	0.610	1.261	
STANDARD DEVIATION	0.374	0.482	0.492	0.553	0.065	0.084	0.086	0.097	
COEFFICIENT OF VARIATION (%)	41.093	14.032	14.118	7.673	41.093	14.032	14.118	7.673	

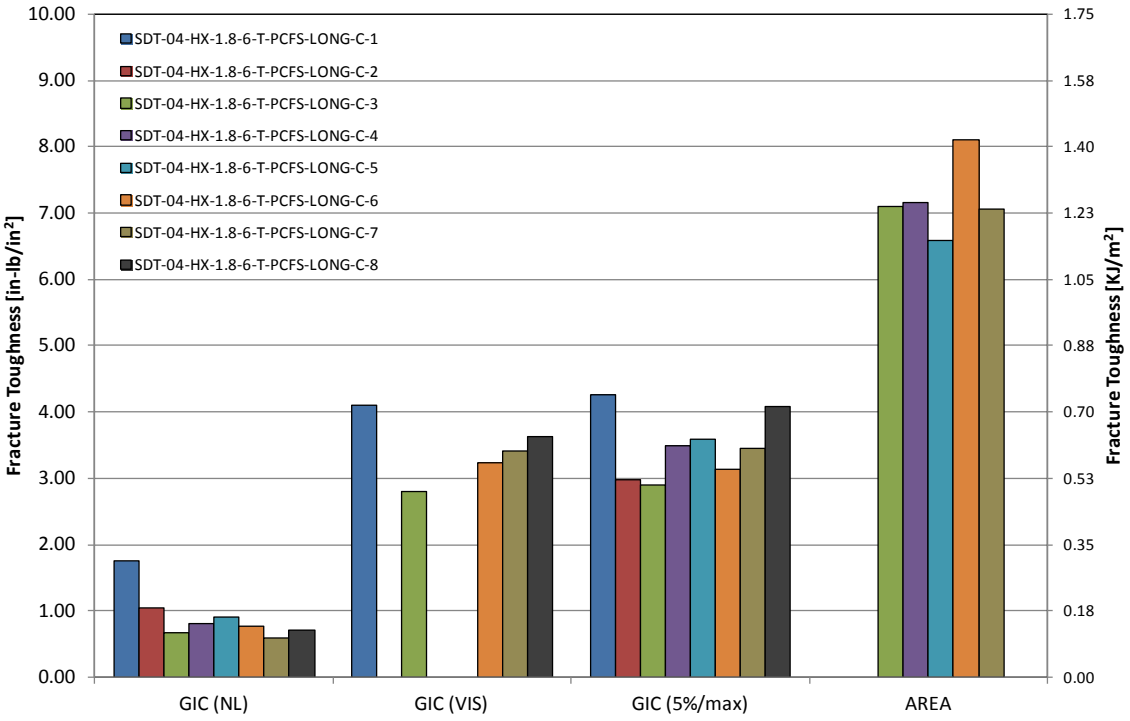

Figure A-49. GIC for HRH-10–1/8–6.0 longitudinal ribbon direction with top disbond (center)

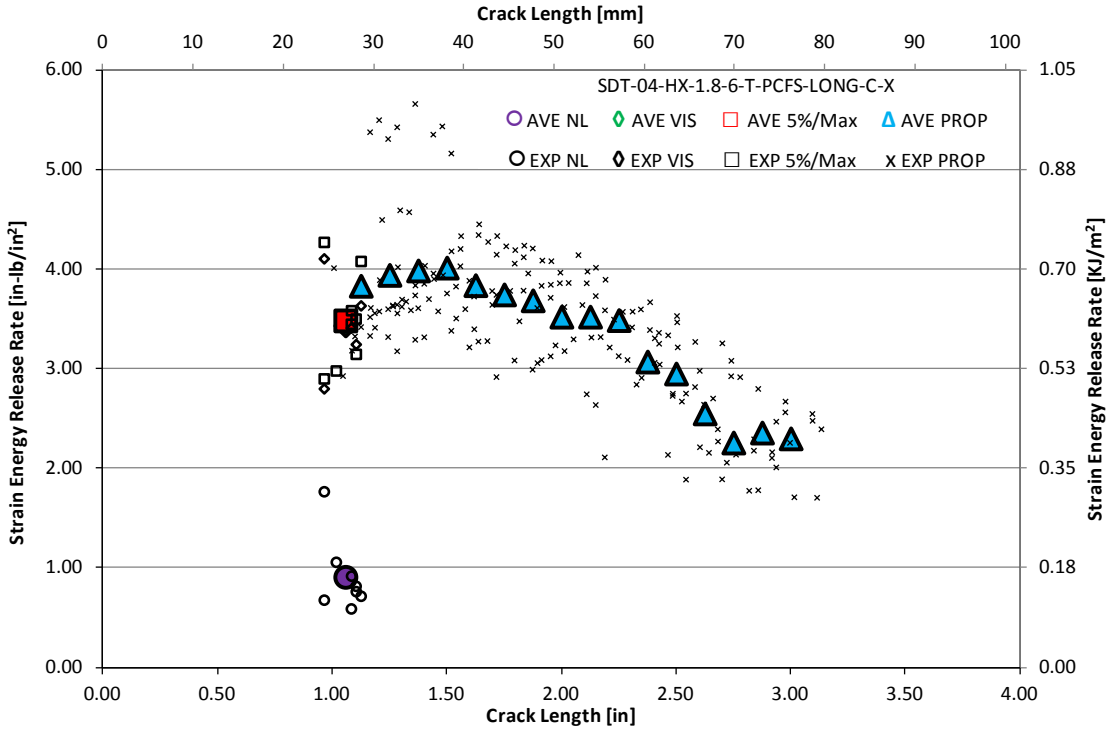

Figure A-50. Resistance curve for HRH-10–1/8–6.0 longitudinal ribbon direction with top disbond (center)

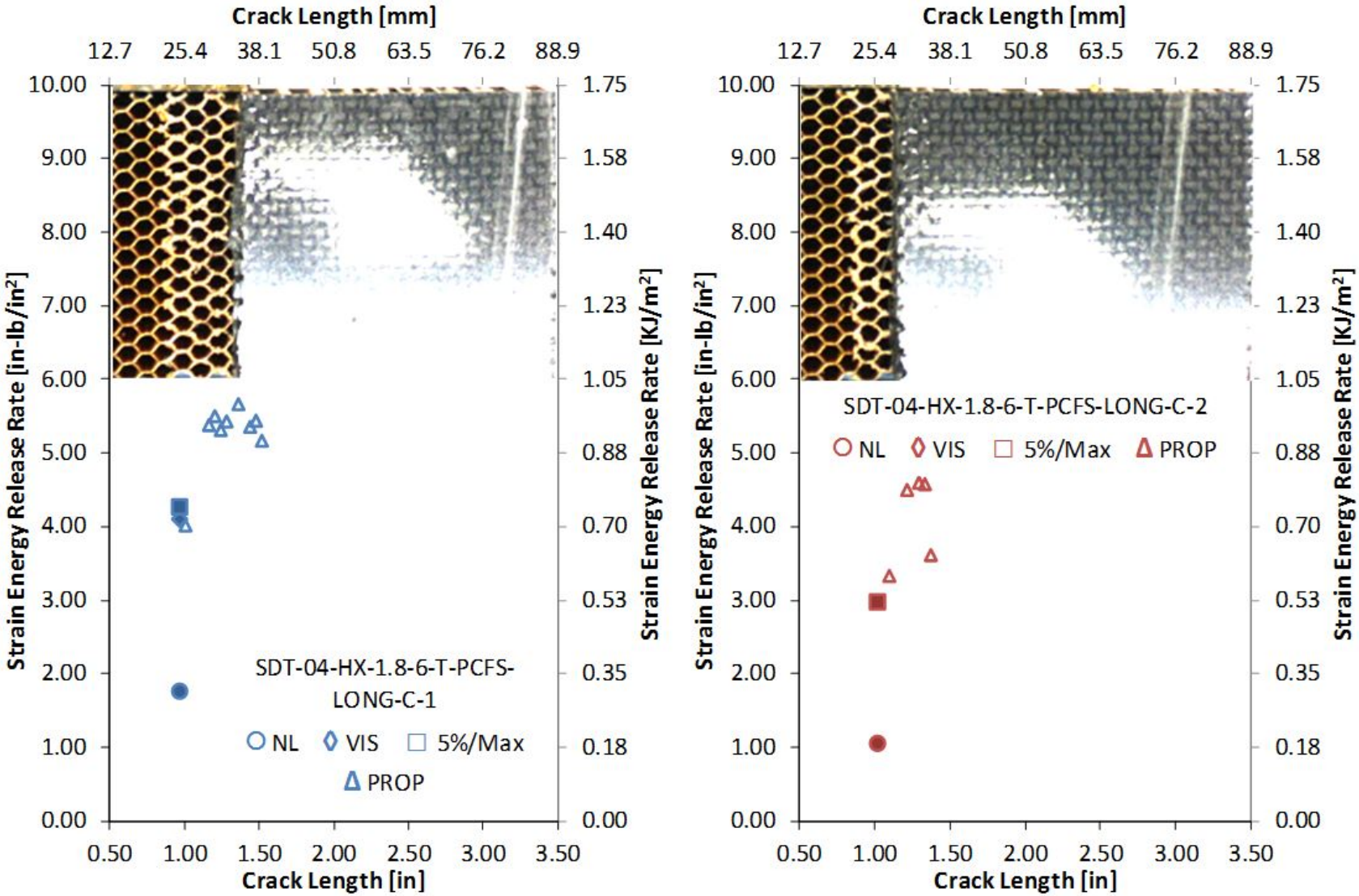

Figure A-51. Failure mode image and resistance curve of SDT-04-HX-1.8-6-T-PCFS-LONG-C-X #1 and #2

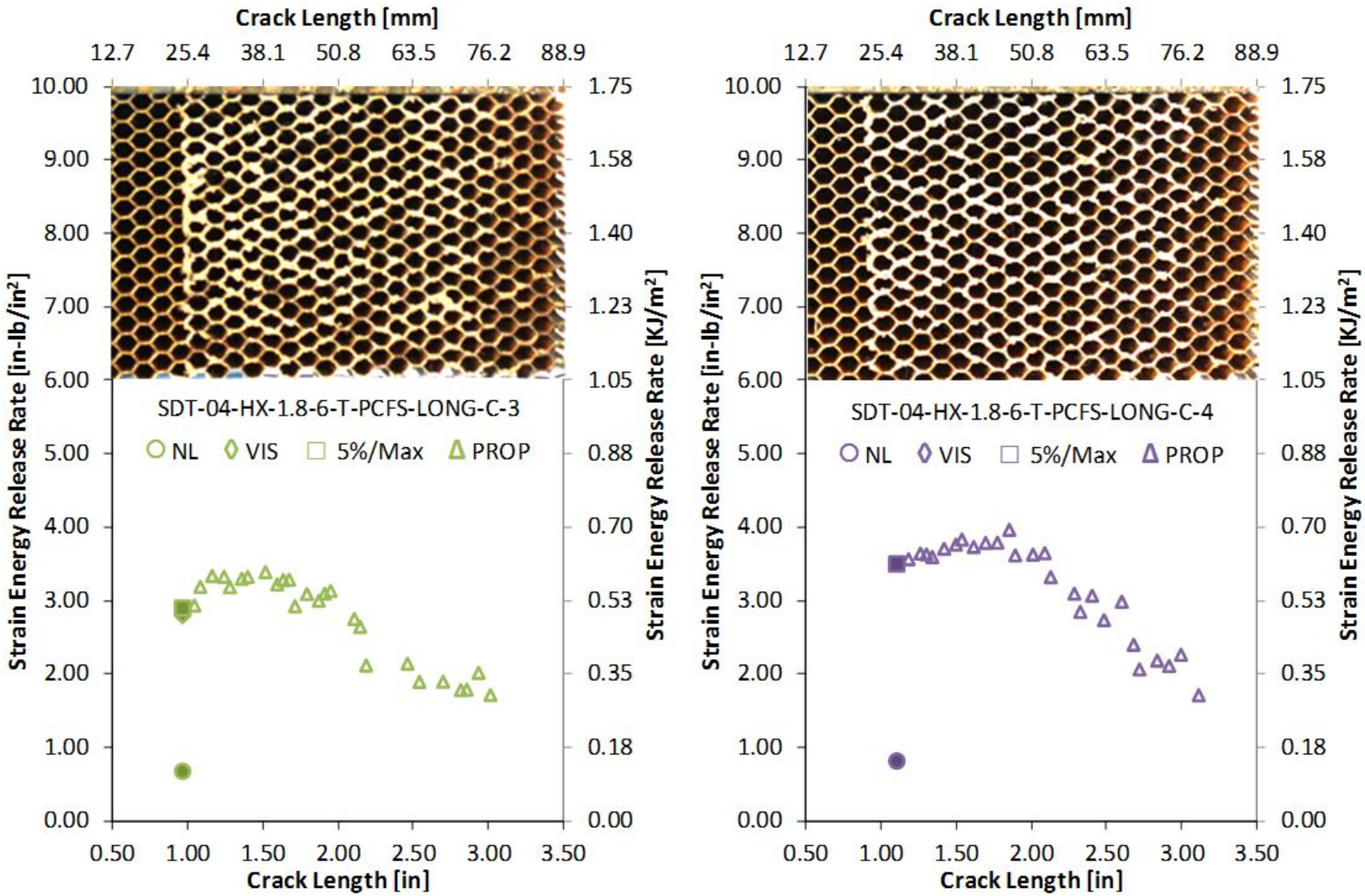

Figure A-52. Failure mode image and resistance curve of SDT-04-HX-1.8-6-T-PCFS-LONG-C-X #3 and #4

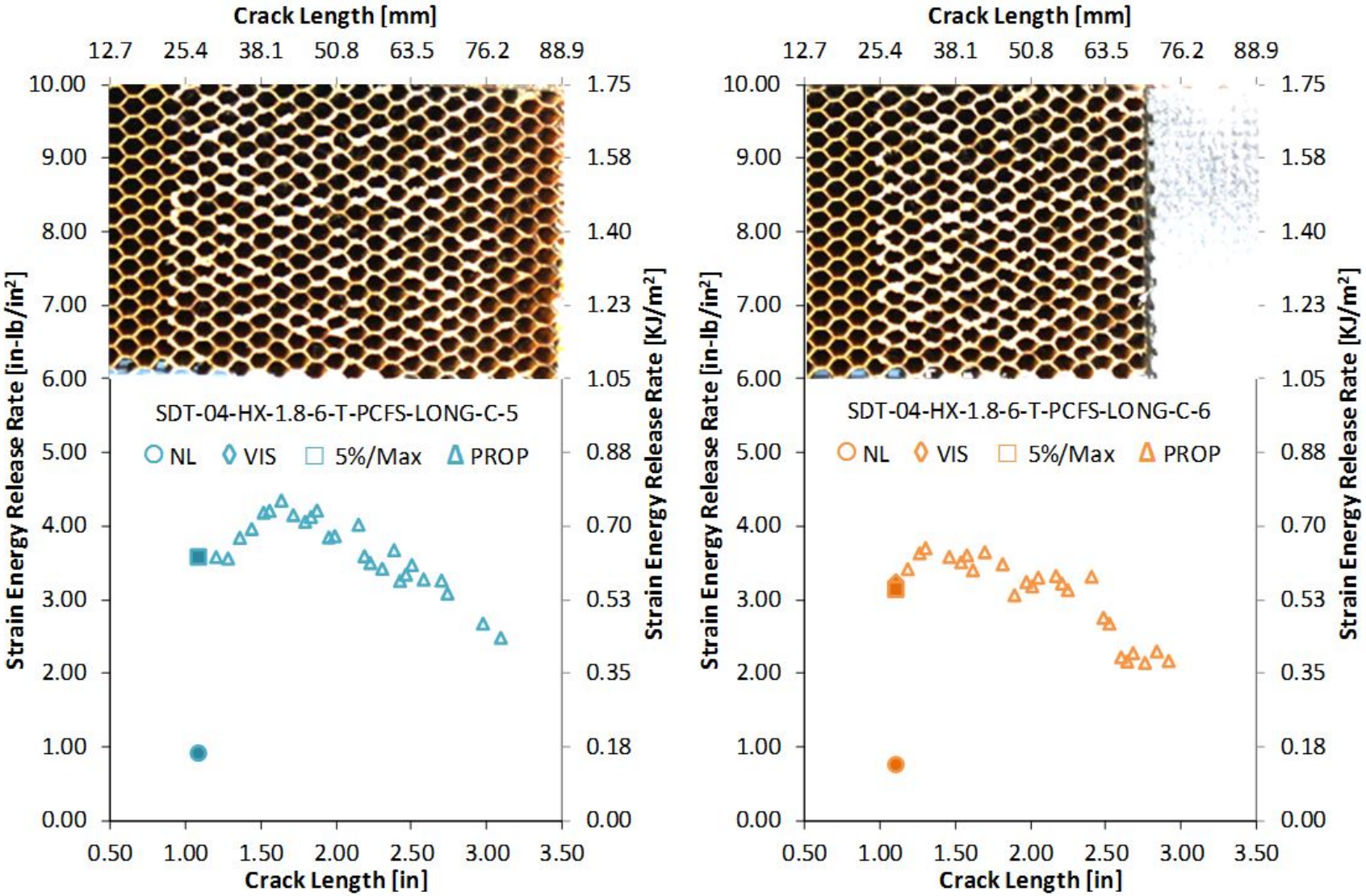

Figure A-53. Failure mode image and resistance curve of SDT-04-HX-1.8-6-T-PCFS-LONG-C-X #5 and #6

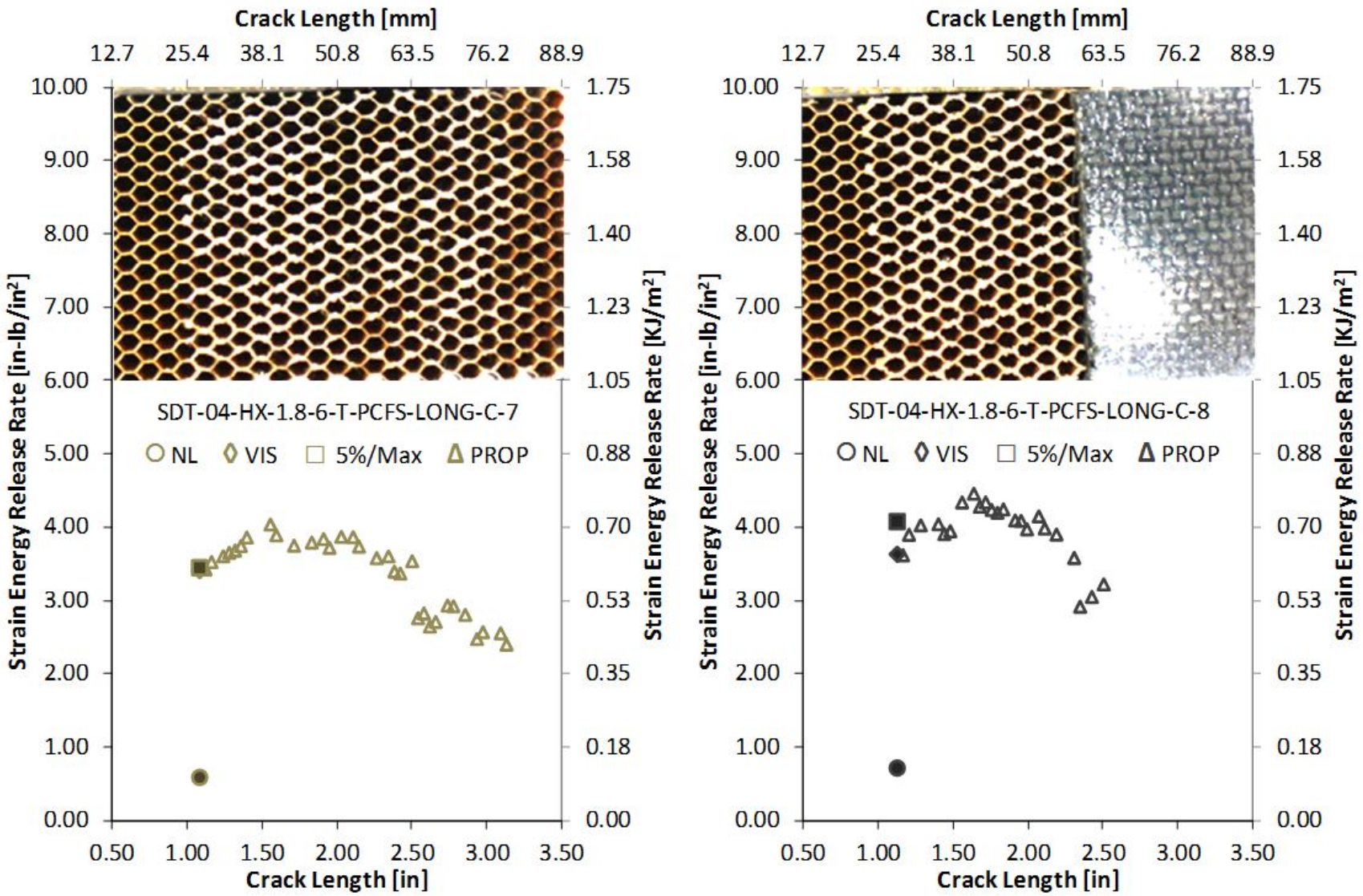

Figure A-54. Failure mode image and resistance curve of SDT-04-HX-1.8-6-T-PCFS-LONG-C-X #7 and #8

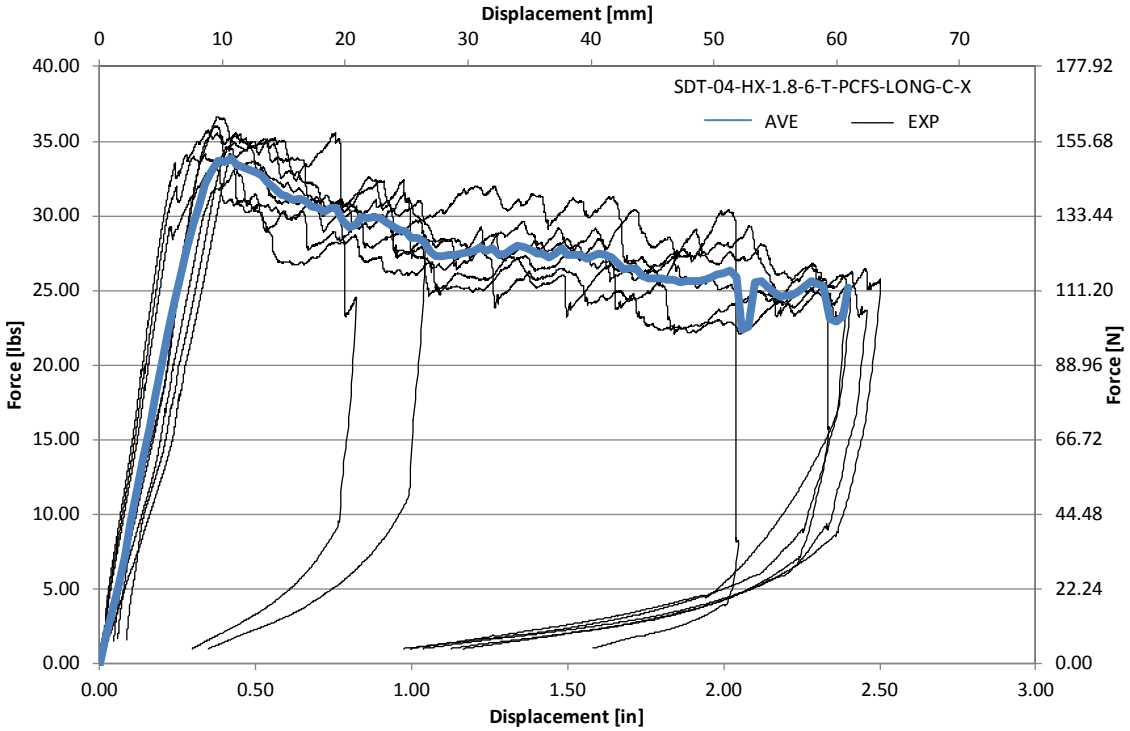

Figure A-55. Load vs. displacement curve for HRH-10–1/8–6.0 longitudinal ribbon direction with top disbond (center)

A.3.2 HRH-10–1/8–6.0 LONGITUDINAL RIBBON DIRECTION WITH BOTTOM DISBOND (CENTER) DATA

Table A-19. Test summary for HRH-10–1/8–6.0 longitudinal ribbon direction with bottom disbond (center) pre-crack

Specimen	GIC (in-lb/in^2)			GIC (KJ/m^2)			Failure Mode
	NL	VIS	5%/max	NL	VIS	5%/max	
SDT-04-HX-1.8-6-B-PCFS-LONG-C-1	1.854	N/A	3.093	0.325	N/A	0.542	Primarily APO
SDT-04-HX-1.8-6-B-PCFS-LONG-C-2	1.285	4.204	4.253	0.225	0.736	0.745	Primarily APO
SDT-04-HX-1.8-6-B-PCFS-LONG-C-3	0.951	N/A	4.310	0.166	N/A	0.755	Primarily APO
SDT-04-HX-1.8-6-B-PCFS-LONG-C-4	1.762	N/A	4.007	0.309	N/A	0.702	Primarily APO
SDT-04-HX-1.8-6-B-PCFS-LONG-C-5	0.785	N/A	2.618	0.137	N/A	0.459	Primarily APO
SDT-04-HX-1.8-6-B-PCFS-LONG-C-6	2.102	N/A	4.096	0.368	N/A	0.717	Primarily APO
SDT-04-HX-1.8-6-B-PCFS-LONG-C-7	2.669	N/A	3.492	0.467	N/A	0.612	Primarily APO
SDT-04-HX-1.8-6-B-PCFS-LONG-C-8	2.781	3.289	3.317	0.487	0.576	0.581	Half a cell in A, then APO
AVERAGE GIC	1.774	3.746	3.648	0.311	0.656	0.639	
STANDARD DEVIATION	0.739	0.647	0.614	0.129	0.113	0.107	
COEFFICIENT OF VARIATION (%)	41.681	17.269	16.822	41.681	17.269	16.822	

Table A-20. Test summary for HRH-10–1/8–6.0 longitudinal ribbon direction with bottom disbond (center)

Specimen	GIC (in-lb/in^2)				GIC (KJ/m^2)				Failure Mode
	NL	VIS	5%/max	AREA	NL	VIS	5%/max	AREA	
SDT-04-HX-1.8-6-B-PCFS-LONG-C-1	0.932	3.383	3.658	N/A	0.163	0.592	0.641	N/A	Primarily APO, then FSF
SDT-04-HX-1.8-6-B-PCFS-LONG-C-2	0.421	3.132	3.406	8.614	0.074	0.549	0.596	1.509	Primarily APO, then FSF
SDT-04-HX-1.8-6-B-PCFS-LONG-C-3	0.377	3.475	3.550	N/A	0.066	0.609	0.622	N/A	Primarily APO, then FSF
SDT-04-HX-1.8-6-B-PCFS-LONG-C-4	0.515	N/A	3.124	7.594	0.090	N/A	0.547	1.330	Primarily APO
SDT-04-HX-1.8-6-B-PCFS-LONG-C-5	0.557	3.227	3.004	7.765	0.097	0.565	0.526	1.360	Primarily APO
SDT-04-HX-1.8-6-B-PCFS-LONG-C-6	0.490	N/A	3.386	7.672	0.086	N/A	0.593	1.344	Primarily APO
SDT-04-HX-1.8-6-B-PCFS-LONG-C-7	0.450	N/A	2.452	7.521	0.079	N/A	0.429	1.317	Primarily APO
SDT-04-HX-1.8-6-B-PCFS-LONG-C-8	1.124	1.851	2.711	6.746	0.197	0.324	0.475	1.181	Primarily APO
AVERAGE GIC	0.608	3.014	3.161	7.652	0.107	0.528	0.554	1.340	
STANDARD DEVIATION	0.270	0.664	0.421	0.597	0.047	0.116	0.074	0.105	
COEFFICIENT OF VARIATION (%)	44.374	22.017	13.316	7.798	44.374	22.017	13.316	7.798	

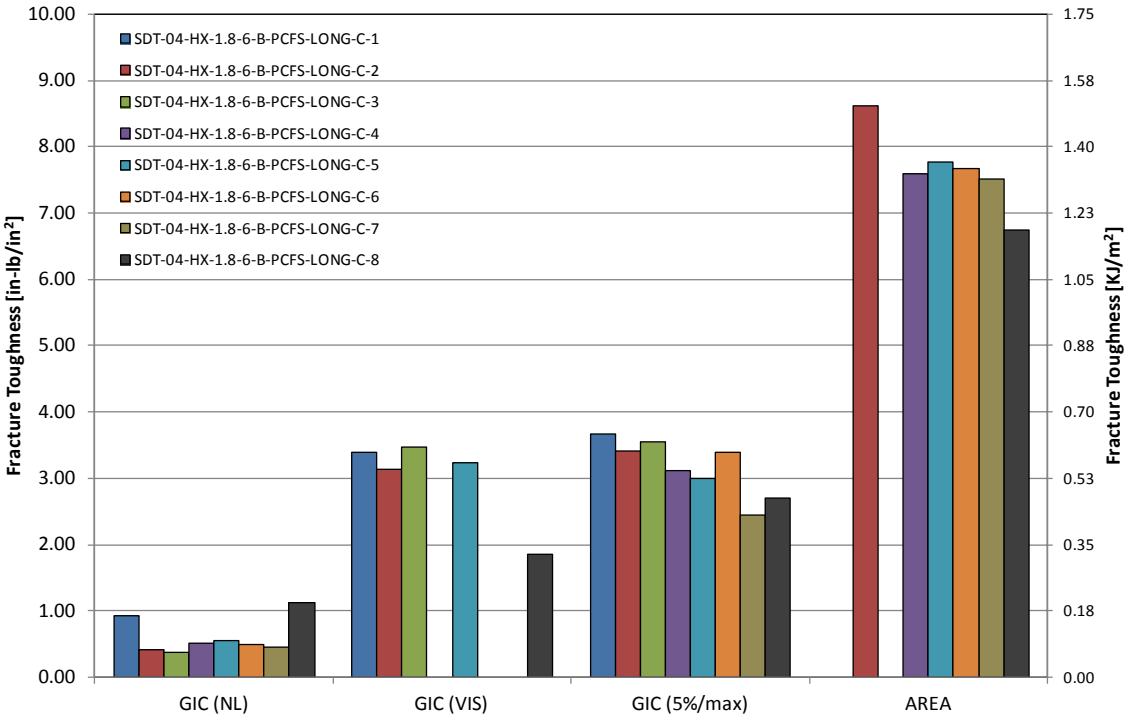

Figure A-56. GIC for HRH-10–1/8–6.0 longitudinal ribbon direction with bottom disbond (center)

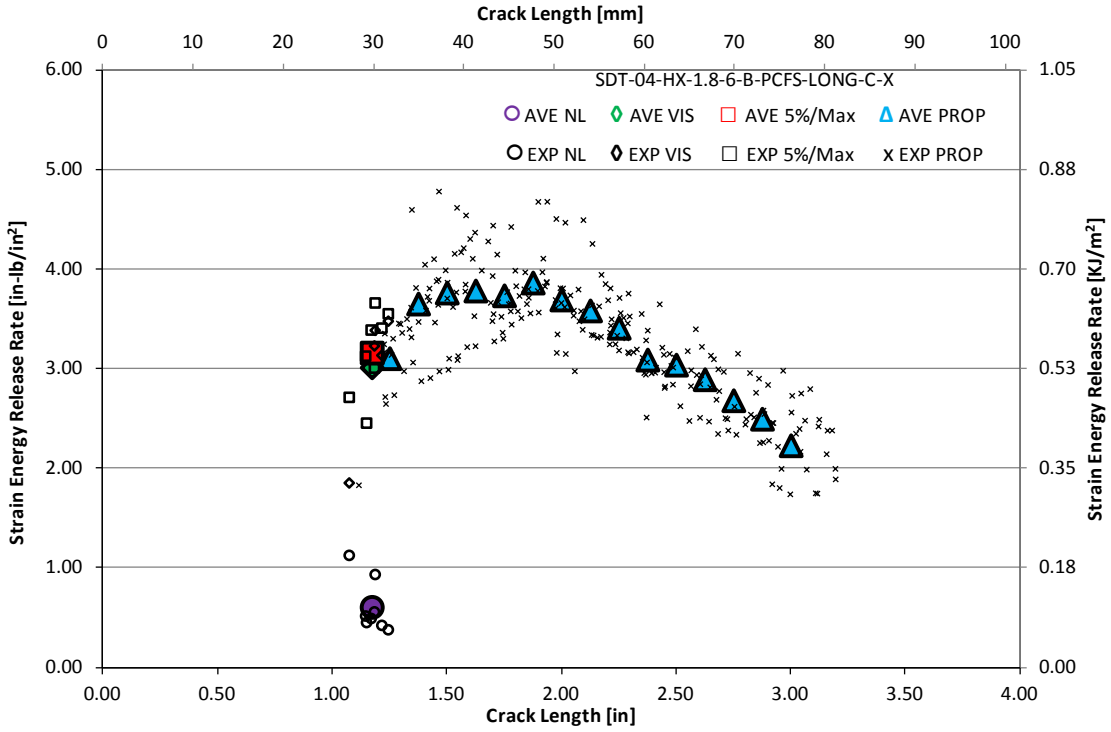

Figure A-57. Resistance curve for HRH-10–1/8–6.0 longitudinal ribbon direction with bottom disbond (center)

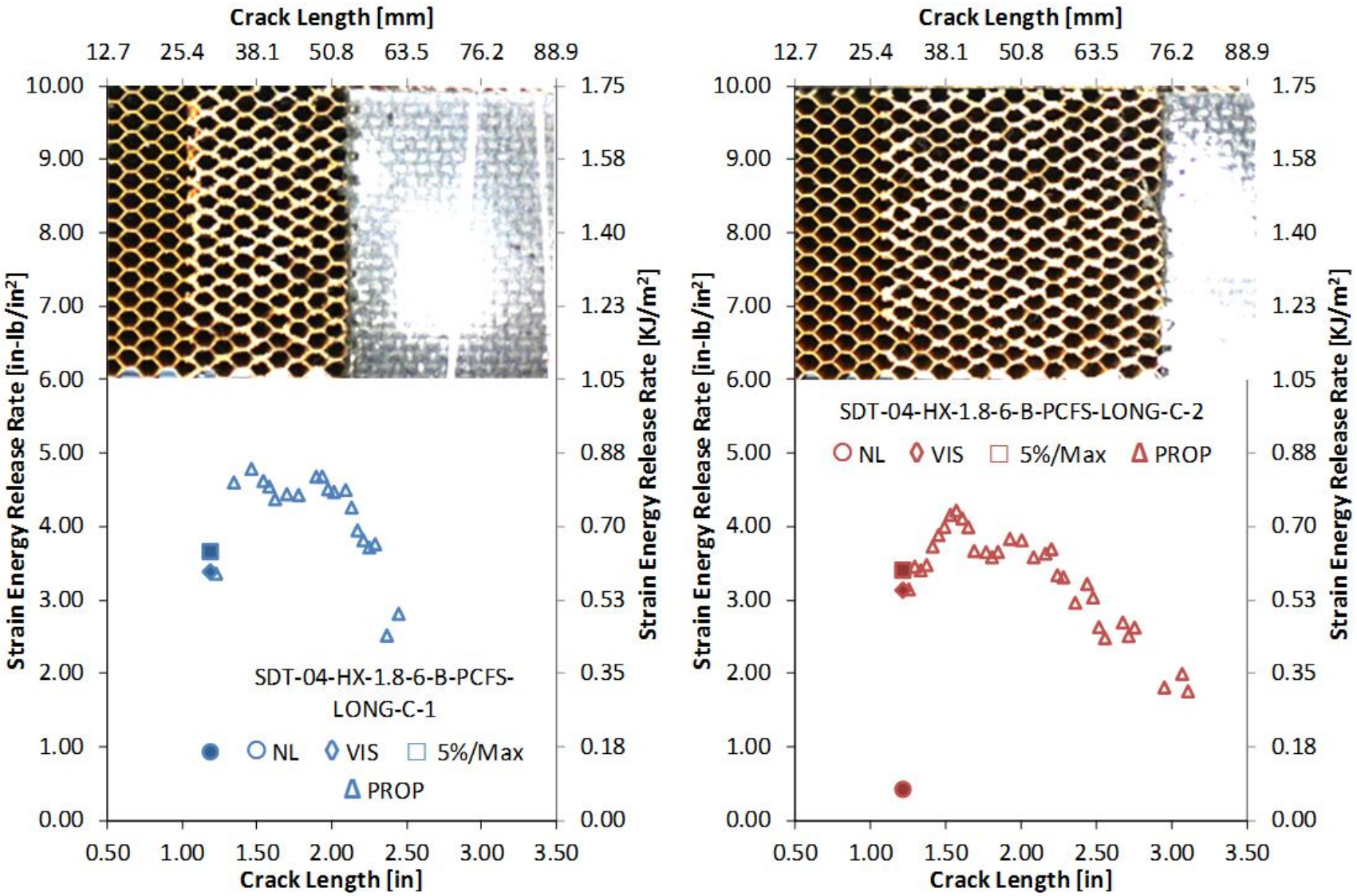

Figure A-58. Failure mode image and resistance curve of SDT-04-HX-1.8-6-B-PCFS-LONG-C-X #1 and #2

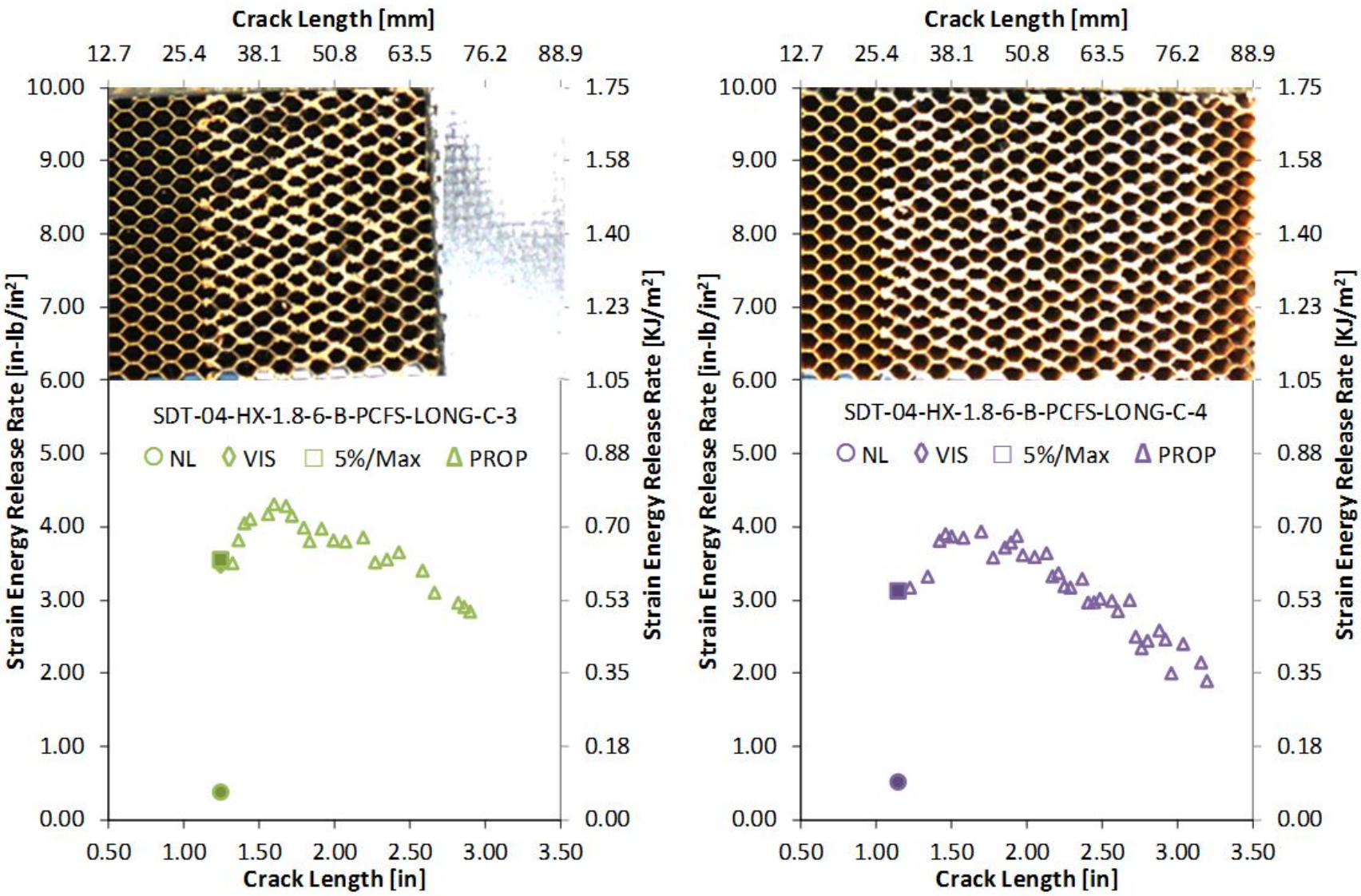

Figure A-59. Failure mode image and resistance curve of SDT-04-HX-1.8-6-B-PCFS-LONG-C-X #3 and #4

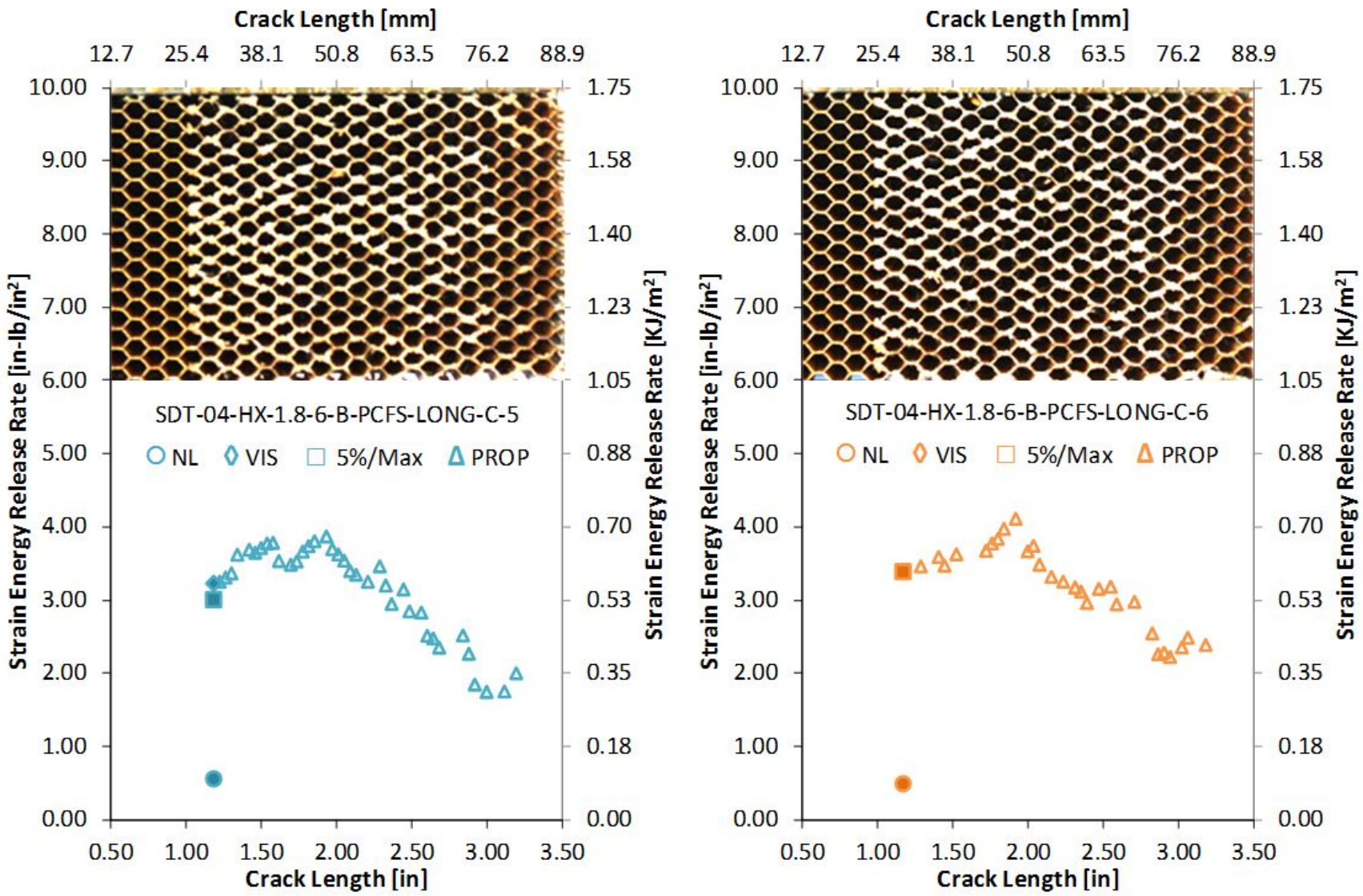

Figure A-60. Failure mode image and resistance curve of SDT-04-HX-1.8-6-B-PCFS-LONG-C-X #5 and #6

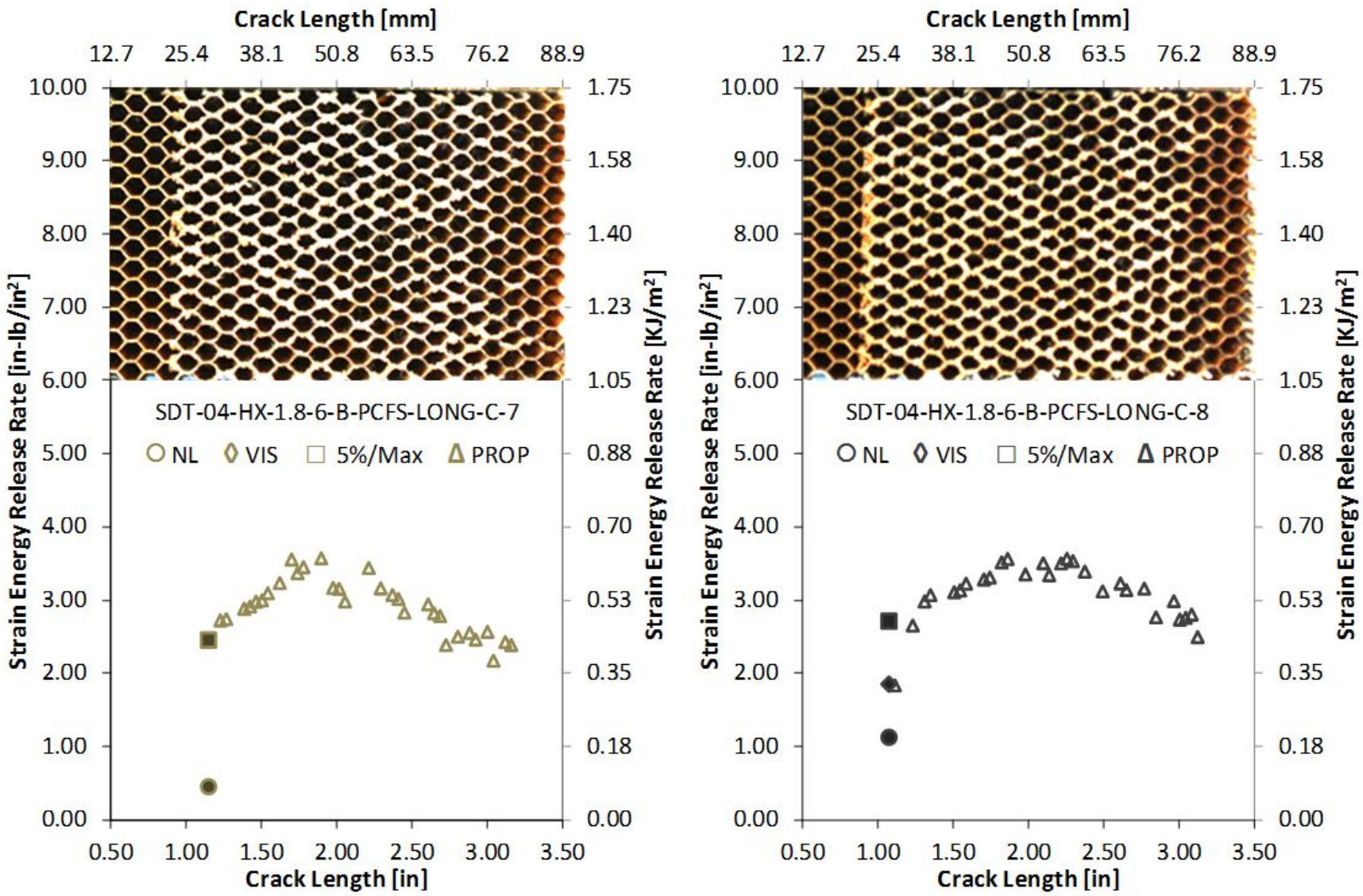

Figure A-61. Failure mode image and resistance curve of SDT-04-HX-1.8-6-B-PCFS-LONG-C-X #7 and #8

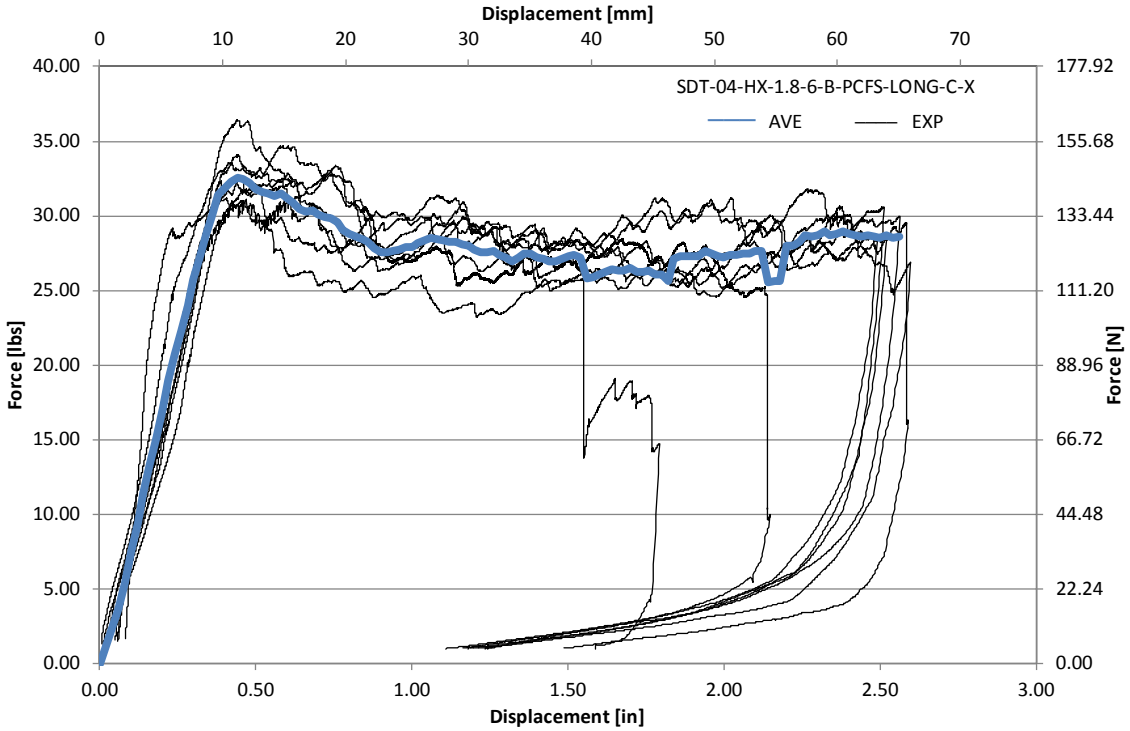

Figure A-62. Load vs. displacement curve for HRH-10–1/8–6.0 longitudinal ribbon direction with bottom disbond (center)

A.4 HRH-10–3/16–2.0 DATA

A.4.1 HRH-10–3/16–2.0 LONGITUDINAL RIBBON DIRECTION WITH TOP DISBOND (CENTER) DATA

Table A-21. Test summary for HRH-10–3/16–2.0 longitudinal ribbon direction with top disbond (center) pre-crack

Specimen	GIC (in-lb/in^2)			GIC (KJ/m^2)			Failure Mode
	NL	VIS	5%/max	NL	VIS	5%/max	
SDT-04-HX-3.16-2-T-PCFS-LONG-C-1	1.320	2.366	2.416	0.231	0.414	0.423	Primarily C
SDT-04-HX-3.16-2-T-PCFS-LONG-C-2	1.129	N/A	1.757	0.198	N/A	0.308	Primarily C
SDT-04-HX-3.16-2-T-PCFS-LONG-C-3	1.000	N/A	1.549	0.175	N/A	0.271	Primarily C
SDT-04-HX-3.16-2-T-PCFS-LONG-C-4	0.929	N/A	1.484	0.163	N/A	0.260	Primarily C
SDT-04-HX-3.16-2-T-PCFS-LONG-C-5	0.823	0.965	0.965	0.144	0.169	0.169	Primarily C
SDT-04-HX-3.16-2-T-PCFS-LONG-C-6							
SDT-04-HX-3.16-2-T-PCFS-LONG-C-7	0.985	N/A	1.572	0.172	N/A	0.275	Primarily C
SDT-04-HX-3.16-2-T-PCFS-LONG-C-8							
AVERAGE GIC	1.031	1.665	1.624	0.181	0.292	0.284	
STANDARD DEVIATION	0.173	0.991	0.471	0.030	0.174	0.082	
COEFFICIENT OF VARIATION (%)	16.780	59.493	28.987	16.780	59.493	28.987	

Table A-22. Test summary for HRH-10–3/16–2.0 longitudinal ribbon direction with top disbond (center)

Specimen	GIC (in-lb/in^2)				GIC (KJ/m^2)				Failure Mode
	NL	VIS	5%/max	AREA	NL	VIS	5%/max	AREA	
SDT-04-HX-3.16-2-T-PCFS-LONG-C-1	0.892	2.425	2.425	2.740	0.156	0.425	0.425	0.480	Primarily C
SDT-04-HX-3.16-2-T-PCFS-LONG-C-2	0.846	N/A	1.905	2.783	0.148	N/A	0.334	0.487	Primarily C
SDT-04-HX-3.16-2-T-PCFS-LONG-C-3	0.422	1.802	2.323	2.321	0.074	0.316	0.407	0.406	Primarily C
SDT-04-HX-3.16-2-T-PCFS-LONG-C-4	0.614	1.602	1.894	2.400	0.108	0.281	0.332	0.420	Primarily C
SDT-04-HX-3.16-2-T-PCFS-LONG-C-5	0.593	1.766	2.662	2.363	0.104	0.309	0.466	0.414	Primarily C
SDT-04-HX-3.16-2-T-PCFS-LONG-C-6									
SDT-04-HX-3.16-2-T-PCFS-LONG-C-7	0.714	2.024	2.083	2.547	0.125	0.354	0.365	0.446	Primarily C
SDT-04-HX-3.16-2-T-PCFS-LONG-C-8									
AVERAGE GIC	0.680	1.924	2.215	2.526	0.119	0.337	0.388	0.442	
STANDARD DEVIATION	0.174	0.318	0.307	0.198	0.031	0.056	0.054	0.035	
COEFFICIENT OF VARIATION (%)	25.616	16.525	13.861	7.854	25.616	16.525	13.861	7.854	

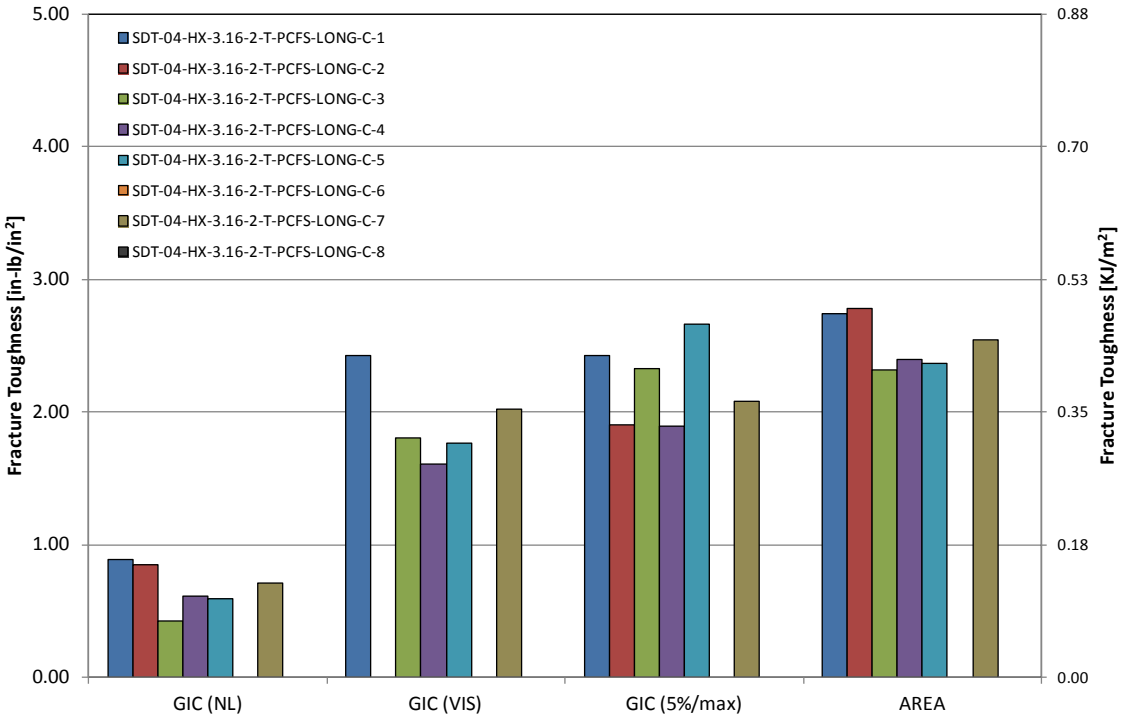

Figure A-63. GIC for HRH-10–3/16–2.0 longitudinal ribbon direction with top disbond (center)

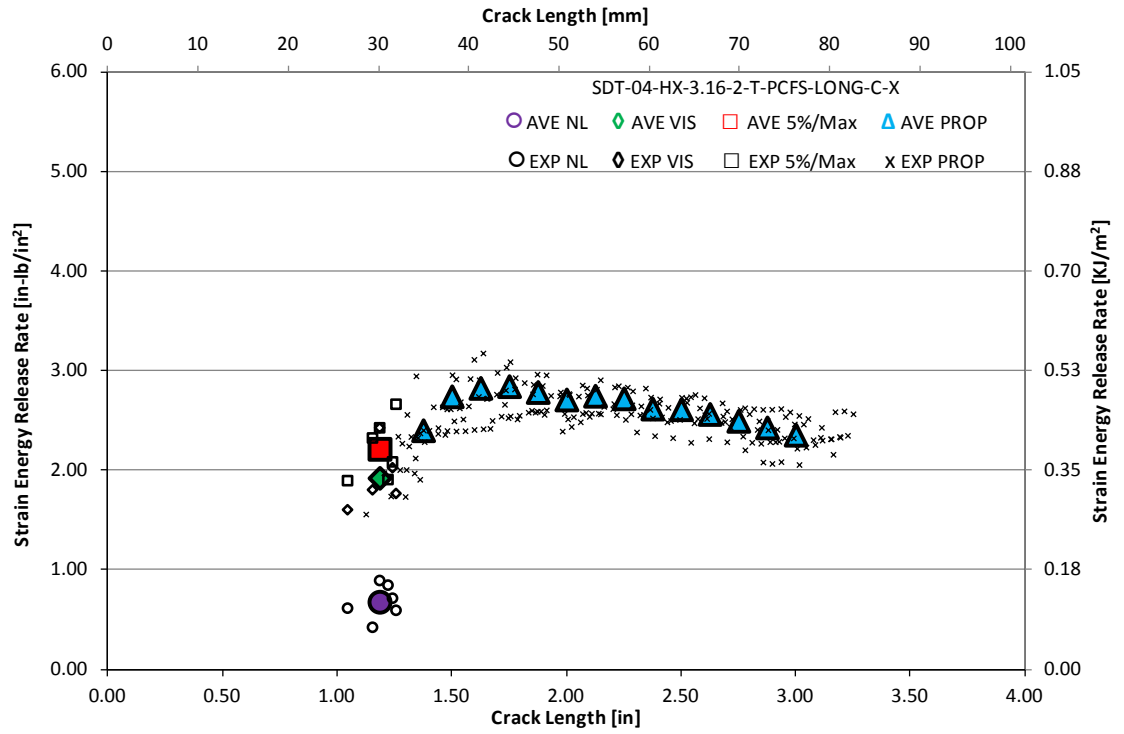

Figure A-64. Resistance curve for HRH-10–3/16–2.0 longitudinal ribbon direction with top disbond (center)

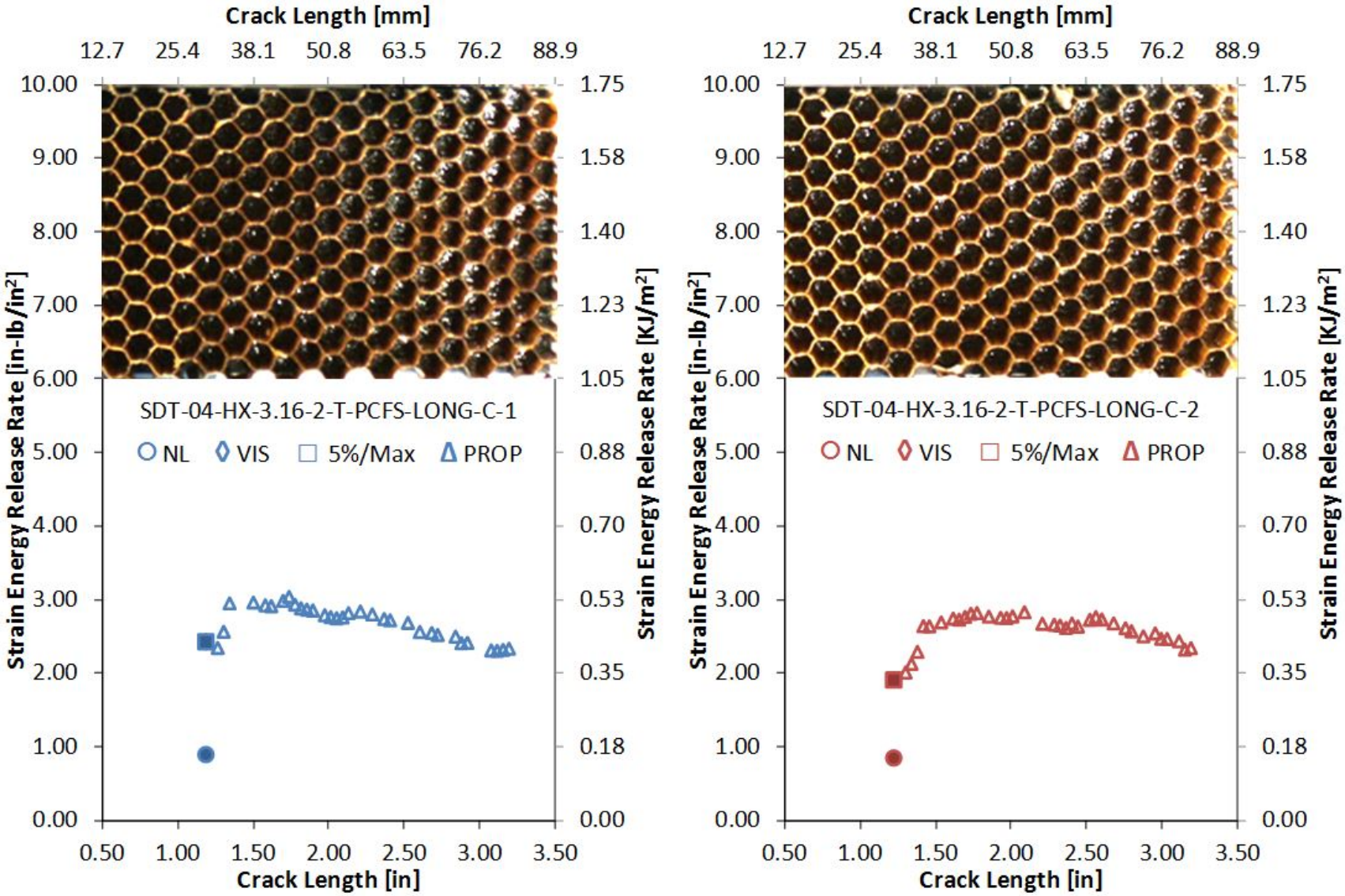

Figure A-65. Failure mode image and resistance curve of SDT-04-HX-3.16-2-T-PCFS-LONG-C-X #1 and #2

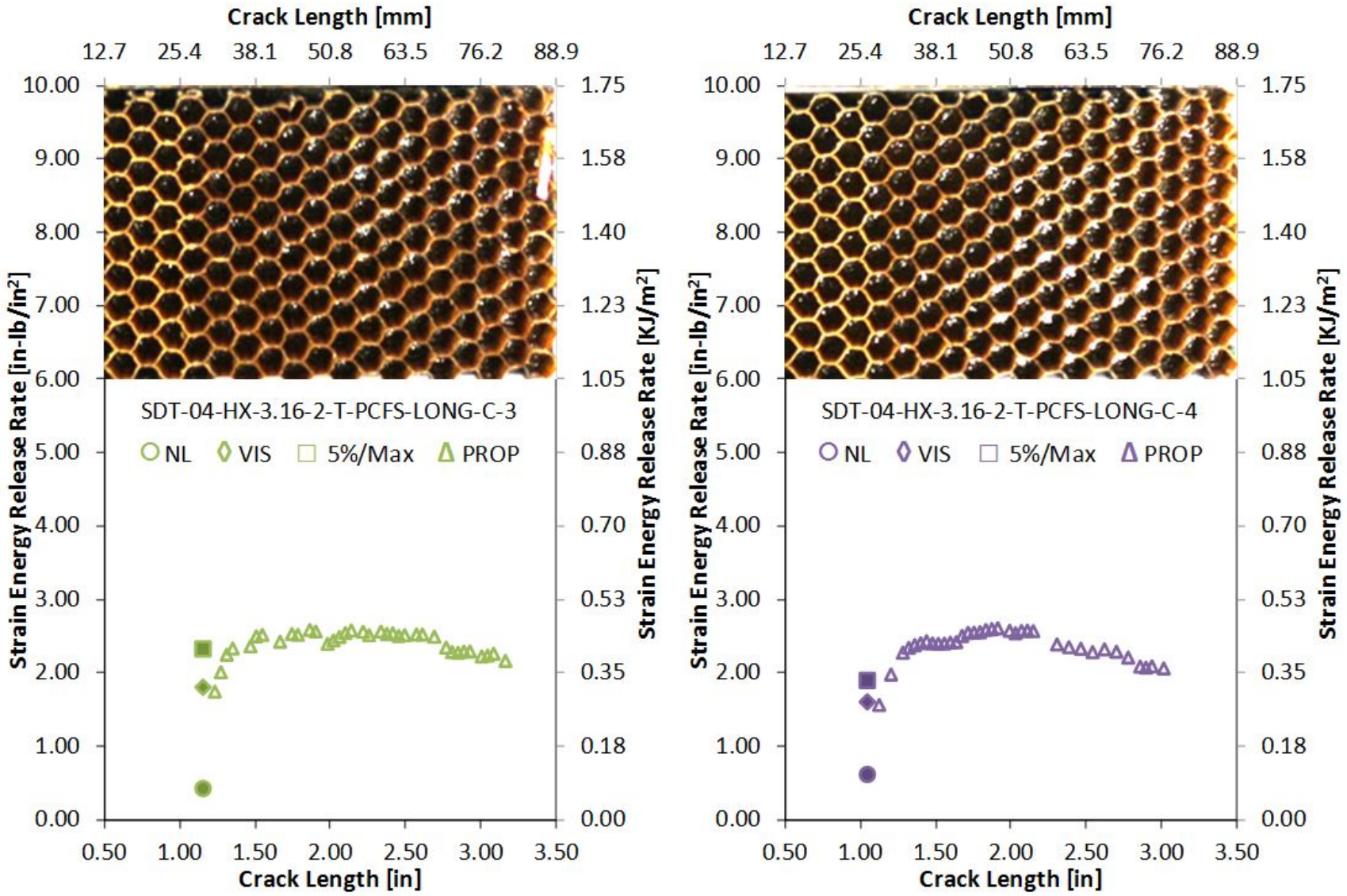

Figure A-66. Failure mode image and resistance curve of SDT-04-HX-3.16-2-T-PCFS-LONG-C-X #3 and #4

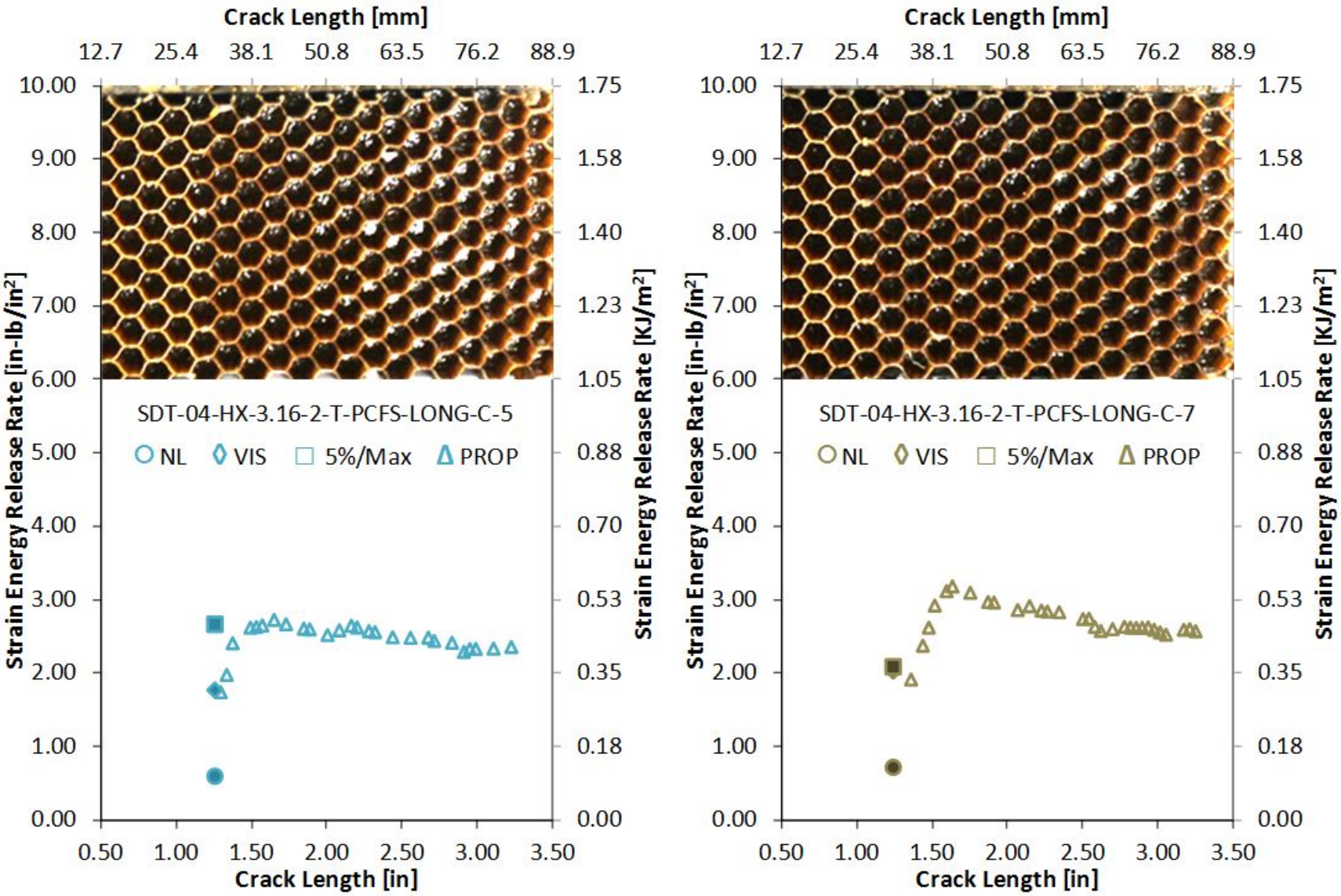

Figure A-67. Failure mode image and resistance curve of SDT-04-HX-3.16-2-T-PCFS-LONG-C-X #5 and #7

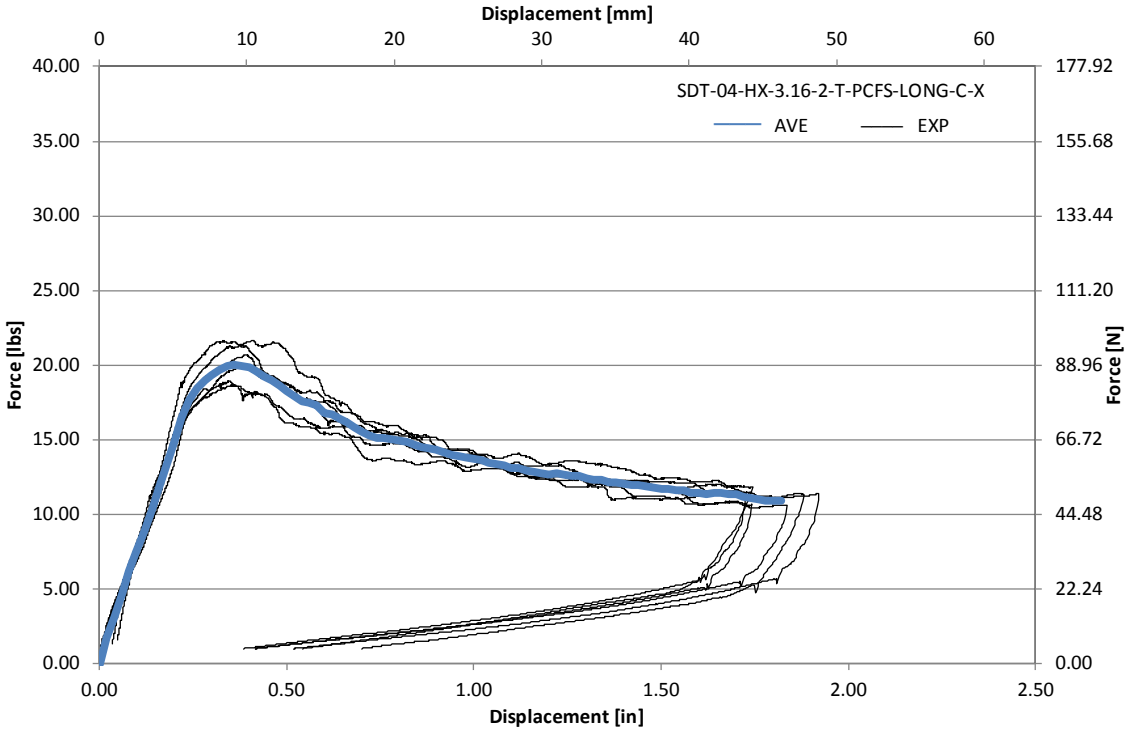

Figure A-68. Load vs. displacement curve for HRH-10–3/16–2.0 longitudinal ribbon direction with top disbond (center)

A.4.2 HRH-10–3/16–2.0 LONGITUDINAL RIBBON DIRECTION WITH BOTTOM DISBOND (CENTER) DATA

Table A-23. Test summary for HRH-10–3/16–2.0 longitudinal ribbon direction with bottom disbond (center) pre-crack

Specimen	GIC (in-lb/in^2)			GIC (KJ/m^2)			Failure Mode
	NL	VIS	5%/max	NL	VIS	5%/max	
SDT-04-HX-3.16-2-B-PCFS-LONG-C-1	1.294	N/A	2.158	0.227	N/A	0.378	Primarily C
SDT-04-HX-3.16-2-B-PCFS-LONG-C-2	1.635	N/A	1.923	0.286	N/A	0.337	Primarily C
SDT-04-HX-3.16-2-B-PCFS-LONG-C-3	1.556	N/A	1.915	0.273	N/A	0.335	Primarily C
SDT-04-HX-3.16-2-B-PCFS-LONG-C-4	1.420	N/A	1.856	0.249	N/A	0.325	Primarily C
SDT-04-HX-3.16-2-B-PCFS-LONG-C-5	1.176	2.020	2.020	0.206	0.354	0.354	Primarily C
SDT-04-HX-3.16-2-B-PCFS-LONG-C-6	0.987	N/A	1.705	0.173	N/A	0.299	Primarily C
SDT-04-HX-3.16-2-B-PCFS-LONG-C-7							
SDT-04-HX-3.16-2-B-PCFS-LONG-C-8							
AVERAGE GIC	1.345	2.020	1.929	0.235	0.354	0.338	
STANDARD DEVIATION	0.242	N/A	0.153	0.042	N/A	0.027	
COEFFICIENT OF VARIATION (%)	18.025	N/A	7.906	18.025	N/A	7.906	

Table A-24. Test summary for HRH-10–3/16–2.0 longitudinal ribbon direction with bottom disbond (center)

Specimen	GIC (in-lb/in^2)				GIC (KJ/m^2)				Failure Mode
	NL	VIS	5%/max	AREA	NL	VIS	5%/max	AREA	
SDT-04-HX-3.16-2-B-PCFS-LONG-C-1	0.869	2.330	2.354	2.550	0.152	0.408	0.412	0.447	Primarily C
SDT-04-HX-3.16-2-B-PCFS-LONG-C-2	0.945	2.022	2.204	2.404	0.165	0.354	0.386	0.421	Primarily C
SDT-04-HX-3.16-2-B-PCFS-LONG-C-3	0.821	2.671	2.688	2.346	0.144	0.468	0.471	0.411	Primarily C
SDT-04-HX-3.16-2-B-PCFS-LONG-C-4	0.904	2.243	2.268	2.193	0.158	0.393	0.397	0.384	Primarily C
SDT-04-HX-3.16-2-B-PCFS-LONG-C-5	0.951	1.915	2.288	2.119	0.166	0.335	0.401	0.371	Primarily C
SDT-04-HX-3.16-2-B-PCFS-LONG-C-6	0.719	N/A	2.224	2.244	0.126	N/A	0.390	0.393	Primarily C
SDT-04-HX-3.16-2-B-PCFS-LONG-C-7									
SDT-04-HX-3.16-2-B-PCFS-LONG-C-8									
AVERAGE GIC	0.868	2.236	2.338	2.309	0.152	0.392	0.409	0.404	
STANDARD DEVIATION	0.088	0.295	0.180	0.156	0.015	0.052	0.031	0.027	
COEFFICIENT OF VARIATION (%)	10.109	13.176	7.680	6.760	10.109	13.176	7.680	6.760	

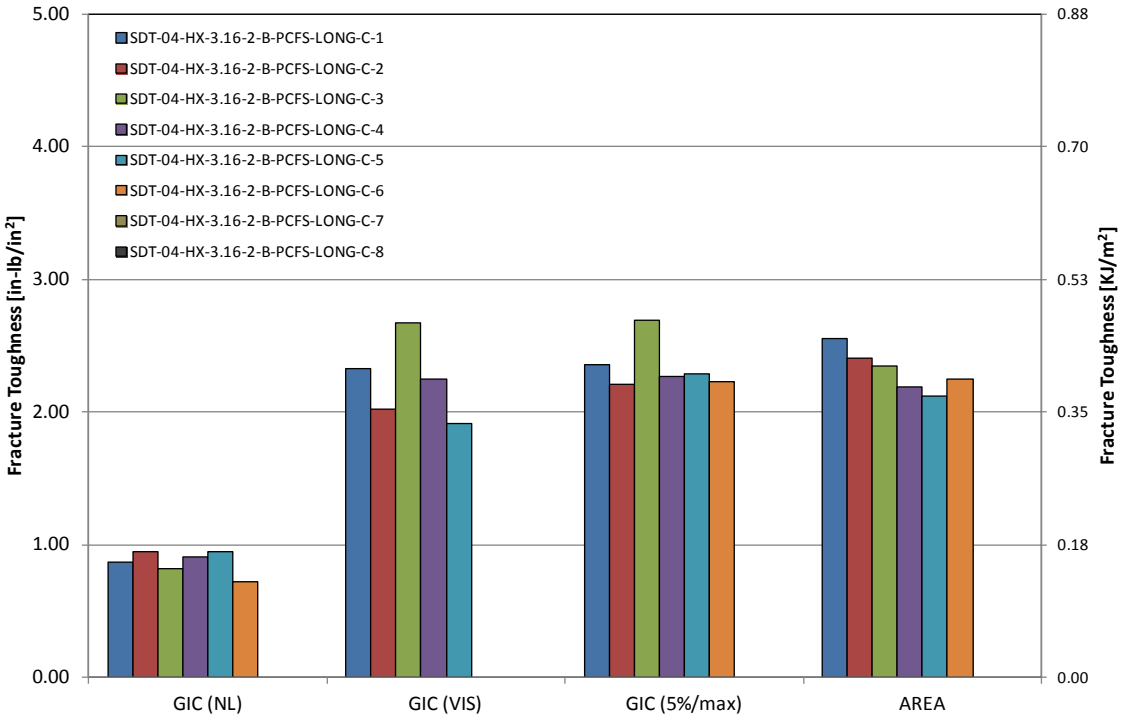

Figure A-69. GIC for HRH-10–3/16–2.0 longitudinal ribbon direction with bottom disbond (center)

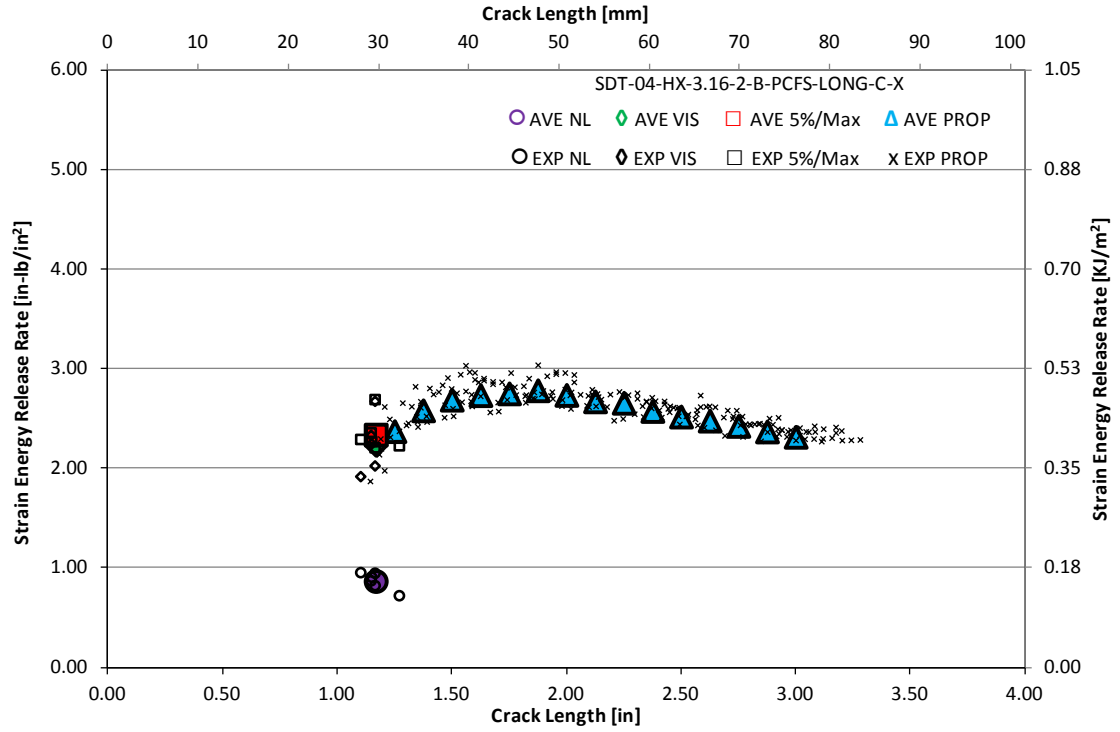

Figure A-70. Resistance curve for HRH-10–3/16–2.0 longitudinal ribbon direction with bottom disbond (center)

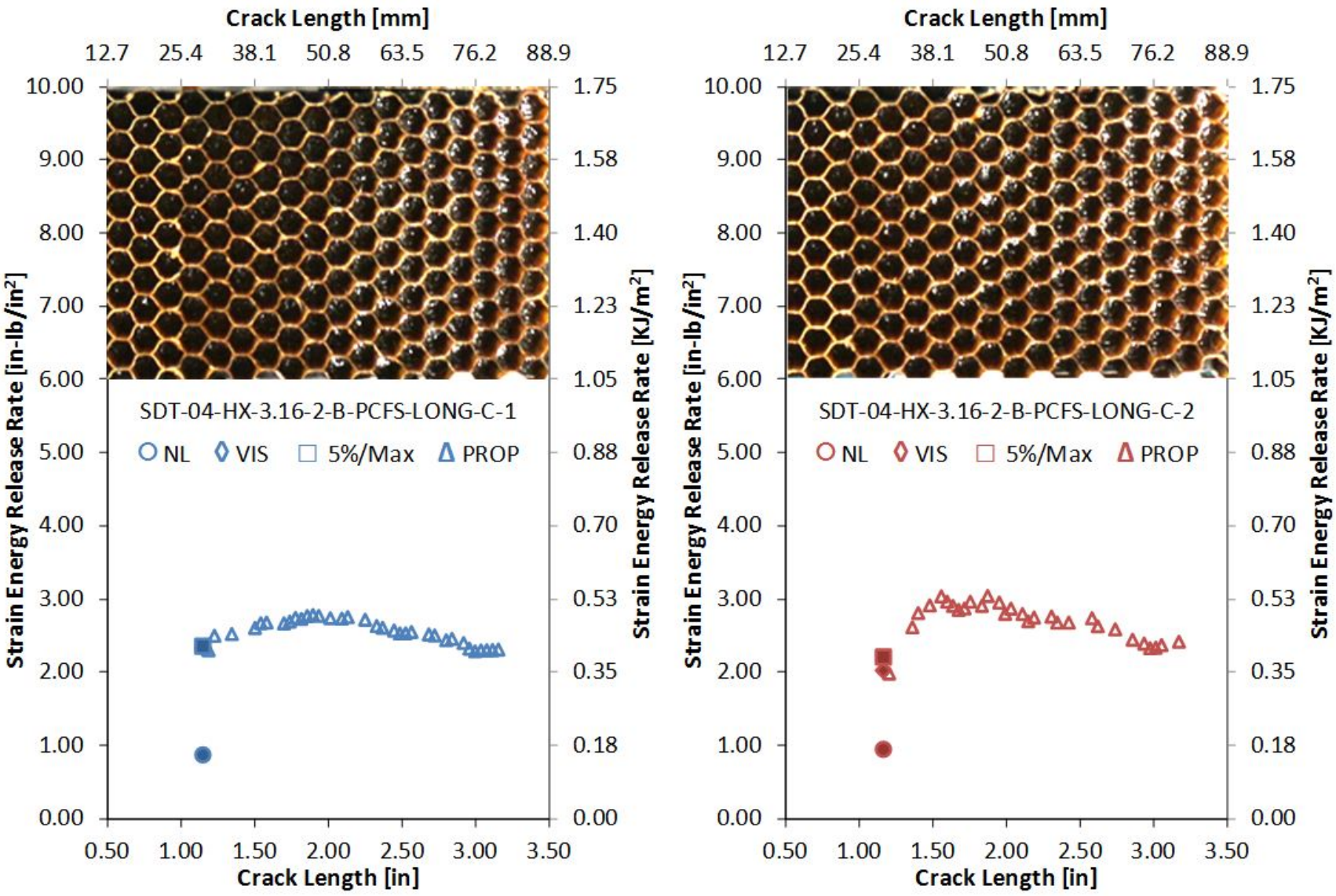

Figure A-71. Failure mode image and resistance curve of SDT-04-HX-3.16-2-B-PCFS-LONG-C-X #1 and #2

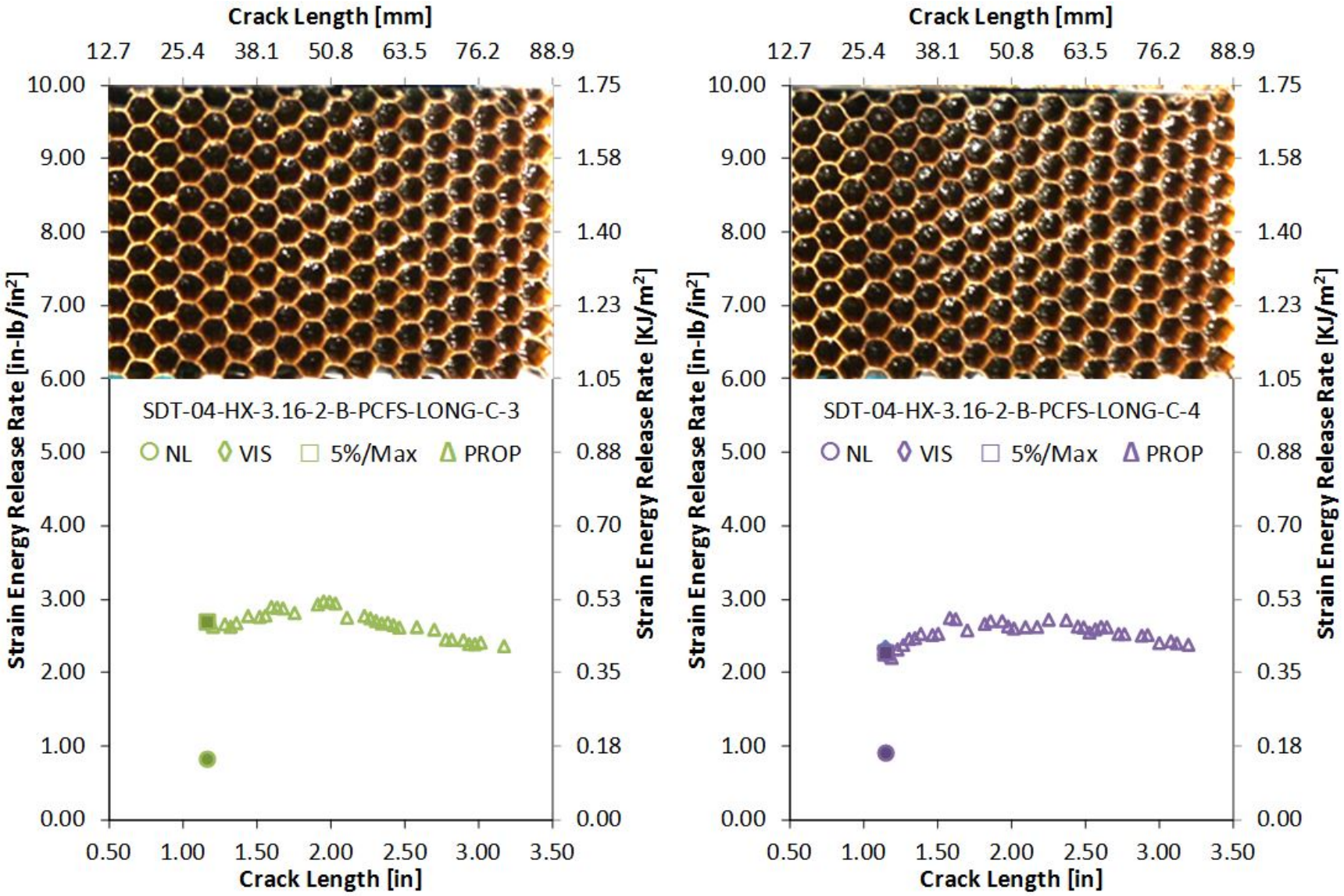

Figure A-72. Failure mode image and resistance curve of SDT-04-HX-3.16-2-B-PCFS-LONG-C-X #3 and #4

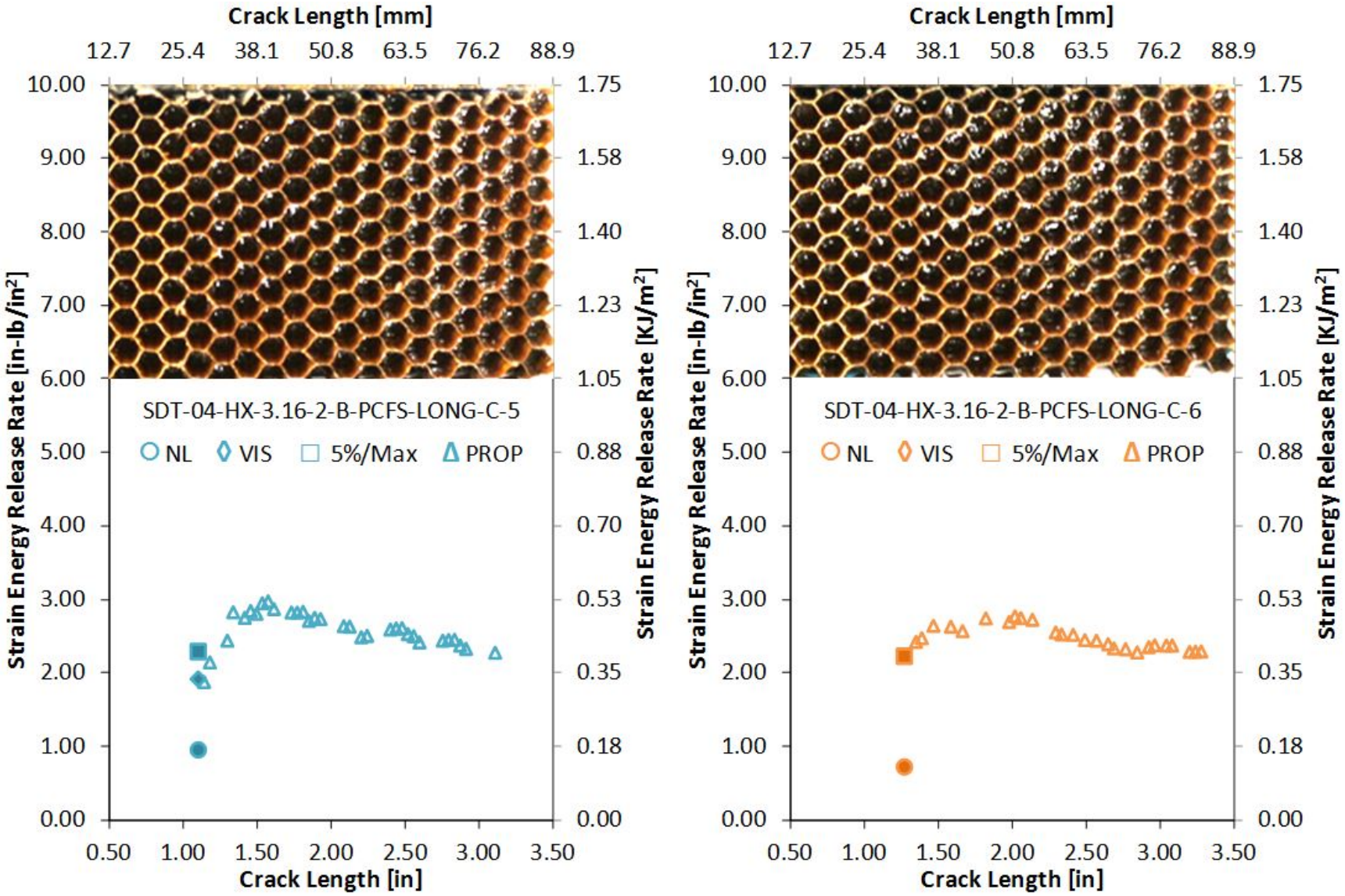

Figure A-73. Failure mode image and resistance curve of SDT-04-HX-3.16-2-B-PCFS-LONG-C-X #5 and #6

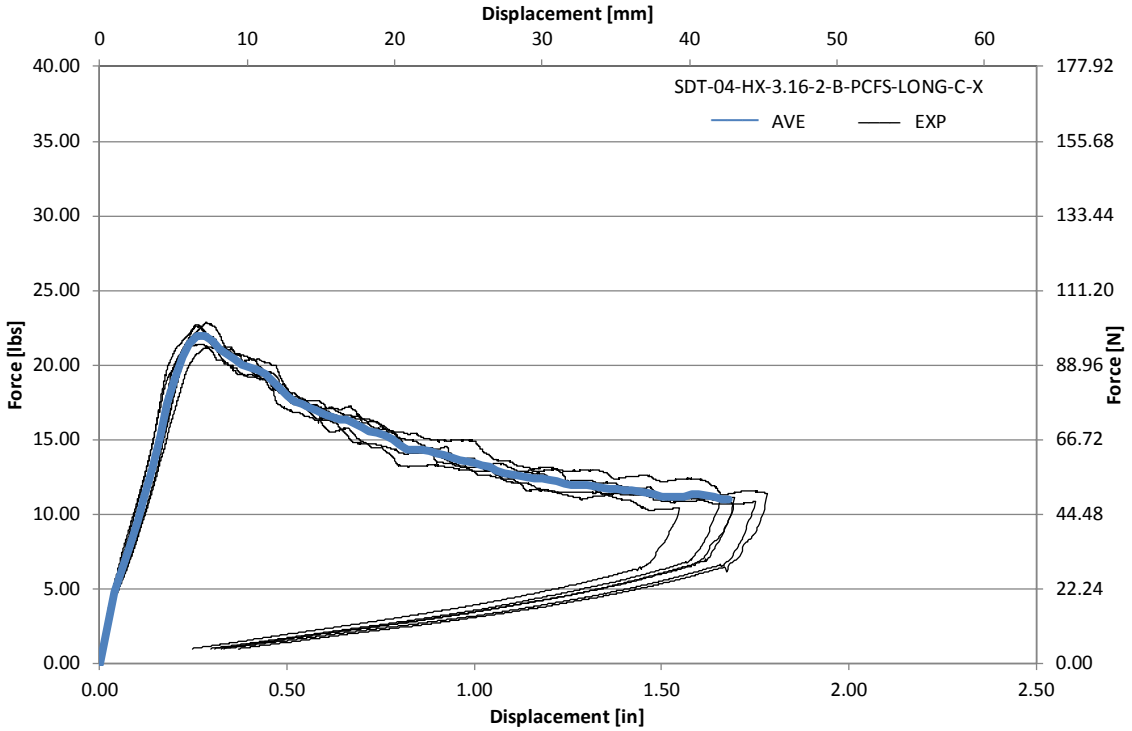

Figure A-74. Load vs. displacement curve for HRH-10–3/16–2.0 longitudinal ribbon direction with bottom disbond (center)

A.5 HRH-10–3/16–3.0 DATA

A.5.1 HRH-10–3/16–3.0 LONGITUDINAL RIBBON DIRECTION WITH TOP DISBOND (CENTER) DATA

Table A-25. Test summary for HRH-10–3/16–3.0 longitudinal ribbon direction with top disbond (center) pre-crack

Specimen	GIC (in-lb/in^2)			GIC (KJ/m^2)			Failure Mode
	NL	VIS	5%/max	NL	VIS	5%/max	
SDT-04-HX-3.16-3-T-PCFS-LONG-C-1	2.185	N/A	2.807	0.383	N/A	0.492	*
SDT-04-HX-3.16-3-T-PCFS-LONG-C-2	2.154	N/A	3.154	0.377	N/A	0.552	*
SDT-04-HX-3.16-3-T-PCFS-LONG-C-3	1.563	1.835	1.835	0.274	0.321	0.321	*
SDT-04-HX-3.16-3-T-PCFS-LONG-C-4	2.403	N/A	3.114	0.421	N/A	0.545	*
SDT-04-HX-3.16-3-T-PCFS-LONG-C-5	1.506	2.295	2.295	0.264	0.402	0.402	*
SDT-04-HX-3.16-3-T-PCFS-LONG-C-6	1.660	N/A	2.198	0.291	N/A	0.385	*
SDT-04-HX-3.16-3-T-PCFS-LONG-C-7							
SDT-04-HX-3.16-3-T-PCFS-LONG-C-8							
AVERAGE GIC	1.912	2.065	2.567	0.335	0.362	0.450	
STANDARD DEVIATION	0.381	0.325	0.538	0.067	0.057	0.094	
COEFFICIENT OF VARIATION (%)	19.912	15.729	20.954	19.912	15.729	20.954	

Notes	*	Mix of C and APO, with the APO occurring primarily on the double cell walls in the ribbon direction.

Table A-26. Test summary for HRH-10–3/16–3.0 longitudinal ribbon direction with top disbond (center)

Specimen	GIC (in-lb/in^2)				GIC (KJ/m^2)				Failure Mode
	NL	VIS	5%/max	AREA	NL	VIS	5%/max	AREA	
SDT-04-HX-3.16-3-T-PCFS-LONG-C-1	0.900	N/A	3.033	3.435	0.158	N/A	0.531	0.602	*
SDT-04-HX-3.16-3-T-PCFS-LONG-C-2	0.725	N/A	2.682	3.876	0.127	N/A	0.470	0.679	*
SDT-04-HX-3.16-3-T-PCFS-LONG-C-3	1.264	3.228	3.327	3.958	0.221	0.565	0.583	0.693	*
SDT-04-HX-3.16-3-T-PCFS-LONG-C-4	0.753	2.823	2.874	3.598	0.132	0.494	0.503	0.630	*
SDT-04-HX-3.16-3-T-PCFS-LONG-C-5	0.946	1.902	1.918	3.516	0.166	0.333	0.336	0.616	*
SDT-04-HX-3.16-3-T-PCFS-LONG-C-6	0.995	2.777	2.954	3.758	0.174	0.486	0.517	0.658	*
SDT-04-HX-3.16-3-T-PCFS-LONG-C-7									
SDT-04-HX-3.16-3-T-PCFS-LONG-C-8									
AVERAGE GIC	0.931	2.683	2.798	3.690	0.163	0.470	0.490	0.646	
STANDARD DEVIATION	0.195	0.558	0.480	0.207	0.034	0.098	0.084	0.036	
COEFFICIENT OF VARIATION (%)	20.970	20.814	17.161	5.618	20.970	20.814	17.161	5.618	

Notes	*	Primarily C with many cells partially in APO; APO is primarily on the double cell walls in the ribbon direction.

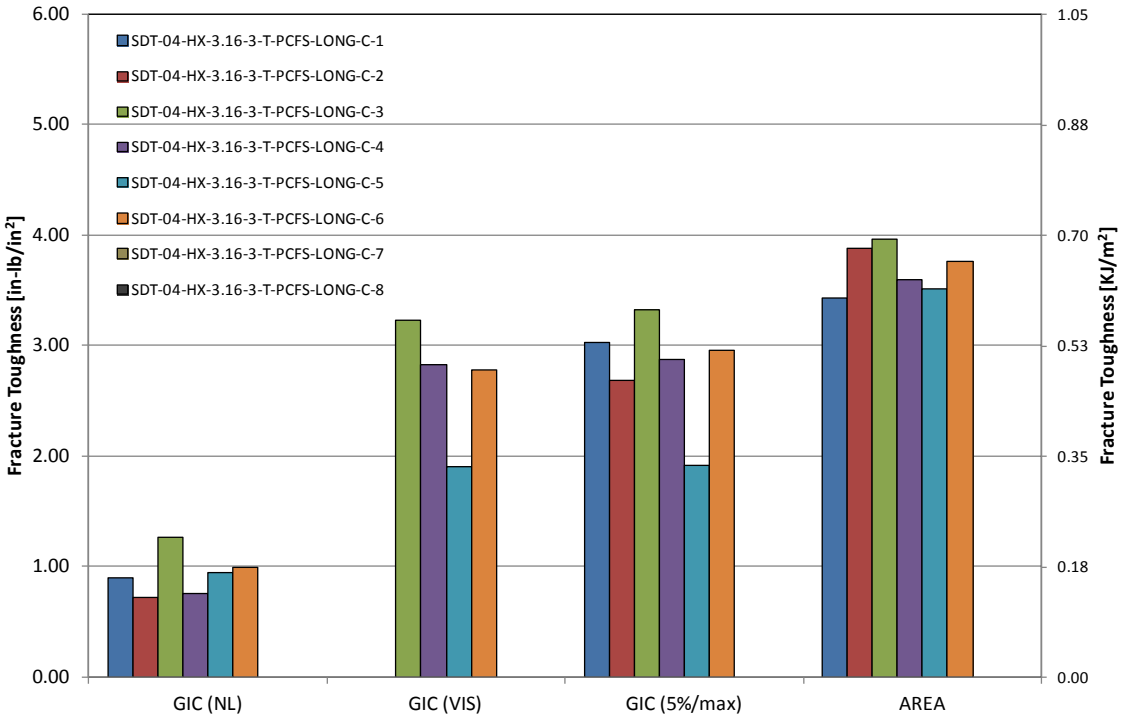

Figure A-75. GIC for HRH-10–3/16–3.0 longitudinal ribbon direction with top disbond (center)

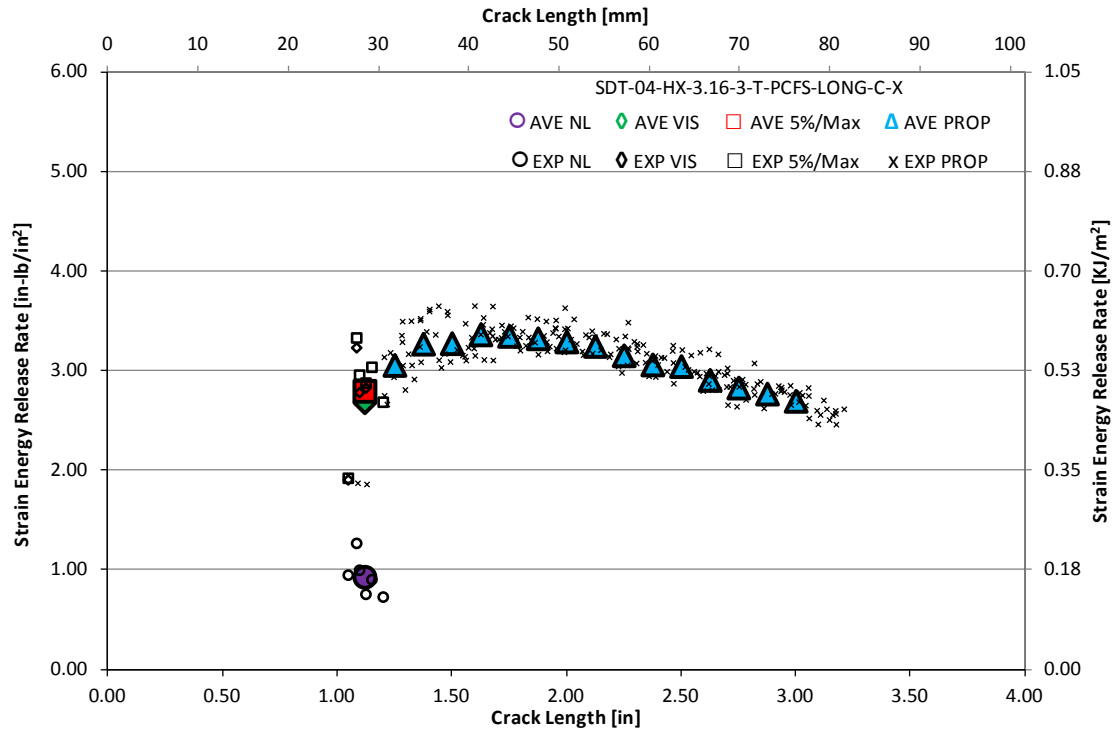

Figure A-76. Resistance curve for HRH-10–3/16–3.0 longitudinal ribbon direction with top disbond (center)

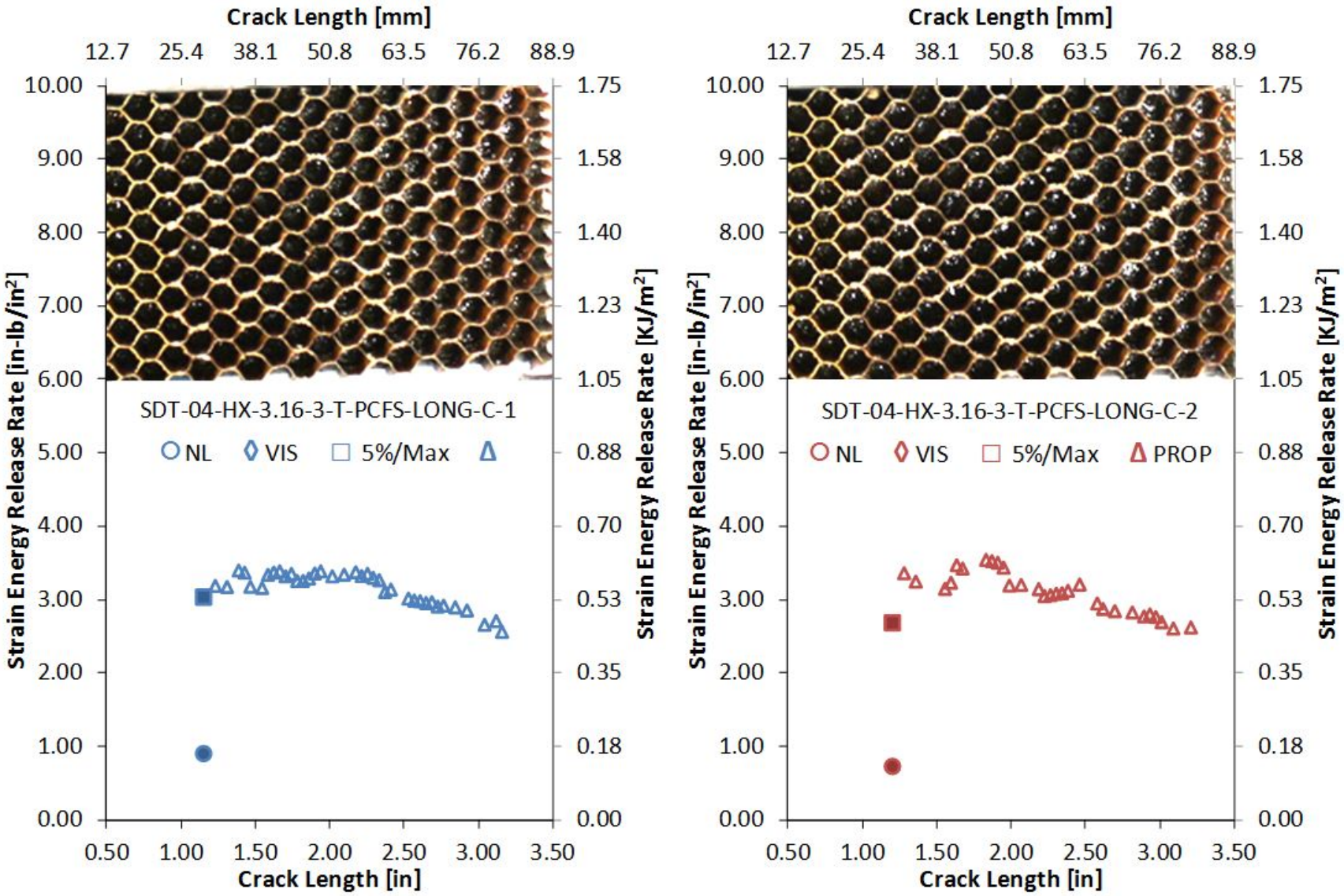

Figure A-77. Failure mode image and resistance curve of SDT-04-HX-3.16-3-T-PCFS-LONG-C-X #1 and #2

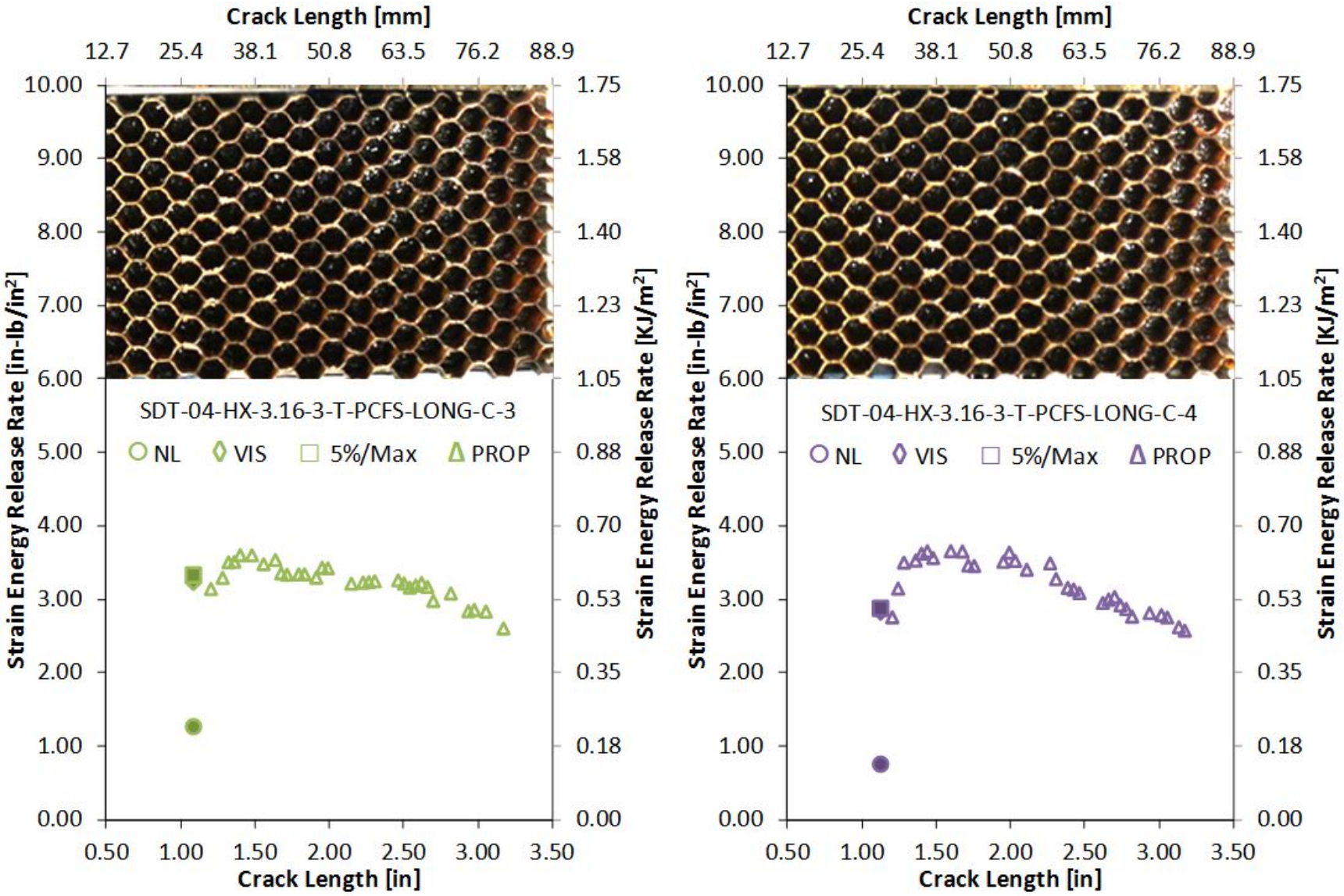

Figure A-78. Failure mode image and resistance curve of SDT-04-HX-3.16-3-T-PCFS-LONG-C-X #3 and #4

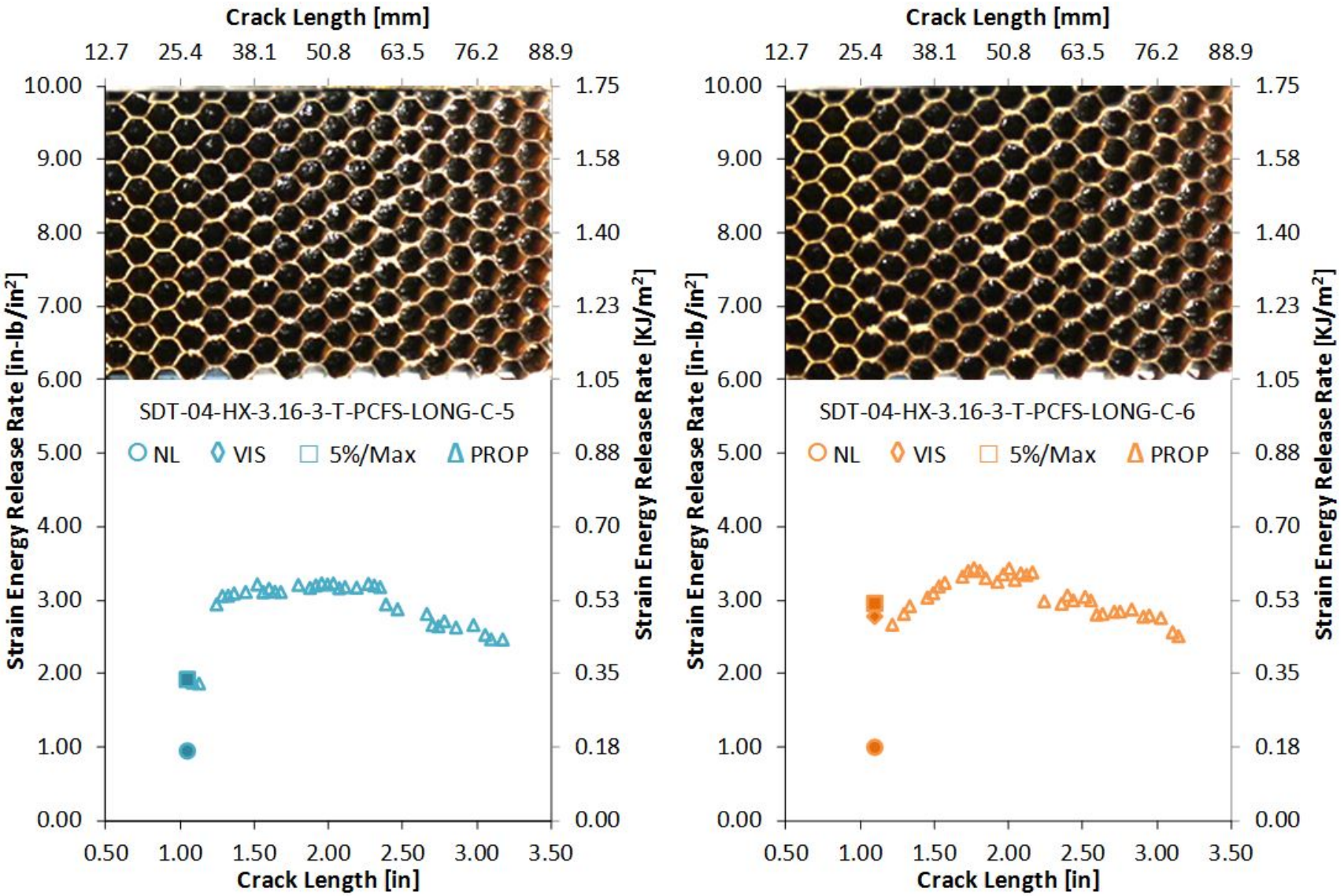

Figure A-79. Failure mode image and resistance curve of SDT-04-HX-3.16-3-T-PCFS-LONG-C-X #5 and #6

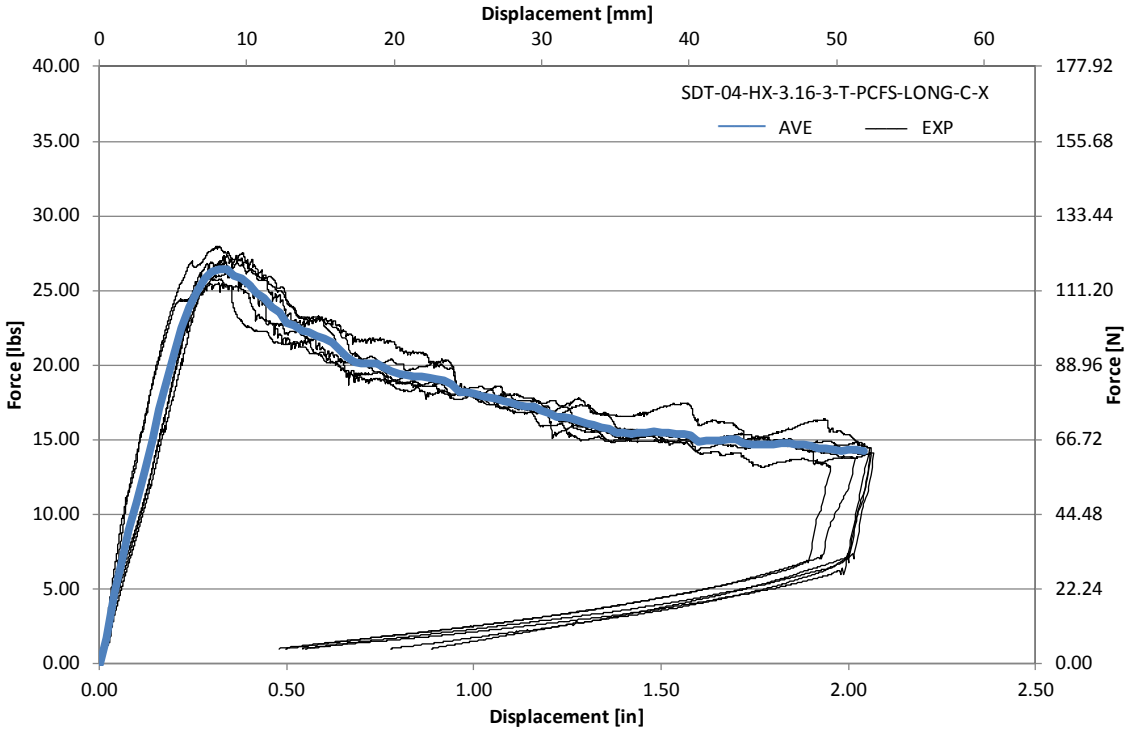

Figure A-80. Load vs. displacement curve for HRH-10–3/16–3.0 longitudinal ribbon direction with top disbond (center)

A.5.2 HRH-10–3/16–3.0 LONGITUDINAL RIBBON DIRECTION WITH BOTTOM DISBOND (CENTER) DATA

Table A-27. Test summary for HRH-10–3/16–3.0 longitudinal ribbon direction with bottom disbond (center) pre-crack

Specimen	GIC (in-lb/in^2)			GIC (KJ/m^2)			Failure Mode
	NL	VIS	5%/max	NL	VIS	5%/max	
SDT-04-HX-3.16-3-B-PCFS-LONG-C-1	1.524	N/A	2.291	0.267	N/A	0.401	*
SDT-04-HX-3.16-3-B-PCFS-LONG-C-2	1.335	2.155	2.204	0.234	0.377	0.386	*
SDT-04-HX-3.16-3-B-PCFS-LONG-C-3	1.560	N/A	2.192	0.273	N/A	0.384	*
SDT-04-HX-3.16-3-B-PCFS-LONG-C-4	1.324	N/A	2.619	0.232	N/A	0.459	*
SDT-04-HX-3.16-3-B-PCFS-LONG-C-5	1.521	2.475	2.475	0.266	0.433	0.433	*
SDT-04-HX-3.16-3-B-PCFS-LONG-C-6	1.691	N/A	2.679	0.296	N/A	0.469	*
SDT-04-HX-3.16-3-B-PCFS-LONG-C-7							
SDT-04-HX-3.16-3-B-PCFS-LONG-C-8							
AVERAGE GIC	1.492	2.315	2.410	0.261	0.405	0.422	
STANDARD DEVIATION	0.141	0.226	0.212	0.025	0.040	0.037	
COEFFICIENT OF VARIATION (%)	9.415	9.781	8.789	9.415	9.781	8.789	

Notes	*	Primarily in APO with some partial cells in C

Table A-28. Test summary for HRH-10–3/16–3.0 longitudinal ribbon direction with bottom disbond (center)

Specimen	GIC (in-lb/in^2)				GIC (KJ/m^2)				Failure Mode
	NL	VIS	5%/max	AREA	NL	VIS	5%/max	AREA	
SDT-04-HX-3.16-3-B-PCFS-LONG-C-1	0.751	2.352	2.685	3.160	0.131	0.412	0.470	0.553	*
SDT-04-HX-3.16-3-B-PCFS-LONG-C-2	1.501	1.993	3.248	3.174	0.263	0.349	0.569	0.556	*
SDT-04-HX-3.16-3-B-PCFS-LONG-C-3	1.126	2.459	2.577	3.316	0.197	0.431	0.451	0.581	*
SDT-04-HX-3.16-3-B-PCFS-LONG-C-4	1.826	N/A	2.171	3.151	0.320	N/A	0.380	0.552	*
SDT-04-HX-3.16-3-B-PCFS-LONG-C-5	1.786	1.941	2.149	2.921	0.313	0.340	0.376	0.512	*
SDT-04-HX-3.16-3-B-PCFS-LONG-C-6	0.714	3.066	3.166	3.489	0.125	0.537	0.554	0.611	*
SDT-04-HX-3.16-3-B-PCFS-LONG-C-7									
SDT-04-HX-3.16-3-B-PCFS-LONG-C-8									
AVERAGE GIC	1.284	2.362	2.666	3.202	0.225	0.414	0.467	0.561	
STANDARD DEVIATION	0.495	0.452	0.471	0.189	0.087	0.079	0.083	0.033	
COEFFICIENT OF VARIATION (%)	38.587	19.148	17.671	5.915	38.587	19.148	17.671	5.915	

Notes	*	Primarily C with many cells in or partially in APO; APO is primarily on the double cell walls in the ribbon direction .

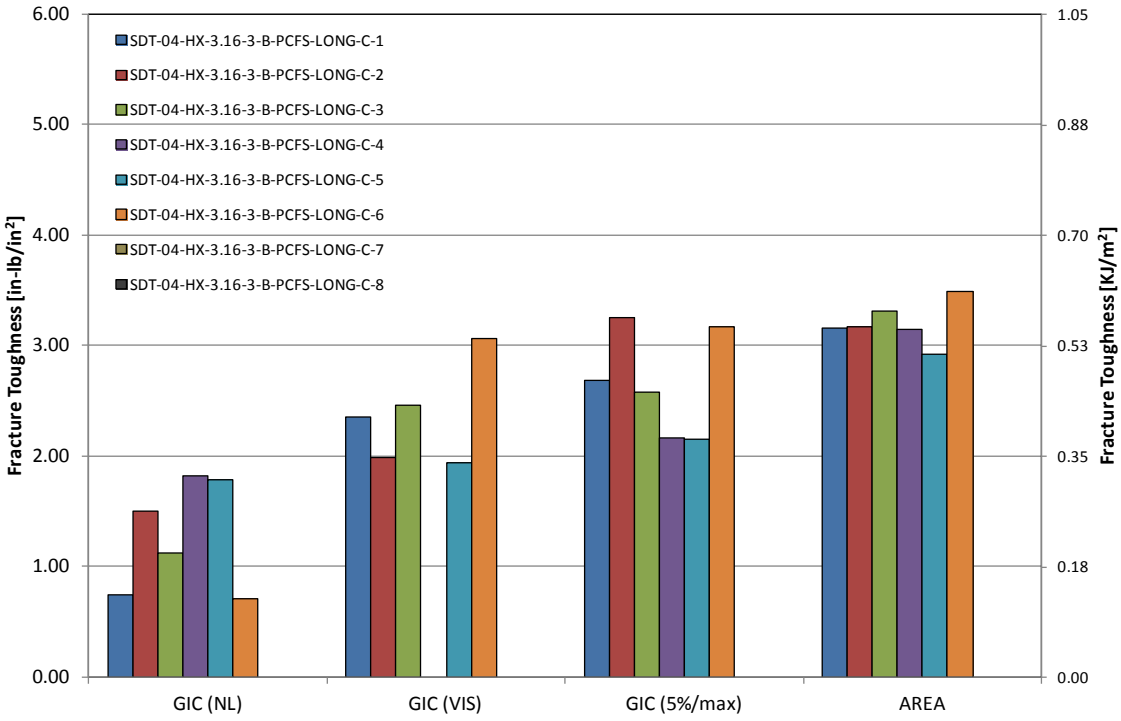

Figure A-81. GIC for HRH-10–3/16–3.0 longitudinal ribbon direction with bottom disbond (center)

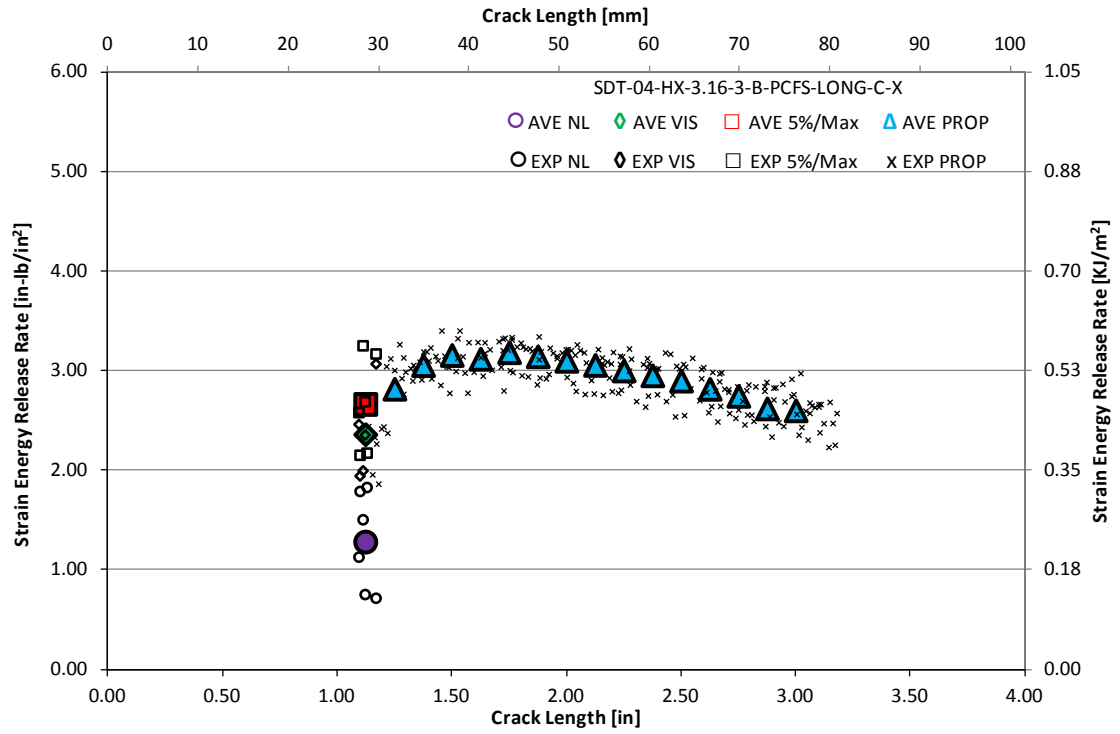

Figure A-82. Resistance curve for HRH-10–3/16–3.0 longitudinal ribbon direction with bottom disbond (center)

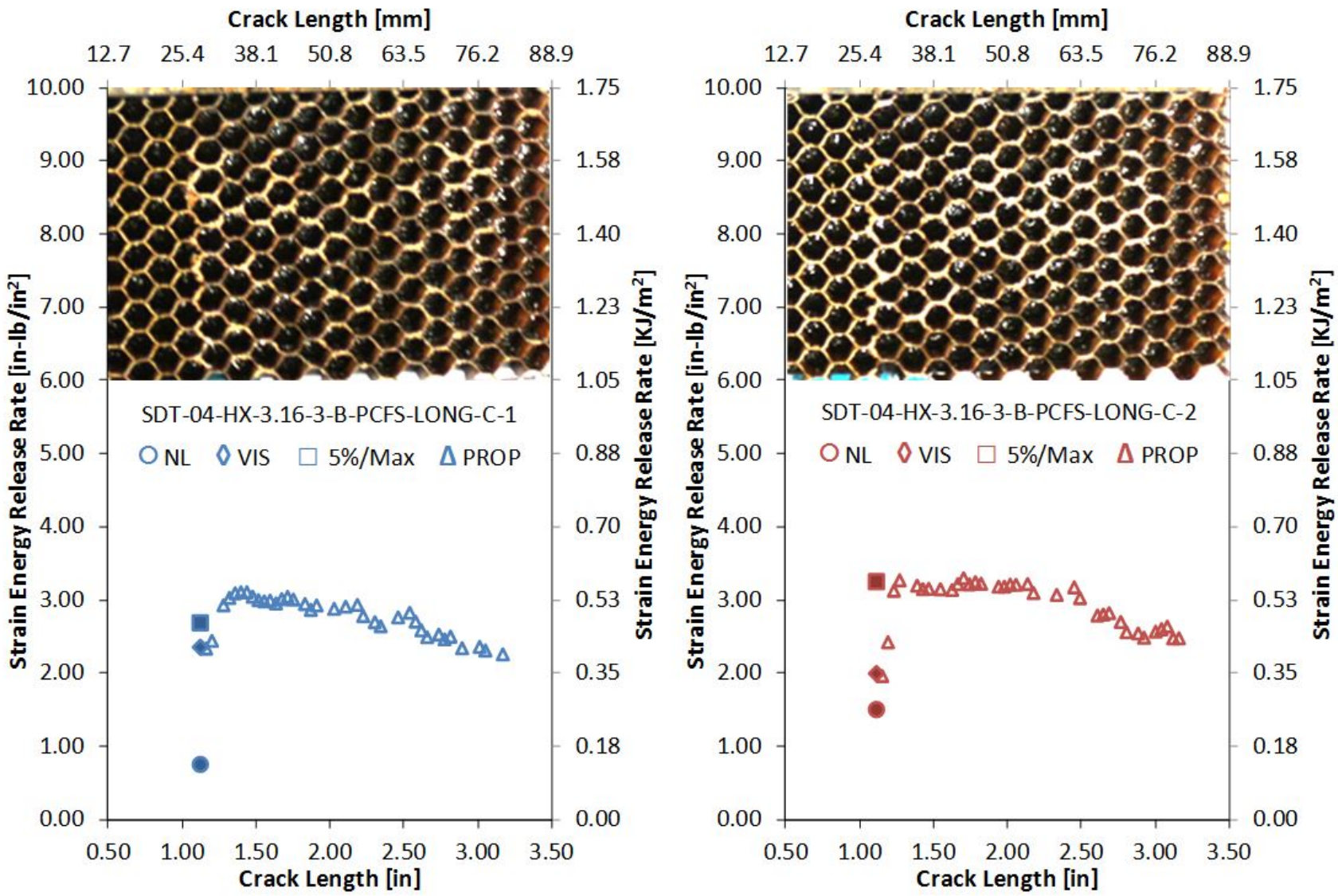

Figure A-83. Failure mode image and resistance curve of SDT-04-HX-3.16-3-B-PCFS-LONG-C-X #1 and #2

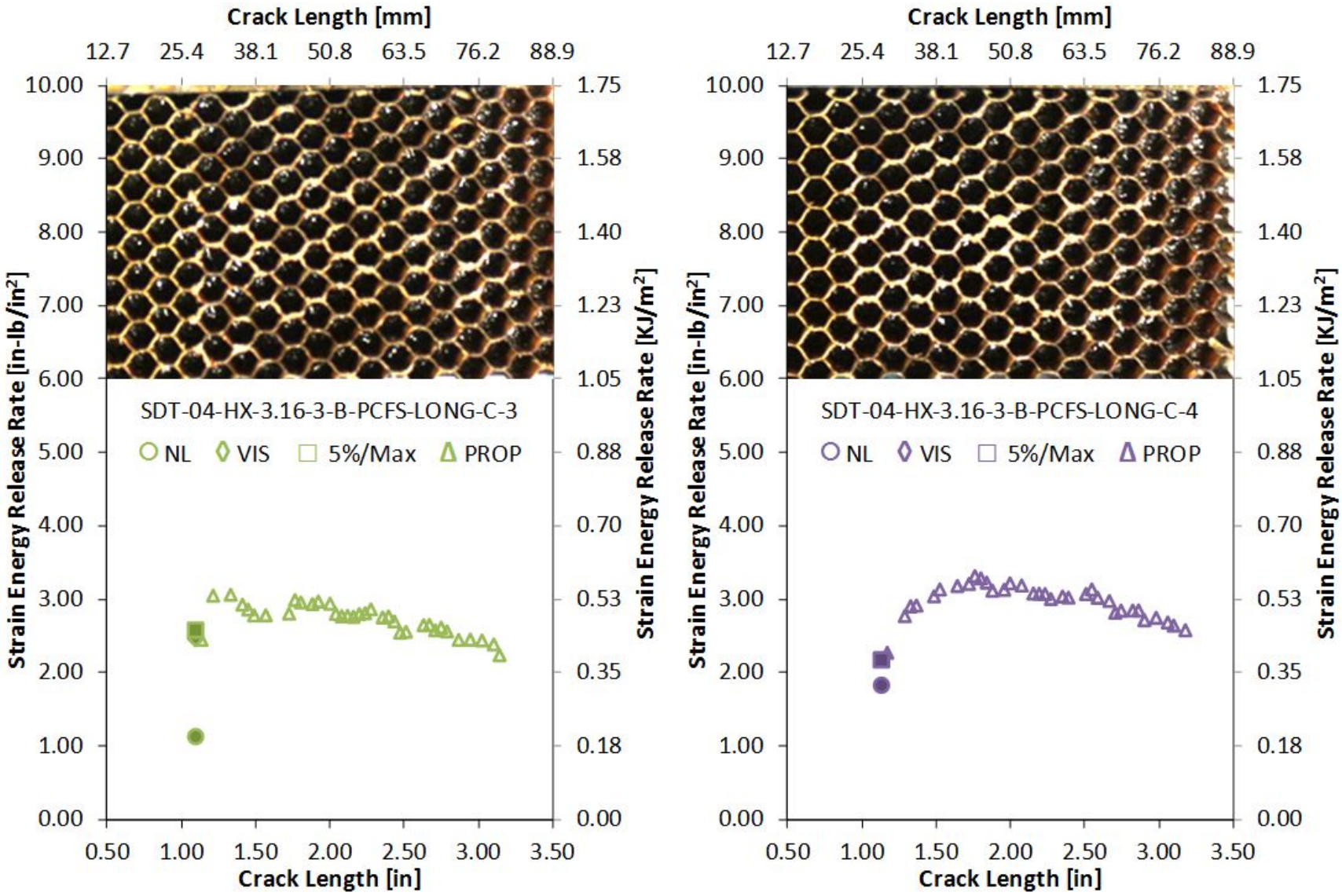

Figure A-84. Failure mode image and resistance curve of SDT-04-HX-3.16-3-B-PCFS-LONG-C-X #3 and #4

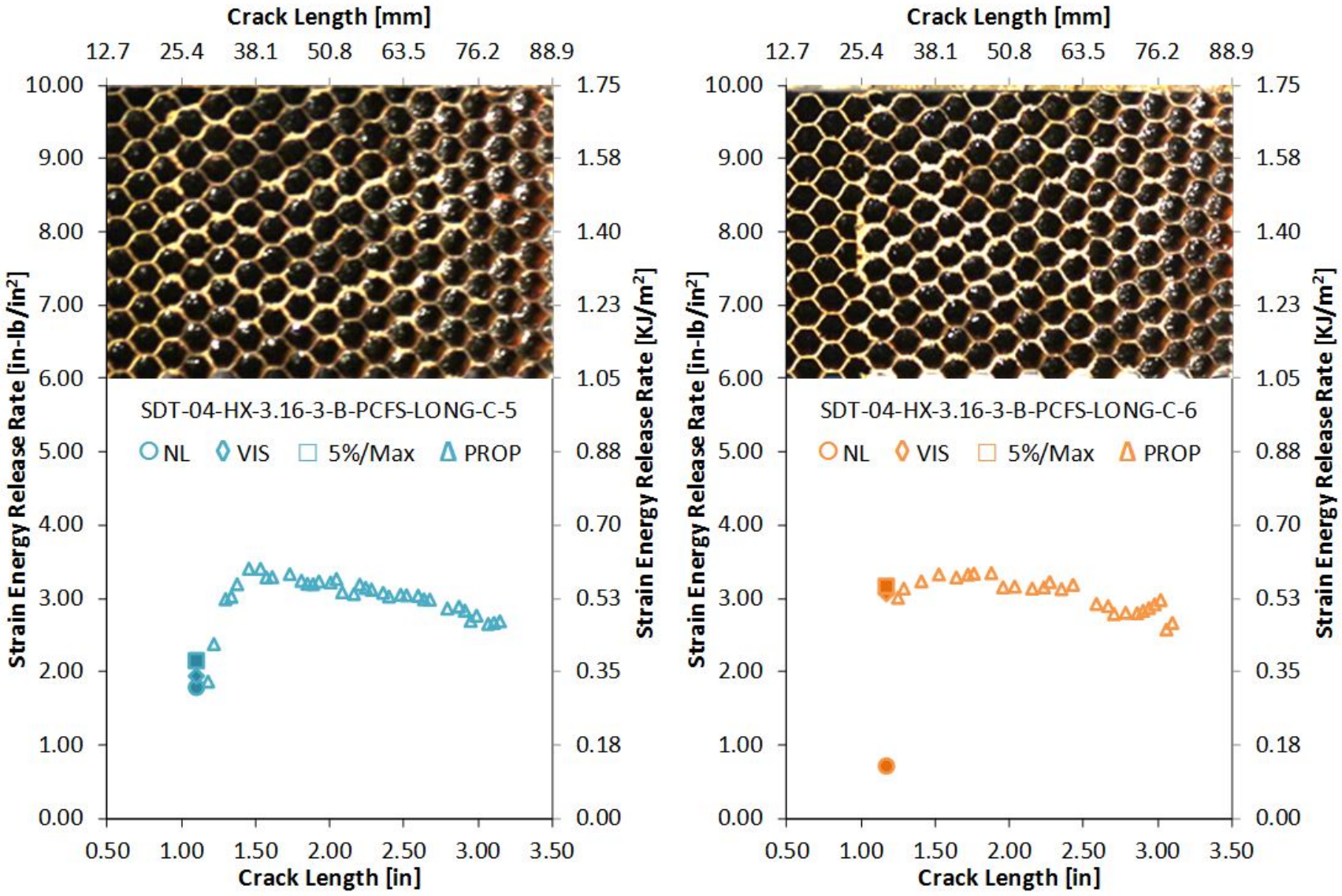

Figure A-85. Failure mode image and resistance curve of SDT-04-HX-3.16-3-B-PCFS-LONG-C-X #5 and #6

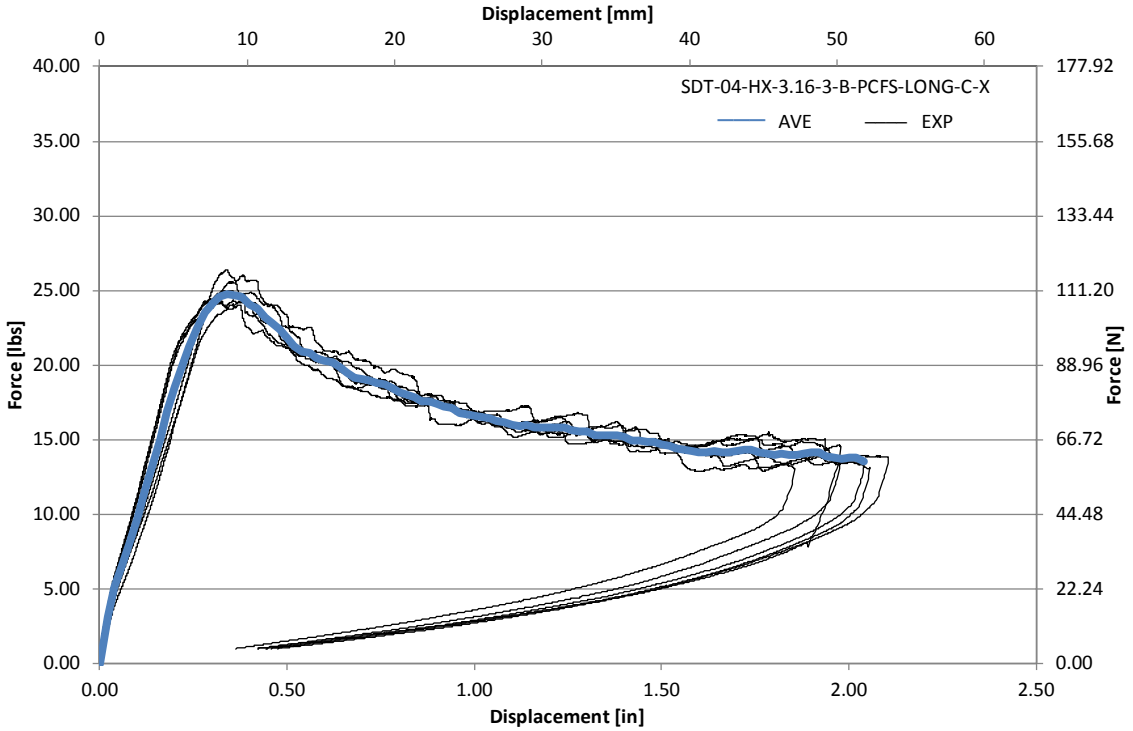

Figure A-86. Load vs. displacement curve for HRH-10–3/16–3.0 longitudinal ribbon direction with bottom disbond (center)

A.5.3 HRH-10–3/16–3.0 LATERAL RIBBON DIRECTION WITH TOP DISBOND (CENTER) DATA

Table A-29. Test summary for HRH-10–3/16–3.0 lateral ribbon direction with top disbond (center) pre-crack

Specimen	GIC (in-lb/in^2)			GIC (KJ/m^2)			Failure Mode
	NL	VIS	5%/max	NL	VIS	5%/max	
SDT-04-HX-3.16-3-T-PCFS-LAT-C-1	1.752	2.141	2.213	0.307	0.375	0.388	Primarily in C
SDT-04-HX-3.16-3-T-PCFS-LAT-C-2	1.570	N/A	2.074	0.275	N/A	0.363	Primarily in C
SDT-04-HX-3.16-3-T-PCFS-LAT-C-3	1.637	N/A	2.349	0.287	N/A	0.411	Primarily in C
SDT-04-HX-3.16-3-T-PCFS-LAT-C-4	1.615	N/A	2.267	0.283	N/A	0.397	Primarily in C
SDT-04-HX-3.16-3-T-PCFS-LAT-C-5	1.359	N/A	2.545	0.238	N/A	0.446	Primarily in C
SDT-04-HX-3.16-3-T-PCFS-LAT-C-6	1.894	2.461	2.495	0.332	0.431	0.437	Primarily in C
SDT-04-HX-3.16-3-T-PCFS-LAT-C-7							
SDT-04-HX-3.16-3-T-PCFS-LAT-C-8							
AVERAGE GIC	1.638	2.301	2.324	0.287	0.403	0.407	
STANDARD DEVIATION	0.180	0.227	0.177	0.032	0.040	0.031	
COEFFICIENT OF VARIATION (%)	10.986	9.848	7.620	10.986	9.848	7.620	

Table A-30. Test summary for HRH-10–3/16–3.0 lateral ribbon direction with top disbond (center)

Specimen	GIC (in-lb/in^2)				GIC (KJ/m^2)				Failure Mode
	NL	VIS	5%/max	AREA	NL	VIS	5%/max	AREA	
SDT-04-HX-3.16-3-T-PCFS-LAT-C-1	0.841	N/A	2.120	3.602	0.147	N/A	0.371	0.631	Primarily C
SDT-04-HX-3.16-3-T-PCFS-LAT-C-2	1.100	N/A	2.152	3.502	0.193	N/A	0.377	0.613	*
SDT-04-HX-3.16-3-T-PCFS-LAT-C-3	0.843	N/A	1.768	3.304	0.148	N/A	0.310	0.579	*
SDT-04-HX-3.16-3-T-PCFS-LAT-C-4	0.712	N/A	2.351	3.434	0.125	N/A	0.412	0.601	*
SDT-04-HX-3.16-3-T-PCFS-LAT-C-5	0.828	N/A	2.170	3.459	0.145	N/A	0.380	0.606	*
SDT-04-HX-3.16-3-T-PCFS-LAT-C-6	0.920	N/A	2.104	3.355	0.161	N/A	0.368	0.588	*
SDT-04-HX-3.16-3-T-PCFS-LAT-C-7									
SDT-04-HX-3.16-3-T-PCFS-LAT-C-8									
AVERAGE GIC	0.874	N/A	2.111	3.443	0.153	N/A	0.370	0.603	
STANDARD DEVIATION	0.130	N/A	0.190	0.106	0.023	N/A	0.033	0.019	
COEFFICIENT OF VARIATION (%)	14.822	N/A	9.009	3.080	14.822	N/A	9.009	3.080	

Notes	*	Primarily C, with a couple of cells partially in APO; APO is primarily on the double cell walls in the ribbon direction.

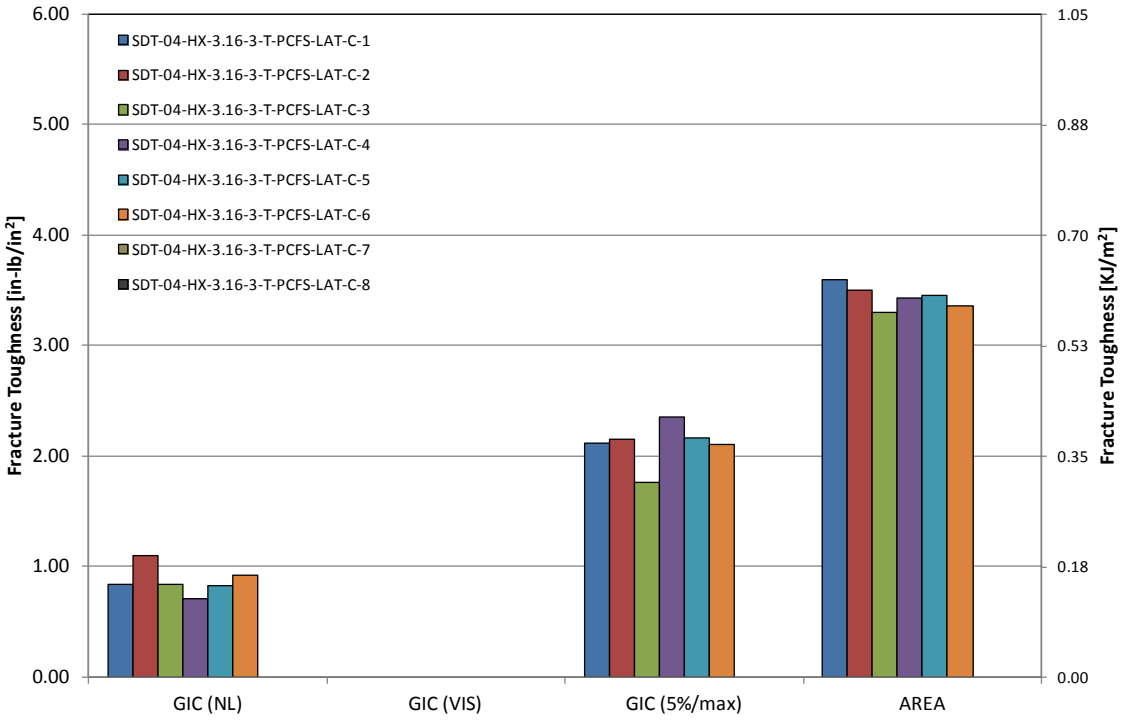

Figure A-87. GIC for HRH-10–3/16–3.0 lateral ribbon direction with top disbond (center)

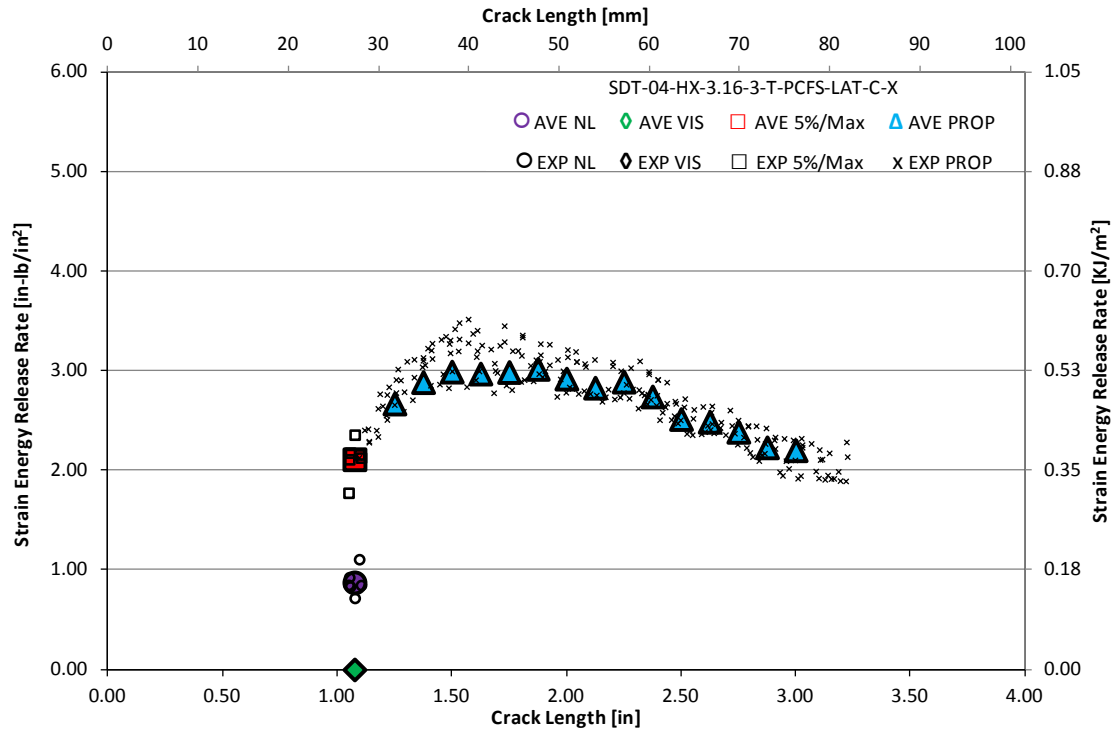

Figure A-88. Resistance curve for HRH-10–3/16–3.0 lateral ribbon direction with top disbond (center)

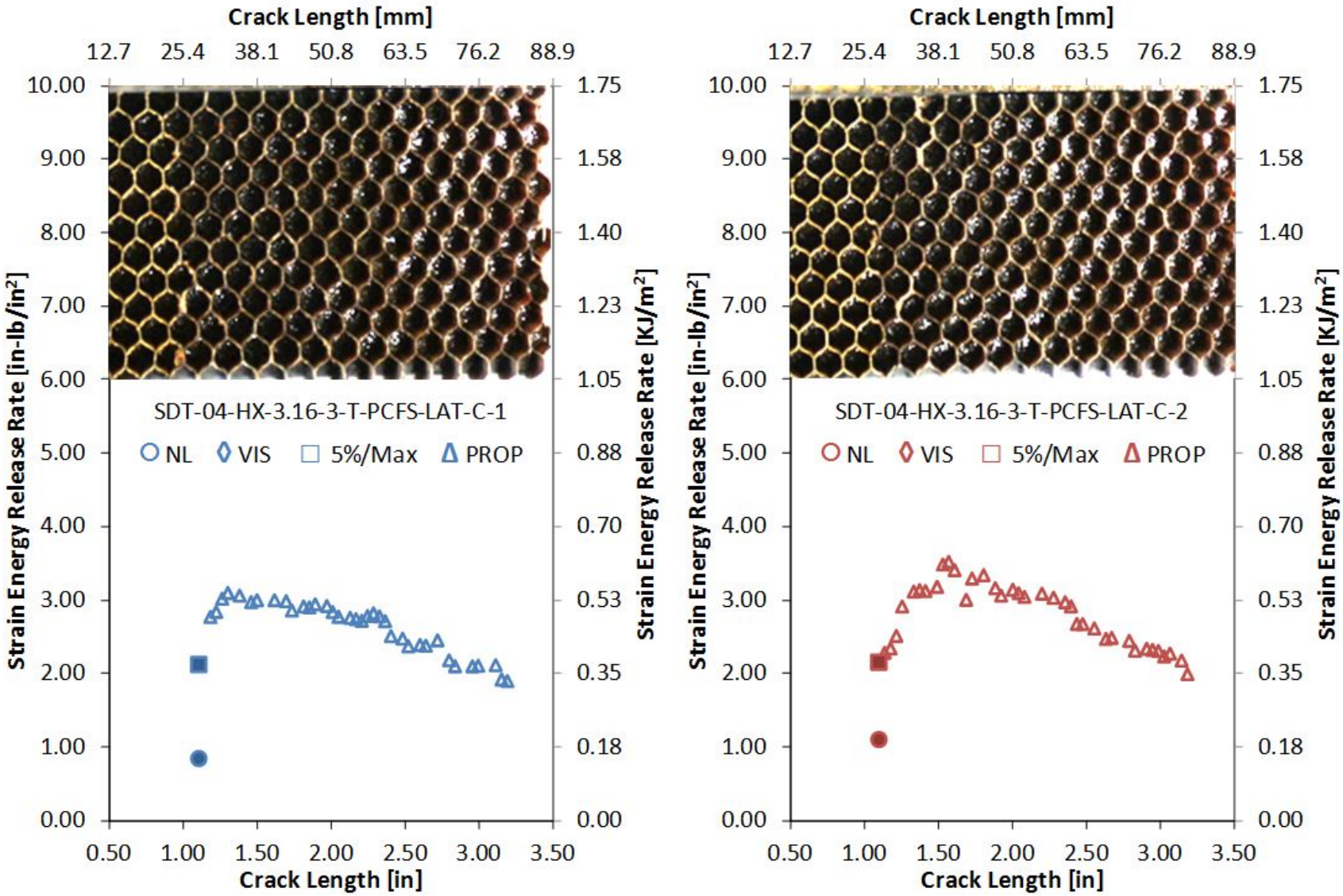

Figure A-89. Failure mode image and resistance curve of SDT-04-HX-3.16-3-T-PCFS-LAT-C-X #1 and #2

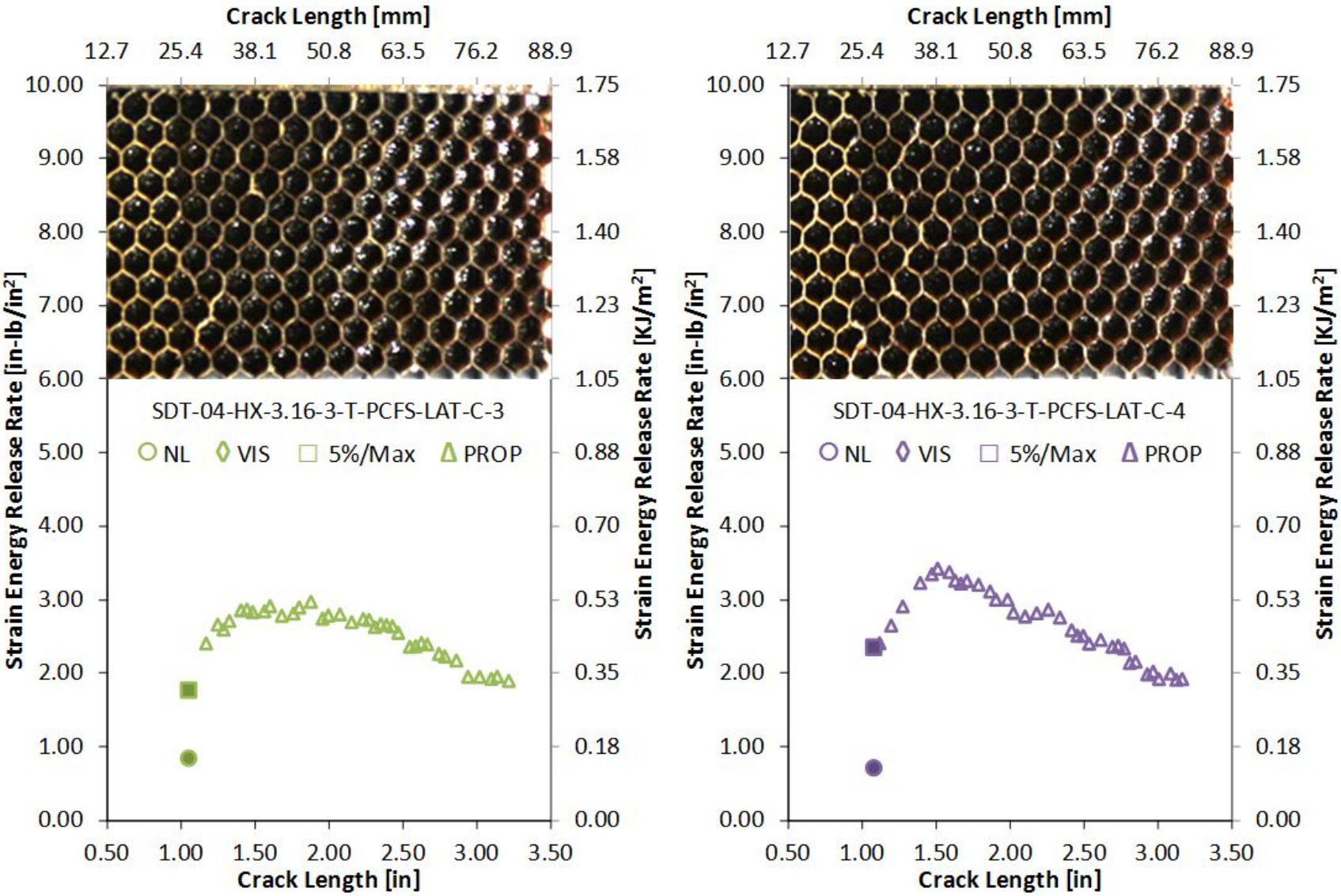

Figure A-90. Failure mode image and resistance curve of SDT-04-HX-3.16-3-T-PCFS-LAT-C-X #3 and #4

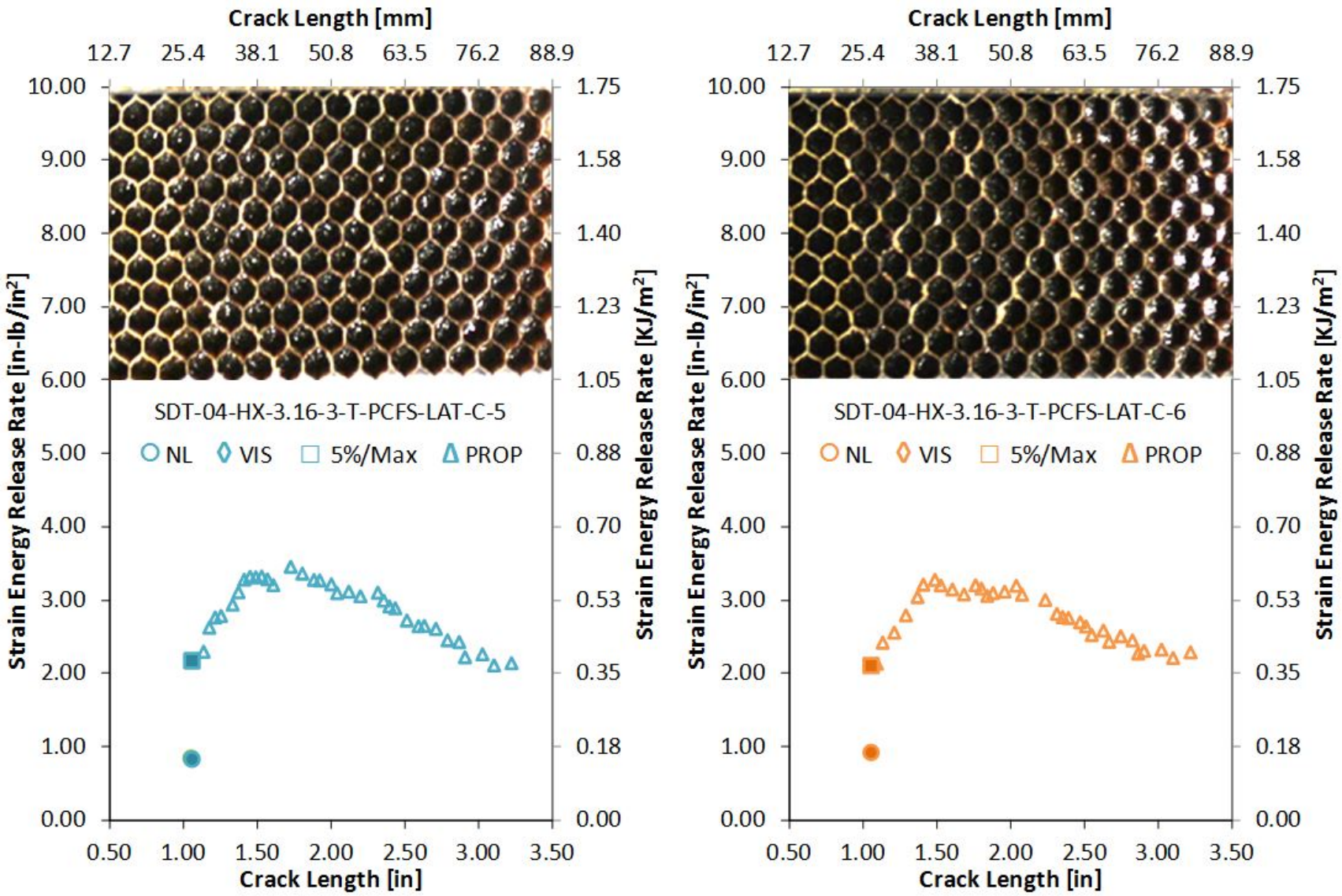

Figure A-91. Failure mode image and resistance curve of SDT-04-HX-3.16-3-T-PCFS-LAT-C-X #5 and #6

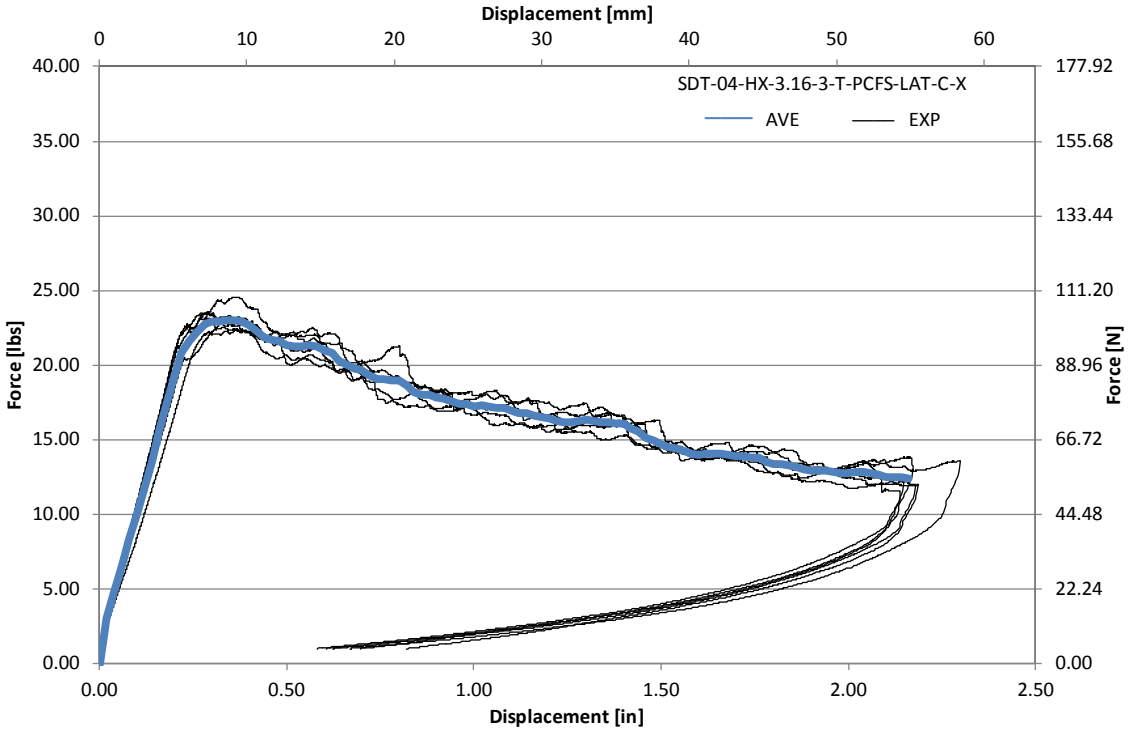

Figure A-92. Load vs. displacement curve for HRH-10–3/16–3.0 lateral ribbon direction with top disbond (center)

A.5.4 HRH-10–3/16–3.0 LATERAL RIBBON DIRECTION WITH BOTTOM DISBOND (CENTER) DATA

Table A-31. Test summary for HRH-10–3/16–3.0 lateral ribbon direction with bottom disbond (center) pre-crack

Specimen	GIC (in-lb/in^2)			GIC (KJ/m^2)			Failure Mode
	NL	VIS	5%/max	NL	VIS	5%/max	
SDT-04-HX-3.16-3-B-PCFS-LAT-C-1	1.250	N/A	2.401	0.219	N/A	0.421	*
SDT-04-HX-3.16-3-B-PCFS-LAT-C-2	1.450	N/A	2.359	0.254	N/A	0.413	*
SDT-04-HX-3.16-3-B-PCFS-LAT-C-3	2.081	N/A	2.505	0.365	N/A	0.439	*
SDT-04-HX-3.16-3-B-PCFS-LAT-C-4	1.457	N/A	2.633	0.255	N/A	0.461	*
SDT-04-HX-3.16-3-B-PCFS-LAT-C-5	1.854	2.696	2.774	0.325	0.472	0.486	*
SDT-04-HX-3.16-3-B-PCFS-LAT-C-6	1.761	N/A	2.486	0.308	N/A	0.435	*
SDT-04-HX-3.16-3-B-PCFS-LAT-C-7							
SDT-04-HX-3.16-3-B-PCFS-LAT-C-8							
AVERAGE GIC	1.642	2.696	2.527	0.288	0.472	0.442	
STANDARD DEVIATION	0.309	N/A	0.154	0.054	N/A	0.027	
COEFFICIENT OF VARIATION (%)	18.792	N/A	6.087	18.792	N/A	6.087	

Notes	*	Mix of C and APO, with the APO occurring primarily on the double cell walls in the ribbon direction.

Table A-32. Test summary for HRH-10–3/16–3.0 lateral ribbon direction with bottom disbond (center)

Specimen	GIC (in-lb/in^2)				GIC (KJ/m^2)				Failure Mode
	NL	VIS	5%/max	AREA	NL	VIS	5%/max	AREA	
SDT-04-HX-3.16-3-B-PCFS-LAT-C-1	0.651	N/A	2.458	3.650	0.114	N/A	0.430	0.639	*
SDT-04-HX-3.16-3-B-PCFS-LAT-C-2	0.876	2.469	2.595	3.867	0.153	0.432	0.454	0.677	*
SDT-04-HX-3.16-3-B-PCFS-LAT-C-3	0.886	1.871	1.904	3.868	0.155	0.328	0.333	0.677	*
SDT-04-HX-3.16-3-B-PCFS-LAT-C-4	0.672	N/A	2.314	3.545	0.118	N/A	0.405	0.621	*
SDT-04-HX-3.16-3-B-PCFS-LAT-C-5	1.256	N/A	2.190	3.472	0.220	N/A	0.384	0.608	*
SDT-04-HX-3.16-3-B-PCFS-LAT-C-6	1.000	N/A	2.814	3.472	0.175	N/A	0.493	0.608	*
SDT-04-HX-3.16-3-B-PCFS-LAT-C-7									
SDT-04-HX-3.16-3-B-PCFS-LAT-C-8									
AVERAGE GIC	0.890	2.170	2.379	3.646	0.156	0.380	0.417	0.638	
STANDARD DEVIATION	0.224	0.423	0.319	0.184	0.039	0.074	0.056	0.032	
COEFFICIENT OF VARIATION (%)	25.185	19.488	13.397	5.040	25.185	19.488	13.397	5.040	

Notes	*	Primarily C with many cells in APO and partially in APO; APO is primarily on the double cell walls in the ribbon direction.

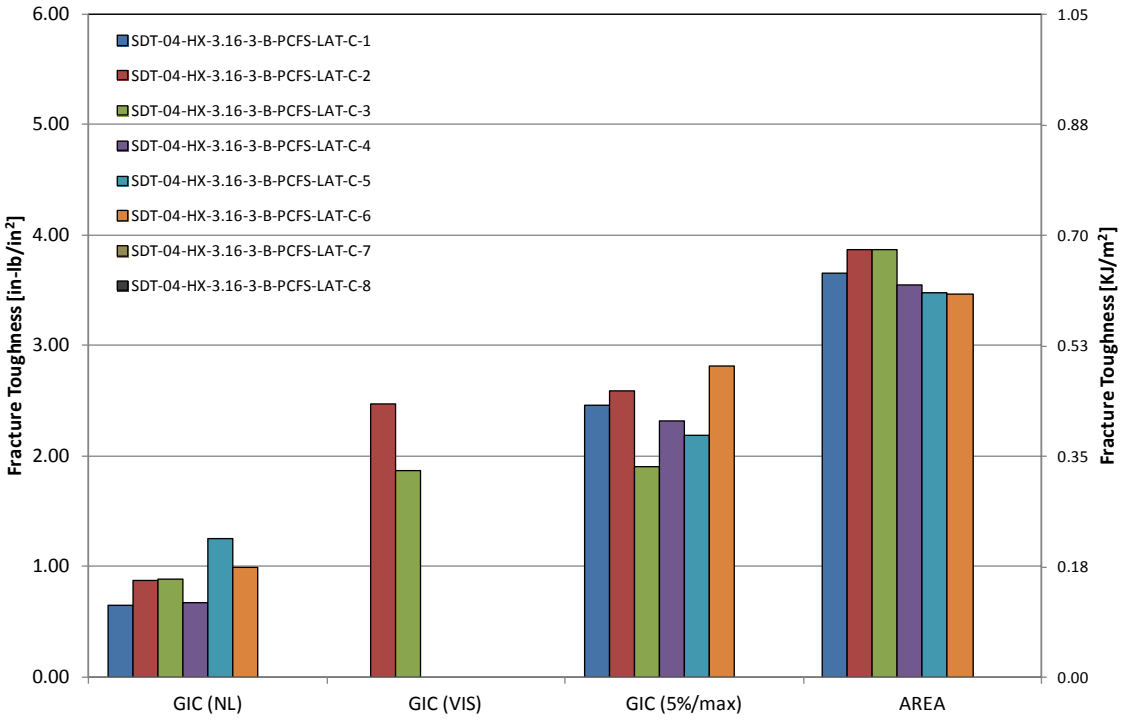

Figure A-93. GIC for HRH-10–3/16–3.0 lateral ribbon direction with bottom disbond (center)

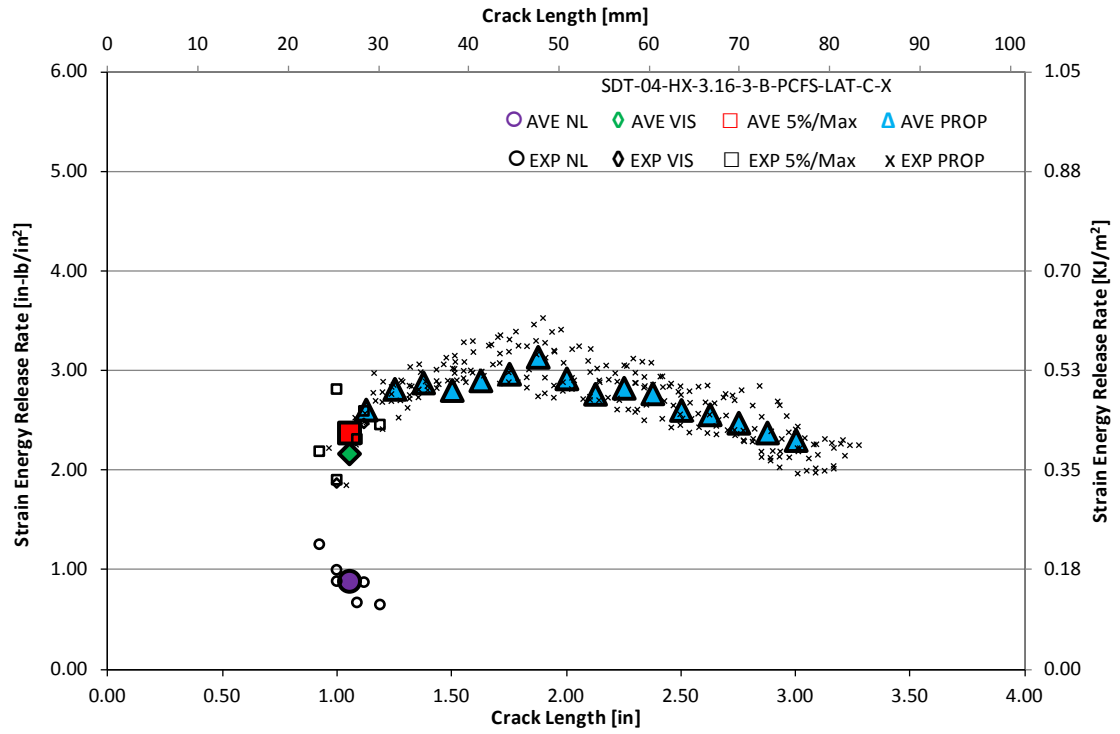

Figure A-94. Resistance curve for HRH-10–3/16–3.0 lateral ribbon direction with bottom disbond (center)

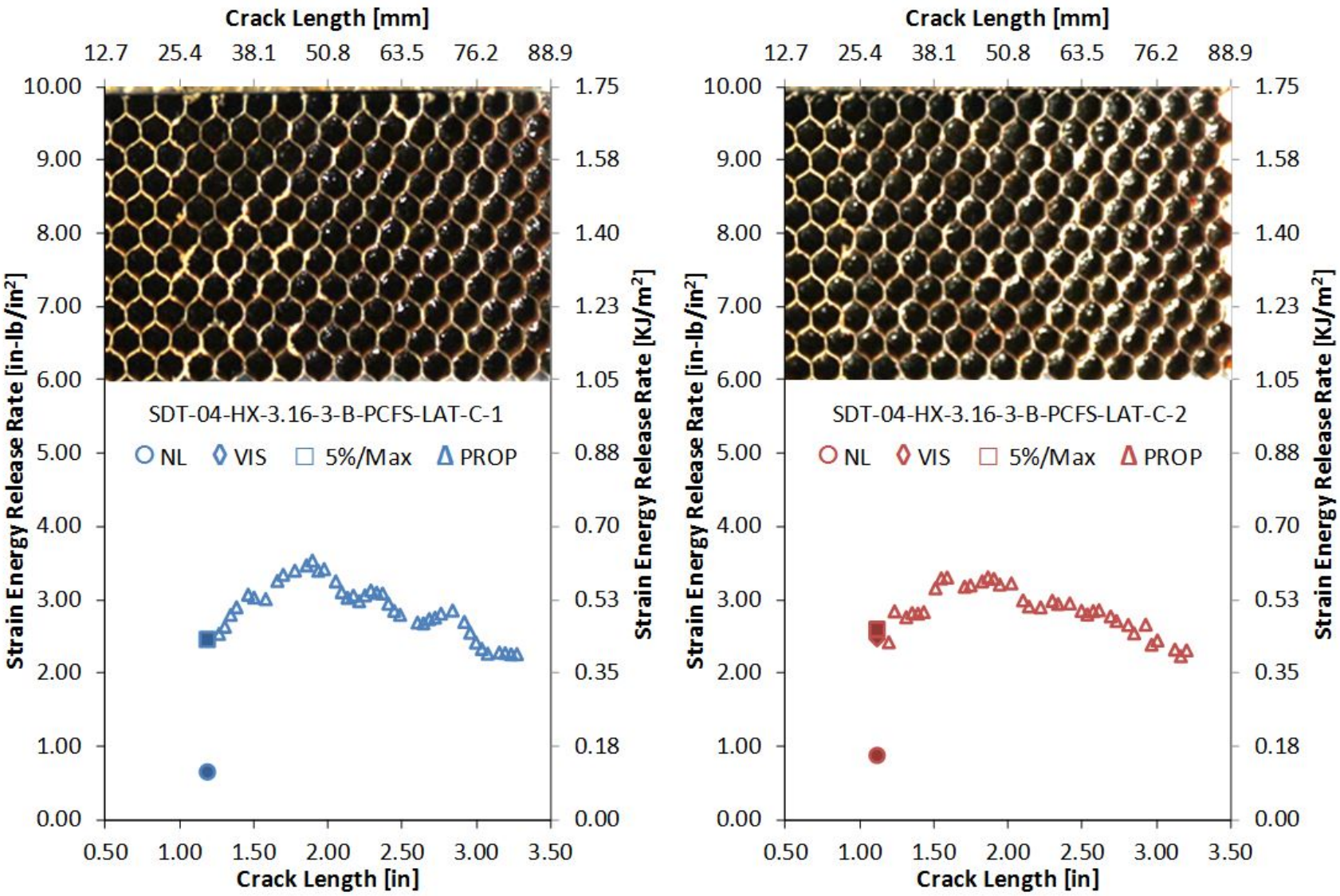

Figure A-95. Failure mode image and resistance curve of SDT-04-HX-3.16-3-B-PCFS-LAT-C-X #1 and #2

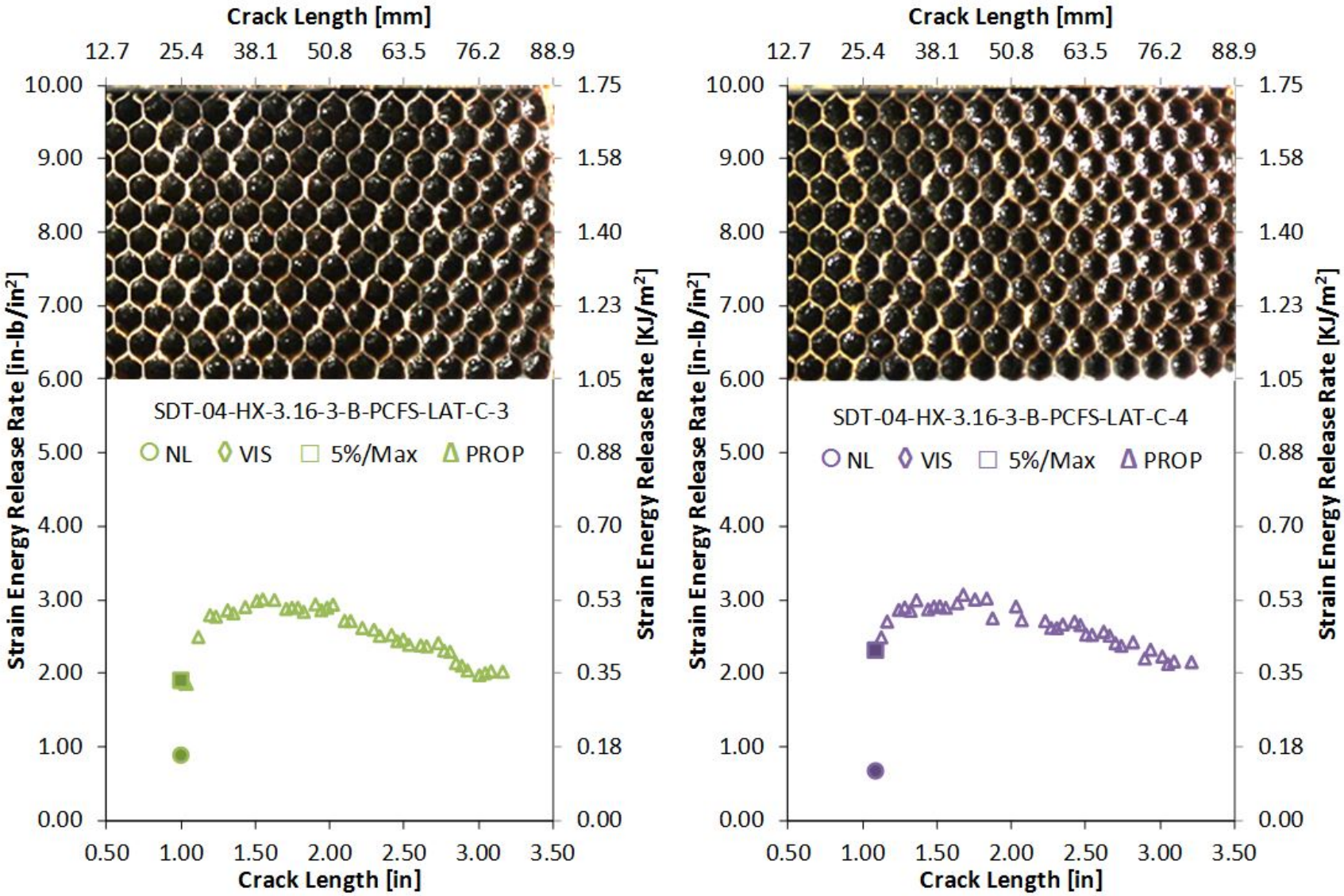

Figure A-96. Failure mode image and resistance curve of SDT-04-HX-3.16-3-B-PCFS-LAT-C-X #3 and #4

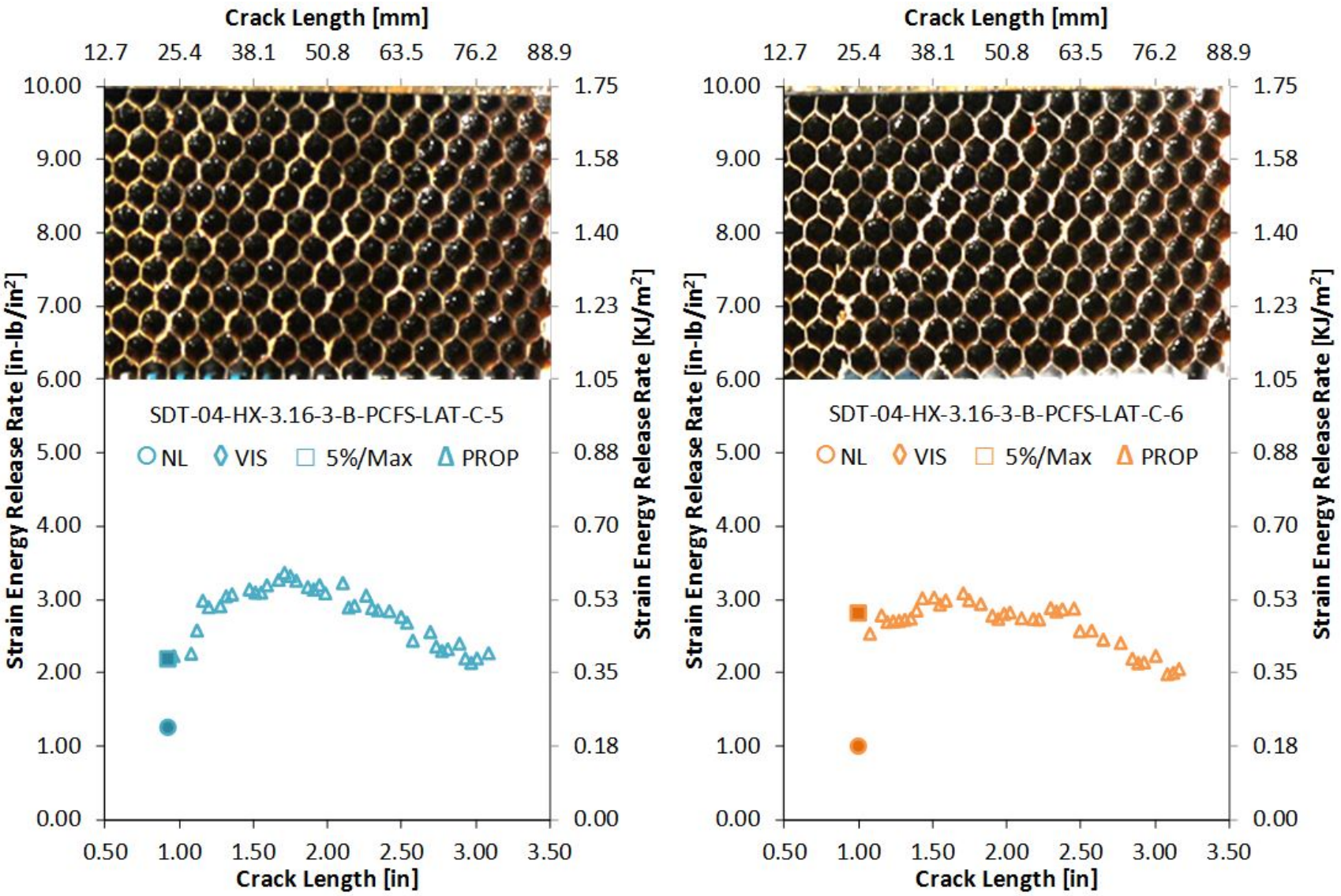

Figure A-97. Failure mode image and resistance curve of SDT-04-HX-3.16-3-B-PCFS-LAT-C-X #5 and #6

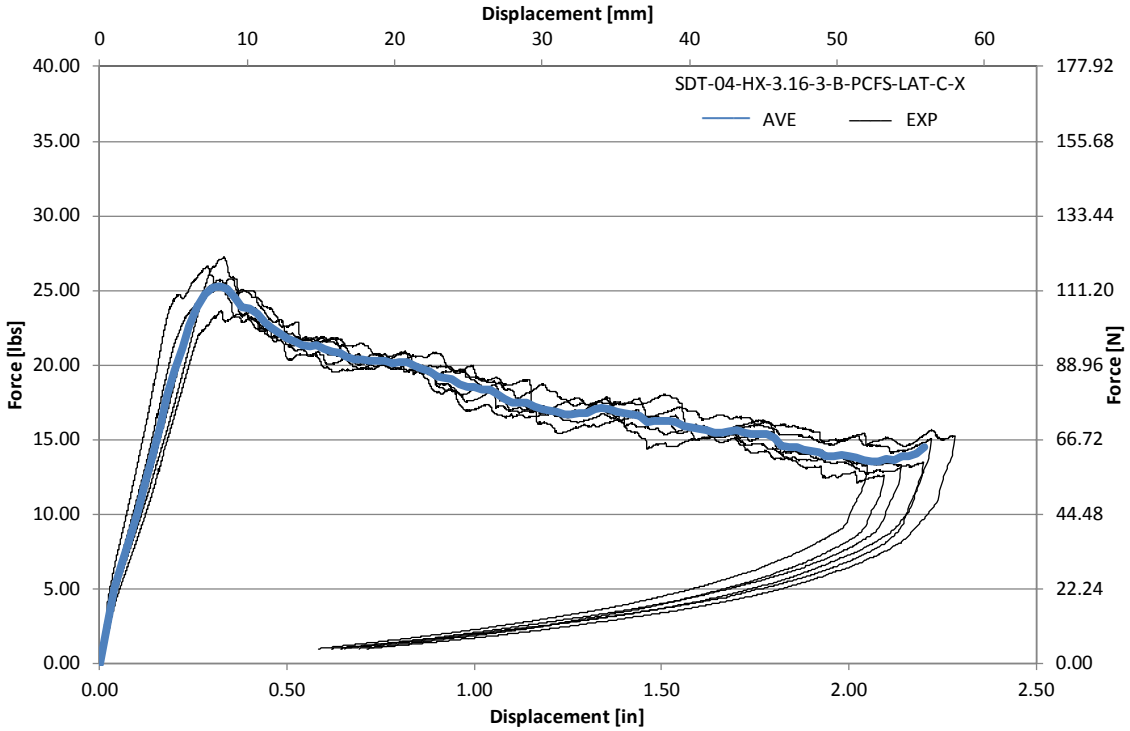

Figure A-98. Load vs. displacement curve for HRH-10–3/16–3.0 lateral ribbon direction with bottom disbond (center)

A.6 HRH-10–3/16–6.0 DATA

A.6.1 HRH-10–3/16–6.0 LONGITUDINAL RIBBON DIRECTION WITH TOP DISBOND (CENTER) DATA

Table A-33. Test summary for HRH-10–3/16–6.0 longitudinal ribbon direction with top disbond (center) pre-crack

Specimen	GIC (in-lb/in^2)			GIC (KJ/m^2)			Failure Mode
	NL	VIS	5%/max	NL	VIS	5%/max	
SDT-04-HX-3.16-6-T-PCFS-LONG-C-1	1.249	N/A	2.315	0.219	N/A	0.405	Primarily APO
SDT-04-HX-3.16-6-T-PCFS-LONG-C-2	1.475	2.268	2.290	0.258	0.397	0.401	Primarily APO
SDT-04-HX-3.16-6-T-PCFS-LONG-C-3	1.189	N/A	2.307	0.208	N/A	0.404	Primarily APO
SDT-04-HX-3.16-6-T-PCFS-LONG-C-4	1.149	N/A	2.047	0.201	N/A	0.358	Primarily APO
SDT-04-HX-3.16-6-T-PCFS-LONG-C-5	1.299	N/A	2.209	0.227	N/A	0.387	Primarily APO
SDT-04-HX-3.16-6-T-PCFS-LONG-C-6	1.201	N/A	2.534	0.210	N/A	0.444	Primarily APO
SDT-04-HX-3.16-6-T-PCFS-LONG-C-7							
SDT-04-HX-3.16-6-T-PCFS-LONG-C-8							
AVERAGE GIC	1.260	2.268	2.284	0.221	0.397	0.400	
STANDARD DEVIATION	0.117	N/A	0.159	0.021	N/A	0.028	
COEFFICIENT OF VARIATION (%)	9.297	N/A	6.954	9.297	N/A	6.954	

Table A-34. Test summary for HRH-10–3/16–6.0 longitudinal ribbon direction with top disbond (center)

Specimen	GIC (in-lb/in^2)				GIC (KJ/m^2)				Failure Mode
	NL	VIS	5%/max	AREA	NL	VIS	5%/max	AREA	
SDT-04-HX-3.16-6-T-PCFS-LONG-C-1	0.333	N/A	1.782	4.594	0.058	N/A	0.312	0.805	*
SDT-04-HX-3.16-6-T-PCFS-LONG-C-2	0.662	1.876	2.009	4.174	0.116	0.328	0.352	0.731	*
SDT-04-HX-3.16-6-T-PCFS-LONG-C-3	0.789	2.207	2.234	4.642	0.138	0.386	0.391	0.813	*
SDT-04-HX-3.16-6-T-PCFS-LONG-C-4	0.406	N/A	1.932	4.854	0.071	N/A	0.338	0.850	*
SDT-04-HX-3.16-6-T-PCFS-LONG-C-5	0.736	2.437	2.472	4.783	0.129	0.427	0.433	0.838	*
SDT-04-HX-3.16-6-T-PCFS-LONG-C-6	0.845	N/A	1.858	5.191	0.148	N/A	0.325	0.909	*
SDT-04-HX-3.16-6-T-PCFS-LONG-C-7									
SDT-04-HX-3.16-6-T-PCFS-LONG-C-8									
AVERAGE GIC	0.628	2.173	2.048	4.706	0.110	0.381	0.359	0.824	
STANDARD DEVIATION	0.211	0.282	0.260	0.335	0.037	0.049	0.045	0.059	
COEFFICIENT OF VARIATION (%)	33.526	12.993	12.672	7.122	33.526	12.993	12.672	7.122	

Notes	*	Primarily APO, with a few partial cells in A.

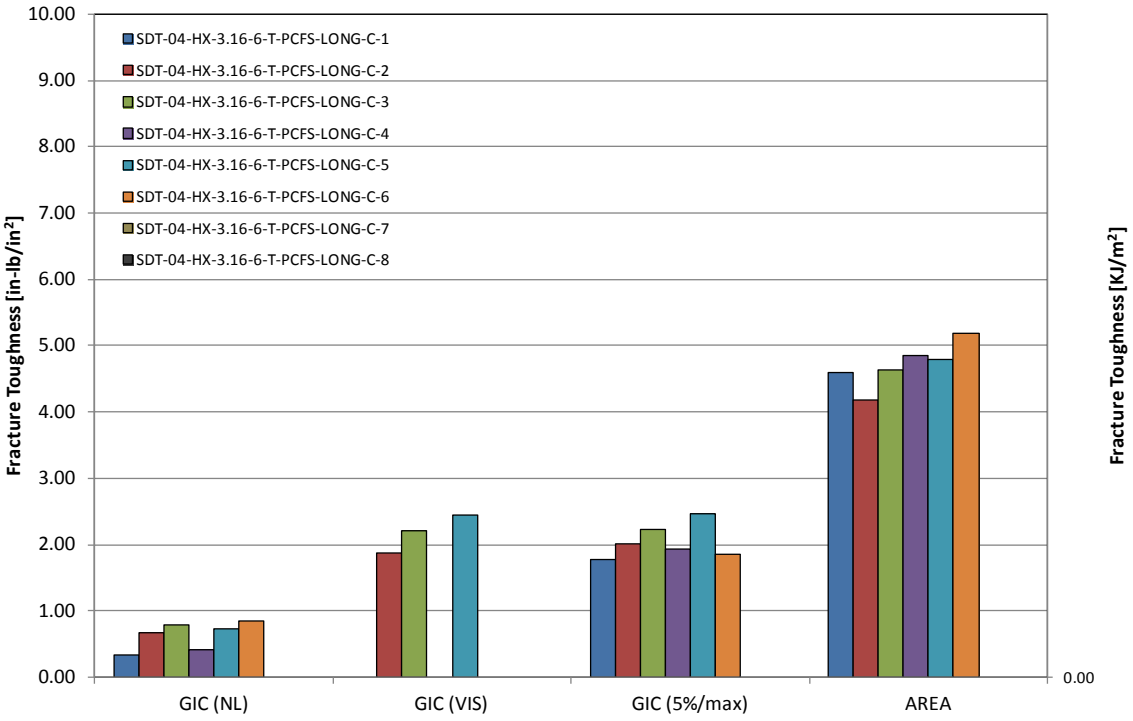

Figure A-99. GIC for HRH-10–3/16–6.0 longitudinal ribbon direction with top disbond (center)

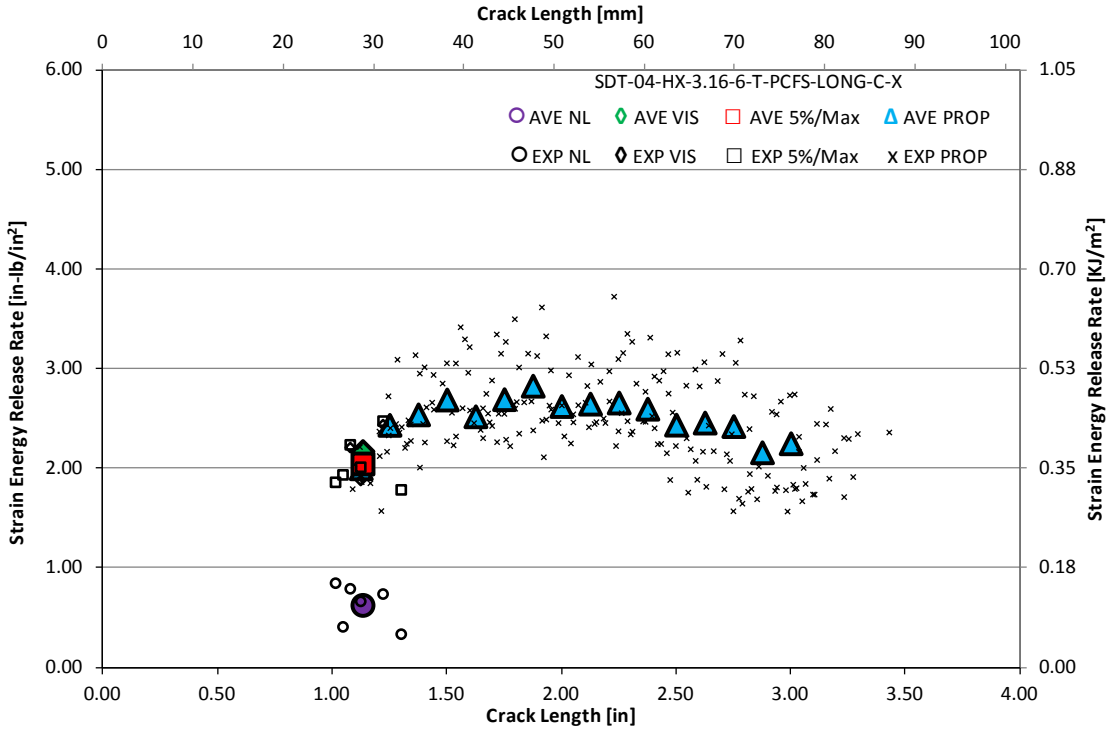

Figure A-100. Resistance curve for HRH-10–3/16–6.0 longitudinal ribbon direction with top disbond (center)

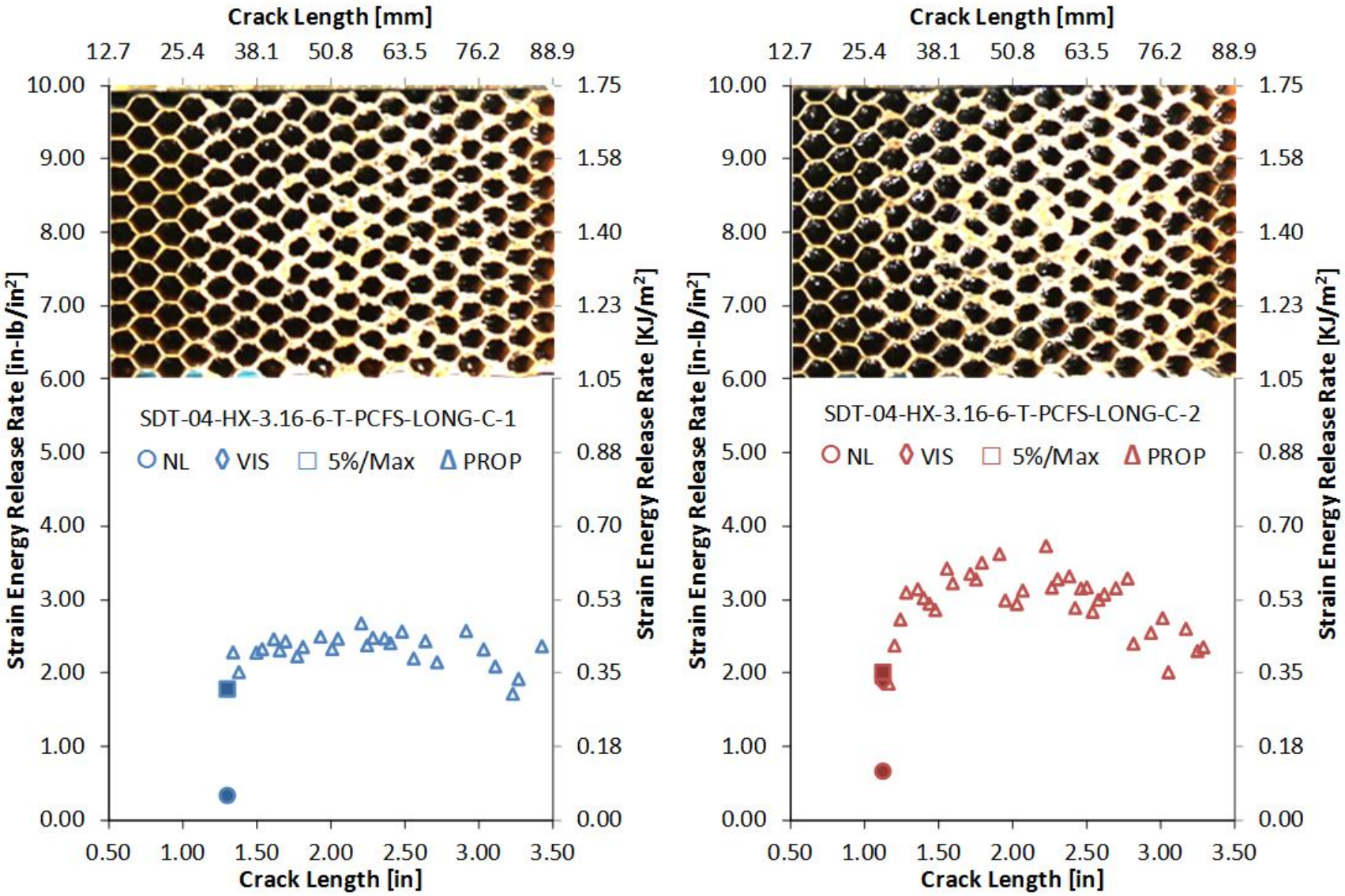

Figure A-101. Failure mode image and resistance curve of SDT-04-HX-3.16-6-T-PCFS-LONG-C-X #1 and #2

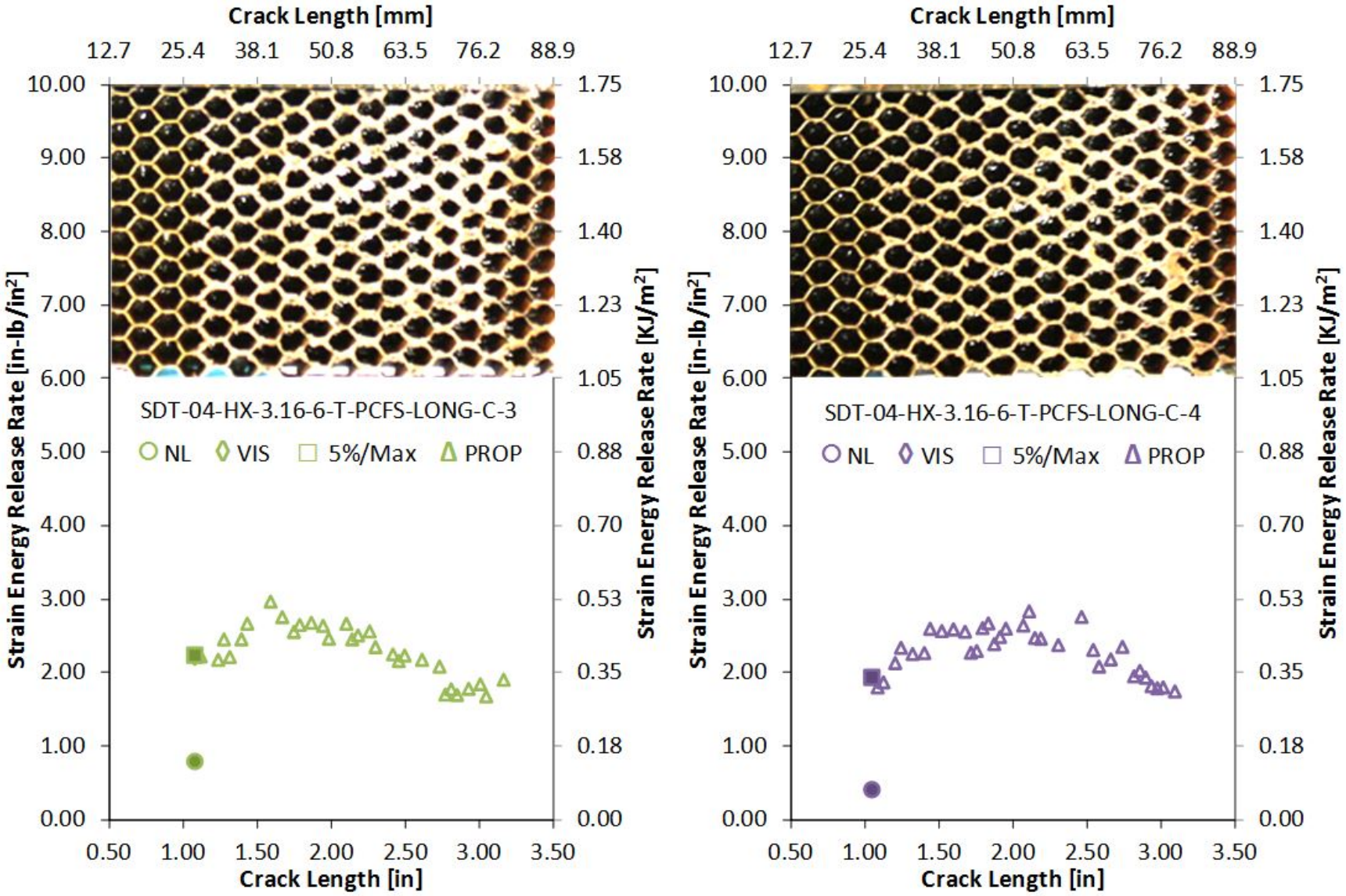

Figure A-102. Failure mode image and resistance curve of SDT-04-HX-3.16-6-T-PCFS-LONG-C-X #3 and #4

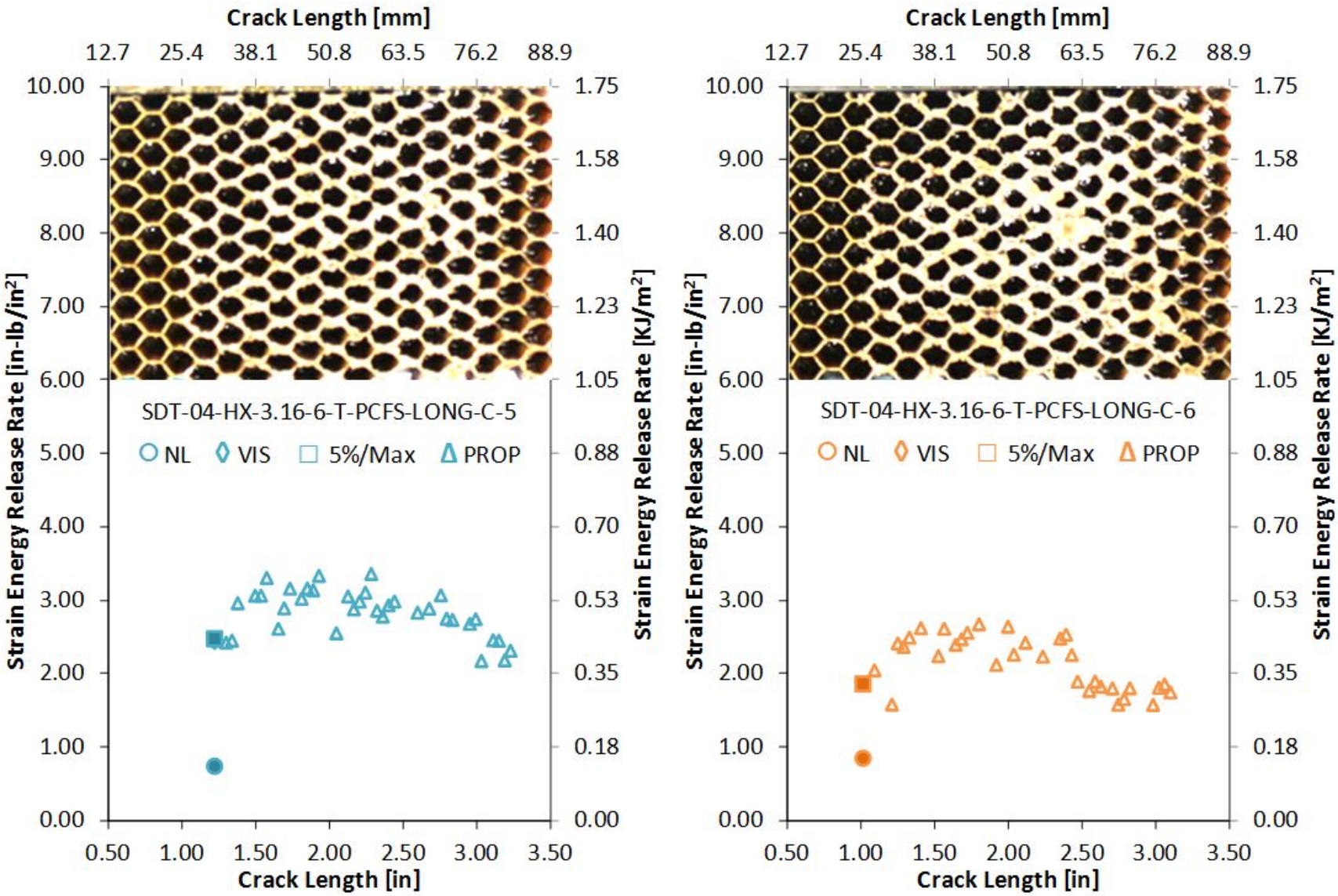

Figure A-103. Failure mode image and resistance curve of SDT-04-HX-3.16-6-T-PCFS-LONG-C-X #5 and #6

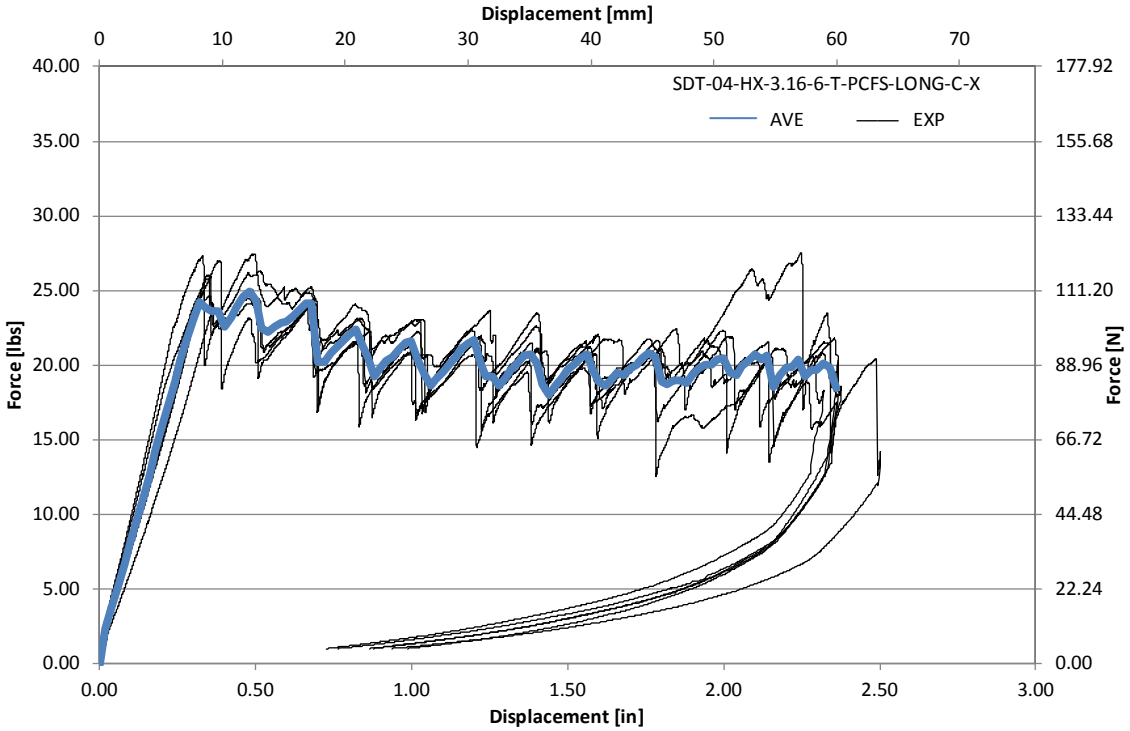

Figure A-104. Load vs. displacement curve for HRH-10–3/16–6.0 longitudinal ribbon direction with top disbond (center)

A.6.2 HRH-10–3/16–6.0 LONGITUDINAL RIBBON DIRECTION WITH BOTTOM DISBOND (CENTER) DATA

Table A-35. Test summary for HRH-10–3/16–6.0 longitudinal ribbon direction with bottom disbond (center) pre-crack

Specimen	GIC (in-lb/in^2)			GIC (KJ/m^2)			Failure Mode
	NL	VIS	5%/max	NL	VIS	5%/max	
SDT-04-HX-3.16-6-B-PCFS-LONG-C-1	1.343	N/A	1.906	0.235	N/A	0.334	Primarily APO with one cell in A
SDT-04-HX-3.16-6-B-PCFS-LONG-C-2	1.185	N/A	1.746	0.208	N/A	0.306	Primarily APO with a cell partially in A
SDT-04-HX-3.16-6-B-PCFS-LONG-C-3	1.516	N/A	2.495	0.265	N/A	0.437	Primarily APO with a cell partially in A
SDT-04-HX-3.16-6-B-PCFS-LONG-C-4	1.377	N/A	2.815	0.241	N/A	0.493	Primarily APO
SDT-04-HX-3.16-6-B-PCFS-LONG-C-5	1.257	N/A	2.615	0.220	N/A	0.458	Primarily APO with one cell in A
SDT-04-HX-3.16-6-B-PCFS-LONG-C-6	1.460	N/A	2.565	0.256	N/A	0.449	Primarily APO with one cell in A and a couple of cells partially in A
SDT-04-HX-3.16-6-B-PCFS-LONG-C-7							
SDT-04-HX-3.16-6-B-PCFS-LONG-C-8							
AVERAGE GIC	1.356	N/A	2.357	0.238	N/A	0.413	
STANDARD DEVIATION	0.123	N/A	0.428	0.022	N/A	0.075	
COEFFICIENT OF VARIATION (%)	9.077	N/A	18.147	9.077	N/A	18.147	

Table A-36. Test summary for HRH-10–3/16–6.0 longitudinal ribbon direction with bottom disbond (center)

Specimen	GIC (in-lb/in^2)				GIC (KJ/m^2)				Failure Mode
	NL	VIS	5%/max	AREA	NL	VIS	5%/max	AREA	
SDT-04-HX-3.16-6-B-PCFS-LONG-C-1	0.679	N/A	1.488	4.252	0.119	N/A	0.261	0.745	*
SDT-04-HX-3.16-6-B-PCFS-LONG-C-2	0.363	2.136	2.461	3.868	0.064	0.374	0.431	0.677	*
SDT-04-HX-3.16-6-B-PCFS-LONG-C-3	1.328	N/A	2.132	3.173	0.233	N/A	0.373	0.556	*
SDT-04-HX-3.16-6-B-PCFS-LONG-C-4	0.974	2.503	3.522	3.195	0.170	0.438	0.617	0.560	*
SDT-04-HX-3.16-6-B-PCFS-LONG-C-5	0.703	2.087	2.811	3.556	0.123	0.365	0.492	0.623	*
SDT-04-HX-3.16-6-B-PCFS-LONG-C-6	0.402	N/A	2.646	3.584	0.070	N/A	0.463	0.628	*
SDT-04-HX-3.16-6-B-PCFS-LONG-C-7									
SDT-04-HX-3.16-6-B-PCFS-LONG-C-8									
AVERAGE GIC	0.742	2.242	2.510	3.605	0.130	0.393	0.440	0.631	
STANDARD DEVIATION	0.364	0.228	0.681	0.411	0.064	0.040	0.119	0.072	
COEFFICIENT OF VARIATION (%)	49.057	10.150	27.152	11.408	49.057	10.150	27.152	11.408	

Notes	*	Primarily APO, with several cells in A and several partial cells in A.

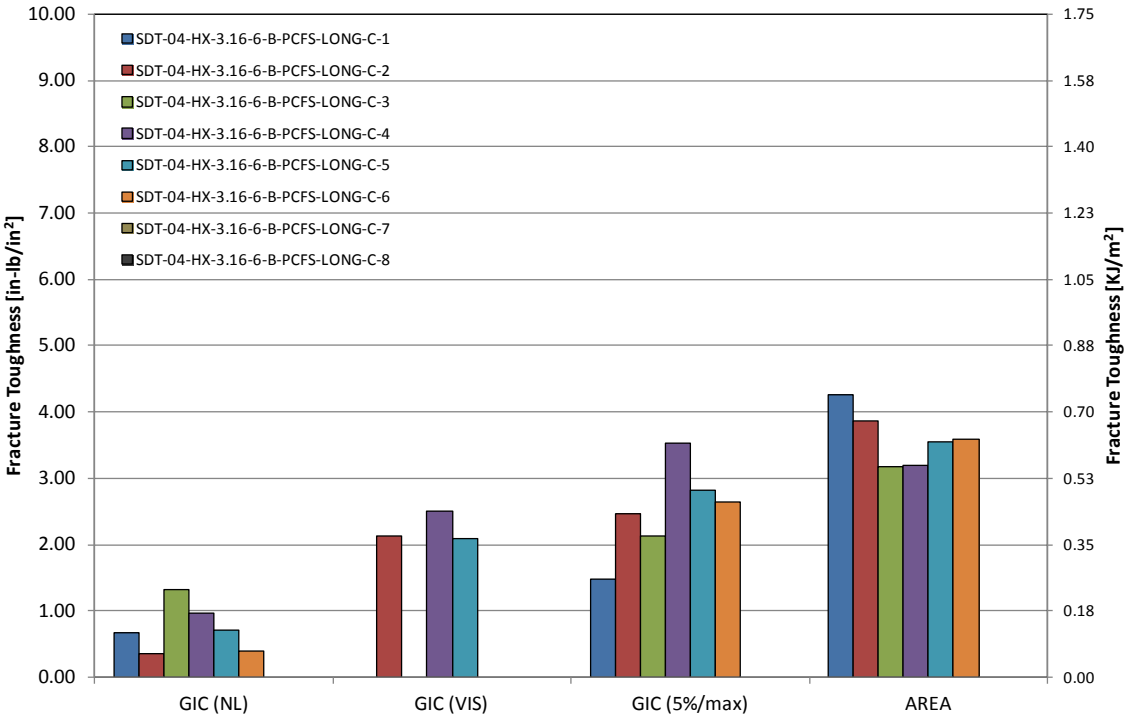

Figure A-105. GIC for HRH-10–3/16–6.0 longitudinal ribbon direction with bottom disbond (center)

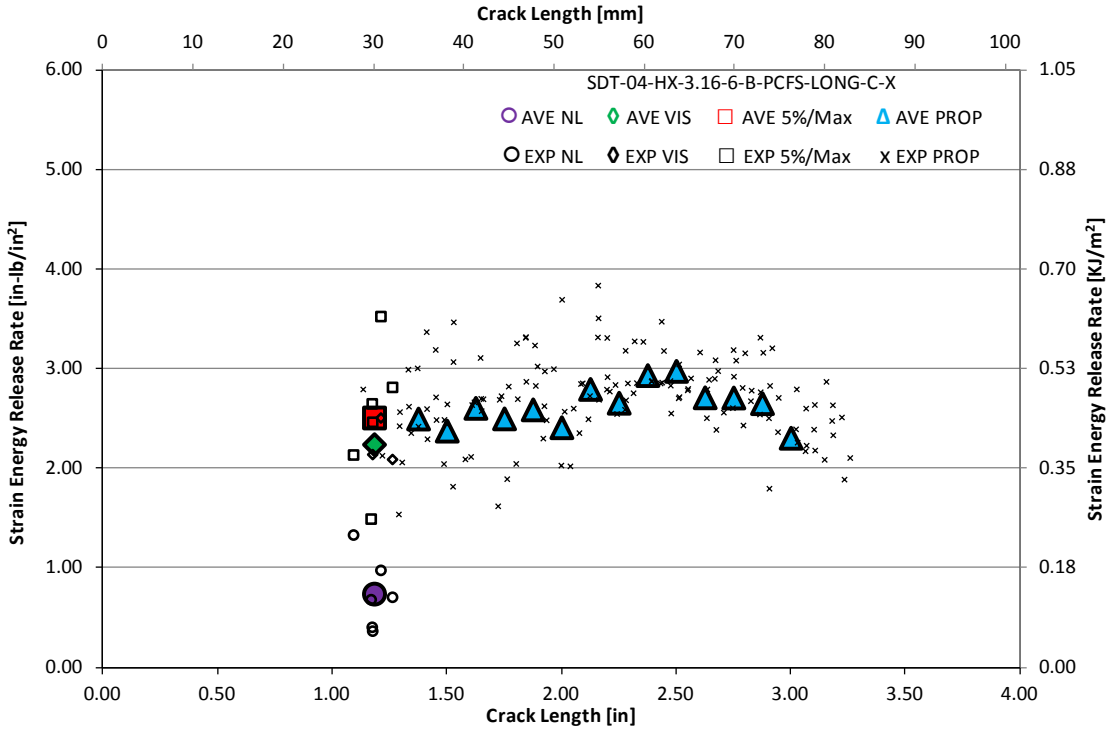

Figure A-106. Resistance curve for HRH-10–3/16–6.0 longitudinal ribbon direction with bottom disbond (center)

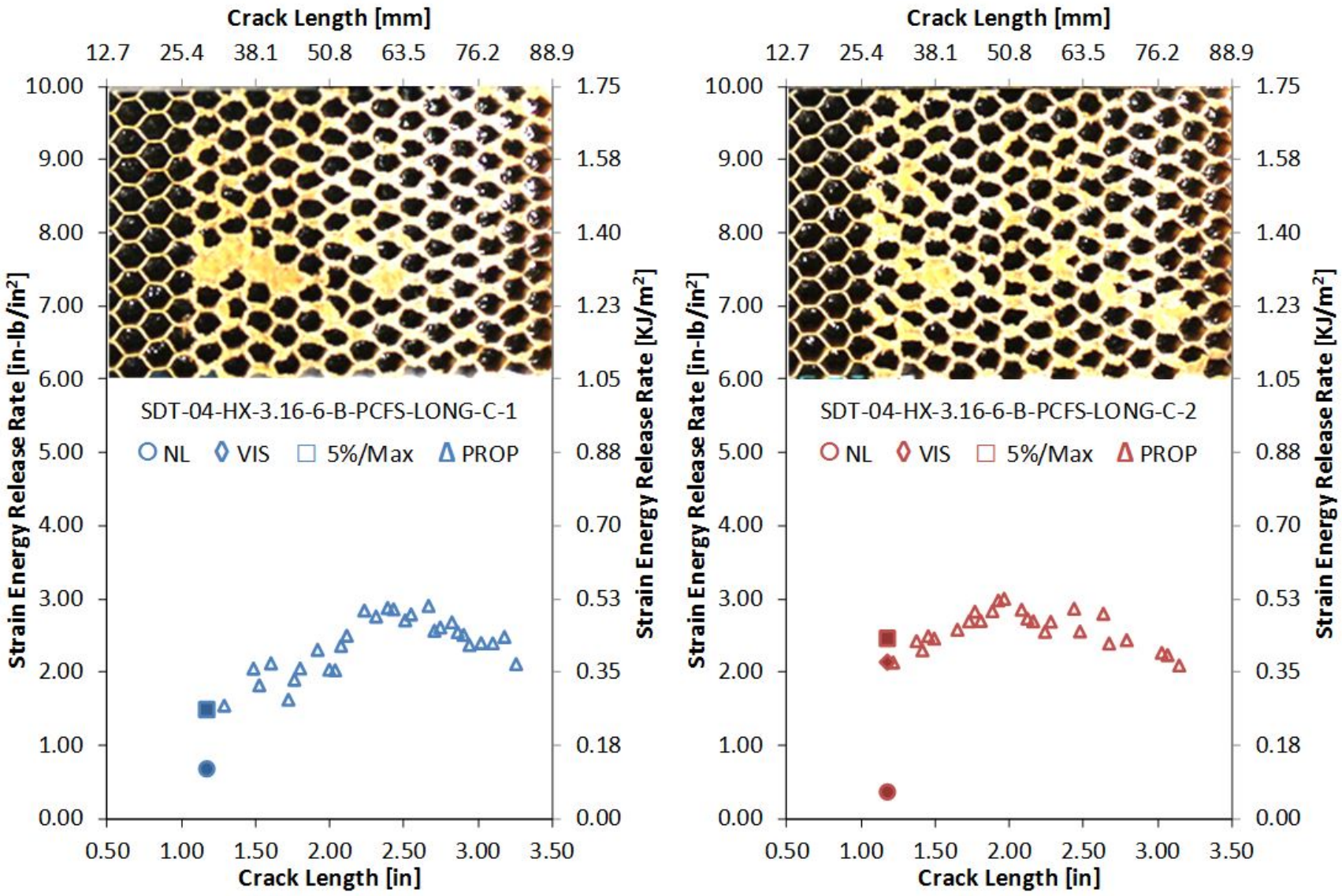

Figure A-107. Failure mode image and resistance curve of SDT-04-HX-3.16-6-B-PCFS-LONG-C-X #1 and #2

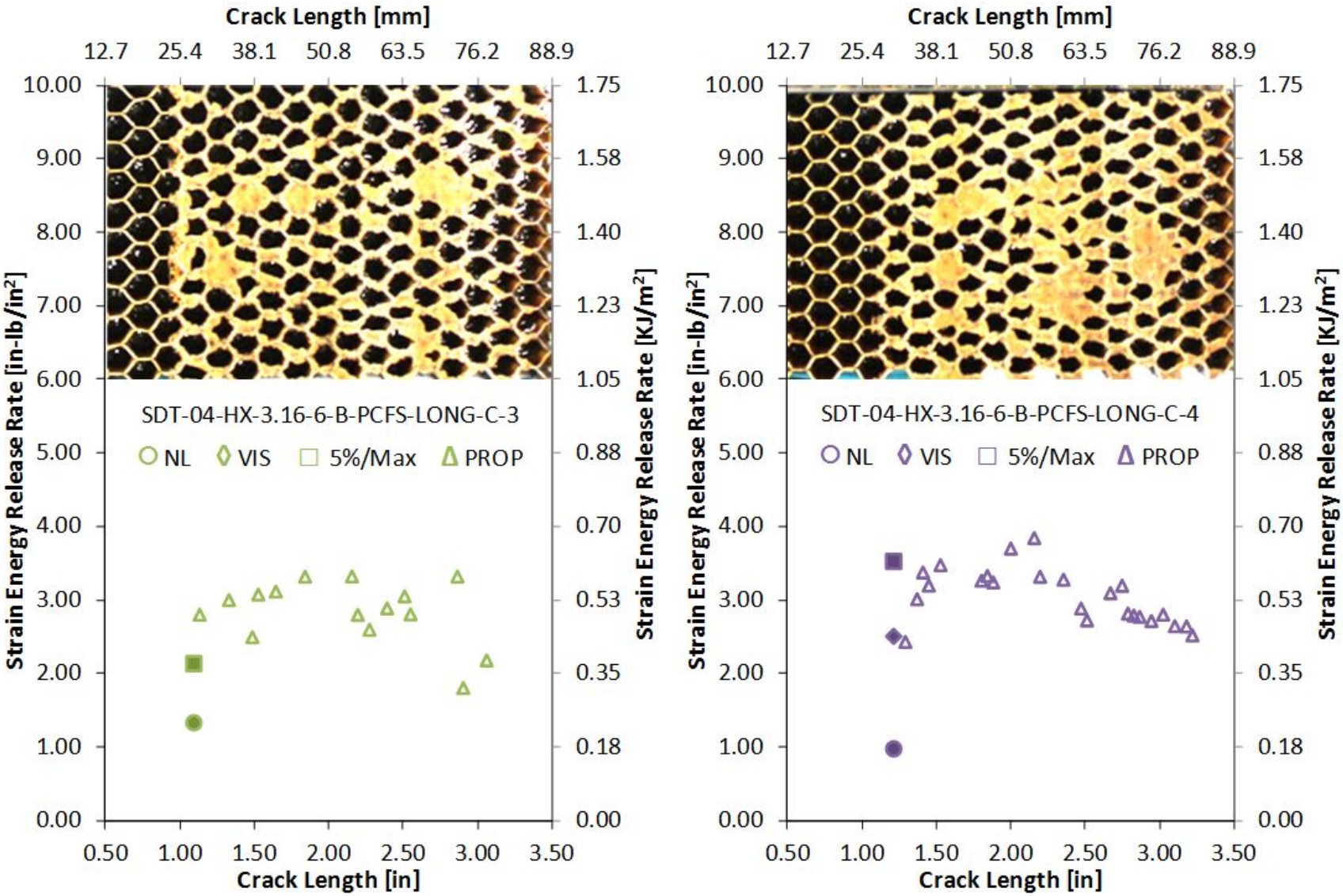

Figure A-108. Failure mode image and resistance curve of SDT-04-HX-3.16-6-B-PCFS-LONG-C-X #3 and #4

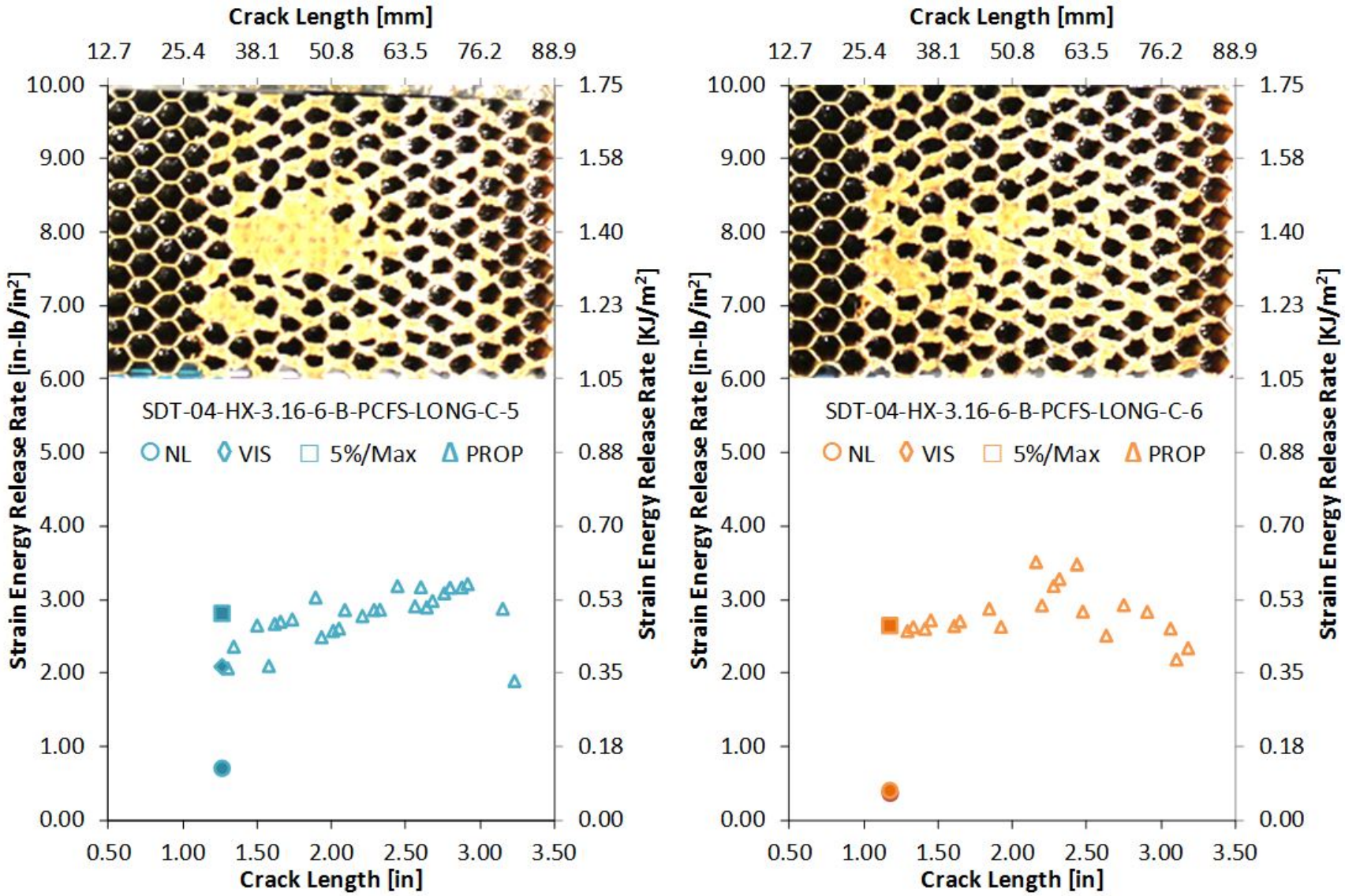

Figure A-109. Failure mode image and resistance curve of SDT-04-HX-3.16-6-B-PCFS-LONG-C-X #5 and #6

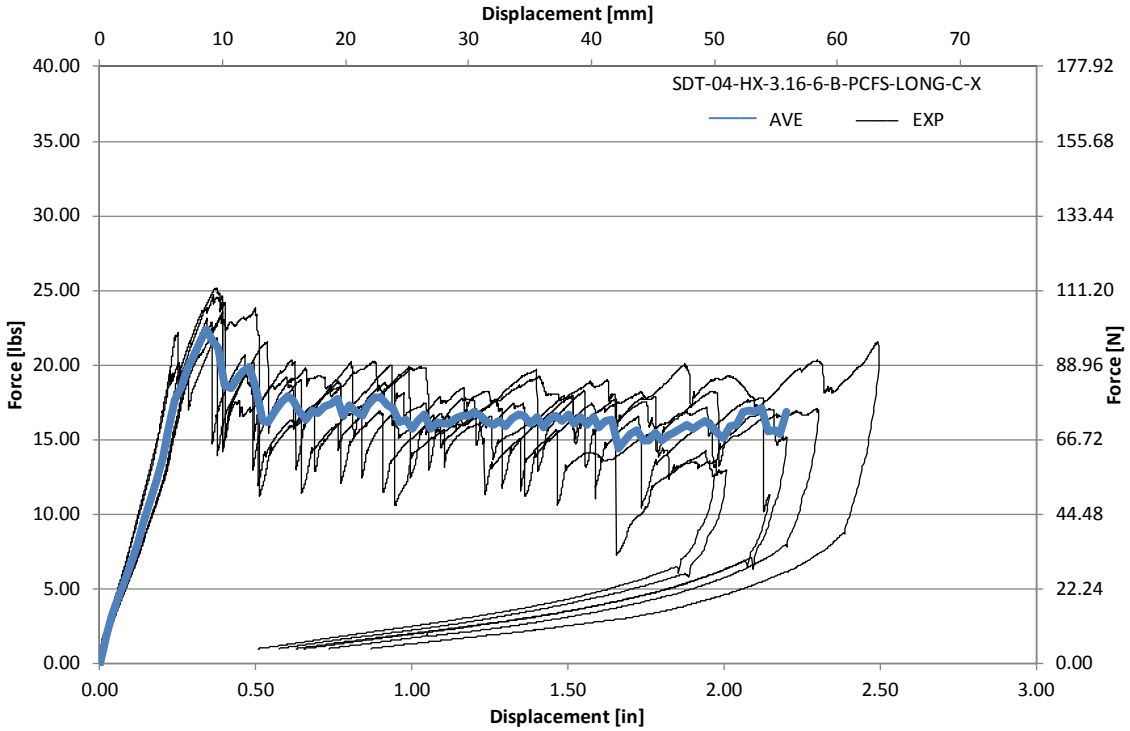

Figure A-110. Load vs. displacement curve for HRH-10–3/16–6.0 longitudinal ribbon direction with bottom disbond (center)

A.7 HRH-10–3/8–2.0 DATA

A.7.1 HRH-10–3/8–2.0 LONGITUDINAL RIBBON DIRECTION WITH TOP DISBOND (CENTER) DATA

Table A-37. Test summary for HRH-10–3/8–2.0 longitudinal ribbon direction with top disbond (center) pre-crack

Specimen	GIC (in-lb/in^2)			GIC (KJ/m^2)			Failure Mode
	NL	VIS	5%/max	NL	VIS	5%/max	
SDT-04-HX-3.8-2-T-PCFS-LONG-C-1	1.027	1.037	1.049	0.180	0.182	0.184	Primarily APO
SDT-04-HX-3.8-2-T-PCFS-LONG-C-2	0.606	1.098	1.120	0.106	0.192	0.196	Primarily APO
SDT-04-HX-3.8-2-T-PCFS-LONG-C-3	1.157	N/A	1.519	0.203	N/A	0.266	*
SDT-04-HX-3.8-2-T-PCFS-LONG-C-4	0.997	1.306	1.306	0.175	0.229	0.229	*
SDT-04-HX-3.8-2-T-PCFS-LONG-C-5	1.047	N/A	1.526	0.183	N/A	0.267	*
SDT-04-HX-3.8-2-T-PCFS-LONG-C-6	0.588	0.816	0.816	0.103	0.143	0.143	*
SDT-04-HX-3.8-2-T-PCFS-LONG-C-7							
SDT-04-HX-3.8-2-T-PCFS-LONG-C-8							
AVERAGE GIC	0.904	1.064	1.223	0.158	0.186	0.214	
STANDARD DEVIATION	0.244	0.202	0.280	0.043	0.035	0.049	
COEFFICIENT OF VARIATION (%)	26.976	18.934	22.918	26.976	18.934	22.918	

Notes	*	Primarily APO on the surface with many cells partially in C right below the surface; C is primarily not on the double cell walls in the ribbon direction.

Table A-38. Test summary for HRH-10–3/8–2.0 longitudinal ribbon direction with top disbond (center)

Specimen	GIC (in-lb/in^2)				GIC (KJ/m^2)				Failure Mode
	NL	VIS	5%/max	AREA	NL	VIS	5%/max	AREA	
SDT-04-HX-3.8-2-T-PCFS-LONG-C-1	0.499	1.150	1.165	N/A	0.087	0.201	0.204	N/A	*
SDT-04-HX-3.8-2-T-PCFS-LONG-C-2	0.829	1.100	1.113	1.323	0.145	0.193	0.195	0.232	*
SDT-04-HX-3.8-2-T-PCFS-LONG-C-3	0.513	N/A	1.551	1.300	0.090	N/A	0.272	0.228	*
SDT-04-HX-3.8-2-T-PCFS-LONG-C-4	0.664	N/A	1.227	N/A	0.116	N/A	0.215	N/A	*
SDT-04-HX-3.8-2-T-PCFS-LONG-C-5	0.474	N/A	1.394	N/A	0.083	N/A	0.244	N/A	*
SDT-04-HX-3.8-2-T-PCFS-LONG-C-6	0.554	1.090	1.376	1.263	0.097	0.191	0.241	0.221	*
SDT-04-HX-3.8-2-T-PCFS-LONG-C-7									
SDT-04-HX-3.8-2-T-PCFS-LONG-C-8									
AVERAGE GIC	0.589	1.113	1.304	1.295	0.103	0.195	0.228	0.227	
STANDARD DEVIATION	0.135	0.032	0.165	0.031	0.024	0.006	0.029	0.005	
COEFFICIENT OF VARIATION (%)	22.971	2.907	12.652	2.361	22.971	2.907	12.652	2.361	

Notes	*	Primarily APO on the surface with many cells partially in C, right below the surface; C is primarily not on the double cell walls in the ribbon direction.

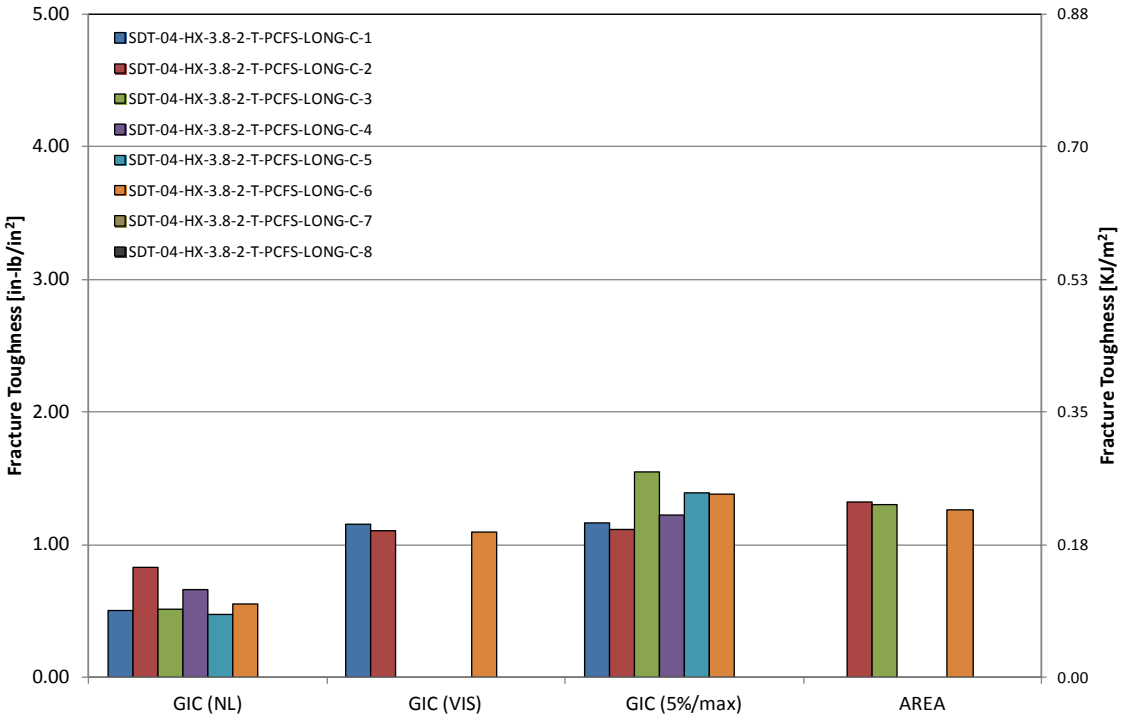

Figure A-111. GIC for HRH-10–3/8–2.0 longitudinal ribbon direction with top disbond (center)

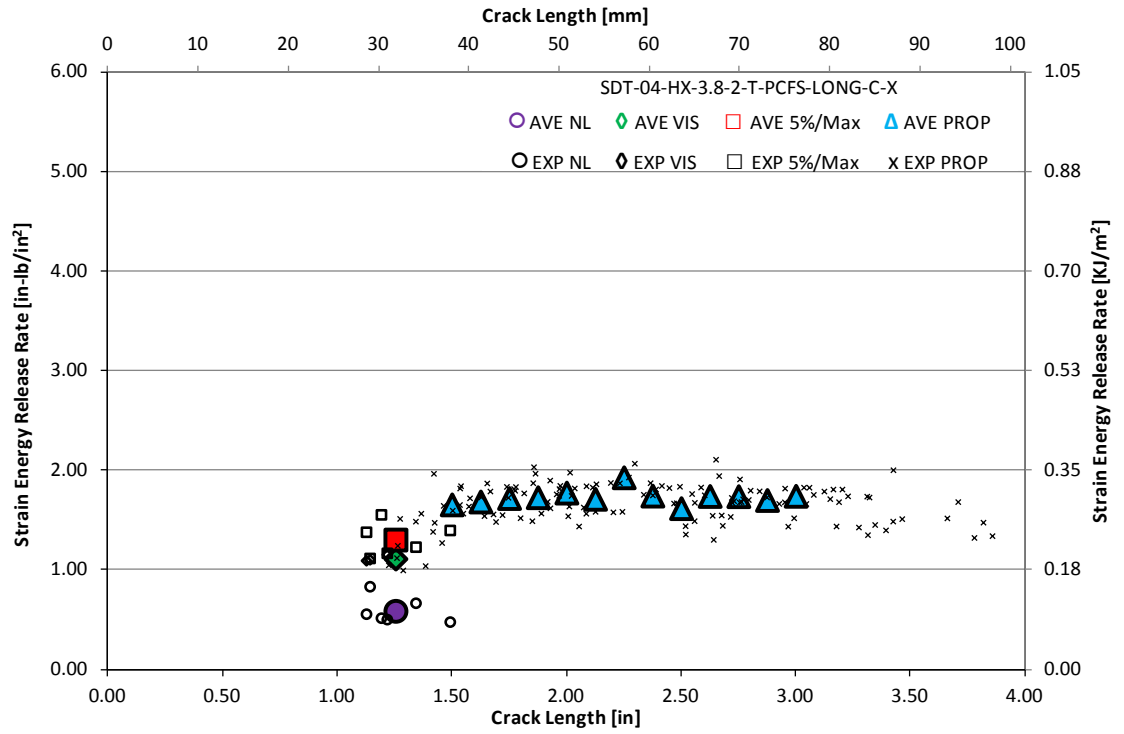

Figure A-112. Resistance curve for HRH-10–3/8–2.0 longitudinal ribbon direction with top disbond (center)

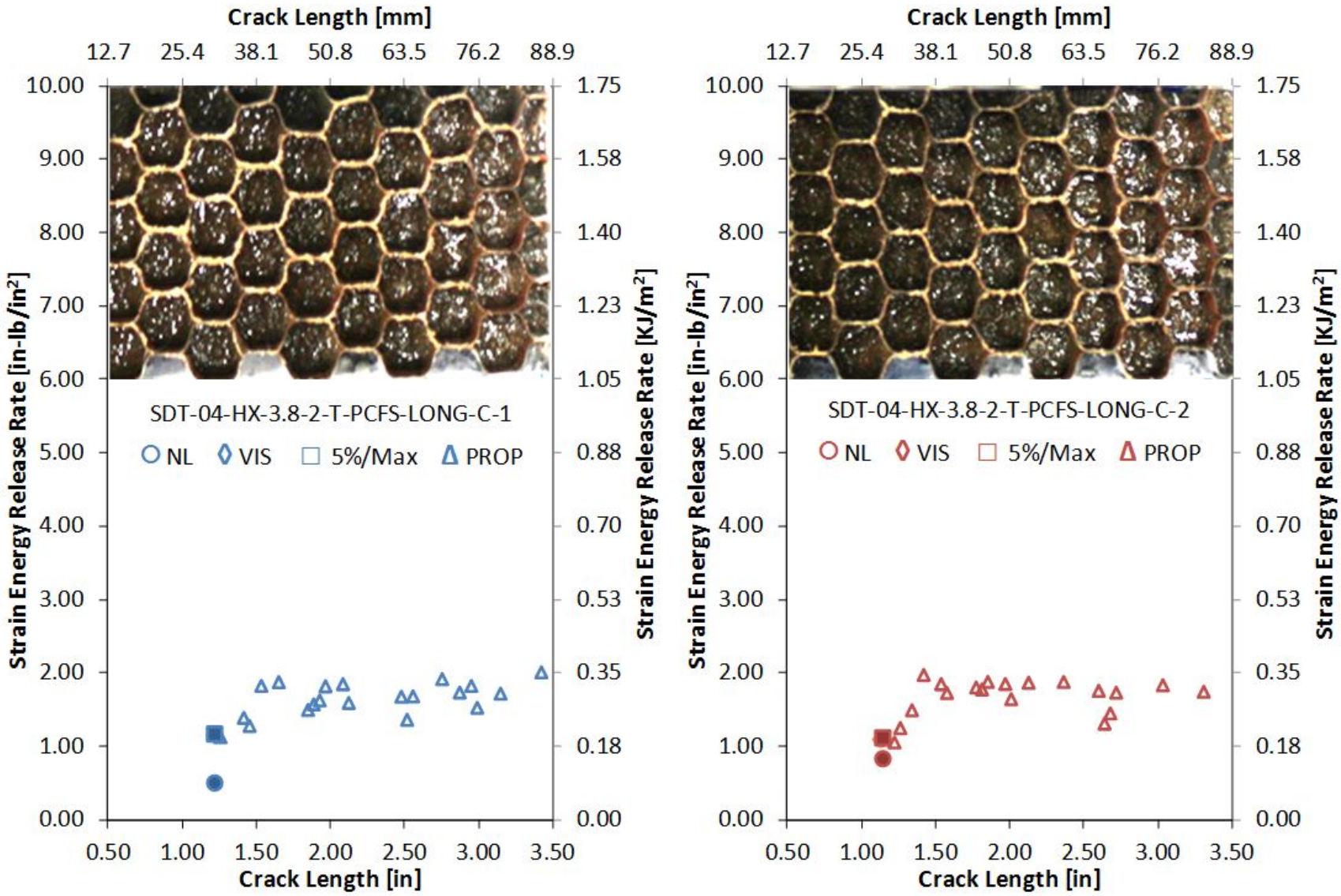

Figure A-113. Failure mode image and resistance curve of SDT-04-HX-1.8-2-T-PCFS-LONG-C-X #1 and #2

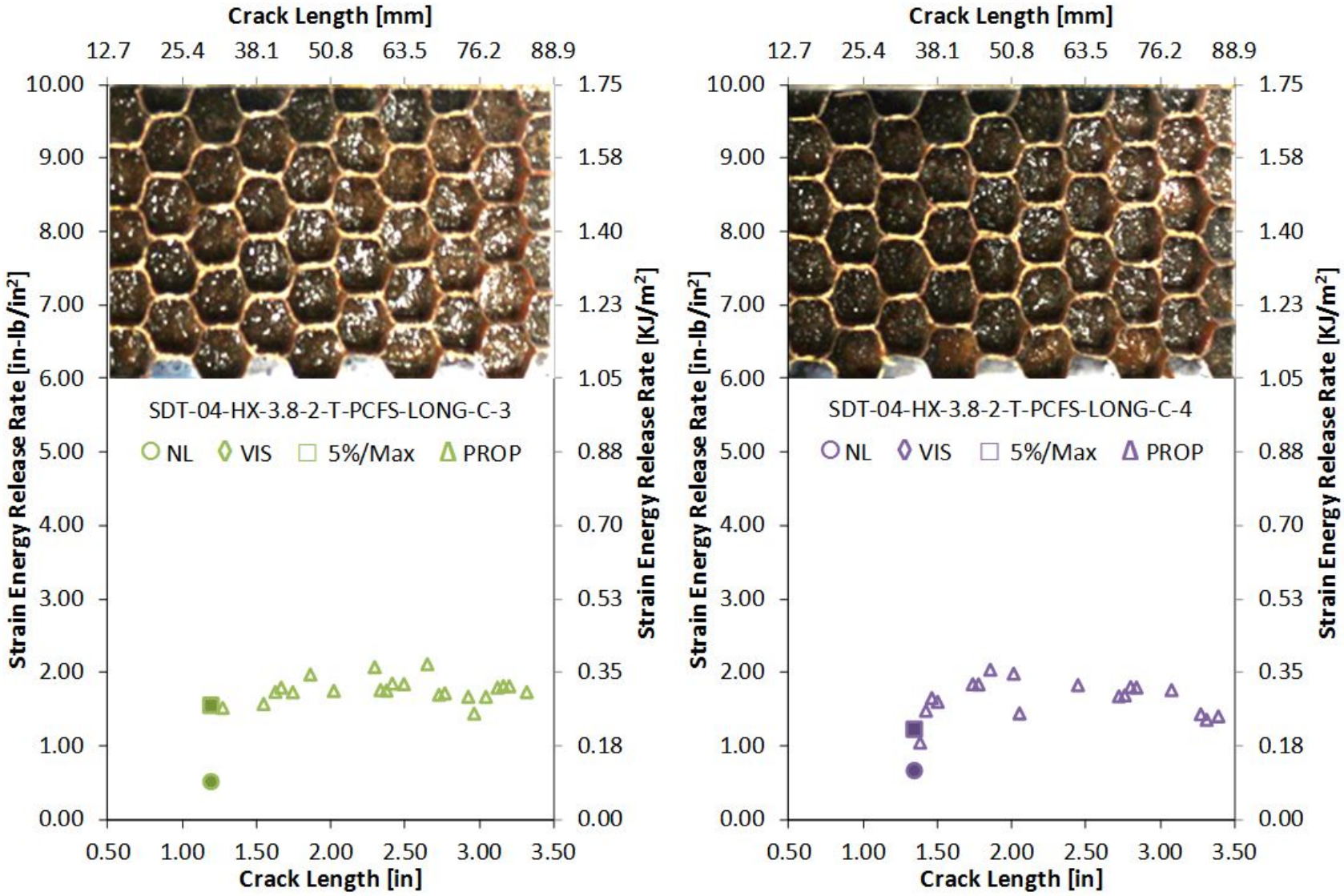

Figure A-114. Failure mode image and resistance curve of SDT-04-HX-1.8-2-T-PCFS-LONG-C-X #3 and #4

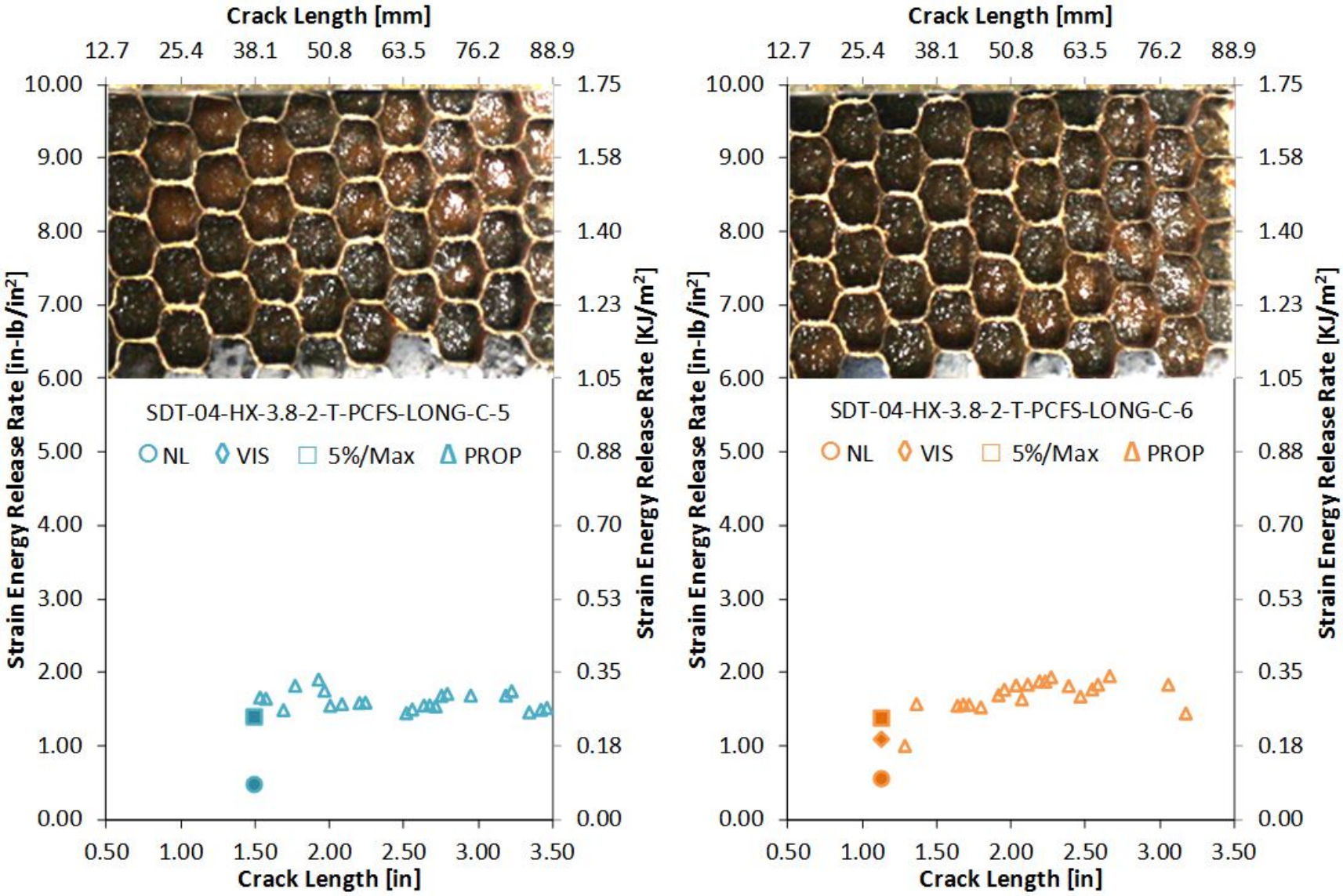

Figure A-115. Failure mode image and resistance curve of SDT-04-HX-1.8-2-T-PCFS-LONG-C-X #5 and #6

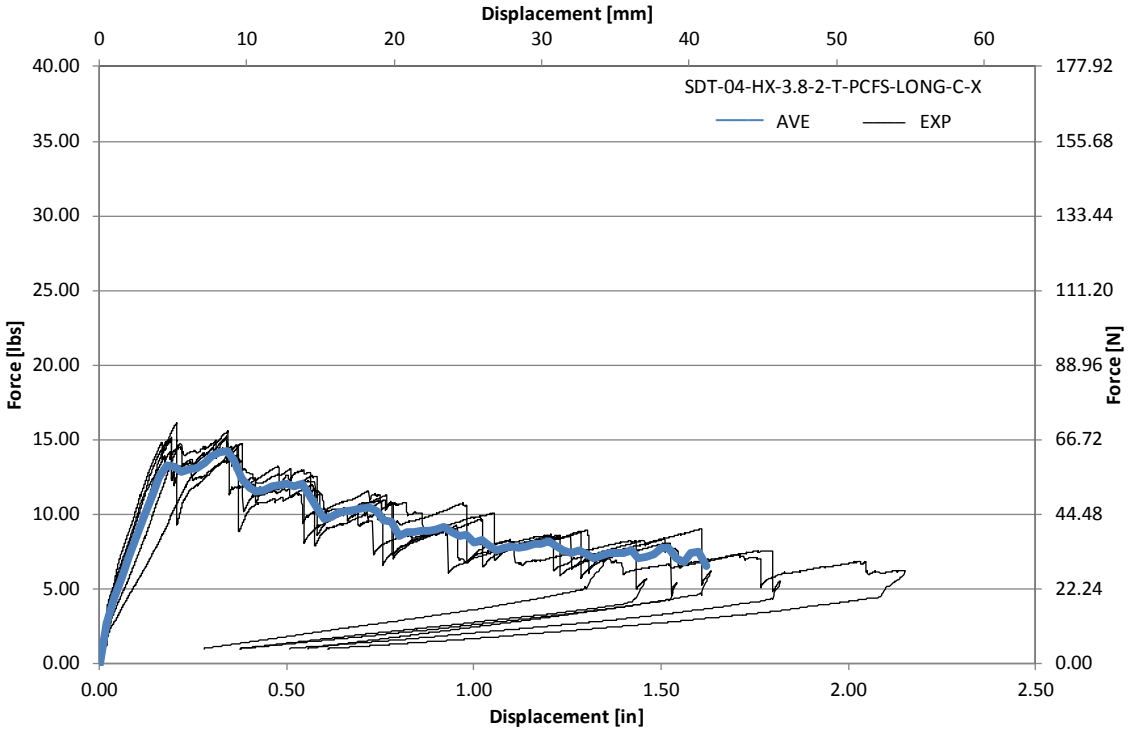

Figure A-116. Load vs. displacement curve for HRH-10–3/8–2.0 longitudinal ribbon direction with top disbond (center)

A.7.2 HRH-10–3/8–2.0 LONGITUDINAL RIBBON DIRECTION WITH BOTTOM DISBOND (CENTER) DATA

Table A-39. Test summary for HRH-10–3/8–2.0 longitudinal ribbon direction with bottom disbond (center) pre-crack

Specimen	GIC (in-lb/in^2)			GIC (KJ/m^2)			Failure Mode
	NL	VIS	5%/max	NL	VIS	5%/max	
SDT-04-HX-3.8-2-B-PCFS-LONG-C-1	0.925	N/A	2.059	0.162	N/A	0.361	*
SDT-04-HX-3.8-2-B-PCFS-LONG-C-2	1.051	1.517	1.517	0.184	0.266	0.266	Primarily APO
SDT-04-HX-3.8-2-B-PCFS-LONG-C-3	1.055	2.651	2.651	0.185	0.464	0.464	*
SDT-04-HX-3.8-2-B-PCFS-LONG-C-4	0.610	2.411	2.432	0.107	0.422	0.426	*
SDT-04-HX-3.8-2-B-PCFS-LONG-C-5	0.800	2.063	2.177	0.140	0.361	0.381	*
SDT-04-HX-3.8-2-B-PCFS-LONG-C-6	0.805	2.472	2.472	0.141	0.433	0.433	Primarily APO
SDT-04-HX-3.8-2-B-PCFS-LONG-C-7							
SDT-04-HX-3.8-2-B-PCFS-LONG-C-8							
AVERAGE GIC	0.874	2.223	2.218	0.153	0.389	0.388	
STANDARD DEVIATION	0.171	0.448	0.404	0.030	0.079	0.071	
COEFFICIENT OF VARIATION (%)	19.578	20.178	18.216	19.578	20.178	18.216	

Notes	*	Primarily APO on the surface with many cells partially in C, right below the surface; C is primarily not on the double cell walls in the ribbon direction.

Table A-40. Test summary for HRH-10–3/8–2.0 longitudinal ribbon direction with bottom disbond (center)

Specimen	GIC (in-lb/in^2)				GIC (KJ/m^2)				Failure Mode
	NL	VIS	5%/max	AREA	NL	VIS	5%/max	AREA	
SDT-04-HX-3.8-2-B-PCFS-LONG-C-1	0.391	1.014	1.381	1.533	0.068	0.178	0.242	0.268	*
SDT-04-HX-3.8-2-B-PCFS-LONG-C-2	0.492	1.320	1.586	1.578	0.086	0.231	0.278	0.276	*
SDT-04-HX-3.8-2-B-PCFS-LONG-C-3	0.333	1.641	1.662	1.369	0.058	0.287	0.291	0.240	*
SDT-04-HX-3.8-2-B-PCFS-LONG-C-4	0.649	1.627	1.649	1.343	0.114	0.285	0.289	0.235	*
SDT-04-HX-3.8-2-B-PCFS-LONG-C-5	0.388	N/A	1.621	N/A	0.068	N/A	0.284	N/A	*
SDT-04-HX-3.8-2-B-PCFS-LONG-C-6	0.382	1.526	1.532	1.161	0.067	0.267	0.268	0.203	*
SDT-04-HX-3.8-2-B-PCFS-LONG-C-7									
SDT-04-HX-3.8-2-B-PCFS-LONG-C-8									
AVERAGE GIC	0.439	1.426	1.572	1.397	0.077	0.250	0.275	0.245	
STANDARD DEVIATION	0.115	0.264	0.105	0.166	0.020	0.046	0.018	0.029	
COEFFICIENT OF VARIATION (%)	26.231	18.495	6.653	11.917	26.231	18.495	6.653	11.917	

Notes	*	Primarily APO on the surface with many cells partially in C, right below the surface; C is primarily not on the double cell walls in the ribbon direction.

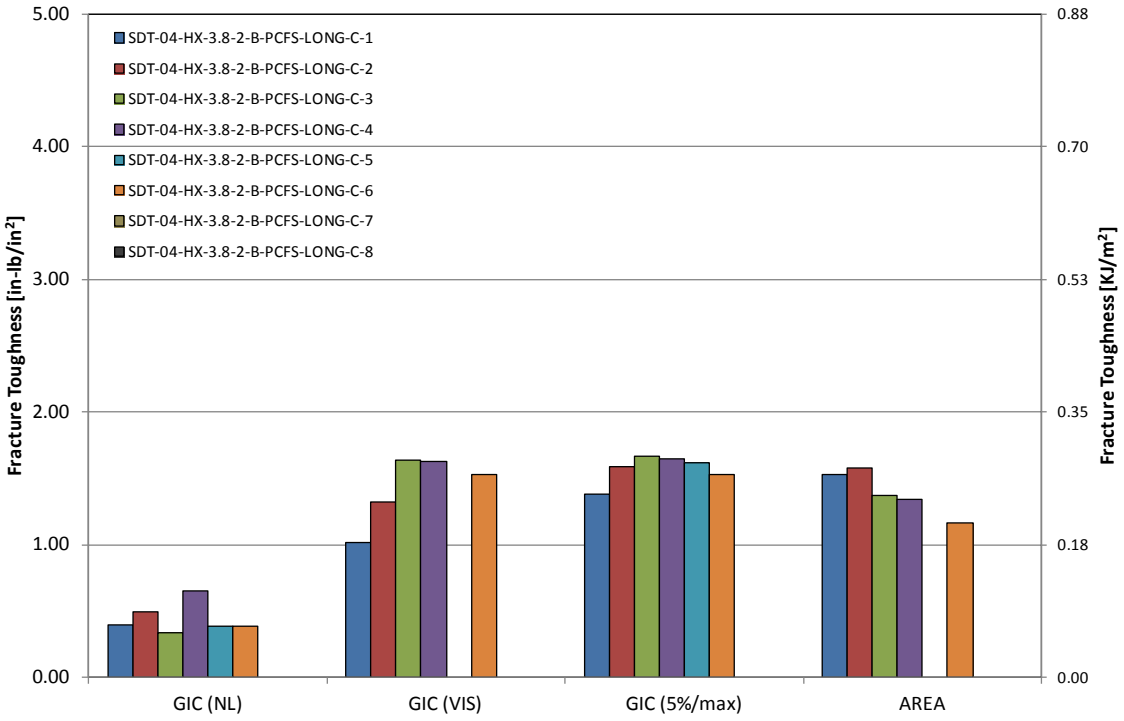

Figure A-117. GIC for HRH-10–3/8–2.0 longitudinal ribbon direction with bottom disbond (center)

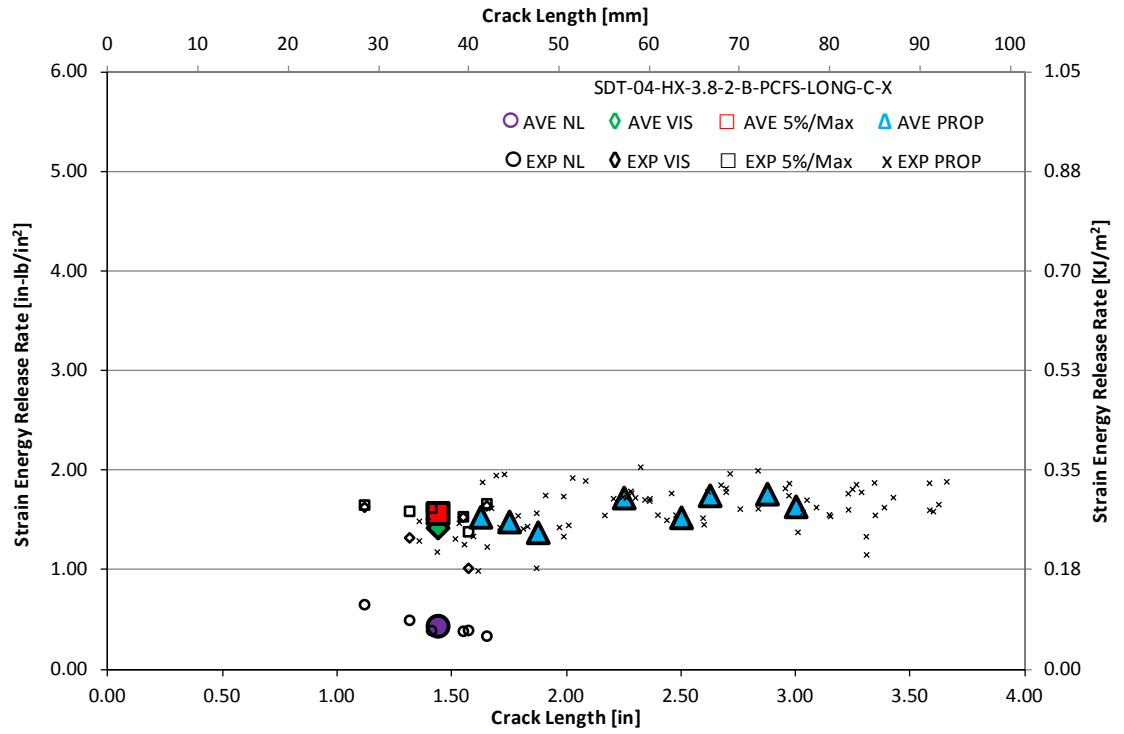

Figure A-118. Resistance curve for HRH-10–3/8–2.0 longitudinal ribbon direction with bottom disbond (center)

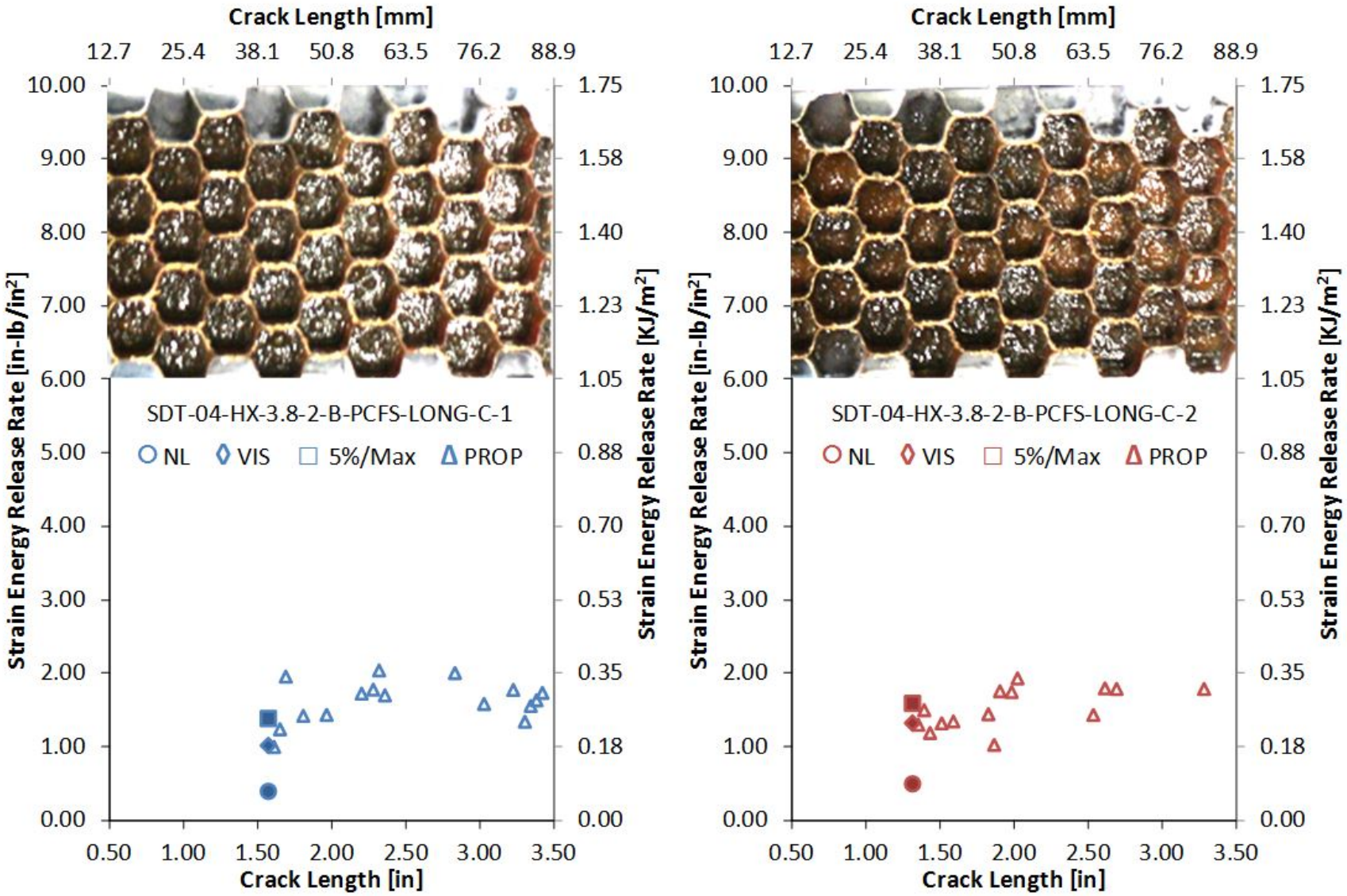

Figure A-119. Failure mode image and resistance curve of SDT-04-HX-3.8-2-B-PCFS-LONG-C-X #1 and #2

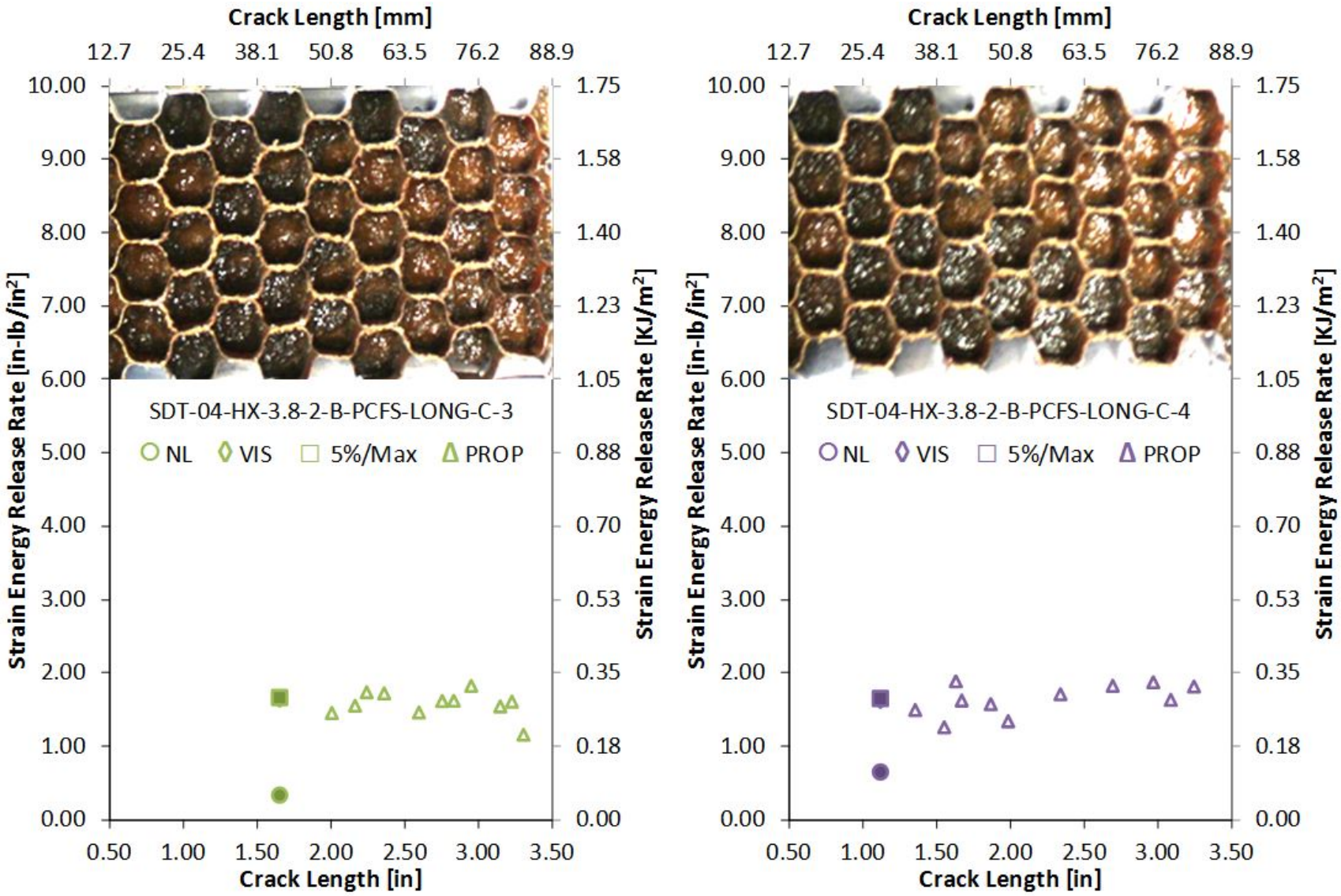

Figure A-120. Failure mode image and resistance curve of SDT-04-HX-3.8-2-B-PCFS-LONG-C-X #3 and #4

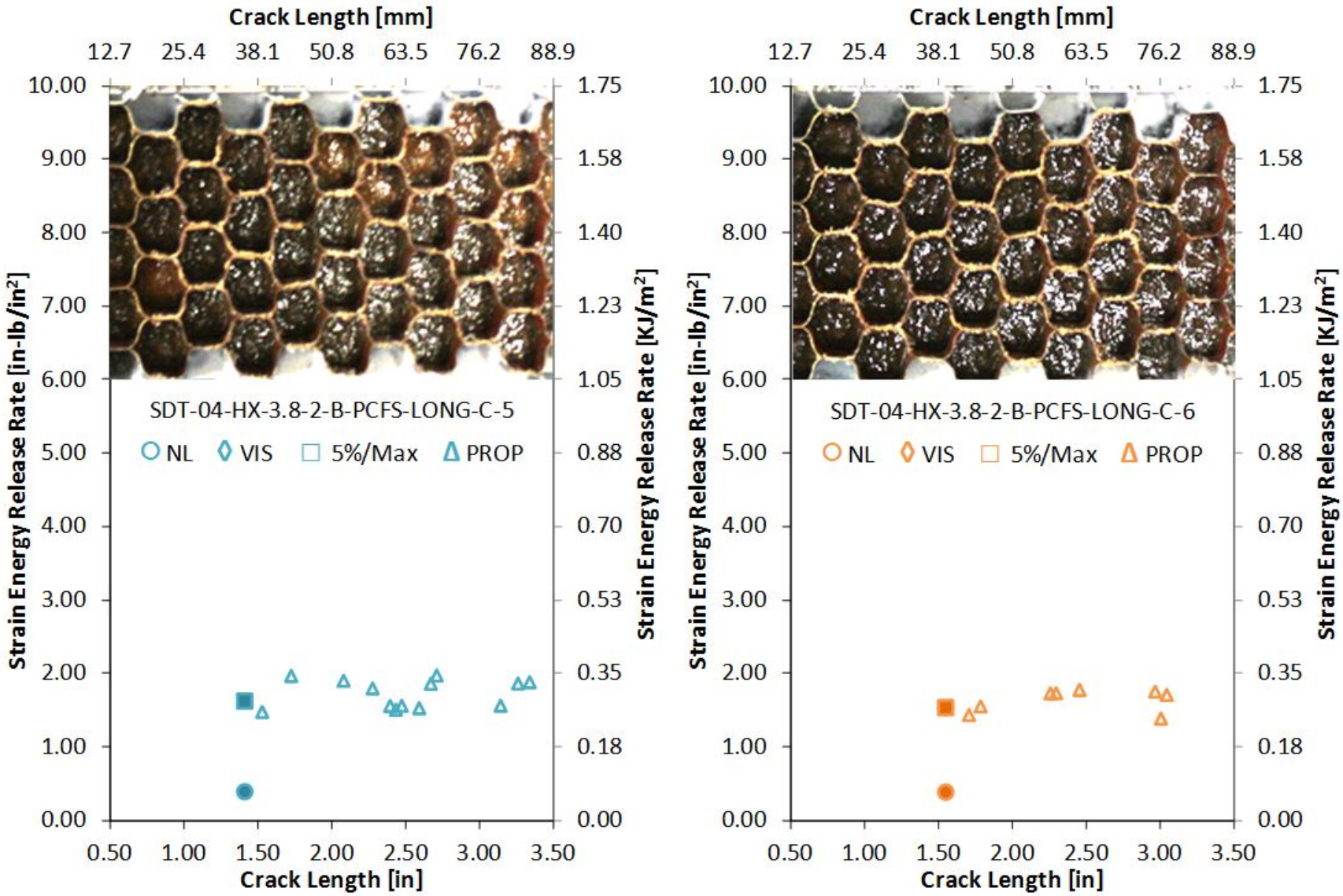

Figure A-121. Failure mode image and resistance curve of SDT-04-HX-3.8-2-B-PCFS-LONG-C-X #5 and #6

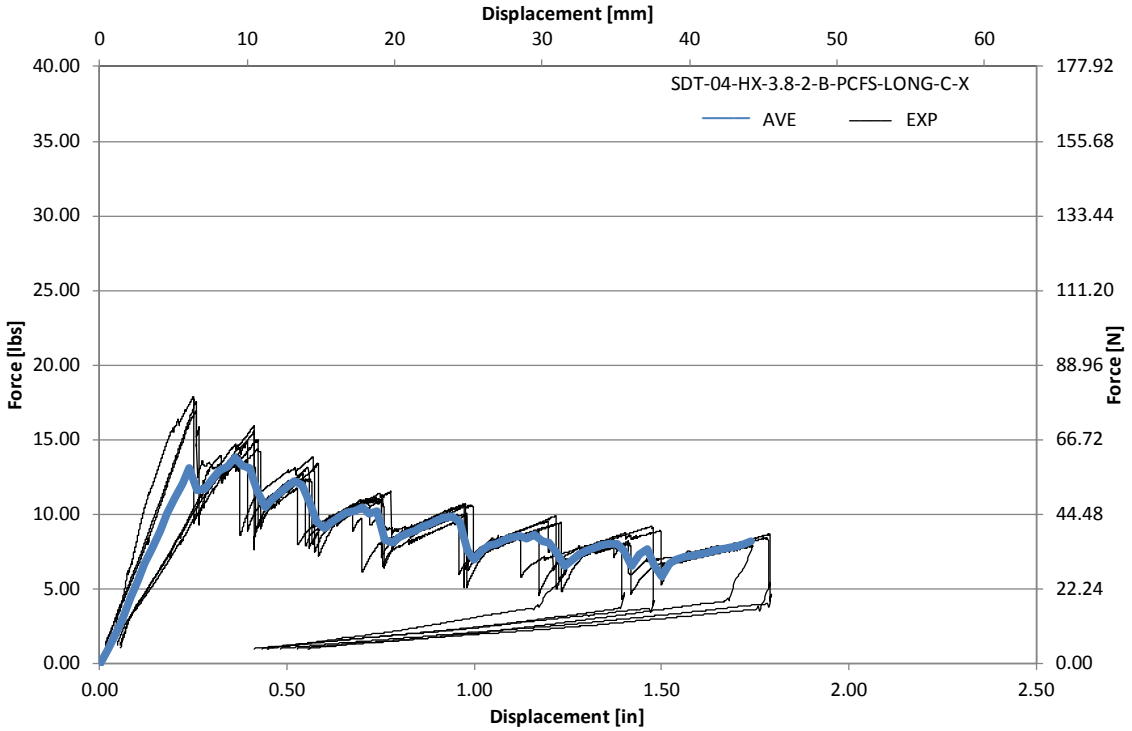

Figure A-122. Load vs. displacement curve for HRH-10–3/8–2.0 longitudinal ribbon direction with bottom disbond (center)

A.8 HRH-10–3/8–3.0 DATA

A.8.1 HRH-10–3/8–3.0 LONGITUDINAL RIBBON DIRECTION WITH TOP DISBOND (CENTER) DATA

Table A-41. Test summary for HRH-10–3/8–3.0 longitudinal ribbon direction with top disbond (center) pre-crack

Specimen	GIC (in-lb/in^2)			GIC (KJ/m^2)			Failure Mode
	NL	VIS	5%/max	NL	VIS	5%/max	
SDT-04-HX-3.8-3-T-PCFS-LONG-C-1	0.574	N/A	0.734	0.100	N/A	0.129	Primarily APO
SDT-04-HX-3.8-3-T-PCFS-LONG-C-2	0.492	N/A	0.693	0.086	N/A	0.121	Primarily APO
SDT-04-HX-3.8-3-T-PCFS-LONG-C-3	0.487	N/A	0.845	0.085	N/A	0.148	Primarily APO
SDT-04-HX-3.8-3-T-PCFS-LONG-C-4	0.650	N/A	0.806	0.114	N/A	0.141	Primarily APO
SDT-04-HX-3.8-3-T-PCFS-LONG-C-5	0.755	N/A	1.054	0.132	N/A	0.185	Primarily APO
SDT-04-HX-3.8-3-T-PCFS-LONG-C-6	0.421	N/A	1.031	0.074	N/A	0.180	Primarily APO
SDT-04-HX-3.8-3-T-PCFS-LONG-C-7							
SDT-04-HX-3.8-3-T-PCFS-LONG-C-8							
AVERAGE GIC	0.563	#####	0.860	0.099	#####	0.151	
STANDARD DEVIATION	0.123	#####	0.151	0.022	#####	0.026	
COEFFICIENT OF VARIATION (%)	21.830	#####	17.541	21.830	#####	17.541	

Table A-42. Test summary for HRH-10–3/8–3.0 longitudinal ribbon direction with top disbond (center)

Specimen	GIC (in-lb/in^2)				GIC (KJ/m^2)				Failure Mode
	NL	VIS	5%/max	AREA	NL	VIS	5%/max	AREA	
SDT-04-HX-3.8-3-T-PCFS-LONG-C-1	0.492	N/A	2.301	N/A	0.086	N/A	0.403	N/A	Primarily APO
SDT-04-HX-3.8-3-T-PCFS-LONG-C-2	0.914	2.005	2.016	2.214	0.160	0.351	0.353	0.388	Primarily APO
SDT-04-HX-3.8-3-T-PCFS-LONG-C-3	0.480	N/A	2.871	N/A	0.084	N/A	0.503	N/A	Primarily APO
SDT-04-HX-3.8-3-T-PCFS-LONG-C-4	0.860	2.459	2.547	2.446	0.151	0.431	0.446	0.428	Primarily APO
SDT-04-HX-3.8-3-T-PCFS-LONG-C-5	0.238	2.557	2.648	2.218	0.042	0.448	0.464	0.388	Primarily APO
SDT-04-HX-3.8-3-T-PCFS-LONG-C-6	0.338	N/A	2.178	N/A	0.059	N/A	0.381	N/A	Primarily APO
SDT-04-HX-3.8-3-T-PCFS-LONG-C-7									
SDT-04-HX-3.8-3-T-PCFS-LONG-C-8									
AVERAGE GIC	0.554	2.341	2.427	2.292	0.097	0.410	0.425	0.401	
STANDARD DEVIATION	0.276	0.294	0.318	0.133	0.048	0.052	0.056	0.023	
COEFFICIENT OF VARIATION (%)	49.764	12.578	13.122	5.788	49.764	12.578	13.122	5.788	

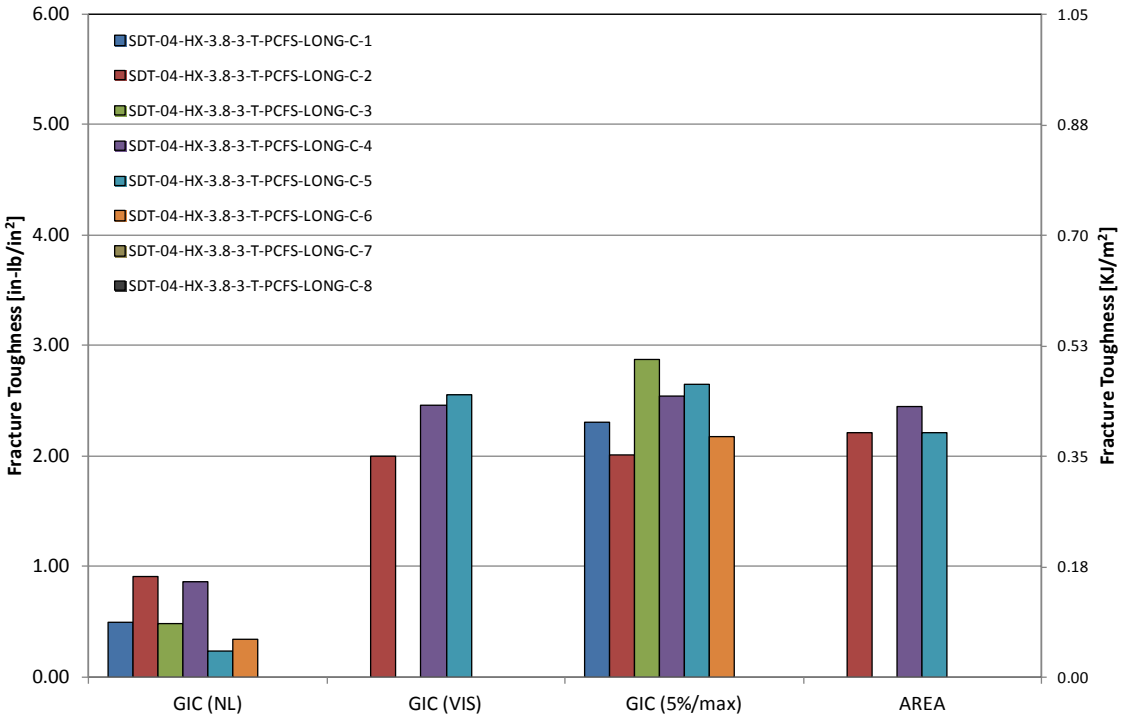

Figure A-123. GIC for HRH-10–3/8–3.0 longitudinal ribbon direction with top disbond (center)

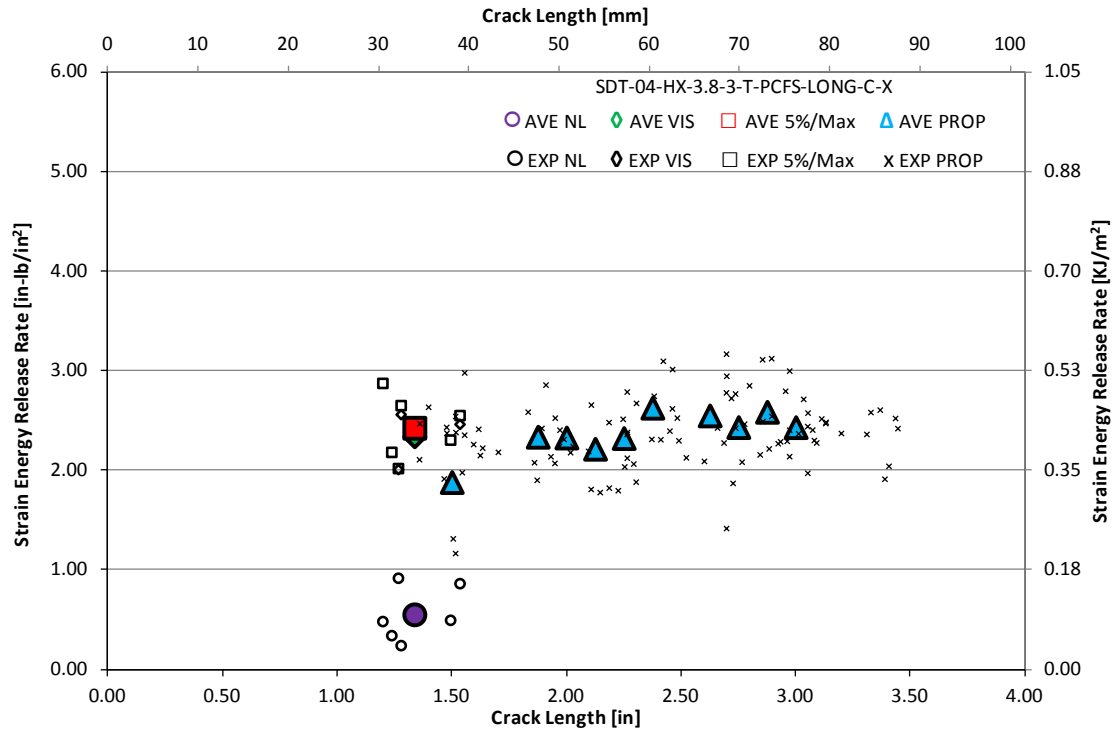

Figure A-124. Resistance curve for HRH-10–3/8–3.0 longitudinal ribbon direction with top disbond (center)

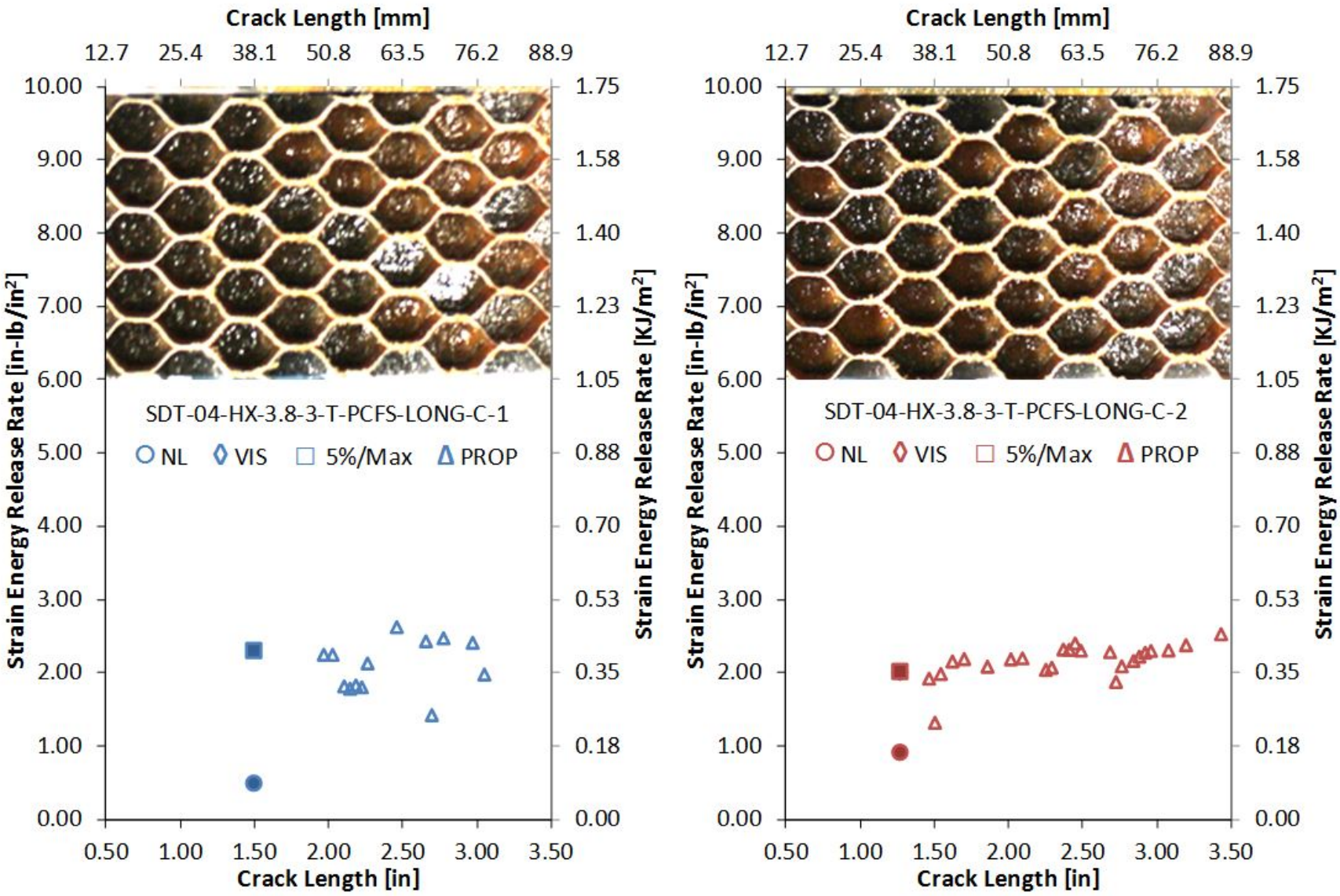

Figure A-125. Failure mode image and resistance curve of SDT-04-HX-3.8-3-T-PCFS-LONG-C-X #1 and #2

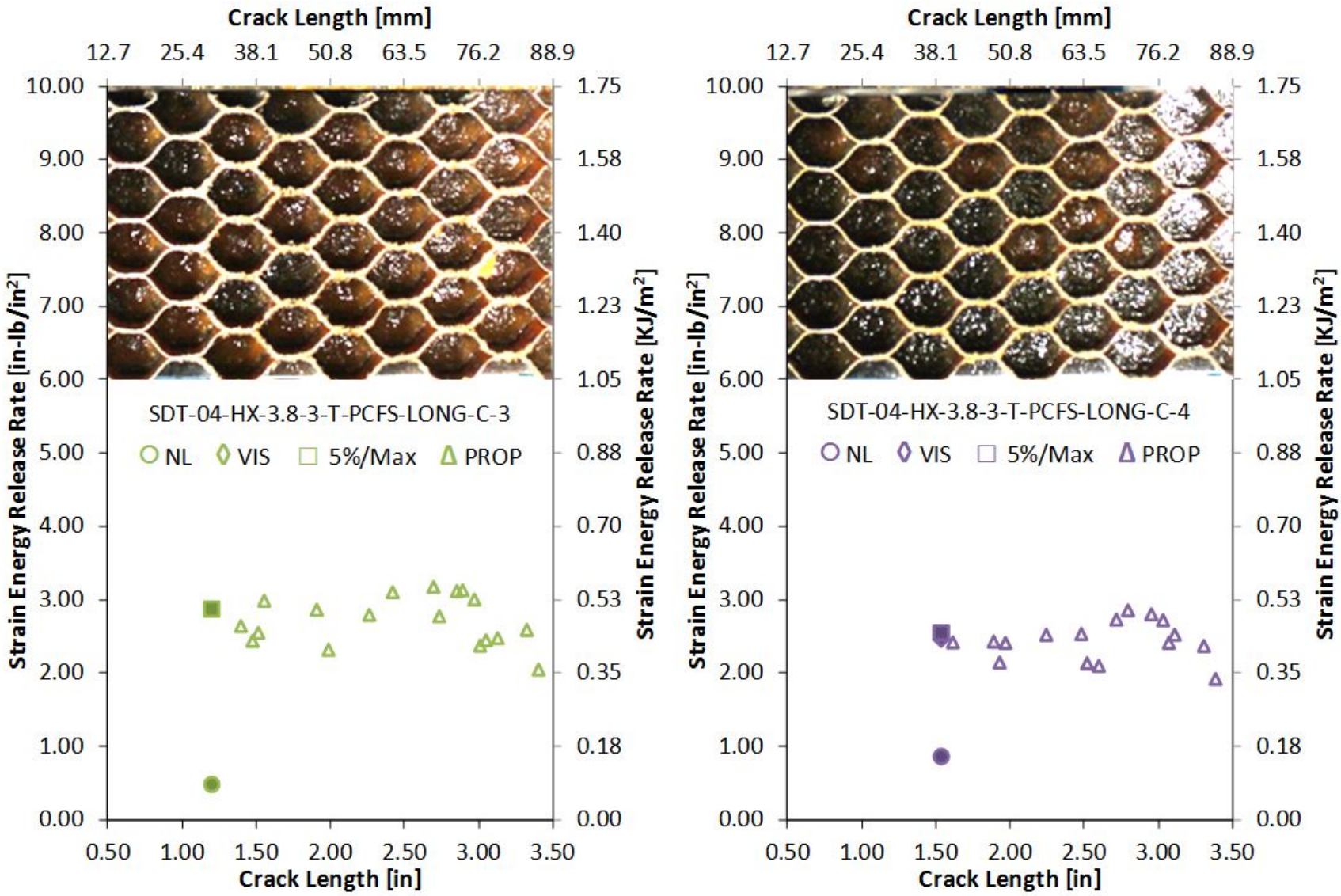

Figure A-126. Failure mode image and resistance curve of SDT-04-HX-3.8-3-T-PCFS-LONG-C-X #3 and #4

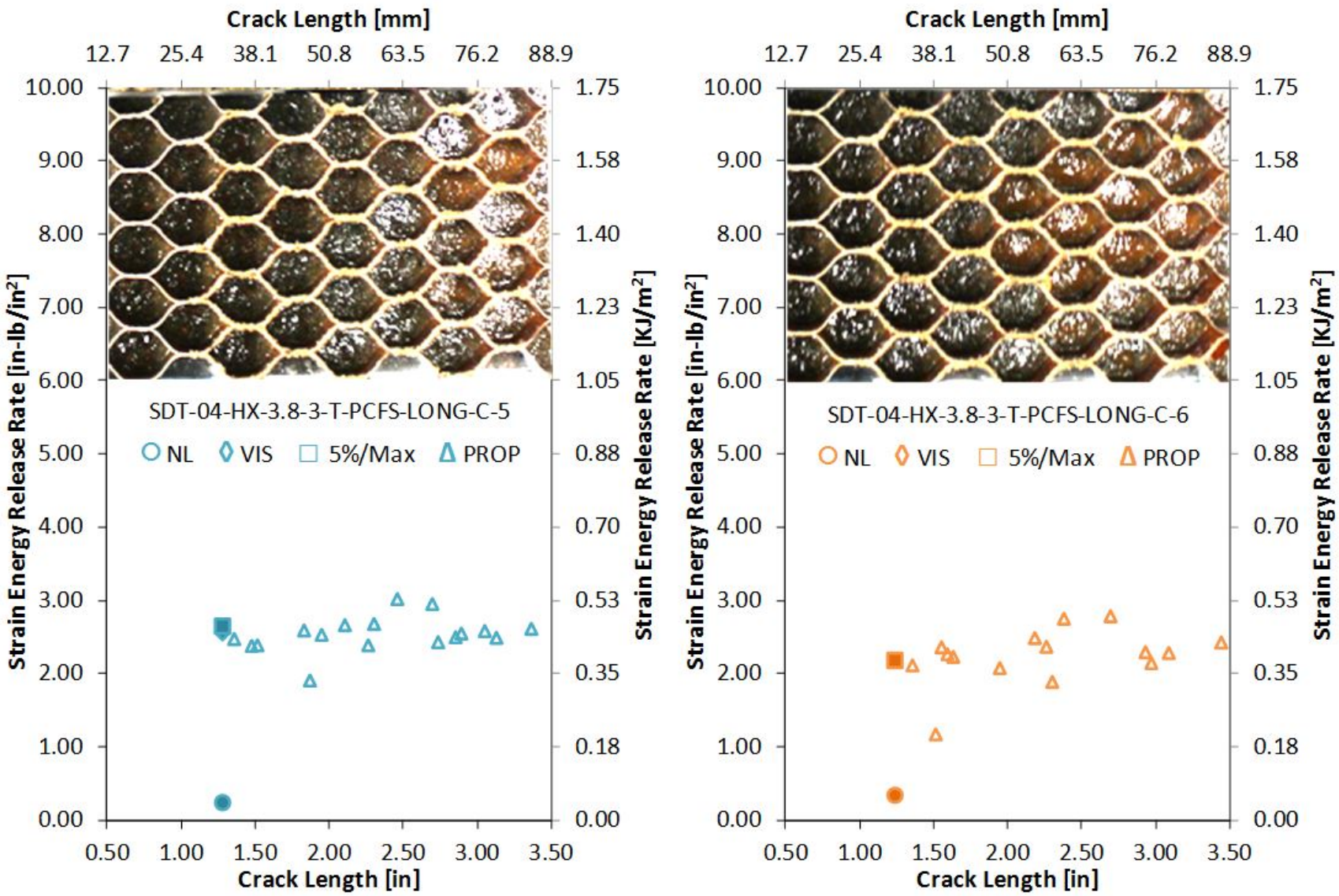

Figure A-127. Failure mode image and resistance curve of SDT-04-HX-3.8-3-T-PCFS-LONG-C-X #5 and #6

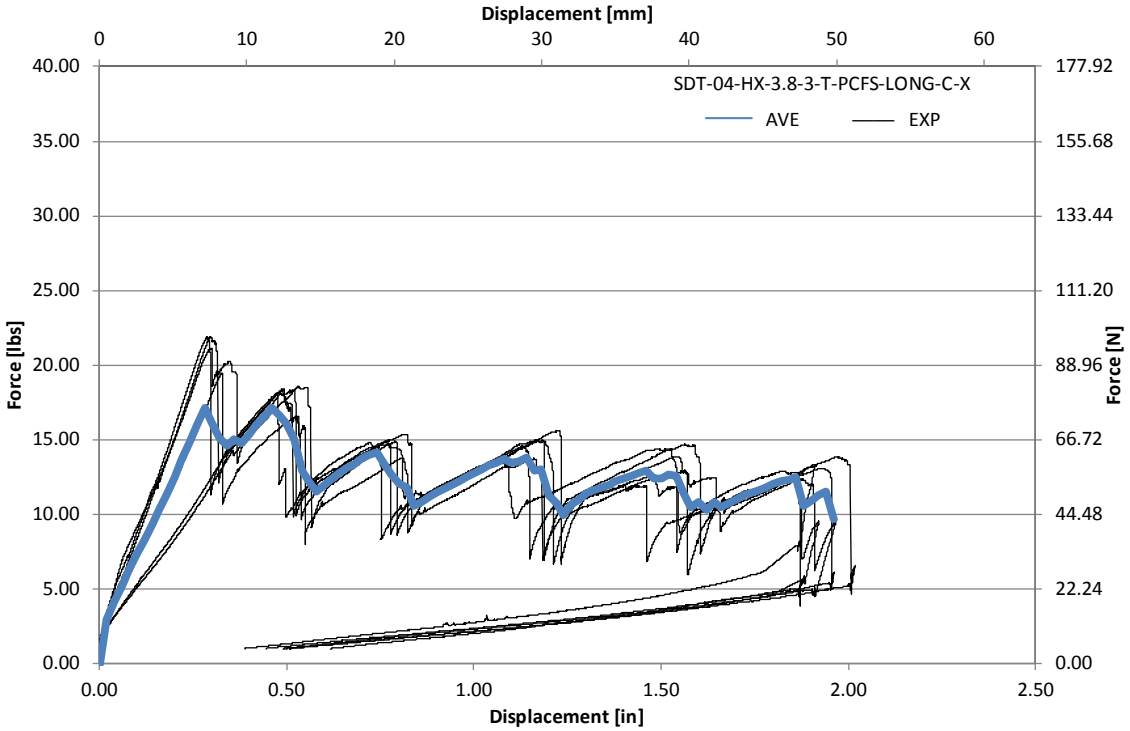

Figure A-128. Load vs. displacement curve for HRH-10–3/8–3.0 longitudinal ribbon direction with top disbond (center)

A.8.2 HRH-10–3/8–3.0 LONGITUDINAL RIBBON DIRECTION WITH BOTTOM DISBOND (CENTER) DATA

Table A-43. Test summary for HRH-10–3/8–3.0 longitudinal ribbon direction with bottom disbond (center) pre-crack

Specimen	GIC (in-lb/in^2)			GIC (KJ/m^2)			Failure Mode
	NL	VIS	5%/max	NL	VIS	5%/max	
SDT-04-HX-3.8-3-B-PCFS-LONG-C-1	0.846	N/A	1.430	0.148	N/A	0.250	Primarily APO
SDT-04-HX-3.8-3-B-PCFS-LONG-C-2	1.473	N/A	2.229	0.258	N/A	0.390	Primarily APO
SDT-04-HX-3.8-3-B-PCFS-LONG-C-3	1.336	N/A	1.796	0.234	N/A	0.314	Primarily APO
SDT-04-HX-3.8-3-B-PCFS-LONG-C-4	1.440	N/A	2.214	0.252	N/A	0.388	Primarily APO
SDT-04-HX-3.8-3-B-PCFS-LONG-C-5	1.859	N/A	2.280	0.326	N/A	0.399	Primarily APO
SDT-04-HX-3.8-3-B-PCFS-LONG-C-6	1.447	2.195	2.219	0.253	0.384	0.389	Primarily APO
SDT-04-HX-3.8-3-B-PCFS-LONG-C-7							
SDT-04-HX-3.8-3-B-PCFS-LONG-C-8							
AVERAGE GIC	1.400	2.195	2.028	0.245	0.384	0.355	
STANDARD DEVIATION	0.326	N/A	0.343	0.057	N/A	0.060	
COEFFICIENT OF VARIATION (%)	23.263	N/A	16.901	23.263	N/A	16.901	

Table A-44. Test summary for HRH-10–3/8–3.0 longitudinal ribbon direction with bottom disbond (center)

Specimen	GIC (in-lb/in^2)				GIC (KJ/m^2)				Failure Mode
	NL	VIS	5%/max	AREA	NL	VIS	5%/max	AREA	
SDT-04-HX-3.8-3-B-PCFS-LONG-C-1	0.826	N/A	1.827	2.068	0.145	N/A	0.320	0.362	Primarily APO
SDT-04-HX-3.8-3-B-PCFS-LONG-C-2	0.656	2.058	2.071	2.156	0.115	0.360	0.363	0.378	Primarily APO
SDT-04-HX-3.8-3-B-PCFS-LONG-C-3	0.789	N/A	1.789	2.084	0.138	N/A	0.313	0.365	Primarily APO
SDT-04-HX-3.8-3-B-PCFS-LONG-C-4	0.566	N/A	1.560	1.975	0.099	N/A	0.273	0.346	Primarily APO
SDT-04-HX-3.8-3-B-PCFS-LONG-C-5	0.972	N/A	1.963	2.442	0.170	N/A	0.344	0.428	Primarily APO
SDT-04-HX-3.8-3-B-PCFS-LONG-C-6	0.942	N/A	1.719	2.209	0.165	N/A	0.301	0.387	Primarily APO
SDT-04-HX-3.8-3-B-PCFS-LONG-C-7									
SDT-04-HX-3.8-3-B-PCFS-LONG-C-8									
AVERAGE GIC	0.792	2.058	1.821	2.156	0.139	0.360	0.319	0.378	
STANDARD DEVIATION	0.158	N/A	0.180	0.162	0.028	N/A	0.032	0.028	
COEFFICIENT OF VARIATION (%)	19.996	N/A	9.891	7.494	19.996	N/A	9.891	7.494	

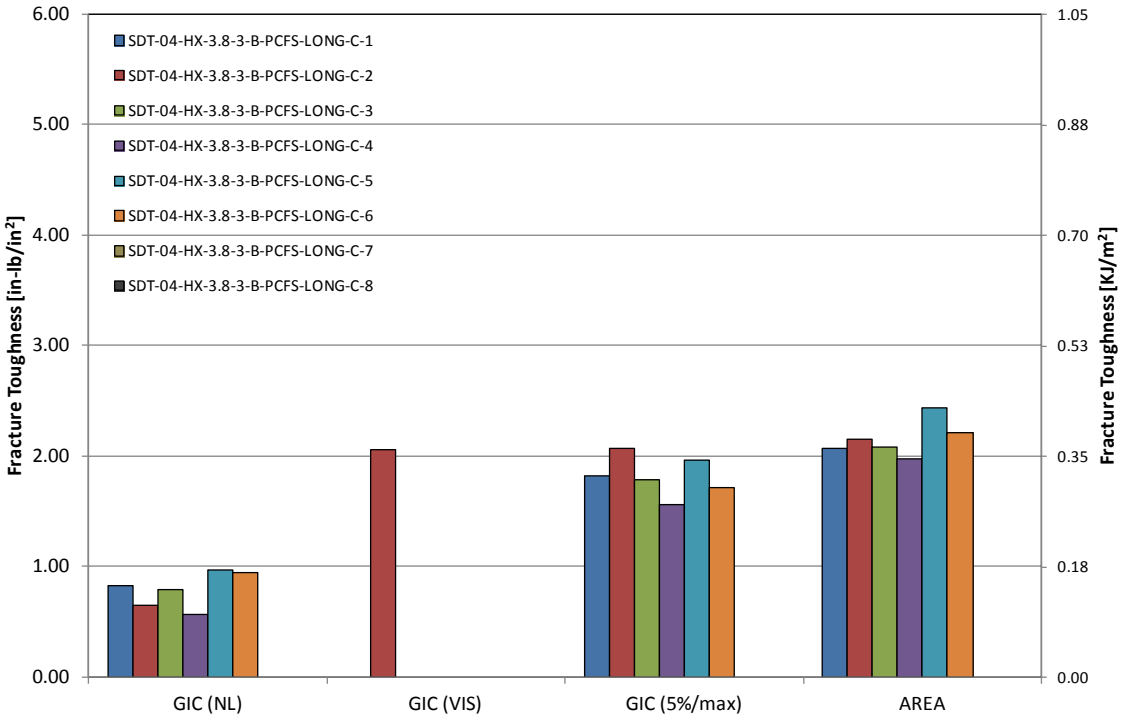

Figure A-129. GIC for HRH-10–3/8–3.0 longitudinal ribbon direction with bottom disbond (center)

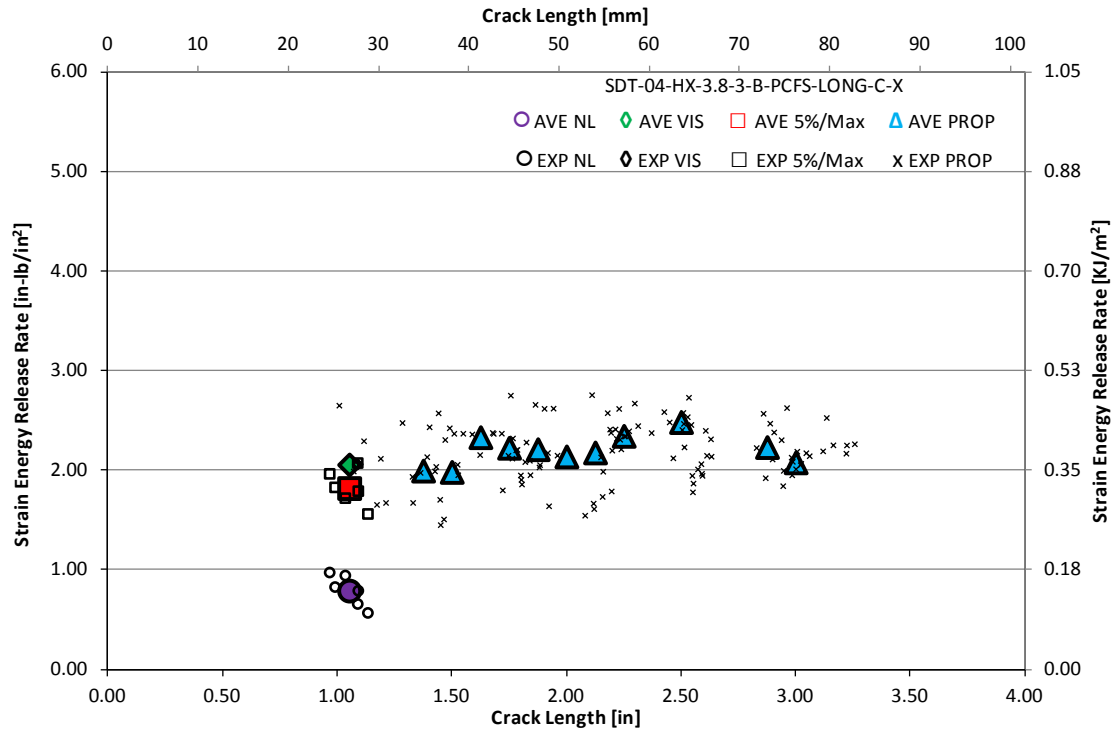

Figure A-130. Resistance curve for HRH-10–3/8–3.0 longitudinal ribbon direction with bottom disbond (center)

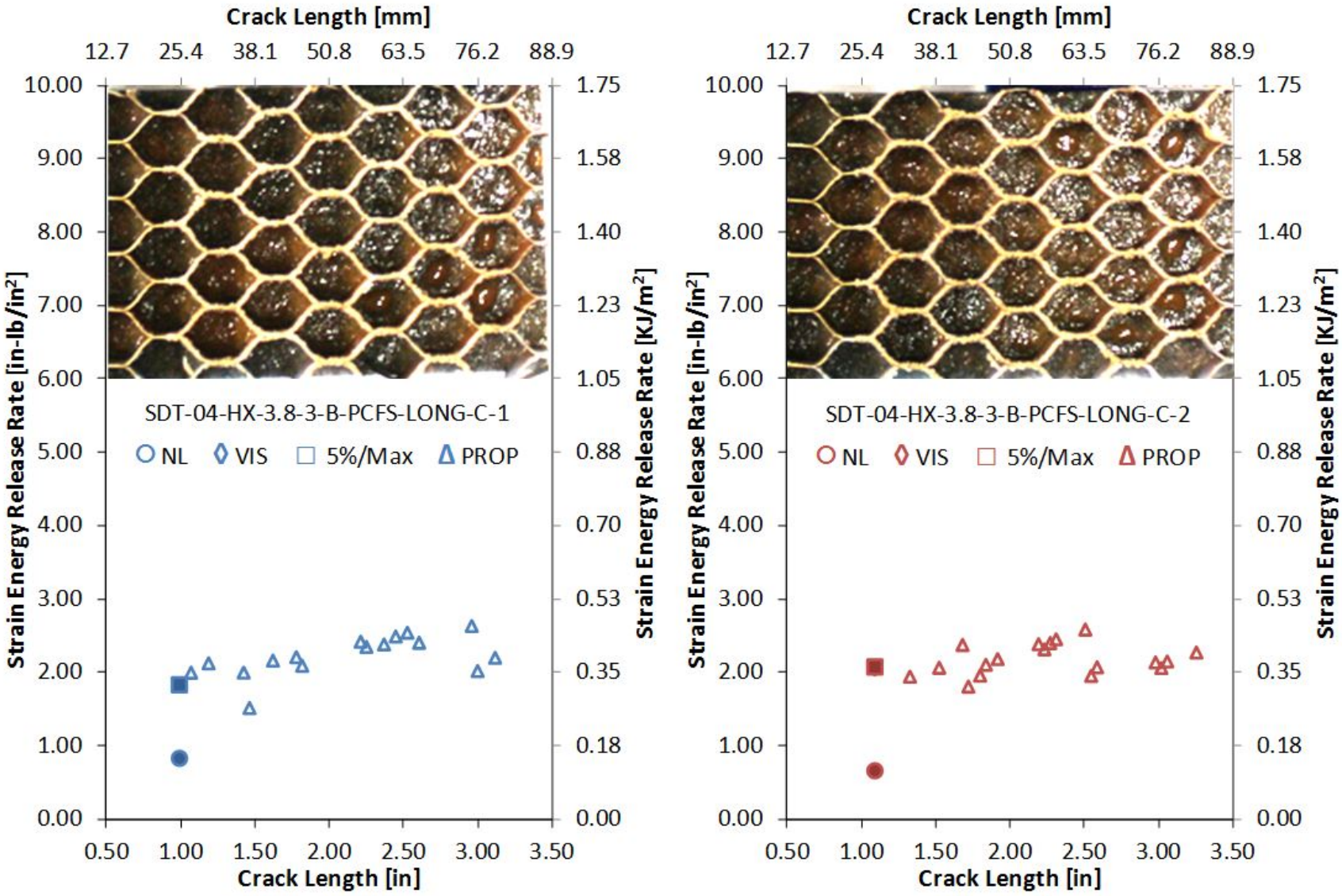

Figure A-131. Failure mode image and resistance curve of SDT-04-HX-3.8-3-B-PCFS-LONG-C-X #1 and #2

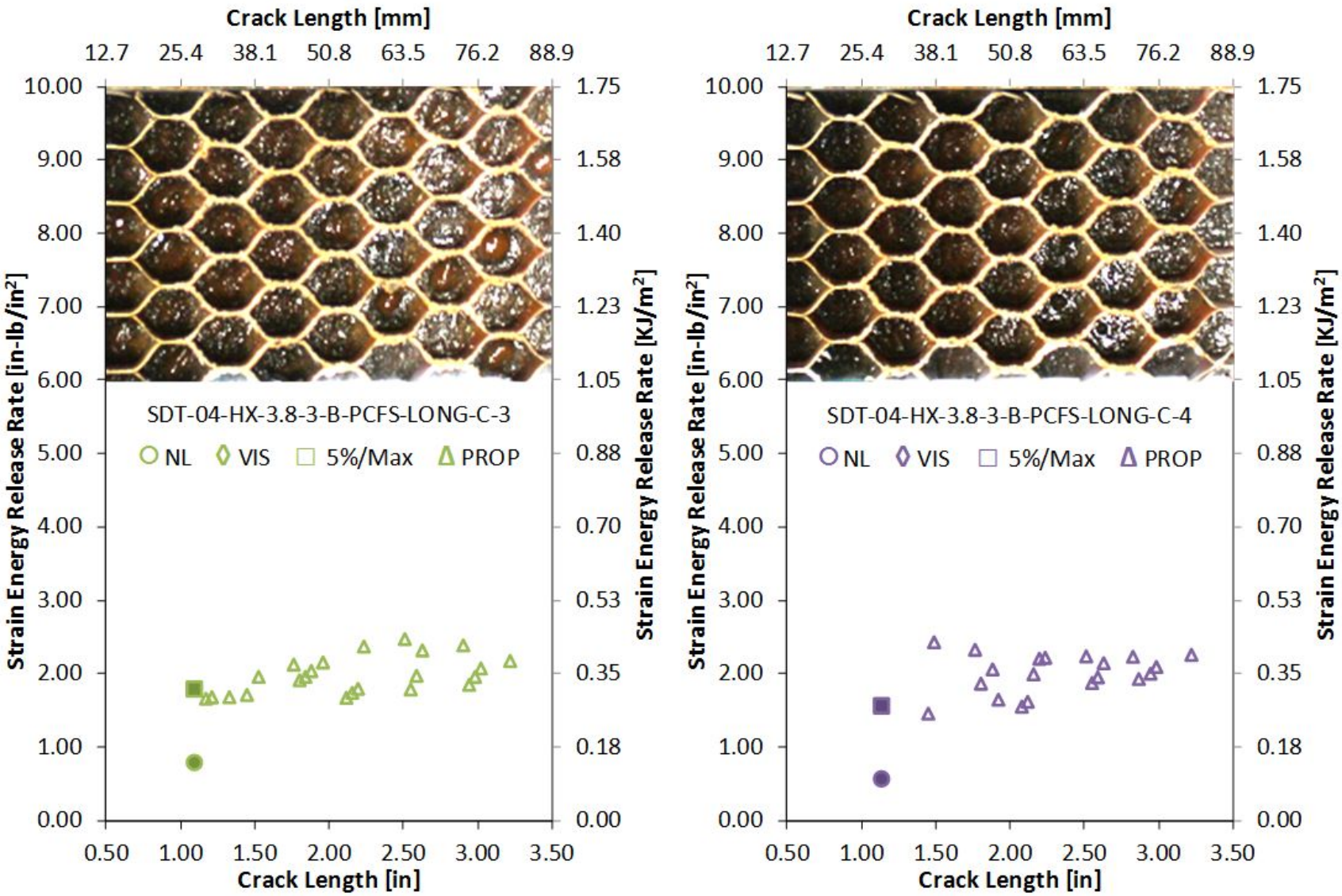

Figure A-132. Failure mode image and resistance curve of SDT-04-HX-3.8-3-B-PCFS-LONG-C-X #3 and #4

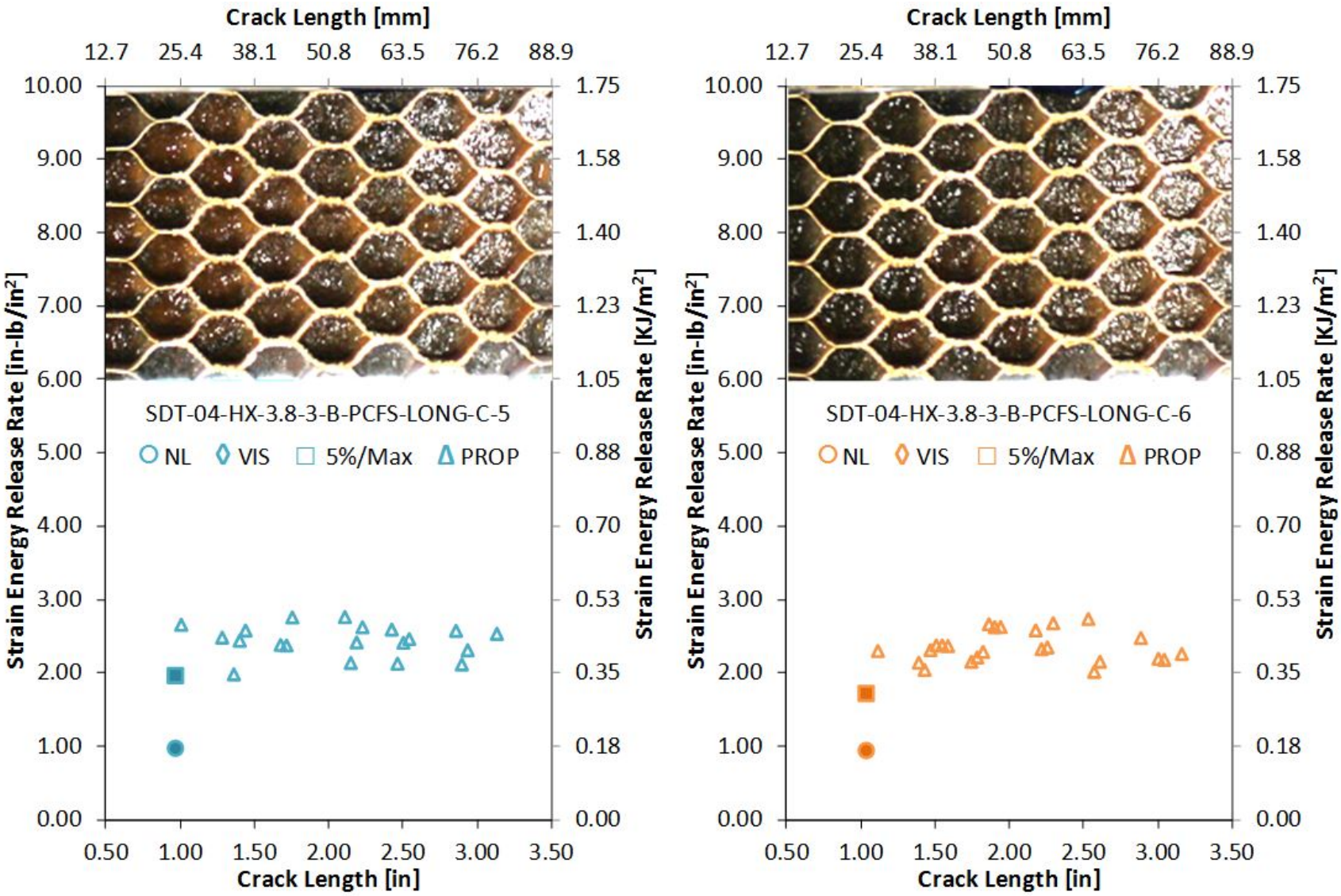

Figure A-133. Failure mode image and resistance curve of SDT-04-HX-3.8-3-B-PCFS-LONG-C-X #5 and #6

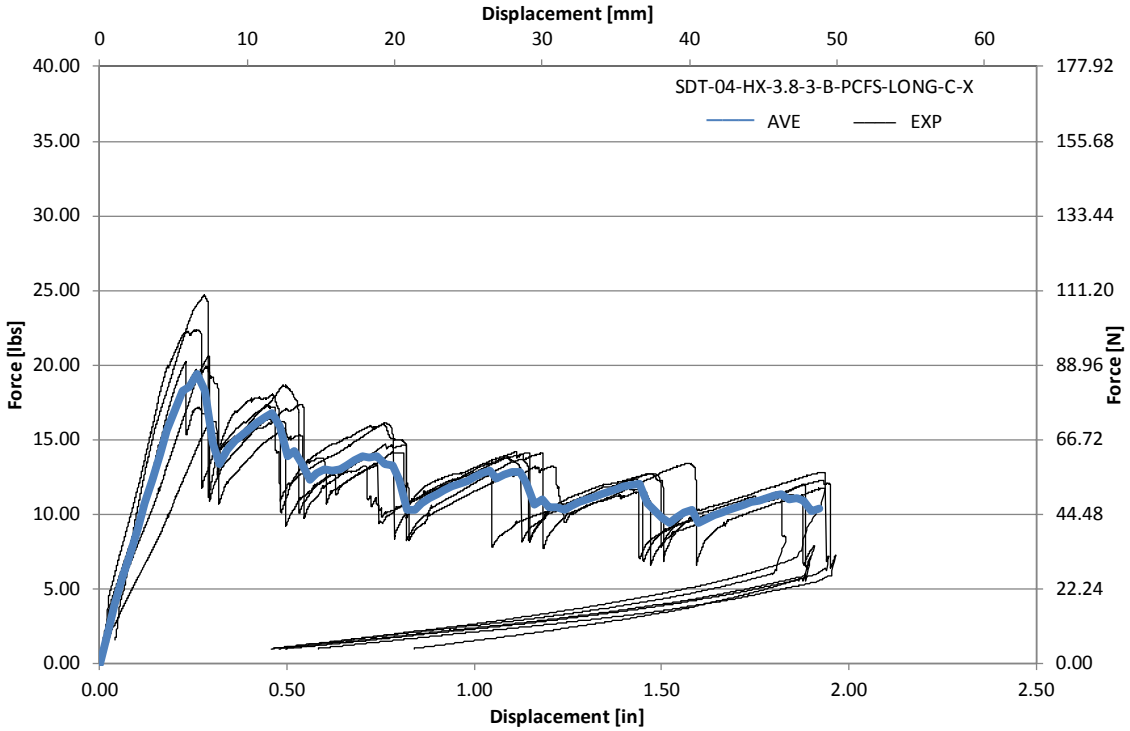

Figure A-134. Load vs. displacement curve for HRH-10–3/8–3.0 longitudinal ribbon direction with bottom disbond (center)

A.8.3 HRH-10–3/8–3.0 LONGITUDINAL RIBBON DIRECTION WITH BOTTOM DISBOND (EDGE) DATA

Table A-45. Test summary for HRH-10–3/8–3.0 longitudinal ribbon direction with bottom disbond (edge) pre-crack

Specimen	GIC (in-lb/in^2)			GIC (KJ/m^2)			Failure Mode
	NL	VIS	5%/max	NL	VIS	5%/max	
SDT-04-HX-3.8-3-B-PCFS-LONG-E-1							
SDT-04-HX-3.8-3-B-PCFS-LONG-E-2	1.192	1.920	1.920	0.209	0.336	0.336	Primarily APO
SDT-04-HX-3.8-3-B-PCFS-LONG-E-3	1.208	N/A	1.212	0.212	N/A	0.212	Primarily APO
SDT-04-HX-3.8-3-B-PCFS-LONG-E-4	0.841	N/A	0.841	0.147	N/A	0.147	Primarily APO
SDT-04-HX-3.8-3-B-PCFS-LONG-E-5	1.352	1.649	1.673	0.237	0.289	0.293	Primarily APO
SDT-04-HX-3.8-3-B-PCFS-LONG-E-6	1.144	N/A	2.131	0.200	N/A	0.373	Primarily APO
SDT-04-HX-3.8-3-B-PCFS-LONG-E-7	1.222	1.772	1.772	0.214	0.310	0.310	Primarily APO
SDT-04-HX-3.8-3-B-PCFS-LONG-E-8							
AVERAGE GIC	1.160	1.781	1.592	0.203	0.312	0.279	
STANDARD DEVIATION	0.171	0.136	0.479	0.030	0.024	0.084	
COEFFICIENT OF VARIATION (%)	14.724	7.625	30.079	14.724	7.625	30.079	

Table A-46. Test summary for HRH-10–3/8–3.0 longitudinal ribbon direction with bottom disbond (edge)

Specimen	GIC (in-lb/in^2)				GIC (KJ/m^2)				Failure Mode
	NL	VIS	5%/max	AREA	NL	VIS	5%/max	AREA	
SDT-04-HX-3.8-3-B-PCFS-LONG-E-1									
SDT-04-HX-3.8-3-B-PCFS-LONG-E-2	0.620	N/A	1.314	1.974	0.109	N/A	0.230	0.346	Primarily APO
SDT-04-HX-3.8-3-B-PCFS-LONG-E-3	0.505	1.728	2.559	N/A	0.088	0.303	0.448	N/A	Primarily APO
SDT-04-HX-3.8-3-B-PCFS-LONG-E-4	0.335	2.131	2.179	2.294	0.059	0.373	0.382	0.402	Primarily APO
SDT-04-HX-3.8-3-B-PCFS-LONG-E-5	0.432	1.000	1.055	N/A	0.076	0.175	0.185	N/A	Primarily APO
SDT-04-HX-3.8-3-B-PCFS-LONG-E-6	0.713	1.962	2.283	N/A	0.125	0.344	0.400	N/A	Primarily APO
SDT-04-HX-3.8-3-B-PCFS-LONG-E-7	1.499	2.012	2.072	2.107	0.263	0.352	0.363	0.369	Primarily APO
SDT-04-HX-3.8-3-B-PCFS-LONG-E-8									
AVERAGE GIC	0.684	1.767	1.910	2.125	0.120	0.309	0.335	0.372	
STANDARD DEVIATION	0.421	0.453	0.591	0.161	0.074	0.079	0.103	0.028	
COEFFICIENT OF VARIATION (%)	61.556	25.636	30.926	7.578	61.556	25.636	30.926	7.578	

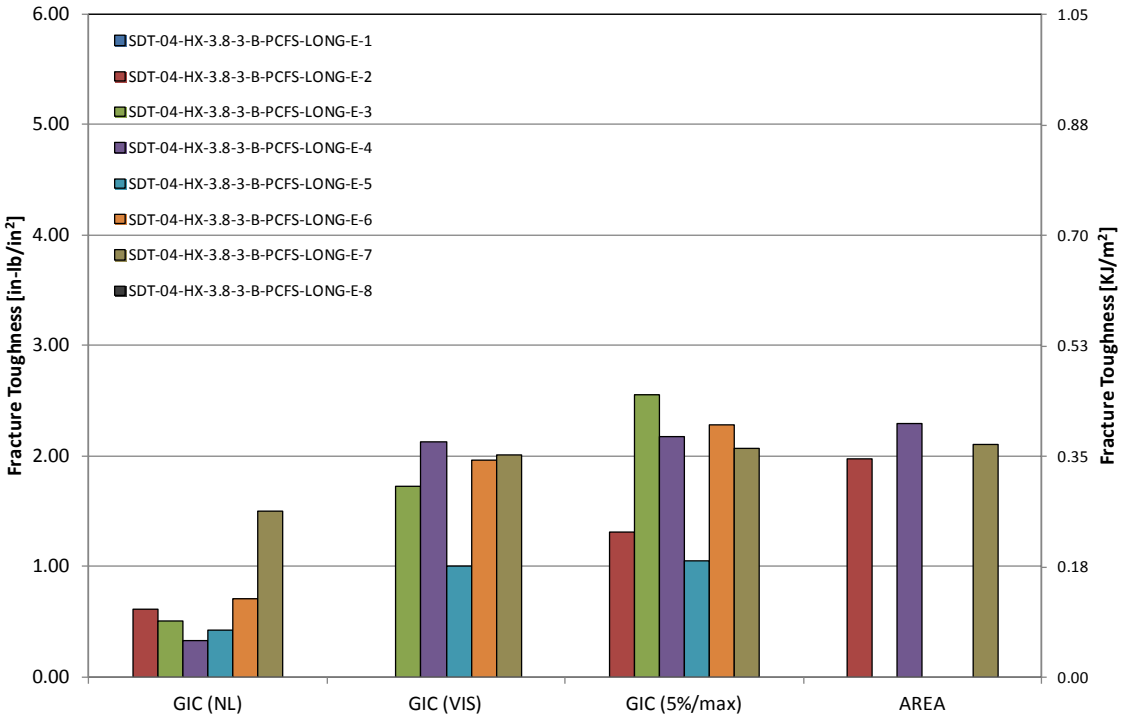

Figure A-135. GIC for HRH-10–3/8–3.0 longitudinal ribbon direction with bottom disbond (edge)

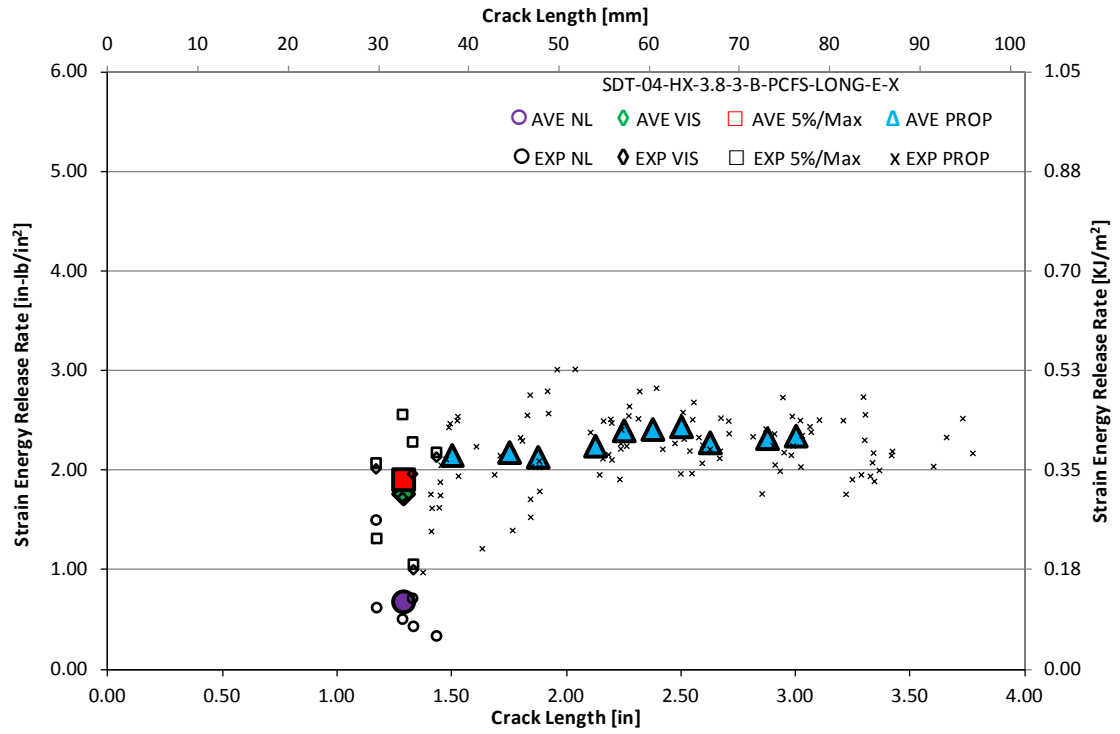

Figure A-136. Resistance curve for HRH-10–3/8–3.0 longitudinal ribbon direction with bottom disbond (edge)

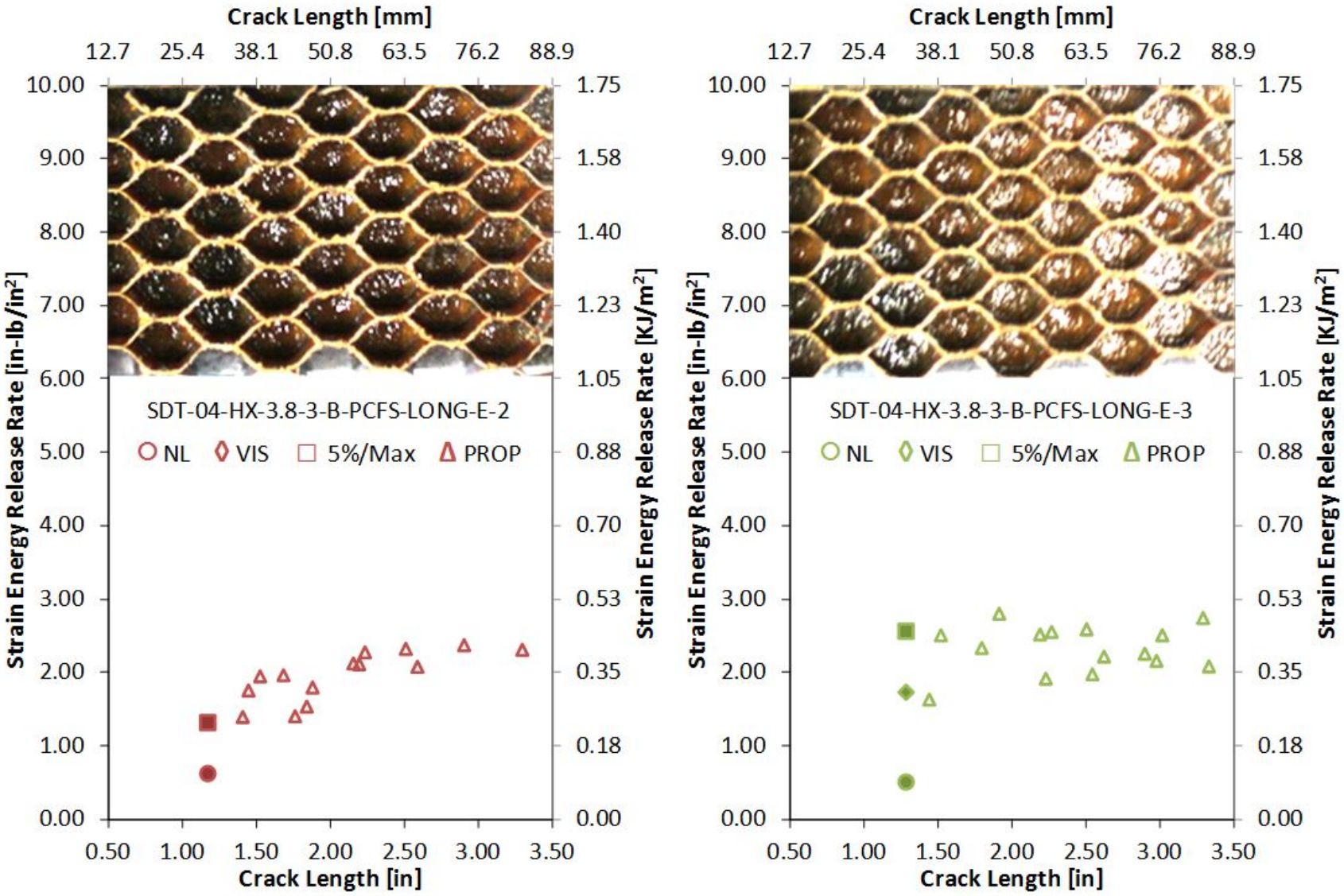

Figure A-137. Failure mode image and resistance curve of SDT-04-HX-3.8-3-B-PCFS-LONG-E-X #2 and #3

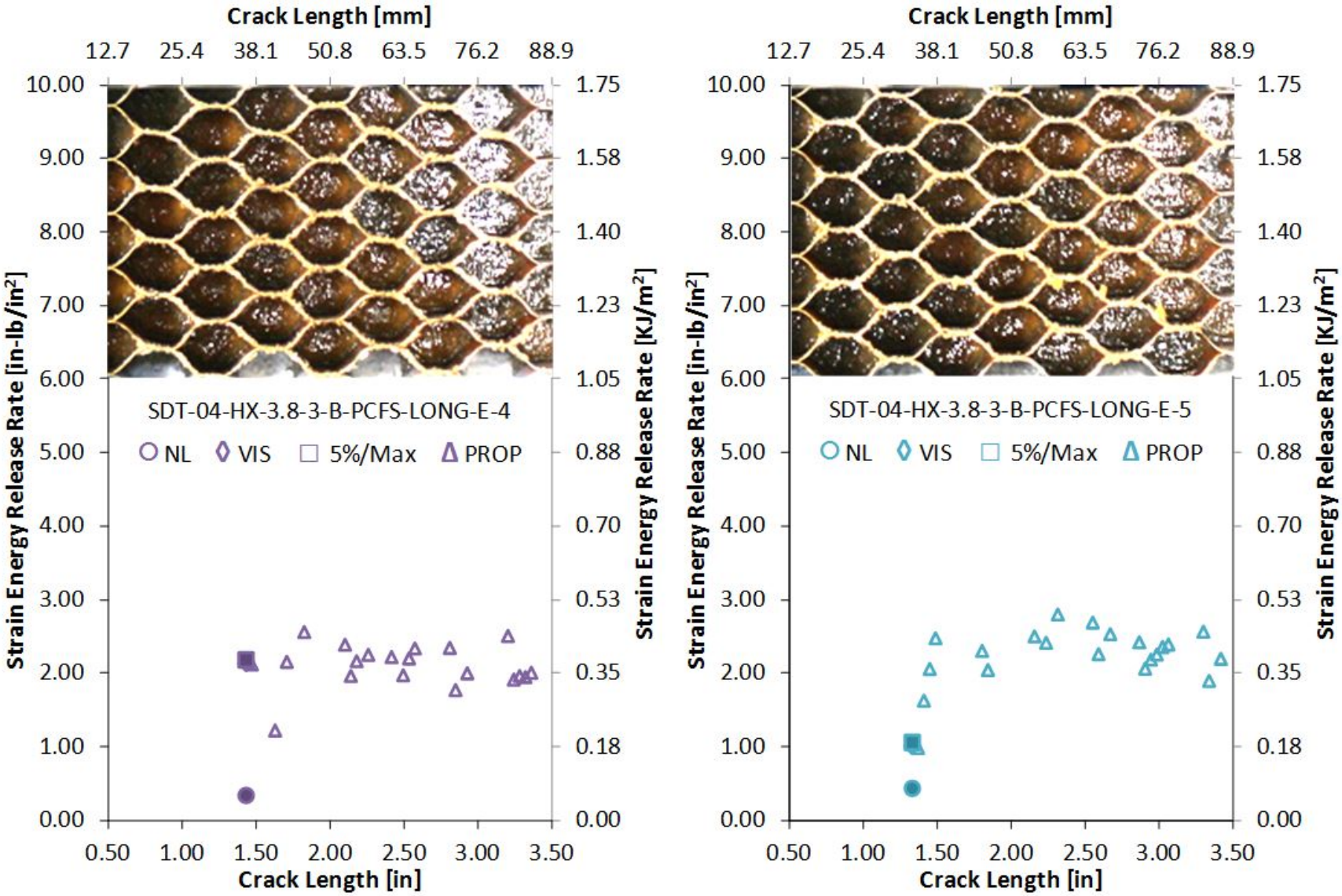

Figure A-138. Failure mode image and resistance curve of SDT-04-HX-3.8-3-B-PCFS-LONG-E-X #4 and #5

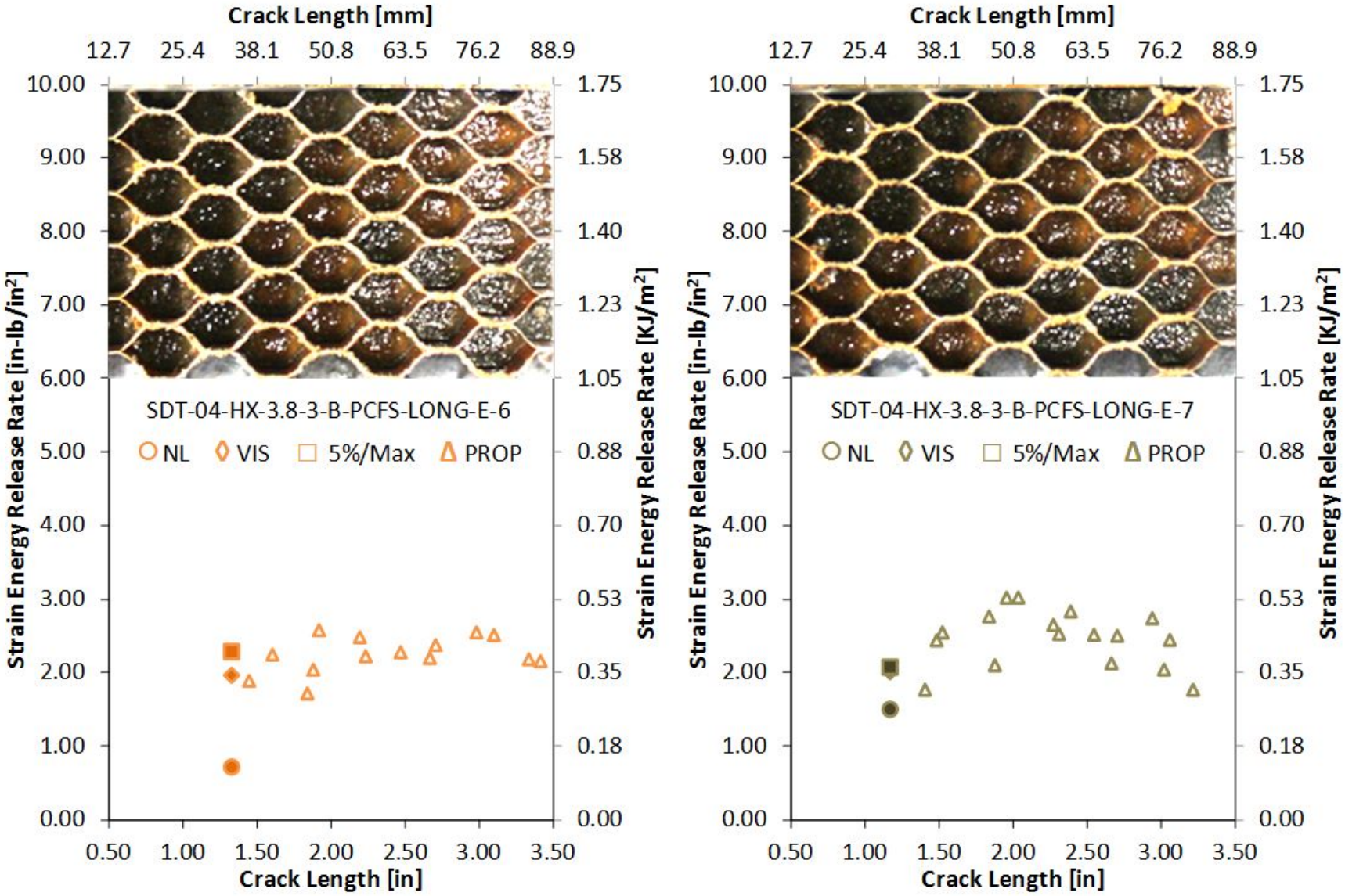

Figure A-139. Failure mode image and resistance curve of SDT-04-HX-3.8-3-B-PCFS-LONG-E-X #6 and #7

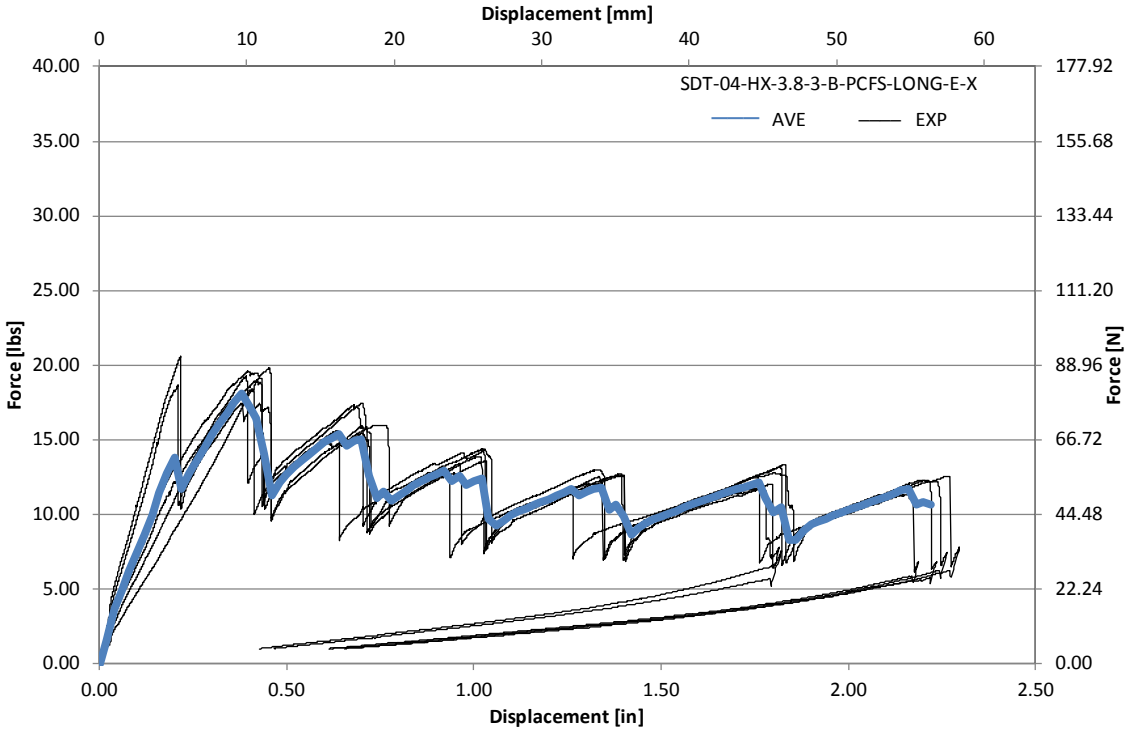

Figure A-140. Load vs. displacement curve for HRH-10–3/8–3.0 longitudinal ribbon direction with bottom disbond (edge)

A.8.4 HRH-10–3/8–3.0 LATERAL RIBBON DIRECTION WITH TOP DISBOND (CENTER) DATA

Table A-47. Test summary for HRH-10–3/8–3.0 lateral ribbon direction with top disbond (center) pre-crack

Specimen	GIC (in-lb/in^2)			GIC (KJ/m^2)			Failure Mode
	NL	VIS	5%/max	NL	VIS	5%/max	
SDT-04-HX-3.8-3-T-PCFS-LAT-C-1	0.801	1.699	1.697	0.140	0.298	0.297	Primarily APO
SDT-04-HX-3.8-3-T-PCFS-LAT-C-2	1.306	2.091	2.091	0.229	0.366	0.366	Primarily APO
SDT-04-HX-3.8-3-T-PCFS-LAT-C-3	1.291	1.597	2.071	0.226	0.280	0.363	Primarily APO
SDT-04-HX-3.8-3-T-PCFS-LAT-C-4	1.378	N/A	2.252	0.241	N/A	0.394	Primarily APO
SDT-04-HX-3.8-3-T-PCFS-LAT-C-5	0.937	1.447	1.447	0.164	0.253	0.253	Primarily APO
SDT-04-HX-3.8-3-T-PCFS-LAT-C-6							
SDT-04-HX-3.8-3-T-PCFS-LAT-C-7	0.964	1.903	1.903	0.169	0.333	0.333	Primarily APO
SDT-04-HX-3.8-3-T-PCFS-LAT-C-8							
AVERAGE GIC	1.113	1.747	1.910	0.195	0.306	0.335	
STANDARD DEVIATION	0.241	0.253	0.295	0.042	0.044	0.052	
COEFFICIENT OF VARIATION (%)	21.637	14.507	15.447	21.637	14.507	15.447	

Table A-48. Test summary for HRH-10–3/8–3.0 lateral ribbon direction with top disbond (center)

Specimen	GIC (in-lb/in^2)				GIC (KJ/m^2)				Failure Mode
	NL	VIS	5%/max	AREA	NL	VIS	5%/max	AREA	
SDT-04-HX-3.8-3-T-PCFS-LAT-C-1	0.897	N/A	1.514	2.630	0.157	N/A	0.265	0.461	Primarily APO
SDT-04-HX-3.8-3-T-PCFS-LAT-C-2	0.580	1.867	1.877	2.952	0.102	0.327	0.329	0.517	Primarily APO
SDT-04-HX-3.8-3-T-PCFS-LAT-C-3	0.576	1.638	1.681	3.083	0.101	0.287	0.294	0.540	Primarily APO
SDT-04-HX-3.8-3-T-PCFS-LAT-C-4	0.978	N/A	1.717	3.046	0.171	N/A	0.301	0.533	Primarily APO
SDT-04-HX-3.8-3-T-PCFS-LAT-C-5	0.423	0.822	0.840	2.950	0.074	0.144	0.147	0.517	Primarily APO, with one cell partially in A
SDT-04-HX-3.8-3-T-PCFS-LAT-C-6									
SDT-04-HX-3.8-3-T-PCFS-LAT-C-7	0.559	N/A	2.075	2.928	0.098	N/A	0.363	0.513	Primarily APO
SDT-04-HX-3.8-3-T-PCFS-LAT-C-8									
AVERAGE GIC	0.669	1.442	1.617	2.932	0.117	0.253	0.283	0.513	
STANDARD DEVIATION	0.218	0.549	0.425	0.160	0.038	0.096	0.075	0.028	
COEFFICIENT OF VARIATION (%)	32.537	38.084	26.309	5.449	32.537	38.084	26.309	5.449	

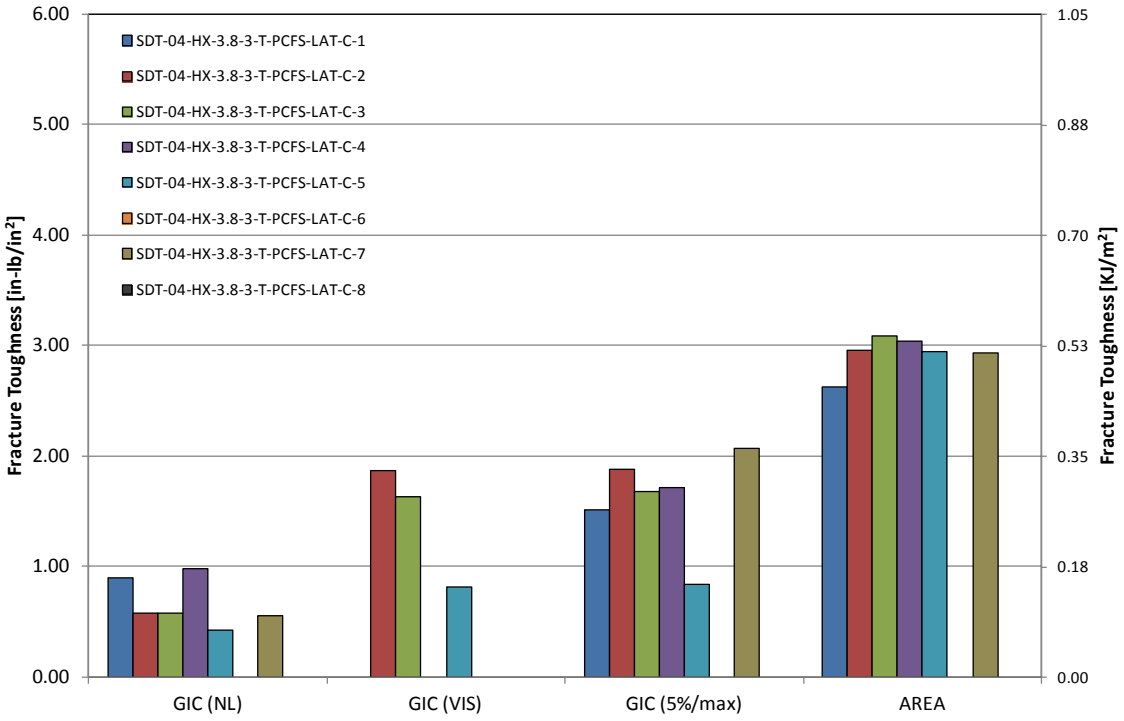

Figure A-141. GIC for HRH-10–3/8–3.0 lateral ribbon direction with top disbond (center)

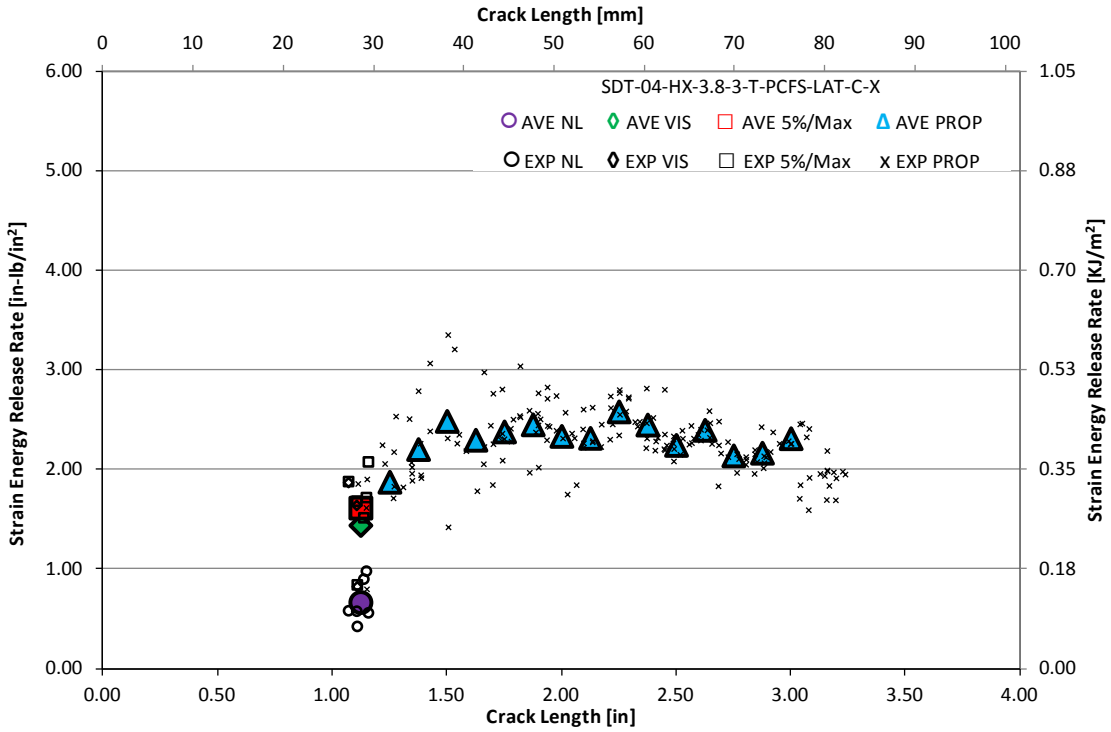

Figure A-142. Resistance curve for HRH-10–3/8–3.0 lateral ribbon direction with top disbond (center)

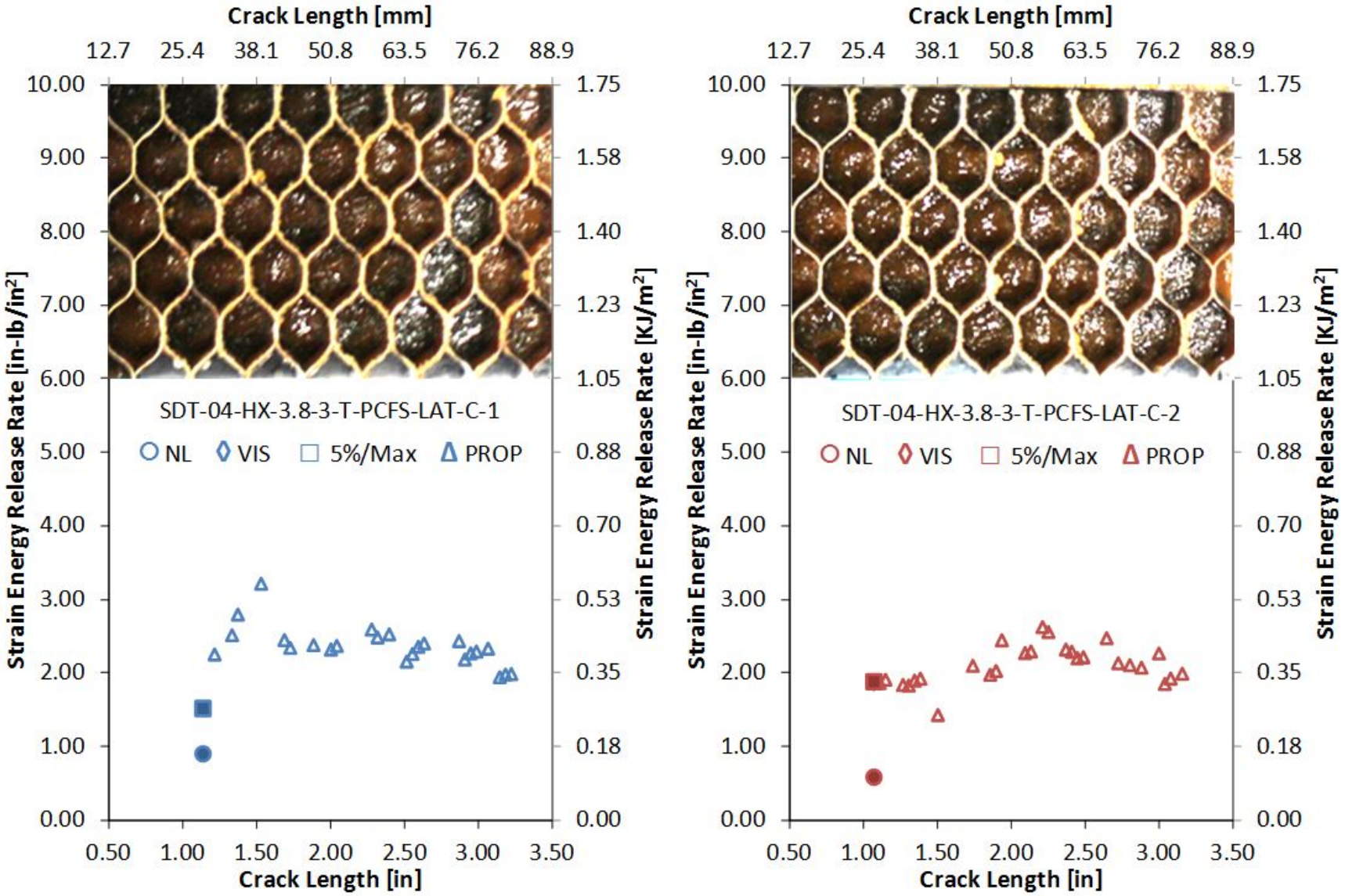

Figure A-143. Failure mode image and resistance curve of SDT-04-HX-3.8-3-T-PCFS-LAT-C-X #1 and #2

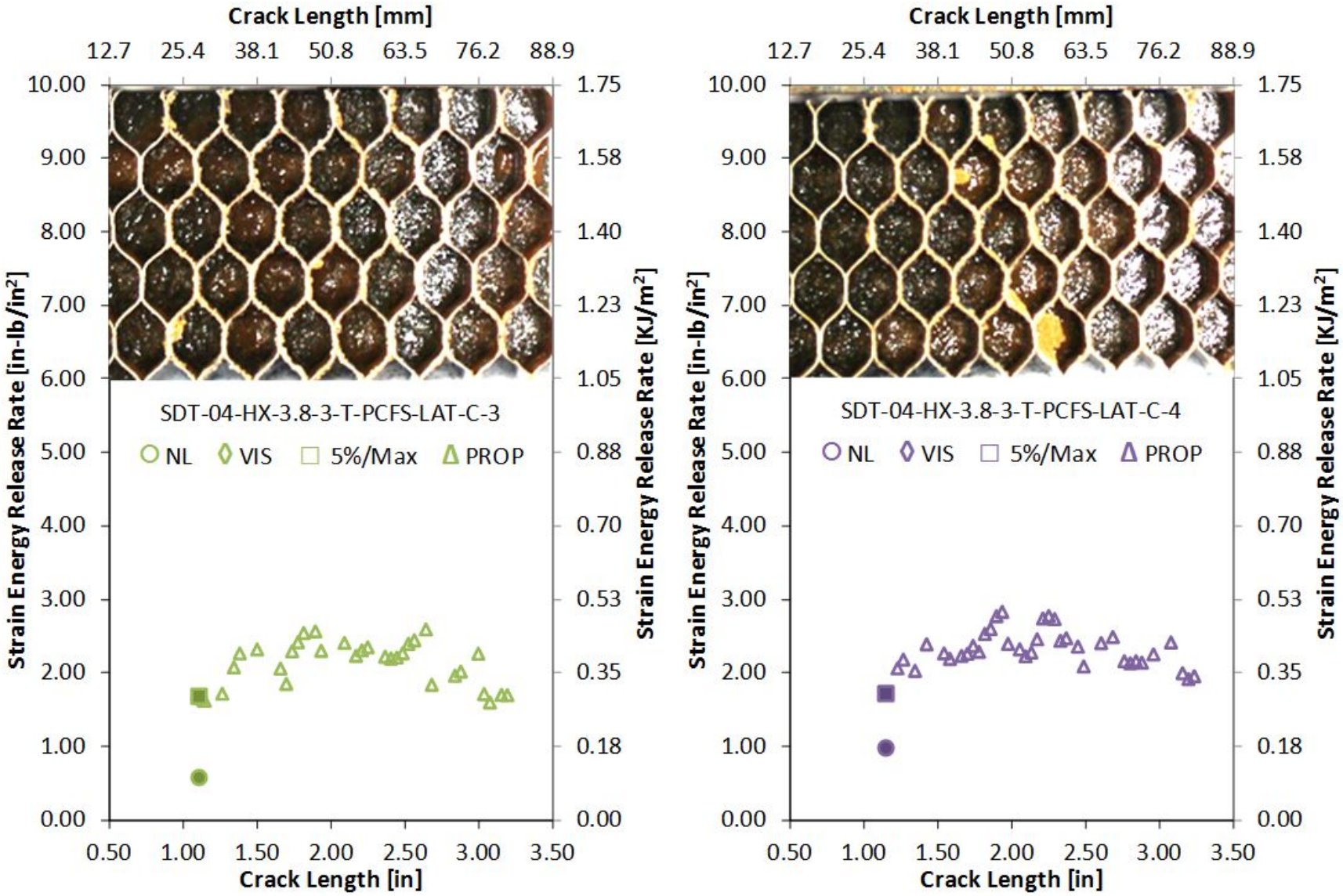

Figure A-144. Failure mode image and resistance curve of SDT-04-HX-3.8-3-T-PCFS-LAT-C-X #3 and #4

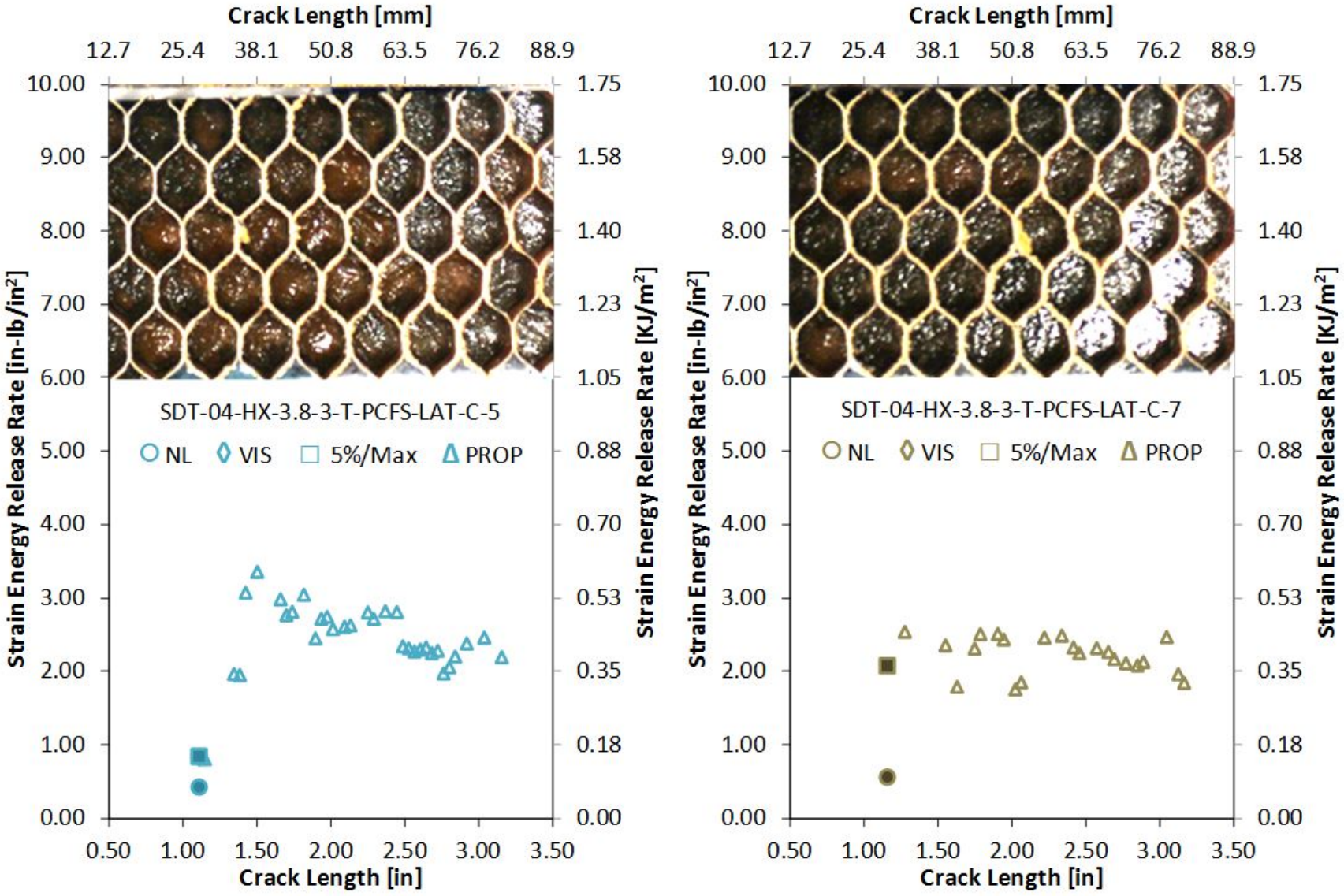

Figure A-145. Failure mode image and resistance curve of SDT-04-HX-3.8-3-T-PCFS-LAT-C-X #5 and #7

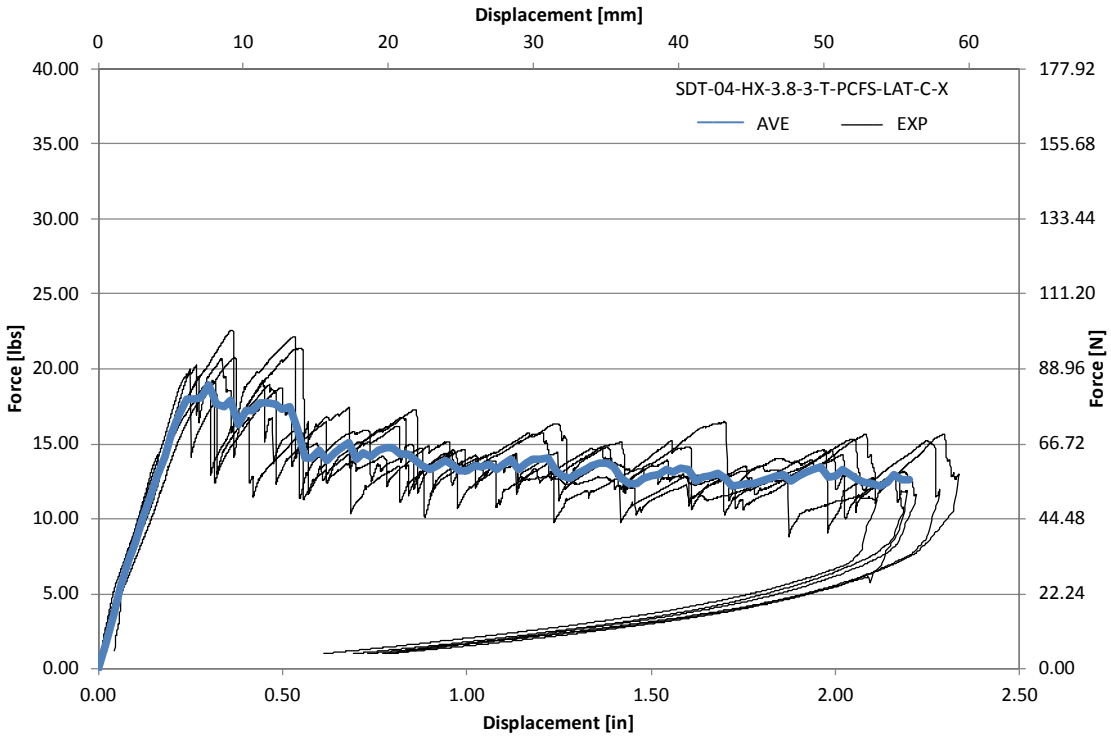

Figure A-146. Load vs. displacement curve for HRH-10–3/8–3.0 lateral ribbon direction with top disbond (center)

A.8.5 HRH-10–3/8–3.0 LATERAL RIBBON DIRECTION WITH BOTTOM DISBOND (CENTER) DATA

Table A-49. Test summary for HRH-10–3/8–3.0 lateral ribbon direction with bottom disbond (center) pre-crack

Specimen	GIC (in-lb/in^2)			GIC (KJ/m^2)			Failure Mode
	NL	VIS	5%/max	NL	VIS	5%/max	
SDT-04-HX-3.8-3-B-PCFS-LAT-C-1	1.057	N/A	1.506	0.185	N/A	0.264	Primarily APO
SDT-04-HX-3.8-3-B-PCFS-LAT-C-2	1.724	N/A	2.143	0.302	N/A	0.375	Primarily APO
SDT-04-HX-3.8-3-B-PCFS-LAT-C-3	1.223	2.412	2.412	0.214	0.422	0.422	Primarily APO
SDT-04-HX-3.8-3-B-PCFS-LAT-C-4	1.635	N/A	2.047	0.286	N/A	0.358	Primarily APO
SDT-04-HX-3.8-3-B-PCFS-LAT-C-5	1.274	N/A	1.805	0.223	N/A	0.316	Primarily APO
SDT-04-HX-3.8-3-B-PCFS-LAT-C-6	0.998	N/A	1.414	0.175	N/A	0.248	Primarily APO
SDT-04-HX-3.8-3-B-PCFS-LAT-C-7							
SDT-04-HX-3.8-3-B-PCFS-LAT-C-8							
AVERAGE GIC	1.318	2.412	1.888	0.231	0.422	0.331	
STANDARD DEVIATION	0.299	N/A	0.385	0.052	N/A	0.067	
COEFFICIENT OF VARIATION (%)	22.684	N/A	20.408	22.684	N/A	20.408	

Table A-50. Test summary for HRH-10–3/8–3.0 lateral ribbon direction with bottom disbond (center)

Specimen	GIC (in-lb/in^2)				GIC (KJ/m^2)				Failure Mode
	NL	VIS	5%/max	AREA	NL	VIS	5%/max	AREA	
SDT-04-HX-3.8-3-B-PCFS-LAT-C-1	0.816	N/A	1.742	2.333	0.143	N/A	0.305	0.409	Primarily APO
SDT-04-HX-3.8-3-B-PCFS-LAT-C-2	1.026	2.078	2.124	2.605	0.180	0.364	0.372	0.456	Primarily APO
SDT-04-HX-3.8-3-B-PCFS-LAT-C-3	1.124	1.563	1.578	2.191	0.197	0.274	0.276	0.384	Primarily APO
SDT-04-HX-3.8-3-B-PCFS-LAT-C-4	0.543	1.547	1.553	2.554	0.095	0.271	0.272	0.447	Primarily APO
SDT-04-HX-3.8-3-B-PCFS-LAT-C-5	0.827	N/A	2.308	2.528	0.145	N/A	0.404	0.443	Primarily APO
SDT-04-HX-3.8-3-B-PCFS-LAT-C-6	0.812	1.403	1.636	2.639	0.142	0.246	0.287	0.462	Primarily APO
SDT-04-HX-3.8-3-B-PCFS-LAT-C-7									
SDT-04-HX-3.8-3-B-PCFS-LAT-C-8									
AVERAGE GIC	0.858	1.648	1.823	2.475	0.150	0.289	0.319	0.433	
STANDARD DEVIATION	0.201	0.295	0.316	0.175	0.035	0.052	0.055	0.031	
COEFFICIENT OF VARIATION (%)	23.474	17.932	17.350	7.084	23.474	17.932	17.350	7.084	

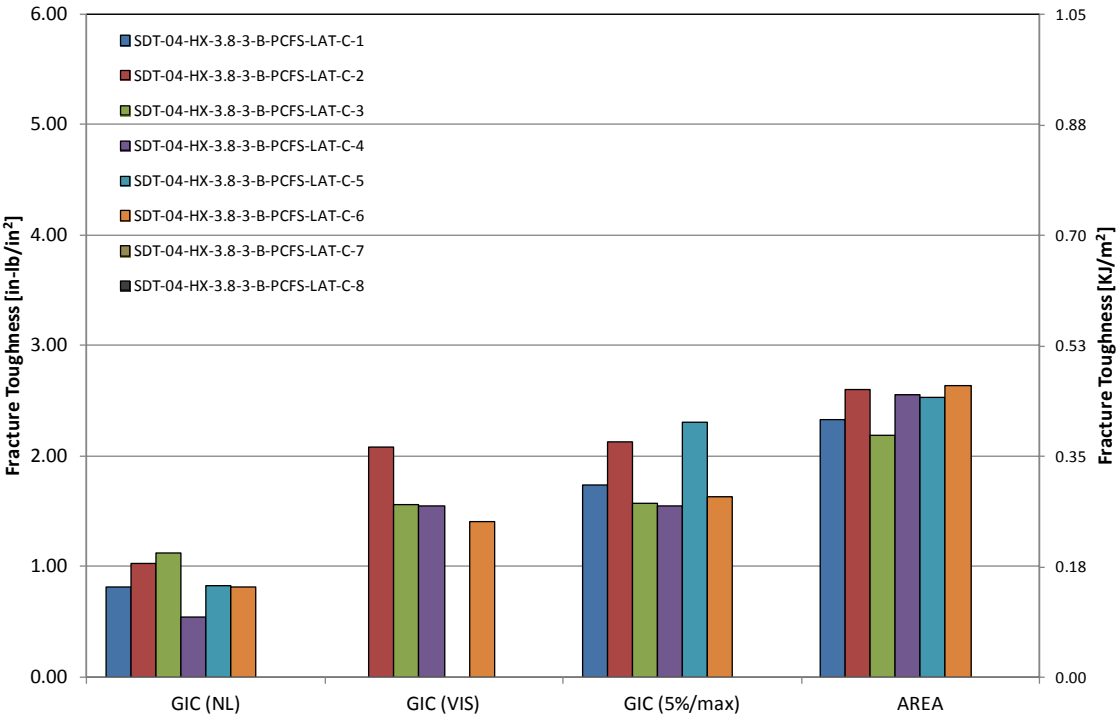

Figure A-147. GIC for HRH-10–3/8–3.0 lateral ribbon direction with bottom disbond (center)

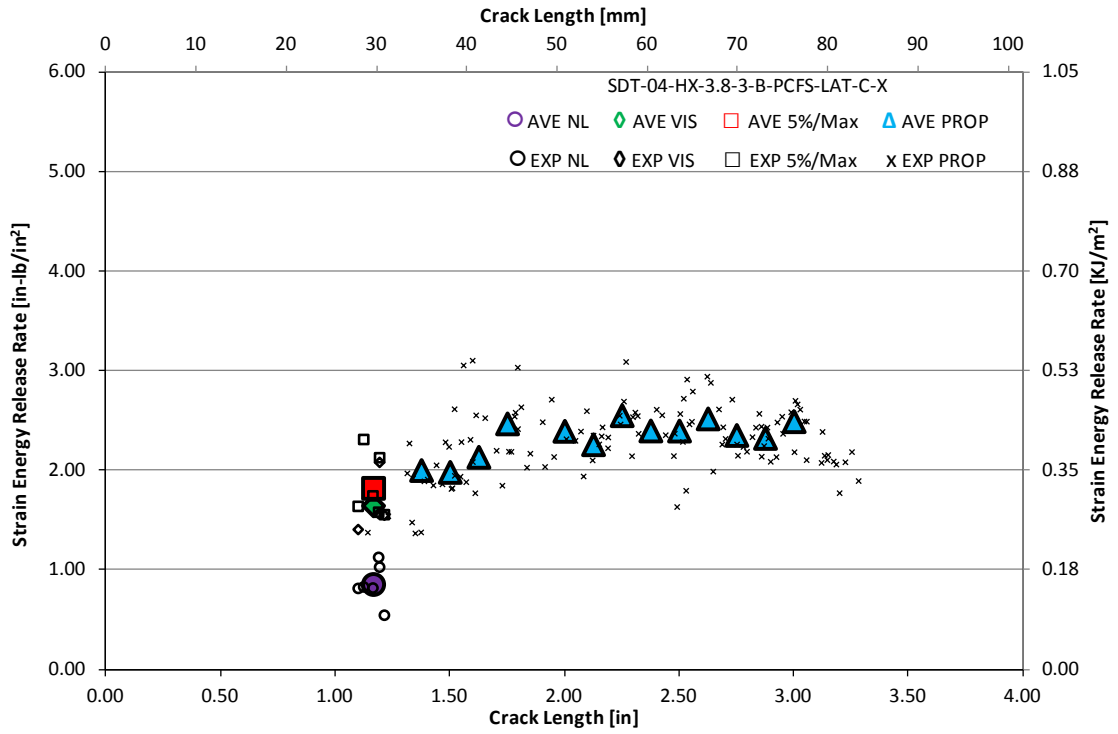

Figure A-148. Resistance curve for HRH-10–3/8–3.0 lateral ribbon direction with bottom disbond (center)

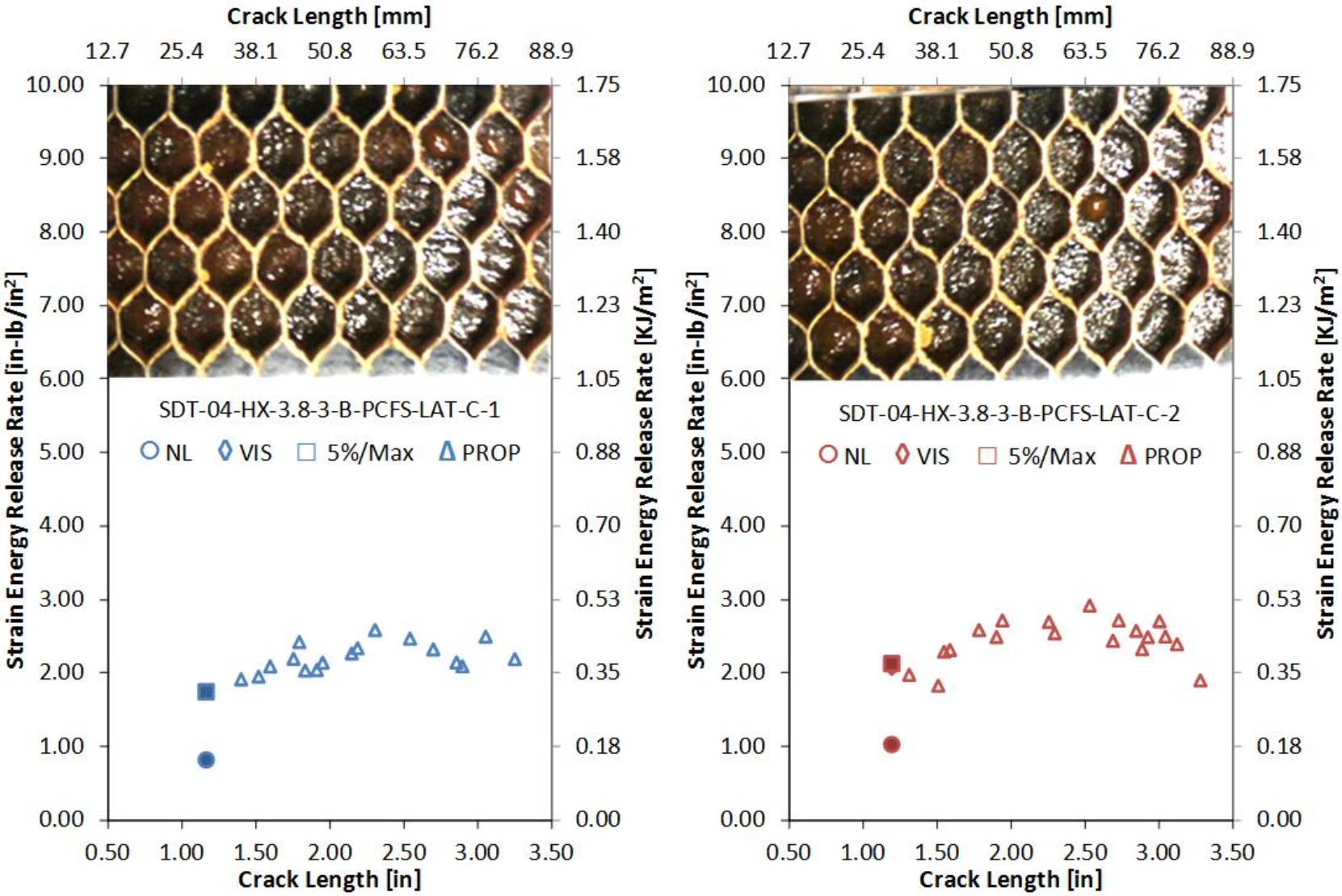

Figure A-149. Failure mode image and resistance curve of SDT-04-HX-3.8-3-B-PCFS-LAT-C-X #1 and #2

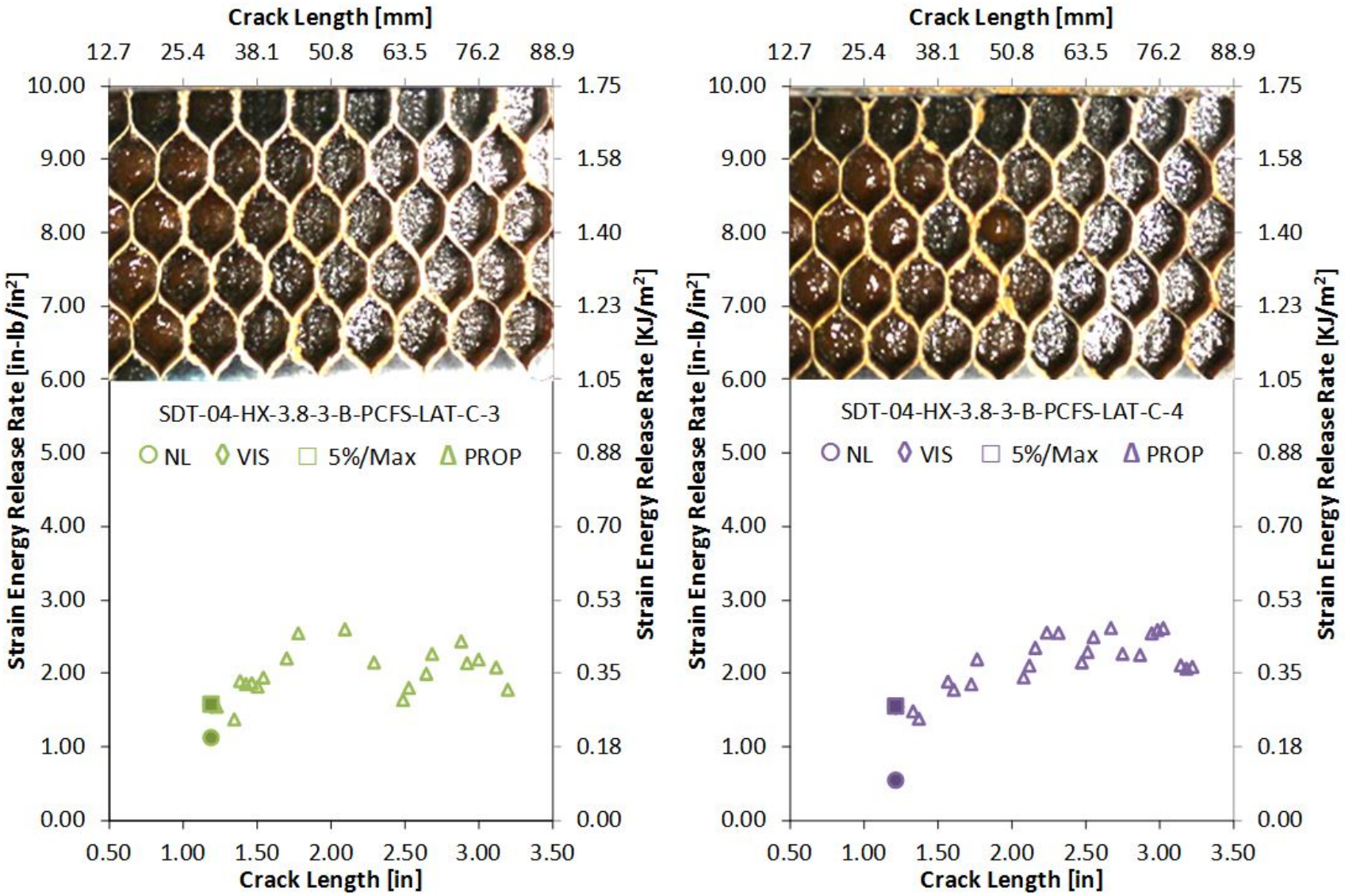

Figure A-150. Failure mode image and resistance curve of SDT-04-HX-3.8-3-B-PCFS-LAT-C-X #3 and #4

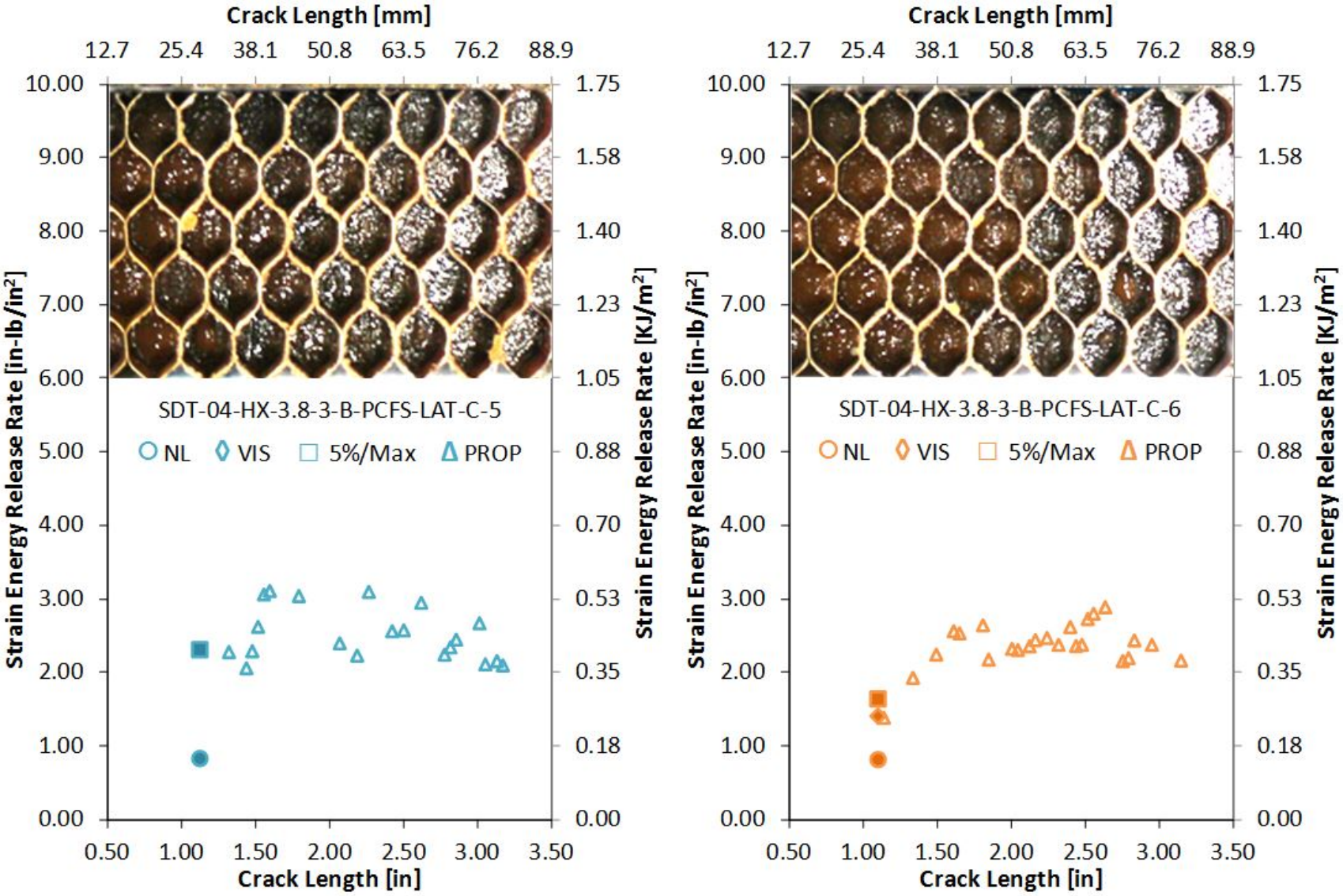

Figure A-151. Failure mode image and resistance curve of SDT-04-HX-3.8-3-B-PCFS-LAT-C-X #5 and #6

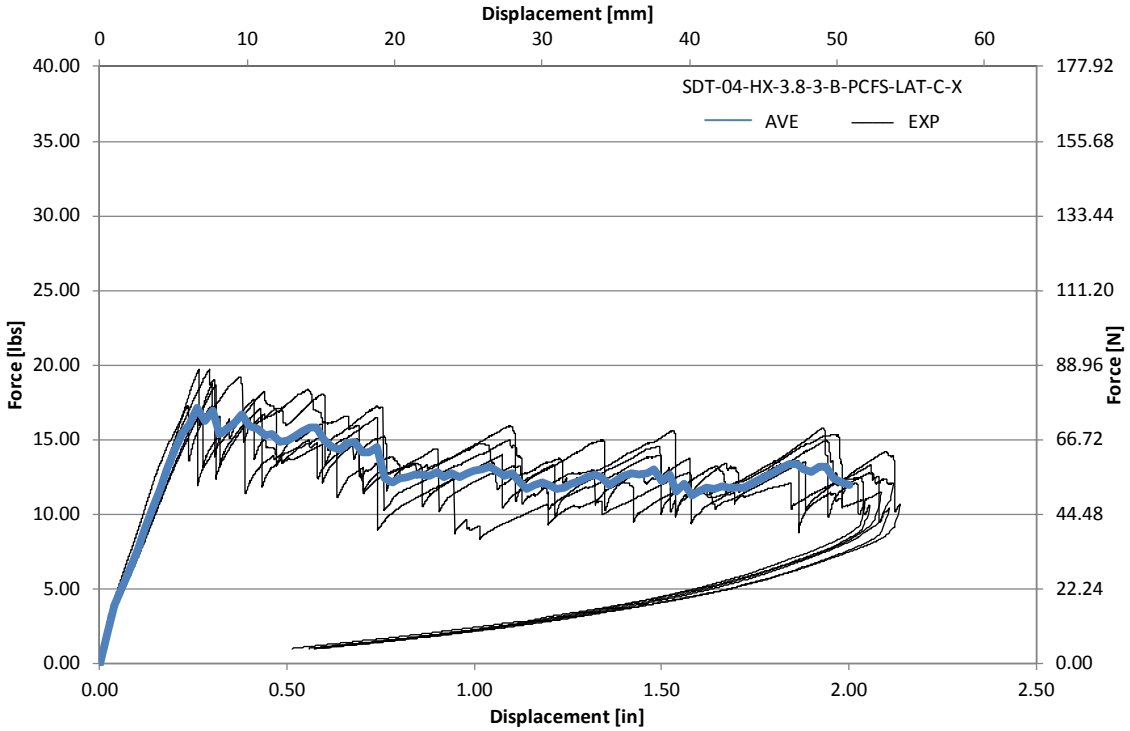

Figure A-152. Load vs. displacement curve for HRH-10–3/8–3.0 lateral ribbon direction with bottom disbond (center)

A.8.6 HRH-10–3/8–3.0 LATERAL RIBBON DIRECTION WITH BOTTOM DISBOND (EDGE) DATA

Table A-51. Test summary for HRH-10–3/8–3.0 lateral ribbon direction with bottom disbond (edge) pre-crack

Specimen	GIC (in-lb/in^2)			GIC (KJ/m^2)			Failure Mode
	NL	VIS	5%/max	NL	VIS	5%/max	
SDT-04-HX-3.8-3-B-PCFS-LAT-E-1	0.926	3.142	3.142	0.162	0.550	0.550	Primarily APO
SDT-04-HX-3.8-3-B-PCFS-LAT-E-2	1.091	N/A	2.910	0.191	N/A	0.510	Primarily APO
SDT-04-HX-3.8-3-B-PCFS-LAT-E-3	1.259	2.114	2.136	0.220	0.370	0.374	Primarily APO
SDT-04-HX-3.8-3-B-PCFS-LAT-E-4	1.007	2.349	2.371	0.176	0.411	0.415	Primarily APO
SDT-04-HX-3.8-3-B-PCFS-LAT-E-5	1.198	2.451	2.451	0.210	0.429	0.429	Primarily APO
SDT-04-HX-3.8-3-B-PCFS-LAT-E-6	1.392	2.550	2.550	0.244	0.447	0.447	Primarily APO
SDT-04-HX-3.8-3-B-PCFS-LAT-E-7							
SDT-04-HX-3.8-3-B-PCFS-LAT-E-8							
AVERAGE GIC	1.145	2.521	2.593	0.201	0.442	0.454	
STANDARD DEVIATION	0.171	0.383	0.369	0.030	0.067	0.065	
COEFFICIENT OF VARIATION (%)	14.945	15.182	14.241	14.945	15.182	14.241	

Table A-52. Test summary for HRH-10–3/8–3.0 lateral ribbon direction with bottom disbond (edge)

Specimen	GIC (in-lb/in^2)				GIC (KJ/m^2)				Failure Mode
	NL	VIS	5%/max	AREA	NL	VIS	5%/max	AREA	
SDT-04-HX-3.8-3-B-PCFS-LAT-E-1	0.496	N/A	1.673	1.966	0.087	N/A	0.293	0.344	Primarily APO
SDT-04-HX-3.8-3-B-PCFS-LAT-E-2	0.388	1.915	1.917	2.713	0.068	0.335	0.336	0.475	Primarily APO, with one cell partially in A
SDT-04-HX-3.8-3-B-PCFS-LAT-E-3	1.581	2.458	2.480	2.041	0.277	0.430	0.434	0.357	Primarily APO, with one cell partially in A
SDT-04-HX-3.8-3-B-PCFS-LAT-E-4	1.068	2.318	2.329	N/A	0.187	0.406	0.408	N/A	Primarily APO
SDT-04-HX-3.8-3-B-PCFS-LAT-E-5	0.444	N/A	1.456	N/A	0.078	N/A	0.255	N/A	Primarily APO
SDT-04-HX-3.8-3-B-PCFS-LAT-E-6	0.761	1.332	1.378	2.470	0.133	0.233	0.241	0.433	Primarily APO
SDT-04-HX-3.8-3-B-PCFS-LAT-E-7									
SDT-04-HX-3.8-3-B-PCFS-LAT-E-8									
AVERAGE GIC	0.790	2.006	1.872	2.298	0.138	0.351	0.328	0.402	
STANDARD DEVIATION	0.463	0.504	0.455	0.355	0.081	0.088	0.080	0.062	
COEFFICIENT OF VARIATION (%)	58.613	25.152	24.330	15.454	58.613	25.152	24.330	15.454	

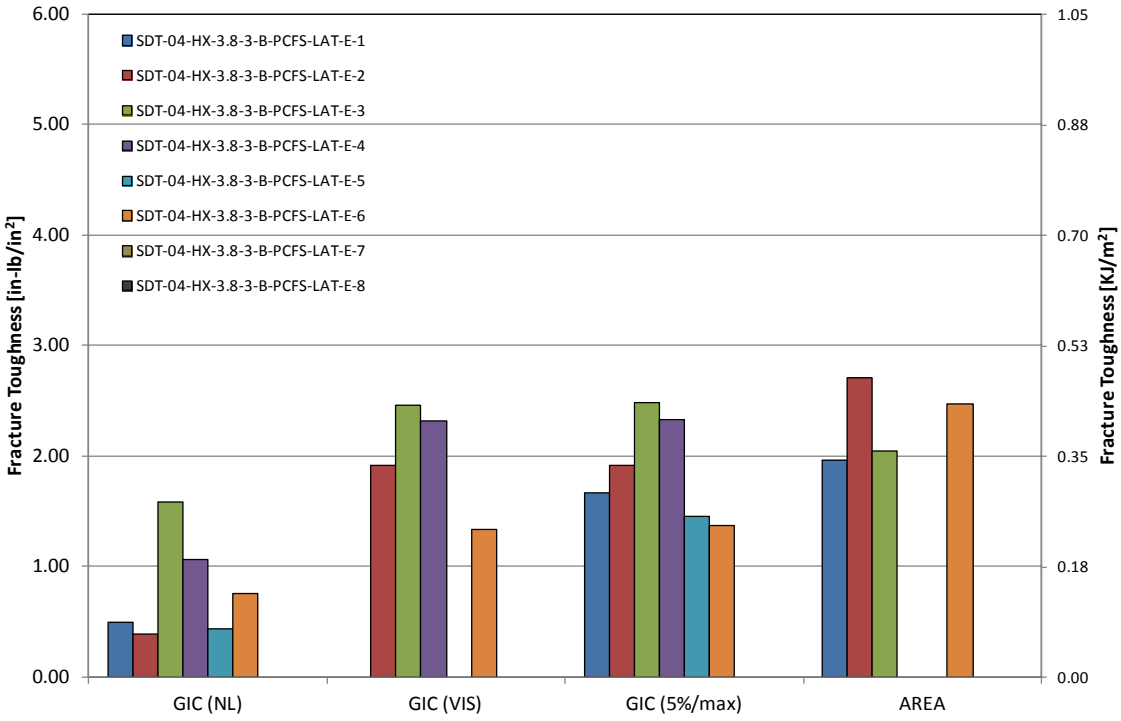

Figure A-153. GIC for HRH-10–3/8–3.0 lateral ribbon direction with bottom disbond (edge)

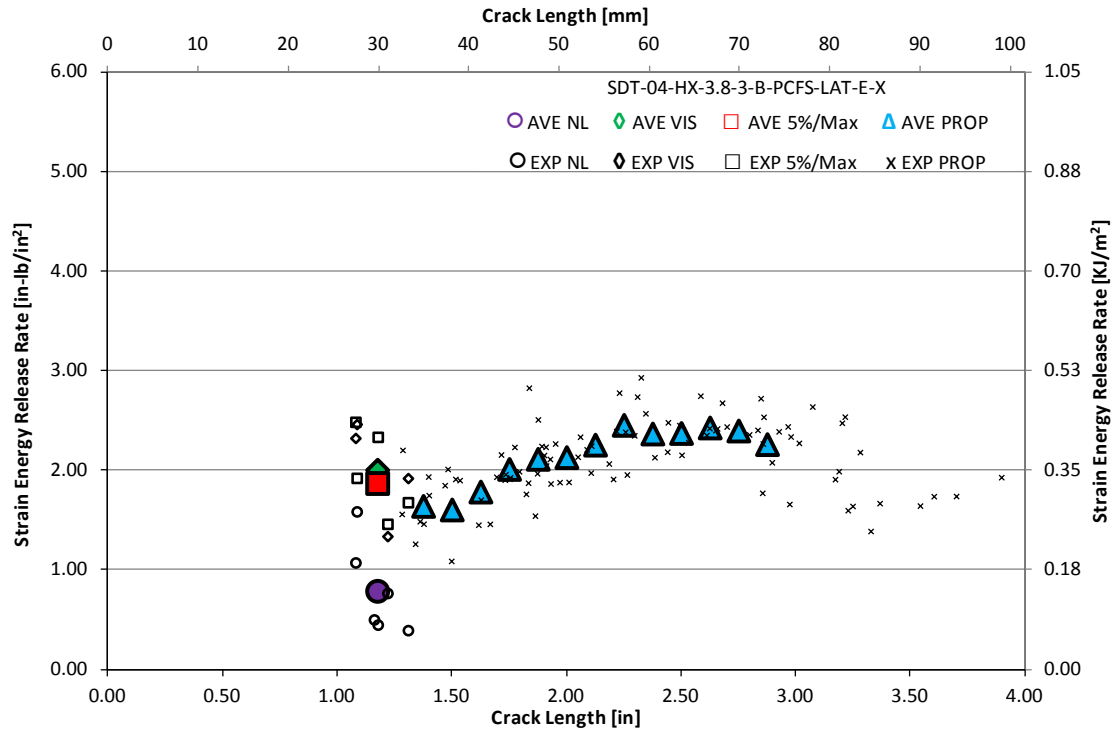

Figure A-154. Resistance curve for HRH-10–3/8–3.0 lateral ribbon direction with bottom disbond (edge)

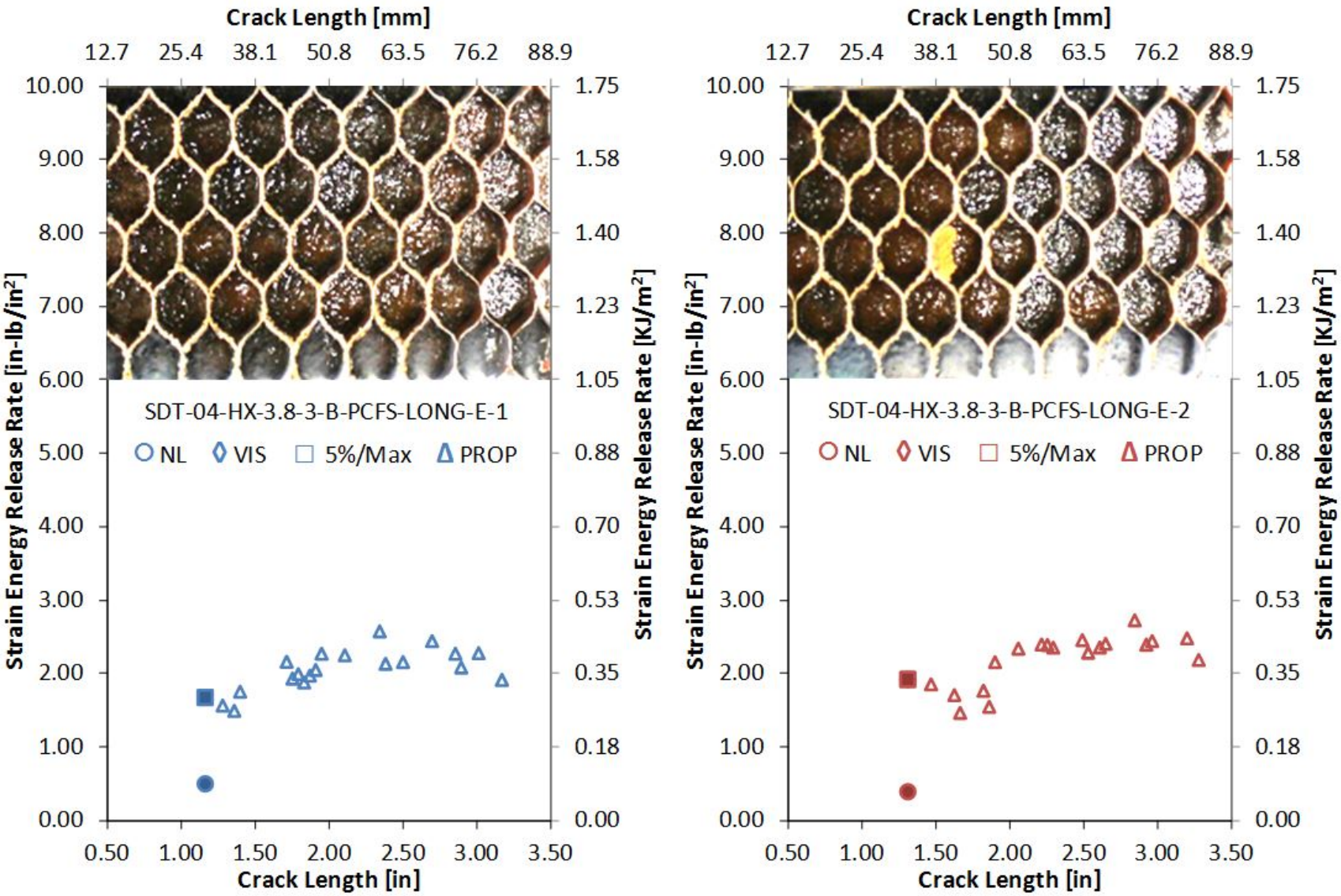

Figure A-155. Failure mode image and resistance curve of SDT-04-HX-3.8-3-B-PCFS-LAT-E-X #1 and #2

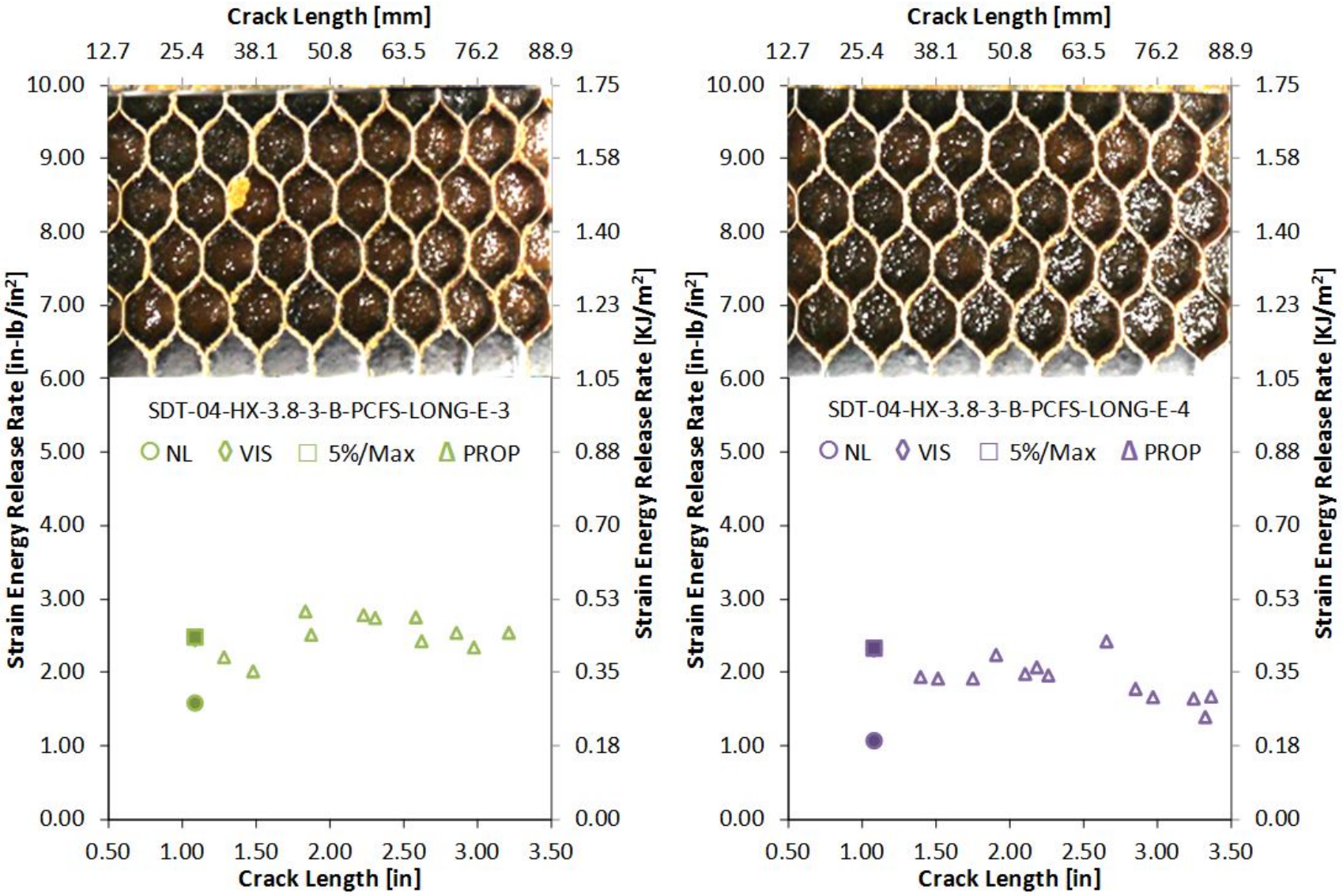

Figure A-156. Failure mode image and resistance curve of SDT-04-HX-3.8-3-B-PCFS-LAT-E-X #3 and #4

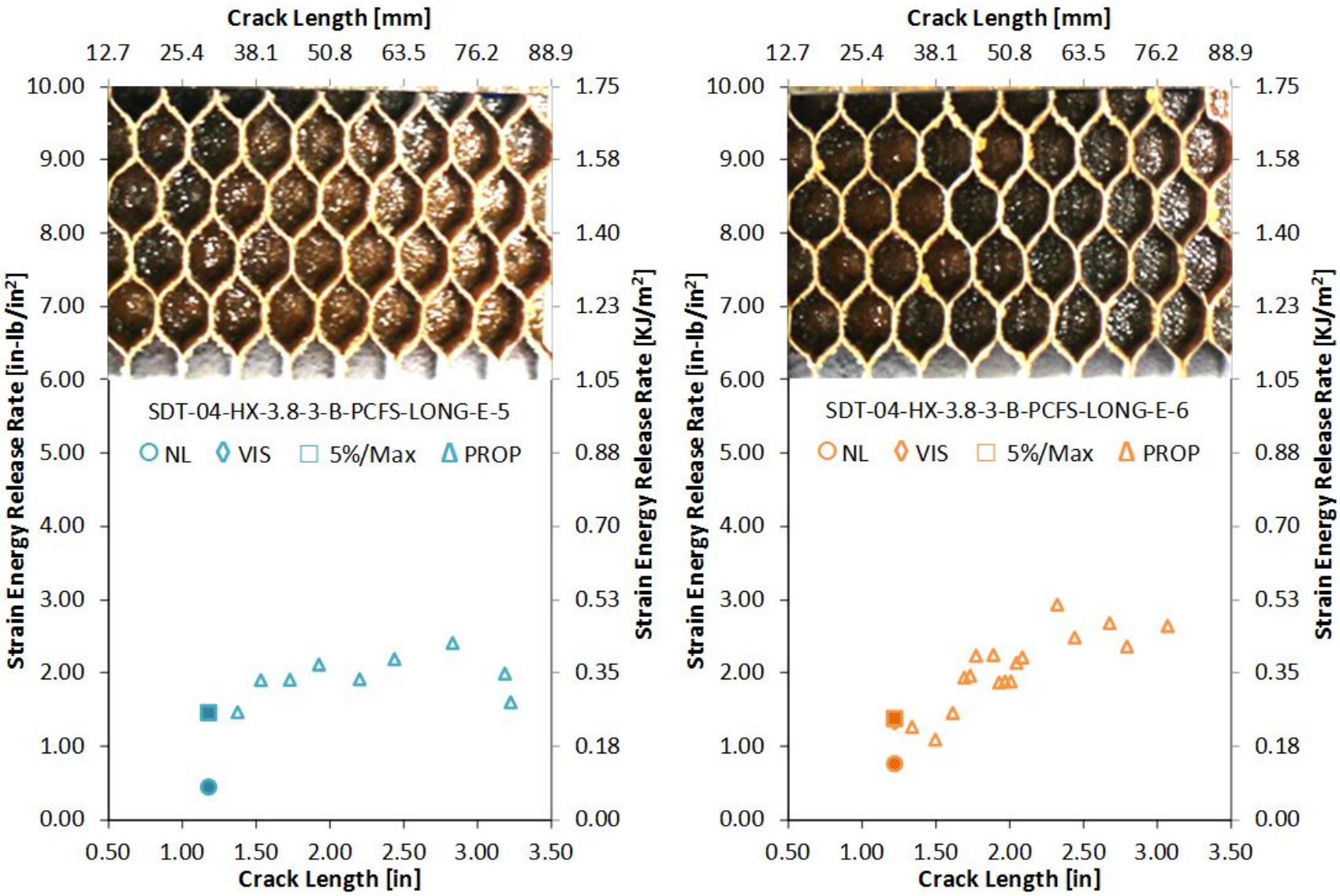

Figure A-157. Failure mode image and resistance curve of SDT-04-HX-3.8-3-B-PCFS-LAT-E-X #5 and #6

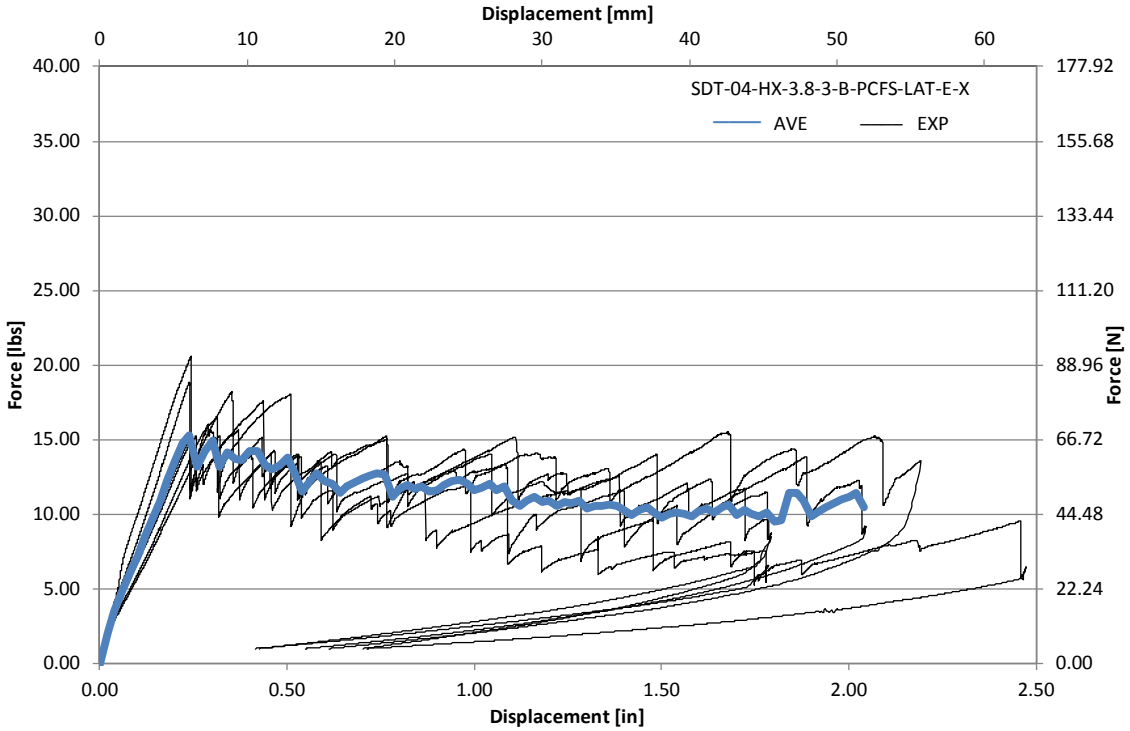

Figure A-158. Load vs. displacement curve for HRH-10–3/8–3.0 lateral ribbon direction with bottom disbond (edge)

APPENDIX B—STATIC RESULTS FOR THIN CO-CURED FACESHEET (4-PLY) AND HRH-10 HEXAGONAL CORES TESTED AS SINGLE-CANTILEVER BEAMS

B.1 HRH-10–1/8–3.0 DATA

B.1.1 HRH-10–1/8–3.0 LONGITUDINAL RIBBON DIRECTION WITH TOP DISBOND (CENTER) DATA

Table B-1. Test summary for HRH-10–1/8–3.0 longitudinal ribbon direction with top disbond (center) pre-crack

Specimen	GIC (in-lb/in^2)			GIC (KJ/m^2)			Failure Mode
	NL	VIS	5%/max	NL	VIS	5%/max	
SDT-04-HX-1.8-3-T-CCFS-LONG-C-1	1.272	N/A	1.996	0.223	N/A	0.350	Half a cell in A, then C
SDT-04-HX-1.8-3-T-CCFS-LONG-C-2	1.446	N/A	2.092	0.253	N/A	0.366	Half a cell in A, then C
SDT-04-HX-1.8-3-T-CCFS-LONG-C-3	1.035	N/A	3.706	0.181	N/A	0.649	Half a cell in A, then C
SDT-04-HX-1.8-3-T-CCFS-LONG-C-4							
SDT-04-HX-1.8-3-T-CCFS-LONG-C-5	1.293	N/A	1.861	0.227	N/A	0.326	Primarily C, with a couple of cells half A
SDT-04-HX-1.8-3-T-CCFS-LONG-C-6	1.459	N/A	2.965	0.256	N/A	0.519	Primarily C
SDT-04-HX-1.8-3-T-CCFS-LONG-C-7	2.017	3.341	3.341	0.353	0.585	0.585	Primarily C, with a couple of cells half A
SDT-04-HX-1.8-3-T-CCFS-LONG-C-8							
AVERAGE GIC	1.421	3.341	2.660	0.249	0.585	0.466	
STANDARD DEVIATION	0.330	N/A	0.781	0.058	N/A	0.137	
COEFFICIENT OF VARIATION (%)	23.230	N/A	29.371	23.230	N/A	29.371	

Table B-2. Test summary for HRH-10–1/8–3.0 longitudinal ribbon direction with top disbond (center)

Specimen	GIC (in-lb/in^2)				GIC (KJ/m^2)				Failure Mode
	NL	VIS	5%/max	AREA	NL	VIS	5%/max	AREA	
SDT-04-HX-1.8-3-T-CCFS-LONG-C-1	0.988	2.927	3.060	3.320	0.173	0.513	0.536	0.581	Primarily in C
SDT-04-HX-1.8-3-T-CCFS-LONG-C-2	0.638	N/A	2.560	3.874	0.112	N/A	0.448	0.678	Primarily in C
SDT-04-HX-1.8-3-T-CCFS-LONG-C-3	0.458	3.481	3.485	3.852	0.080	0.610	0.610	0.675	Primarily in C
SDT-04-HX-1.8-3-T-CCFS-LONG-C-4									
SDT-04-HX-1.8-3-T-CCFS-LONG-C-5	0.641	N/A	3.128	3.239	0.112	N/A	0.548	0.567	Primarily in C
SDT-04-HX-1.8-3-T-CCFS-LONG-C-6	0.702	2.661	2.866	3.353	0.123	0.466	0.502	0.587	Primarily in C
SDT-04-HX-1.8-3-T-CCFS-LONG-C-7	0.811	2.498	2.633	3.579	0.142	0.437	0.461	0.627	Primarily in C
SDT-04-HX-1.8-3-T-CCFS-LONG-C-8									
AVERAGE GIC	0.706	2.892	2.955	3.536	0.124	0.506	0.518	0.619	
STANDARD DEVIATION	0.179	0.431	0.343	0.277	0.031	0.075	0.060	0.049	
COEFFICIENT OF VARIATION (%)	25.404	14.894	11.616	7.837	25.404	14.894	11.616	7.837	

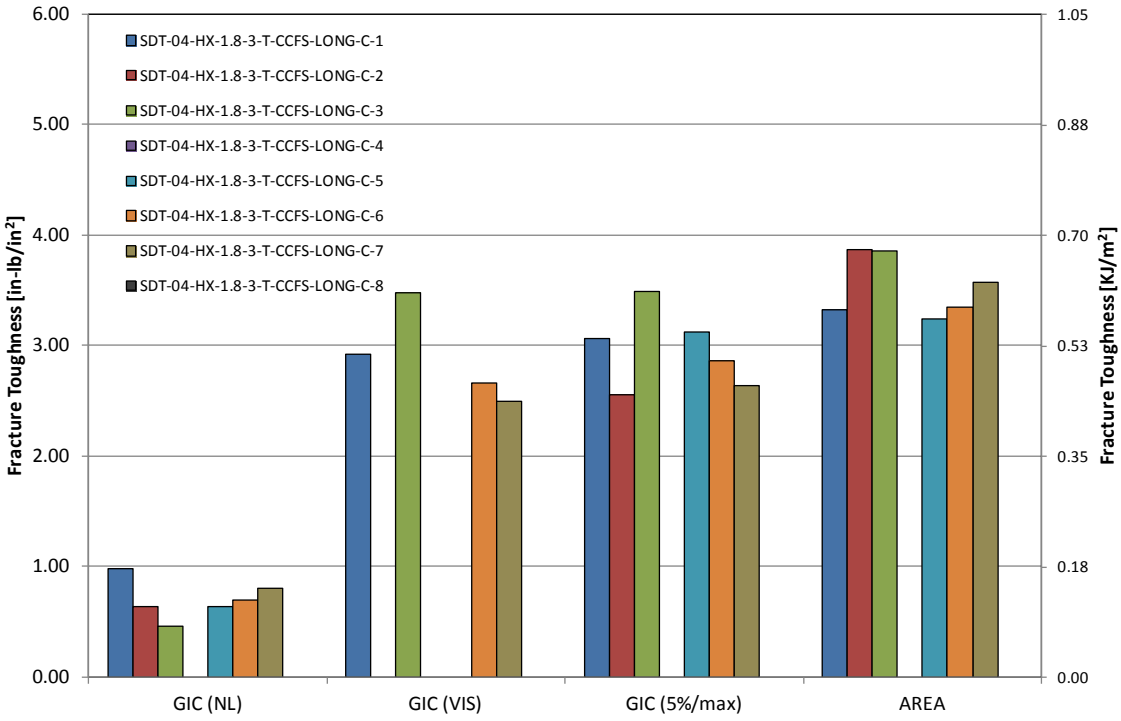

Figure B-1. GIC for HRH-10–1/8–3.0 longitudinal ribbon direction with top disbond (center)

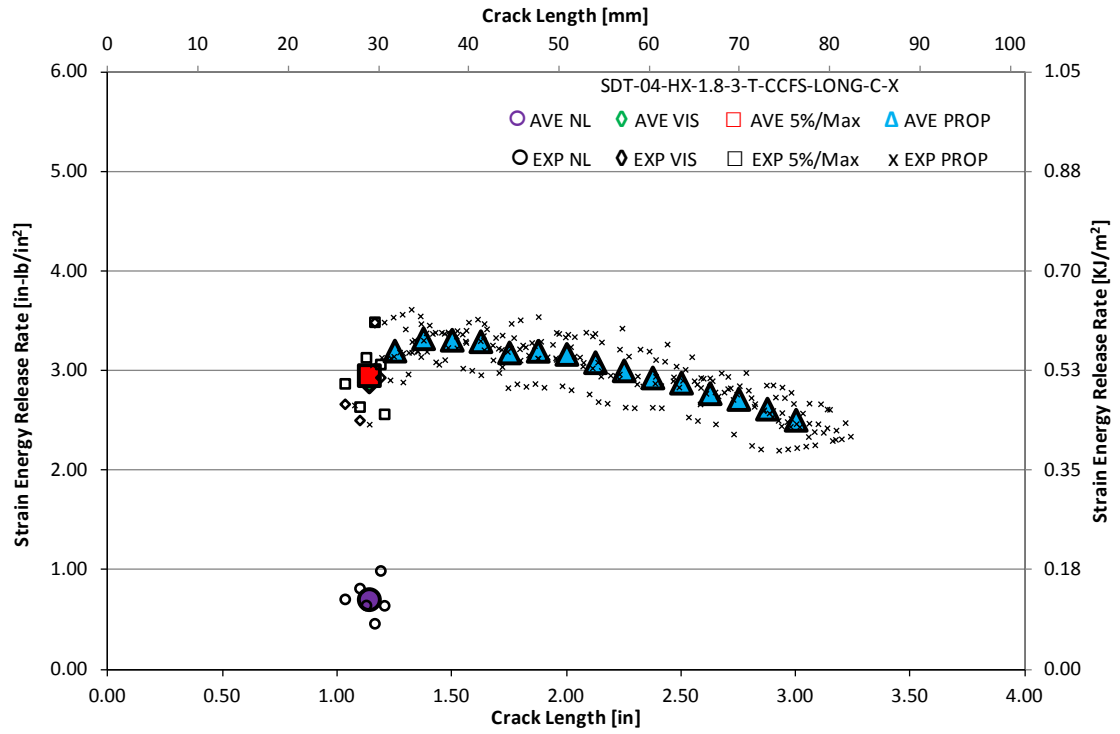

Figure B-2. Resistance curve for HRH-10–1/8–3.0 longitudinal ribbon direction with top disbond (center)

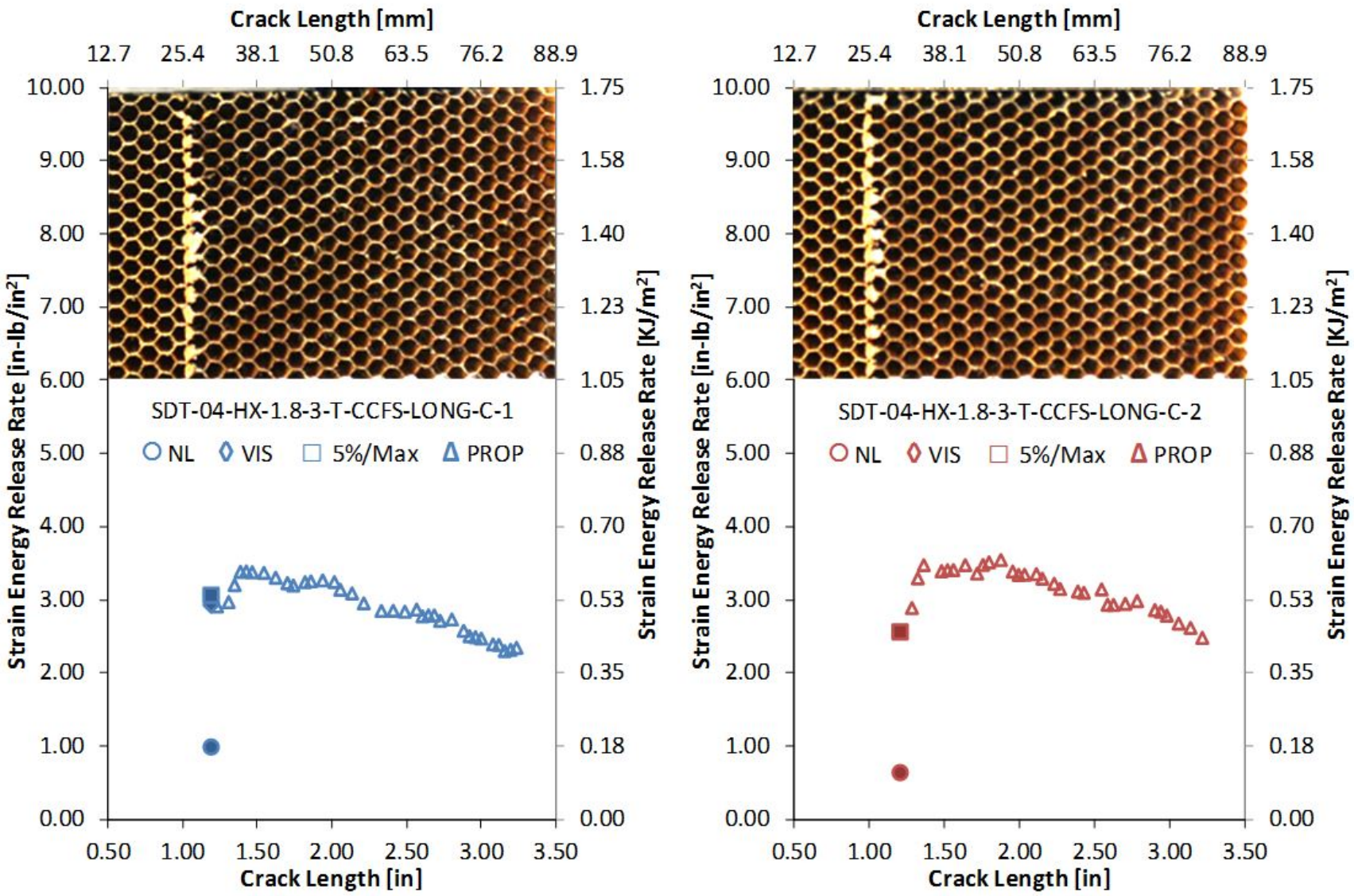

Figure B-3. Failure mode image and resistance curve of SDT-04-HX-1.8-3-T-CCFS-LONG-C-X #1 and #2

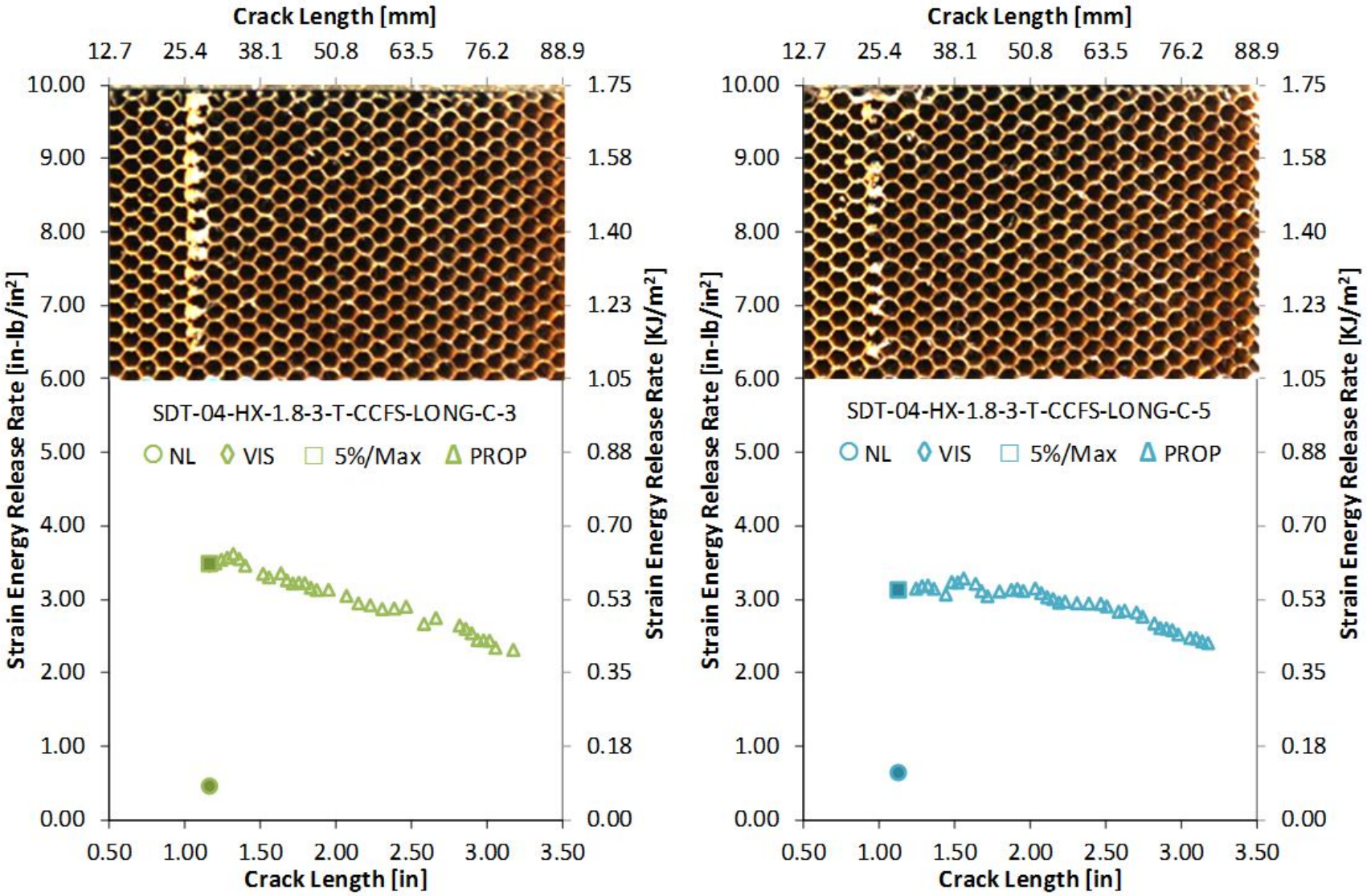

Figure B-4. Failure mode image and resistance curve of SDT-04-HX-1.8-3-T-CCFS-LONG-C-X #3 and #5

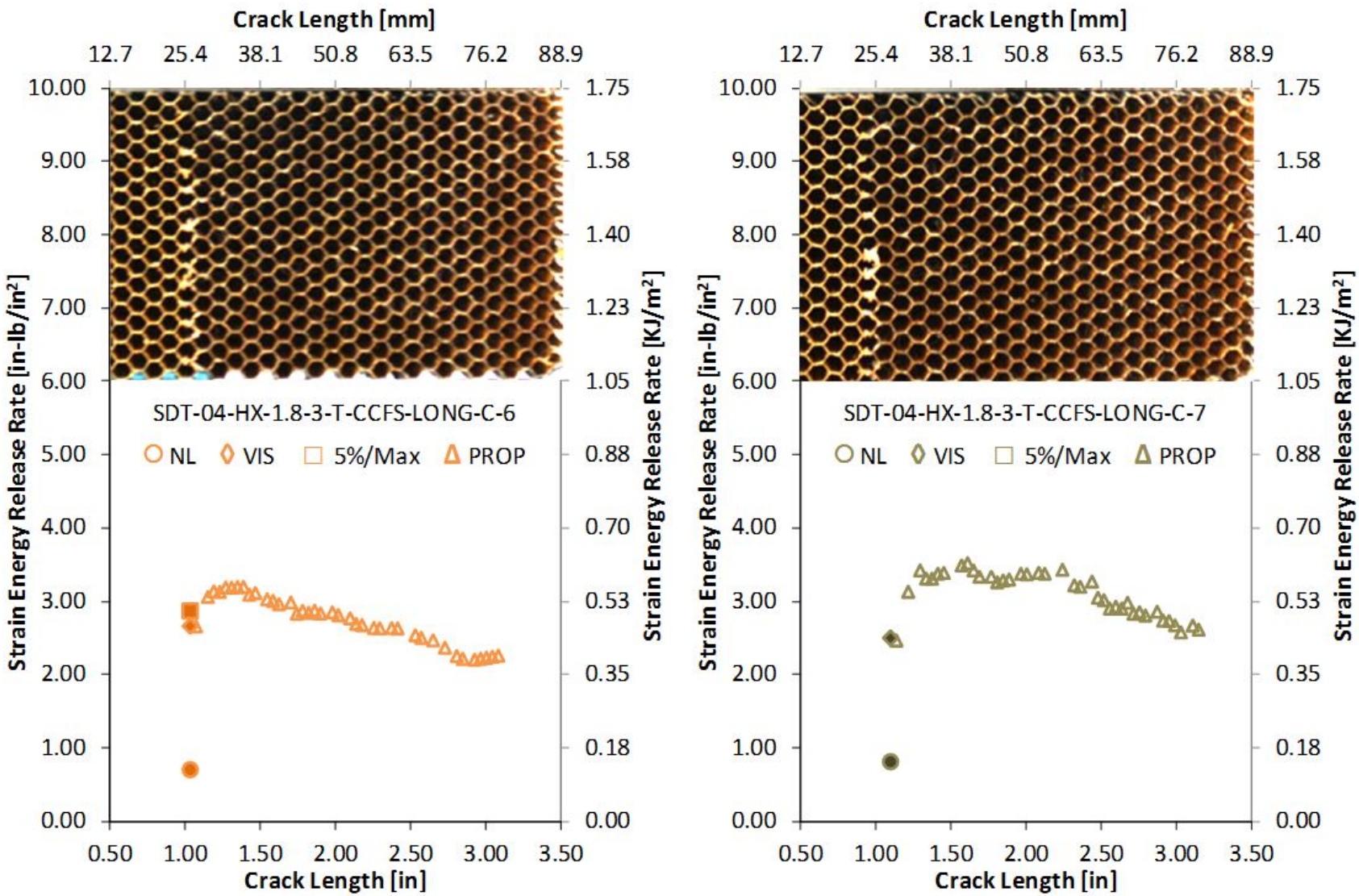

Figure B-5. Failure mode image and resistance curve of SDT-04-HX-1.8-3-T-CCFS-LONG-C-X #6 and #7

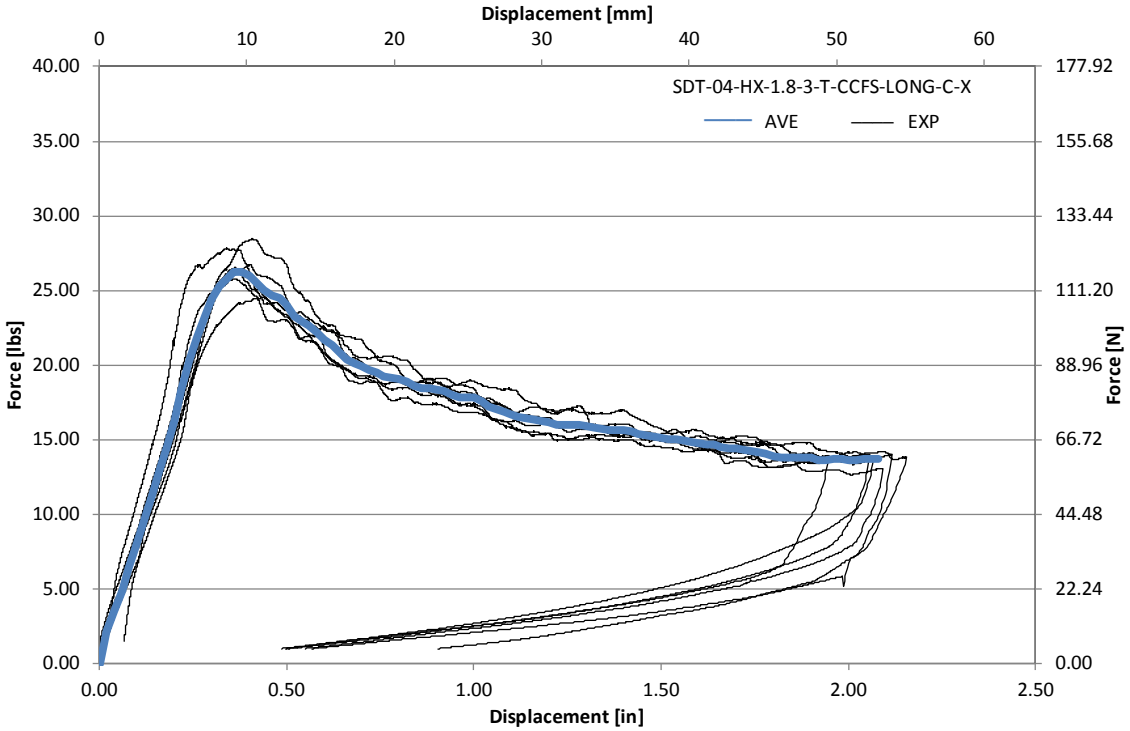

Figure B-6. Load vs. displacement curve for HRH-10–1/8–3.0 longitudinal ribbon direction with top disbond (center)

B.1.2 HRH-10–1/8–3.0 LONGITUDINAL RIBBON DIRECTION WITH BOTTOM DISBOND (CENTER) DATA

Table B-3. Test summary for HRH-10–1/8–3.0 longitudinal ribbon direction with bottom disbond (center) pre-crack

Specimen	GIC (in-lb/in^2)			GIC (KJ/m^2)			Failure Mode
	NL	VIS	5%/max	NL	VIS	5%/max	
SDT-04-HX-1.8-3-B-CCFS-LONG-C-1	1.564	N/A	2.492	0.274	N/A	0.436	Half a cell in A, then C
SDT-04-HX-1.8-3-B-CCFS-LONG-C-2	1.228	N/A	2.402	0.215	N/A	0.421	Half a cell in A, then C
SDT-04-HX-1.8-3-B-CCFS-LONG-C-3	2.014	N/A	2.223	0.353	N/A	0.389	Half a cell in A, then C
SDT-04-HX-1.8-3-B-CCFS-LONG-C-4	1.748	N/A	3.327	0.306	N/A	0.583	Half a cell in A, then C
SDT-04-HX-1.8-3-B-CCFS-LONG-C-5	1.154	N/A	2.457	0.202	N/A	0.430	Half a cell in A, then C
SDT-04-HX-1.8-3-B-CCFS-LONG-C-6	2.369	N/A	3.314	0.415	N/A	0.580	Half a cell in A, then C
SDT-04-HX-1.8-3-B-CCFS-LONG-C-7							
SDT-04-HX-1.8-3-B-CCFS-LONG-C-8							
AVERAGE GIC	1.680	N/A	2.703	0.294	N/A	0.473	
STANDARD DEVIATION	0.466	N/A	0.488	0.082	N/A	0.085	
COEFFICIENT OF VARIATION (%)	27.729	N/A	18.039	27.729	N/A	18.039	

Table B-4. Test summary for HRH-10–1/8–3.0 longitudinal ribbon direction with bottom disbond (center)

Specimen	GIC (in-lb/in^2)				GIC (KJ/m^2)				Failure Mode
	NL	VIS	5%/max	AREA	NL	VIS	5%/max	AREA	
SDT-04-HX-1.8-3-B-CCFS-LONG-C-1	1.193	N/A	3.288	4.192	0.209	N/A	0.576	0.734	Primarily in C
SDT-04-HX-1.8-3-B-CCFS-LONG-C-2	0.664	3.357	3.681	4.125	0.116	0.588	0.645	0.722	Primarily in C
SDT-04-HX-1.8-3-B-CCFS-LONG-C-3	0.639	3.377	3.678	3.943	0.112	0.591	0.644	0.691	Primarily in C
SDT-04-HX-1.8-3-B-CCFS-LONG-C-4	0.682	2.890	3.194	3.930	0.119	0.506	0.559	0.688	Primarily in C
SDT-04-HX-1.8-3-B-CCFS-LONG-C-5	0.796	3.136	3.444	3.974	0.139	0.549	0.603	0.696	Primarily in C
SDT-04-HX-1.8-3-B-CCFS-LONG-C-6	0.772	3.001	3.152	3.952	0.135	0.526	0.552	0.692	Primarily in C
SDT-04-HX-1.8-3-B-CCFS-LONG-C-7									
SDT-04-HX-1.8-3-B-CCFS-LONG-C-8									
AVERAGE GIC	0.791	3.152	3.406	4.019	0.139	0.552	0.597	0.704	
STANDARD DEVIATION	0.206	0.215	0.234	0.111	0.036	0.038	0.041	0.019	
COEFFICIENT OF VARIATION (%)	26.083	6.812	6.878	2.755	26.083	6.812	6.878	2.755	

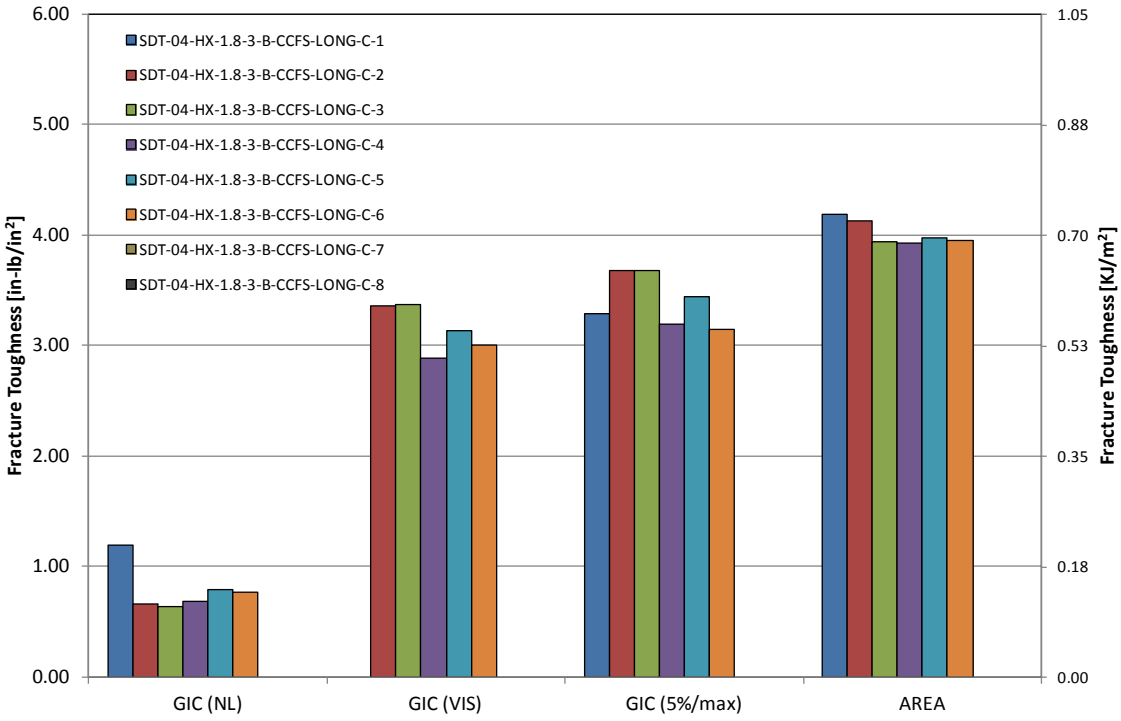

Figure B-7. GIC for HRH-10–1/8–3.0 longitudinal ribbon direction with bottom disbond (center)

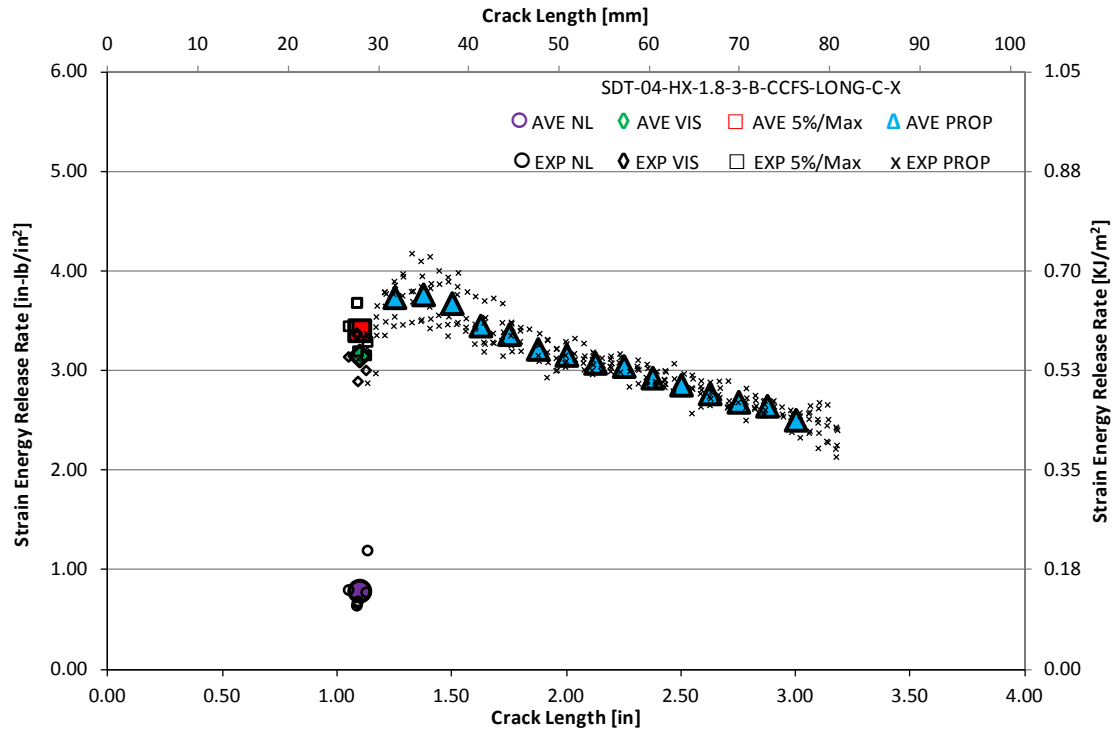

Figure B-8. Resistance curve for HRH-10–1/8–3.0 longitudinal ribbon direction with bottom disbond (center)

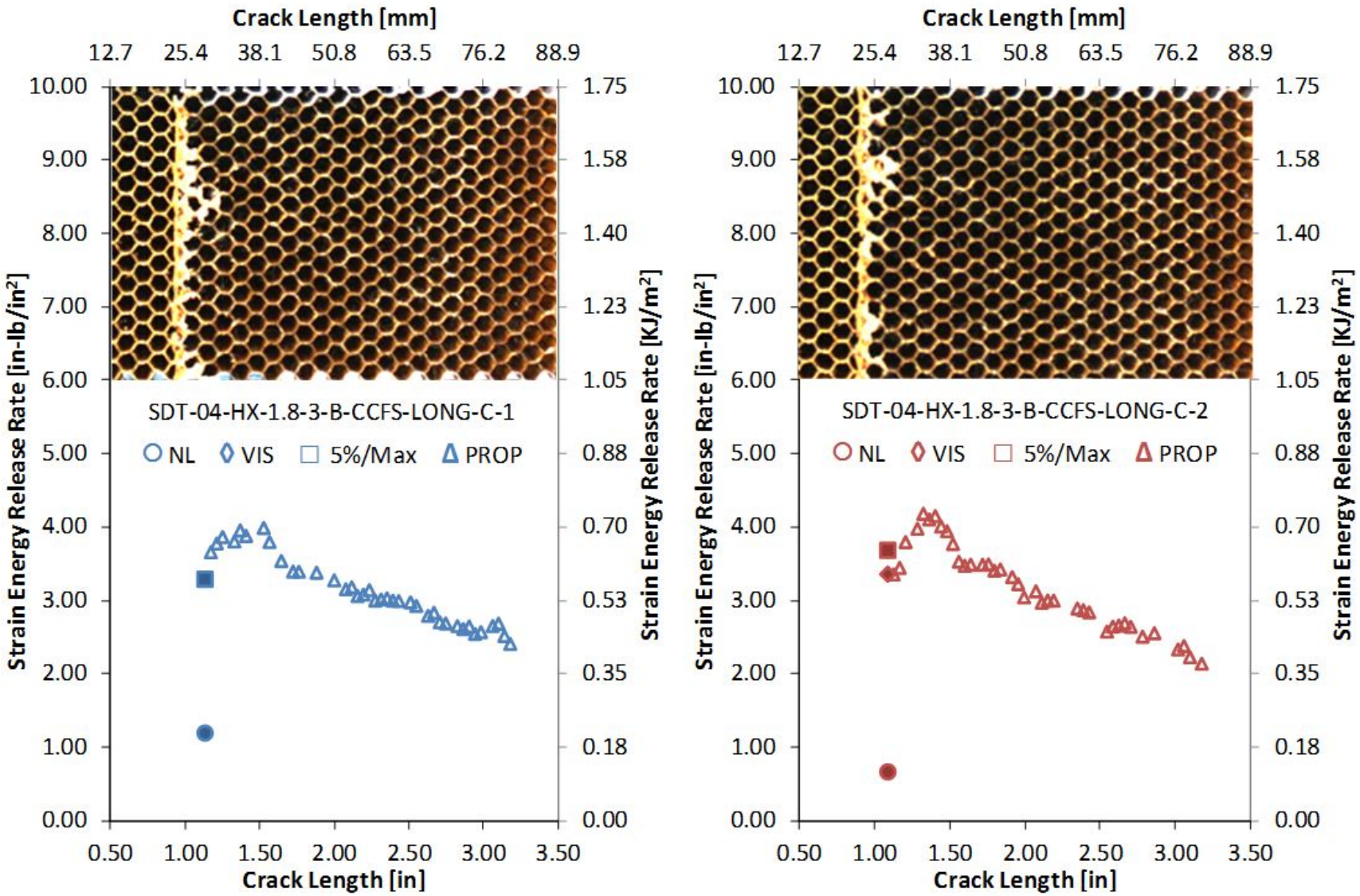

Figure B-9. Failure mode image and resistance curve of SDT-04-HX-1.8-3-B-CCFS-LONG-C-X #1 and #2

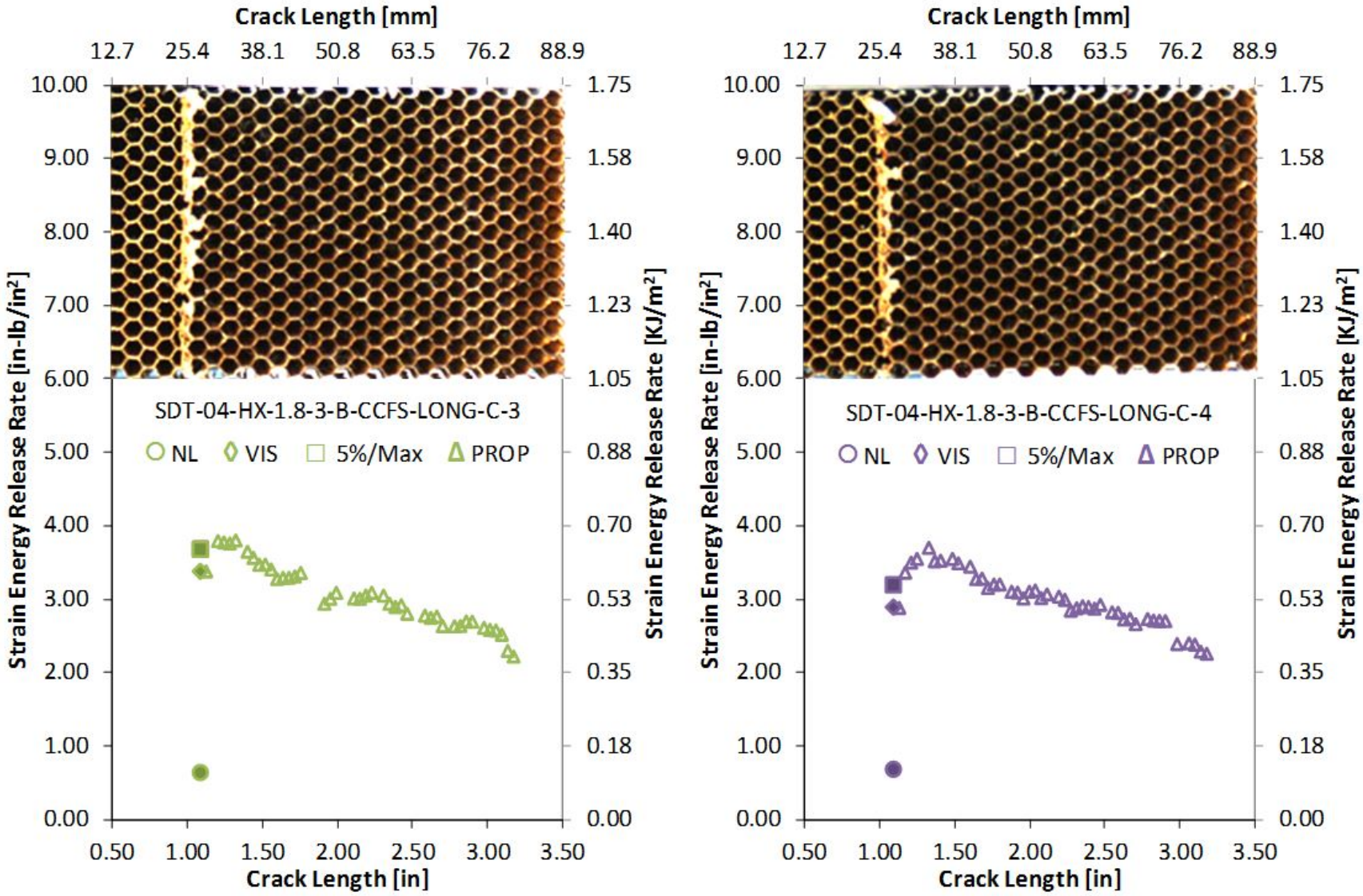

Figure B-10. Failure mode image and resistance curve of SDT-04-HX-1.8-3-B-CCFS-LONG-C-X #3 and #4

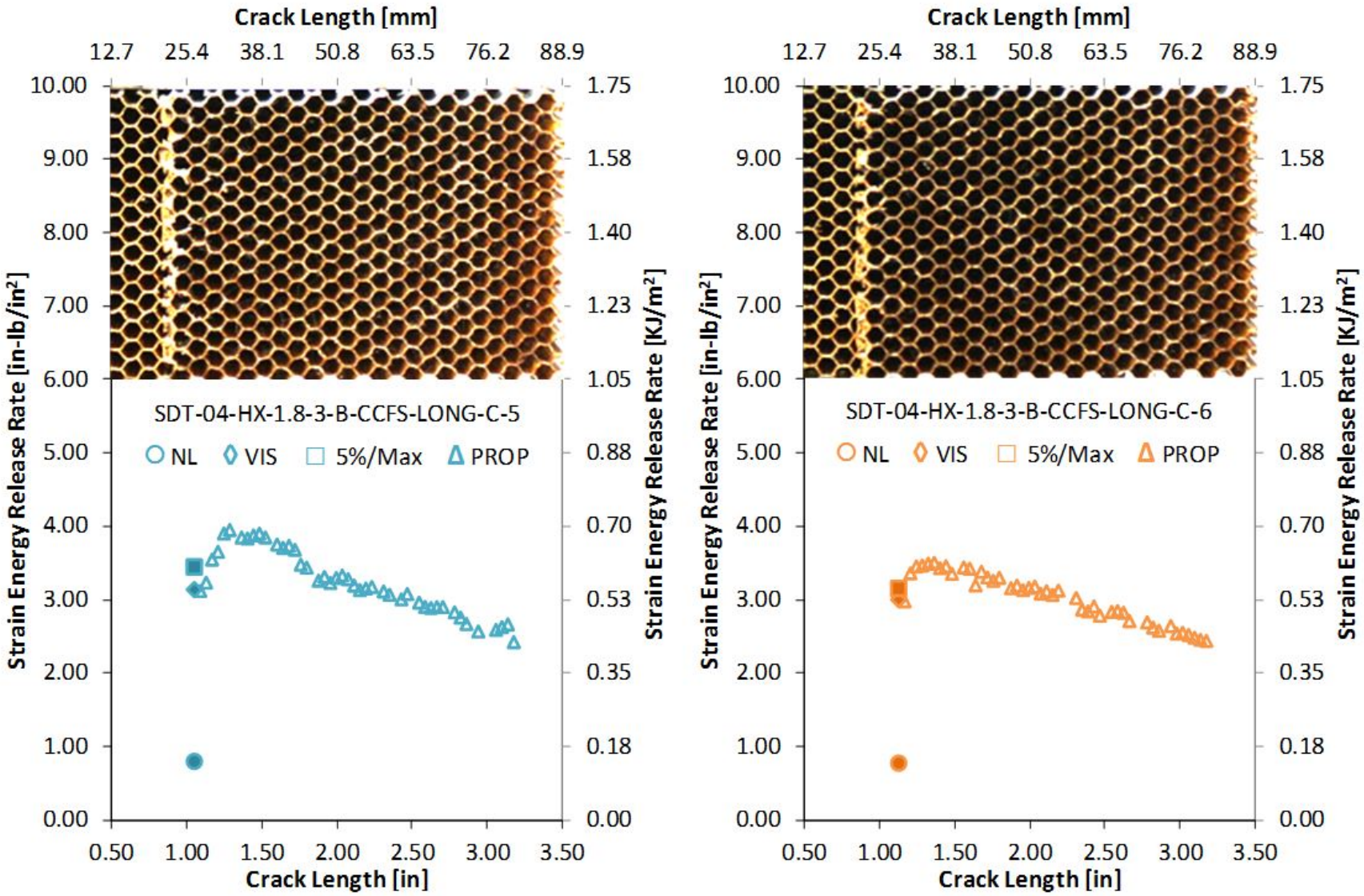

Figure B-11. Failure mode image and resistance curve of SDT-04-HX-1.8-3-B-CCFS-LONG-C-X #5 and #6

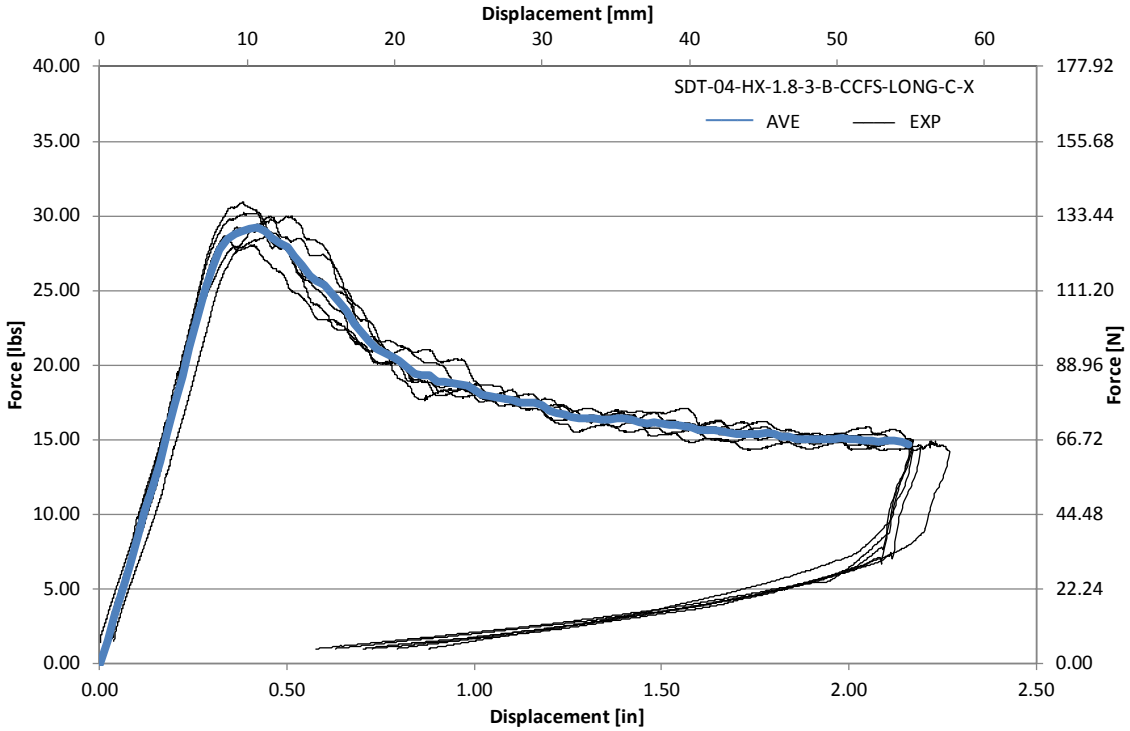

Figure B-12. Load vs. displacement curve for HRH-10–1/8–3.0 longitudinal ribbon direction with bottom disbond (center)

B.2 HRH-10–3/8–3.0 DATA

B.2.1 HRH-10–3/8–3.0 LONGITUDINAL RIBBON DIRECTION WITH TOP DISBOND (CENTER) DATA

Table B-5. Test summary for HRH-10–3/8–3.0 longitudinal ribbon direction with top disbond (center) pre-crack

Specimen	GIC (in-lb/in^2)			GIC (KJ/m^2)			Failure Mode
	NL	VIS	5%/max	NL	VIS	5%/max	
SDT-04-HX-3.8-3-T-CCFS-LONG-C-1	1.324	N/A	2.119	0.232	N/A	0.371	Primarily APO
SDT-04-HX-3.8-3-T-CCFS-LONG-C-2	1.164	N/A	1.685	0.204	N/A	0.295	Primarily APO
SDT-04-HX-3.8-3-T-CCFS-LONG-C-3	1.169	N/A	1.705	0.205	N/A	0.299	Primarily APO
SDT-04-HX-3.8-3-T-CCFS-LONG-C-4	1.000	N/A	1.737	0.175	N/A	0.304	Primarily APO
SDT-04-HX-3.8-3-T-CCFS-LONG-C-5	1.389	N/A	2.194	0.243	N/A	0.384	Primarily APO
SDT-04-HX-3.8-3-T-CCFS-LONG-C-6	1.467	N/A	2.301	0.257	N/A	0.403	Primarily APO
SDT-04-HX-3.8-3-T-CCFS-LONG-C-7	1.381	N/A	2.079	0.242	N/A	0.364	Primarily APO
SDT-04-HX-3.8-3-T-CCFS-LONG-C-8	1.954	N/A	2.234	0.342	N/A	0.391	Primarily APO
AVERAGE GIC	1.356	N/A	2.007	0.238	N/A	0.351	
STANDARD DEVIATION	0.286	N/A	0.256	0.050	N/A	0.045	
COEFFICIENT OF VARIATION (%)	21.063	N/A	12.756	21.063	N/A	12.756	

Table B-6. Test summary for HRH-10–3/8–3.0 longitudinal ribbon direction with top disbond (center)

Specimen	GIC (in-lb/in^2)				GIC (KJ/m^2)				Failure Mode
	NL	VIS	5%/max	AREA	NL	VIS	5%/max	AREA	
SDT-04-HX-3.8-3-T-CCFS-LONG-C-1	0.591	2.551	3.063	N/A	0.104	0.447	0.536	N/A	Primarily APO, then FSF
SDT-04-HX-3.8-3-T-CCFS-LONG-C-2	0.733	2.628	2.762	N/A	0.128	0.460	0.484	N/A	Primarily APO, then FSF
SDT-04-HX-3.8-3-T-CCFS-LONG-C-3	1.075	2.937	3.157	N/A	0.188	0.514	0.553	N/A	Primarily APO, then FSF
SDT-04-HX-3.8-3-T-CCFS-LONG-C-4	0.877	N/A	3.235	N/A	0.154	N/A	0.567	N/A	Primarily APO, then FSF
SDT-04-HX-3.8-3-T-CCFS-LONG-C-5	1.206	2.536	2.730	N/A	0.211	0.444	0.478	N/A	Primarily APO, then FSF
SDT-04-HX-3.8-3-T-CCFS-LONG-C-6	1.142	N/A	2.734	N/A	0.200	N/A	0.479	N/A	Primarily APO, then FSF
SDT-04-HX-3.8-3-T-CCFS-LONG-C-7	1.293	2.517	2.675	4.245	0.226	0.441	0.469	0.743	Primarily APO
SDT-04-HX-3.8-3-T-CCFS-LONG-C-8	1.301	N/A	2.363	3.801	0.228	N/A	0.414	0.666	Primarily APO
AVERAGE GIC	1.027	2.634	2.840	4.023	0.180	0.461	0.497	0.705	
STANDARD DEVIATION	0.265	0.175	0.291	0.314	0.046	0.031	0.051	0.055	
COEFFICIENT OF VARIATION (%)	25.820	6.631	10.233	7.806	25.820	6.631	10.233	7.806	

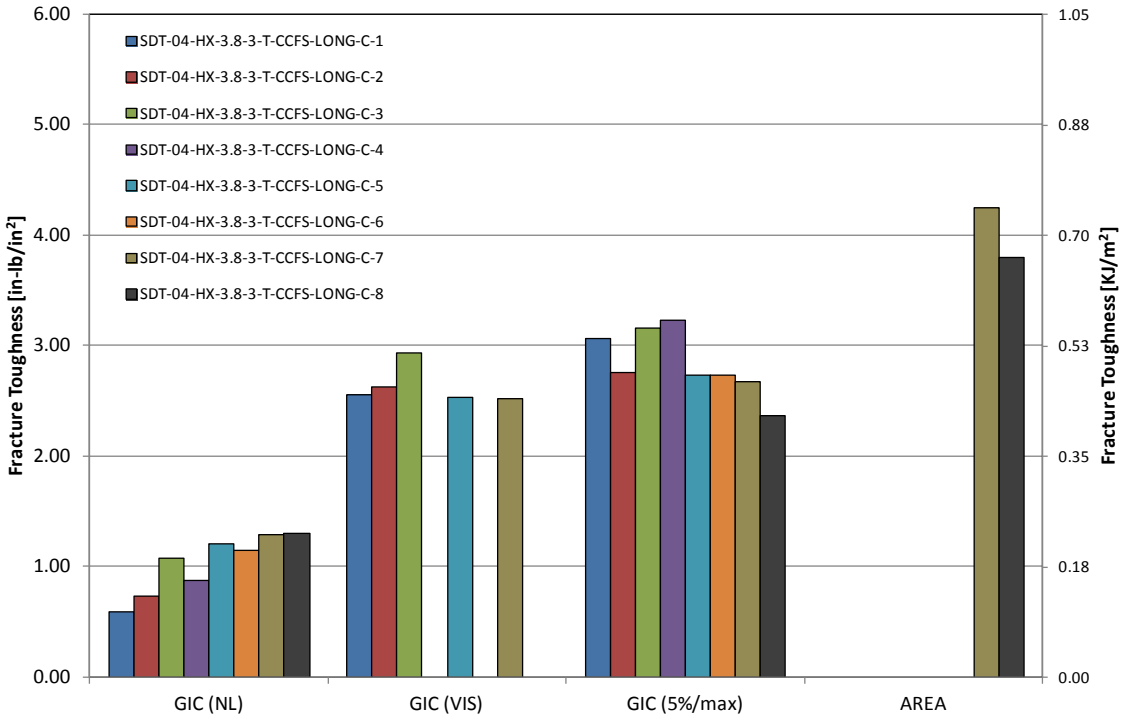

Figure B-13. GIC for HRH-10–3/8–3.0 longitudinal ribbon direction with top disbond (center)

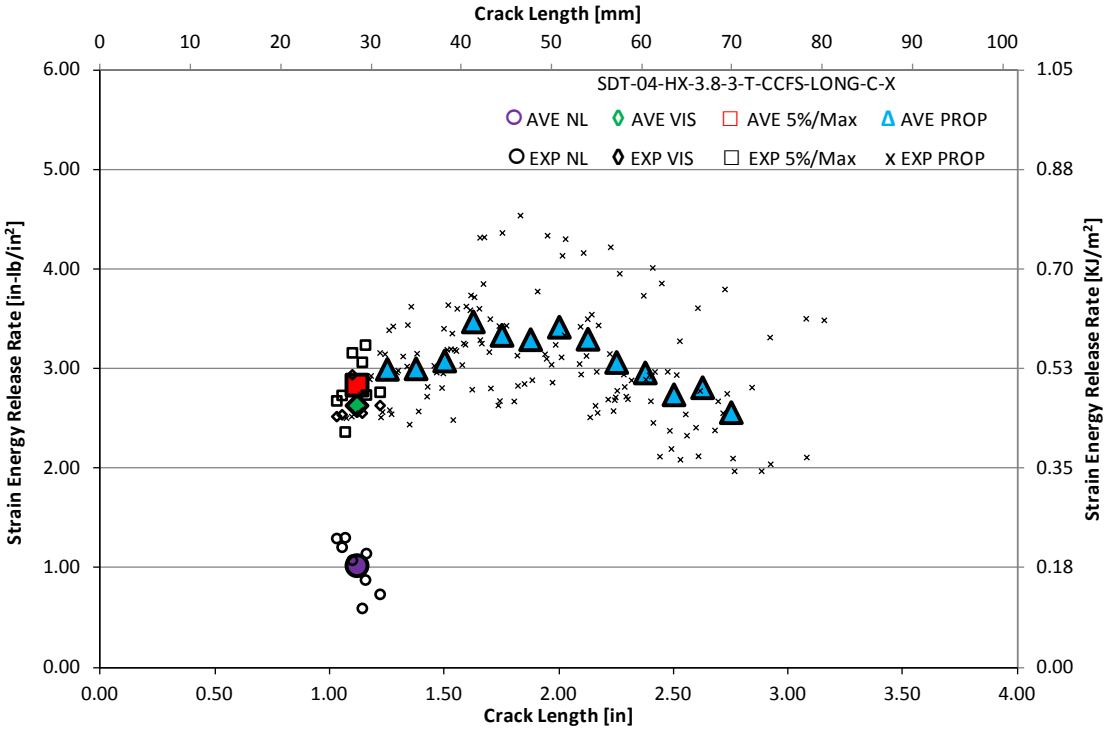

Figure B-14. Resistance curve for HRH-10–3/8–3.0 longitudinal ribbon direction with top disbond (center)

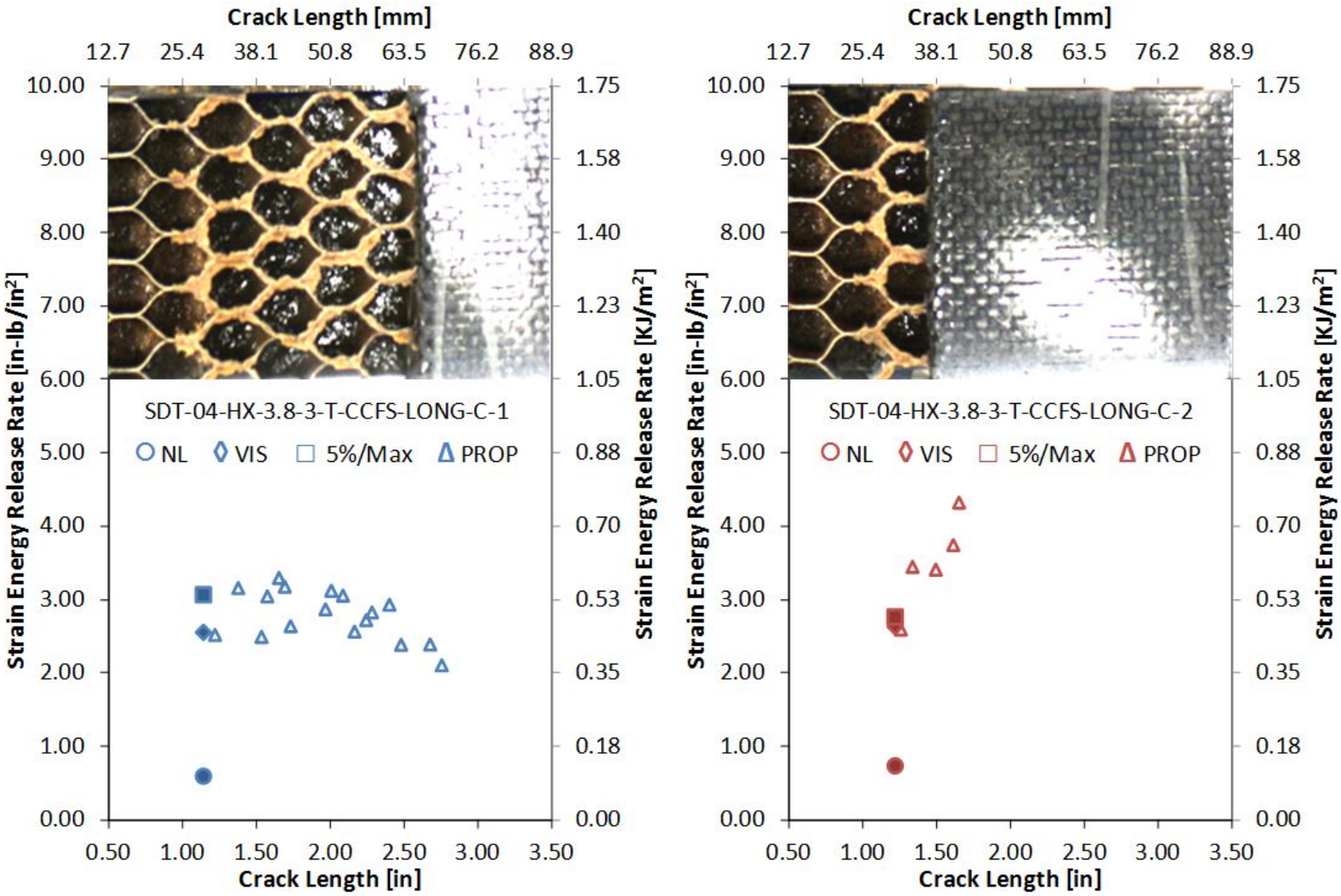

Figure B-15. Failure mode image and resistance curve of SDT-04-HX-3.8-3-T-CCFS-LONG-C-X #1 and #2

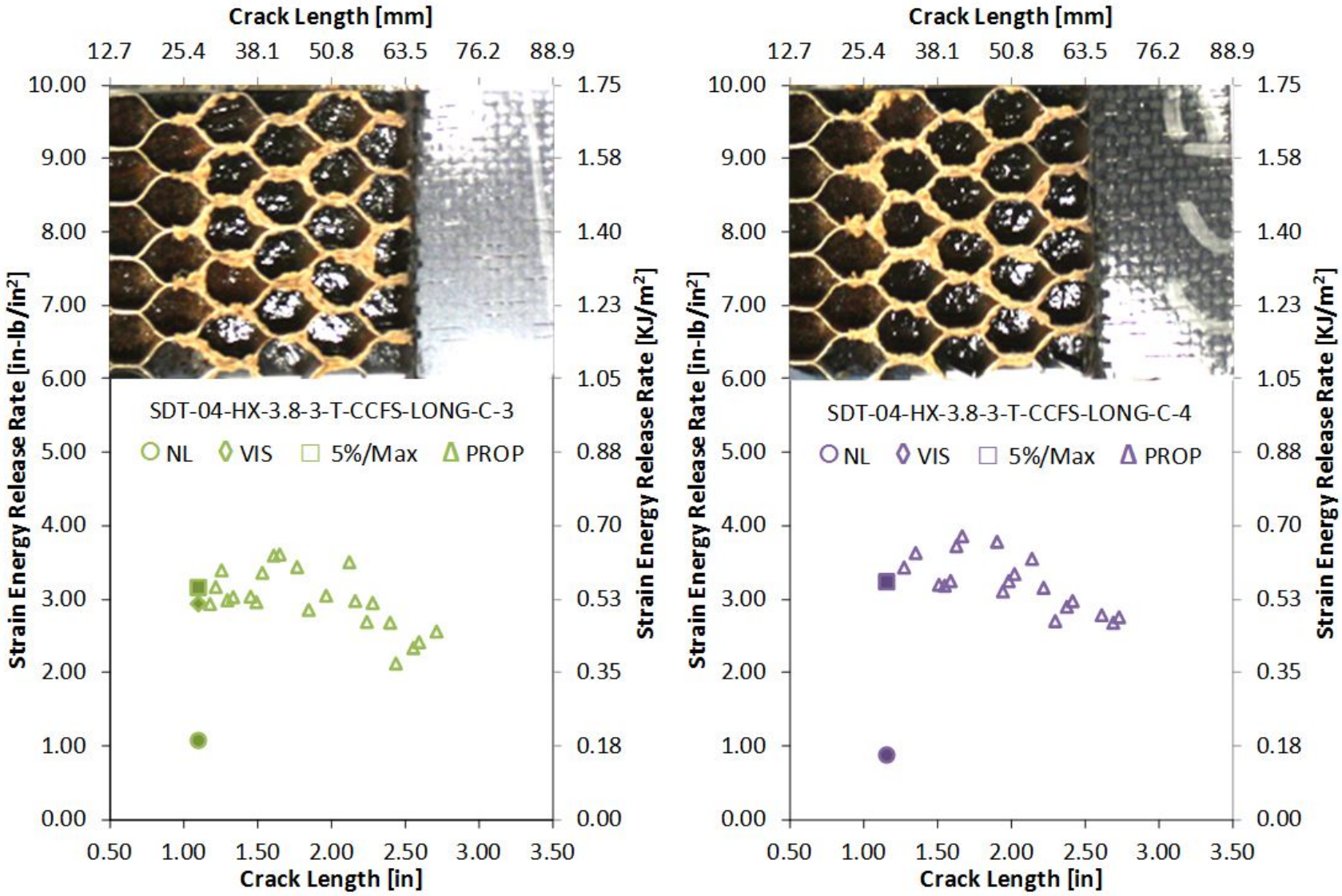

Figure B-16. Failure mode image and resistance curve of SDT-04-HX-3.8-3-T-CCFS-LONG-C-X #3 and #4

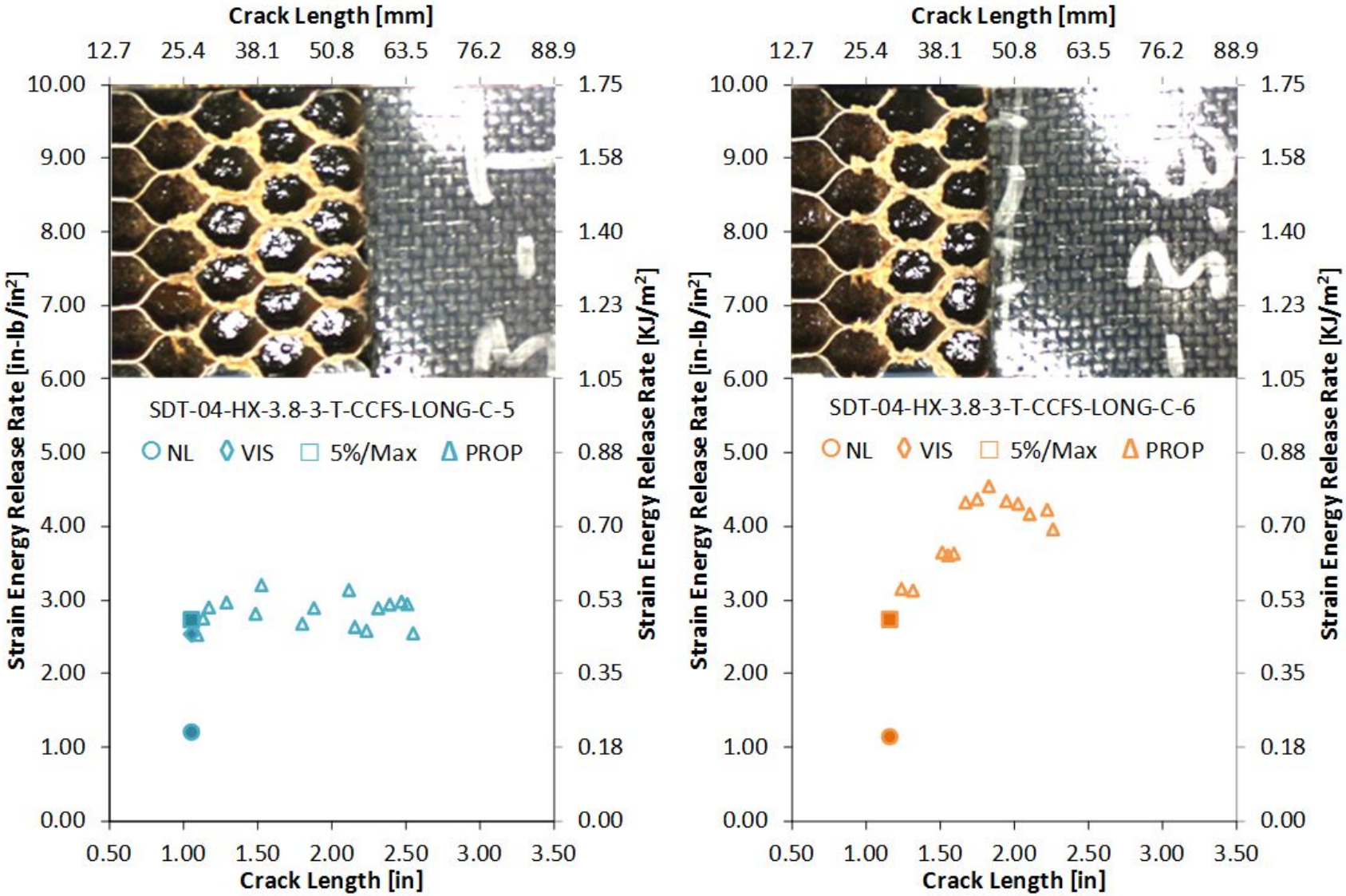

Figure B-17. Failure mode image and resistance curve of SDT-04-HX-3.8-3-T-CCFS-LONG-C-X #5 and #6

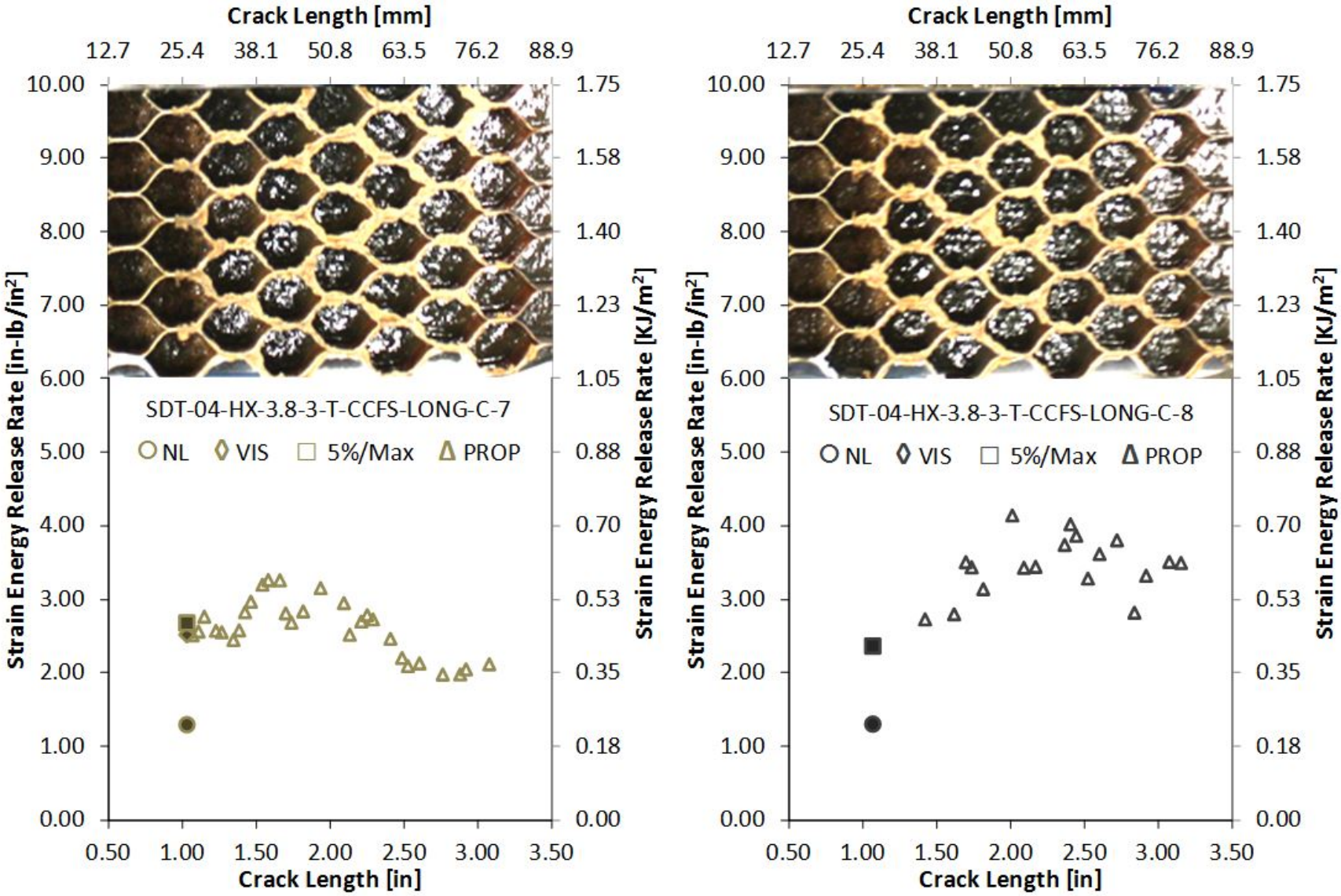

Figure B-18. Failure mode image and resistance curve of SDT-04-HX-3.8-3-T-CCFS-LONG-C-X #7 and #8

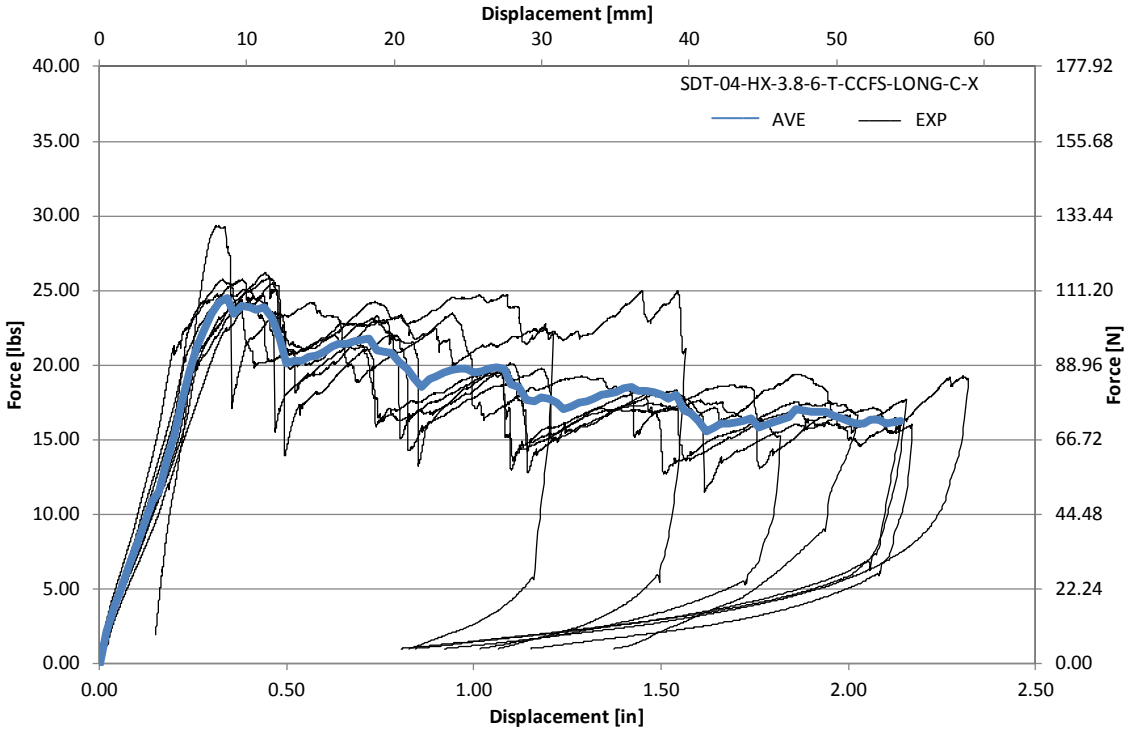

Figure B-19. Load vs. displacement curve for HRH-10–3/8–3.0 longitudinal ribbon direction with top disbond (center)

B.2.2 HRH-10–3/8–3.0 LONGITUDINAL RIBBON DIRECTION WITH BOTTOM DISBOND (CENTER) DATA

Table B-7. Test summary for HRH-10–3/8–3.0 longitudinal ribbon direction with bottom disbond (center) pre-crack

Specimen	GIC (in-lb/in^2)			GIC (KJ/m^2)			Failure Mode
	NL	VIS	5%/max	NL	VIS	5%/max	
SDT-04-HX-3.8-3-B-CCFS-LONG-C-1	0.556	N/A	0.821	0.097	N/A	0.144	Primarily APO
SDT-04-HX-3.8-3-B-CCFS-LONG-C-2	0.464	N/A	0.722	0.081	N/A	0.126	Primarily APO
SDT-04-HX-3.8-3-B-CCFS-LONG-C-3	0.472	N/A	0.860	0.083	N/A	0.151	Primarily APO
SDT-04-HX-3.8-3-B-CCFS-LONG-C-4	1.109	N/A	1.666	0.194	N/A	0.292	Primarily APO
SDT-04-HX-3.8-3-B-CCFS-LONG-C-5	1.029	1.963	1.963	0.180	0.344	0.344	Primarily APO
SDT-04-HX-3.8-3-B-CCFS-LONG-C-6	1.412	N/A	2.378	0.247	N/A	0.416	Primarily APO
SDT-04-HX-3.8-3-B-CCFS-LONG-C-7							
SDT-04-HX-3.8-3-B-CCFS-LONG-C-8							
AVERAGE GIC	0.840	1.963	1.402	0.147	0.344	0.245	
STANDARD DEVIATION	0.398	N/A	0.697	0.070	N/A	0.122	
COEFFICIENT OF VARIATION (%)	47.362	N/A	49.721	47.362	N/A	49.721	

Table B-8. Test summary for HRH-10–3/8–3.0 longitudinal ribbon direction with bottom disbond (center)

Specimen	GIC (in-lb/in^2)				GIC (KJ/m^2)				Failure Mode
	NL	VIS	5%/max	AREA	NL	VIS	5%/max	AREA	
SDT-04-HX-3.8-3-B-CCFS-LONG-C-1	0.320	2.552	3.225	N/A	0.056	0.447	0.565	N/A	Primarily APO, then FSF
SDT-04-HX-3.8-3-B-CCFS-LONG-C-2	0.196	2.811	2.820	3.470	0.034	0.492	0.494	0.608	Primarily APO
SDT-04-HX-3.8-3-B-CCFS-LONG-C-3	0.343	2.025	2.206	3.356	0.060	0.355	0.386	0.588	Primarily APO
SDT-04-HX-3.8-3-B-CCFS-LONG-C-4	0.369	1.495	1.947	4.682	0.065	0.262	0.341	0.820	Primarily APO
SDT-04-HX-3.8-3-B-CCFS-LONG-C-5	0.581	N/A	1.608	4.150	0.102	N/A	0.282	0.727	Primarily APO
SDT-04-HX-3.8-3-B-CCFS-LONG-C-6	0.628	1.798	2.355	4.194	0.110	0.315	0.412	0.734	Primarily APO
SDT-04-HX-3.8-3-B-CCFS-LONG-C-7									
SDT-04-HX-3.8-3-B-CCFS-LONG-C-8									
AVERAGE GIC	0.406	2.136	2.360	3.971	0.071	0.374	0.413	0.695	
STANDARD DEVIATION	0.165	0.540	0.587	0.551	0.029	0.095	0.103	0.097	
COEFFICIENT OF VARIATION (%)	40.654	25.266	24.850	13.886	40.654	25.266	24.850	13.886	

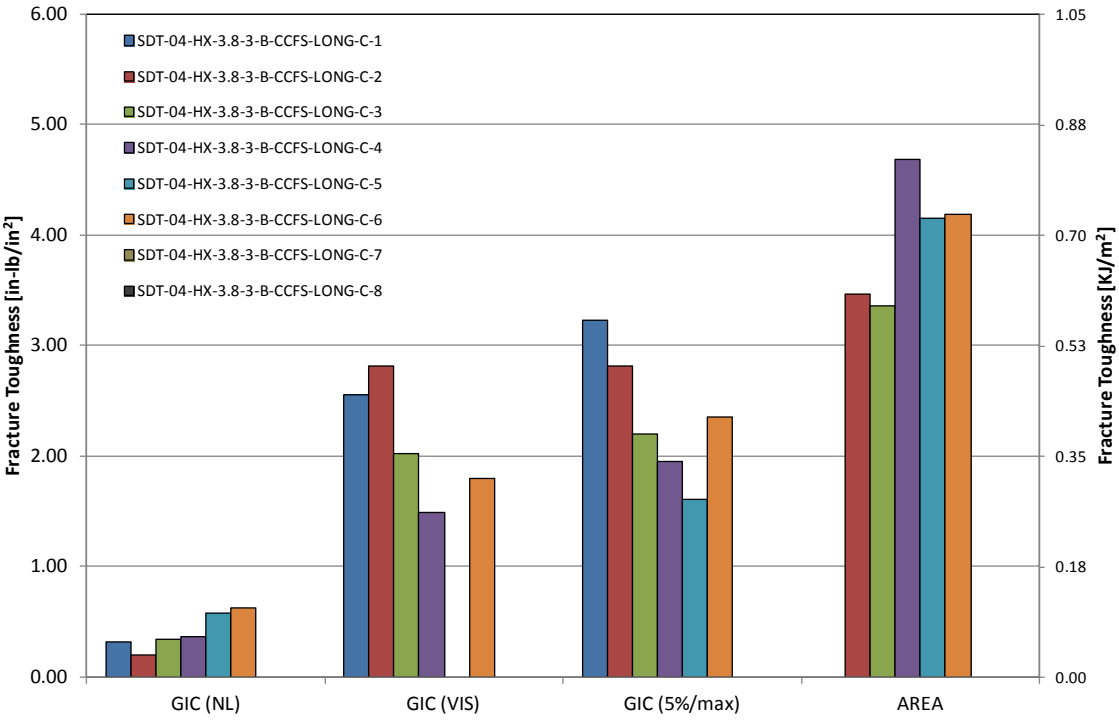

Figure B-20. GIC for HRH-10–3/8–3.0 longitudinal ribbon direction with bottom disbond (center)

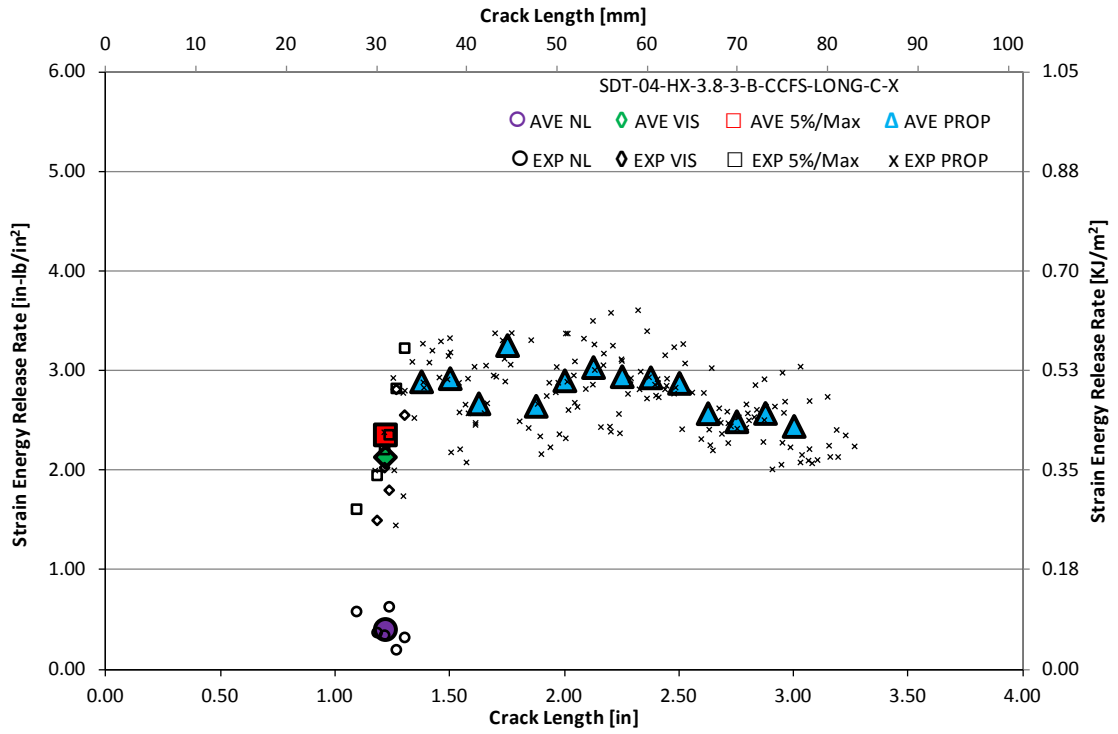

Figure B-21. Resistance curve for HRH-10–3/8–3.0 longitudinal ribbon direction with bottom disbond (center)

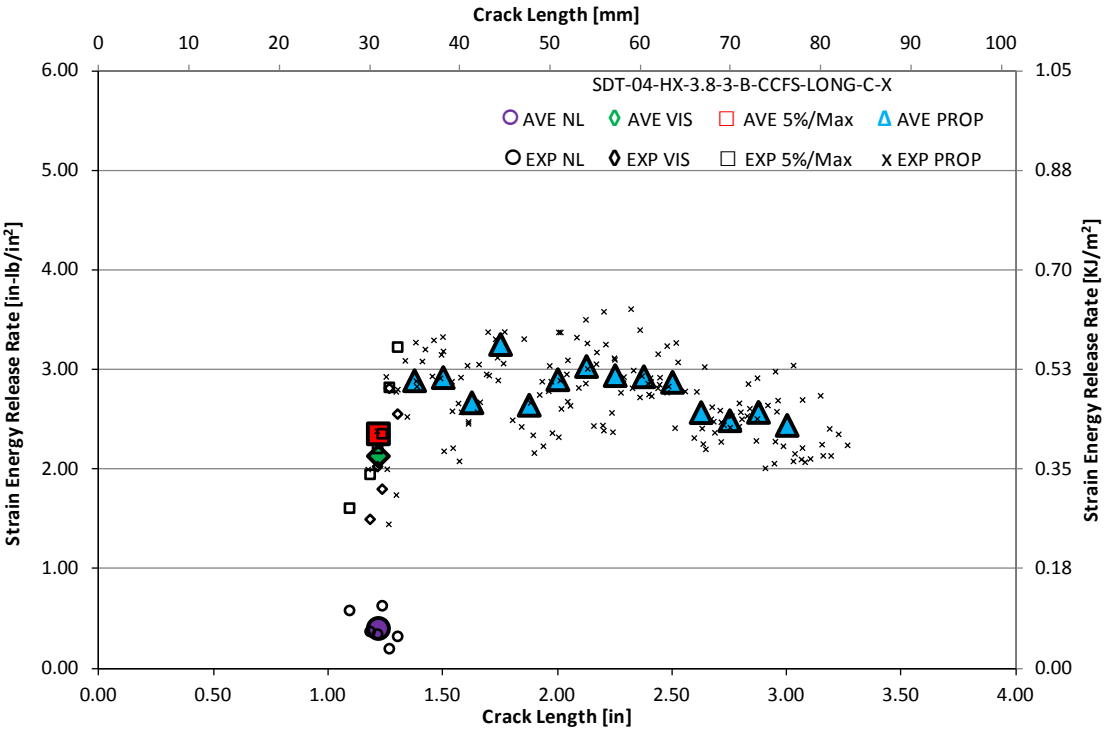

Figure B-22. Resistance curve for HRH-10–3/8–3.0 longitudinal ribbon direction with bottom disbond (center)

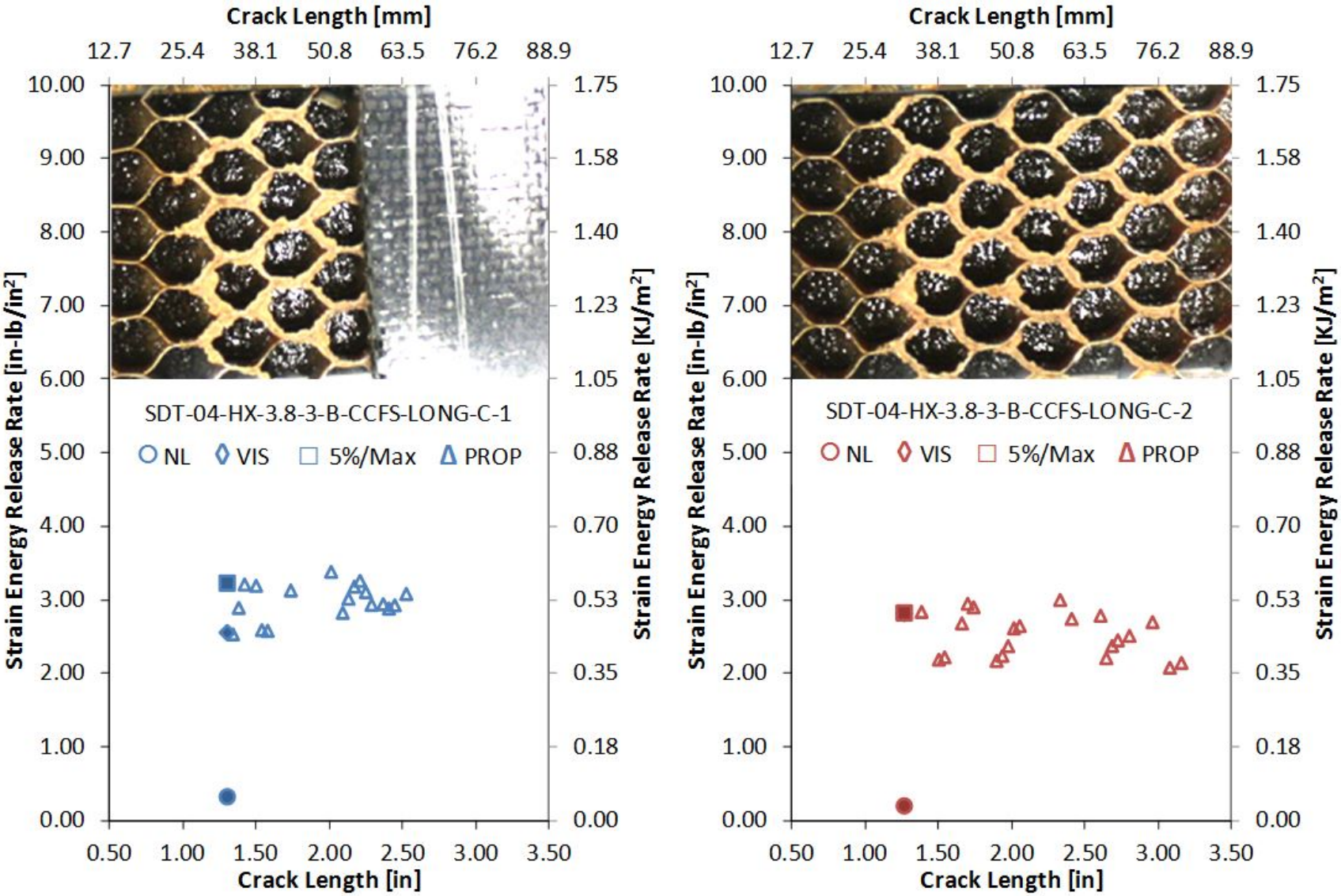

Figure B-23. Failure mode image and resistance curve of SDT-04-HX-3.8-3-B-CCFS-LONG-C-X #1 and #2

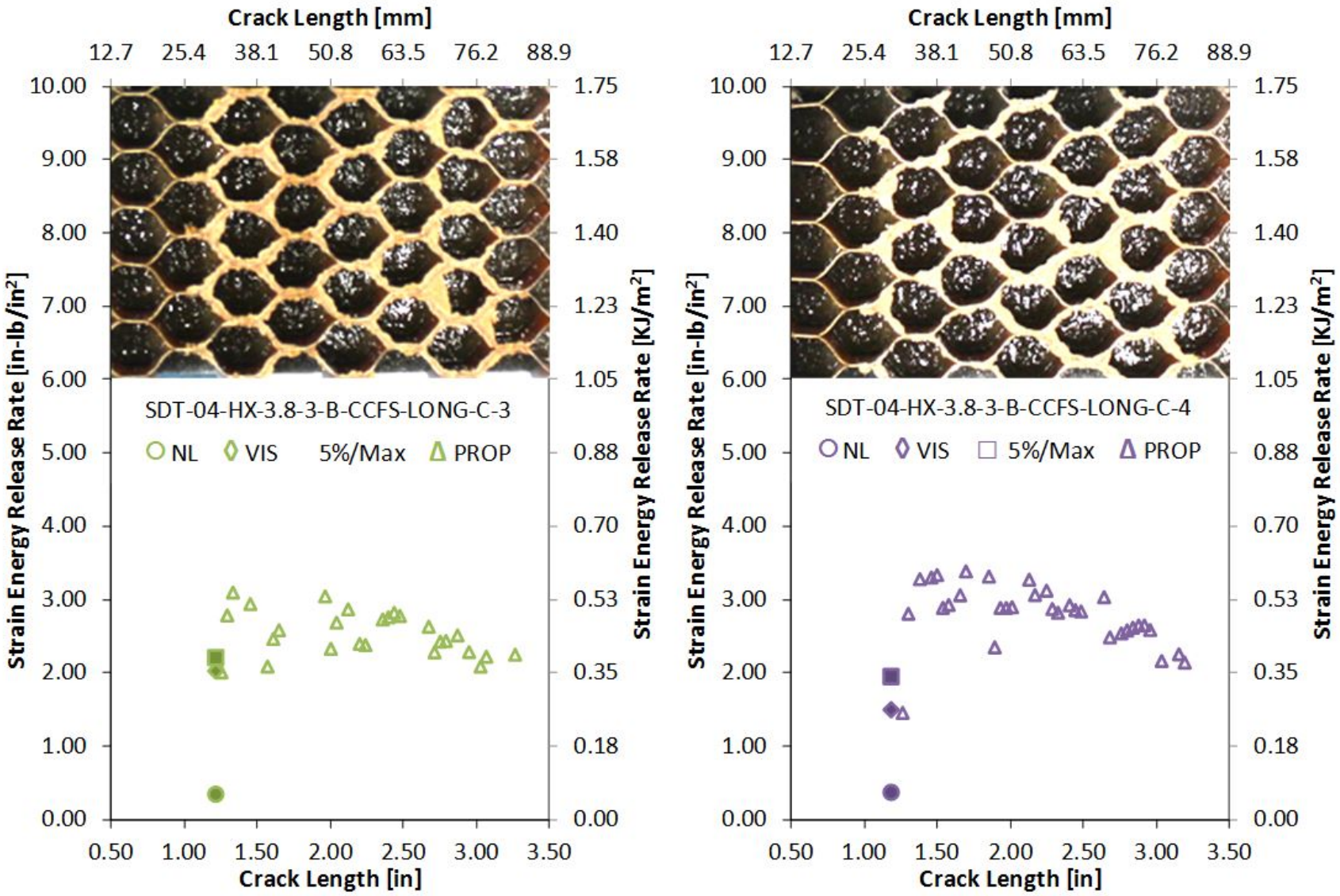

Figure B-24. Failure mode image and resistance curve of SDT-04-HX-3.8-3-B-CCFS-LONG-C-X #3 and #4

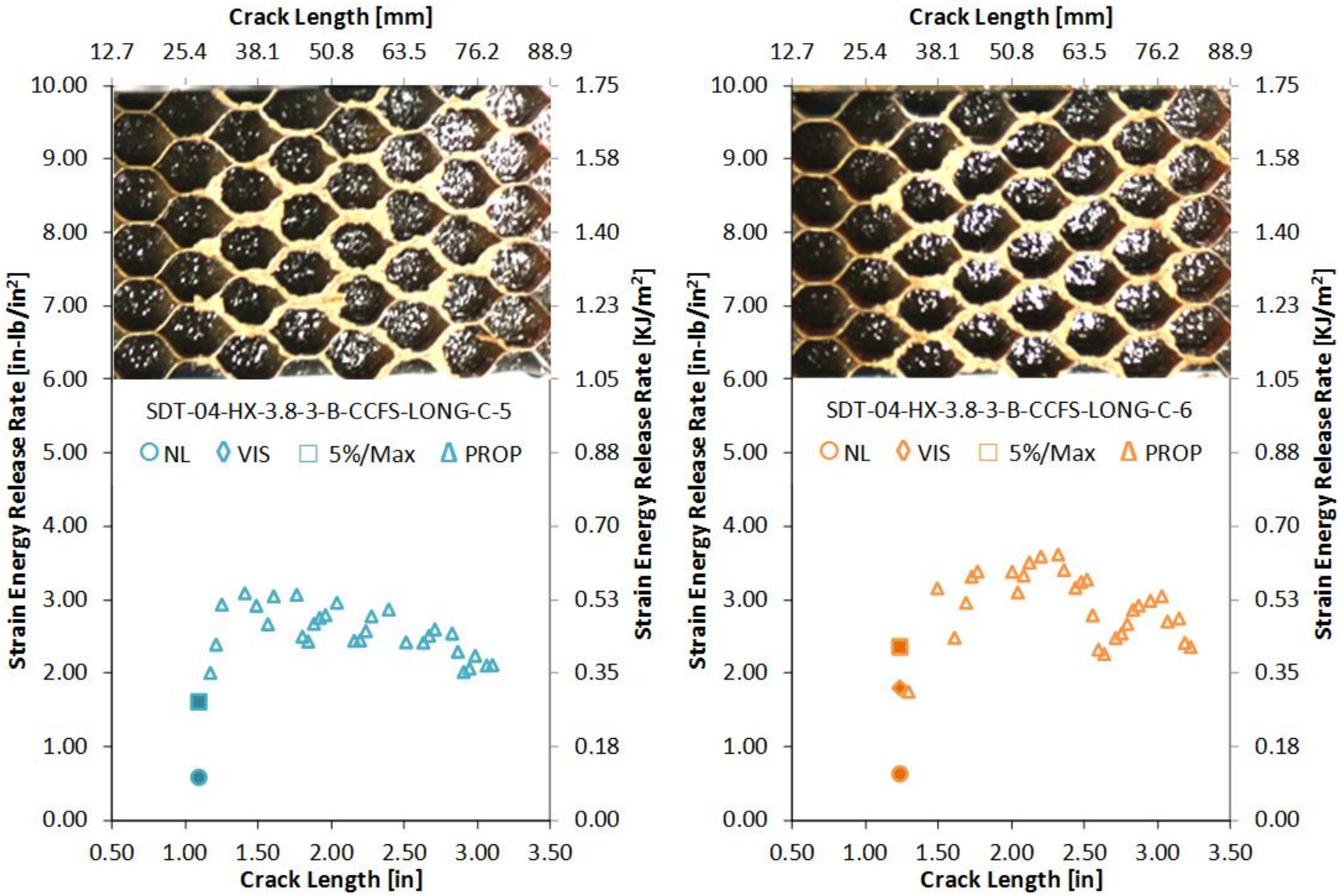

Figure B-25. Failure mode image and resistance curve of SDT-04-HX-3.8-3-B-CCFS-LONG-C-X #5 and #6

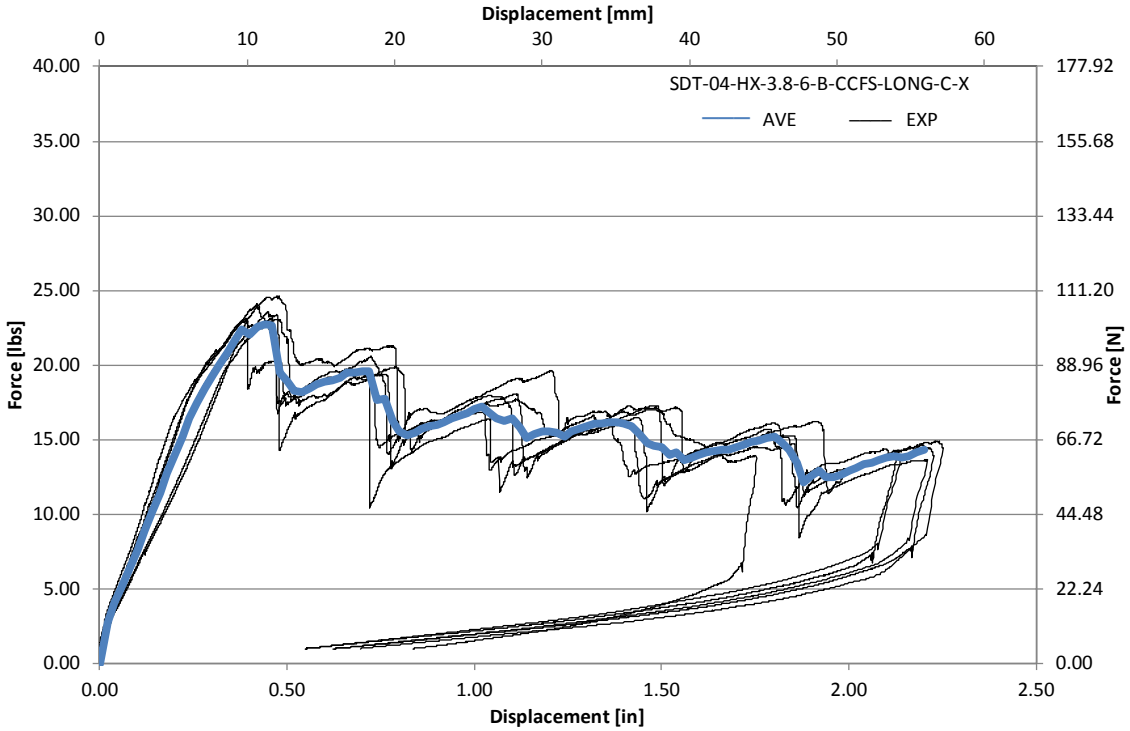

Figure B-26. Load vs. displacement curve for HRH-10–3/8–3.0 longitudinal ribbon direction with bottom disbond (center)

APPENDIX C—STATIC RESULTS FOR THIN PRE-CURED FACESHEET (4-PLY) AND SECONDARILY BONDED HRH-10 OVER-EXPANDED CORES TESTED AS SINGLE-CANTILEVER BEAMS

C.1. HRH-10/OX–3/16–3.0 DATA

C.1.1 HRH-10/OX–3/16–3.0 LONGITUDINAL RIBBON DIRECTION WITH TOP DISBOND (CENTER) DATA

Table C-1. Test summary for HRH-10/OX–3/16–3.0 longitudinal ribbon direction with top disbond (center) pre-crack

Specimen	GIC (in-lb/in^2)			GIC (KJ/m^2)			Failure Mode
	NL	VIS	5%/max	NL	VIS	5%/max	
SDT-04-OX-3.16-3-T-PCFS-LONG-C-1	2.093	N/A	2.545	0.367	N/A	0.446	*
SDT-04-OX-3.16-3-T-PCFS-LONG-C-2	1.650	N/A	2.156	0.289	N/A	0.378	Primarily C
SDT-04-OX-3.16-3-T-PCFS-LONG-C-3	1.838	N/A	2.206	0.322	N/A	0.386	Primarily C
SDT-04-OX-3.16-3-T-PCFS-LONG-C-4	1.687	N/A	2.408	0.295	N/A	0.422	Primarily C
SDT-04-OX-3.16-3-T-PCFS-LONG-C-5	1.353	N/A	2.284	0.237	N/A	0.400	Primarily C
SDT-04-OX-3.16-3-T-PCFS-LONG-C-6	1.383	N/A	2.243	0.242	N/A	0.393	Primarily C
SDT-04-OX-3.16-3-T-PCFS-LONG-C-7							
SDT-04-OX-3.16-3-T-PCFS-LONG-C-8							
AVERAGE GIC	1.667	N/A	2.307	0.292	N/A	0.404	
STANDARD DEVIATION	0.280	N/A	0.145	0.049	N/A	0.025	
COEFFICIENT OF VARIATION (%)	16.776	N/A	6.268	16.776	N/A	6.268	

Notes	*	Primarily C with a few cells partially in APO; APO is primarily on the double cell walls in the ribbon direction.

Table C-2. Test summary for HRH-10/OX–3/16–3.0 longitudinal ribbon direction with top disbond (center)

Specimen	GIC (in-lb/in^2)				GIC (KJ/m^2)				Failure Mode
	NL	VIS	5%/max	AREA	NL	VIS	5%/max	AREA	
SDT-04-OX-3.16-3-T-PCFS-LONG-C-1	0.917	2.749	2.768	2.811	0.161	0.481	0.485	0.492	*
SDT-04-OX-3.16-3-T-PCFS-LONG-C-2	1.042	2.156	2.314	N/A	0.182	0.378	0.405	N/A	*
SDT-04-OX-3.16-3-T-PCFS-LONG-C-3	0.870	N/A	2.575	3.045	0.152	N/A	0.451	0.533	*
SDT-04-OX-3.16-3-T-PCFS-LONG-C-4	0.773	2.644	2.751	2.890	0.135	0.463	0.482	0.506	*
SDT-04-OX-3.16-3-T-PCFS-LONG-C-5	0.849	2.402	2.533	2.785	0.149	0.421	0.444	0.488	*
SDT-04-OX-3.16-3-T-PCFS-LONG-C-6	0.746	2.087	2.145	2.782	0.131	0.365	0.376	0.487	*
SDT-04-OX-3.16-3-T-PCFS-LONG-C-7									
SDT-04-OX-3.16-3-T-PCFS-LONG-C-8									
AVERAGE GIC	0.866	2.407	2.514	2.863	0.152	0.422	0.440	0.501	
STANDARD DEVIATION	0.106	0.291	0.245	0.111	0.019	0.051	0.043	0.019	
COEFFICIENT OF VARIATION (%)	12.290	12.097	9.759	3.867	12.290	12.097	9.759	3.867	

Notes	*	Primarily C with a few cells partially in APO; APO is primarily on the double cell walls in the ribbon direction.

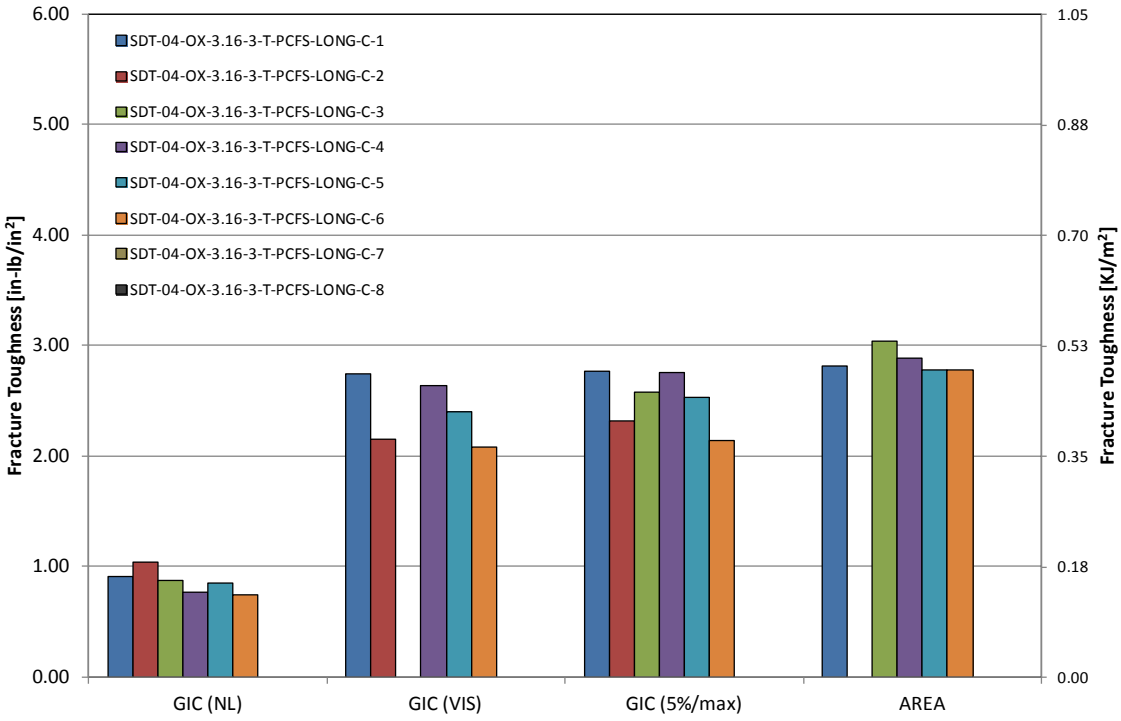

Figure C-1. GIC for HRH-10/OX–3/16–3.0 longitudinal ribbon direction with top disbond (center)

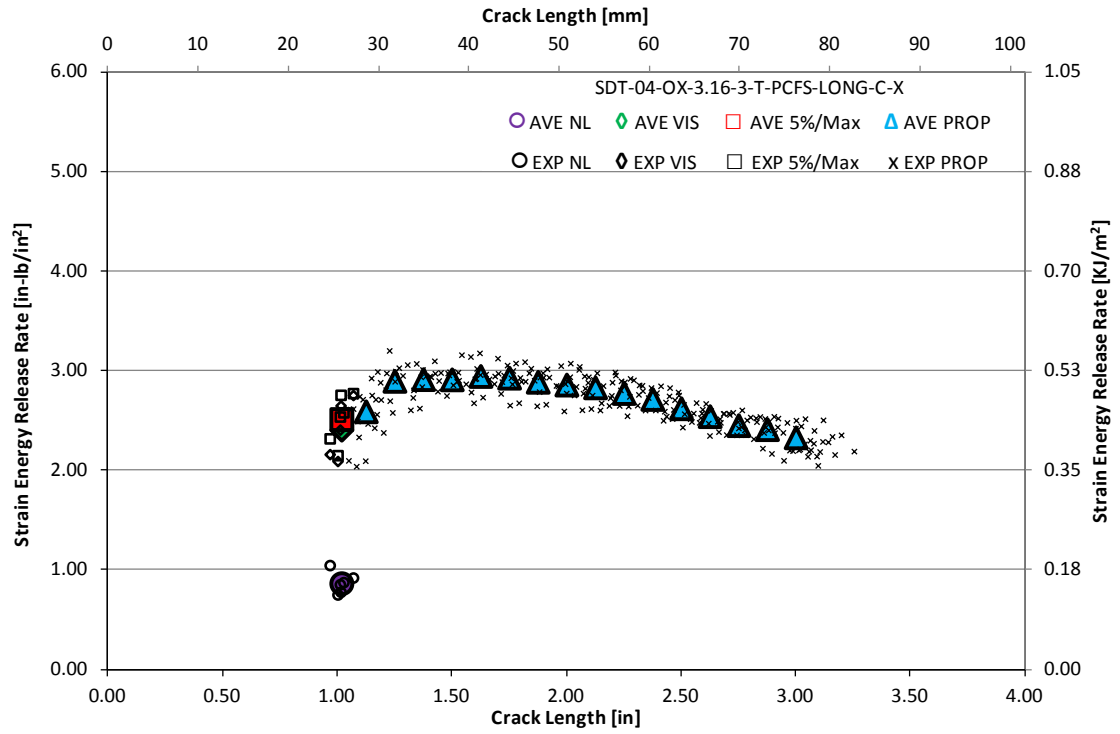

Figure C-2. Resistance curve for HRH-10/OX–3/16–3.0 longitudinal ribbon direction with top disbond (center)

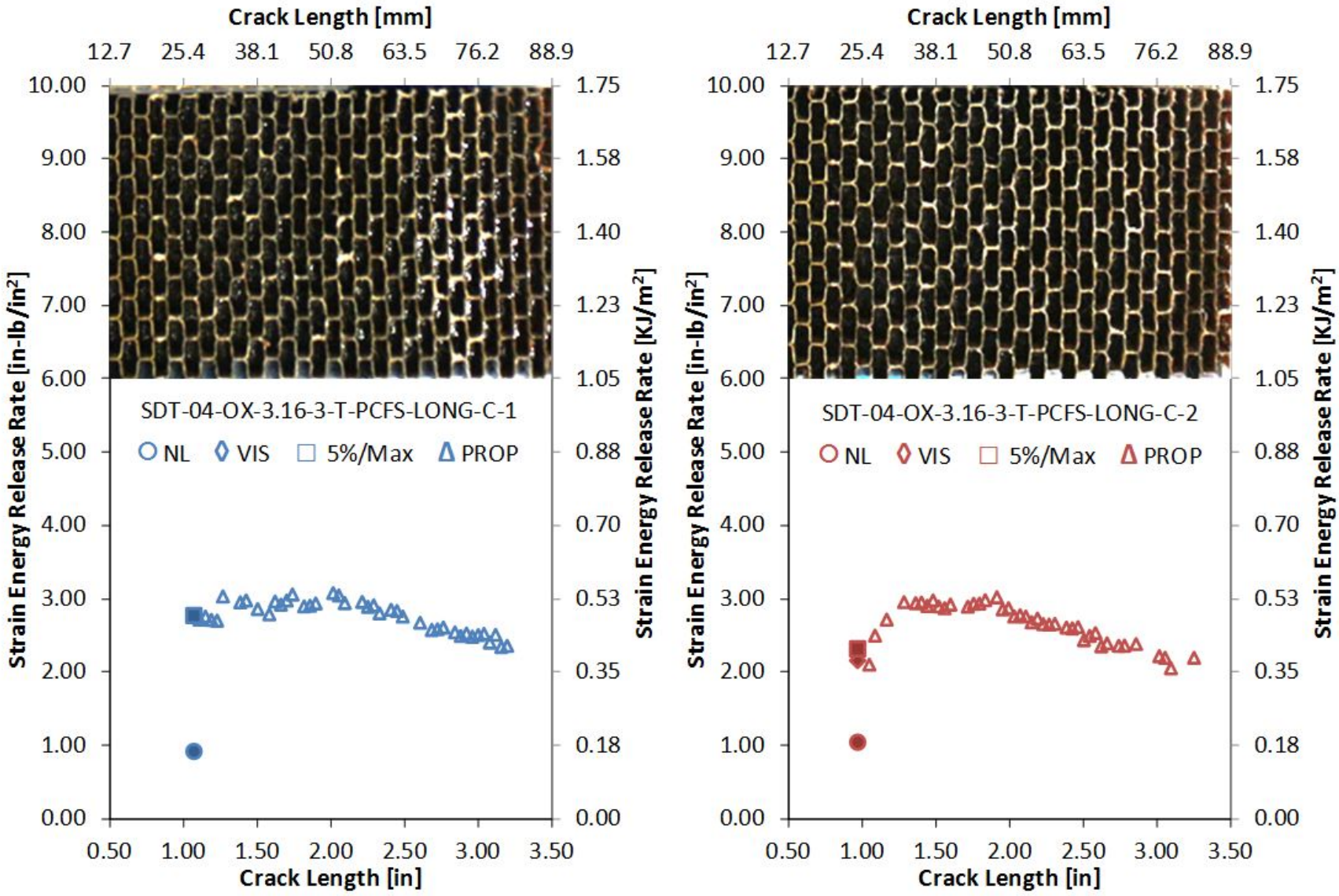

Figure C-3. Failure mode image and resistance curve of SDT-04-OX-3.16-3-T-PCFS-LONG-C-X #1 and #2

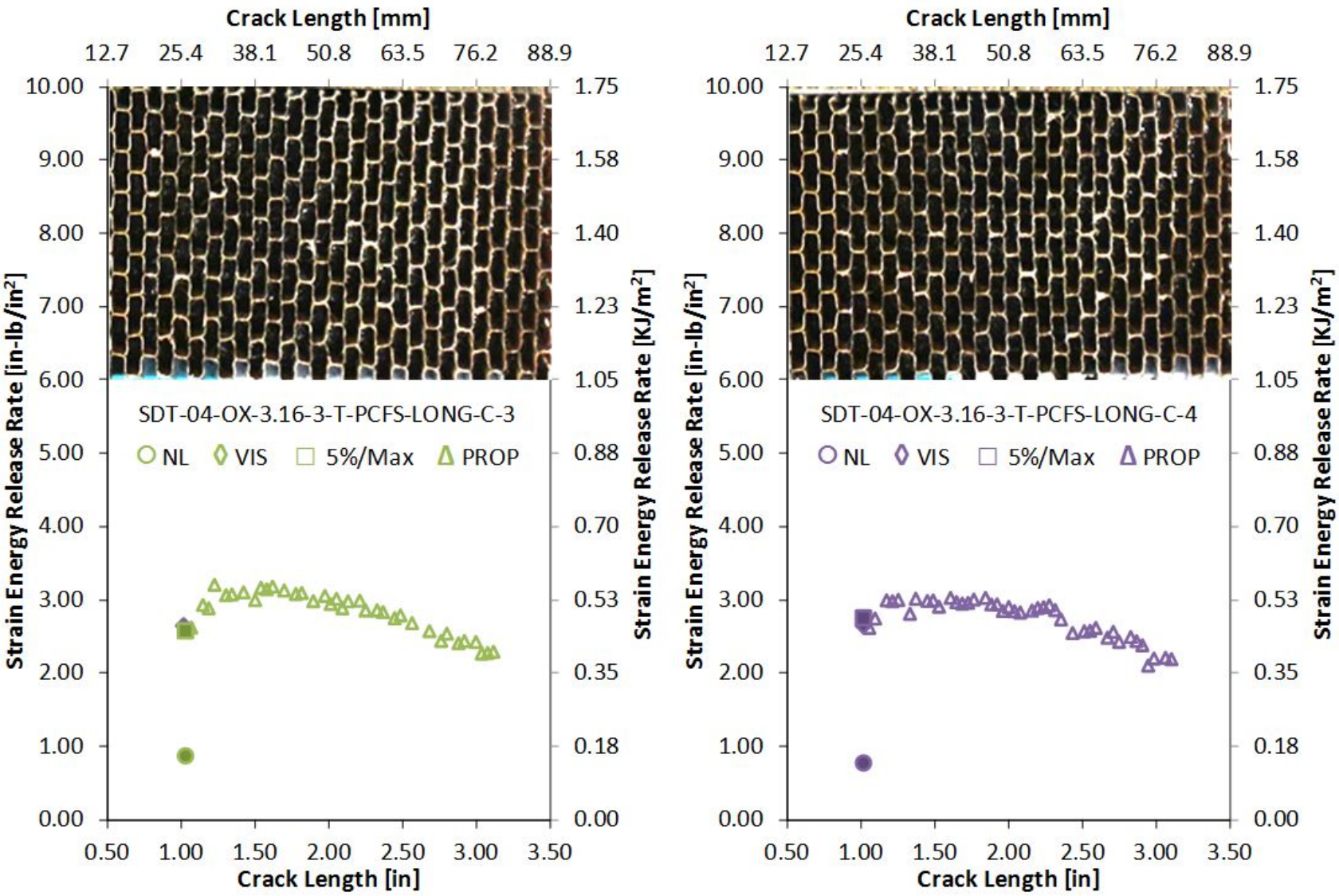

Figure C-4. Failure mode image and resistance curve of SDT-04-OX-3.16-3-T-PCFS-LONG-C-X #3 and #4

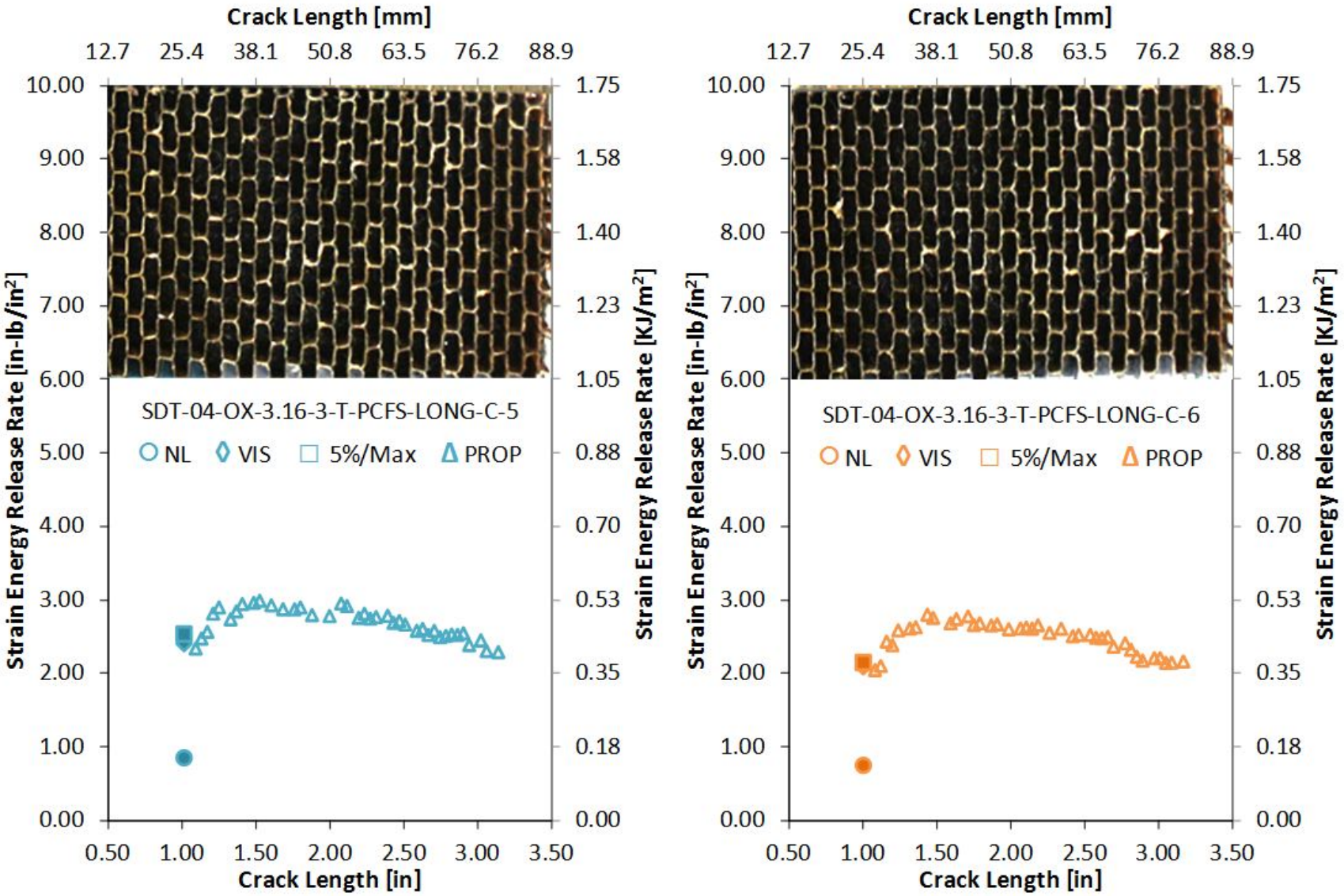

Figure C-5. Failure mode image and resistance curve of SDT-04-OX-3.16-3-T-PCFS-LONG-C-X #5 and #6

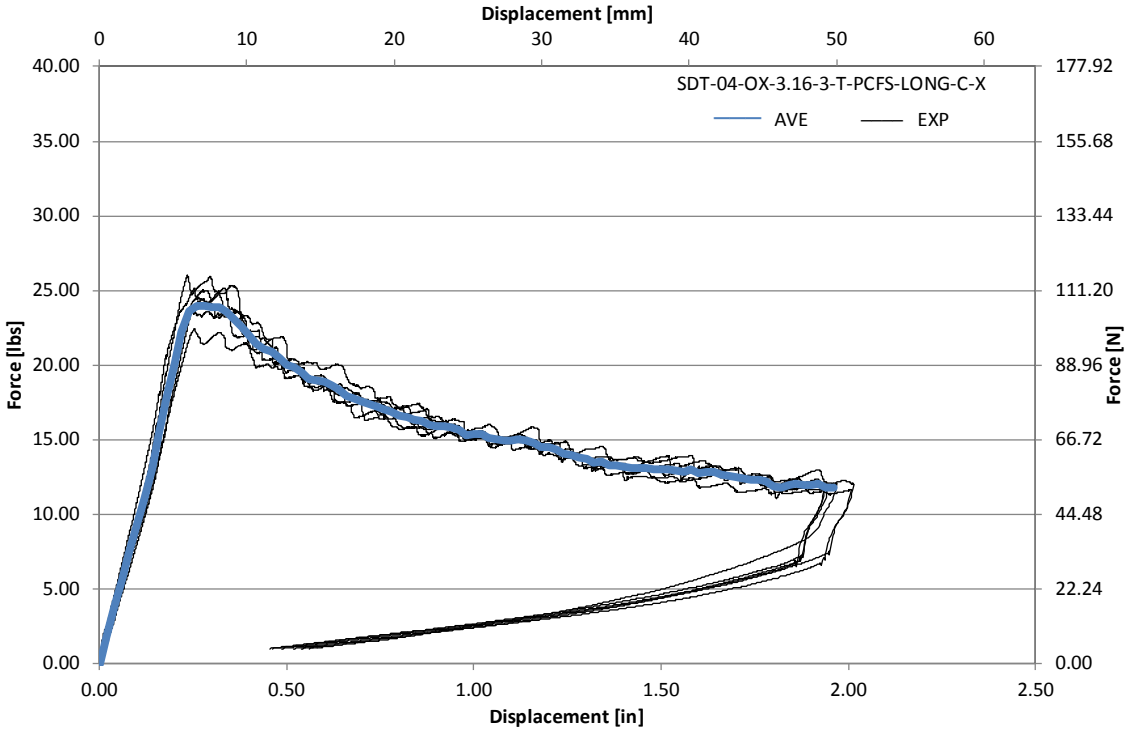

Figure C-6. Load vs. displacement curve for HRH-10/OX–3/16–3.0 longitudinal ribbon direction with top disbond (center)

C.1.2 HRH-10/OX–3/16–3.0 LONGITUDINAL RIBBON DIRECTION WITH BOTTOM DISBOND (CENTER) DATA

Table C-3. Test summary for HRH-10/OX–3/16–3.0 longitudinal ribbon direction with bottom disbond (center) pre-crack

Specimen	GIC (in-lb/in^2)			GIC (KJ/m^2)			Failure Mode
	NL	VIS	5%/max	NL	VIS	5%/max	
SDT-04-OX-3.16-3-B-PCFS-LONG-C-1							
SDT-04-OX-3.16-3-B-PCFS-LONG-C-2	1.909	N/A	2.182	0.334	N/A	0.382	Primarily C
SDT-04-OX-3.16-3-B-PCFS-LONG-C-3	1.356	2.170	2.263	0.238	0.380	0.396	Primarily C
SDT-04-OX-3.16-3-B-PCFS-LONG-C-4	1.460	N/A	2.260	0.256	N/A	0.396	Primarily C
SDT-04-OX-3.16-3-B-PCFS-LONG-C-5	1.071	N/A	2.753	0.188	N/A	0.482	*
SDT-04-OX-3.16-3-B-PCFS-LONG-C-6	1.238	N/A	1.869	0.217	N/A	0.327	Primarily C
SDT-04-OX-3.16-3-B-PCFS-LONG-C-7	1.519	N/A	2.120	0.266	N/A	0.371	Primarily C
SDT-04-OX-3.16-3-B-PCFS-LONG-C-8							
AVERAGE GIC	1.426	2.170	2.241	0.250	0.380	0.393	
STANDARD DEVIATION	0.286	N/A	0.290	0.050	N/A	0.051	
COEFFICIENT OF VARIATION (%)	20.062	N/A	12.933	20.062	N/A	12.933	

Notes	*	Primarily C with a few cells partially in APO; APO is primarily on the double cell walls in the ribbon direction.

Table C-4. Test summary for HRH-10/OX–3/16–3.0 longitudinal ribbon direction with bottom disbond (center)

Specimen	GIC (in-lb/in^2)				GIC (KJ/m^2)				Failure Mode
	NL	VIS	5%/max	AREA	NL	VIS	5%/max	AREA	
SDT-04-OX-3.16-3-B-PCFS-LONG-C-1									
SDT-04-OX-3.16-3-B-PCFS-LONG-C-2	0.674	N/A	2.023	2.861	0.118	N/A	0.354	0.501	*
SDT-04-OX-3.16-3-B-PCFS-LONG-C-3	0.668	2.316	2.327	3.025	0.117	0.406	0.408	0.530	*
SDT-04-OX-3.16-3-B-PCFS-LONG-C-4	0.502	N/A	1.971	2.928	0.088	N/A	0.345	0.513	*
SDT-04-OX-3.16-3-B-PCFS-LONG-C-5	0.651	2.466	2.530	2.975	0.114	0.432	0.443	0.521	*
SDT-04-OX-3.16-3-B-PCFS-LONG-C-6	0.720	N/A	2.003	2.796	0.126	N/A	0.351	0.490	*
SDT-04-OX-3.16-3-B-PCFS-LONG-C-7	0.648	N/A	1.930	2.688	0.114	N/A	0.338	0.471	*
SDT-04-OX-3.16-3-B-PCFS-LONG-C-8									
AVERAGE GIC	0.644	2.391	2.131	2.879	0.113	0.419	0.373	0.504	
STANDARD DEVIATION	0.074	0.106	0.241	0.124	0.013	0.019	0.042	0.022	
COEFFICIENT OF VARIATION (%)	11.545	4.432	11.331	4.309	11.545	4.432	11.331	4.309	

Notes	*	Primarily C with a few cells partially in APO; APO is primarily on the double cell walls in the ribbon direction.

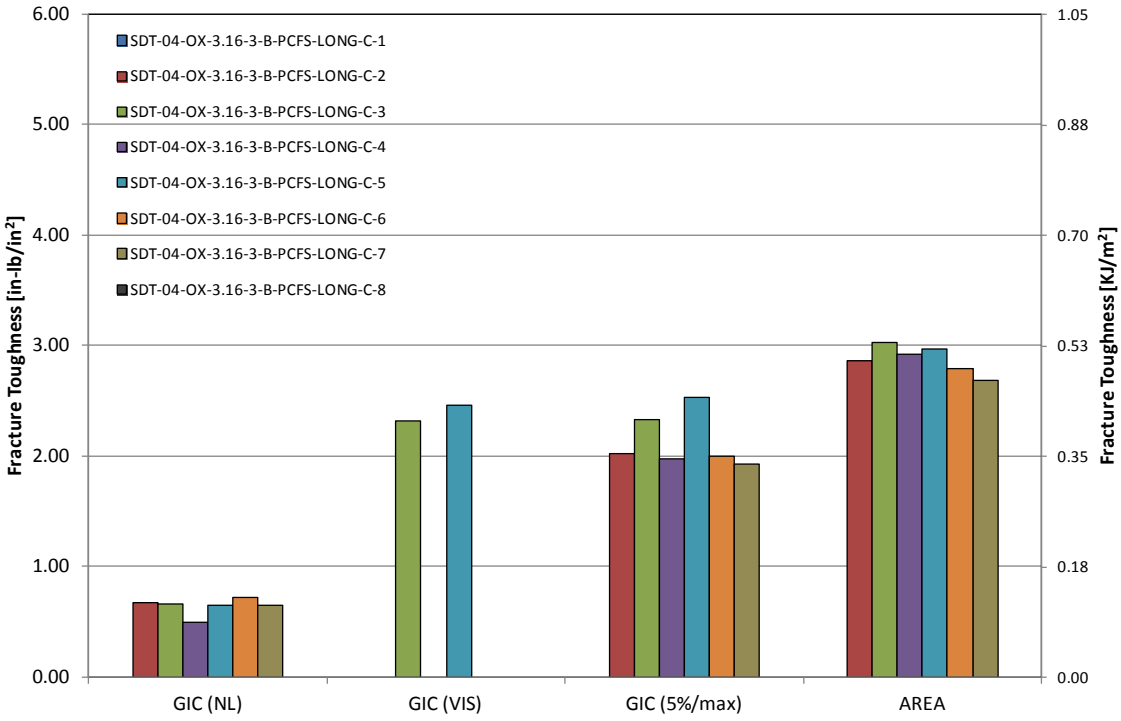

Figure C-7. GIC for HRH-10/OX–3/16–3.0 longitudinal ribbon direction with bottom disbond (center)

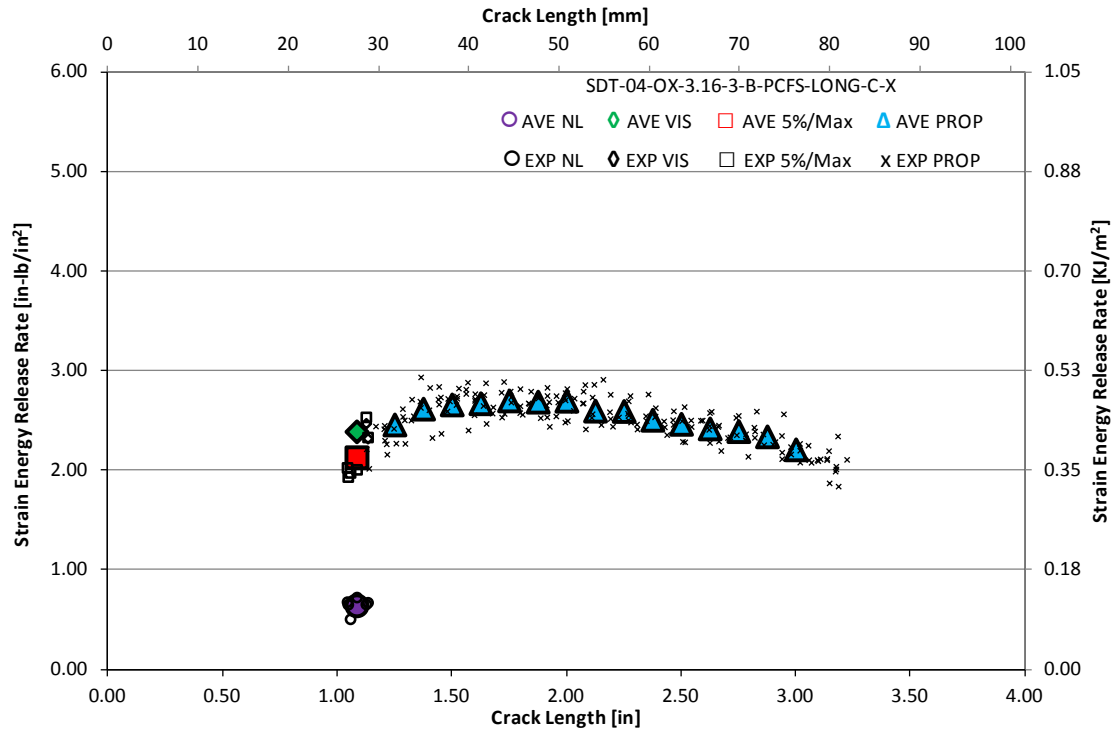

Figure C-8. Resistance curve for HRH-10/OX–3/16–3.0 longitudinal ribbon direction with bottom disbond (center)

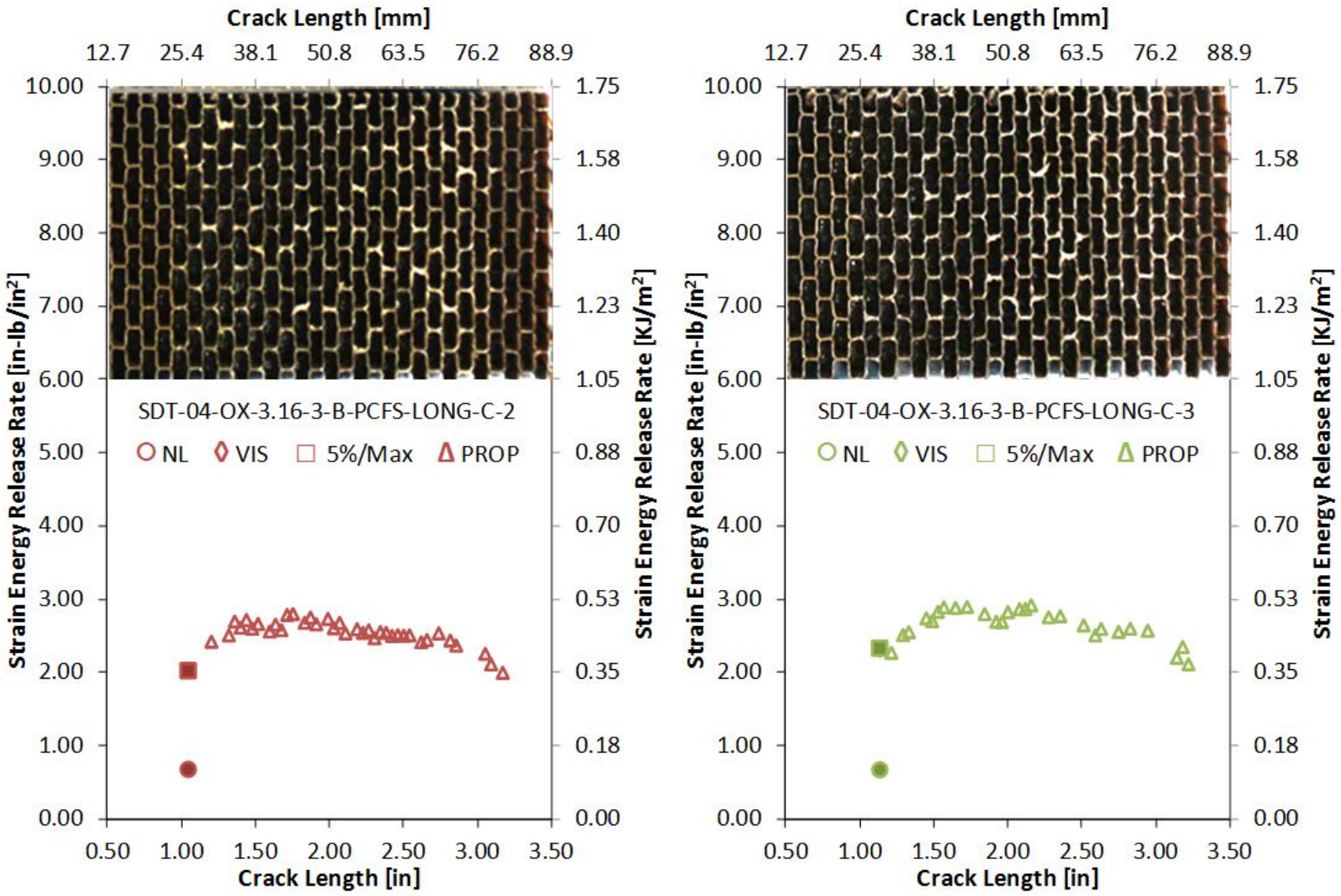

Figure C-9. Failure mode image and resistance curve of SDT-04-OX-3.16-3-B-PCFS-LONG-C-X #2 and #3

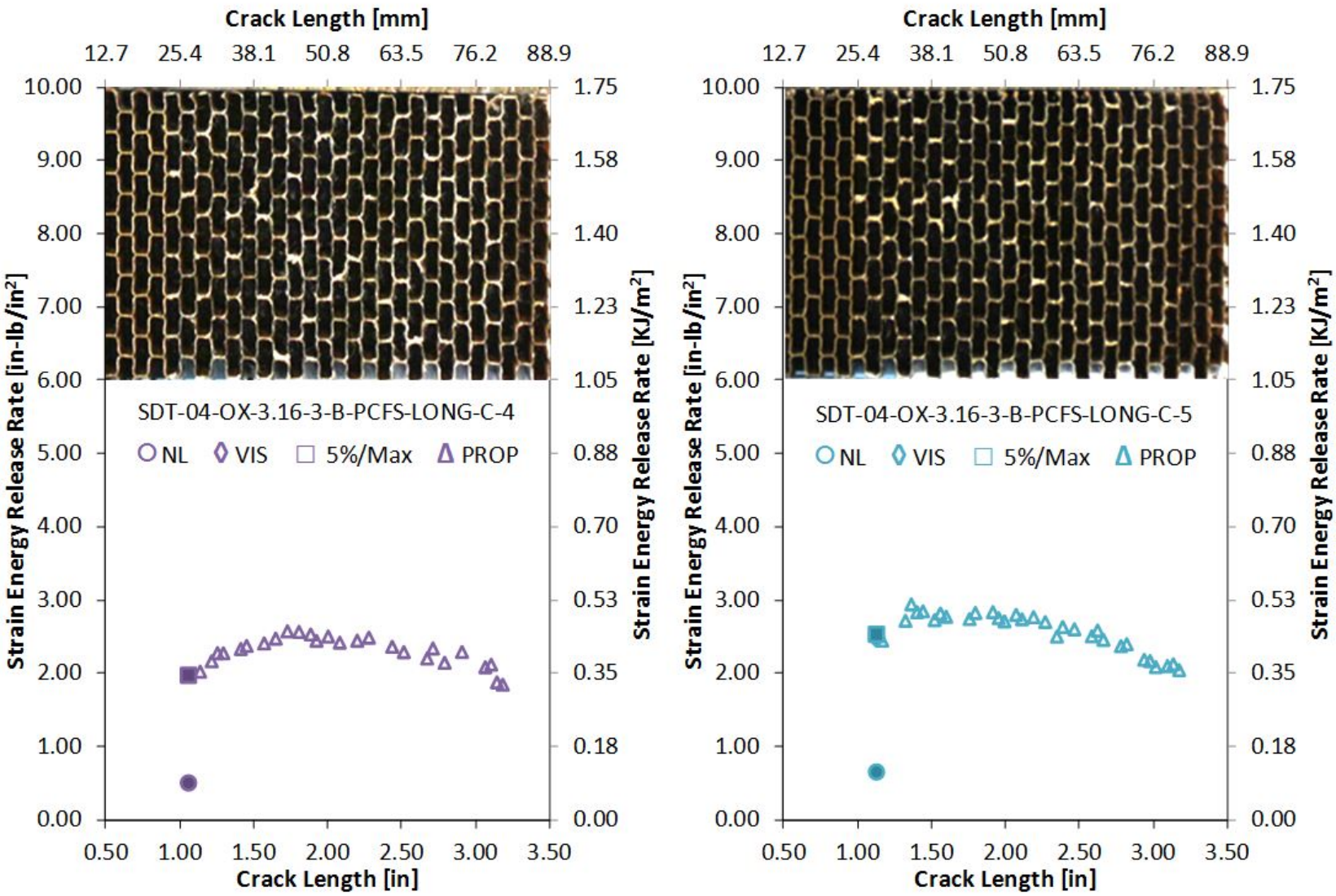

Figure C-10. Failure mode image and resistance curve of SDT-04-OX-3.16-3-B-PCFS-LONG-C-X #4 and #5

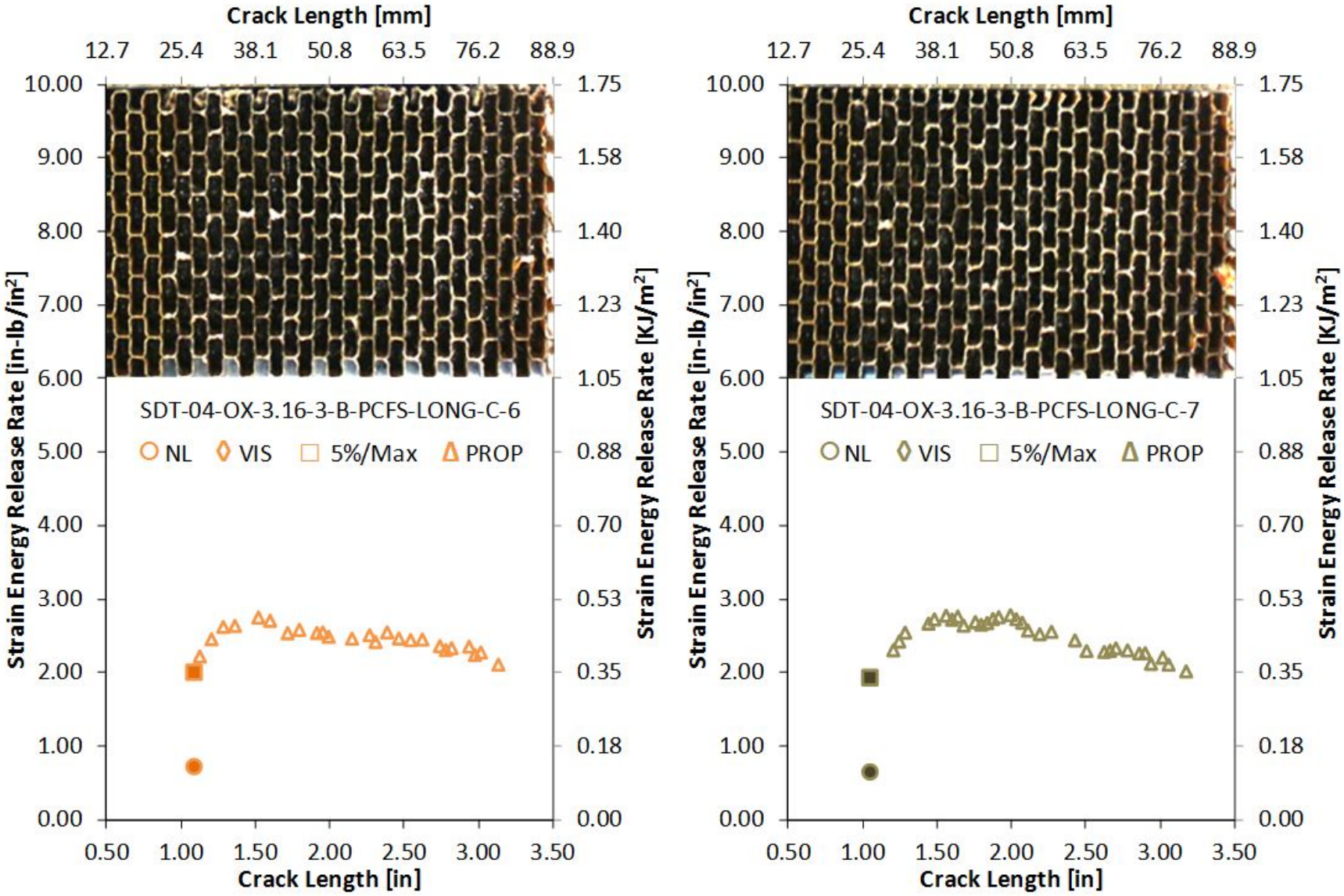

Figure C-11. Failure mode image and resistance curve of SDT-04-OX-3.16-3-B-PCFS-LONG-C-X #6 and #7

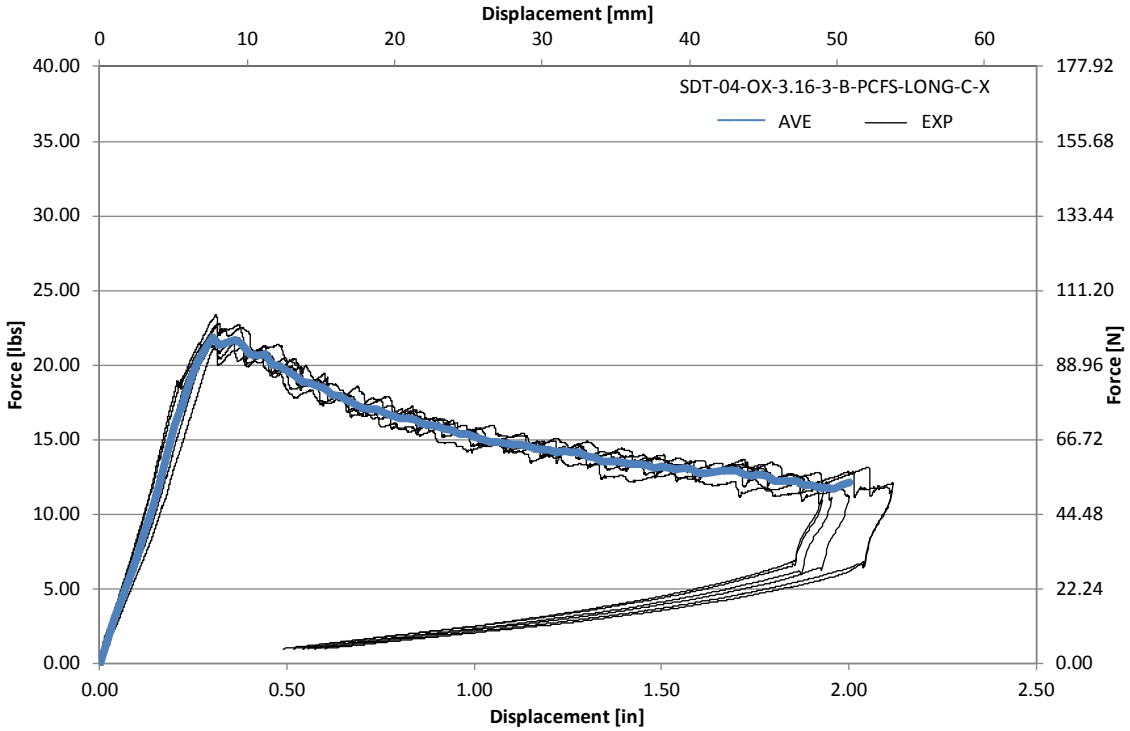

Figure C-12. Load vs. displacement curve for HRH-10/OX–3/16–3.0 longitudinal ribbon direction with bottom disbond (center)

C.1.3 HRH-10/OX–3/16–3.0 LATERAL RIBBON DIRECTION WITH TOP DISBOND (CENTER) DATA

Table C-5. Test summary for HRH-10/OX–3/16–3.0 lateral ribbon direction with top disbond (center) pre-crack

Specimen	GIC (in-lb/in^2)			GIC (KJ/m^2)			Failure Mode
	NL	VIS	5%/max	NL	VIS	5%/max	
SDT-04-OX-3.16-3-T-PCFS-LAT-C-1	1.598	N/A	2.334	0.280	N/A	0.409	*
SDT-04-OX-3.16-3-T-PCFS-LAT-C-2							
SDT-04-OX-3.16-3-T-PCFS-LAT-C-3	1.735	N/A	2.559	0.304	N/A	0.448	*
SDT-04-OX-3.16-3-T-PCFS-LAT-C-4	1.786	N/A	2.576	0.313	N/A	0.451	*
SDT-04-OX-3.16-3-T-PCFS-LAT-C-5	1.823	N/A	2.930	0.319	N/A	0.513	*
SDT-04-OX-3.16-3-T-PCFS-LAT-C-6	1.952	N/A	2.624	0.342	N/A	0.459	*
SDT-04-OX-3.16-3-T-PCFS-LAT-C-7	1.648	N/A	2.299	0.289	N/A	0.403	*
SDT-04-OX-3.16-3-T-PCFS-LAT-C-8							
AVERAGE GIC	1.757	N/A	2.553	0.308	N/A	0.447	
STANDARD DEVIATION	0.127	N/A	0.228	0.022	N/A	0.040	
COEFFICIENT OF VARIATION (%)	7.241	N/A	8.930	7.241	N/A	8.930	

Notes	*	Primarily APO and C with several cells partially in APO; APO is primarily on the double cell walls in the ribbon direction.

Table C-6. Test summary for HRH-10/OX–3/16–3.0 lateral ribbon direction with top disbond (center)

Specimen	GIC (in-lb/in^2)				GIC (KJ/m^2)				Failure Mode
	NL	VIS	5%/max	AREA	NL	VIS	5%/max	AREA	
SDT-04-OX-3.16-3-T-PCFS-LAT-C-1	0.795	2.744	2.759	3.500	0.139	0.481	0.483	0.613	*
SDT-04-OX-3.16-3-T-PCFS-LAT-C-2									
SDT-04-OX-3.16-3-T-PCFS-LAT-C-3	0.841	N/A	2.827	3.362	0.147	N/A	0.495	0.589	*
SDT-04-OX-3.16-3-T-PCFS-LAT-C-4	0.893	N/A	2.844	3.281	0.156	N/A	0.498	0.575	*
SDT-04-OX-3.16-3-T-PCFS-LAT-C-5	0.834	2.928	3.323	3.480	0.146	0.513	0.582	0.609	*
SDT-04-OX-3.16-3-T-PCFS-LAT-C-6	0.958	N/A	2.155	3.386	0.168	N/A	0.377	0.593	*
SDT-04-OX-3.16-3-T-PCFS-LAT-C-7	0.730	3.396	3.418	3.728	0.128	0.595	0.599	0.653	*
SDT-04-OX-3.16-3-T-PCFS-LAT-C-8									
AVERAGE GIC	0.842	3.022	2.888	3.456	0.147	0.529	0.506	0.605	
STANDARD DEVIATION	0.078	0.336	0.454	0.155	0.014	0.059	0.079	0.027	
COEFFICIENT OF VARIATION (%)	9.311	11.119	15.711	4.496	9.311	11.119	15.711	4.496	

Notes	*	Primarily C with many cells partially in APO; APO is primarily on the double cell walls in the ribbon direction.

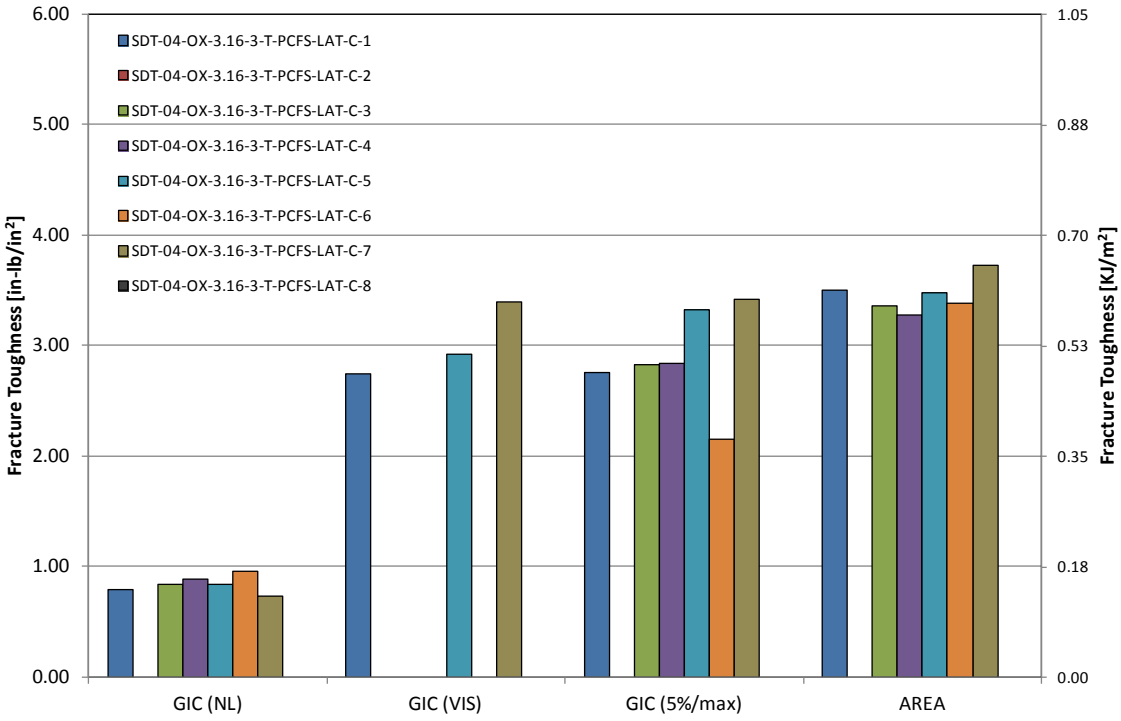

Figure C-13. GIC for HRH-10/OX–3/16–3.0 lateral ribbon direction with top disbond (center)

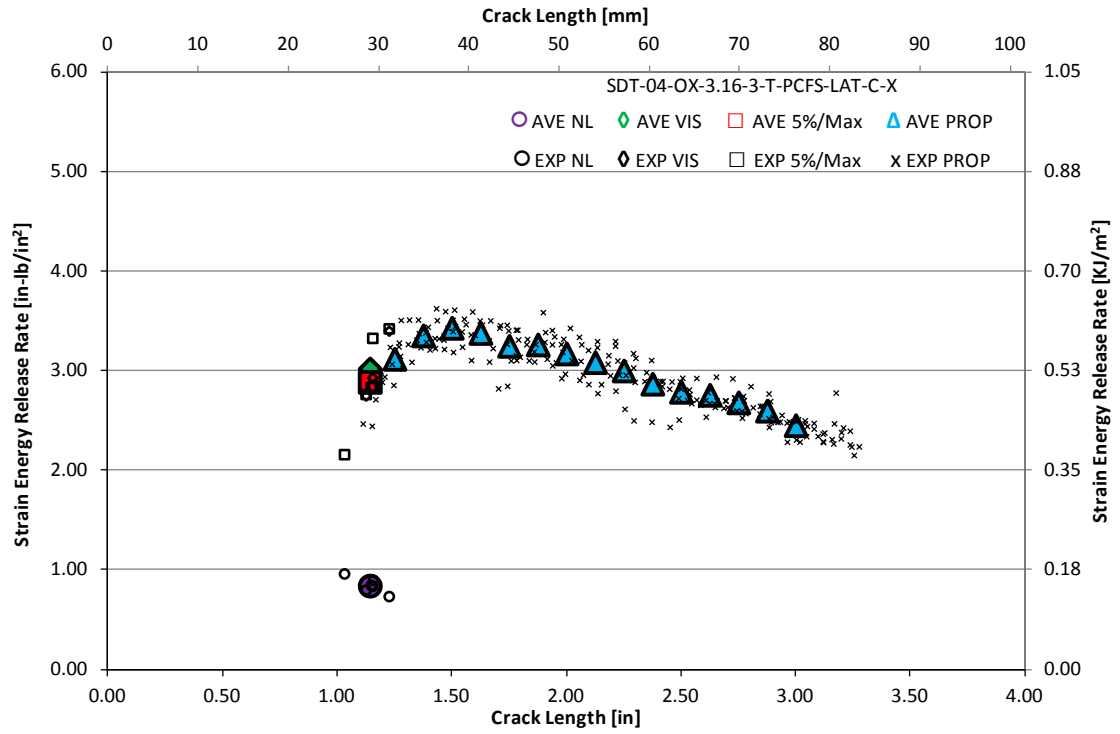

Figure C-14. Resistance curve for HRH-10/OX–3/16–3.0 lateral ribbon direction with top disbond (center)

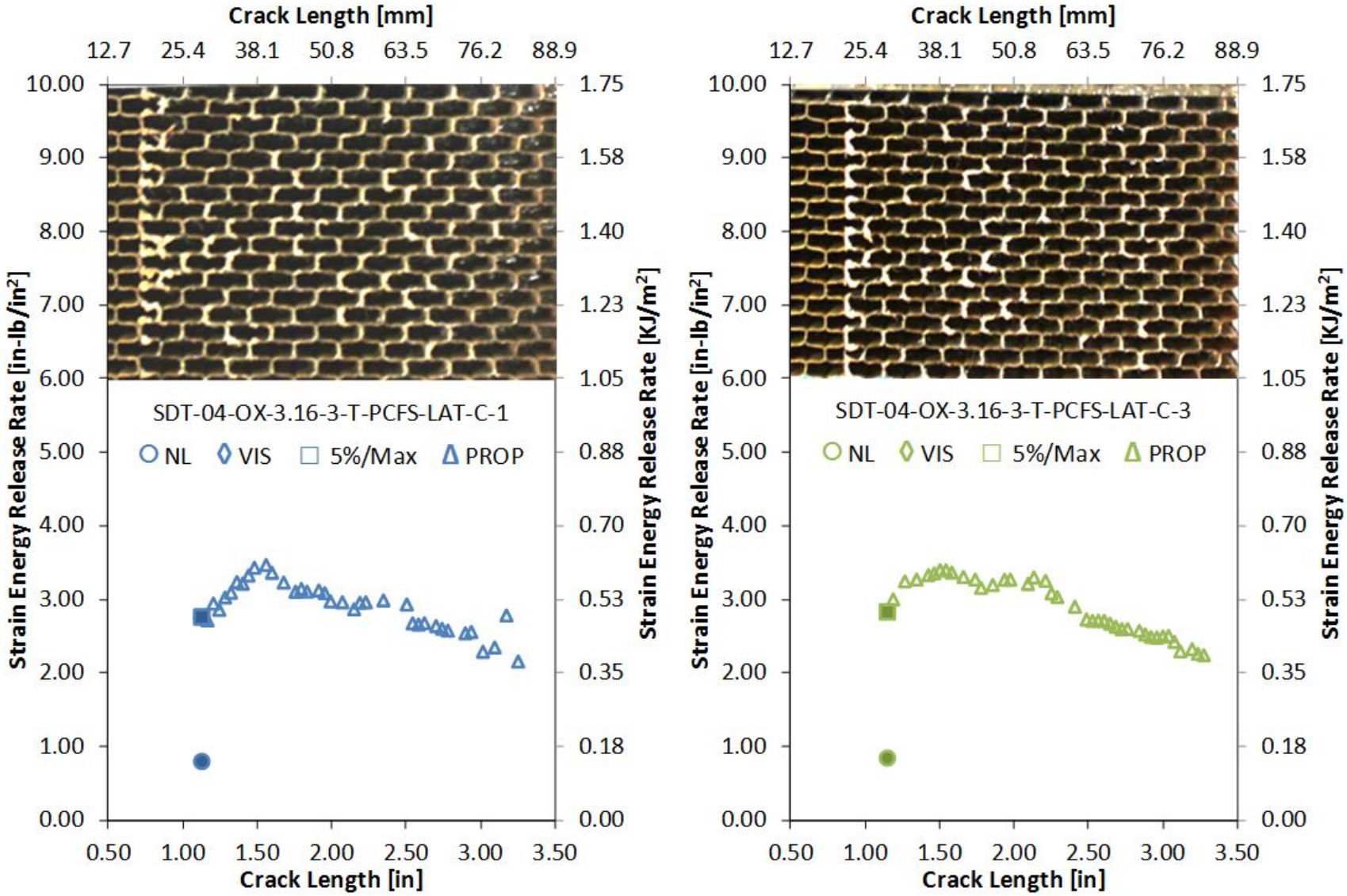

Figure C-15. Failure mode image and resistance curve of SDT-04-OX-3.16-3-T-PCFS-LAT-C-X #1 and #3

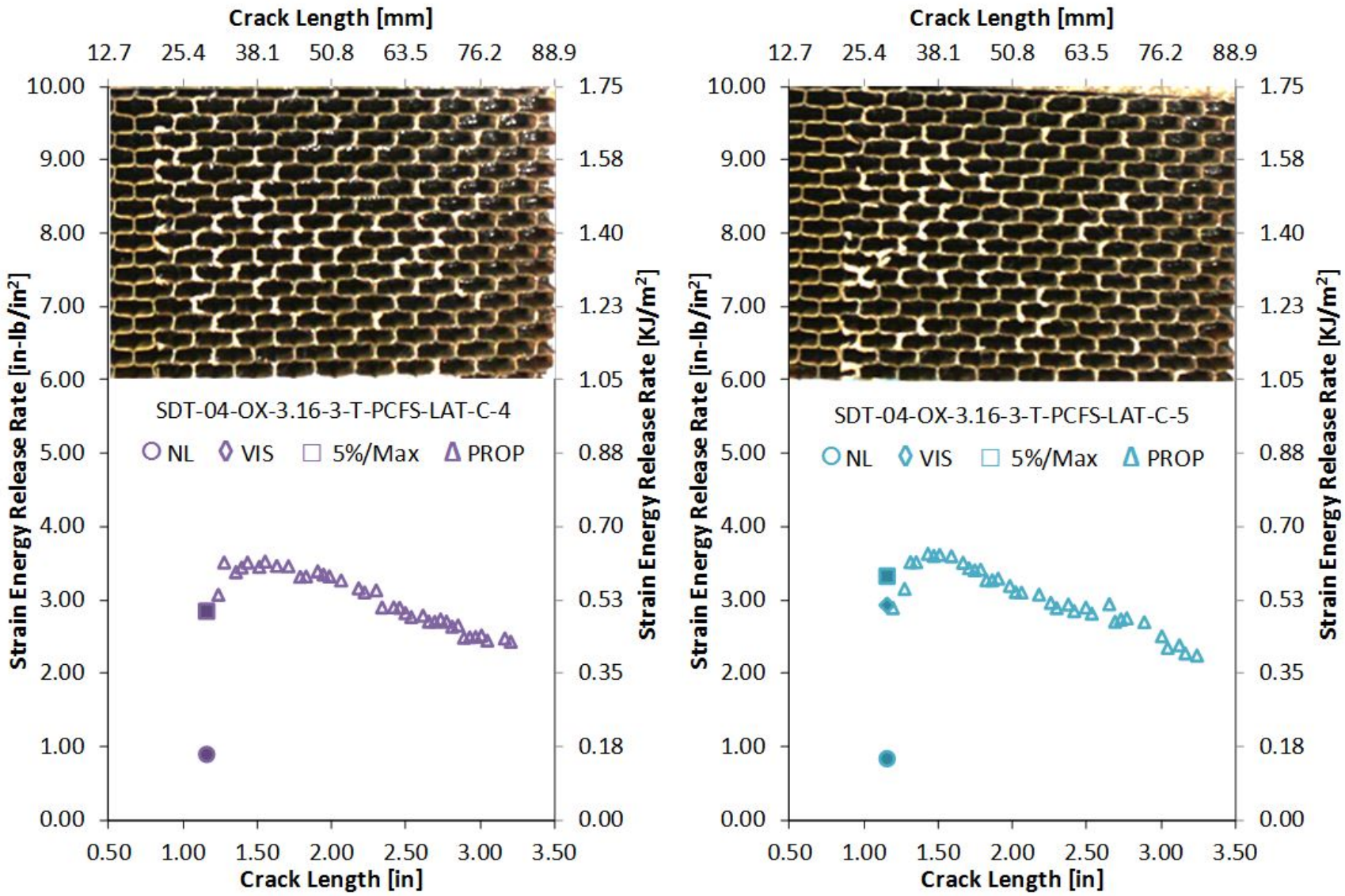

Figure C-16. Failure mode image and resistance curve of SDT-04-OX-3.16-3-T-PCFS-LAT-C-X #4 and #5

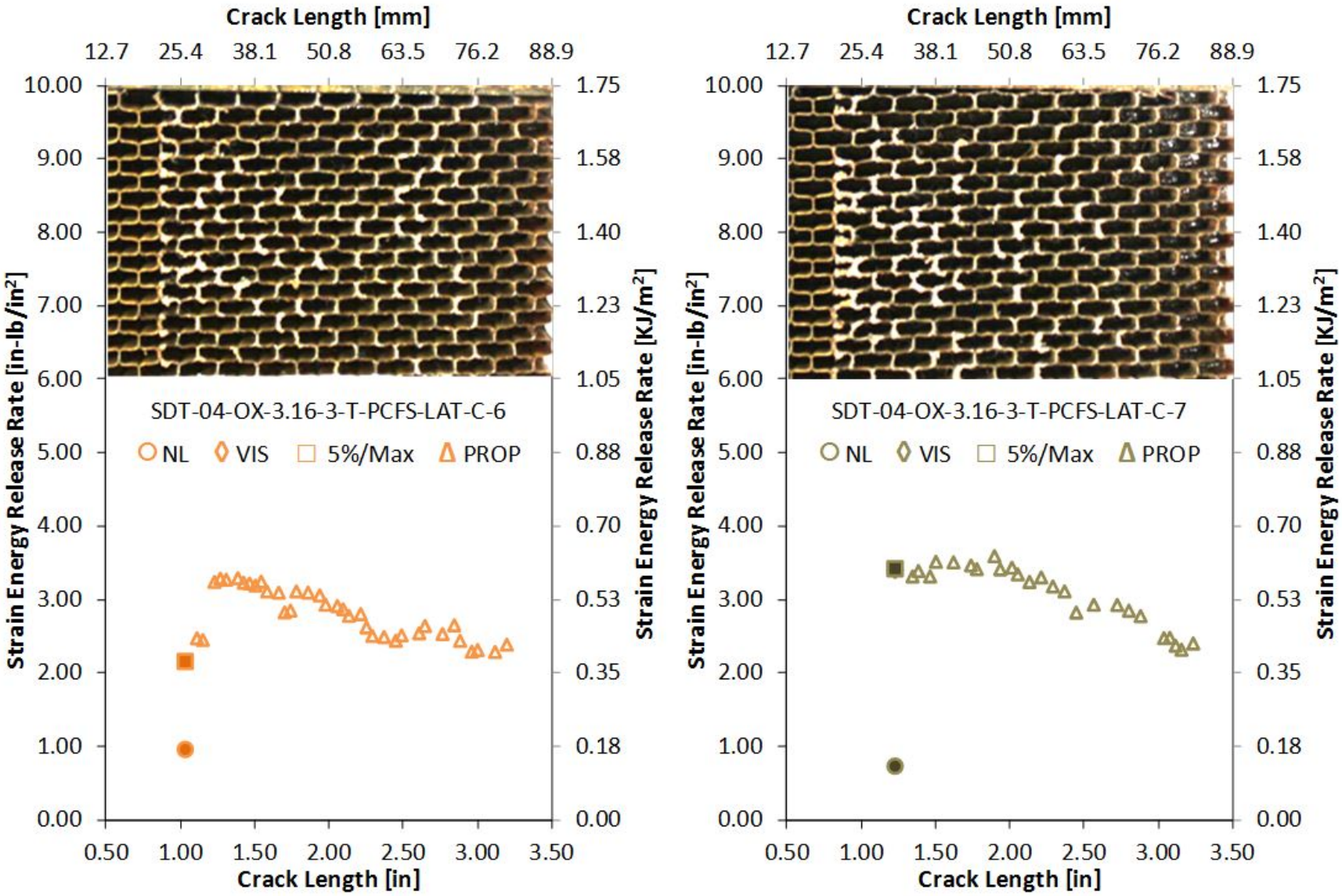

Figure C-17. Failure mode image and resistance curve of SDT-04-OX-3.16-3-T-PCFS-LAT-C-X #6 and #7

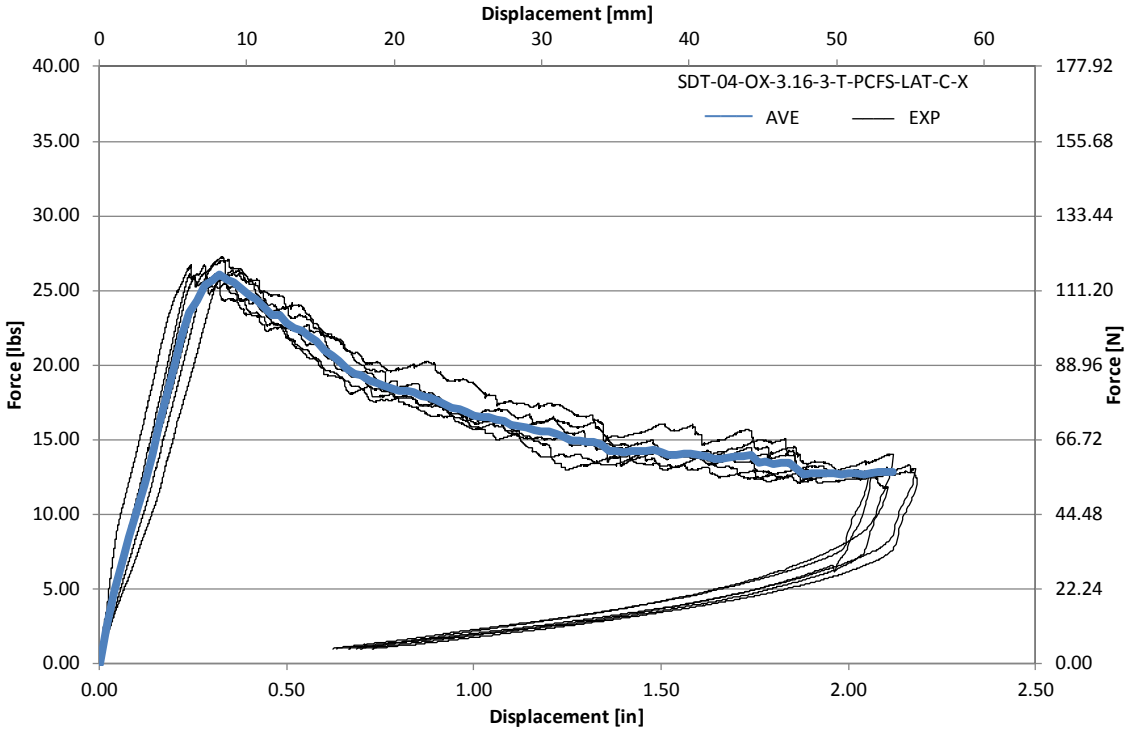

Figure C-18. Load vs. displacement curve for HRH-10/OX–3/16–3.0 lateral ribbon direction with top disbond (center)

C.1.4 HRH-10/OX–3/16–3.0 LATERAL RIBBON DIRECTION WITH BOTTOM DISBOND (CENTER) DATA

Table C-7. Test summary for HRH-10/OX–3/16–3.0 lateral ribbon direction with bottom disbond (center) pre-crack

Specimen	GIC (in-lb/in^2)			GIC (KJ/m^2)			Failure Mode
	NL	VIS	5%/max	NL	VIS	5%/max	
SDT-04-OX-3.16-3-B-PCFS-LAT-C-1	1.481	1.759	1.759	0.259	0.308	0.308	*
SDT-04-OX-3.16-3-B-PCFS-LAT-C-2	1.367	1.638	1.706	0.239	0.287	0.299	*
SDT-04-OX-3.16-3-B-PCFS-LAT-C-3	1.580	2.237	2.251	0.277	0.392	0.394	*
SDT-04-OX-3.16-3-B-PCFS-LAT-C-4	1.595	N/A	2.198	0.279	N/A	0.385	*
SDT-04-OX-3.16-3-B-PCFS-LAT-C-5	1.710	2.070	2.121	0.300	0.362	0.371	*
SDT-04-OX-3.16-3-B-PCFS-LAT-C-6	1.249	1.223	1.249	0.219	0.214	0.219	*
SDT-04-OX-3.16-3-B-PCFS-LAT-C-7							
SDT-04-OX-3.16-3-B-PCFS-LAT-C-8							
AVERAGE GIC	1.497	1.785	1.881	0.262	0.313	0.329	
STANDARD DEVIATION	0.168	0.395	0.385	0.029	0.069	0.067	
COEFFICIENT OF VARIATION (%)	11.207	22.105	20.461	11.207	22.105	20.461	

Notes	*	Primarily APO and C with several cells partially in APO; APO is primarily on the double cell walls in the ribbon direction.

Table C-8. Test summary for HRH-10/OX–3/16–3.0 lateral ribbon direction with bottom disbond (center)

Specimen	GIC (in-lb/in^2)				GIC (KJ/m^2)				Failure Mode
	NL	VIS	5%/max	AREA	NL	VIS	5%/max	AREA	
SDT-04-OX-3.16-3-B-PCFS-LAT-C-1	0.721	N/A	1.497	3.963	0.126	N/A	0.262	0.694	*
SDT-04-OX-3.16-3-B-PCFS-LAT-C-2	0.875	1.228	1.383	3.967	0.153	0.215	0.242	0.695	*
SDT-04-OX-3.16-3-B-PCFS-LAT-C-3	1.456	N/A	1.836	4.006	0.255	N/A	0.322	0.702	*
SDT-04-OX-3.16-3-B-PCFS-LAT-C-4	0.750	2.321	2.321	3.621	0.131	0.406	0.406	0.634	*
SDT-04-OX-3.16-3-B-PCFS-LAT-C-5	0.999	1.659	1.794	3.681	0.175	0.291	0.314	0.645	*
SDT-04-OX-3.16-3-B-PCFS-LAT-C-6	0.742	N/A	1.505	3.903	0.130	N/A	0.264	0.683	*
SDT-04-OX-3.16-3-B-PCFS-LAT-C-7									
SDT-04-OX-3.16-3-B-PCFS-LAT-C-8									
AVERAGE GIC	0.924	1.736	1.722	3.857	0.162	0.304	0.302	0.675	
STANDARD DEVIATION	0.281	0.550	0.343	0.164	0.049	0.096	0.060	0.029	
COEFFICIENT OF VARIATION (%)	30.433	31.700	19.935	4.255	30.433	31.700	19.935	4.255	

Notes	*	Primarily C with many cells partially in APO; APO is primarily on the double cell walls in the ribbon direction.

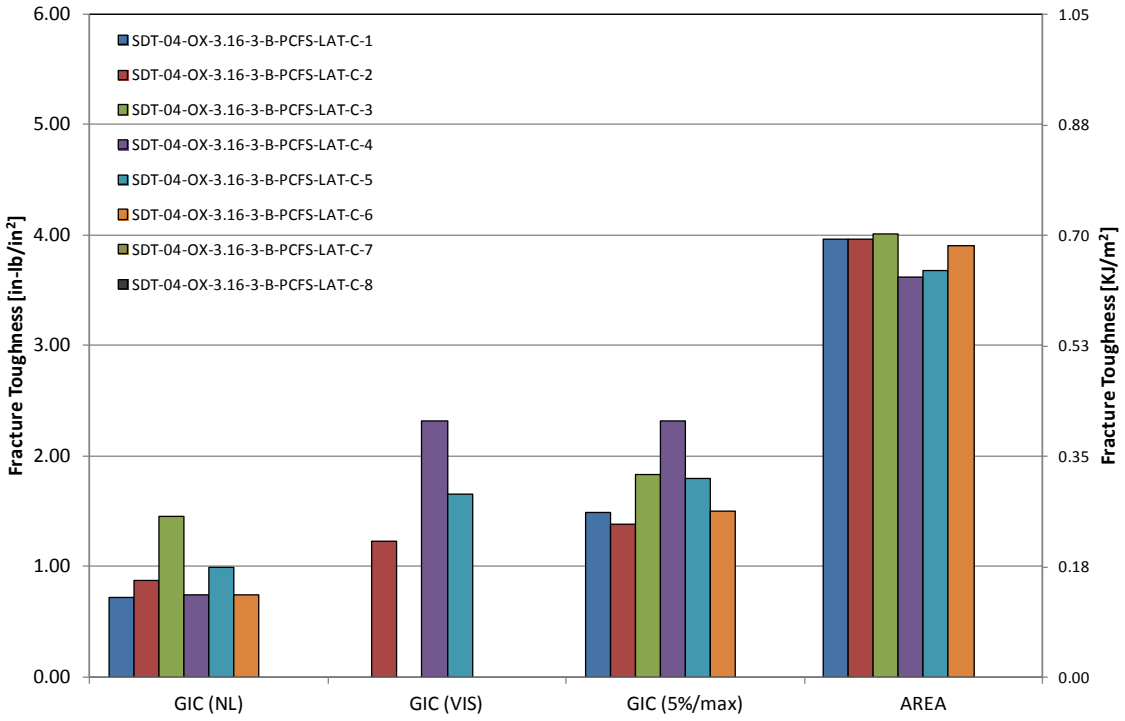

Figure C-19. GIC for HRH-10/OX–3/16–3.0 lateral ribbon direction with bottom disbond (center)

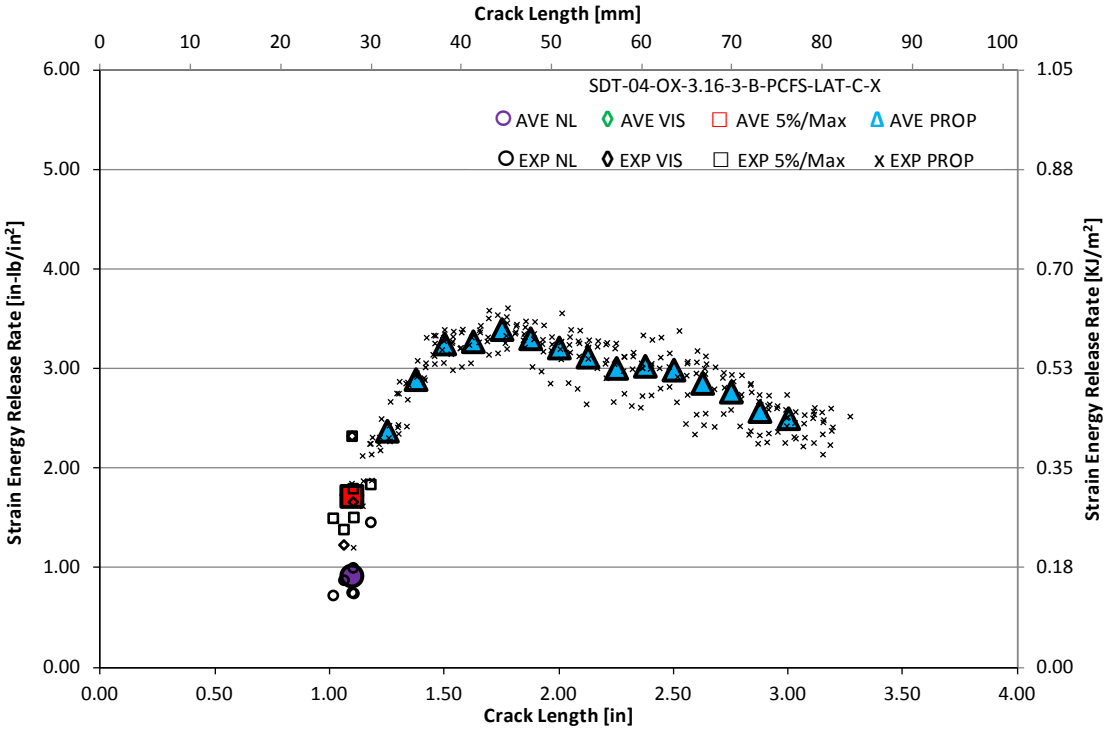

Figure C-20. Resistance curve for HRH-10/OX–3/16–3.0 lateral ribbon direction with bottom disbond (center)

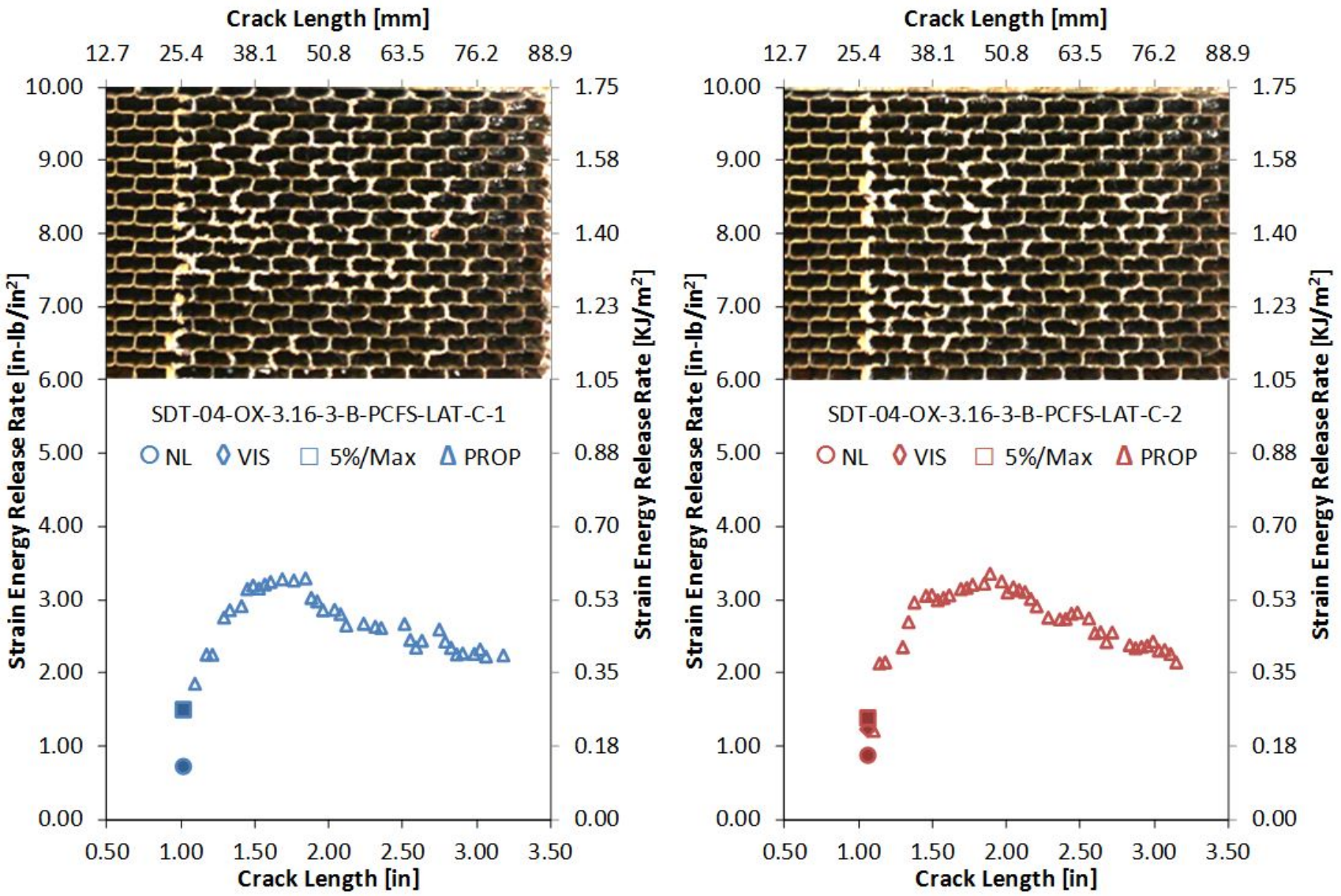

Figure C-21. Failure mode image and resistance curve of SDT-04-OX-3.16-3-B-PCFS-LAT-C-X #1 and #2

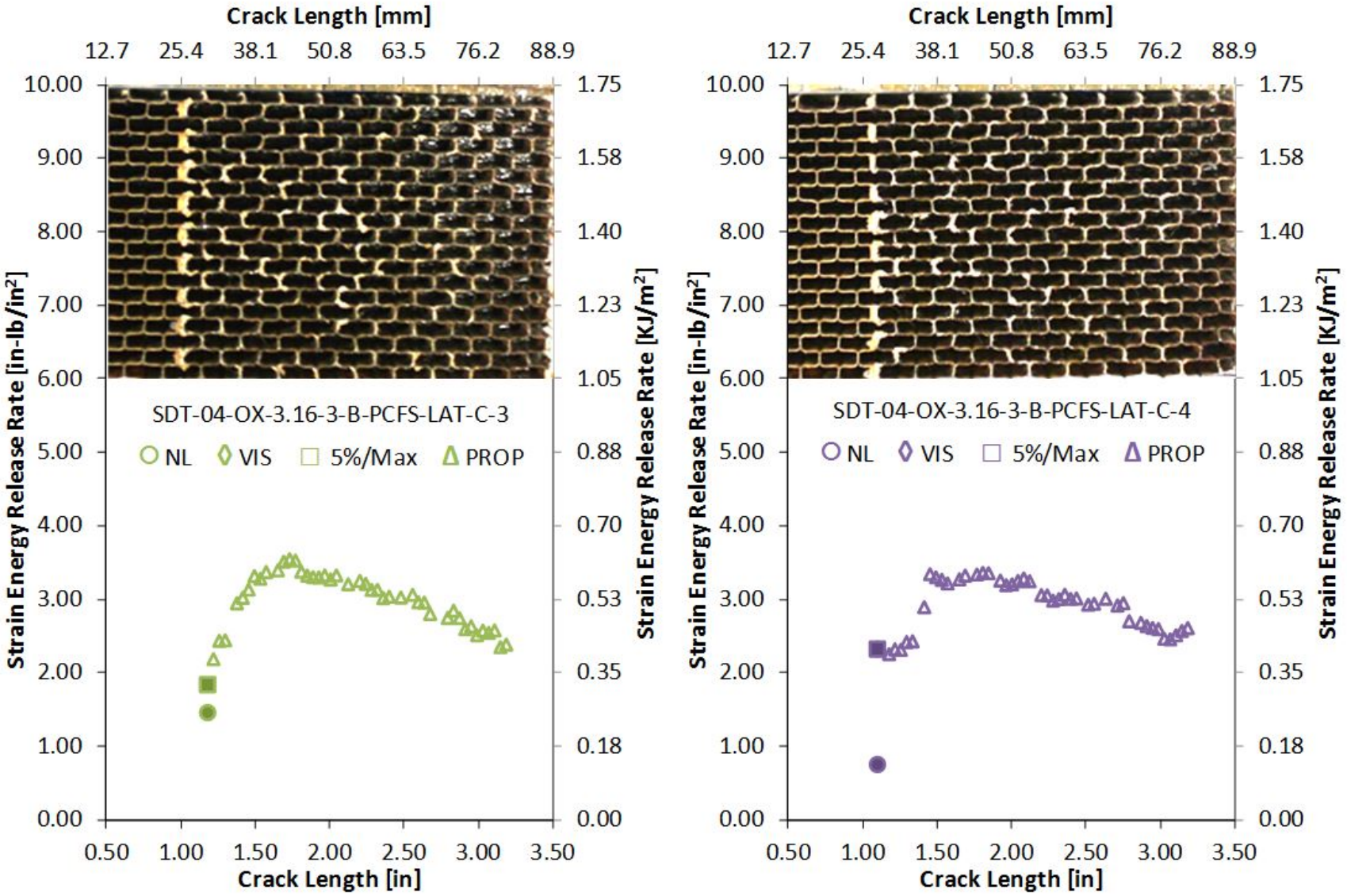

Figure C-22. Failure mode image and resistance curve of SDT-04-OX-3.16-3-B-PCFS-LAT-C-X #3 and #4

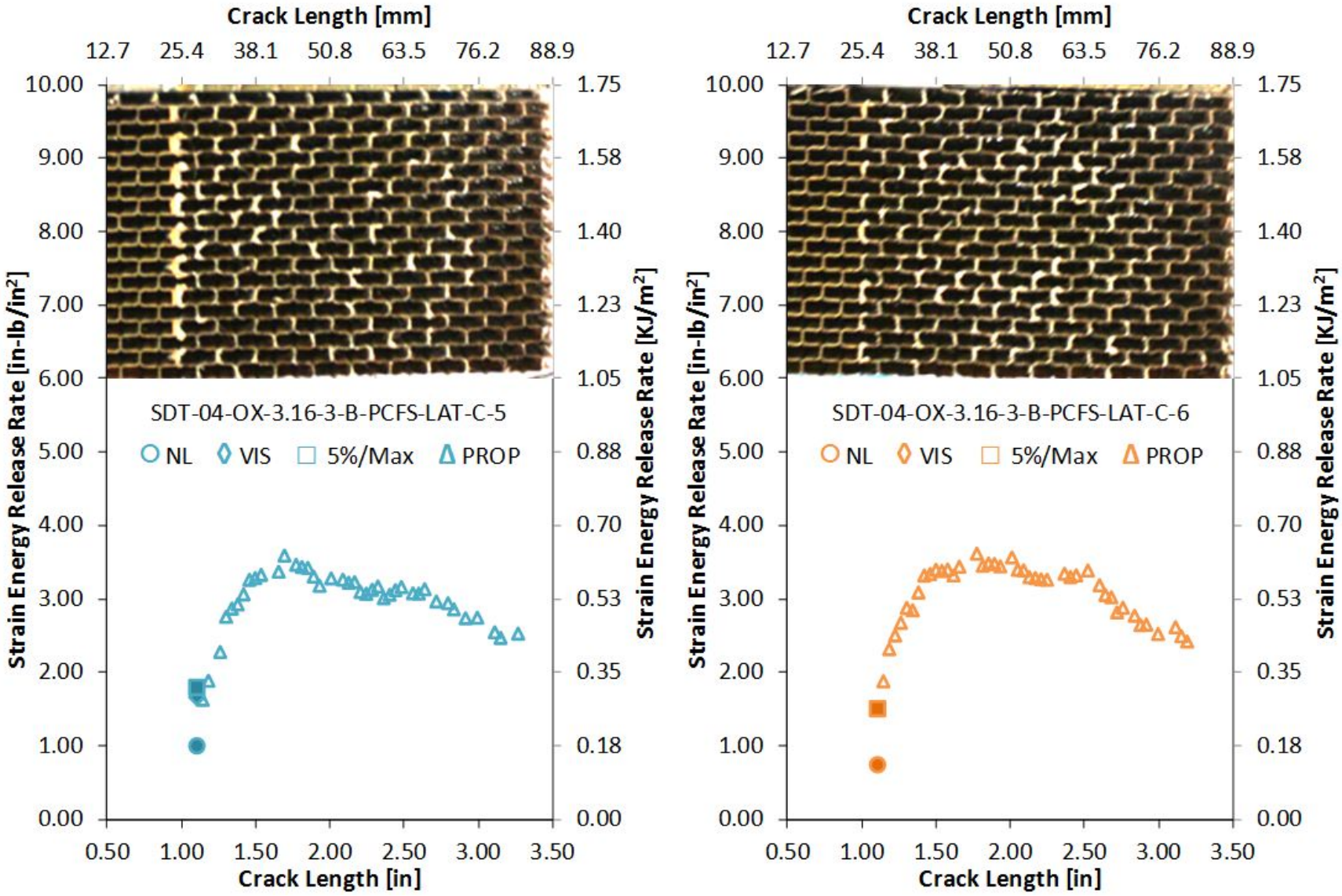

Figure C-23. Failure mode image and resistance curve of SDT-04-OX-3.16-3-B-PCFS-LAT-C-X #5 and #6

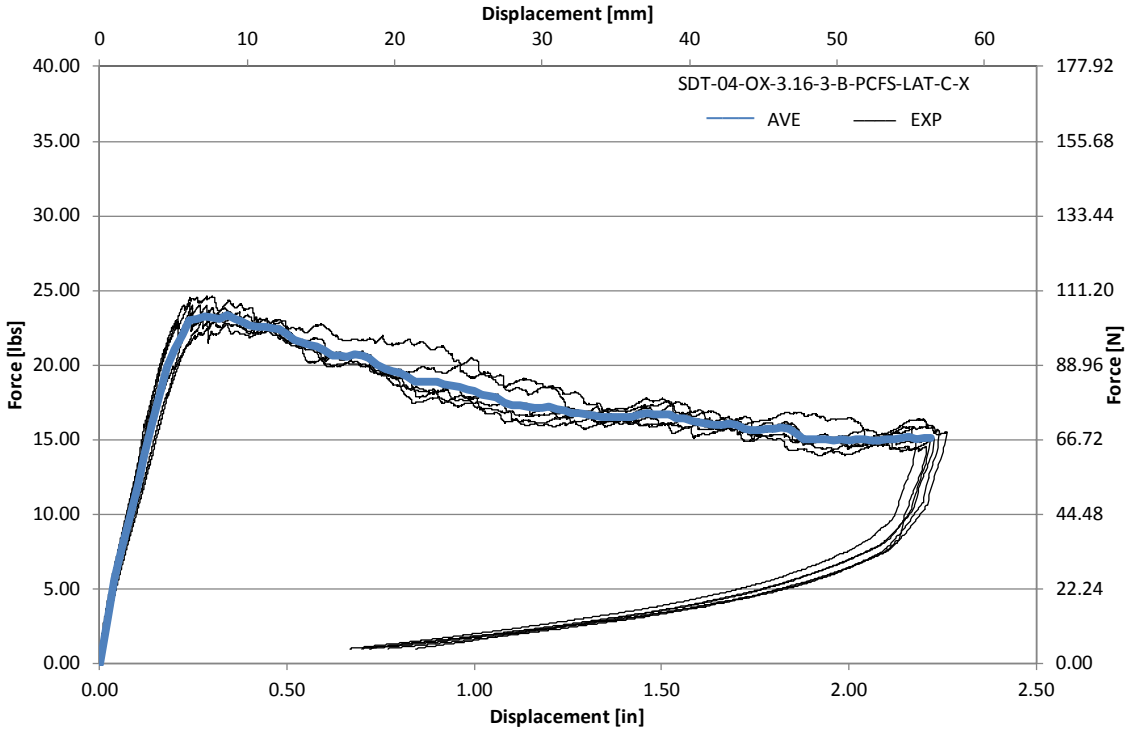

Figure C-24. Load vs. displacement curve for HRH-10/OX–3/16–3.0 lateral ribbon direction with bottom disbond (center)